UNIVERSITY OF OKLAHOMA

GRADUATE COLLEGE

TRILOBITE BIOFACIES, SYSTEMATICS AND FAUNAL TURNOVER IN A SEQUENCE STRATIGRAPHIC FRAMEWORK DURING THE UPPER ORDOVICIAN OF OKLAHOMA AND VIRGINIA

A DISSERTATION

SUBMITTED TO THE GRADUATE FACULTY

In partial fulfillment of the requirements for the

DEGREE OF

DOCTORY OF PHILOSOPHY

By

JESSE R. CARLUCCI
NORMAN, OKLAHOMA
2012

TRILOBITE BIOFACIES, SYSTEMATICS AND FAUNAL TURNOVER IN A SEQUENCE STRATIGRAPHIC FRAMEWORK DURING THE UPPER ORDOVICIAN OF OKLAHOMA AND VIRGINIA

A DISSERTATION APPROVED FOR THE
CONOCOPHILLIPS SCHOOL OF GEOLOGY AND GEOPHYSICS

BY

_____

Dr. Stephen Westrop, Chair

_____

Dr. Richard Lupia

_____

Dr. Richard Cifelli

_____

Dr. Lynn Soreghan

_____

Dr. Carlton Brett

ACKNOWLEDGEMENTS

Thank you to S. Westrop for all of the insight, suggestions, patience, and advice over the last four years. I've learned so much because of your experience. Most importantly, thank you for creating an environment where graduate students are free to pursue their own interests and ideas, and for treating us as colleagues rather than minions. Special thanks to R. Burkhalter for always being available to assist and offer advice. Your technical wizardry kept the SMOMNH lab running safely and smoothly, not an easy task! Thanks to R. Lupia for many discussions, both scientific and otherwise. Your suggestions and ideas have surely improved my teaching and research, and I really appreciate all the time you've taken to write letters on my behalf. I would like to offer my sincerest appreciation to the rest of my committee, G. Soreghan, R. Cifelli, and C. Brett for taking the time to evaluate my work, offer advice, write reference letters, and for teaching great classes that I learned extensively from. The enthusiasm shown by C. Brett for fieldwork is contagious; I'm very thankful for the time you have spent working with me in Oklahoma. Thanks to all of the organizations that funded my research or assistantships: National Science Foundation, ConocoPhillips School of Geology and Geophysics, Sam Noble Oklahoma Museum of Natural History, and the Geological Society of America.

K. Carlucci has provided an immense amount of support throughout this entire process. She has supported me 100% through medical problems, late night's writing papers, and the general frustration that comes with doing a Ph.D. I'm forever thankful for everything you've done for me in the last four years; I couldn't have done it without you.

TABLE OF CONTENTS

LIST OF FIGURES

ABSTRACT

In the Appalachian foreland basin of the eastern United States, major sedimentologic and geochemical changes occured during the Upper Ordovician (Sandbian-Katian). The modification of ocean circulation patterns, introduction of turbid, cool waters across eastern Laurentia, and the transport of fine-grained siliciclastics from the Taconic highlands have been attributed to biofacies replacments and faunal turnover in the basin. This study is a suite of systematic, paleoecological, and sedimentological studies on the trilobite faunas and their associated sedimentary environments during this time interval. High-resolution sequence statigraphic studies provide sea-level context, and facilitate geographic and temporal comparison of trilobite biofacies within similar depositional environments. Cumulatively, these studies demonstrate broad paleoecological and systematic similarities in trilobite faunas during the deposition of late Whiterockian and Mohawkian strata in two different Laurentian basins in Oklahoma and Virginia. These similarities diverge due to the effects of foreland basin development (relative sea level deepening, increase in siliciclastic input, and enhanced upwelling of colder, dysoxic water), which resulted in diachronous trilobite extinction events, and the spread of low diversity deep-water trilobite biofacies in Virginia. Moreover, many classic trilobite associations (e.g., illaenid-chierurid buildup association) were extirpated from the Taconic foreland basin during the same time interval. In regions outside the foreland basin during the same stratigraphic time interval (Bromide-Viola transition) in Oklahoma, diversity actually increases in similar environments, suggesting there is a unique environmental signal in the foreland basin.

CHAPTER 1: INTRODUCTION

In a NSF sponsored workshop in 2006, a series of contributors produced a document called "Future Research Directions in Paleontology" that outlined plans for the DETELO (Deep Time Earth Life Observatories) initiative. These observatories involve integrated teams of paleontologists, sedimentologists and stratigraphers, geochemists and other geoscientists all working on a particular question about Earth's history. These large-scale studies focus on integrating data sets of biologic, sedimentologic, geochemical, and modeling data over an extended research period. Consequently, the research questions must be important enough, and broad enough to justify such a large expenditure of resources. My dissertation is a contribution towards one of these broad interdisciplinary studies (NSF-EAR0819715), with the goal of understanding the effects of the development of the Taconic foreland basin on the associated Laurentian biosphere during the Mohawkian (Upper Ordovician).

In the Appalachian foreland basin of the eastern United States, major sedimentologic and geochemical changes occured during the Upper Ordovician (Sandbian-Katian): a switch from warm to cool water carbonate deposition, an increase in fine-grained siliciclastics and an increase in the relative proportion of phosphatic grains (Patzkowsky and Holland, 1993; Pope and Read, 1995, 1999; Holland and Patzkowsky, 1996). Modification of ocean circulation patterns and the introduction of turbid, nutrient rich, cool waters across the eastern United States were the environmental factors driving the lithologic changes (Patzkowsky and Holland, 1993; Pope and Read, 1995, 1999; Holland and Patzkowsky, 1996), likely as a result of foreland basin development, and possibly as a consequence of early Gondwanan glaciation (Saltzman and Young, 2005).

Biofacies replacements and faunal turnover in the foreland basin (e.g., Patzkowsky and Holland, 1993; Holland and Patzkowsky, 1996; 2007) has been documented in brachiopods and corals, corresponding well to the switch in carbonate types. The replacement dynamics of trilobite biofacies in response to these changes has not been investigated prior to this project.

Far outside the Taconic foreland basin, the Upper Ordovician (Sandbian) Bromide Formation (Simpson Group) of Oklahoma has trilobite faunas that are conspicuous in many different sedimentary environments, from pertidal carbonates to basinal shales and mudstones. For this reason, the trilobite faunas of the Bromide are an ideal "control" to evaluate biotic change in response to changing environmental factors in the foreland basin. Systematic work has been done on some groups of trilobites in the Bromide and Viola Formations (e.g., Esker, 1964; Shaw, 1974; Ludvigsen, 1978; Amati and Westrop, 2004). However, many groups remain poorly known. Proper systematic assignment is essential for any research that uses estimates of abundance and diversity, as they could become biased if specimens are assigned to artificial higher taxonomic groups. The Bromide has previously been interpreted as a transgression-regression cycle, with facies deepening upward until carbonate sedimentation exceeded available accommodation space, reversing the cycle (Longman, 1976; Longman, 1982). In order to provide a context for sea level and accommodation space change during the deposition of the trilobite biofacies, I investigated the facies associations and sequence stratigraphic patterns of the Bromide at a variety of hierarchical scales.

My dissertation focuses on current gaps in knowledge concerning trilobite bioevents in the Sandbian of Oklahoma and Virginia. Specifically on depth related

biofacies (along ramp gradients), during stages two through five (Read, 1980) of the Taconic Orogeny, with the unstudied portions of the Bromide Formation, Oklahoma acting as a control to isolate patterns of trilobite biofacies replacement unique to the foreland basin region. I document new and previously undescribed trilobite species (chapters 2, 3, appendix 3) in Oklahoma, Virginia, and Missouri, and quantitatively analyse their phylogenetic relationships. This allows direct counts of the constituent genera across geographical locations to be compared and analyzed statistically without systematic bias. Using measured sections, petrologic thin sections, hand samples, outcrop gamma ray, well-logs and faunal analyses, I provide updated interpretations of the depositional histories and facies architecture of the Bromide Formation in Oklahoma (chapter 4, appendix 1), and of the Effna Limestone, Liberty Hall facies, and Botetourt Member of the Edinburgh Formation in Virginia (chapter 5, appendix 1). This provides the environmental context and reconstruction of sea level changes that are necessary for the two paleoecologic studies (chapters 5, 6) on trilobite biofacies along depth gradients in the Southern Oklahoma Aulacogen (SOA) and in the Taconic foreland basin.

In chapter 2, I described new species of tetralichine trilobites (*Probolichas kristiae*, *Amphilichas effnensis*) from the Bromide Formation in Oklahoma, and the Effna Limestone in Virginia, as well as all available type species of the group. Descriptive work was supplemented by a quantitative phylogenetic analysis that was conducted using MacClade (Maddison and Maddison, 2005), TNT (Goloboff et al., 2008) and PAUP (Swofford, 2002) software. A strict consensus tree of nine equally most parsimonious trees provides evidence that *Probolichas* Phleger, 1936 is a monophyletic group, and is not synonymous with, or a sub-clade of *Amphilichas* Raymond, 1905. My analysis also

indicated that the genus *Apatolichas* Whittington, 1963 should be revised as it appears to be synonymous with *Amphilichas*, and that the genus *Pseudotupolichas* Phleger, 1936 should be removed from the tribe Tetralichini because of low node support. Since these genera are conspicuous in both the Bromide Formation in Oklahoma, and Effna Limestone in Virginia, this chapter not only contributed to Ordovician trilobite systematics, but improved the biologic resolution of my relative abundance counts.

In chapter 3, I explored the phylogenetic relationships of another problematic trilobite group (*Bumastoides*) that is common in Mohawkian strata in Oklahoma and Virginia. I described three new species (*B. graffhami* sp. nov; *B. moundensis* sp. nov; and *B. kimmswickensis* sp. nov), developed character matrices and conducted a phylogenetic analysis on all the well-documented species within the genus. In doing so, I compared the performance of two separate continous character coding methodologies on my dataset. Finite Mixture Coding (Strait et al., 1996) and coding continuous characters "as such" (Golboloff et al., 2006) were used in the treatment of seven measured characters, included in the larger matrix of 19 discrete characters. Both methodologies yielded similar trees that had very high node support (symmetrical resampling group support and GC values, Golboloff et al., 2005) suggesting that the monophyly of *Bumastoides* required the removal of species that are more similar to the illaenid genus *Stenopareia*. Once again, while my systematic work contributed to the overall study of illaenid trilobites, it was also directly applicable to my estimates of biologic diversity in chapters 5 and 6.

Chapter 4 is a local paleoecological study of trilobite biofacies that were deposited during the initial phases of the Taconic orogeny. The environments I studied

were two carbonate bioherms and their associated biostromes (Effna Limestone), adjoining deep flank deposits (Botetourt Member of the Edinburgh Formation), and the overlying outer-slope to basinal mudstones (Liberty Hall facies of the Edinburgh Formation). I describe the lithofacies of the units, and made trilobite collections from multiple levels within the units. I treated counts of trilobite individuals with QxR mode cluster analysis, ordinations (NMDS, DCA), and rarefaction in PAST (Hammer et al. 2001) to define and characterize biofacies and environmental gradients. Biofacies were clearly delineated along a depth gradient, with gradational compositional changes between associations of trilobites with similar environmental preferences. In addition, the data suggests that there may be faunal differences between the separate buildups. My analysis demonstrates that the standard archetypes of triobite biofacies (e.g., illaenid-cheirurid in buildups, *Ampyx*-nileids in slope settings) were present in the Taconic foreland basin before major regional extirpation and reorganization in similar environments in younger strata. Finally, my study shows quantitative evidence that there are ecological differences between subenvironments in mud-mound complexes. These issues have been discussed elsewhere (e.g., Ross, 1972; Mikulic, 1981) but not subject to robust statistical treatment.

Prior to analyzing the patterns of faunal turnover and trilobite biodiversity in the Bromide Formation, I conducted field work over the course of three years in order to develop a robust sequence stratigraphic depositional model. Stratigraphic biases (much like systematic biases) can distort patterns of faunal change and diversity. Sequence stratigraphic techniques allow for the removal of facies bias, unconformity bias, and condensation bias (Holland, 2000) in paleoecological studies. Moreover, a robust

sequence stratigraphic model also can account for biostratigraphic inconsenstencies due to incomplete preservation of certain systems tracts in parts of a basin. Chapter 5 is my primary sedimentological contribution to the dissertation. It involves describing and reinterpreting the facies associations, bounding surfaces and sequences of the Bromide Formation. My dataset was an assortment of detailed measured sections, portable gamma ray logs, subsurface well logs, thin-sections, polished slabs, over 50 field-collected paleontological collections, museum collections (Shaw, 1974; Sprinkle, 1982; Karim and Westrop, 2002), and hundreds of lithologic samples and photographs. My study revealed the presence of three major 3rd order depositional cycles that document the transition from a siliciclastic-dominated ramp to a carbonate-dominated ramp. Many levels of cyclicity that have not previously been studied (meter-scale, decameter-scale, etc.) suggest rhythmic changes in rates of sea level rise and fall, and available sediment supply. New correlations and facies associations suggests that the Pooleville Member of the Bromide Formation may be condensed downramp, and provide the tools necessary to correlate the sequences into the subsurface. Chapter 5 provides the necessary environmental framework for the discussion of paleoecological trends in chapter 6.

Chapter 6 is a paleoecological study of the trilobite biofacies within the Bromide Formation, their relation to environmental gradients, and how they integrate into the sequence stratigraphic model developed in chapter 5. The statistical methods are similar to chapter 4 (ordination, QxR mode cluster analysis, rarefaction, etc.), but I also made an effort to account for the distribution of biofacies in relation to systems tracts and depositional sequences. The Bromide is dominated by associations of isoteline trilobites and other offshore elements (*Cybeloides*, *Thaleops*, *Remopleurides*, etc.) in the outer-

ramp environment, low diversity *Anataphrus*-illaenid (e.g., *Failleana*) dominated associations in transgressive inner-ramp shoals, a *Thaleops*-*Calyptaulax* association in middle-ramp settings, and a high diversity *Lonchodomas*-*Frencrinuroides* association in middle to outer-ramp environments in the Criner Hills. Rarefaction analyses show that trilobite diversity in comparable environments in the Viola Formation increased when compared to the Bromide trilobite fauna.

Appendices 1-3 are additional work that I completed, but are not explicility illustrated or discussed elsewhere. This includes illustrations and brief discussions of Bromide trilobites not given phylogenetic treatment, annotated measured sections that were not illustrated or have been reduced in size elsewhere in my dissertation, and relative abundance counts of areas in Virginia that are not treated in any of my analyses.

Cumulatively, these chapters are my contribution towards NSF-EAR0819715. They demonstrate broad paleoecological and systematic similarities in trilobite faunas during the deposition of late Whiterockian and Mohawkian strata in two different Laurentian basins. These similarities diverge due to the effects of foreland basin development (relative sea level deepening, increase in siliciclastic input, and enhanced upwelling of colder, dysoxic water), which resulted in diachronous trilobite extinction events, and the spread of low diversity deep-water trilobite biofacies in Virginia. Moreover, many classic trilobite associations (e.g., illaenid-chierurid buildup association) were extirpated from the Taconic foreland basin during the same time interval. Conversely, over the same stratigraphic time interval (Bromide-Viola transition) in Oklahoma, diversity actually increases in similar environments, suggesting there is a unique environmental signal in the foreland basin.

REFERENCES

AMATI, L., and WESTROP, S., 2004, A systematic revision of *Thaleops* (Trilobita: Illaenidae) with new species from the middle and late Ordovician of Oklahoma and New York: Journal of Systematic Palaeontology, v. 2, p. 207-256.

ESKER, G.C., 1964, New species of trilobites from the Bromide Formation (Pooleville Member) of Oklahoma: Oklahoma Geology Notes, v. 24, p. 195-209.

GOLOBOFF, P.A., FARRIS, J.S., KALLERSJO, M., OXELMAN, B., RAMIREZ, M.J., and SZUMIK, C.A., 2005, Improvements to resampling measures of group support: Cladistics, v. 19, p. 324-332.

GOLOBOFF, P.A., MATTONI, C.I., and QUINTEROS, A.S., 2006, Continuous characters analyzed as such: Cladistics, v. 22, p. 589-601.

GOLOBOFF, P., FARRIS, J., and NIXON, K., 2008, TNT, a free program for phylogenetic analysis: Cladistics, v. 24, p. 774-786.

HAMMER, O., HARPER, D., and RYAN, P., 2001, PAST: Paleontological statistics software for education and data analysis: Palaeontologia Electronica, v. 4.

HOLLAND, S., and PATZKOWSKY, M., 1996, Sequence stratigraphy and long-term paleooceanographic changes in the Middle and Upper Ordovician of the eastern United States, *in* Witzke, B., Ludvigson, G., and Day, J., eds., Paleozoic Sequence Stratigraphy: Views from the North American Craton, GSA Special Paper 306: Boulder CO, Geological Society of America.

HOLLAND, S., and PATZKOWSKY, M., 2007, Gradient ecology of a biotic invasion: biofacies of the type Cincinnatian series (Upper Ordovician), Cincinnati, Ohio Region, USA: PALAIOS, v. 22, p. 392-407.

HOLLAND, S.M., 2000, The quality of the fossil record-a sequence stratigraphic perspective, *in* Erwin, D.H., and Wing, S.L., eds., Deep Time: Paleobiologies Perspective: Lawrence, KS, Paleontological Society.

KARIM, T., and WESTROP, S., 2002, Taphonomy and Paleoecology of Ordovician Trilobite Clusters, Bromide Formation, south-central Oklahoma: PALAIOS, v. 17, p. 394-403.

LONGMAN, M.W., 1976, Depositional history, paleoecology, and diagenesis of the Bromide Formation (Ordovician) Arbuckle Mountains, Oklahoma, University of Texas at Austin, 311 p.

LONGMAN, M.W., 1982, Depositional environments, *in* Sprinkle, J., ed., Echinoderm Faunas from the Bromide Formation (Middle Ordovician) of Oklahoma, University of Kansas Paleontological Contributions, Monograph, p. 17-29.

LUDVIGSEN, R., 1978, The trilobites *Bathyurus* and *Eomorachus* from the Middle Ordovician of Oklahoma and their biofacies significance: Life Sciences Contributions ROM, v. 114, p. 1-17.

MADDISON, D., and MADDISON, W., 2005, MacClade: Analysis of Phylogeny and Character Evolution, 4.08: Sunderland, MA, Sinauer Associates Inc.

MIKULIC, D.G., 1981, Trilobites in Paleozoic carbonate buildups: Lethaia, v. 14, p. 45-56.

PATZKOWSKY, M., and HOLLAND, S., 1993, Biotic response to a Middle Ordovician paleoceanographic event in eastern North America: Geology, v. 21, p. 619-622.

PATZKOWSKY, M., and HOLLAND, S., 1999, Biofacies Replacement in a Sequence Stratigraphic Framework: Middle and upper Ordovician of the Nashville Dome, Tennessee, USA: PALAIOS, v. 14, p. 301-323.

PHLEGER, F., 1936, Lichadian Trilobites: Journal of Paleontology, v. 10, p. 593-615.

POPE, M.C., and READ, J.F., 1995, Sequences and meter-scale cyclicity of Middle to Late Ordovician cool water carbonates and clastics, *in* Cooper, J.D., Droser, M.L., and Finney, S.C., eds., Ordovician Odyssey: Short Papers for the Seventh International Symposium on the Ordovician System: Pacific Section, Society for Sedimentary Geology, p. 333-336.

READ, J.F., 1980, Carbonate ramp-to-basin transitions and foreland basin evolution, Middle Ordovician, Virginia Appalachians: AAPG Bulletin, v. 64, p. 1575-1612.

ROSS, J., 1972, Fossils from the Ordovician bioherm at Meiklejohn Peak, Nevada: Geological Survey Professional Paper v. 685, p. 1-47.

SALTZMAN, M.R., and YOUNG, S.A., 2005, Long-lived glaciation in the Late Ordovician? Isotopic and sequence stratigraphic evidence from western Laurentia: Geology, v. 33, p. 109-112.

SHAW, F., 1974, Simpson Group (Middle Ordovician) Trilobites of Oklahoma: Journal of Paleontology Memoir, v. 48, p. 1-54.

SPRINKLE, J., 1982, Echinoderm zones and faunas, *in* Sprinkle, J., ed., Echinoderm Faunas from the Bromide Formation (Middle Ordovician) of Oklahoma, University of Kansas Paleontological Contributions, Monograph 1, p. 47-56.

STRAIT, D., MONIZ, M., and STRAIT, P., 1996, Finite Mixture Coding: A new approach to coding continuous characters: Systematic Biology, v. 45, p. 67-78.

SWOFFORD, D.L., 2002, PAUP* Phylogentic Analysis Using Parsimony (*and other methods), Version 4.0b10: Sunderland, MA, Sinauer Associates.

WHITTINGTON, H.B., 1963, Middle Ordovician trilobites from Lower Head, western Newfoundland: Bulletin of the Museum of Comparative Zoology, v. 129, p. 1-118.

CHAPTER 2: TETRALICHINE TRILOBITES FROM THE UPPER ORDOVICIAN OF OKLAHOMA AND VIRGINIA, AND PHYLOGENETIC SYSTEMATICS OF THE TETRALICHINI

ABSTRACT—New material, including a complete exoskeleton, from the Bromide Formation of Oklahoma, allows a complete evaluation of *Probolichas* Phleger, 1936 and necessitates a quantitative revision of the lichid tribe Tetralichini Phleger, 1936. A strict consensus tree of nine equally parsimonious trees generated from a branch and bound analysis indicates that the genus *Probolichas* is monophyletic, and should no longer be restricted as synonymous with, or as a sub-clade of *Amphilichas* Raymond, 1905. The genus *Apatolichas* Whittington, 1963 is revised as a synonym of *Amphilichas*, and the Tetralichini is defined as clade with three genera: *Amphilichas*, *Probolichas*, and *Lyralichas* Weber, 1948. *Probolichas kristiae* from the Bromide Formation and *Amphilichas effnensis* from the Effna Formation of Virginia are new species.

INTRODUCTION

THE GENUS *Probolichas* was erected by Phleger (1936) to describe tetralichine trilobites with an anterior projection (proboscis) from the median lobe, and an otherwise *Amphilichas*-like grade of organization. Some authors have questioned the taxonomic validity of *Probolichas* (Phleger, 1936) as a genus (Warburg, 1939; Thomas and Holloway, 1988), because the presence of a proboscis was not viewed as a genus level characteristic, especially when no pygidia have been associated with *Probolichas* cranidia. There are three competing hypotheses presented in the literature: *Probolichas* is a distinct genus (Phleger, 1936), *Probolichas* is a subgenus of *Amphilichas* (Evitt, 1951),

and *Probolichas* is a synonym of *Amphilichas* (Warburg, 1939). We agree with Thomas and Holloway (1988) that these hypotheses can be evaluated only when *Probolichas* cranidia and pygidia are correctly associated with each other. Here, we describe new, completely articulated material of *Probolichas kristiae* n. sp., from the Bromide Formation (Cooper, 1956) of Oklahoma. In addition to new material, some of the relevant *Probolichas* and *Amphilichas* specimens originally described from the Bromide by Shaw (1974) are re-illustrated and re-described herein. These data are supplemented by comparison to new tetralichine material from the Viola Springs Group of Oklahoma (Finney, 1986; Amati and Westrop, 2006) and the Effna Limestone (Cooper, 1944; Cooper, 1956; Read, 1980) of Virginia.

Pollitt et al., (2005) recognized the Tetralichini as a monophyletic group in their extensive phylogenetic analysis of the Lichidae Hawle and Corda, 1847. However, support for the Tetralichini as a clade was low, and their work focused on the higher taxonomic groupings of the Lichidae (see Pollitt et al., 2005, fig. 9), so there remain unanswered questions regarding the relationships of ingroup Tetralichini. Phleger (1936) erected the genera *Tetralichas* and *Kerakephalichas* within (what is now) the Tetralichini, but Thomas and Holloway (1988) treated them as synonyms of *Amphilichas* based on their estimation of characters of generic importance. Furthermore, various authors (Phleger, 1936; Tripp, 1957, Thomas and Holloway, 1988) have noted the significant variation within *Amphilichas*, especially in comparison to the type species (*A. lineatus* Angelin, 1854), which has markedly different longitudinal furrow morphology than most species assigned to this genus. These issues combined with uncertainties over the correct

sclerite associations for *Probolichas* demonstrate the need for a modern systematic revision of the Tetralichini.

Herein we: 1) illustrate and describe *Probolichas kristiae* n. sp., *Amphilichas effnensis* n.sp., and other tetralichine species from the Simpson Group of Oklahoma and Effna Limestone of Virginia; 2) re-illustrate and re-describe (where necessary) type specimens of tetralichine genera; 3) conduct a phylogenetic analysis of all genera within the Tetralichini (*Amphilichas*, *Probolichas*, *Apatolichas*, *Lyralichas*, and *Pseudotupolichas* Phleger, 1936); 4) Revise the Tetralichini using the results of the phylogenetic analysis.

GEOLOGIC SETTING

Locality and collection information.—Two localities in Oklahoma, and one in Virginia yielded the trilobite collections used in this work. The Oklahoma collections are from: Rock Crossing (RC) located 9 km southwest of Ardmore, OK and Tyson's Quarry (TQ), located 8 km southwest of Ardmore, OK (Figs. 1 and 2). We made additional collections from RC and TQ to supplement those already made by Thomas Eckert (Eckert, 1951, unpublished M.S. thesis) and those donated by Allen Graffham (Geological Enterprises Ltd) to the Sam Noble Oklahoma Museum of Natural History. The collections at TQ are taken from the upper Pooleville, in rudstone pavements (interpreted as tempesites) that top blue massive carbonate wackestone (see Fig. 2). The collections at RC were taken from 30.48-36.6 m (Eckert, 1951) below the Viola contact in a light tan mudstone/wackestone facies of the Lower Pooleville (see Sprinkle, 1982, p. 363 for a detailed measured section).

Porterfield Quarry (PQ, Fig 3) is an abandoned facility located approximately 7 km southwest of Saltville (Smyth County), Virginia. The quarry is exposed approximately 1 km down the unlabeled service road (off VA 610), and consists of over 2 km of exposed rock along strike (SW to NE, see Fig. 3.3), although most of the Effna buildup has been quarried out. The PQ collections are from boulders in the Effna biohermal (Read, 1982) limestone (Fig. 3.3), left behind when the quarry ceased operation.

Oklahoma stratigraphy and depositional setting.—The Bromide Formation (Ulrich, 1911) is an Upper Ordovician (Sandbian; Turinian) mostly carbonate succession that is the youngest unit in the Simpson Group, which also includes the Joins, Oil Creek, McLish, and Tulip Creek formations (Cooper, 1956; Harris, 1957). In south-central Oklahoma, the Bromide Formation is well exposed throughout the Arbuckle Mountains and Criner Hills regions. It was deposited along a carbonate ramp that extended from the Arbuckle Platform into the Southern Oklahoma Aulacogen (Fig. 1). The Southern Oklahoma Aulacogen was a subsiding trough within the Oklahoma Basin, an arm of a failed triple rift system (Longman, 1982a, b). The two sub-units of the Bromide Formation are the stratigraphically older Mountain Lake Member, and the overlying Pooleville Member (Cooper, 1956). The facies composition and fauna of these units changes dramatically based on their location within the platform to aulacogen transition. A lowstand systems tract of massive sandstones and sandy crinoidal grainstone characterizes the lower Mountain Lake Member. These are overlain by meter scale deep ramp cycles of carbonate mudstone, wackestone, and occasional rudstone. The cycle tops are irregular, mineralized, starved surfaces, commonly associated with bryozoan obrution

horizons. Up-ramp, the Pooleville member consists of an early highstand interval of shallow subtidal carbonate mudstone, wackestone, and grainstone, with heavily reworked brachiopod and trilobite tempesites commonplace. The overlying late highstand peritidal carbonates are commonly referred to as the Corbin Ranch Submember (Harris, 1957; Amsden and Sweet, 1983).

The Bromide Formation faunas are very diverse. Bromide ostracods, conodonts, brachiopods, acritarchs, bryozoans, and graptolites have been relatively well studied, consisting of over 300 described species (see Fay and Graffham, 1982 for compilation). Trilobites from the Bromide Formation have been studied (Esker, 1964; Shaw, 1974; Ludvigsen, 1978; Karim and Westrop, 2002; Amati and Westrop, 2004; Amati and Westrop, 2006), but there still remains much work in terms of the trilobite systematics, biostratigraphy, and paleoecology. Preliminary observations indicate that the Mountain Lake Member is characterized by low diversity assemblages dominated by "*Homotelus"*, with diversity rapidly increasing in the early highstand interval of the Pooleville. *Calyptaulax* Cooper, 1930, *Thaleops* Conrad, 1843, *Bumastoides* Whittington, 1954, *Ceraurus*, Green, 1832, *Dolichoharpes* Whittington, 1949, *Harpidella* M'Coy,1849, *Remopleurides* Portlock, 1843, *Failleana* Chatterton and Ludvigsen, 1976, *Lonchodomas* Angelin, 1854, *Amphilichas*, and *Probolichas* occur in rudstone pavements in the Pooleville. The majority of these genera become locally extinct or migrate out of the area when peritidal conditions develop (see Amati and Westrop, 2006) during the Corbin Ranch interval, indicating that trilobite diversity in the Bromide is highest in mid-ramp to inner ramp environments.

Virginia stratigraphy and depositional setting.—The Upper Ordovician (Sandbian) carbonate ramp to basin transition in the Valley and Ridge province of Virginia (see Read, 1982, fig. 1) contains numerous local buildup facies, referred to as the Ward Cove, Rockdell, Murat, and Effna limestones. These build-ups are similar to Carboniferous Waulsortian mounds (Wilson, 1975, Read, 1982) in that frame building organism are of minor importance, and marine cementation in combination with baffling of carbonate fines by bryozoans and pelmatazoan crinoids likely helped mound development (Read, 1982; King, 1986). The Effna Formation (Fig. 3) is composed of downslope buildups, which overlie shallower inner to midramp facies that include wackestone of the Lincolnshire Limestone (referred to as the Lenoir downramp), and the fenestral carbonates of the Mosheim Limestone. The Effna underlies the Liberty Hall Formation, which is an interbedded basinal shale and carbonate mudstone facies. The Effna Formation consists of two sub-units (Sabol, 1958; Ruppel and Walker, 1977; Read 1982). The lower unit is a pelmatazoan and bryozoan grainstone, presumably biostromal, which formed as debris was shed from the buildups. The other unit is the buildups (or pods) themselves, which are primarily carbonate mudstone and wackestone, although ramose, lacy, and encrusting bryozoans often form bafflestone. The Botetourt Limestone (Cooper and Cooper, 1946) is a dark, nodular grainstone (wackestone and packstone are developed locally) that flanks, interfingers, and overlies the Effna build-ups. At some localities, (PQ for example, Fig. 3.3) the Botetourt extends across the younger buildup facies. The lateral expression of the Botetourt is dynamic, and is best represented by detailed facies maps (Read, 1982, figs. 6a, 7c). The Botetourt is generally interpreted as a deeper water facies that formed on the flanks of downslope build-ups, and is transitional

between the Effna and basinal Liberty Hall facies (Read, 1982). The entire sequence (Mosheim, Lincolnshire, Effna, Botetourt, Liberty Hall) is a transgressive ramp to basin sequence, part of the regional onlap sequence during the early and middle stages of downwarping during the Taconic foreland basin formation (Read, 1980).

Ramose bryozoans, lacy and encrusting bryozoans, pelmatozoans, brachiopods, trilobites, mollusks, and calcareous algae dominate the fauna of the Effna buildup (see Read, 1982, table 2 for fauna constituent percentages). Trilobites are a relatively low percentage of the total abundance in the build-ups, but are fairly diverse. Our collections in the Effna have yielded the following genera: *Sphaerexochus* Beyrich, 1845, *Bumastoides*, *Amphilichas*, *Illaenus* Dalman, 1827, *Kawina* Barton, 1916, *Ceraurus*, *Calyptaulax*, and *Thaleops*. Raymond (1925) described some of this fauna from his work in the Holston (Effna) of Virginia.

PHYLOGENETIC ANALYSIS

Notes on taxa.— Lichas laciniatus (Dalman, 1827) was chosen as an outgroup taxon based on its plesiomorphic glabellar and pygidial morphology (Thomas and Holloway 1988), and on the results of previously published work (Pollitt et al., 2005). Pollitt et al., (2005) constructed a cladogram of the family Lichidae with polarity determined by reference to a lichakephalid outgroup taxon. Their 50% majority rule tree placed the genus *Lichas* Dalman, 1827 as directly basal to the sister clades Tetralichini and Echinolichini Phleger, 1936 (see Pollitt et al., 2005, fig. 8). Some plesiomorphic characters (relative to tetralichines) possessed by *Lichas* are: the possession of furrow S1 (joining of the axial and longitudinal furrows), the presence of a bullar lobe, the lack of pleural spines on the pygidium, and a subsemicircular pygidium (both shared with more

basal lichids like *Lichakephalina* Sdzuy, 1955 and *Acidaspidina* Lazarenko, 1960). The presence of distinct lateral lobes is a primitive character not only in relation to the Tetralichini, but the Trilobita as a whole. Fused lateral lobes such as those of *Amphilichas* are surely a derived characteristic. The lobation pattern in *Lichas* represents an intermediate step before complete fusion of the lateral lobes, and therefore is an ideal taxon to assess character polarity in taxa with composite lobes. Although several authors (Phleger, 1936; Thomas and Holloway, 1988) considered *Metopolichas* Gürich, 1901 a basal genus to tetralichines, we will not use it as an outgroup because the type material is incompletely preserved (Thomas and Holloway, 1988).

The subfamily Tetralichinae (Phleger, 1936) as defined by Thomas and Holloway (1988) includes *Amphilichas*, *Probolichas*, *Lyralichas*, and *Apatolichas*. They regarded *Kerakephalichas* (Phleger, 1936) and following Warburg (1925), *Acrolichas* (Foerste, 1919) as junior synonyms of *Amphilichas*. Thomas and Holloway's (1988) synonymy of *Kerakephalichas* was based on their estimation that cranidial spinosity was not a character of generic importance. We cannot investigate the relationship of *Kerakephalichas* (i.e., *Amphilichas rhinoceros* Slocom, 1913) to other tetralichines because the type material lacks a hypostome and pygidium, although we redescribe and reillustrate the holotype cranidium (Fig. 7.1).

Pollitt et al. (2005) expanded the tribe Tetralichini to include *Pseudotupolichas* (Phleger, 1936) based on their majority rule tree (Pollitt et al., 2005, fig. 9). However, this clade was unresolved in their strict consensus tree, and the support for the Tetralichini node in the majority rule tree was extremely low. Thomas and Holloway (1988) assigned *Pseudotupolichas* to the subfamily Lichinae, so the relationships of this

genus need to be evaluated. The taxa used in our analysis include the type species of every genus within the Tetralichini: *Probolichas robbinsi*, *Amphilichas lineatus*, *Apatolichas jukesi*, *Lyralichas bronnikovi*, and *Pseudotupolichas ornatus*. The type specimens of *Amphilichas*, *Probolichas*, and "*Kerakephalichas*" are re-illustrated here. We were unable to secure loans of the types of *Apatolichas*, *Lyralichas* and *Pseudotupolichas*, and our coding is based on published illustrations (Weber, 1932; Phleger, 1936; Whittington, 1963; Thomas and Holloway, 1988), and evaluation of other available material of the respective type species. We also consulted the literature for illustrated non-type species (Evitt, 1951; Tripp, 1957; Shaw, 1974; Chatterton and Ludvigsen, 1976; Owen, 1981; Westrop and Ludvigsen, 1983; Edgecombe et al. 2004) to supplement physical material. In some instances we accept the pygidial assignment of later authors to a particular species. For example, we follow the assignment of pygidia to *A*. *lineatus* by Owen (1981). The taxa used here also represent all known species within *Probolichas*, *Apatolichas*, and *Lyralichas*. *Amphilichas* is known from approximately 50 species; but in many instances, there is broad overlap in morphology, or the material is fragmentary and sclerite associations are unknown. In some cases, we had to exclude some species with unique characters, because they are incompletely known. For example, *A*. *hexadactylus* (Öpik, 1937*)* and *A*. *narrawayi* (Foerste, 1920) have elongated first and second pleural furrows, but both are only known from pygidia (Thomas and Holloway, 1988). Correct association of exoskeletal parts should be completed on these species (as well as other species known only from partial exoskeletons) before they are included in any analysis. The species that we use here represent relatively complete specimens with a broad range of morphology including different degrees of longitudinal furrow

effacement, sculpture, and convexity. Our primary concern is the relationship between *Amphilichas* and *Probolichas*, so we believe this is an adequate pool of species to represent *Amphilichas* in the phylogenetic analysis.

It is important to note that even though we were unable to secure access to the type material of *Apatolichas jukesi* (GSC 671a), our coding is primarily based on the type species (Whittington,1963, pl. 32, figs. 4-11; pl. 33, 34) rather than the material we illustrated here (*A*. cf. *A*. *jukesi* of Ross, 1972). *Amphilichas cucullus (*Meek and Worthen, 1865; Foerste, 1920) codes the same as the Oklahoma material illustrated here (*A*. cf. *A*. *cucullus*). *Amphilichas* cf. *A*. *encyrtos* (Edgecombe et al., 2004) was chosen over *A*. *encyrtos* (Webby, 1974) because a more complete exoskeleton is known.

CHARACTERS AND CODING

The character terminology used here follows Thomas and Holloway (1988), Whittington and Kelly (1997) and Pollitt et al. (2005). The dataset includes 13 ingroup taxa, one outgroup taxon, and 28 characters with 70 states. These characters code morphological features of the cranidium (13 characters), hypostome (4 characters) and pygidium (11 characters). All the characters are binned into their respective states based only on clearly discrete differences. Ratio based characters are also only used when there are discrete (i.e. not a continuum of size ranges) differences in states, so that quantitative methods such as gap weighting (Thiele, 1993) or finite mixture coding (Strait et al. 1996) are not necessary. All characters are treated as unordered and (initially) weighted equally. Parsimony uninformative characters (autapomorphic characters, e.g., the extra interpleural furrow of *Lyralichas* or the effaced axial furrow of *Apatolichas*) and redundant (i.e., similar sculptural characters in different parts of the exoskeleton)

characters are omitted. Characters with states that were inapplicable for some species (Characters 4-6, which describe the variation of the glabellar proboscis) were coded using reductive coding (Strong and Lipscomb, 1999): inapplicable states were coded as "?". Characters 7, 8, 9, 18 are from Pollitt et al. (2005).

Cranidium.—

1. Posterior extent of longitudinal glabellar furrow: (0) doesn't reach SO (e.g., *Lyralichas bronnikovi*, Thomas and Holloway, 1988, pl. 12, fig. 260); (1) extends to SO (e.g., *Amphilichas subpunctatus*, Fig. 10.1); (2) remnant longitudinal furrow (e.g. *Amphilichas lineatus*, Fig. 9.2).

2. Path of posterior end of longitudinal furrow: (0) curves abaxially below the palpebral lobe (e.g., *Pseudotupolichas ornatus*, Thomas and Holloway, 1988, pl. 4, fig. 70); (1) straight (e.g., *Amphilichas subpunctatus*, Fig. 10.1).

3. Anterior projection: (0) absent (e.g., *Amphilichas lineatus*, Fig. 9.4) (1) blunt anterior or dorsal swelling of median lobe (e.g., *Amphilichas* cf. *A*. *cucullus*, Fig. 8.9); (2) present as a proboscis (e.g., *Probolichas kristiae*, Fig. 7.3).

4. Proboscis width: (1) wide (e.g., *Probolichas robbinsi*, Fig. 6.1); (2) narrow (e.g., *Probolichas kristiae*, Fig. 7.3).

5. Longitudinal profile of proboscis: (1) straight (e.g., *Probolichas robbinsi*, Fig. 6.2); (2) down-curved (e.g., *Probolichas kristiae*, Fig. 7.6).

6. Proboscis tuberculation: (1) circular along entire length of proboscis (e.g., *Probolichas robbinsi*, Fig. 6.1); (2) progressively more elongate along length (e.g., *Probolichas kristiae*, Fig. 7.6).

7. Glabellar lobe L1a: (0) present, strongly expressed (e.g., *Lichas laciniatus*, Warburg, 1925, pl. 8, fig. 20); (1) present, weakly expressed (e.g., *Apatolichas jukesi*, Whittington, 1963, pl. 34, fig.11); (2) completely incorporated into a composite lateral lobe (e.g., *Amphilichas subpuctatus*, Fig. 9.11).

8. Width (tr) of palpebral lobe: (0) narrow relative to glabellar width (e.g., *Pseudotupolichas ornatus*, Thomas and Holloway, 1988, pl. 4, fig. 70); (1) wide relative to glabellar width (e.g., *Apatolichas jukesi*, Whittington, 1963, pl. 34, fig. 10).

9. Glabellar lobation: (0) bullar lobe present (e.g., *Lichas laciniatus*, Warburg, 1925, pl. 8, fig. 20); (1) composite lateral lobe present, bullar lobe fused with other lateral glabellar lobes (e.g., *Amphilichas effnensis*, Fig. 11.2).

10. Shape of SO: (0) transverse (e.g., *Lichas laciniatus*, Warburg, 1925, pl. 8, fig. 20); (1) transverse medially, then deflected posteriorly (e.g., *Probolichas robbinsi*, Fig. 6.1).

11. Lateral incisions of longitudinal furrows at eye level: (0) absent (e.g., *Probolichas robbinsi*, Fig. 6.1); (1) present (e.g., *Probolichas kristiae*, Fig. 6.6).

12. Anterior portion of median lobe: (0) non-punctate (e.g., *Amphilichas aspratilis*, Shaw, 1974, pl. 12, fig. 6); (1) punctate (e.g., *Amphilichas subpunctatus*, Fig. 9.11).

13. Preglabellar furrow: (0) complete (e.g., *Amphilichas subpunctatus*, Fig. 10.2); (1) medially effaced (e.g., *Amphilichas effnensis*, Fig. 11.3)

Hypostome.—

14. Hypostome tuberculation: (0) absent (e.g., *Pseudotupolichas ornatus*, Thomas and Holloway, 1988, pl. 4, fig. 67); (1) present (e.g., *Probolichas kristiae*, Fig. 9.10).

15. Hypostome median body: (0) proportionally long length (sag) (e.g., *Pseudotupolichas ornatus*, Thomas and Holloway, 1988, pl. 4, fig. 67); (1) reduction in length (sag) (e.g., *Amphilichas subpunctatus*, Fig. 10.7).

16. Hypostome anterior lobe: (0) sub-circular (e.g., *Pseudotupolichas ornatus*, Thomas and Holloway, 1988, pl. 4, fig. 67); (1) sub-trapezoidal (e.g., *Amphilichas subpunctatus* Fig. 10.7).

17. Hypostome posterior lobe: (0) long (sag), strongly anteriorly deflected (e.g., *Lichas laciniatus*, Thomas and Holloway, 1988, pl. 1, fig. 10); (1) reduced in length (sag) (e.g., *Probolichas kristiae*, Fig. 9.10); (2) long (sag), transverse or slightly anteriorly deflected (e.g., *Amphilichas subpunctatus*, Fig. 10.7).

Pygidium.—

18. Number of pleural furrow pairs (excluding post axial band): (0) three (e.g., *Lichas laciniatus*, Thomas and Holloway, 1988, pl. 1, fig. 5); (1) two (e.g., *Probolichas kristiae*, Fig. 8.3); (2) one (e.g., *Apatolichas jukesi*, Whittington, 1963, pl. 33, fig. 10); (3) four (e.g., *Lyralichas bronnikovi*, Thomas and Holloway, 1988, pl. 12, fig. 264).

19. Extent of 1st pleural furrow: (0) terminates at pleural tip (e.g., *Pseudotupolichas ornatus*, Thomas and Holloway, 1988, pl. 4, fig. 76); (1) terminates near fulcrum (e.g., *Amphilichas subpunctatus*, Fig. 9.12); (2) terminates near base of marginal spines (e.g., *Probolichas kristiae*, Fig. 8.3).

20. Number of complete axial ring furrows: (0) two (e.g., *Lyralichas bronnikovi*, Thomas and Holloway, 1988, pl. 12, fig. 264); (1) one (e.g., *Amphilichas effnensis* Fig. 10.10).

21. Postaxial band: (0) well defined (e.g., *Probolichas kristiae*, Fig. 7.3); (1) absent or poorly defined (e.g., *Apatolichas jukesi*, Whittington, 1963, pl. 33, fig. 10)

22. Pygidial shape in dorsal view: (0) subcircular (e.g., *Probolichas kristiae*, Fig. 7.3); (1) subtriangular (e.g., *Apatolichas jukesi*, Whittington 1963, pl. 33, fig. 10); (2) subquadrate (e.g., *Pseudotupolichas ornatus*, Thomas and Holloway, 1988, pl. 4, fig. 76).

23. Ratio of pygidial length (sag) to width (tr): (0) length of pygidium approximately ¾ of of width (e.g., *Probolichas kristiae*, Fig. 8.3); (1) proportionally long and narrow, approaching 1:1 ratio (e.g., *Pseudotupolichas ornatus*, Thomas and Holloway, 1988, pl. 4, fig. 76); (2) length of pygidium approximately ½ of width (e.g., *Amphilichas* cf. *encyrtos*, Edgecombe et al. 2004, fig. 11H).

24. Shape of 2nd axial ring furrow: (0) horizontal (tr) (e.g., *Amphilichas conradi*, Chatterton and Ludvigsen, 1976, pl. 18, fig. 56); (1) weakly chevron shaped (e.g., *Amphilichas subpunctatus*, Fig. 9.12); (2) strongly chevron shaped (e.g., *Probolichas kristiae*, Fig. 8.3).

25. Sculpture of pygidium: (0) tubercles coarse and uniform in size (e.g., *Amphilichas subpunctatus*, Fig. 9.12); (1) tubercles variable in size (e.g., *Probolichas kristiae*, Fig. 7.4).

26. Shape of post-axial band: (0) parallel sided or gently expanding posteriorly (e.g., *Probolichas kristiae*, Fig. 8.3); (1) narrowing posteriorly (e.g., *Amphilichas subpunctatus*, Fig. 10.4).

27. Basal width (tr) distance between posterior-most (3^{rd} or 4^{th}) pair of pygidial pleural spines: (0) Posterior most spine lost (e.g., *Lichas laciniatus*, Thomas and Holloway, 1988, pl. 1 fig. 5); (1) very narrow, only an extremely shallow embayment separating spines (e.g., *Apatolichas jukesi*, Whittington 1963, pl. 33, fig. 10); (2) narrow embayment relative to transverse width of pleural spines (e.g., *Amphilichas subpunctatus*, Fig. 10.4);

(3) wide embayment relative to transverse width of pleural spines (e.g., *Probolichas kristiae*, Fig. 8.3); (4) wide embayment because of reduction in pleural spine size (e.g., *Pseudotupolichas ornatus*, Thomas and Holloway, 1988, pl. 4, fig. 76).

28. Shape of posterior-most pleurae: (0) short and broad (e.g., *Amphilichas conradi*, Chatterton and Ludvigsen, 1976, pl. 18, fig. 56); (1) long and broad (e.g., *Probolichas kristiae*, Fig. 8.3); (2) long and slender (e.g., *Pseudotupolichas ornatus*, Thomas and Holloway, 1988, pl. 4, fig. 76).

Parsimony analysis.—All analyses were conducted in PAUP* version 4.0b10 (Swofford, 2002) using a branch and bound search algorithm, and the results were checked using TNT (Goloboff et al., 2008; implicit enumeration). The settings for the branch and bound analysis were as follows: gaps were treated as missing, the initial upper bound was computed heuristically, addition sequence was furthest, zero length branches were not collapsed, topological constraints were not enforced, and trees were treated as un-rooted. Successive approximations reweighting (Farris, 1969) of the rescaled consistency index (RC) was used to down-weight homoplastic characters. PAUP* was also used to run additional analyses, such as calculation of the tree length frequency distribution from 10,000 equally sampled random trees, and computation of 1,000 replicate bootstrap probabilities via a branch and bound algorithm. Bremer support values (Bremer, 1994) were calculated by continually keeping trees with length values of N+1 in PAUP*, where N = the tree length of the strict consensus tree. This was done until all nodes collapsed. Character state optimization was performed in PAUP* and Winclada v. 1.00.08 (Nixon, 2002), and the results are shown in Fig. 5.

Systematic methods.—Systematic diagnoses are primarily based on the unambiguous state changes (i.e. those that occur at the same node under the assumptions of both ACCTRAN and DELTRAN optimization), although in some instances we added ambiguous state changes (and autapomorphic characters not included in the analysis) to develop a more complete picture of the characters held by the group being diagnosed. We have also provided node-based clade definitions (de Queiroz and Gauthier, 1990; De Queiroz, 2007; modified by Maletz et al., 2009) based on the strict consensus tree, in order to constrain the outcome of common ancestry relationships (i.e., a clade), while the description and diagnoses provide data on how the components of that particular clade are recognized. Clade definitions also clearly document synonymous taxa (e.g., *Amphilichas* and *Apatolichas* have the same clade definition; therefore they are synonymous in an unambiguous fashion). In instances where a taxon cannot be defined as the most recent common ancestor of two taxa (*Lyralichas* is only known from one species), branch based definitions are used (de Queiroz and Gauthier, 1990; de Queiroz, 2007). We have opted to use a conventional Linnean classification with named ranks, so the clade definitions are not used as the basis of the formal taxonomy, but as additional information, documenting the clades exact location, and synonymy.

RESULTS

Parsimony analyses.—PAUP* retained 36 equally most parsimonious trees (MPTs) with a tree length of 53+ steps. Successive approximations by the rescaled consistency index (RC) down-weighted nine homoplastic characters, producing nine MPTs. A strict consensus of these nine trees (Fig. 4) has a length of 34 steps, consistency index (CI) of 0.79, retention index (RI) of 0.69, and RC of 0.55. We calculated 10,000

random trees using the same specifications as the branch and bound analysis, resulting in a frequency distribution with a mean tree length of 51.2 steps. No trees with a length approaching 34 steps were retained, so the probability of getting a tree of 34 steps at random is less than 1/10000, or $p < 0.0001$, suggesting there is a strong phylogenetic signal in our data. The bootstrap values indicate that nodes 2-5, 9, and 10 (Fig. 4) are supported in more than 50% of trees found in the analysis. The Bremer support value for node 2 is three, nodes 3, 4, 6, 9, and 10 have values of two, and all other nodes have a value of one.

Pseudotupolichas is the most basal ingroup taxon. *Amphilichas*, *Probolichas*, *Lyralichas* and *Apatolichas* are united at node 2 (characters 2, state 1; 10, state 1; 15, state 1; 17, state 2; 19, state 2) forming the Tetralichini clade. We exclude *Pseudotupolichas* from the Tetralichini (following Thomas and Holloway, 1988) because of the high number of supporting synapomorphies and bootstrap support (100%) at node 2. This suggests the possession of a composite lobe is not diagnostic of the Tetralichini (which is supported by the fact that some echinolichines have completely fused composite lobes). *Lyralichas* is a sister taxon to the rest of the tetralichines. *Amphilichas*, "*Apatolichas*", and *Probolichas* form a clade at node 3, based on hypostome tuberculation (character 14, state 1) and hypostome anterior lobe shape (character 16, state 1). *Probolichas* is monophyletic, and is a sister taxon to *Amphilichas* and "*Apatolichas*". The presence of a proboscis (character 3, state 2; node 4) unites all species of *Probolichas*, while at node 5 *P. kristiae* and *P. pandus* are sister taxa based on their shared longitudinal furrow incisions (character 11, state 1). Monophyly of *Amphilichas* (including "*Apatolichas*") is supported by the extent of the 1st pleural furrow (character

19, state 1; node 6). An *Amphilichas* subclade is formed at node 7 based on the shape of the 2nd pygidial axial furrow (character 24, state 1). Within that clade, *A. subpunctatus*, *A. lineatus*, and *A. effnensis* are united by their punctate anterior median lobe (character 12, state 1; node 8). At node 9, *A. effnensis* and *A. lineatus* are sister taxa based on the effacement of the pre-glabellar furrow (character 13, state 1). *Apatolichas jukesi* and *A.* cf. *encyrtos* are united by the shape, pleural furrow number, and length/width ratio of the pygidium (characters 18, state 1; 22, state 1; 23, state 1; node 10).

Classification.—The taxonomy that results from the strict consensus tree (Fig. 4) defines three genera within the Tetralichini, and collapses *Apatolichas* into *Amphilichas*. Under this interpretation, removing *Apatolichas* from *Amphilichas* would render *Amphilichas* paraphyletic. This is perhaps the most striking change to the taxonomy of the Tetralichini. It is necessary based on our hypothesis of common ancestry, since the majority of MPTs support this interpretation. Modifying the placement of node 10 on the MPTs (or consensus trees) results in a significantly less parsimonious result. Collapsing the node would also have no effect on the resulting taxonomy. Our analysis diagnoses the *Amphilichas* clade (node 6) based on the length of the pleural furrows, which are shorter than those of *Probolichas* and *Lyralichas*. Although ambiguous based on the character optimization, *Amphilichas* and *Apatolichas* also have identical hypostomal characters (15-17), while *Probolichas* and *Lyralichas* only possess some, but not all of the same states. For example, the hypostome of *Probolichas* is similar to *Amphilichas*, except the posterior lobe is reduced in length (Fig. 9.10).

Our data also clearly support separation of *Probolichas* from *Amphilichas*, as originally proposed by Phleger (1936). Although Thomas and Holloway (1988)

suggested that the presence of a proboscis did not provide the basis for a new genus, our analysis shows that this character, in combination with other apomorphies, supports monophyly of *Probolichas*.

Phleger (1936) erected *Tetralichas* for species with complete (extending to occipital furrow) longitudinal furrows, and restricted *Amphilichas* to those with incomplete longitudinal furrows, as in *A*. *lineatus*. There is no support for *Tetralichas* in our analysis, as *A*. *conradi*, another species with incomplete longitudinal furrows (character 1), is not part of the same sub-clade as *A*. *lineatus.* Furthermore, *Lyralichas* also has incomplete longitudinal furrows, but is not a sister taxon to *A*. *conradi* or *A*. *lineatus*.

SYSTEMATIC PALEONTOLOGY

Illustrated material (Figs. 6-11) was photographed at 1mm intervals with a Canon E05 5D camera equipped with an 80 or 120mm lens. Images were then stacked using Helicon focus 4.0.4 pro Multiprocessor (Helicon Soft, Ltd) with depth map rendering. References to "length" refer to sagittal or exsagittal directions, and "width" refers to transverse. Characters in diagnoses without state numbers are autapomorphies (separated from the rest of the diagnosis by a semicolon), and weren't included in the analysis. Repository acronyms: OU: Sam Noble Oklahoma Museum of Natural History, USNM: United States National Museum (Smithsonian), Ar: Swedish Museum of Natural History, FMNH: Chicago Field Museum of Natural History.

Order: LICHIDA Moore, 1959

Family LICHIDAE Hawle & Corda, 1847

Subfamily LICHINAE Hawle & Corda, 1847

Tribe TETRALICHINI Phleger, 1936

Diagnosis.—Longitudinal furrow straight (character 2, state 1), SO deflected posteriorly (character 10, state 1), hypostome median body reduced in length (sag) (character 15, state 1), hypostome posterior lobe transverse or reduced and slightly anteriorly deflected (character 17, states 1 and 2) pleural furrows terminate at fulcrum or near base of marginal spine (character 19, states 1 and 2).

Definition.—The clade stemming from the most recent common ancestor of *Lyralichas bronnikovi* and *Amphilichas cf. A. encyrtos* and all of its descendants (node 2, Fig. 4).

Genus PROBOLICHAS Phleger, 1936

Type Species.—Hoplolichas robbinsi Ulrich 1892, from the Sandbian of Minnesota (by original designation).

Diagnosis.—Tetralichini with an elongated anterior projection (proboscis) (character 3), strongly chevron shaped 2nd pygidial axial ring furrow (character 24), wide embayment between posterior most pleural spines (character 27), long and broad posterior most pleurae (character 28).

Definition.—The clade stemming from the most recent common ancestor of *Probolichas robbinsi* and *Probolichas pandus* and all of its descendants (node 4, Fig. 4).

Discussion.—Probolichas was erected by Phleger (1936) who emphasized the presence of an anterior projection from the median glabella in his diagnosis. Species within this genus were otherwise thought to resemble *Amphilichas*. Evitt (1951) treated *Probolichas* as a subgenus of *Amphilichas* because he believed all other glabellar features to be identifical to *Amphilichas*. Warburg (1939) felt the proboscis was of little

importance because similar structures occurred in other genera (e.g. *Platylichas* Gürich, 1901). Thomas and Holloway (1988) shared Warburg's doubts about the taxonomic utility of the prolongation, but tentatively accepted *Probolichas* as a valid genus, pending confirmation of the sclerite association suggested by material from the Bromide Formation (Thomas and Holloway, 1988, pl. 12, figs. 265, 270, 273). They reviewed material of *P. robbinsi* and *P. pandus*, and concluded that further morphological information was necessary before the genus could be properly assessed.

The complete material described herein, and the cladistic analysis presented in the preceding sections allows for the status of *Probolichas* to be determined. Not all of the synapomorphies (see diagnosis) that unite this genus were available for evaluation by previous authors, who considered the proboscis the only relevant character for discussion. Both Shaw (1974) and Thomas and Holloway (1988) noted that incomplete *Probolichas* pygidia from the Bromide were distinct from those of *Amphilichas*, and pygidial characters are tentatively (pygidia from *P. pandus* and *P. robbinsi* are not known) used to diagnose the genus in addition to the presence of a proboscis.

PROBOLICHAS ROBBINSI (Ulrich, 1892)

Figures 6.1-6.3

Hoplolichas robbinsi, Ulrich, 1892, figs. 1a, 1b.

Probolichas robbinsi, Phleger, 1936, figs. 43, 44.

Diagnosis.—Probolichas with a wide (character 4, state 1), straight (character 5, state 1) proboscis that has circular tubercles along its entire length (character 6, state 1); transverse posterior occipital margin, proportionally short proboscis.

Description.— Cranidium subtriangular in outline, width across the base of proboscis 20% of cranidial length, and width across palpebral lobes 89% of its length. Convexity of longitudinal profile very low, nearly flat in lateral view; slopes very gently downward near the anterior end of cranidia (excluding proboscis). In anterior view, convexity weak, sloping gently abaxially away from median line. Axial furrows narrow, clearly defined grooves, bowed gently inward and descending almost vertically at anterior; curved around edge of LO posteriorly. Glabella subrectangular in outline, occupies 61% of cranidial width opposite palpebral lobes, narrows anteriorly. Short, wide proboscis emerges from median lobe dorsally, occupying 40% of cranidial length, equal to 23% of cranidial width opposite palpebral lobes. Proboscis width 40% of its length; circular in cross section, abruptly rounded at anterior end, with flat longitudinal profile. SO narrow, well-incised groove, transverse between longitudinal furrows, then abruptly turning posteriorly at angle of approximately 20 degrees. Width of LO 61% of cranidial width (across palpebral lobes), and length 5% of cranidial length. Posterior margin of LO transverse. Longitudinal furrows are similar in depth to axial furrows, roughly parallel between SO and glabellar mid-length, then diverging anteriorly, before descending ventrally. They outline "bulb-shaped" medial lobe, comprising 42% of glabellar width opposite palpebral lobes, but expanding anteriorly. Composite lobe curves abaxially, accounting for 71% of cranidial length (excluding proboscis), and 29% of glabellar width opposite palpebral lobes. Fixigena comprising 28% of maximum cranidial length in dorsal view. Palpebral lobe and area incompletely preserved; palpebral furrow apparently finely etched groove, curved strongly. Preocular area narrow, descending steeply forward; posterior area slightly depressed just posterior of the palpebral lobe, descends

less steeply than preocular area, with posterolateral projection much wider than postocular area. Posterior border furrow slightly wider and deeper than axial furrow, extends to sutural margin. Posterior border rectangular in outline, length at axial furrow equal to about 3% of total cranidial length, slightly anteriorly directed, widening laterally (exsag.). Suture incompletely preserved, appears strongly curved outward behind palpebral lobe.

Dorsal exoskeleton ornamented by tubercles of three different sizes. Each successive size class approximately 30-40% larger than the next lowest size, reaching up to 0.33 mm in diameter. Smallest and medium sized tubercles densely and evenly scattered across entire cranidium, largest size more prominent on the proboscis. One large tubercle present in the middle anterior portion of both composite lobes.

Material Examined.—Holotype cranidium (USNM 41950, Figs. 6.1-6.3).

Occurrence.—Sandbian-Katian (Upper Ordovician) of the Galena group of Minnesota (Evitt, 1951; Emerson et al., 2004).

Discussion.—Phleger (1936) designated *Probolichas robbinsi* as the type species for *Probolichas*. His illustrations (Phleger, 1936, figs. 43, 44) are simple line drawings, and the material was not redescribed. *Probolichas robbinsi* differs from *P. pandus* and *P. kristiae* sp. nov in that the proboscid tubercles are not elongate, and the posterior margin of the occipital ring is transverse rather than anteriorly curved. *Probolichas robbinsi* also lacks lateral incisions to the longitudinal furrow, and has a proportionally shorter proboscis than *P. kristiae*.

PROBOLICHAS KRISTIAE new species

Figures 6.4-6.6, 7.2-7.8, 8.2-8.3, 9.1, 9.10

Probolichas sp. Shaw, 1974, pg. 46, pl. 12, figs. 17, 19, 20

Probolichas? sp. Thomas and Holloway, 1988, pl. 12, figs. 265, 270, 273.

Diagnosis.—*Probolichas* with proboscis that is narrow (character 4, state 2), down-curved (character 5, state 2), has elongate tubercles (character 6, state 2), pronounced lateral incisions of longitudinal furrows opposite palpebral lobes (character 11, state 1); proportionally long proboscis.

Description.—Cranidium accounts for 40% of dorsal exoskeletal length, subtriangular in outline, width across base of proboscis 24% of cranidial length, width at palpebral lobes 66% of length; longitudinal profile is weakly convex, increasing in slope slightly near anterior end of the median lobe. Axial furrows deep, convex adaxially in dorsal view, diving ventrally anterior of palpebral lobe until termination point, curved around edge of LO posteriorly; preglabellar furrow not preserved. Glabella subrectangular in outline (excluding proboscis), widest at palpebral lobes, tapering gently towards the anterior border, glabellar width occupies 66% of cranidial width opposite palpebral lobe. Proboscis originates from within median lobe, occupies 43% of total cranidial length, equal to 15% of cranidial width at palpebral lobes; circular in cross-section, bluntly rounded at anterior end. Proboscis width between 21-30% of its length. Longitudinal profile of posterior part of proboscis slightly depressed, whereas anterior end slightly raised, producing a down-curved appearance in lateral view. SO similar in depth and width to axial furrow, with longitudinal furrows terminating at two equidistant points along its width. LO wide (comprising 62% of cranidial width), slightly narrowing (exsag.) abaxially. Posterior margin of LO curved forward in dorsal view. Longitudinal furrows similar in depth and width to axial furrows, extending to SO, shallowing slightly

posterior of lateral incisions; outline forwardly expanding median lobe, which comprises 41-44% of glabellar width across palpebral lobes. Longitudinal furrows abaxially outline subrectangular composite lobes and curve strongly ventrally until intersecting with axial furrow; lateral incisions opposite palpebral lobes strong, distorting slightly shape of composite lobe. Composite lobes maintain even width over their longitudinal extent; curving gently abaxially opposite palpebral lobe, then diving strongly ventrally. They comprise 54-55% of cranidial length at most anterior extent, and 26-29% of glabellar width across palpebral lobes. Fixigena curve adaxially, semielliptical in outline, slightly narrowing anteriorly, comprising 28% of maximum cranidial length in dorsal view. Flat, semicircular palpebral lobe lies opposite lateral incisions, equal to 14% of cranidial length; outlined adaxially by shallow, curved palpebral furrow. Preocular area of fixigena slightly curved, descending ventrally steeply; palpebral area approximately same width as preocular area, curved slightly abaxially, accounting for 9-12% of cranidial width across palpebral lobes; posterior area flat, with short, abruptly terminated posterolateral projection that is approximately double width of preocular area. Posterior border furrows shallow, slightly anteriorly directed, abaxially terminates at the sutural edge. Posterior border short, subrectangular in outline, little change in length (exsag.) abaxially. Free cheek broad and bluntly rounded, with maximum length 37% of cranidial length (excluding proboscis), but narrowing gently (exsag.) distally; posterior margin flexed backward, paralleling curvature of anterior thoracic segments.

Hypostome elliptical in outline, with length 55% of maximum width; well-defined median notch in posterior border equal to 22% of hypostomal length. Anterior margin well rounded, gently tapering abaxially into lateral notch, anterior border absent

or incompletely preserved. Lateral border expands backward, passing without interruption into broad, flat posterior border. Posterior border varies little in length except at median notch, slightly raised dorsally in a band just forward of median notch, maximum length (exsag.) equal to 48% of hypostomal length. Lateral border furrows slightly sigmoidal, converging posteriorly, shallowing along margin of posterior lobe. Median body sub-trapezoidal, comprises 71% of hypostomal length. Anterior lobe of median body "bulb" shaped in outline, accounts for 96% of median body length. Middle furrow shallow, present only abaxially, loosely defining the separation between posterior and anterior lobes. Posterior lobe reduced in length (sag) and strongly curved. Posterior border furrow transverse, deeper than lateral border furrow, clearly separating median body from the posterior border.

Thorax of eleven segments, subrectangular in outline and slightly narrows backwards; strongly convex (tr), length 53% of width. Axial lobe narrows backwards, occupies 24% of thorax width at anterior. Axial furrow wider and deeper than cranidial axial furrow, ring furrows shallow. Axial rings well defined, rectangular in outline, and of roughly equal length. Pleurae horizontal for approximately 25% of their width, flexed downward at fulcrum at approximately 30° from horizontal; narrowing gently into bluntly spinose terminations. Pleural furrows shallow, extending beyond fulcrum, slightly curved, anterior pleural bands slightly longer than posterior bands.

Pygidium sub-semicircular in outline, length 65-74% of maximum width, with three pairs of pleurae. Axis accounts for 33-39% of pygidial length, and 20-21% of pygidial width at first axial ring; tapers gently into a bluntly rounded U-shaped terminal axial piece. First axial ring approximately the same length as last thoracic axial ring, but

slightly narrower in width. Second axial ring slightly longer and less wide than the first; bounded anteriorly by transverse axial ring furrow and posteriorly by strongly chevron shaped ring furrow. Interpleural furrows finely etched, very gently sinuous, curving outwards and backwawrd, extending to pygidial margin; furrows (interpleural?) on adaxial sides of third pair parallel sided, joining axial furrows and outlining a post axial band. Three pairs of broad and flat pleurae that become progressively wider and more curved distally towards the rear; each terminates at blunt marginal spine. Interspine region narrow (tr., exsag.), and sharply pointed adaxially between first and and second pleurae, becoming wider (tr., exsag.) and more bluntly pointed between the 2nd and 3rd pair; 3rd pair separated by more rounded embayment. Pleural furrows finely etched grooves, extending across 40-45% of pleural width from axis, divide pleurae into sub-equal anterior and posterior bands.

Dome shaped tubercles of primarily two sizes present on cranidial surface and thorax; on a few specimens, 3rd set of larger tubercles is present on cranidial surface. Each larger size is approximately 30-40% larger than next lowest size, largest size reaching up to 0.8 mm diameter on crandium. Tubercles on cranidium and thorax evenly distributed. Tubercles on proboscis elongate, hollow, progressively more tilted towards the anterior. Hypostomal median body heavily tuberculate, three separate sizes of tubercle, effaced near posterior margin of anterior lobe. Terrace ridges present on outer parts of lateral and posterior borders, becoming thinner adaxially, not extending to median notch. Posterior border with widely spaced punctae. Pygidial tubercles are less homogeneous, consisting of at least four different sizes. Extremely large dome-shaped tubercles present only on pygidial surface, reaching up to 1.5 mm in diameter, without

discernable pattern to their distribution. Thoracic tubercles are less prominent than those of cranidium or pygidium.

Etymology.—After Kristi Carlucci.

Types.— Holotype, one complete specimen in dorsal view (OU 11260, Figs. 7.2-7.3). paratypes, five partial cranidia (OU 11262, Figs. 7.5-7.6; 11263, Fig. 7.8; 8096, Fig.7.7; 12483, Fig. 8.2; 12484; Fig. 9.4) two nearly complete pygidia (OU 11269, Fig. 8.3; 5203, Fig. 7.4), one thoracopygon (OU 11265, Fig. 6.4), one hypostome (OU 8091, Fig. 9.10). Type locality is Rock Crossing (RC) at Hickory Creek, Carter County Oklahoma.

Material Examined.— In addition to types, four additional partial cranidia and five partial pygidia. One cranidium (OU 11271, Thomas and Holloway, 1988, pl. 12, fig. 265) and two pygidia (OU 11267, 11268, Thomas and Holloway, 1988, pl. 12, figs. 270, 273) have been illustrated. All material is stored in the Sam Noble Oklahoma Museum of Natural History.

Occurrence.—Upper Ordovician (Turinian) of the Pooleville Member of the Bromide Formation, Arbuckle Mountains, Oklahoma. Localities include Rock Crossing (RC) and Tysons quarry (TQ), both near Ardmore, Oklahoma.

Discussion.—*Probolichas kristiae* n. sp. is the only species known from a complete exoskeleton. Comparisons with the type species, *P*. *robbinsi* (Ulrich, 1892) were made above. The proboscis of *P*. *pandus* is very robust and relatively short and stands in stark contrast to the long and slender proboscis of *P*. *kristiae*. The pygidia of *P*. *robbinsi* and P. *pandus* are currently not known, so comparison to *P*. *kristiae* is not

possible. The pygidial characters used to supplement the diagnosis of *Probolichas* are based solely on *P. kristiae*.

Genus AMPHILICHAS Raymond, 1905

Type Species.—*Platymetopus lineatus* Angelin, 1854, from the Boda Limestone Formation, Sweden (by original designation).

Diagnosis.—Tetralichini with 1st pleural furrow extending to fulcrum (character 19, state 1), post axial band absent or narrows posteriorly (character 26, state 1), narrow embayment of pygidial margin between posterior-most marginal spines (character 27, states 1 and 2).

Definition.—The clade stemming from the most recent common ancestor of *Amphilichas subpunctatus* and *Amphilichas* cf. *A. encyrtos* and all of its descendants (node 6, Fig. 4).

Discussion.—The diagnosis presented by Thomas and Holloway (1988) states that *Amphilichas* is a tetralichine with a complete axial furrow, and varying levels of effacement of the longitudinal furrow. The results of our analysis indicate that *Amphilichas* is better diagnosed as a clade based on the extent of the pleural furrow, thus incorporating *Apatolichas* into *Amphilichas*. The results section of this paper elaborates on why this is necessary taxonomically. We follow previous authors (Warburg, 1939; Tripp, 1957; Thomas and Holloway, 1988) in considering *Acrolichas* to be a junior subjective synonym of *Amphilichas*. Our results also support those same authors' treatment of *Tetralichas* as a junior subjective synonym of *Amphilichas*.

AMPHILICHAS LINEATUS (Angelin, 1854)

Figures 9.2-9.4

Platymetopus lineatus Angelin, 1854, pl. 38, figs. 12, 12a.

Lichas lineatus Tornquist 1884, p. 36

Amphilichas lineatus Foerste, 1920, pl. 4, figs. 12a, 12b*;* Warburg, 1925, p.326, pl. 8, figs. 39, 40; Warburg, 1939, p. 14; Owen, 1981, pl. 16, figs. 7-15; Thomas and Holloway, 1988, pl. 12, figs. 262, 266.

Diagnosis.—*Amphilichas* with remnant longitudinal furrow (character 1, state 2), pre-glabellar furrow medially effaced (character 13, state 1); glabella extremely expanded in width.

Description.—Cranidial length 80% of cranidial width opposite approximate level of palpebral lobes. Longitudinal profile convexity very strong, overhanging the anterior border; convexity (tr) of glabella relatively weak. Preglabellar furrow shallow, effaced medially. Axial furrows deeper than preglabellar furrow, slightly converging posteriorly, clearly defined grooves, curving around LO, anteriorly descending ventrally (nearly vertical) before intersecting longitudinal furrow. Glabella subcircular in outline, narrows slightly anteriorly, very wide compared to total cranidial width; widest opposite the anterior-most extent of fixigena (in dorsal view), strongly rounded. SO nearly transverse medially, slightly posteriorly directed abaxially, terminating at intersection with axial furrow. LO subelliptical, edges very rounded, transverse medially, slightly posteriorly directed towards lateral margins; length comprises 11% of cranidial length, and is widest part of glabella, with width equal to 110% of glabellar width at (approximate) palpebral level. Very shallow longitudinal expressed at anterior only and curves forward and outward to intersect axial furrow near anterior end of glabella. Border furrow approximately same depth and width as axial furrow.

Irregularly scattered tubercles of three different sizes present on LO, fixigena, posterior portion of glabella; each size class approximately 20-30% larger than the next smallest size, largest tubercles reaching up to 0.21 mm, tubercles gradually become effaced anteriorly, disappearing completely beyond level of palpebral lobe. Anteriorly, glabella has evenly distributed punctae.

Material Examined.—Lectotype cranidium, (Ar 6040, Fig. 9.2-9.4).

Occurrence.—Ashgillian (Upper Ordovician) Boda Limestone of Dalarne, Sweden (Angelin, 1854) and the Kjorrven, Bønsnes, and Husbergøya formations of the Oslo region of Norway (Owen, 1981)

Discussion.— *Amphilichas lineatus* is distinct from most other species because the longitudinal furrows are largely effaced and the glabella is very wide. Owen (1981, pl. 16, figs. 7-15) assigned sclerites from Norway to this species. Although these specimens are more tuberculate than the holotype and the longitudinal furrow is less effaced, we tentatively follow Owen's interpretation (see also Thomas and Holloway, 1988).

AMPHILICHAS CF. A CUCULLUS (Meek and Worthen, 1865)

Figures 8.4-8.10

cf. *Lichas cucullus* Meek and Worthen, 1865, p. 266; Whiteaves, 1897, p. 236.

cf. *Platymetopus cucullus* Clarke, 1894, p.746, figs. 66, 67.

cf. *Acrolichas cucullus* Foerste, 1920, p. 30, pl. 1, figs a-g; Bradley, 1930, p. 264, pl. 29, figs. 1-9; Shimer and Shrock, 1944, p. 649, pl. 170, figs. 19-22.

cf. *Amphilichas cucullus* Tripp, 1957, fig. 4q; Tripp, 1959, p. 498, fig. 395, 1c

non *Amphilichas cf. cucullus* Westrop and Ludvigsen, 1983, pl. 9 figs 1, 6, pl. 10, figs. 1-7.

Description.—Cranidium subtriangular in outline, with length 63% of cranidial width opposite palpebral lobe. Longitudinal profile of cranidium very strongly convex, particularly anteriorly. In anterior view, median lobe stands well above level of composite lobes. Axial furrow uniformly narrow and deep; slightly curved inward opposite palpebral lobe, then descends almost vertically in front of palpebral lobe to join preglabellar furrow; posteriorly, axial furrows curve outward around margins of LO. Glabella subpectangular in outline, with width comprising 68% of cranidial width between palpebral lobes. SO same depth and width as axial furrow, transverse medially, then posteriorly directed at about 30 degrees behind composite lobes. LO slightly arched towards anterior, narrowing abaxially, accounting for 16-21% of cranidial length, and 64% of cranidial width opposite palpebral lobes. Longitudinal furrows deep, curved gently outward anteriorly before descending steeply downward to terminate at axial furrow. Median lobe expands anteriorly, comprising 38-41% of glabellar width opposite palpebral lobes. Anterior portion of median lobe very prominent, swollen in appearance, and bluntly pointed anteriorly. Composite lobes widen slightly anteriorly; subrectangular in outline in dorsal view, c-shaped in lateral view. Composite lobes constitute 28-30% of glabellar width opposite palpebral lobes, 66-67% of glabellar length. Fixigena strongly curved laterally, boomerang shaped in outline (dorsal view), occupying 51% of cranidial length in dorsal view. Palpebral lobe incompletely preserved, apparently semicircular; palpebral furrow apparently curved, finely etched groove. Preocular area a very narrow band that descends steeply forward; palpebral area slightly wider than preocular area,

gently inflated, accounting for 8% of width across palpebral lobes; posterior area flat, with posteriolateral projection of approximately double width of preocular area. Posterior border short, nearly transverse and widens slightly abaxially. Posterior border furrow narrowly etched groove, shallower than axial furrow, extending to sutural margin.

Hypostome elliptical in outline, with length 51% of width, well-defined median notch in posterior border equal to 17% of hypostomal length. Anterior border obsolete medially, expanding abaxially. Anterior margin well rounded, gently tapers abaxially into lateral notch. Lateral border expands backwards dramatically, subtriangular in outline, descends slightly ventrally into posterior border. Posterior border wide and flat, narrowing gradually between shoulder and conspicuous median notch, length (exsag.) equal to about 43% of hypostomal length. Lateral border furrows deep and wide, converging adaxially until it intersects posterior border furrow. Median body subtrapezoidal in outline, occupying 75% of hypostomal length. Anterior lobe large, bulb-shaped in outline. Middle furrow present only abaxially, same depth and width as lateral furrow, clearly delineating anterior and posterior lobes. Posterior lobe short, transverse, subrectangular in outline, constituting 24% of median body length (sag.). Posterior border furrow same depth and width as lateral furrow, transverse, clearly separating median body from very weakly convex (tr) posterior border region.

Tubercles on cranidial surface of five different sizes. Size classes 1-4 are approximately 30-40% larger than next lowest size; largest tubercles reaching up to 0.66 mm in diameter. Smaller sizes scattered randomly on cranidial surface, largest dome shaped tubercles are aligned exsagitally on composite lobes (Fig. 8.5), but not on median lobe. On LO, larger tubercles occur along posterior margin. On hypostome, median body

heavily tuberculate, three separate sizes of tubercle, uniformly distributed on anterior lobe. Terrace ridges minimally present on outer parts of lateral and posterior borders, not extending to median notch. Tightly-packed tubercles on lateral border, posterior border with widely spaced punctae.

Material Examined.— One almost complete cranidium (OU 12149, Figs. 8.7, 8.9-8.10), one partial cranidium (OU 12147, Figs. 8.5-8.6, 8.8) and one complete hypostome (OU 12146, Fig. 8.4).

Occurrence.—Upper Ordovician (Sandbian) of Oklahoma (Viola Springs Formation). OU 12146 and OU 12147 are from the Highway 99 section (41 and 46.5m collections, see Amati and Westrop 2006, fig. 7), Pontotoc County Oklahoma. OU 12149 is from undifferentiated Viola Springs Formation, Lawrence Quarry, Pontotoc County, Oklahoma.

Discussion.—Cranidia of *Amphilichas* cf. *A*. *cucullus* figured here (Figs. 8.4-8.10), are very similar to those from the Kimmswick Limestone of Missouri (Meek and Worthen, 1865, pg. 266; Foerste, 1920, pl. 1, c, d, e; Shimer and Shrock, 1944, pl. 170, figs. 19-22) and the Trenton Group of the Ottawa region, Ontario (Foerste, 1920, pl. 1 a, b). The dimensions of the composite lobes, glabella, and occipital lobes are very similar, and both possess a slight dorsally projected swelling of the median lobe. The hypostome of *A*. cf. *A*. *cucullus* (Fig. 8.4) is also nearly identical to the *A*. *cucullus* hypostome from the Kimmswick (Foerste, 1920, fig. 1g). There is no pygidium available for *A*. cf. *A*. *cucullus* and *A*. *cucullus* itself is poorly known, so we prefer to use open nomenclature until a complete association of exoskeletal parts can be made. Westrop and Ludvigsen (1983, pl. 9 figs 1, 6, pl. 10, figs. 1-7) also identified sclerites from southern Manitoba as

A. cf. *A*. *cucullus.* Their cranidia are similar to ours, except the swelling of the median lobe is greater and producing a more pointed lateral profile (compare Westrop and Ludvigsen, 1983, pl. 10, fig. 2 with Figs. 8.7, 8.10), the sculpture is slightly less coarse, and the median lobe is relatively wider (tr) and longer (sag), so they are likely not conspecific.

AMPHILICHAS RHINOCEROS (Slocom, 1913)

Figure 7.1

Amphilichas rhinoceros, Slocom, 1913, pl. 15, figs. 5, 6; Walter, 1924, pl. 18, figs. 7, 8; Thomas and Holloway, 1988, pl. 12, fig. 255.

Kerakephalichas rhinoceros, Phleger, 1936, fig. 42.

Diagnosis.—*Amphilichas* with dorsal/anterior swelling of the median lobe (character 3; state 1); one pair of spines developed on the anterior portion of the median lobe, one spine developed on each composite lobe.

Description.—Cranidium incomplete but apparently subpentangular in outline. Axial furrow finely etched groove, straight between posterior margin and a point just behind posterior tip of palpebral lobe, then gradually diverging forward. Glabella apparently subpentagonal in outline, widest in front of palpebral lobes. Longitudinal furrows are shallow but clearly-defined grooves, roughly parallel between SO and point opposite base of spine on composite lateral lobe, then diverging forward; anterior termination point not preserved. SO somewhat deeper than axial and longitudinal furrows, slightly curved towards the anterior. LO with gently rounded margins, width equal to 63% of cranidial width between palpebral lobes, narrows slightly abaxially. Posterior margin of LO transverse to slightly curved forward, showing doublure.

Longitudinal furrows extend forward from SO; subparallel posteriorly but diverge along curved path anteriorly; median lobe apparently bulb-shaped in outline. Minimum width of median lobe at SO 71% of its maximum preserved width; width of median lobe comprises 31% of glabellar width opposite palpebral lobes. Near anterior end of median lobe, two dorsally elevated nodes form the base of vertically directed curved spines. Composite lobes incompletely preserved, apparently subrectangular in outline, widest between palpebral lobes, curving gently abaxially. Composite lobe accounts for about 35% of glabellar width opposite palpebral lobe. Each composite lobe carries long, stout curved spine near axial furrow and opposite palpebral lobe (only based preserved on left side of cranidium as ill-defined inflation). Fixigena incompletely preserved; palpebral area apparently narrow (tr.); postocular area apparently flat, with posterolateral projection approximately equal in width to palpebral area.

Cranidium has regularly scattered tubercles of four sizes present on exoskeletal surface. Size classes 1-3 are 20-30% larger than next lowest size class. Largest size tubercles are disproportionately large, reaching up to 1.25 mm in diameter, elliptical shaped, denser on median lobe.

Material Examined.—Holotype cranidium (FMNH 11181, Fig. 7.1)

Occurrence.— Upper Ordovician (lower Maquoketa Formation) of Elgin, Iowa, USA.

Discussion.—The specimen illustrated here is the holotype of *Amphilichas rhinoceros* Slocom 1913, a species that was designated later as the type species of *Kerakaphalichas* Phleger 1936. Following previous authors (Warburg, 1939; Tripp, 1957; Thomas and Holloway, 1988) *Kerakaphalichas* is treated as a junior synonym of

Amphilichas. The spines on the cranidium are unique within the Tetralichini, but this species shares all other features with *Amphilichas*, including the general lobation and furrow patterns; the broadly inflated median lobe resembles those of both *A*. *cucullus* and A. *bicornis*. The holotype specimen is compacted and incomplete anteriorly, so it is impossible to tell if the convexity most resembles other species of *Amphilichas*, or a less convex tetralichine such as *Probolichas*.

The specimen FMNH 11181 is an external mold, and was illustrated by Slocom (1913) and Walter (1924), although both authors presented interpretive line drawings of the dorsal cranidial exoskeleton (also Phleger, 1936, fig. 42). Although these reconstructions seem to capture the cranidial morphology well, the length and orientation of the spines is largely speculation. Our illustration (Fig. 7.1) is the first silicon cast of FMNH 11181.

AMPHILICHAS SUBPUNCTATUS (Esker, 1964)

Figures 9.7-9.8, 9.11-9.12, 10.1-10.4, 10.7-10.8

Amphilichas subpunctatus Esker, 1964, pl. 3 figs. 1-4.

Amphilichas subpunctatus Shaw 1974, pl. 11, figs. 1-4; 7, 8, 11; pl. 12, figs. 1, 2, 4, 7-9, 11-14.

Diagnosis.—*Amphilichas* with a punctae dominated anterior portion of the median lobe (character 12, state 1), small consistently sized tubercles (character 25, state 0), strongly punctate hypostome (covaries with character 14, state 0); macula on hypostomal median body very well defined.

Description.— Cranidium subtriangular in outline, with length 65-72% of cranidial width across palpebral lobes. Longitudinal profile strongly convex, median lobe

overhanging the anterior border, convexity (tr) also high, with composite lobes depressed below level of median lobe. Axial furrows finely etched grooves, gently convergent between posterior margin and point just behind posterior tip of palpebral lobe, then diverge gradually forward; in front of palpebral lobes, axial furrows descend almost vertically downward to join preglabellar furrow. Glabella subpentagular in outline; width opposite palpebral lobes 88-96% of length, widest just in front of palpebral lobes. SO slightly deeper than axial furrow, transverse medially but deflected backward behind composite lobes. LO width 78-79% of cranidial width at palpebral level, 15-16% of cranidial length, narrows slightly abaxially. Posterior margin of LO very slightly arched forward, flattening horizontally (tr) below fixigena. Longitudinal furrows clearly defined, approximately same depth as axial furrows, subparallel between SO and point opposite mid-length of palpebral lobe, then curving outward and steeply downward to terminate at axial furrow. In dorsal view, median lobe bulb-shaped in outline, narrowest posteriorly, expanding dramatically beyond palpebral lobes. In lateral view, median lobe very prominent, overhanging anterior border, curving postero-ventrally beyond composite lateral lobe. In dorsal view, composite lobes are bands that curve gently outward, approximately equal width for their duration, length occupying 59-61% of cranidial length, and 26-32% of glabellar width opposite palpebral lobes; in front of palpebral lobes, composite lobes descend almost vertically forward. Palpebral lobe semielliptical in outline, length equal to a little more than 20% of cranidial length, and centered behind cranidial mid-length; elevated slightly above palpebral area of fixigena. Palpebral furrow gently curved and shallows markedly opposite middle of palpebral lobe. Preoccular area of fixigena is narrow band that descends steeply forward; palpebral area somewhat wider

than preoccular area, accounting for 16-18% of cranidial width across palpebral lobes, and gently inflated; posterior area less steeply sloping than preoccular area, with relatively narrow (tr.) posterolateral projection that is roughly double width of postocular area. Posterior border furrow nearly transverse, comparable in depth to SO and extends to sutural margin. Posterior border convex, length at axial furrow equal to about 6% of cranidial length, but expanding slightly abaxially. Sutural margin in front of palpebral lobe not preserved; posterior branches diverge backward in sigmoid curve.

Hypostome elliptical in outline, with length 54% of width, with well-defined median notch in posterior border equal to 18% of hypostomal length. Anterior margin rounded; anterior border very short, narrowing abaxially, and is obsolete at sagittal line. Lateral border expands backward, subtriangular in outline, and passes without interruption into broad, nearly flat posterior border. Posterior border varies little in length aside from at median notch; maximum length (exsag.) equal to about 40% of hypostomal length. Lateral border furrows firmly impressed grooves that converge gradually backward to join roughly transverse posterior border furrow. Median body subtrapezoidal in outline; comprises 69% of hypostomal length. Anterior lobe also sub-trapezoidal in outline, accounts for 74% of median body length. Middle furrow slightly shallower than lateral border furrow, present only abaxially, slightly posteriorly directed, terminates at macula. Posterior lobe sub-rectangular in outline, widening slightly abaxially. Macula very pronounced, sub-rectangular in outline, orientated about 30˚ from vertical.

Available pygidia incomplete but apparently subellipitcal in outline and weakly convex. Axis comprises two segments plus long terminal piece, and occupies at least 41-

43% (estimated) of pygidial length, and 30-36% of pygidial width at first axial ring; tapers backward and rounded posteriorly. Posterior end of axis defined by change in slope between it and post-axial band. First axial ring furrow transverse, well-incised and extends across entire width of axis; second ring furrow shallower, weakly chevron shaped, effaced abaxially. One axial ring complete, rectangular in outline; second axial ring incomplete, more rounded irregularly shape because of partial effacement of 2nd ring furrow. Interpleural furrows same depth and width as pleural furrows, but shallow abruptly for final 40% of their extent, curve outwards and backward; furrows (interpleural?) on adaxial sides of third pair trend obliquely forward from pygidial margin, joining axial furrows, outlining a posteriorly narrowing post-axial band. Three pairs of flat, broad pleurae. First pleurae terminates in sharply pointed spine; others not preserved. Interspine embayment somewhat larger (tr., exsag.) between 1st and 2nd pleurae than between between 2nd and 3rd. Pleural furrows expressed on first two pairs of pleurae only, similar in depth to 1st axial ring furrow; shallowing gradually posteriorly, terminating at point immediately behind fulcrum. Pleurae divided into subequal anterior and posterior bands.

Cranidium has three tubercle sizes, evenly scattered and densely packed on exoskeletal surface. Each tubercle size is 20-30% larger than next smallest size, with largest reaching up to 0.5 mm in diameter. Anteriorly, tubercles are effaced; widely spaced punctae dominate the median lobe anteriorly. Pygidial sculpture consists of three primary tubercle sizes on the axis, slightly elongate, largest size also reaching 0.5 mm in diameter. At mid-point of pleurae, tubercles become more homogeneous, with loss of largest size class. Hypostome median body strongly punctate; pits packed more tightly on

lateral margins of anterior lobe, sparsely distributed near mid-line and on posterior lobe. Prominent terrace ridges present on outer parts of lateral and posterior borders, extending to a point just forward of median notch. Tubercles of two sizes also present on borders. Widely spaced pits present on median portion of posterior border, behind posterior lobe. Band of smooth exoskeleon occurs along margins of median notch.

Material Examined.— Material illustrated: One complete holotype cranidium (OU 5202, Figs. 10.1-10.3), two nearly complete cranidia (OU 12485, Figs. 9.7-9.8, 9.11; 12490, Fig. 10.8), two partial pygidia (OU 5201, Fig. 9.12; 12486, Fig. 10.4), one complete hypostome (OU 12489, Fig. 10.7). Unfigured material includes two nearly complete cranidia, three partial cranidia, one partial pygidia, one partial thorax, and one complete hypostome.

Occurrence.— Upper Ordovician (Sandbian) Pooleville Member of the Bromide Formation, Arbuckle Mountains, Oklahoma. Localities include Rock Crossing (RC) and Tysons quarry (TQ), both near Ardmore, Oklahoma.

Discussion.—Esker (1964) regarded the punctation on the ventral portion of the median lobe as diagnostic of *Amphilichas subpunctatus*. However, as Shaw (1974) also noted, there are numerous species that possess this character including *A. minganensis*, *A. jukesi*, *A. lineatus*, and *A. effnensis*. Our phylogenetic analysis suggests the punctation of the median lobe is characteristic of an *Amphilichas* subclade that includes *A. subpunctatus*, *A. lineatus* and *A. effnensis* (Fig. 5). It should be noted that the removal of tubercles on the composite lobes of the holotype (Figs. 10.1-10.3) is an artifact of preparation. The natural anterior punctation is primarily on the median lobe (see Figs. 9.8, 9.11).

Shaw (1974) discussed the similar morphology between *A*. *aspratalis* (Bradley, 1930) from the Kimswick Limestone of Missouri, and *A*. *subpuctatus*. However, these two species are distinct from one another, with *A*. *subpunctatus* possessing a more prominent median lobe, more convex (sag) cranidium, more evenly distributed, fine tuberculation, and punctation on the anterior part of the median lobe.

Two distinct types of tetralichine hypostome have been recovered from the Pooleville Member, and only two tetralichine species (*Amphilichas subpunctatus* and *Probolichas kristiae*) are known from this unit. One of these includes the hypostome assigned by Shaw (1974, pl. 12, fig.2; Fig. 9.10 here) to *A*. *subpunctatus*. This hypostome is distinct from other species of *Amphilichas* in possessing a very reduced posterior lobe of the median body, and is highly tuberculate. These observations, in addition to tubercle shape and density, suggest this hypostome is better assigned to *Probolichas kristiae*. The more *Amphilichas*-like, strongly punctate hypostome (Fig. 10.7) is assigned to *A*. *subpunctatus*, whose cranidia are also punctate anteriorly. Shaw (1974, p. 43) mentioned, but did not illustrate four other hypostomata, which he claimed showed a size-related change in sculpture of the median body from coarse punctae to tubercles or smooth surfaces. Our material shows no evidence of such a size-related gradient in sculpture, as similar sized specimens are either tubercle- or punctae-dominated, and possess different median body morphology. Shaw (1974, pl. 11, figs. 2, 8) illustrated one complete specimen of *A*. *subpunctatus* (although this specimen cannot be located in the collections of the Oklahoma Museum of Natural History), so the thorax of the species is known. In general the appearance of Shaw's specimens is similar to Figure 8.1. However, because

the latter is incomplete, and thoracic segments are fairly similar across *Amphilichas* species, a confident identification is not possible.

AMPHILICHAS CF. A. JUKESI (Billings, 1865)

Figures 9.5-9.6, 9.9

cf. *Lichas jukesi* Billings,1865, fig. 269 a, b.

cf. *Acrolichas jukesi* Foerste, 1920, pl. 2, fig 1.

cf. *Apatolichas jukesi* Whittington,1963, pl. 32, figs. 4-11; pl. 33, 34; Thomas and Holloway, 1988, pl. 12, 259, 263, 267, 271.

Apatolichas cf. A. jukesi Ross, 1972, pl. 18 figs. 1-8; Fortey and Droser 1999, fig. 5.12).

Material Examined.—Material illustrated: One incomplete cephalon, USNM 167232c, Ross (1972; Figs. 9.5-9.6, 9.9). Unfigured material includes two incomplete cephala, USNM 167232 a, b, Ross (1972 pl. 18, figs. 1-5) one incomplete pygidia, USNM 495786 Fortey and Droser (1999, fig. 5.12).

Occurrence.—Middle Ordovician (Whiterockian) from the bioherm at Meiklejohn Peak, Nevada (Ross, 1972) and the Antelope Valley Limestone, Whiterock Canyon, Nevada (Fortey and Droser, 1999).

Discussion.—For a more complete systematic treatment of *Amphilichas jukesi*, see Whittington (1963), and Ross (1972) for *Amphilichas* cf. *A. jukesi*. Tripp (1957) assigned *Apatolichas jukesi* to *Amphilichas*, but later authors (Whittington, 1963; Ross, 1972; Fortey and Droser, 1999) considered the genus *Apatolichas* to be valid. Here, both *Apatolichas* cf. *A. jukesi* (Ross, 1972; Fortey and Droser, 1999) and *Apatolichas jukesi* (Whittington, 1963) are treated as species of *Amphilichas*. *Amphilichas jukesi* differs from other species of *Amphilichas* because the axial furrow is effaced from

approximately the midpoint of the palpebral lobe back to the occipital furrow, and there is independent convexity in the composite lobe, where L1a would be located. However, the genus *Amphilichas* is diagnosed here as a clade based on pleural furrow length and other pygidial characters, and *A. jukesi* possesses these traits. According to our analysis, *Apatolichas* is nested within *Amphilichas*.

We agree with Fortey and Droser (1999) that there is circumstantial evidence for treating the pygidium that they identified as *Amphilichas* cf. *A. jukesi* as conspecific with the cranidia that Ross (1972) illustrated under the same name. It is likely that *A.* cf. *A. jukesi* is not conspecific with *Amphilichas jukesi* (Whittington, 1963). The pygidium of *A.* cf. *A. jukesi* (Fortey and Droser, 1999, fig. 5.12) has considerably narrower (tr) posterior-most spines, a more complete 2nd axial ring furrow, and slightly longer pleural furrows. The cranidia of *A.* cf. *A. jukesi* are quite similar to those of *A. jukesi* (compare Figs. 9.5-9.6, 9.9 to Whittington, 1963, pl. 32 figs. 4-6), but the latter exhibits more pronounced effacement of the axial furrow, and a longer (sag), more angular shaped LO.

AMPHILICHAS EFFNENSIS new species

Figures 10.5-10.6, 10.10, 11.1-11.6

Diagnosis.—Amphilichas with densely punctate median lobe (character 12, state 1), preglabellar furrow effaced medially (character 13, state 1), post axial band poorly defined (character 21, state 1); glabella slightly expanded in width (tr), subelliptical composite lobes, dorso-ventrally compressed cranidium. Third pair of pygidial pleura with near straight posterior margins with rounded, rather spinose termination.

Description.— Cranidium subcircular in outline, with length equal to 63-65% of cranidial width across palpebral lobes. Longitudinal profile weakly convex except

anteriorly, where it descends in a steep, forwardly convex curve. In anterior view, median lobe rises well above composite lobes. Axial furrows well defined grooves, nearly parallel between SO and palpebral lobes, then becoming bowed outward before descending to join preglabellar furrow; preglabellar furrow shallows adaxially and is effaced medially (Fig. 11.2). Glabella wide, subcircular in outline, length equal to 78-84% of glabellar width opposite palpebral lobes. SO similar in depth to axial furrow, transverse behind median lobe but deflected backward behind composite lobes at an angle of about 20 degrees LO width 68-69% of cranidial width opposite palpebral lobes, constitutes 13-16% of cranidial length. Posterior margin of LO transverse medially but very slightly anteriorly directed abaxially. Longitudinal furrows comparable in depth to axial furrows along most of their course but shallowing slightly near SO; parallel between SO and palpebral lobes, then diverging forward and downward along curved path. Median lobe accounts for 37-41% of glabellar width opposite palpebral lobes but expands considerably at anterior. . Lateral composite lobes suboval in outline, widest just forward of palpebral lobes, comprising 29-32% of glabellar width and 62-65% of length in dorsal view. Palpebral lobe incompletely preserved but apparently small and centered behind cranidial mid-length. Preocular area of fixigena narrow bands that slope steeply forward. Palpebral area incompletely preserved but stands slightly above level of palpebral lobe. Posterior area of fixigena slopes steeply downward; posterolateral projection is about twice width of postocular area. Posterior border furrow well-incised, directed slighly forward and extends to sutural margin. Posterior border short, subrectangular in outline, widens abaxially.

Pygidium appears subcircular in outline with maximum width 93% of maximum length, with broad, flat pleural field. Axis tapers backward, length equal to about 55% of maximum length, and occupies about 37% of pygidial width at anterior-most axial ring; separated from triangular postaxial band only by slight change in slope. Axis with two axial rings and a terminal piece composed of two segments. Articulating half-ring semielliptical in outline, length (sag.) equal to minimum length (sag) of first axial ring; articulating furrow finely etched, nearly transverse groove. First axial furrow curved forward shallowing; first axial ring shortest medially but expands abaxially. Second axial ring furrow curved backwards, nearly effaced medially and expressed abaxially as fine, slit-like grooves that terminate before reaching axial furrows; second axial ring is subelliptical in outline. Terminal piece accounts for about half of axis length and subequally divided into two segments by barely perceptible, backwardly-curved furrow that terminates short of axial furrows. Post-axial band poorly differentiated from axis. Interpleural furrows separating first and second pairs of pleurae are shallow but clearly defined and curve outward and backward; furrows (interpleural?) on adaxial sides of third pair trend obliquely forward from pygidial margin, joining axial furrows and outlining postaxial band. Three pairs of broad, flat pleurae; embayments of pygidial margin separating pleural tips are narrow, slit-like. First and 2nd pairs of pleurae approximately same length (exsag) with strongly curved lateral margins; second pair have spinose terminations oriented backward and inward, tips of first pair not preserved. Third pair of pleurae have nearly straight posterior margins, with rounded, rather than spinose adaxial termination. Pleural furrows expressed only on first pair of pleurae as shallow, oblique

grooves that terminate just short of fulcrum. Where evident, anterior and posterior pleural bands subequal in length.

Sculpture. Cranidial exoskeleton strongly punctate, pits more closely packed on median lobe, less conspicuous on composite lobe and LO. Cranidial tubercles of two sizes, larger size reaching 0.40 mm in diameter and 20-30% larger than smaller size, rounded and smooth, barely raised above exoskeletal surface; become ill-defined or absent beyond palpebral lobes, leaving anterior median glabella punctae-dominated. Pygidial tubercles of three primary sizes, each size class approximately 10-20% larger than next lowest, largest size reaching 0.35 mm in diameter, very rounded, flat, spacing tighter on axis.

Etymology.—After the Effna Formation.

Types.—Holotype cranidium (OU 12493, Figs. 11.1-11.3), paratype cranidia (OU 12487, Fig. 10.5; OU 12488, Fig. 10.6; OU 12494, Figs. 11.4-11.6), paratype pygidia (OU 12492, Fig. 10.10). Type locality is Porterfield Quarry (PQ) in Smyth County Virginia, Upper Ordovician (Sandbian) of the Effna Formation.

Material Examined.—In addition to types, unfigured material includes two partial cranidia.

Occurrence.—Known only from the type locality.

Discussion.—The only other species reported from the Effna Formation of Virginia are *Amphilichas minganensis* (Billings, 1865) and *A. prominulus* (Raymond, 1925, pl. 8, figs. 11, 12). The type material of *A. prominulus* from the Effna is very fragmentary, and it is impossible to state with any certainty that the specimen is even a tetralichine, as the entire composite lobe is not preserved. Preservation aside, the

specimen is dissimilar from *A*. *effnensis* because the median lobe protrudes anteriorly and the surface is not punctate. Raymond (1925) claimed to have found sclerites of *A*. *minganensis* Billings 1865 from the Effna, but none were illustrated. Based on his short description, and other illustrations of *A*. *minganensis* (Billings, 1865, pl 181, fig. 163a; Raymond, 1905, pl. 14, figs. 1-3; Raymond, 1910, pl. 19, fig. 14; Shaw, 1968, pl.3, figs. 2-25), this species is morphologically distinct from *A*. *effnensis*. In *A*. *minganensis*, the glabella is not expanded, the composite lobes are much narrower, the glabella is not as dorso-ventrally compressed, and the sculpture is dissimilar.

Based on cranidal morphology, *Amphilichas effnensis* seems most similar to *Amphilichas trentonensis* (Conrad, 1842; Foerste, 1920, pl.1, fig. a-c) from the Trenton of New Jersey. Both share very rounded cranidia and composite lobes, although *A*. *trentonensis* possesses a narrower glabella, less dorso-ventral compression, and more horizontal fixigena. The poorly defined post-axial band of *A*. *effnensis* (e.g., very slight break in slope suggesting the end of the axial piece and start of the post-axial band) is similar to *A*. *jukesi*, although the latter completely lacks a post-axial band. The *A*. *effnensis* pygidium is very similar to other North American tetralichines (*Amphilichas harrisi*, *Amphilichas conifrons*, *Amphilichas minganensis*) pygidia in regards to the effacement of the second pleural furrow. The straight posterior margins of the 3rd pair of pleura are apparently unique to *A*. *effnensis*.

AMPHILICHAS SP. 1

Figure 10.9

Material Examined.—One complete hypostome (OU 12491, Fig. 10.9) and one partial hypostome.

Occurrence.— Upper Ordovician (Sandbian) of the Effna Formation, Porterfield Quarry (PQ) in Smyth County Virginia.

Discussion.—The sculpture of the Effna hypostome (Fig. 10.9) differs from *Amphilichas effnensis* in that the tubercles are smaller, less rounded, and more dorsally elevated above the exoskeletal surface. However, it undoubtedly belongs to a species of *Amphilichas* as the median body is subtrapezoidal, and reduced in length (sag). *Amphilichas* sp. 1 is distinct from the other species claimed to occur in the Effna by Raymond (1925), such as *A*. *minganensis* (Shaw, 1968, pl. 3, fig. 12), because the lateral notches are less prominent, and the median body is tuberculate instead of punctate.

Genus LYRALICHAS Weber, 1948

Type Species.—*Lichas (Amphilichas) bronnikovi* Weber, 1932 from the Ordovician of the Karatau Range, Turkestan (by original designation).

Diagnosis.—Tetralichini with an incomplete longitudinal glabellar furrow (character 1, state 0), four pleural furrow pairs (character 18, state 3), two complete pygidial axial ring furrows (character 20, state 0); three interpleural pygidial furrows, and the abaxial movement of the axial furrow before intersecting with SO.

Definition.—The clade in which all species share a more recent common ancestor with *Lyralichas bronnikovi* than with *Amphilichas* cf. *A. encyrtos* (left branch arising from node 2, Fig. 4).

Discussion.—The monotypic genus *Lyralichas* differs from other tetralichines in having four pleural furrow pairs, three well defined pygidial axial ring furrows, and an abaxial curvature to the axial furrow near SO. *Lyralichas* shares many cranidial

synapomorphies with other tetralichines (see node 2, Fig. 5), even though the pygidial morphology is radically different. Thus, the genus is assigned confidently to Tetralichini.

ACKNOWLEDGEMENTS

This research was funded by NSF grant EAR-0819715 to Amati and Westrop. S. Boyd, R. Burkhalter, K. Carlucci, and A. Thomas assisted in fieldwork, and Burkhalter also provided technical support in the lab. K. Brett and L. Knox collected a number of specimens from the Effna Formation. L. Tyson and A. Graffham provided access to the Tyson (formerly Dunn) Quarry. J. Adrain acquired and generously donated several sclerites of *Probolichas*, including those figured by Thomas and Holloway (1988). F. Read provided helpful locality information in Virginia. Loans of type material were arranged by C. Labandeira and D. Levin at the National Museum of Natural History, P. Mayer at the Field Museum, and C. Franzén and J. Hagström at the Swedish Museum of Natural History. Special thanks to G. Edgecombe and R. Owens who provided reviews that greatly improved the paper.

REFERENCES

AMATI, L., AND S. WESTROP. 2004. A systematic revision of *Thaleops* (Trilobita: Illaenidae) with new species from the Middle and Late Ordovician of Oklahoma and New York. Journal of Systematic Palaeontology, 2(3):207-256.

AMATI, L., AND S. WESTROP. 2006. Sedimentary facies and trilobite biofacies along an Ordovician shelf to basin gradient, Viola Group, South-Central Oklahoma. PALAIOS, 21:516-529.

AMSDEN, T. W., AND W. C. SWEET. 1983 Upper Bromide Formation and Viola Group (Middle and Upper Ordovician) in Eastern Oklahoma. Oklahoma Geological Survey Bulletin, 132:1-76.

ANGELIN, N. P. 1854. Palaeontologica Scandinavica Pars II. Academiae Regiae Scientarium Suecanae (Holmiae), 21-92.

BARTON, D. C. 1916. A revision of the Cheirurinae, with notes on their evolution. Washington University Studies in Science, 3:101-152.

BEYRICH, E. 1845. Ueber einige böhmische Trilobiten, Berlin, 47 p.

BILLINGS, E. 1865. Palaeozoic fossils, containing descriptions and figures of new or little known species of organic remains from the Silurian rocks. Dawson Brothers, Montreal, 426 p.

BRADLEY, J. H. 1930. Fauna of the Kimmswick Limestone of Missouri and Illinois. Walker Museum, University of Chicago Contributions, 2(219-290).

BREMER, K. 1994. Branch support and tree stability. Cladistics, 10(3):295-304.

CHATTERTON, B. D. E., AND R. LUDVIGSEN. 1976. Silicified Middle Ordovician trilobites from the South Nahanni river area, District of Mackenzie, Canada. Palaeontographica, 154:1-106.

CLARKE, J. M. 1894. The Lower Silurian trilobites of Minnesota. Minnesota Geology and Natural History Survey:694-759.

CONRAD, T. A. 1842. Observations on the Silurian and Devonian systems of the United States, with descriptions of new organic remains. Journal of the Academy of National Sciences Philadelphia, 8:228-235.

CONRAD, T. A. 1843. Observations on the lead bearing limestone of Wisconsin, and

description of a new genus of trilobites and fifteen new Silurian fossils. Proceedings of the Academy of Natural Sciences of Philadelphia, 1:329-335.

COOPER, G. A. 1930. Upper Ordovician and Lower Devonian stratigraphy and palaeontology of Percé, Quebec: part 2; new species from the Upper Ordovician of Percé. American Journal of Science, 5(20):385-392.

COOPER, B. N. 1944. Geology and mineral resources of the Rukes Garden quadrangle, Virginia. Virginia Geological Survey Bulletin, 60.

COOPER, B. N., AND G. A. COOPER. 1946. Lower Middle Ordovician stratigraphy of the Shenandoah Valley, Virginia. Bulletin of the Geological Society of America, 57(35-114).

COOPER, G. A. 1956. Chazyan and related brachiopods. Smithsonian Miscellaneous Collections 127(Pt 1, 2):1-245.

DALMAN, J. W. 1827. Om Palaeaderna, eller de sa kallade Trilobiterna. Kongliga Svenska vetenskapsadademiens handlingar:113-152, 226-294.

DE QUEIROZ, K., AND J. GAUTHIER. 1990. Phylogeny as a central principle in taxonomy: phylogenetic definitions of taxon names. Systematic Zoology, 39(4):307-322.

DE QUEIROZ, K. 2007. Toward an integrated system of clade names. Systematic Biology, 56(6):956-974.

ECKERT, T. 1951. The fauna of the upper Bromide Formation. Unpublished M.S. thesis, University of Oklahoma, Norman, 110 p.

EDGECOMBE, G. D., M. R. BANKS, AND D. M. BANKS. 2004. Late Ordovician trilobites from Tasmania: Styginidae, Asaphidae and Lichidae. AAPG Memoir, 30:59-77.

EMERSON, N., J. A. SIMO, C. BYERS, AND J. FOURNELLE. 2004. Correlation of (Ordovican, Mohawkian) K-bentonites in the upper Mississippi valley using apatite

chemistry: implications for stratigraphic interpretation of the mixed carbonate-siliciclastic Decorah Formation. Palaeogeography, Palaeoclimatology, Palaeoecology, 210:215-233.

ESKER, G. C. 1964. New species of trilobites from the Bromide Formation (Poolevillve Member) of Oklahoma. Oklahoma Geology Notes, 24:195-209.

EVITT, W. 1951. Some Middle Ordovician trilobites of the families Cheiruridae, Harpidae and Lichidae. Journal of Paleontology, 25(5):587-616.

FARRIS, J. S., 1969. A Successive Approximations Approach to Character Weighting. Systematic Zoology, 18(4):374-385.

FAY, R. O., AND A. A. GRAFFHAM. 1982. Biostratigraphic and paleontological studies, p. 195-209. *In* J. Sprinkle (ed.), Echinoderm Faunas from the Bromide formation (Middle Ordovician) of Oklahoma.Volume 1. University of Kansas Paleontological Contributions, Monograph 1.

FINNEY, S. C. 1986. Graptolite biofacies and correlation of eustatic, subsidence, and tectonic events in the Middle to Upper Ordovician of North America. PALAIOS, 1:435-461.

FOERSTE, A. F. 1919. Notes on *Isotelus*, *Acrolichas*, *Calymene* and *Encrinurus*. Bulletin of the scientific labs of Denison University, 19:65-81.

FOERSTE, A. F. 1920. The generic relations of the American Ordovician Lichadidae. American Journal of Science, 4(49):26-50.

FORTEY, R., AND M. DROSER. 1999. Trilobites from the base of the type Whiterockian (Middle Ordovician) in Nevada. Journal of Paleontology, 73(2):182-201.

GOLOBOFF, P., J. FARRIS, AND K. NIXON. 2008. TNT, a free program for phylogenetic analysis. Cladistics, 24:774-786.

GREEN, J. 1832. A monograph of the trilobites of North America. Joseph Brano, Philadelphia,

93 p.

GÜRICH, G. 1901. Ueber eine neue *Lichas*-art aus dem Devon von Neu-Süd Wales und über die Gattung *Lichas* überhaupt. Neues Jahr-buch für Mineralogie, Geologie und Paläontologie, 14:519-539.

HARRIS, R. W. 1957. Ostracoda of the Simpson Group. Oklahoma Geological Survey Bulletin, 75(1-333).

HAWLE, I., AND A. J. C. CORDA. 1847. Prodrom einer monographie der böhmischen Trilobiten. Abhandlungen Koeniglichen Böehmischen Gesellschaft der Wissenschaften. J.G Calve, Prague.

HOLLAND, S., AND M. PATZKOWSKY. 1996. Sequence stratigraphy and long-term paleooceanographic changes in the Middle and Upper Ordovician of the eastern United States. *In* B. Witzke, G. Ludvigson, and J. Day (eds.), Paleozoic Sequence Stratigraphy: Views from the North American Craton, GSA Special Paper 306. Geological Society of America, Boulder CO.

KARIM, T., AND S. WESTROP. 2002. Taphonomy and paleoecology of Ordovician trilobite clusters, Bromide Formation, South-central Oklahoma. PALAIOS, 17:394-403.

KING, D. T. 1986. Waulsortian-type buildups and resedimented (carbonate-turbidite) facies, early Mississippian Burlington shelf, central Missouri. Journal of Sedimentary Petrology, 56:471-479.

LAZARENKO, N. P. 1960. Some new Upper Cambrian trilobites of the northwest part of the Siberian Platform. Trudy Nauchno-Issledovatel'skogo Instituta Geologii Arktiki, 20:38-41.

LONGMAN, M. W. 1982a. Depositional environments, p. 17-29. *In* J. Sprinkle (ed.),

Echinoderm faunas from the Bromide Formation (Middle Ordovician) of Oklahoma.Volume 1. University of Kansas Paleontological Contributions, Monograph 1.

LONGMAN, M. W. 1982b. Depositional setting and regional characteristics. *In* J. Sprinkle (ed.), Echinoderm faunas from the Bromide Formation (Middle Ordovician) of Oklahoma. The University of Kansas Paleontological Contributions, Monograph 1.

LUDVIGSEN, R. 1978. The trilobites *Bathyurus* and *Eomonorachus* from the Middle Ordovician of Oklahoma and their biofacies significance. Royal Ontario Museum Life Sciences Contributions, 114:1-18.

MADDISON, D., AND W. MADDISON. 2005. MacClade: Analysis of Phylogeny and Character Evolution, 4.08. Sinauer Associates Inc, Sunderland, MA.

MALETZ, J., J. CARLUCCI, AND C. MITCHELL. 2009. Graptoloid cladistics, taxonomy and phylogeny. Bulletin of Geosciences, 84(1):7-19.

M'COY, F. 1849. On the classification of some British fossil Crustacea, with notces of new forms in the University collection at Cambridge. Annual Magazine of Natural History (London), 2(4):161-179.

MEEK, F. B., AND A. H. WORTHEN. 1865. Contributions to the palaeontology of Illinois and other western states. Proceedings of the Academy of Natural Sciences of Philadelphia, 17(5):245-273.

MOORE, R. C. 1959. Treatise on invertebrate paleontology, Part O, Arthropoda 1. Geological Society of America and University of Kansas, Boulder, CO and Lawrence, KA, 560 p.

NIXON, K. 2002. WinClada ver. 1.00.08.

ÖPIK, A. A. 1937. Trilobiten aus Estland. Publications of the Geologic Institutions of the University of Tartu, 52:1-163.

OWEN, A. W. 1981. The Ashgill trilobites of the Oslo Region, Norway. Palaeontographica, A 175:1-88.

PHLEGER, F. 1936. Lichadian Trilobites. Journal of Paleontology, 10(7):593-615.

POLLITT, J., R. FORTEY, AND M. WILLS. 2005. Systematics of the trilobite families Lichidae Hawle & Corda, 1847 and Lichakephalidae Tripp, 1957: The application of bayesian inference to morphological data. Journal of Systematic Palaeontology, 3(3):225-241.

PORTLOCK, J. E. 1843. Report on the geology of the Country of Londonderry and of parts of Tyrone and Fermanagh. Longman, Brown, Green, and Longmans, London, 475 p.

RAYMOND, P. E. 1905. Notes on the names *Amphion*, *Harpina* and *Platymetopus*. American Journal of Science, 4(19):377-378.

RAYMOND, P. E. 1910. Notes on Ordovician trilobites IV, new and old species from the Chazy. Annals of the Carnegie Museum, 7:60-80.

RAYMOND, P. E. 1925. Some trilobites of the lower Middle Ordovician of eastern North America. Bulletin of the Museum of Comparative Zoology, 67:1-180.

READ, J. F. 1980. Carbonate ramp-to-basin Transitions and foreland basin evolution, Middle Ordovician, Virginia Appalachians. AAPG Bulletin, 64(10):1575-1612.

READ, J. F. 1982. Geometry, facies, and development of Middle Ordovician carbonate buildups, Virginia Appalachians. AAPG Bulletin, 66(2):189-209.

ROSS, J. 1972. Fossils from the Ordovician bioherm at Meiklejohn Peak, Nevada. U.S. Government Printing Office, Washington, 685, 1-47 p.

RUPPEL, S., AND K. WALKER. 1977. The ecostratigraphy of the Middle Ordovician of the Southern Appalachians (Kentucky, Tennessee, and Virginia), U.S.A: A Field Excursion.

Studies in Geology, University of Tennessee Department of Geological Sciences, 77-1.

SABOL, J. W. 1958. Geology of the Porterfield Quarry area, Smyth County, Virginia, Unpublished M.S. thesis, Virginia Polytechnic Institute, 81 p.

SDZUY, K. 1955. Die Fauna der Leimintz-Schiefer (Tremadoc). Abhandlungen der Senckenbergischen Naturforschenden Gesellschaft, 492:1-74.

SHAW, F. C. 1968. Early Middle Ordovician Chazy trilobites of New York. New York State Museum and Science Services Memoir 17, 163 p.

SHAW, F. 1974. Simpson Group (Middle Ordovician) Trilobites of Oklahoma. Journal of Paleontology Memoir, 48(6):1-54.

SHIMER, H. W., AND R. R. SHROCK. 1944. Index Fossils of North America. M.I.T. Press, 837 p.

SLOCOM, A. W. 1913. New trilobites from the Maquoketa beds of Fayette County, Iowa. Field Museum of Natural History Geological Series, 4:43-83.

SPRINKLE, J. 1982. Introduction. *In* J. Sprinkle (ed.), Echinoderm faunas from the Bromide Formation (Middle Ordovician) of Oklahoma. University of Kansas Paleontological Contributions, Monograph 1.

STRAIT, D., M. MONIZ, AND P. STRAIT. 1996. Finite Mixture Coding: A new approach to coding continuous characters. Systematic Biology, 45(1):67-78.

STRONG, E.E., AND D. LIPSCOMB. 1999. Character coding and inapplicable characters. Cladistics, 15: 363-371.

SWOFFORD, D. L. 2002. PAUP* Phylogentic Analysis Using Parsimony (*and other methods), Version 4.0b10. Sinauer Associates, Sunderland, MA.

THIELE, K. 1993. The holy grail of the perfect character: the cladistic treatment of

morphometric data. Cladistics, 9:275-304.

THOMAS, A. T., AND D. J. HOLLOWAY. 1988. Classification and phylogeny of the trilobite order Lichida. Philosophical Transactions of the Royal Society of London, 321(1205):179-262.

TÖRNQUIST, S. L. 1884. Undersökningar öfver Siljansområdets trilobitfauna. Sveriges Geologiska Undersokning Afh, 436:1-191.

TRIPP, R. P. 1957. The classification and evolution of the superfamily Lichacea (Trilobita). Geological Magazine, 94:104-122.

TRIPP, R. P. 1959. Family Lichidae, p. 579. *In* R. C. Moore (ed.), Treatise on Invertebrate Paleontology, Part O, Arthropoda I. Geological Society of America.

ULRICH, E. O. 1892. Two new Lower Silurian species of *Lichas* (Subgenus *Hoplolichas*). American Geologist, 10:271-272.

ULRICH, E. O. 1911. Revision of the Paleozoic systems. Geological Society of America Bulletin, 22:281-680.

WALTER, O. T. 1924. Trilobites of Iowa and some related Paleozoic forms. Iowa Geological Survey Annual Reports 1923 and 1924, 31:1-388.

WARBURG, E. 1925. The trilobites of the Leptaena Limestone in Dalarne. Bulletin of the Geologic Institute of the University of Upsala, 27:1-446.

WARBURG, E. 1939. The Swedish Ordovician and Lower Silurian Lichidae. Kungliga Svenska Vetenskapsakademiens Handlingar, Stockholm, 17(4):1-162.

WEBBY, B. D. 1974. Upper Ordovician Trilobites from Central New South Wales. Palaeontology, 17(2):203-252.

WEBER, V. N. 1932. Trilobites of the Turkestan. Monographs of the Palaeontology of the

USSR, 178:3-151.

WEBER, V. N. 1948. Trilobites of the Silurian deposits of the USSR. Part 1. The Lower Silurian trilobites. Monografii po Paleontologii SSR, 69:1-111.

WESTROP, S. R., AND R. LUDVIGSEN. 1983. Systematics and Paleoecology of Upper Ordovician Trilobites from the Selkirk Member of the Red River Formation, Southern Manitoba. Manitoba Department of Energy and Mines Geological Report GR 82-2, Winnipeg, 51 p.

WHITEAVES, J. F. 1897. The fossils of the Galena-Trenton and Black River Formations of Lake Winnipeg and its vicinity. Geological Survey of Canada, 3:192-242.

WHITTINGTON, H. B. 1949. *Dolichoharpes* and the origin of the harpid fringe. American Journal of Science, 247:276-285.

WHITTINGTON, H. B. 1954. Ordovician trilobites from Silliman's Fossil Mount. Geological Society of America Memoir, 62:119-149.

WHITTINGTON, H. B. 1963. Middle Ordovician trilobites from Lower Head, western Newfoundland. Bulletin of the Museum of Comparative Zoology, 129:1-118.

WHITTINGTON, H. B., AND S. R. A. KELLY. 1997. Morphological terms applied to Trilobita. *In* R. L. Kaesler (ed.), Treatise on Invertebrate Paleontology, Pt. O, Arthropoda 1. Trilobita (revised). Volume 1. Introduction, Order Agnostida, Order Redlichiida. Geological Society of America and University of Kansas, Lawrence.

WILSON, J. L. 1975. Carbonate facies in geologic history. Springer-Verlag, New York, 471 p.

FIGURE *1*—Map of South-Central Oklahoma showing the localities where lichid material was collected for this study. Rock Crossing is a creek bed exposure at the intersection of Hickory Creek and D3265 Rd in the Criner Hills of Carter County, OK. Map coordinates for RC are 34.071, 97.169 (Lat/Long) and 14S, E0668976, N3771981 (UTM, NAD27). Tyson's Quarry (TQ) (formerly Dunn Quarry) is a privately operated quarry southwest of Ardmore, OK. Map coordinates and a specific topographic position for TQ are withheld at the request of the quarry owner. Darkly shaded area indicates the approximate extent of the southern Oklahoma aulacogen; lightly shaded area indicates the approximate extent of the Arbuckle Mountains (modified from Karim and Westrop, 2002; Amati and Westrop, 2004).

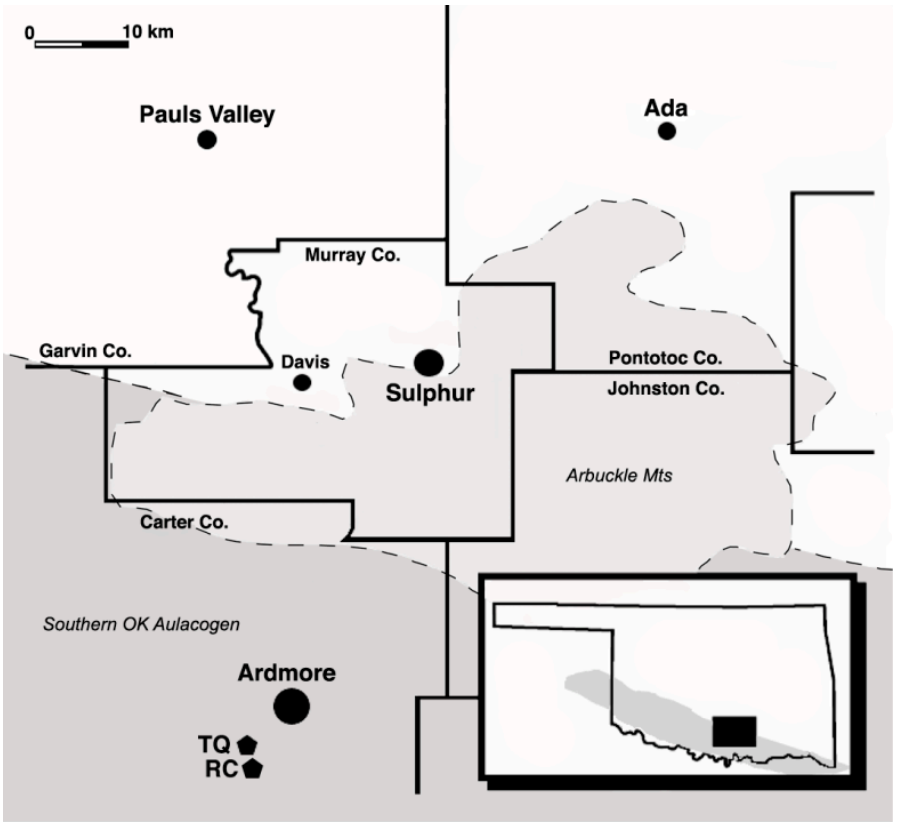
0
10 km
Pauls Valley
Ada
Murray Co.
Garvin Co.
Davis
Sulphur
Pontotoc Co.
Johnston Co.
Arbuckle Mts
Carter Co.
Southern OK Aulacogen
Ardmore
TQ
RC

FIGURE *2*—Stratigraphic section (TQ) in the Pooleville Member of the Bromide Formation, arrows denote horizons collections were taken from. See Sprinkle, (1982, pg. 363) for a measured section of the RC locality. Key to abbreviations: ms = mudstone, ws = wackestone, ps = packstone, gs = grainstone or rudstone.

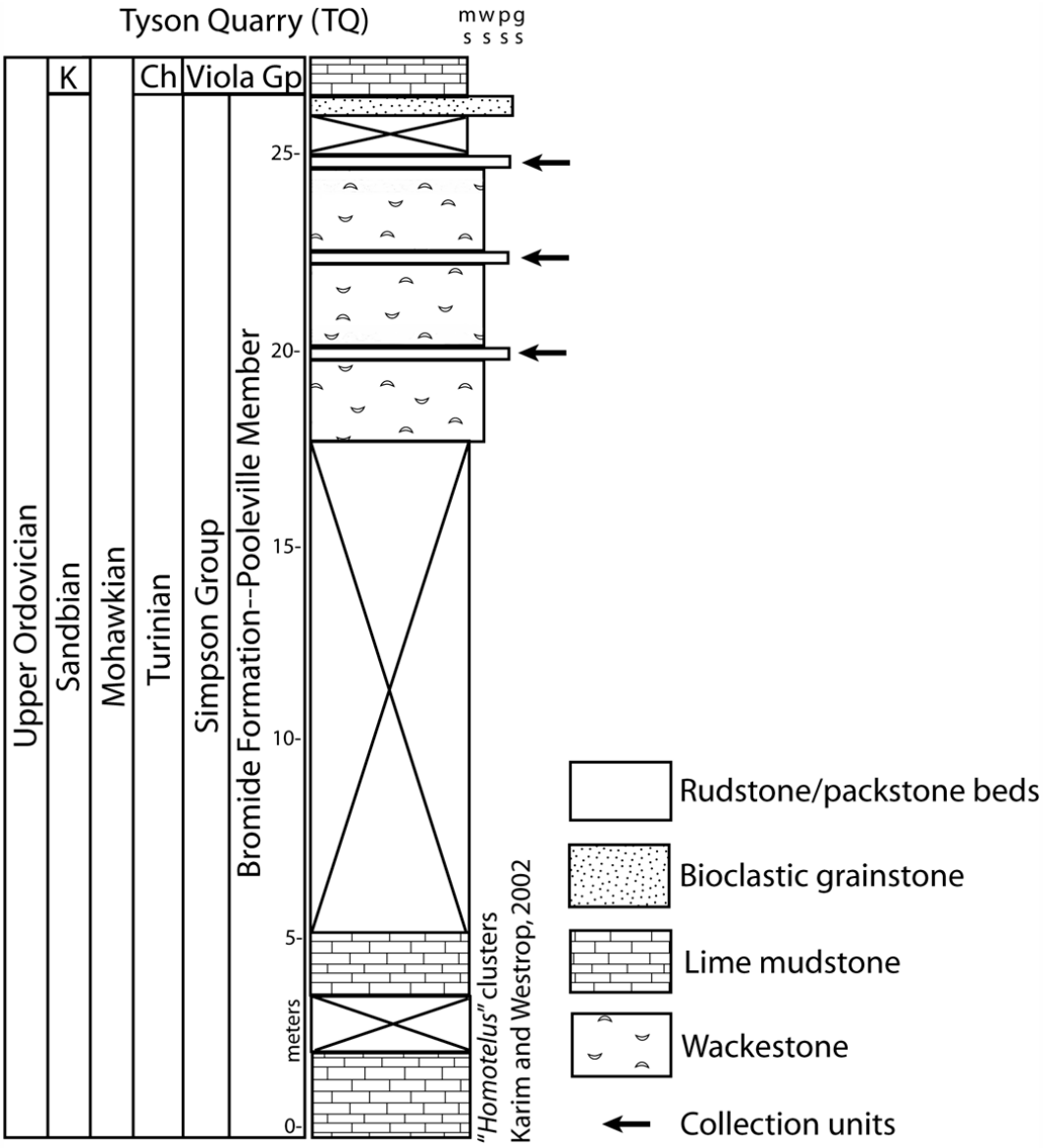
Tyson Quarry (TQ)
mwpg
s s s s
K
Ch
Viola Gp
Upper Ordovician
Sandbian
Mohawkian
Turinian
Simpson Group
Bromide Formation--Pooleville Member
25-
20-
15-
10-
5-
0-
meters
"Homotelus" clusters
Karim and Westrop, 2002
Rudstone/packstone beds
Bioclastic grainstone
Lime mudstone
Wackestone
Collection units

FIGURE *3—1*, Stratigraphic section of the PQ locality, abbreviations are the same as Figure 2. *2*, South-western Virginia locality map showing the southern portion of the Broadford Quadrangle, and the Porterfield Quarry (PQ) locality. The quarry is on VA 610/Valley Rd 4.8 km east of the intersection of VA 610 and VA 635. Map coordinates for PQ are 36.878, -81.681 (Lat/Long) and 17S, 439250, 4081420 (UTM, NAD27). *3*, Complete quarry map (modified from Read, 1982) based on multiple measured sections (collected and compiled by Sabol, 1958; Read, 1982, lithologic terminology modified here). Black arrow denotes location of stratigraphic section in Figure 3.1. The dotted line denotes the uncertain stratigraphic placement of the base of the Mohawkian and Turinian. Holland and Patzkowsky (1996) show the top half of the build-up in the Mohawkian and the bottom in the Whiterockian. Rather than picking an arbitrary dividing line, we placed the base of the Effna at the base of the Mohawkian.

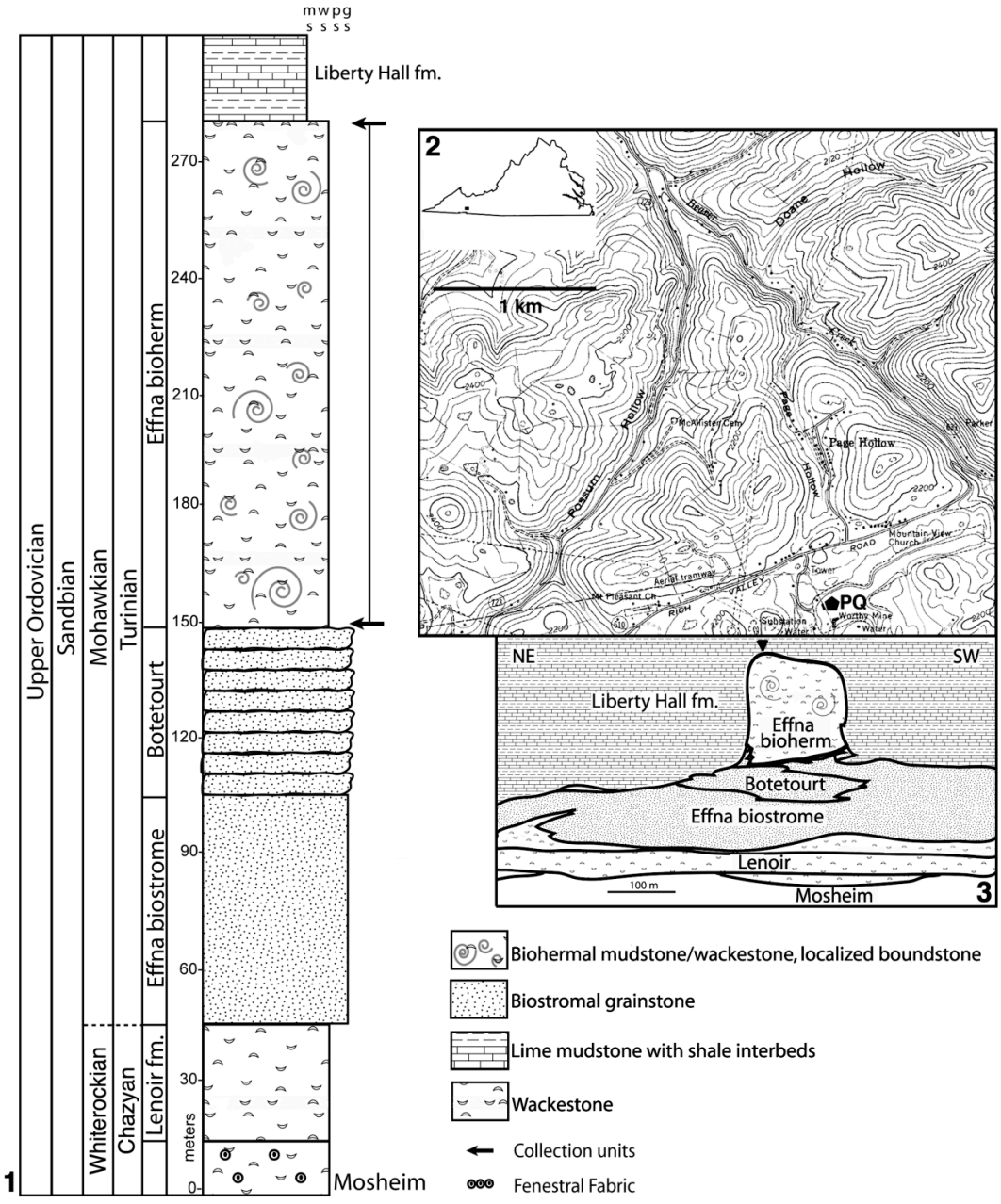
mwpg
s s s s
Liberty Hall fm.
Upper Ordovician
Sandbian
Mohawkian
Whiterockian
Chazyan
Turinian
Lenoir fm.
Effna biostrome
Botetourt
Effna bioherm
270
240
210
180
150
120
90
60
30
0
meters
1
Mosheim
2
1 km
Hollow
Branch
Doane
Creek
Possum
Hollow
McAlister Cem
Page Hollow
Parker
Mountain View Church
ROAD
Aerial tramway
Mt Pleasant Ch
VALLEY
RIDGE
Tower
PQ
Worthy Mine
Water
Substation
NE
SW
Liberty Hall fm.
Effna bioherm
Botetourt
Effna biostrome
Lenoir
100 m
Mosheim
3
Biohermal mudstone/wackestone, localized boundstone
Biostromal grainstone
Lime mudstone with shale interbeds
Wackestone
Collection units
Fenestral Fabric

FIGURE *4*—Strict consensus tree of the nine MPTs retained from the parsimony analysis, and recommended taxonomy of the Tetralichini. Tree length is 34 steps, CI is 0.79, RI is 0.69, and RC is 0.55. Nodes are numbered for easy reference within the text. Nodes with bootstrap support values >50%: (2) 100%, (3) 84%, (4) 63% (5) 61% (9) 62% (10) 77%. Bremer support value for node 2 is three; nodes 3, 4, 6, 9, and 10 are two, all other nodes are one.

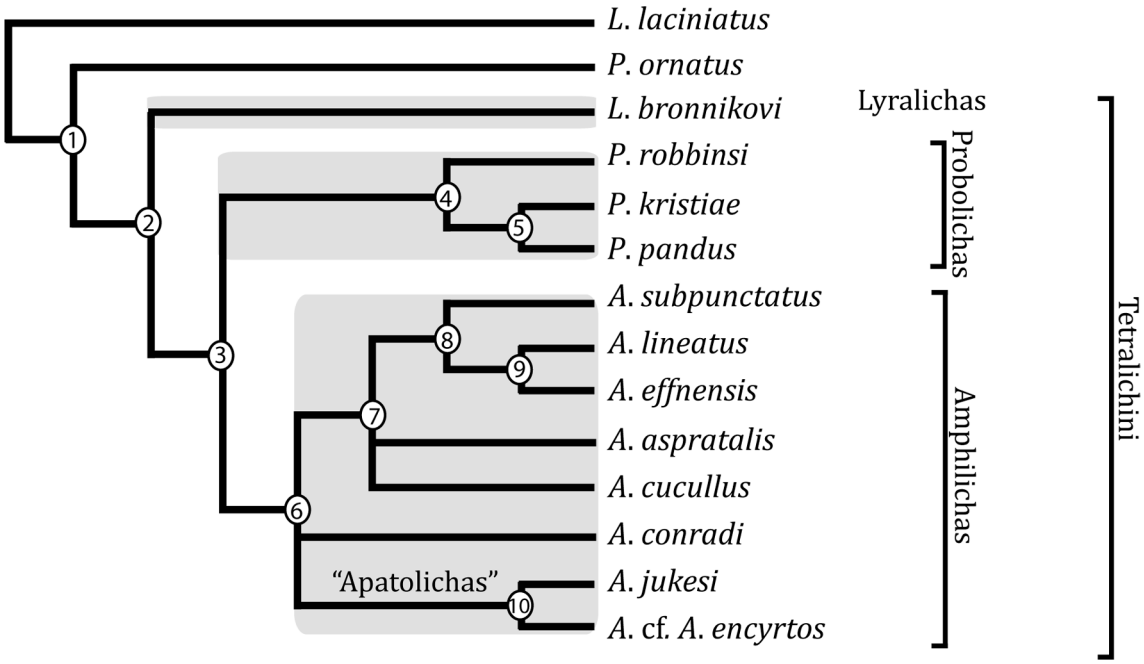
L. laciniatus
P. ornatus
L. bronnikovi
P. robbinsi
P. kristiae
P. pandus
A. subpunctatus
A. lineatus
A. effnensis
A. aspratalis
A. cucullus
A. conradi
A. jukesi
A. cf. A. encyrtos
"Apatolichas"
Lyralichas
Probolichas
Amphilichas
Tetralichini
1
2
3
4
5
6
7
8
9
10

FIGURE *5*—Optimized character distribution showing character states that change unambiguously on one of the nine MPTs (chosen because its topology is closest to the strict consensus tree). Black circles indicate synapomorphic character states, and white circles indicate homoplastic character states. Optimization was performed in PAUP* and checked in Winclada.

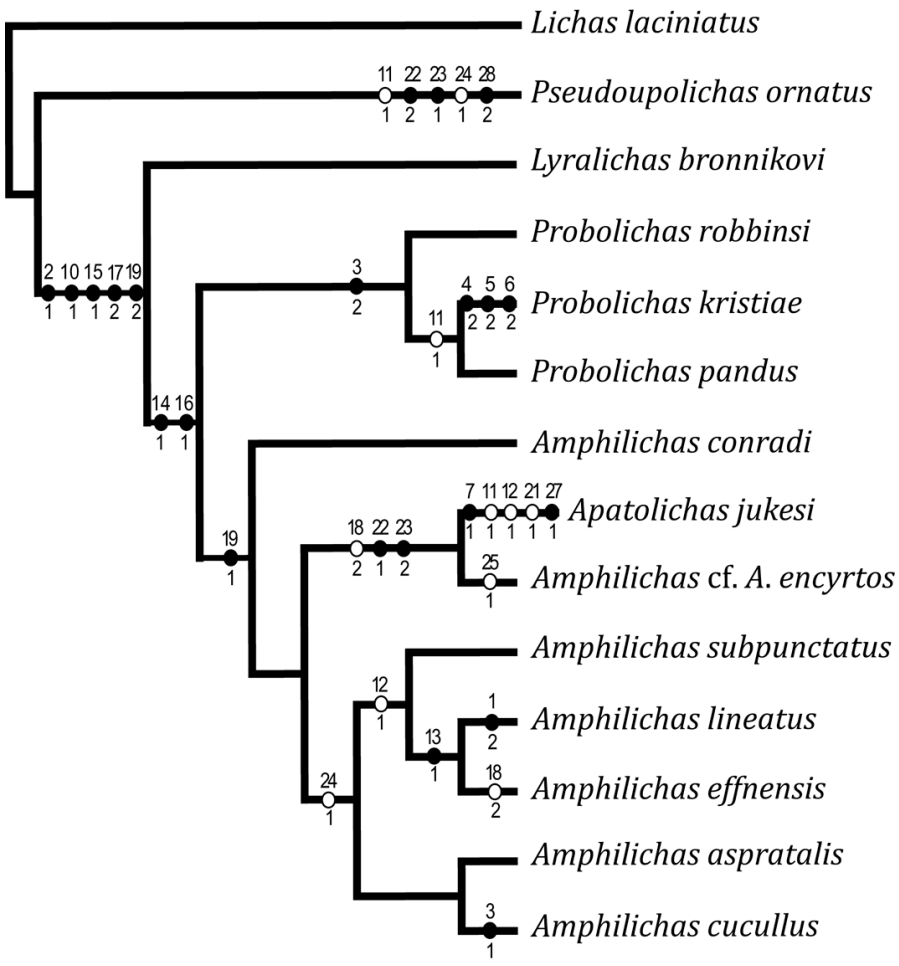
Lichas laciniatus
11 22 23 24 28
1 2 1 1 2
Pseudoupolichas ornatus
Lyralichas bronnikovi
Probolichas robbinsi
2 10 15 17 19
1 1 1 2 2
3
2
4 5 6
2 2 2
Probolichas kristiae
11
1
Probolichas pandus
14 16
1 1
Amphilichas conradi
7 11 12 21 27
1 1 1 1 1
Apatolichas jukesi
19
1
18 22 23
2 1 2
25
1
Amphilichas cf. A. encyrtos
Amphilichas subpunctatus
12
1
1
2
Amphilichas lineatus
13
1
18
2
Amphilichas effnensis
24
1
Amphilichas aspratalis
3
1
Amphilichas cucullus

FIGURE *6*—*Probolichas* Phleger, 1936. All from the Bromide Formation, Upper Ordovician, Oklahoma, except 1, 2 and 3, which are from the Prosser limestone, Upper Ordovician of Minnesota. *1-3*, *Probolichas robbinsi* (Ulrich, 1892, figs. 1a, 1b) holotype cranidium, dorsal, lateral, and anterior views, x3, USNM 041950. *4-6*, *Probolichas kristiae* n. sp. *4*, thoracopygon, dorsal view, x1, OU 11265. *5*, *6*, cranidium, lateral and dorsal views, x1.5, OU 11261.

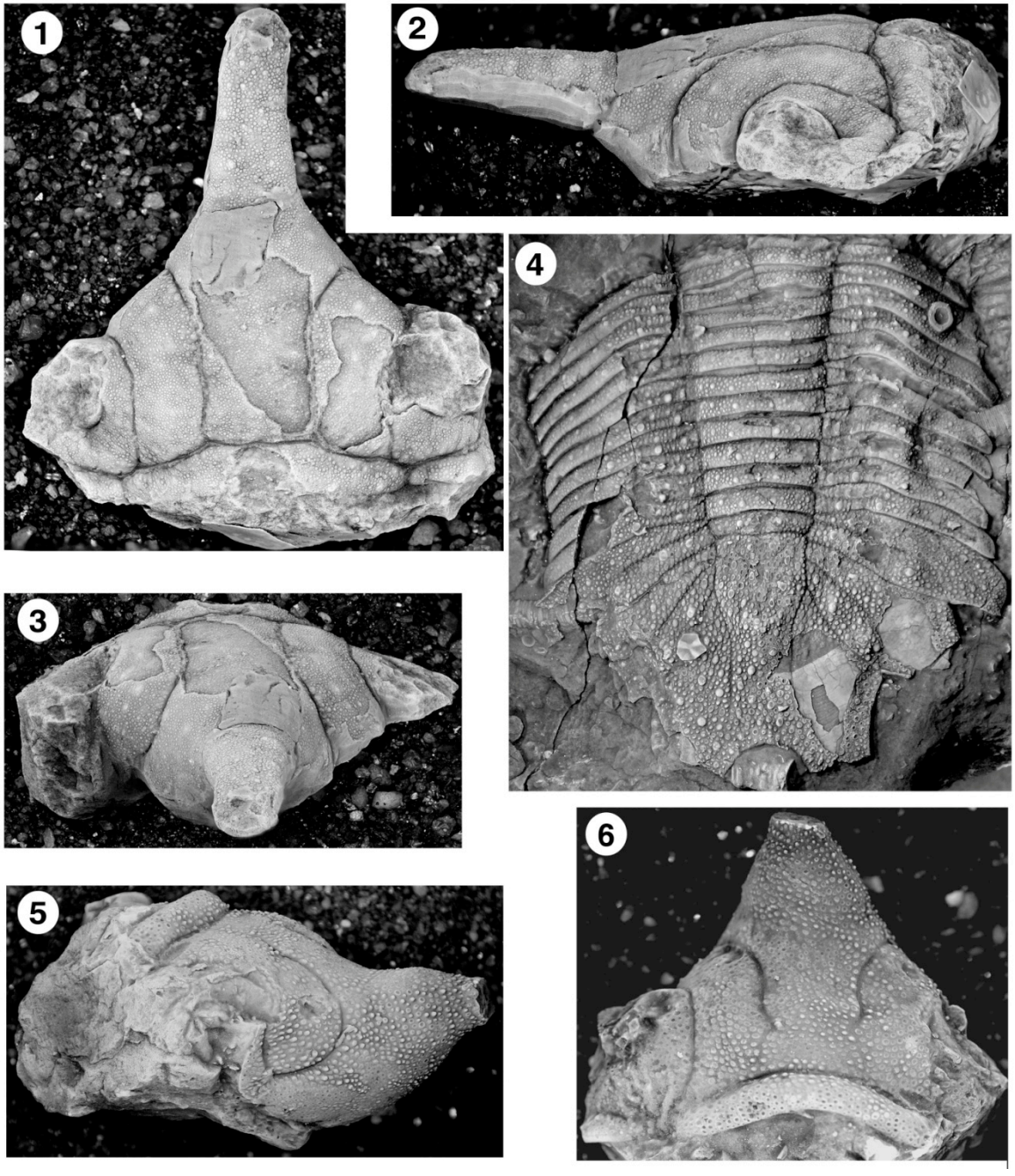
1
2
3
4
5
6

FIGURE *7*—Tetralichine trilobites. All from the Bromide Formation, Upper Ordovician of Oklahoma, except 1, which is from the Middle Ordovician (lower Maquoketa) of Iowa. *1*, *Amphilichas rhinoceros* (Slocom, 1913 pl. 15, figs. 5, 6) cranidium, dorsal view, x1.6, FMNH 11181. Only the base of the dorsal median lobe spine is visible on the cast. *2*, *3*, *Probolichas kristiae*, holotype, lateral view, x4, dorsal view, x3, OU 11260. *4*, *P. kristiae* (Shaw, 1974, pl. 12, fig. 17) pygidium, dorsal view, x1.3, OU 5203. *5*, *6*, *P. kristiae* proboscis, dorsal and lateral views, x2, OU 11262. *7*, *P. kristiae* (Shaw, 1974, pl.12 fig. 19) cranidium, dorsal view, x2.5, OU 8096. *8*, *P. kristiae* cranidium, dorsal view, x3, OU 11263.

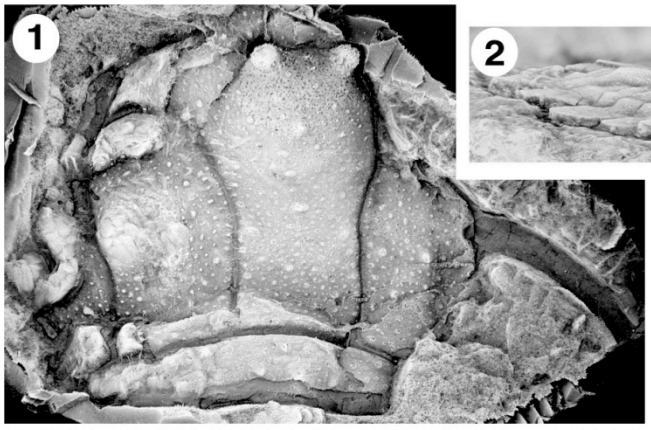
1


2

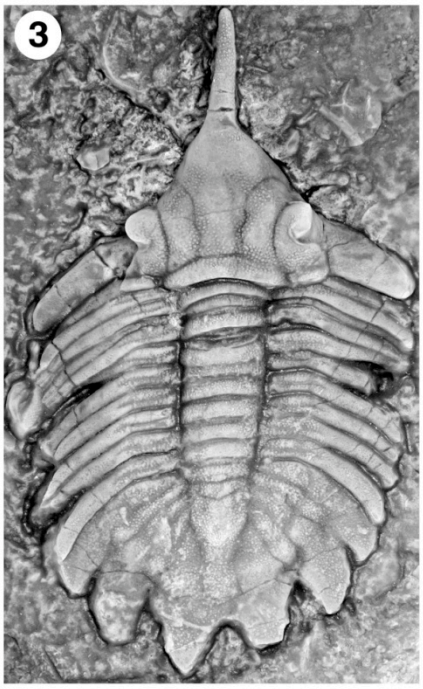
3


4

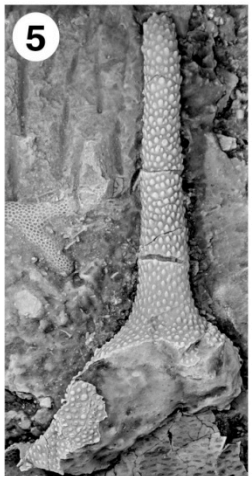
5


6

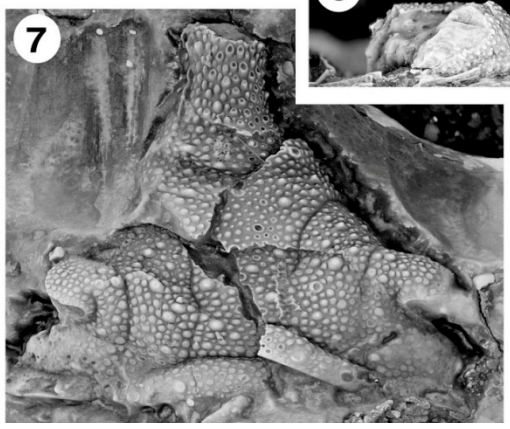
7

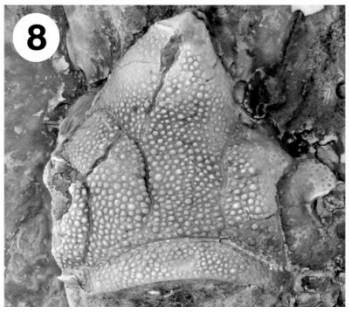
8

FIGURE *8*—Oklahoma tetralichines. 1-3 are from the Bromide Formation, 4-10 are from the Viola Springs Formation, both (Upper Ordovician) of Oklahoma. *1*. *Amphilichas* sp. thorax, lateral view, x1.5, OU 12482. *2*. *Probolichas kristiae* proboscis, dorsal view, x1.5, OU 12483. *3*. *P*. *kristiae* pygidium, dorsal view, x2, OU 11269. *4*, *Amphilichas* cf. *A*. *cucullus* hypostome, dorsal view, x3, OU 12146. *5*, *6*, *8*, *A*. cf. *A*. *cucullus* cranidium, dorsal, lateral, anterior views, x3, OU 12147. *7*, *9*, *10*, *A*. cf. *A*. *cucullus* cranidium, anterior, dorsal, lateral views, x4, OU 12149.


1


2

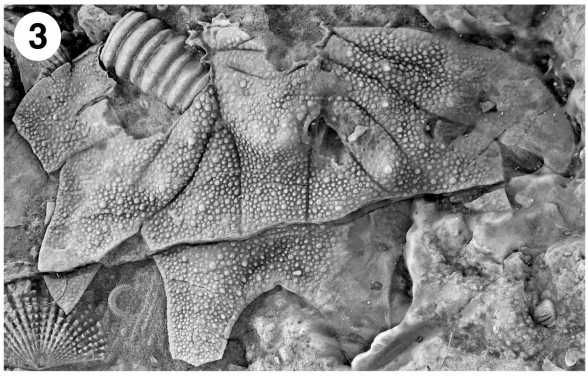
3


4

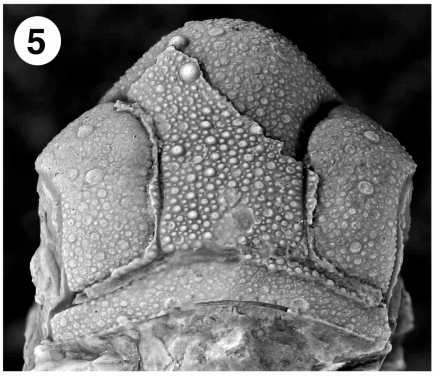
5

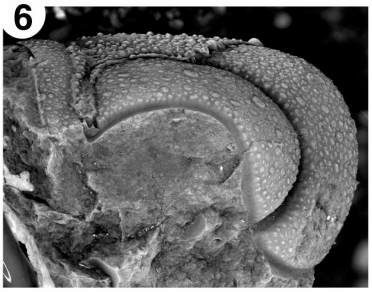
6


7

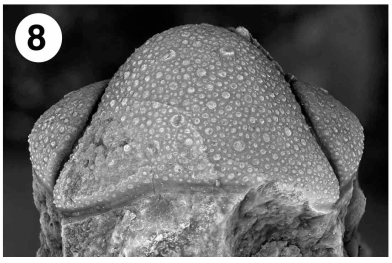
8


9


10

FIGURE *9*—Tetralichines trilobites. 1, 7-8, 10-12 from the Bromide Formation (Upper Ordovician) of Oklahoma, 2-4 are from the Boda Limestone Formation (Upper Ordovician) of Sweden, 5, 6, 9 are from the Middle Ordovician (Whiterockian) bioherm at Meiklejohn Peak, Nevada. *1*, *Probolichas kristiae* proboscis, dorsal view, x1.5, OU 12484. *2-4*, *Amphilichas lineatus* (Angelin, 1854, pl. 38, figs. 12, 12a), lectotype cranidium, lateral, anterior, dorsal views, x6, Ar 6040. *5*, *6*, *9*, *Amphilichas* cf. *A*. *jukesi* (Ross, 1972 pl. 18, figs.6-8), dorsal view x5, lateral, anterior views, x6, USNM 167232c. *7*, *8*, *11*, *Amphilichas subpunctatus*, dorsal, lateral, anterior views, x2, OU 12485. *10*, *Probolichas kristiae* (Shaw, 1974, pl. 12, fig. 2) hypostome, dorsal view, x1.5, OU 8091 *12*, *A*. *subpunctatus* (Shaw, 1974, pl. 12, fig. 14) pygidium, dorsal view, x2, OU 5201.

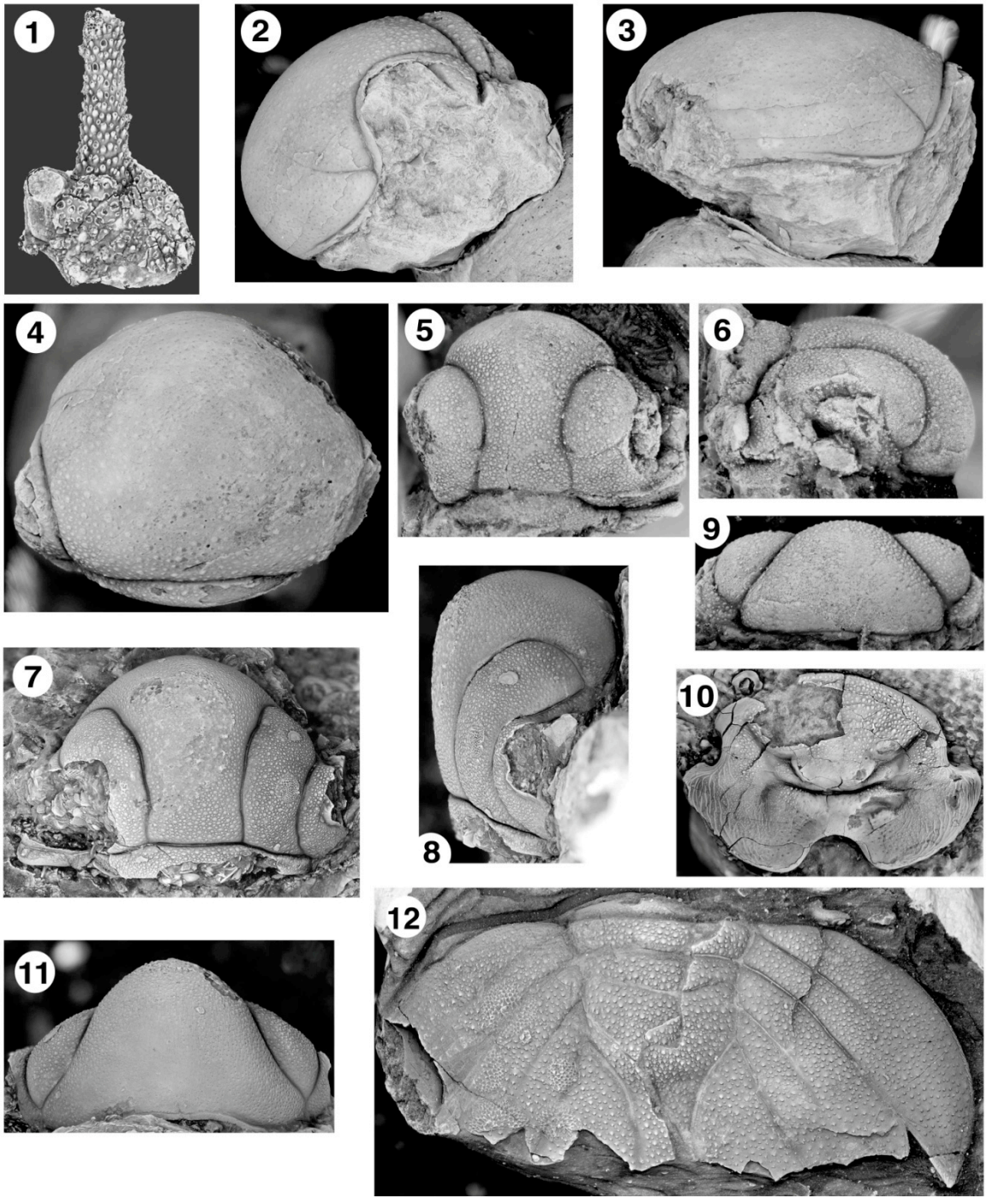
1
2
3
4
5
6
9
8
7
10
12
11

FIGURE *10—Amphilichas* Raymond, 1905. 1-4, 7-8 are from the Bromide Formation (Upper Ordovician) of Oklahoma, 5-6, 9-10 are from the Effna Formation (Upper Ordovician) of Virginia. *1-3*, *Amphilichas subpunctatus* (Esker, 1964, pl. 3 figs. 1-4) holotype cranidium, dorsal, anterior, lateral views, x2, OU 5203. *4*, *A*. *subpunctatus* pygidium, dorsal view, x2, OU 12486. *5*, *Amphilichas effnensis*, cranidium, dorsal view, x4, OU 12487. *6*. *A*. *effnensis* cranidium, dorsal view, x3, OU 12488. *7*, *A*. *subpunctatus* hypostome, dorsal view, x3, OU 12489. *8*, *A*. *subpunctatus* cranidium, dorsal view, x2, OU 12490. *9*, *Amphilichas* sp. 1 hypostome, dorsal view, x2.5, OU 12491. *10*, *A*. *effnensis* pygidium, dorsal view, x2.9, OU 12492.

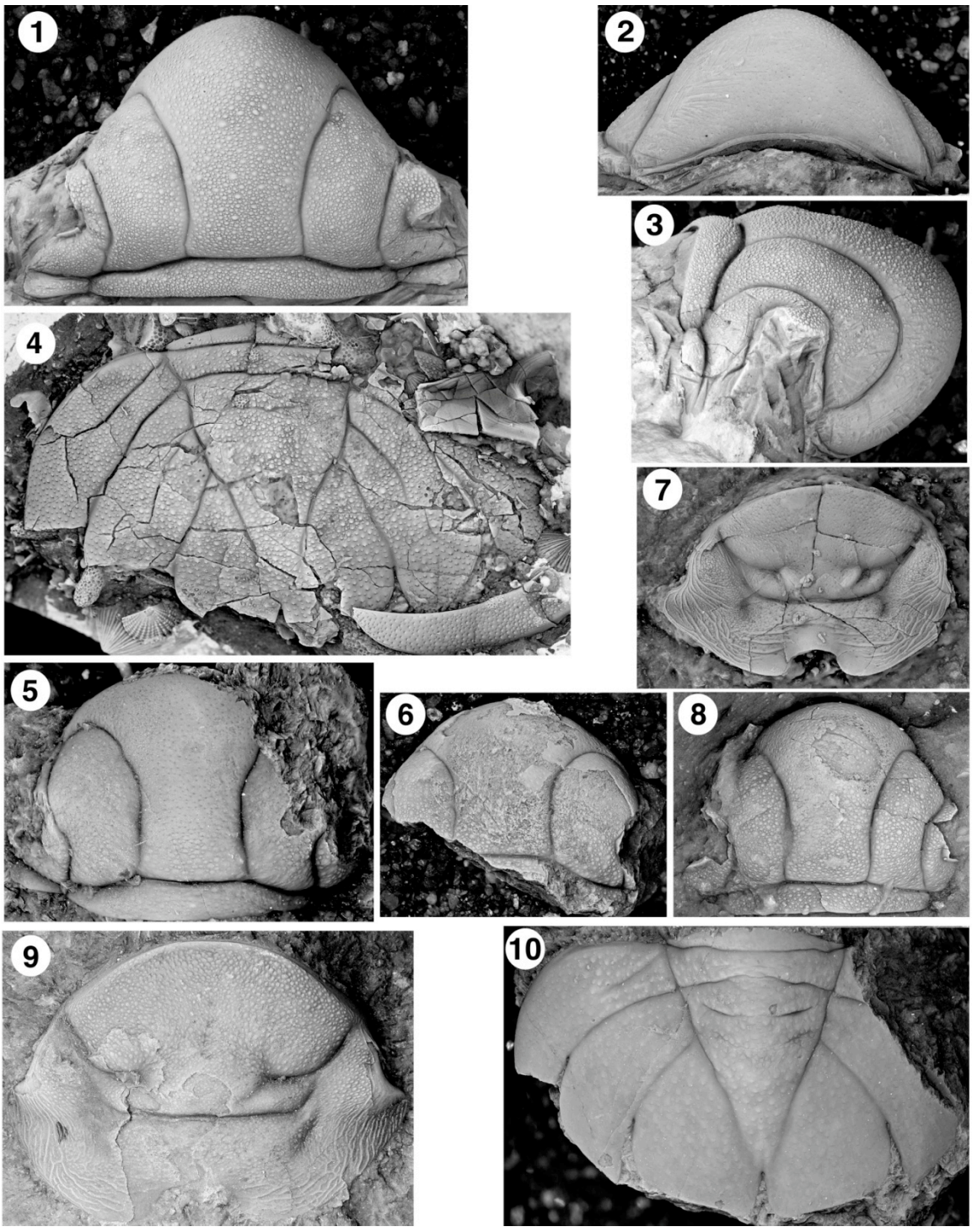
1
2
3
4
7
5
6
8
9
10

FIGURE *11—Amphilichas effnensis*. All are from the Effna Formation (Upper Ordovician) of Virginia. *1-3*, *A. effnensis*, holotype cranidium, dorsal, lateral, anterior views, x2.5, OU 12493. *4-6*, *A. effnensis*, cranidium, dorsal, lateral, anterior views, x4, OU 12494.

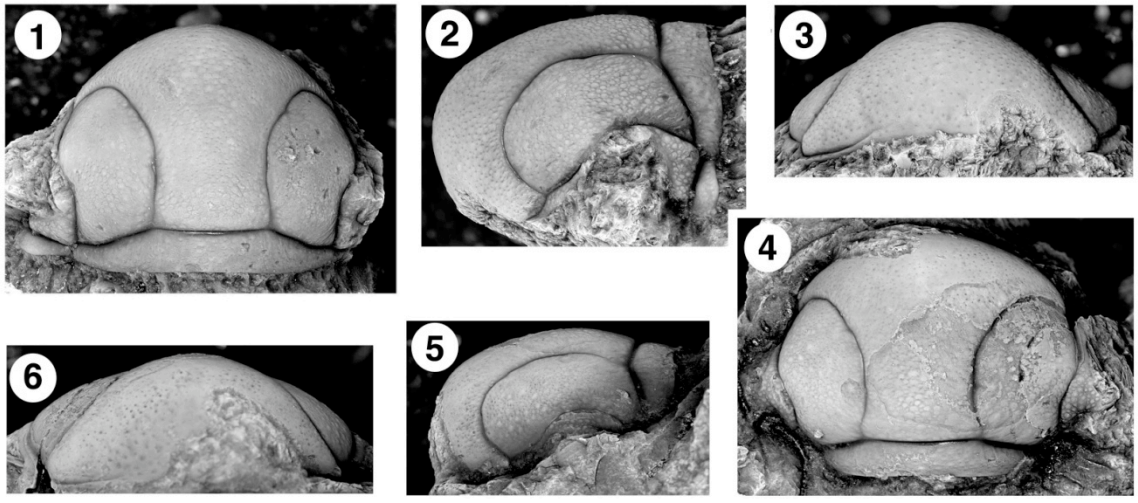
1
2
3
4
5
6

APPENDIX *1*—Character matrix for the cladistics analysis. A question mark (?) indicates missing data.

Taxon	1	2	3	4	5	6	7	8	9	10	11	12	13	14	15	16	17	18	19	20	21	22	23	24	25	26	27	28
L. laciniatus	0	0	0	?	?	?	0	0	0	0	0	0	0	0	0	0	0	0	0	0	0	0	0	0	0	0	0	0
P. kristiae	1	1	2	2	2	2	2	1	1	1	1	0	?	1	1	1	1	1	2	1	0	0	0	2	1	0	3	1
P. pandus	1	1	2	1	1	1	2	1	1	1	1	0	?	?	?	?	?	?	?	?	?	?	?	?	?	?	?	?
P. robbinsi	1	1	2	1	1	1	2	1	1	1	0	0	?	?	?	?	?	?	?	?	?	?	?	?	?	?	?	?
A. lineatus	2	1	0	?	?	?	2	1	1	1	0	1	1	1	1	1	2	1	1	?	?	0	0	?	0	?	?	0
A. subpunctatus	1	1	0	?	?	?	2	1	1	1	0	1	0	1	1	1	2	1	1	1	0	0	0	1	0	1	2	0
A. aspratilis	1	1	0	?	?	?	2	1	1	1	0	0	0	1	1	1	2	1	1	1	0	0	0	1	0	1	2	0
A. conradi	0	1	0	?	?	?	2	1	1	1	0	0	0	1	1	1	2	1	1	1	0	0	0	0	0	1	2	0
A. cucullus	1	1	1	?	?	?	2	1	1	1	0	0	0	1	1	1	2	1	1	1	0	0	0	1	0	1	2	0
A. jukesi	1	1	0	?	?	?	1	1	1	1	1	1	0	1	1	1	2	2	1	1	1	1	2	0	0	?	1	0
L. bronnikovi	0	1	0	?	?	?	2	?	1	1	0	0	0	0	0	0	2	3	2	0	0	0	0	0	0	1	2	0
P. ornatus	1	0	0	?	?	?	2	0	1	0	1	0	0	0	0	0	0	0	0	1	0	2	1	1	0	0	4	2
A. cf. *encyrtos*	1	1	0	?	?	?	2	1	1	1	0	0	?	?	1	1	2	2	1	1	0	1	2	0	1	1	2	0
A. effnensis	1	1	0	?	?	?	2	1	1	1	0	1	1	?	?	?	?	2	1	1	1	0	?	1	0	?	2	0

CHAPTER 3: A SYSTEMATIC REVISION OF THE UPPER ORDOVICIAN TRILOBITE GENUS BUMASTOIDES (TRILOBITA: ILLENIDAE) WITH NEW SPECIES FROM OKLAHOMA, VIRGINIA, AND MISSOURI

Abstract

Species of the Ordovician illaenid trilobite genus *Bumastoides* Whittington, 1954, have been notoriously difficult to classify because of their high degree of exoskeletal effacement. New species from Oklahoma (*B*. *graffhami*, sp. nov), Virginia (*B*. *moundensis* sp. nov), and Missouri (*B*. *kimmswickensis* sp. nov) provide more data for a phylogenetic analysis on the genus. Continuous characters were treated as such, and analyzed with finite mixture coding in two separate parsimony analyses. A strict consensus tree of eight equally most parsimonious trees, and a weighted best-fit tree both indicate that many species previously assigned to *Bumastoides* should be removed from the genus. Both methods yielded a tree with similar topology, supporting the removal of three *Stenopareia*-like species from *Bumastoides*. Based on the optimized character distribution, the supporting synapomorphies for *Bumastoides* are: weak to effaced cranidial axial furrow and lack of glabellar differentiation even by change in convexity, dicuspid inner margin of pygidial doublure, subtrapezoidal pygidium, undifferentiated or minimally expressed pygidial axis, long pygidial doublure, and maximum pygidial width at half-length. The pygidial outline shape, length of pygidial doublure, and degree of independent convexity on the cranidium are characters that may be useful in separating species of *Stenopareia* and *Bumastoides*.

Introduction

The Ordovician (Darriwilian-Hirnantian) illaenid trilobite genus *Bumastoides* was originally erected by Whittington (1954) as a subgenus of *Bumastus* Murchison, 1839. The former has, among other characters, fainter axial furrows, a distinctive lunette, proportionally smaller palpebral lobes, and 8-10 segments in the thorax. Ludvigsen & Chatterton (1980) elevated *Bumastoides* to full generic status, and placed the genus in the Illaeninae. Later workers (e.g., Whittington 1997a) cited thoracic morphology to reiterate that *Bumastoides* is an illaenid, rather than a styginid (as is *Bumastus*). Although the taxonomic position of *Bumastoides* itself is currently well constrained, recognizing taxonomic divisions within the genus has been problematic. The extremely high level of exoskeletal effacement makes discrete differences difficult to identify, resulting in species diagnoses that are not truly diagnostic. Shape differences that describe variation along a curve for instance, are often relative, and not easily binned into discrete character states. Chatterton & Ludvigsen (1976, p. 35) considered imperceptible axial furrows, prominent lunettes, a steeply curved anterior cephalic profile, absence of a median pustule, and an ovate to rounded subpentagonal pygidium to be diagnostic characters of *Bumastoides lenzi*. While undoubtedly characteristic of *B. lenzi*, the same combination of characters can also be used to describe other *Bumastoides* species. The vague diagnoses of illanid genera closely related to *Bumastoides* (e.g., *Stenopareia* Holm, 1886; most recent diagnosis by Curtis & Lane 1997, p. 18) further exacerbates the problem of distinguishing between the taxa. Certain species could be placed in either *Bumastoides* or *Stenopareia* according to current diagnoses. These issues, combined with new species data from the Sandbian-Katian interval, demonstrate the need for a systematic revision of

Bumastoides. Ideally, any revision of the genus should effectively deal with the difficulties inherent in diagnosing species, and that is the approach taken here.

A cladistic analysis allows the relationships of ingroup *Bumastoides* to be explored, and character optimization provides discrete apomorphies with which to construct new diagnoses. Finite mixture coding (FMC) (Strait et al. 1996) allows for subtle differences in quantitative characteristics to be binned into discrete states, and is contrasted with a method that treats continuous characters as such (Goloboff et al. 2006). The optimized character distribution is synthesized with descriptions and diagnoses of previously documented *Bumastoides* species (including types) and new material from the Upper Ordovician (Sandbian-Katian) of Oklahoma, Virginia, and Missouri.

Geologic setting of new material

Oklahoma

The Bromide Formation (Ulrich 1911) is an Upper Ordovician (Sandbian; Turinian) carbonate-dominated succession that is the youngest unit of the Simpson Group (Cooper 1956; Harris 1957). It is exposed throughout the Arbuckle Mountains and Criner Hills region of south-central Oklahoma (see Fay et al. 1982, fig. 77; Carlucci et al. 2010, fig. 1), and was deposited along a depth gradient from the Arbuckle Platform up-ramp, to the subsiding Southern Oklahoma aulacogen down-ramp (Longman 1982a; 1982b) (Fig. 1A). Siliclastic material is common in the stratigraphically lower Mountain Lake Member (Cooper 1956), often forming meter-scale cyclic packages with bryozoan and pelmatozoan rich wackestone, packstone, and grainstone. Cycle tops are commonly mineralized, starved surfaces, often associated with bryozoan rudstone horizons. Up-ramp, the younger Pooleville Member is characterized by massive to thick-bedded

carbonate mudstone, wackestone, and grainstone, with reworked tempestites commonplace. A thin cap of peritidal carbonate is referred to as the Corbin Ranch Submember (Harris 1957; Amsden & Sweet 1983). Down-ramp, the Pooleville is composed of fine-grained, thickly bedded, laminated carbonate mudstone, and resembles the overlying Viola Formation. Shaw (1974) and Carlucci et al. (2010) present discussions of the trilobite fauna of the Bromide.

Three localities in the Bromide Formation yielded material of *Bumastoides graffhami* sp. nov. Tyson's Quarry (TQ) is a private quarry approximately 8 km southwest of Ardmore, (Fig. 1A) in the Criner Hills region of Carter County (Carlucci et al. 2010). The type specimen of *B. graffhami* was collected from the upper Pooleville Member, in an interval of rudstone pavements (interpreted here as tempesites) that top blue massive carbonate wackestone (see Carlucci et al. 2010, fig. 2 for a measured section and approximate collection levels). Shaw (1974) assigned this material to the nearby Rudd Quarry, but the original label specifies the "upper" quarry (TQ here, formerly the Dunn quarry). The Daube Ranch (DRa) (formerly the Johnston Ranch) locality (Fig. 1A) exposes the Bromide Formation along Spring Creek, below the dam forming the upper Humbolt Lake in Murray County. The *B. graffhami* material was collected 21.3m below the Viola contact, in a light tan, thinly bedded wackestone (with localized packstone) that alternates with fissile tan shale (see Fay et al. 1982, pg. 336 for a detailed measured section). The final locality is a roadcut along U.S. Highway 177 at its intersection with Goddard Youth Road (Fig. 1A), approximately 13 km south of the town of Sulphur, Murray County. The material of *B. graffhami* was collected at two collection levels (Fig. 2). The lower collection is from thinly interbedded marly shale and

wackestone. The shale layers thin very slightly upwards, and the percentage of bioclasts increases upwards in the wackestone. The upper collection is from an interbedded laminated carbonate mudstone, and brachiopod-rich fossiliferous wackestone. Rudstone pavements often cap the wackestone beds, and are likely coeval with the pavements at TQ from which the type specimen was collected.

Sclerites assigned to *B*. cf. *B. milleri* (Billings, 1859) were collected from the Viola Springs Formation (Viola Group; Upper Ordovician, Katian) at the Highway 99 section, near Fittstown, south-central Oklahoma (Amati & Westrop, 2004, fig. 1; Amati & Westrop 2006, figs 3 and 7). They occur in a bryozoan grainstone-to rudstone facies (Amati & Westrop 2006, p. 521) between 18 — 34 m above the base of the Viola Springs Formation.

Virginia

All material of *Bumastoides moundensis* sp. nov is from either the Effna Formation or the Botetourt limestone (Cooper & Cooper 1946) in the Valley and Ridge Province of Virginia (Read 1982, fig. 1). The Effna Formation was deposited in downslope carbonate mud-mound buildups that are composed of a series of biohermal pods flanked by grainstone (see Read 1998, fig. 4). These buildups form primarily by marine cementation and baffling of carbonate fines by bryozoans and pelmatazoans, with frame building organisms of little importance (Read 1982; King 1986). The first (often-pod surrounding) unit of the Effna is a biostromal grainstone, which formed as debris was shed from the mudstone pods (Sabol 1958; Ruppel and Walker 1977; Read 1982). The other unit is the biohermal mudstone of the buildups, which is the primary constituent of the pod facies. Both units are highly fossiliferous; Carlucci et al. (2010) provided a list of

trilobite genera commonly found in the Effna. The Botetourt limestone is a dark, shaly, nodular wackestone, packstone and grainstone that flanks, interfingers with, and overlies the Effna. The Botetourt is considered to be transitional between the Effna and the basinal Liberty Hall facies (Read 1982).

Two localities provided new material of *Bumastoides moundensis*. Porterfield Quarry (PQ) is an abandoned facility located 7 km southwest of Saltville, in Smyth County. The quarry is exposed approximately 1 km down an unlabeled service road off VA 610 (see Carlucci et al. 2010 fig. 3-2 for a locality map). The PQ collections (Carlucci et al. 2010, fig. 3-1) are from boulders of biohermal mudstone left behind when the quarry ceased operation. The mudstone is massive and very fine grained with bryozoans locally forming boundstone. Additional *B*. *moundensis* material was collected from a roadcut along Interstate 77 near the town of Bland, in Bland County. The roadcut is less than 1 km north of the Big Walker Mountain Tunnel exit. The material was collected from 1 meter above the Effna/Botetourt contact in a black, nodular wackestone. See Read (1982, fig. 7A) for a facies mosaic, 'nodular, shaly skeletal limestone' is here referred to as the Botetourt.

Missouri and Illinois

Archival material from Missouri that was described by Bradley (1930) and assigned here to *B*. *billingsi* (Raymond & Narraway, 1908) was collected from the Upper Ordovician (Katian) "Kimmswick Limestone" (now Dunleith Formation of the Kimmswick Subgroup; Templeton & Willman 1963) along the Mississippi River at Batchtown, Illinois, and Glen Park, Missouri (Bradley 1925). New material of *B. kimmswickensis* sp. nov. is from a previously undocumented roadcut along Missouri State

Highway M, 0.5 km south of Antonia and about 6 km west of its intersection with Interstate 55 at Barnhart (Fig. 1B). It occurs at a single horizon 90 cm above the base of the Dunleith Formation, within a 44 cm thick interval of gray shale with bioclastic packstone lenses and lime mudstone nodules; the House Springs Bentonite (Kolata et al. 1998, figs. 5, 8) forms the basal 8 cm of this interval.

Phylogenetic analysis

Taxonomic notes

The analysis used 16 ingroup species and one outgroup species, of which 15 have been classified previously as *Bumastoides*, and two as *Stenopareia* Holm, 1886. *Stenopareia* is an illaenid genus that is considered to be closely related to *Bumastoides* because it also exhibits a high degree of exoskeletal effacement, has prominent lunettes, and has an inflated, highly convex cranidium with the eyes positioned just forward of the posterior border. The type species of *Stenopareia*, *S. linnarssoni* Holm, 1882 was chosen as the outgroup taxon because its morphology has been well documented, and it occupies a relatively basal position within *Stenopareia*. The pygidia of species of *Stenopareia* are clearly distinct from those of *Bumastoides* (subsemicircular, with faint expression of the axis), and they possess more pronounced axial furrows over all three tagmata.

Whiteley et al. (2002) treated *Bumastus globosus* Billings, 1859 as a species of *Bumastoides*, though it has never formally been placed in the genus. Based on evaluation of the lectotype (GSC1090b; Shaw 1968, pl. 17, figs. 20-21, 22, 24) and hypotypes, this species does not belong to *Bumastoides*, and was not used in our analysis. The deeply incised axial furrows (Shaw 1968, pl. 17, fig. 15), wide cephalic axis, and highly convex thoracic axis are unlike any species of *Bumastoides*, and Westrop & Ludvigsen (1983)

placed it in *Stenopareia*. All species formally named as *Bumastoides* were considered for inclusion, but some were omitted from the analysis because the known material is too incomplete to code properly (e.g., *B. scoticus*, Tripp, 1965; *B. fornax*, Tripp, 1980; *B. tricuspidatus*, Edgecombe et al. 2006). *B. rivilus* was the only Scottish species included. The types of other Scottish species placed in *Bumastoides* (*B. fornax* Tripp, 1980, pl. 1, figs. 6-10; *B. scoticus* Tripp, 1965) were borrowed by us, but both were far too damaged and incomplete to code for the parsimony analysis. The type material for *B. fornax* is so badly damaged we would hesitate to identify it to the genus level. *Bumastus lioderma* Raymond, 1925 may belong to *Bumastoides*, but is only known from a partial cranidium, so it cannot be adequately assessed phylogenetically.

Characters and coding

The dataset includes 20 unordered characters (10 binary, 10 multistate) with a total of 52 states (see Appendix 1). These characters code morphological features of the cranidium (7 characters), thorax (2 characters), and pygidium (11 characters). All characters were binned into their states based on clearly discrete differences or statistically defined bins (see Finite Mixture Coding below). Characters that could not reliably be placed into discrete categories, parsimony uninformative characters, or those that dramatically covary with each other were removed in the initial analysis. A second analysis (20 discrete, 6 measured) retained continuous characters (Appendix 2) that could not be discretized (Goloboff et al. 2006). There is some small degree of covariation in the pygidial characters. For example, the location of maximum (tr) width has some bearing on the overall pygidial shape, but is only one component of a more complex feature. In all such instances the characters code differently from each other. Characters with

inapplicable states for some species were coded using reductive coding (Strong & Lipscomb 1999) (e.g., species with a completely effaced axial furrow in character 1, were not coded again in character 5); inapplicable states were coded as '?'. In *Bumastoides*, sculptural characters of the cranidium and pygidium are often decoupled (e.g., terrace lines on the cranidium are not always associated with lines on the pygdium, and vice versa), so similar sculptural characters (e.g., terrace lines) are coded independently on the two tagmata. Finally, some characters were omitted simply because the variation in preservation made it impossible to detect discrete states where they may have existed (e.g., the presence or absence of a pygidial articulating facet border, or the number of terrace lines on the thoracic articulating facets).

The simple morphology and furrow effacement in *Bumastoides* makes the use of continuous measured characters an attractive option. Some measured character data were taken from literature sources (*Bumastoides tenuirugosus*, Troedsson, 1928; Westrop & Ludvigsen 1983; *Bumastoides lenzi*, Chatterton & Ludvigsen, 1976; *Bumastoides solangeae*, Hunda et al., 2003; *Stenopareia linnarssoni*, Holm, 1882; Warburg 1925; *Stenopareia grandis*, Billings, 1859; Chatterton & Ludvigsen 2004). Literature illustrations were only used if the orientation of the specimens was comparable to those used in our figures (Figs. 6-26). The majority of measured data are taken from the material illustrated here and non-illustrated material of the same species in our collections. The proportions we used are those that can be confidently measured in a majority of species included in the analysis. To avoid large amounts of missing data, some measured features used in the systematic descriptions were not used in the analysis

(e.g., proportion of eye length in lateral view). Material that has obviously been flattened (e.g., Fig. 19E) was not measured.

Finite Mixture Coding. We follow the approach developed in Strait et al. (1996), automated by the program FMC Box (Sheets 2003). This method identifies a number of possible normal distribution models that best describe the character data, and then uses the Aikake Information Criterion (AIC, Akaike 1974) to assess the goodness of fit for each model. The model with the lowest AIC score and the highest weight (probability of that model being correct compared to the others) is the optimal distribution for binning character states. Characters that show a high relative probability of a one-model distribution were removed from the analysis; others were binned into their respective distribution by a group probability assignment based on the magnitude of the normal function at the specimen value. Finite Mixture Coding (FMC) is a particularly good approach for binning measured character states here because it potentially allows for the isolation of discrete character data from a genus which otherwise has very few ingroup apomorphies. In six of the seven measured ratio characters, a one-distribution model was clearly best supported (Figs. 3A-F have AIC values of 0, and relative probability of a one distribution model being correct of >99.7%). These characters were removed from the first analysis because their values cannot confidently be assigned to discrete bins: cranidial length (sag.) in proportion to width (tr.) across palpebral lobes (Fig. 3A), maximum length (sag.) of lunettes in proportion to cranidial length (exsag.) in dorsal view (Fig. 3B), maximum width (tr.) of one lunette in proportion to width (tr.) across palpebral lobes (Fig. 3C), percentage of total exoskeletal length occupied by the cranidium (in lateral view) (Fig. 3D), percentage of total exoskeletal length occupied by

the pygidium (in lateral view) (Fig. 3E), width of one palpebral lobe as a percentage of cranidial width across palpebral lobes (Fig. 3F). The maximum length/width ratio of the pygidium best fits a four-distribution model (Fig. 3G) and it was retained for the first phylogenetic analysis. The inability of FMC to bin measured characters into more than one discrete state highlights the difficulty of diagnosing new species of *Bumastoides* with concrete, unequivocal evidence. We suggest that vague references to character proportions be omitted from diagnoses of new species (e.g., lunettes proportionally wide, long, etc.), and instead only be used for pairwise comparisons (e.g, *B*. *holei* has proportionally wider lunettes than *B*. *moundensis*). These data also show that measured characters with clear gaps in their distribution still best fit a one-bin model, suggesting that some workers may be overestimating the utility of measured characters (unless they are treated as such).

Continuous characters coded as such. Goloboff et al. (2006) suggested analyzing continuous characters as such, rather than applying methods that make the data discrete. The characters that were removed based on the results of the FMC analysis were retained in a second analysis that treated them as additive characters with terminal ranges from -1/+1 standard error (SE). Following Goloboff et al. (2006), scaling problems associated with increased branch-lengths were controlled by using implied weights (Goloboff 1993) with a concavity constant (k) of three. The implied weight ratio is less than the ratio implied by the difference of scale, and is one method of balancing the contributions of the characters, making them more even.

Measured characters are identified with an asterix (*) in the list below.

Cranidium. 1. Axial furrow: (0) well-defined and with glabella expressed by independent convexity (e.g., *B*. *aplatus*, Fig. 26F); (1) weak or effaced and glabella not differentiated even by change in convexity (e.g., *B*. *graffhami*, Fig. 19B).

2. Path of posterior branch of facial suture: (0) nearly straight backwards to posterior margin (no posterolateral projection) (e.g., *B*. *holei*, Fig. 14E); (1) backwards and outwards, forming a small subtriangular posterolateral projection (e.g., *B*. *kimmswickensis*, Fig. 23E).

3. Median tubercle near posterior margin: (0) absent (e.g., *B*. *moundensis*, Fig. 20C); (1) present-circular (e.g., *B*. *bellevillensis*, Fig. 10A); (2) present-elliptical (e.g., *B*. *graffhami*, Fig. 19E).

4. Predominant shape of lunette: (0) crescentic; deeply incised adaxially, shallowing dramatically abaxially (e.g., *B*. *moundensis*, Fig. 21B); (1) elliptical; relatively consistent impression (e.g., *B*. *holei*, Fig. 13C); (2) lunettes absent (e.g., *B*. *gardensis*, Fig. 26G).

5. Path of the axial furrow: (0) straight (e.g., *S*. *grandis*, Chatteron & Ludvigsen 2004, pl. 2, fig. 10); (1) converging inwards (e.g., *B*. *bellevillensis*, Fig. 10A).

6. Pitting on internal mould: (0) absent (e.g., *B*. *aplatus*, Fig. 26C); (1) present and widely spaced (e.g., *B*. *graffhami*, Fig. 19C); (2) present; densely distributed (e.g., *B*. *moundensis*, Fig. 21A).

7. Cranidial terrace lines: (0) absent (e.g., *S*. *linnarssoni*, Warburg 1925, pl. 2, fig. 17); (1) only present anteriorly and ventrally (e.g., *B*. *graffhami*, Fig. 19B); (2) present on most of cranidial exoskeletal surface (e.g., *B*. *beckeri*, Fig. 11A).

Thorax. 8. Number of thoracic segments: (0) 9 (e.g., *B*. *milleri*, Fig. 7H); (1) 8 (e.g., *B*. *bellevillensis,* Fig. 10D.); (2) 10 (e.g., *B*. *porrectus*, Fig. 16E).

9. Dorsal extent of the articulating facet: (0) below the axial furrow (e.g., *B. porrectus*, Fig. 15D); (1) to the axial furrow (e.g., *B. graffhami*, Fig. 18B).

Pygidium. 10. Number of cusps on dorsal inner margin of doublure: (0) one (e.g., *S. linnarssoni*, Jaanusson 1954, fig. 10F); (1) none (e.g., *B. rivilus*, Fig. 26A); (2) two (e.g., *B. kimmswickensis*, Fig. 22H).

11. Large paired pygidial muscle scars on exfoliated material: (0) absent (e.g., *B. tenuirugosus*, Fig. 17A); (1) present (e.g., *B. billingsi*, Fig. 8B).

12. Shape in outline: (0) semicircular (e.g., *B. rivilus*, Fig. 26A); (1) subtrapezoidal to rounded subtrapezoidal (e.g., *B. porrectus*, Fig. 15G); (2) elliptical (e.g., *B. gardensis*, Fig. 26H).

13. Median depression on dorsal surface (ventral ridge) of doublure inner margin: (0) absent (e.g., *Bumastoides solangeae*, Hunda et al. 2003, pl. 1 fig. 2); (1) complete (e.g., *B. kimmswickensis*, Fig. 23H); (2) effaced posteriorly (e.g., *B. bellevillensis*, Fig. 10E).

14. Concentric terrace lines on dorsal exoskeleton: (0) absent (e.g., *B. kimmswickensis*, Fig. 22D); (1) present (e.g., *B. holei*, Fig. 14D)

15. Undulating terrace lines directed inward from lateral margins on dorsal exoskeleton: (0) present (e.g., *B. graffhami*, Fig. 18C); (1) absent (e.g., *B. porrectus*, Fig. 16D).

16. *Ratio of max pygidial length (sag.) to max pygidial width (tr.): (0) (e.g., *B. gardensis*, Fig. 26H); (1) (e.g., *B. graffhami*, Fig. 18F); (2) (e.g., *B. porrectus*, Fig. 15A); (3) (e.g., *B. moundensis*, Fig. 20F).

17. Expression of axial furrow: (0) minor lateral notches that flank medial anterior margin (e.g., *B. aplatus*, Fig. 26D); (1) present; outline a convex and well-defined axis (e.g., *B. gardensis*, Fig. 26H); (2) completely effaced (e.g., *B. beckeri*, Fig. 11F).

18. Location of pygidial maximum width (tr.): (0) at or near the anterior end (e.g., *B*. *rivilus*, Fig. 26A); (1) at half-length (sag.) (e.g., *B*. *kimmswickensis*, Fig. 22D).

19. Length (sag.) of doublure: (0) short; approximately 30% of pygidial length (e.g., *B*. *rivilus*, Fig. 26A) (1) long; approximately 60% of pygidial length (e.g., *B*. *billingsi*, Fig. 9E).

20. Pitting on pygidial dorsal exoskeleton: (0) present (e.g., *B*. *gardensis*, Fig. 26H); (1) absent (e.g., *B*. *porrectus*, Fig. 16B).

Results

Parsimony analysis

The data matrix was constructed in MacClade 4.08 OS X (Maddison & Maddison 2005), and parsimony and related analyses were conducted in PAUP* version 4.0b10 (Swofford 2002), and checked in TNT (Goloboff et al. 2008; implicit enumeration). A branch and bound search algorithm was used with the following settings: the initial upper bound was computed heuristically, addition sequence was furthest, zero length branches were not collapsed, topological constraints were not enforced, and trees were treated as unrooted. All characters were unordered, weighted equally, and parsimony informative. PAUP* retained eight equally most parsimonious trees (MPTs) with a tree length of 56 steps, a consistency index (CI) of 0.57, retention index (RI) of 0.69, and a rescaled consistency index (RC) of 0.40; the strict consensus tree is shown in Fig. 4, and one of the eight MPTs in Fig. 5A (chosen because it retains some relationships that are present in multiple MPTs, e.g., *Bumastoides holei*, and *B*. *billingsi* as sister taxa). Calculation of a tree length distribution of 10,000 equally sampled random trees (with the same settings as the parsimony analysis) resulted in a mean tree length of 91.5 steps, with no retained

trees approaching 56 steps. The probability of getting a tree of 56 steps at random is less than 0.0001. Symmetric resampling (33% probability) group support (see Fig. 4) and GC values (frequency differences, see Goloboff et al. 2005) were calculated by a 1,000 replicate implicit enumeration algorithm, with two clades (nodes 4 and 9) appearing in at least 50% of the replicates. Bremer support values (Bremer 1994) were calculated by continually keeping trees with length values of N + 1 in PAUP* (checked in TNT), where N = the tree length of the strict consensus tree. Three clades have Bremer support values (Bremer 1994) of higher than 1 (nodes 1, 4 and 9: see Fig. 4).

A second analysis (continuous characters as such) used the same search algorithm (implicit enumeration) and settings in TNT as the first, with the exception of the implied weights. One tree (Fig. 5B) with a best-fit value of 8.47 was retained. Symmetric resampling group support of greater than 50% is present on the equivalents of node 2 and 4 (Fig. 4). *Bumastoides milleri* and *B. graffhami* (node 9) still have relatively high support, as does an arrangement not found in the initial analysis (*B. beckeri* and *B. moundensis*). In general, the support values are higher on the more basal nodes in the second analysis (compare Fig. 4 to Fig. 5B), but much of the resolved portions of the *Bumastoides* clade have contradictory (i.e. negative) GC values. The second tree also has more homoplasy in the optimization of the discrete characters (CI of 0.53, RI: 0.62, RC: 0.33). The broad topology of the second tree is similar to the first, with high support (82/80 in the former, 61/60 in the latter) for the same *Bumastoides* clade that excludes *B. rivulus*, *B. aplatus*, and *B. gardensis*. These data indicate that changing the treatment of continuous characters has little effect on the most important question here: what taxa belong in *Bumastoides*? The second analysis retains some other arrangements not found

in the first (e.g., *B*. *holei* and *B*. *bellevillensis* as sister taxa), but this relationship is not well supported, and has little bearing on the overall goals of revision. We think it is best to use the FMC driven results (Fig.4) as the basis of the taxonomy because the strict consensus tree conservatively collapses much of the poorly supported in-group *Bumastoides*, and in general contains fewer assumptions than the second analysis.

The strict consensus tree (Fig. 4) is partially pectinate, and demonstrates a well-supported monophyletic group (*Bumastoides*) at node 4. *B*. *aplatus* Raymond, 1925, *B*. *rivilus* Ingham & Tripp, 1991, and *B*. *gardensis* Shaw, 1968 are excluded from *Bumastoides* because of the clade support and high number of apomorphies at node 4 (Fig. 5A). Nearly all of the pygidial characteristics shared by *Bumastoides* (characters 10, 12, 17, 18, 19) and one cranidial characteristic (character 1) exclude these three taxa, all of which generally share more features with *Stenopareia*. These three taxa (nodes 1-3 on Fig. 4) appear to render *Stenopareia* paraphyletic in the context of this analysis, but the species included here are inadequate to assess the monophyly of the genus as a whole (an option beyond the scope of this study). In the absence of an updated systematic revision of *Stenopareia*, we chose to provisionally regard these taxa as *Stenopareia* sensu lato. In this way, no new superfluous genera are formed within the Illaenidae, and the placement is consistent with the assessment of later authors who doubted the original assignment of *B*. *gardensis* and *B*. *aplatus* to *Bumastoides* (Chatterton & Ludvigsen 1976; Westrop & Ludvigsen 1983). Whittington (1954) also expressed concern about his placement of *B*. *aplatus* in *Bumastoides*, suggesting that the pygidial attributes of the species were not characteristic of the rest of the genus. Similarly, Shaw (1968) hesitantly placed *B*.

gardensis in *Bumastoides* because of its similarity with *B*. *aplatus*, and Ingham & Tripp (1991) referred to their new species as '*Bumastoides*? r*ivilus*'.

Character optimization

Figure 5A is a character state optimization of unambiguous state changes (those present at the same node under both the assumptions of ACCTRAN and DELTRAN optimization) on one of the eight MPTs. *Stenopareia grandis* is the most basal ingroup taxon. The rest of the ingroup is united at node 1 based on converging inward axial furrows (character 5, state 1) and the loss of one cusp on the pygidial doublure (character 10, state 1). At node 2, cranidial terrace lines are present only anteriorly and ventrally (character 7, state 1), and at node 3, pitting on the pygidial dorsal exoskeleton is lost (character 20, state 1). *Bumastoides* species are united at node 4 by their shared axial furrow impression (character 1, state 1), two cusps on the doublure (character 10, state 2), subtrapezoidal pygidial shape (character 12, state 1), lack of axis expression (character 17, state 2), half-length location of maximum pygidial width (character 18, state 1), and long length of doublure (character 19, state 1). The pygidial median depression (ventral ridge) is complete at node 5 (character 13, state 1). At node 6, the pitting on the cranidial internal mould changes to densely distributed (character 6, state 2), and at node 7 the median posterior tubercle is present (character 3, state 1), and the shape of the lunette is elliptical (character 4, state 1). The pitting on the cranidial internal mould changes from densely to loosely distributed at node 8 (character 6, state 1). *B*. *milleri* and *B*. *graffhami* are sister taxa at node 9, based on a predominantly crescentic lunette (character 4, state 0) and pygidial undulating terrace lines (character 15, state 0). *B*. *beckeri* and *B*.

kimmswickensis are sister taxa at node 10 based on terrace lines covering the entire cranidial exoskeleton (character 7, state 2).

Systematic palaeontology

Illustrated material was photographed at 1mm intervals with a Canon E05 5D camera equipped with a 65, 80, or 120 mm lens. Images were stacked using Helicon Focus 4.04 Pro Multiprocessor (Helicon Soft, Ltd). References to length are in the sagittal direction, and width in transverse, unless otherwise noted. Outline shapes (e.g., crescentic) refer to dorsal view, unless specified otherwise. For the standard cranidial dorsal view, the midpoint of the lunette is approximately opposite the top of the palpebral lobe. The palpebral lobe (or eye if preserved) was oriented horizontal for the standard lateral view. Diagnostic characters which do not reference a character from the cladistic analysis are autapomorphies of that species, and are separated from the rest of the characters with a semicolon. Systematic diagnoses are based primarily on unambiguous state changes in Figure 5A, although ambiguous states (e.g., number of thoracic segments) and autapomorphies are also used to create a complete (and unique) character assemblage for each species. The clade definitions (de Queiroz & Gauthier 1990; de Queiroz 2007) for *Bumastoides* are based on the strict consensus tree. We are using a Linnean classification with named ranks, so the clade definitions are not the basis of the formal taxonomy, but additional information that specifies the clades exact location on the consensus tree. Repository acronyms are as follows: OU, Sam Noble Oklahoma Museum of Natural History; NYSM, New York State Museum, Albany; GLAHM; Hunterian Museum and Art Gallery, Glasgow; MCZ, Museum of Comparative Zoology, Harvard University; CM, Carnegie Museum of Natural History, Pittsburgh; GSC,

Geological Survey of Canada, Ottawa; SUI, University of Iowa Paleontology Repository, Iowa City; UC, P, Field Museum of Natural History, Chicago.

Class **TRILOBITA** Walch, 1771

Order **CORYNEXOCHIDA** Kobayashi, 1935

Suborder **ILLAENINA** Jaanusson, 1959

Family **ILLAENIDAE** Hawle & Corda, 1847

Genus ***BUMASTOIDES*** Whittington, 1954

Type Species. *Illaneus milleri*, Billings, 1859 from the Trenton Group of Ontario, by original designation.

Definition. The clade *Bumastoides* is the common ancestor of *B*. *porrectus* and *B*. *solangea* and all of its descendants (Fig. 4, node 4). To underscore the importance of character 1, an apomorphy-based definition may also be useful: *Bumastoides* is the clade stemming from the first ancestor to possess an axial furrow that is weak or effaced and glabella not differentiated even by change in convexity from the rest of the cranidium.

Diagnosis. Cranidial axial furrow weak or effaced and glabella not differentiated even by change in convexity from the rest of the cranidium (character 1, state 1), dicuspid inner margin of pygidial doublure (character 10, state 2), pygidia subtrapezoidal or rounded subtrapezoidal (character 12, state 1), pygidial axis expression is undifferentiated or minimally expressed (character 17, states 0, 2), location of maximum pygidial width is at half-length (sag.) (character 18, state 1), pygidial doublure length (sag.) is long (character 19, state 1).

Remarks. Raymond (1916) and Troedsson (1928) recognized that Ordovician species referred to as *Bumastus* were a distinct group from Silurian bumastids, but did not

propose a new taxonomic group to describe them. In his work on a trilobite fauna from Baffin Island, Whittington (1954) erected *Bumastoides* as a subgenus of *Bumastus* based on the following differences: axial furrows are faint or absent, the lunette is distinctive, the palpebral lobe is smaller and placed farther back from the midline, there are 8-10 segments in the thorax, and the maximum width of the pygidium is at half length (sag.). He originally placed *B. milleri*, *B. bellevillensis*, *B. beckeri*, *B. billingsi*, *B. porrectus*, and *B. tenuirugosus* into this taxon, and speculated that species with distinctive pygidia like *B. aplatus* might also belong in it because their cranidia were similar to *Bumastoides*. We show here that these species differ in an important cranidial feature (character 1), and a wide variety of pygidial characters, and are best placed in *Stenopareia* (or at the very least excluded from *Bumastoides*). Ludvigsen & Chatterton (1980) elevated *Bumastoides* to full generic status, and placed it in the Illaeninae based on the presence of a forward turning rostral flange in *B. lenzi*. This placement was supported by Whittington (1997a) because *Bumastoides* also shares a wide variety of other features with illaenids: a down-curving doublure with the anterior edge lying below the ventral ridge, a virtually non-fulcrate thorax, narrow pleurae and a wide thoracic axis.

Besides the effacement of the *Bumastoides* exoskeleton, one of the largest barriers to the construction of accurate phylogenetic reconstructions has been the inconsistent assessment of the number of thoracic segments by some authors (see *B. milleri* remarks below for examples). Material with anywhere from 8-10 thoracic segments have been placed into the same species because of the lack of identifying features. There is no evidence that the number of thoracic segments varies in holaspids, so the number of segments should be considered diagnostic in material that is obviously morphologically

mature. Ludvigsen & Chatterton (1980) and Chatterton (1980) demonstrated that illaenid trilobites could vary dramatically during their holaspid ontogeny (but not in the number of thoracic segments). Coupled with the lack of morphology in the group, it is clear that extreme rigor is necessary to delineate new species of *Bumastoides*.

Bumastoides milleri **(**Billings, 1859)

(Figs. 6-7)

1859 *Illaenus milleri* Billings: 375, fig. 10

1877 *Illaenus milleri* Walcott: 71.

1908 *Bumastus milleri* Raymond & Narraway: 254, pl. 61, figs. 3-5, 9-10.

? 1927 *Bumastus milleri* Walter: 222, pl. 17, fig. 2.

1954 *Bumastoides milleri* Whittington: 224, pl. 62, figs. 16-18, 20, 25-26, 29.

1957 *Bumastus trentonensis* Fisher: 16, pl. 6, fig. 9.

1987 *Bumastoides milleri* DeMott: 91, pl. 6, figs. 20-23.

1997b *Bumastoides milleri* Whittington: 12, fig. 9, 1-4.

non 2002 *Bumastoides milleri* Whiteley et al.: 211, pl. 6.

Diagnosis. Median tubercle present and circular (character 3, state 1), lunette predominantly crescentic (character 4, state 0), nine thoracic segments (character 8, state 0), low length to width ratio of pygidia (51-58%) (character 16, state 0).

Material. Figured material includes four incomplete individuals (holotype GSC 1319b, Figs. 6A-D; NYSM 10757, Figs. 7A-B, E, F; SUI 125988, Figs. 7C, G; and SUI 125975, Figs. 7D, H), one incomplete cranidium (MCZ 145734, Figs. 6E-G). Unfigured material includes one thoracopygon (MCZ 107232, DeMott 1987, pl. 6, figs. 20-21), one nearly

complete individual (MCZ107233, DeMott 1987, pl. 6, figs. 22-23), and ten other partial specimens (SUI 125976-79, 125981-82, 125985-87, 125989).

Occurrence. Upper Ordovician (Sandbian-Katian) of the Selby Formation and "Rockland Formations" (lower Trenton Group), New York and Ontario, the Platteville Group (Iowa, Wisconsin, and Illinois), and the Maquoketa Formation of Iowa.

Description. Cranidium occupies 36-38% of total exoskeletal length; elliptical, length 66-70% of width across palpebral lobes; inflated, longitudinal and transverse profiles strongly convex, anterior part of the cranidium curving downwards strongly. Anterior margin convex forwards, posterior margin slightly convex backwards, flattened medially. Axial furrows weak, terminating just posterior of lunettes. Lunettes just forward of palpebral lobe, comprise 18-23% of cranidial length (exsag.), each equal to 6-7% of cranidial width opposite palpebral lobes, crescentic, deeply impressed adaxially then shallowing abaxially; expressed on both external surface (Fig. 6F) and internal mould (Fig. 7B). Eyes large, crescentic, situated close to posterior margin, account for 31-35% of cranidial length in lateral view. Palpebral lobes semicircular, each equal to 22-25% of cranidial length and 4-5% of width, palpebral furrow extremely weak, primarily defined by change in slope at fixigena, curved slightly inwards. Posterior branch of facial suture extends backwards and outwards to the posterior margin, posterolateral projection subtriangular, sharply terminating at a point behind the eye. Anterior branches converge forward and downward along curved paths, joining rostral suture at a point approximately in front of lunette. Librigena subsemicircular with rounded genal angle, dorsal surface smooth except terrace lines which extend over sutural margin onto posterior margin of librigena. Exoskeletal surface smooth posteriorly, slightly undulating closely packed

terrace lines present only abaxially, becoming more widely spaced, prominent, and medially complete towards anterior margin. Widely spaced pits present on cranidial internal mould. Circular median tubercle present on dorsal surface, close to posterior margin (Fig. 7A, B).

Thorax of nine segments; strongly convex (tr.), longitudinal profile nearly flat. Axial furrows very weak, defined only by slight change in pleural angle at fulcrum. Axis wide, evenly arched (tr.), subrectangular in outine, comprising approximately 79-80% of thoracic width. Axial rings subrectangular, narrowing (sag.) very slightly backwards. Pleura without furrows, slightly narrower (sag.) than axial rings, directed primarily outwards and downwards (minimally fulcrate), terminations rounded. Articulating facets rounded subtriangular, with eight to nine terrace lines that initially nearly parallel each other, than converge upwards, extend to just below the axial furrow, well-defined border.

Pygidium wide (tr.) and short (sag.), accounts for 28-32% of total exoskeletal length; subtrapezoidal with rounded anterior corners, sharp posterior corners, and well-rounded posterior margin, length equal to 51-58% of maximum width, longitudinal profile initially convex backwards lightly, then strongly convex backwards towards posterior end, convex (tr.) abaxially, flat medially. Axis undifferentiated. Dorsal inner margin of pygidial doublure appears bicuspid and curved backward, terrace lines extend inward and slightly downward, dorsal most terrace lines mirror angle of inner margin. Articulating facet subsemicircular with well-defined border, rounded ventral margin, six undulating terrace lines converge upwards, extends dorsally to axial furrow. Dorsal exoskeleton smooth except three straight terrace lines that follow lateral margins, and

three undulating terrace lines that extend inward and upward from lateral margins. Widely spaced pits present on pygidial internal mould.

Remarks. *Bumastoides milleri* has been used as a catch-all for *Bumastoides*-type trilobites since it was first described by Billings (1859). Clarke (1897) and Whittington (1954) assigned holaspid material with anywhere from eight to ten thoracic segments to *B*. *milleri*. Walter (1927) assumed a cranidium from the Platteville Limestone in Iowa was *B*. *milleri*, even though it was damaged and indistinct. Whiteley et al. (2002, p. 211, pl. 6) assigned a specimen with ten thoracic segments to *B*. *milleri*. As advocated by DeMott (1987), and from the type material from Ontario, *B*. *milleri* should be restricted to species with nine thoracic segments. Species with eight or ten segments show consistent character assemblages that separate them from *B*. *milleri* (see other diagnoses).

Clarke (1897) considered *Bumatoides milleri* a synonym of *Illaenus trentonensis* Emmons, 1842. The location of the original *I*. *trentonensis* material is not known, but the small illustration (Emmons 1842, p. 390, fig. 3) shows a trilobite with well-incised axial furrows, eight thoracic segments, a subtriangular pygidium, and a rather flattened cranidial profile. An assignment of this species to *Bumastoides* is doubtful at best (see also Raymond 1925). Later hypotypes (Clarke 1897; Fisher 1957) of '*B*. *trentonensis*' can confidently be assigned to other Trenton species of *Bumastoides* (*B*. *milleri*, NYSM 10757, Figs. 7A-B, E, F; *B*. *porrectus*, NYSM 4158, Figs. 16A-E).

Bumastoides billingsi (Raymond & Narraway, 1908)

(Figs. 8-9)

1908 *Bumastus billingsi* Raymond & Narraway: 253, pl. 62, figs. 1-2.

1913 *Bumastus billingsi* Raymond: 34, pl. 3, fig 12.

1930 *Bumastus billingsi* Bradley: 254-256, pl. 28, figs. 1-7.

1979 *Bumastoides billingsi* Ludvigsen: 47, figs. 28C-D.

Diagnosis. Predominant shape of lunette is elliptical (character 4, state 1), path of the cranidial axial furrow is straight (character 5, state 0), ten thoracic segments (character 8, state 2), large paired muscle scars present on pygidium (character 11, state 1), ratio of pygidial length to width is high (76-83%) (character 16, state 3), axial furrow expressed as notches flanking center of the pygidial anterior margin (character 17, state 0).

Material. Figured material includes two exfoliated, nearly complete individuals (plastotype CM 5472, Figs.8A-E, see also Ludvigsen 1979, fig. 28C, D for images of the actual specimen; UC 10776, Figs. 9F, I-J), one exfoliated cranidium (UC 20700a, Figs. 9A-C), and two exfoliated pygidia (UC 20710a Figs. 9D-E; UC 20710b, Figs. 9G, H). Unfigured material includes one librigena (UC 5858a), four incomplete pygidia (UC5858b-d; UC20710c), and two exfoliated cranidia (UC5858e-f).

Occurrence. Upper Ordovician (Katian) of the Trenton Group, Hull Quebec, and the "Kimmswick Limestone" (Dunleith Formation) of Missouri and Illinois.

Description. Cranidium occupies approximately 34% of total exoskeletal length, semicircular, length 67-74% of width across palpebral lobes; inflated, longitudinal and transverse profile strongly convex, anterior part of cranidium curving downwards strongly. Anterior margin strongly convex forwards, posterior margin gently convex backwards. Axial furrows straight, approximately 25% of maximum lunette width, terminating at adaxial side of lunette. Lunettes just forward of palpebral lobe, comprise 17-21% of cranidial length (exsag.), each equal to 8% of cranidial width opposite palpebral lobes, elliptical, deeply impressed only as a narrow adaxial band, otherwise

uniform impression throughout. Eyes small, crescentic, situated close to posterior margin, accounts for 23-26% of cranidial length in lateral view. Palpebral lobes apparently semicircular. Anterior branches of facial suture converge forward and downward along curved paths. Anterior margin of rostral plate gently bowed, rostral plate apparently subtriangular. Librigena subsemicircular with strongly rounded genal angle, border well-defined, barely perceptible loosely spaced pitting on dorsal surface, terrace lines developed at a point anterior and ventral of palpebral lobes. Widely spaced pitting present on cranidial internal mould, median tubercle absent.

Thorax of ten segments; strongly convex (tr.), longitudinal profile flat. Axial furrows defined only by slight change in pleural angle at fulcrum. Axis wide, evenly arched (tr.), subrectangular. Axial rings subrectangular, gradually narrowing (sag.) posteriorly. Pleura without furrows, slightly narrower (sag.) than axial rings, directed outwards and downwards (minimally fulcrate), terminations bluntly rounded. Thoracic dorsal exoskeleton smooth.

Pygidium accounts for 35% of total exoskeletal length; subtrapezoidal, anterior corners and posterior margin well rounded, length equal to 76-83% of maximum width, longitudinal profile initially flat, then convex towards the posterior end, gently convex (tr.). Axis expressed as a slight protrusion medially, slight depressions laterally flanking axis. Anterior ventral ridge pronounced, following curvature of the anterior margin. Doublure inner margin dicuspid, median depression on doublure wide, terminates just above posterior margin. Paired subrectangular muscle scars, evenly distributed pits, and median ridge expressed on internal mould.

Remarks. Raymond & Narraway (1908) described *Bumastoides billingsi* as a new species, citing its large size, stronger cranidial dorsal furrows, wider thoracic axis, and stronger lunettes as the primary differences between it and *B*. *milleri*. They also suggested that *B*. *billingsi* could be synonymous with Emmon's (1842) larger specimen of *Bumastus trentonensis* (Emmons, 1842, p. 390, fig. 1). Like the smaller specimen (Emmons 1842, p. 390, fig. 3, see remarks under *B*. *milleri*) this specimen almost certainly does not belong to *Bumastoides*. The elongated pygidium and well-incised axial furrows that diverge beyond the lunettes strongly suggest this material is best assigned to *Failleana* Chatterton & Ludvigsen, 1976.

Bradley (1930) described material from the Kimmswick Limestone (Fig. 9) that we consider conspecific with the material from Quebec. He noted the similarity with *B*. *holei*, a sister taxon relationship present in 3/8 of our MPTs. Both are of generally very large size, have deep, elliptical lunettes, a wide thoracic axis, and well-defined, paired pygidial muscle scars. *B*. *billingsi* differs from *B*. *holei* in the length/width ratio of the pygidium (70-74% in the latter, 76-83% in the former), the residual axis expression at the pygidial anterior border, and the density of cranidial internal mould pitting.

Bumastoides bellevillensis (Raymond & Narraway, 1908)

(Fig. 10)

1908 *Bumastus bellevillensis* Raymond & Narraway: 253, pl. 61, figs. 6-7.

Diagnosis. Median cranidial tubercle present (character 3, state 1), eight thoracic segments (character 8, state 1), median pygidal depression on doublure effaced posteriorly (character 13, state 2); median ridge on cranidial internal mould.

Material. One incomplete entire individual (holotype CM 1900, Figs. 10A-E).

Occurrence. Upper Ordovician (Katian) of the Trenton Group (almost certainly Verulam Formation; Ludvigsen 1979, fig. 3), Belleville, Ontario.

Description. Cranidium comprises 36% of total exoskeletal length; elliptical, length 66% of width at palpebral lobes; inflated, longitudinal and transverse profile strongly convex, anterior part of cranidium curving downwards strongly. Anterior margin convex forwards, posterior margin gently convex backwards. Median cranidial ridge present on internal mould, extends from just above anterior margin to a point near lunette base. Axial furrows narrow, converging gently forward, terminating at adaxial side of lunette, width approximately 20% of maximum lunette width. Lunettes just forward of palpebral lobe, occupying 21% of cranidial length (exsag.) each equal to 8% of width across palpebral lobes, deeply impressed adaxially, shallowing abaxially. Eyes crescentic, located close to posterior margin, account for 32% of cranidial length in lateral view. Palpebral lobes semicircular, each equal to 21% of cranidial length and 5% of cranidial width, palpebral furrow extremely weak, defined largely by change in slope at fixigena. Posterior branch of facial suture extends straight backwards to posterior margin (posterolateral projection absent). Anterior branches converge forward and downward along gently curved paths, joining rostral suture at a point in front of lunette. Anterior margin of rostral plate nearly transverse. Librigena apparently subsemicircular with rounded genal angle, dorsal surface smooth, well defined terrace lines present on rounded lateral and ventral margins of librigena. Tightly packed, transverse terrace lines on rostral plate. Pitting on cranidial internal mould widely spaced and evenly distributed. Circular posterior median tubercle present on cranidial internal mould.

Thorax of eight segments; strongly convex (tr.), longitudinal profile nearly flat. Axial furrows very weak, bowed outwards near mid-length of thorax. Axis wide, evenly arched (tr.), subrectangular. Axial rings subrectangular, narrowing (sag.) slightly backwards. Pleura without furrows, directed strongly downwards, slightly backwards and outwards at fulcrum. Articulating facets broad, slightly overlapping each other; subtriangular, extend upwards to axial furrow, six terrace lines converge upwards. Dorsal surface smooth.

Pygidium occupies 33% of total exoskeletal length; subtrapezoidal, with gently rounded anterior corners, and well-rounded posterior margin, length equal to 66% of maximum width, longitudinal profile initially flat, then convex backwards towards the posterior end, convex (tr.) abaxially, nearly flat medially, axis undifferentiated. Dorsal inner margin of doublure curved backwards and bicuspid, median depression present only anteriorly. Evenly spaced, slightly undulating terrace lines transverse across doublure, near inner margin terrace lines extend dorsally along cusps, effaced medially.

Remarks. *Bumastoides bellevillensis* is easily distinguishable from other species because it has three autapomorphies: a sagittal ridge on the cranidum, eight thoracic segments, and a depression on the dorsal surface of doublure that is only expressed anteriorly.

Bumastoides beckeri (Slocom, 1913)

(Figs. 11-12)

1913 *Bumastus beckeri* Slocom: 54, pl. 14, figs. 1-4.

1927 *Bumastus milleri* Walter: 220, pl. 18, figs. 10-11.

Diagnosis. Continuous terrace lines cover entire cranidial exoskeleton (character 7, state 2), thorax of ten segments (character 8, state 2), concentric terrace lines on pygidium

present (character 14, state 1), undulatory terrace lines directed inwards from pygidial lateral margins present (character 15, state 0); transverse terrace lines present on the first four segments of the thorax.

Material. Figured material includes a nearly complete enrolled specimen (holotype UC 41154, Figs. 11A-E), a nearly complete individual (SUI 125973, Figs. 12A-F), a partially exfoliated individual (SUI 125984, Fig. 12G-H) and an incomplete thoracopygon (P 16708, Figs. 11F-G).

Occurrence. Upper Ordovician (Hirnantian) of the Maquoketa Formation, Fayette County, Iowa.

Description. Cranidium accounts for 32-34% of total exoskeletal length; semicircular, length 70% of width across palpebral lobes; inflated, longitudinal and transverse profiles convex, anterior part of cranidium curving downwards strongly. Anterior margin convex forwards, posterior slightly convex backwards. Axial furrows completely effaced, lunettes just forward of palpebral lobe, elliptical, equal impression throughout, occupying 29% of cranidial length (exsag.), each lunette equal to 4% of cranidial width across palpebral lobes. Eyes small, crescentic, situated close to posterior margin, occupy 28-30% of cranidial length in lateral view. Palpebral lobes semicircular, each comprises 3-4% of cranidial width, equal to 13% of cranidial length, palpebral furrow only defined by change in slope at fixigena. Posterior branch of facial suture extends backwards and outwards forming a small posterolateral projection. Anterior branches converge forward and downward along gently curved paths, intersection with rostral suture not preserved. Librigena subsemicircular, with well-rounded genal angle and well-defined border. Dorsal surface covered in continuous, transverse, slightly undulatory terrace lines

(including librigena), with slight hiatuses near lunette and postocular area; barely perceptible pitting present between terrace lines. Posterior median tubercle absent.

Thorax of ten segments; strongly convex (tr.), axial furrows weak, bowed outwards near thoracic mid-length. Axis wide, subrectangular, evenly arched (tr.), comprising 79-81% of thoracic width. Axial rings subrectangular, narrowing slightly in length (sag.) backwards, four to five terrace lines present on first three segments, two ridges on fourth segment. Pleura without furrows, slightly narrower than axial rings, directed outwards and downwards (minimally fulcrate), terminations transverse, with well-defined border. Articulating facets subtriangular, slightly overlapping, broad, extend to just below axial furrow, nine to ten terrace lines converge upwards. Aside from terrace lines, thoracic dorsal exoskeletal surface smooth.

Pygidium occupies 31-32% of total exoskeletal length; subtrapezoidal with rounded anterior corners and well-rounded posterior margin, length equal to 61-63% of maximum width, longitudinal profile initially flat, abruptly convex backwards towards posterior end, strongly convex (tr.) abaxially, weakly convex medially (tr.). Axis undifferentiated. Articulating facet subtriangular, extending to just below the axial furrow. Three widely spaced concentric terrace lines on dorsal surface mirror pygidial outline, terminating near posterior margin. Undulating terrace lines extend inward from lateral margins, effaced medially.

Remarks. Slocom (1913) considered *Bumastoides beckeri* to be closely allied with *B. billingsi* based on its gross morphology. *Bumastoides beckeri* is more closely related to *B. kimmswickensis* (see remarks below for a comparison), a species not known by Slocom. They are sister taxa, united by their shared possession of terrace lines over the majority of

the cranidial exoskeleton. New material from the Maquoketa of Fayette County, Iowa (Fig. 12), is conspecific with the holotype.

Bumastoides holei (Foerste, 1920)

(Figs. 13-14)

1920 *Bumastus holei* Foerste: 214, pl. 21, figs. 15a, b; pl. 22, figs. a, b.

1925 *Bumastus holei* Raymond: 213, pl. 8, figs. 5, 6.

1999 *Bumastoides holei* Brett et al.: 294, pl. 7, fig. 4.

2002 *Bumastoides holei* Whiteley et al.: 209, pl. 4; 210, pl. 5.

Diagnosis. Path of the posterior branch of the facial suture is straight backwards (character 2, state 0), median tubercle present near posterior margin of cranidium (character 3, state 1), predominant shape of lunette is elliptical (character 4, state 1), pitting on cranidial internal mould densely distributed (character 6, state 2), paired pygidial muscle scars visible (character 11, state 1), concentric terrace lines present on pygidial exoskeleton (character 14, state 1); thoracic and pygidial surface granulose.

Material. Figured material includes two exfoliated but otherwise nearly complete individuals (MCZ 144798, Figs. 13E-F, 14A-C; plesiotype MCZ 101148, Figs. 13A-D), and one complete individual (MCZ 115909, Figs. 14D-H). Unfigured material includes two incomplete whole individuals (MCZ 144799; 145650), and one exfoliated cranidium with partial thorax (NYSM E998).

Occurrence. Upper Ordovician (Katian) of the Rust Formation (Trenton Group), Trenton Falls, New York and the Kimmswick Limestone of Ralls County, Missouri.

Description. Cranidium accounts for 35-36% of total exoskeletal length; semicircular, length 68-69% of width across palpebral lobes; strongly inflated, longitudinal and

transverse profiles convex, anterior part of cranidium curving downwards strongly. Anterior margin convex forwards, posterior margin nearly transverse. Axial furrows weak, converging slightly inwards, terminating on adaxial side of lunette, width approximately 40% of maximum lunette width. Lunettes large, just forward of palpebral lobes, comprise 26-28% of cranidial length (exsag.), each equal to 11-12% of cranidial width across palpebral lobes, elliptical, deeply impressed adaxially, otherwise equal impression throughout. Eyes small, approximately equal in length to lunette, crescentic, situated close to posterior margin, occupies 25-28% of cranidial length in lateral view. Posterior branch of facial suture extends straight backwards (posterolateral projection absent), to posterior margin. Anterior branches initially divergent, then converging forward and downward along gently curved paths, apparently joining rostral suture at a point forward of lunette. Librigena subsemicircular, with well-rounded genal angle. Dorsal surface smooth except for thin, undulating, evenly spaced terrace lines on anterior portion of cranidium, internal mould of cranidia heavily punctate, evenly distributed small pits over entire surface. Circular posterior median tubercle present on cranidial internal mould.

Thorax of ten segments; strongly convex (tr.), longitudinal profile flat. Axial furrows weak, slightly bowed outwards near mid-length of thorax. Axis wide, subrectangular, evenly arched (tr.), comprising 74-76% of thoracic width. Axial rings subrectangular, narrowing (sag.) slightly backwards. Pleura without furrows, slightly narrower than axial rings, directed outwards and downwards (minimally fulcrate), terminations transverse. Articulating facets broad, non-overlapping, subtriangular, extending to just below axial furrow, seven to nine terrace lines converge upwards.

Thoracic dorsal exoskeletal surface covered in very fine granules of approximately even size.

Pygidium accounts for 33-35% of total exoskeletal length; subtrapezoidal with rounded anterior corners and well-rounded posterior margin, length equal to 70-74% of maximum width, longitudinal profile initially flat, gently convex backwards towards posterior end, strongly convex (tr.) abaxially, weakly convex medially. Axis undifferentiated. Depression present medially on doublure, extending to posterior margin. Paired subrectangular muscle scars visible on internal mould. Articulating facet subsemicircular, extending to anterior corner, six terrace lines converge upwards. Six weak, evenly spaced concentric terrace lines on the dorsal surface mimic the pygidial outline, terminating near posterior margin, effaced medially. Granules on exoskeleton similar in shape and distribution to thorax. Pitting on internal mould of same size and distribution as crandia.

Remarks. The original material (a cranidium and associated pygidia) described by Foerste (1920) is from the Kimmswick Limestone, though the location of the type material is currently unknown (Brett et al. 1999). Raymond (1925) redescribed the species based on material from the Trenton Formation collected by Dr. C.D. Walcott, some of which is re-illustrated here. He noted the close similarity between *Bumastoides holei* and *B. billingsi*, citing the possession of the cranidial median tubercle, fainter dorsal furrows, and the strongly punctate appearance of the internal cast as the primary differences. We add to those differences the granulose texture of the surface (covaries with the pitting on the internal mould, but seems absent on the cranidial surface), and the lack of axis expression at the anterior border. Brett et al. (1997) and Whitely et al. (2002)

illustrated more of the Trenton material (MCZ 115909, Figs. 14D-H), but did not describe it.

Bumastoides porrectus (Raymond, 1925)

(Figs. 15-16)

1897 *Bumastus trentonensis* Clarke: 718, fig. 32.

1925 *Bumastus porrectus* Raymond: 213, pl. 8, figs. 7, 8.

1947 *Bumastus porrectus* Wilson: 35, pl. 7, figs. 7-9.

1987 *Bumastoides porrectus* DeMott: 91, pl. 6, figs. 24-28, 30-31.

1999 *Bumastoides porrectus* Brett et al.: 294, pl. 7, fig. 5.

2002 *Bumastoides porrectus* Whiteley et al.: 212, pl. 7.

Diagnosis. Posterior median tubercle faint, but present (character 3, state 1), ten thoracic segments (character 8, state 2), pygidial concentric terrace lines absent (character 14, state 0), undulatory terrace lines on pygidia absent (character 15, state 0).

Material. Figured material includes two complete individuals (holotype MCZ 101147, Figs. 15A-B, D-F; NYSM 4158, Figs 16A-E), one complete cranidium (MCZ 107234, Fig. 15C), one exfoliated cranidium (MCZ 107235, Fig. 15H), and one partially exfoliated pygidium (MCZ 107236, Fig. 15G).

Occurrence. Upper Ordovician (Katian) of the Denley Formation (Trenton Group), Trenton Falls, New York and the Guttenberg Formation (Decorah Group), Iowa and Wisconsin.

Description. Cranidium occupies 37% of total exoskeletal length; semicircular, length 64-70% of width across palpebral lobes; inflated, longitudinal and transverse profile strongly convex. Anterior margin well rounded, convex forward, posterior margin very

slightly convex backwards. Axial furrows very weak, converging slightly inwards, terminating on adaxial side of lunette, width approximately 75% of maximum lunette width. Lunettes just forward of palpebral lobe, comprise 21-25% of cranidial length (exsag.), each equal to 7% of cranidial width opposite palpebral lobes, elliptical, impression relatively even throughout. Eyes crescentic, situated directly in front of posterior margin, occupy 32-33% of cranidial length in lateral view. Palpebral lobes semicircular, each equal to 16-19% of cranidial length and 4-5% of width; palpebral furrow extremely weak, defined largely by change in slope at fixigena, curved slightly inwards. Posterior branch of facial suture extends backwards and outwards to posterior margin, outlining a small, triangular, posterolateral projection which sharply terminates behind the eye. Anterior branches initially subparallel forward, then converging forward and downward on slightly curved paths, apparently terminating at the rostral suture at a point forward and between lunette and palpebral lobe. Librigena narrow (tr.), subsemicircular, genal angle well rounded. Posterior and lateral exoskeletal surface smooth; shallow, discontinuous, undulating terrace lines developed forward of palpebral lobe, becoming straighter and more complete towards the anterior margin; extending just beyond the edge of librigena. Very small circular posterior median tubercle present on cranidial internal mould, barely perceptible on exoskeletal surface.

Thorax of ten segments; strongly convex (tr.), longitudinal profile flat. Axial furrows very weak, defined only by slight change in pleural angle at fulcrum, bowed outwards near mid-length of thorax. Axis wide, subrectangular, evenly arched (tr.), occupying 76-81% of thoracic width. Axial rings subrectangular, maintaining equal length on all ten segments. Pleura without furrows, approximately same length (sag.) as

axial rings, directed outwards and downwards (minimally fulcrate), terminations gently rounded. Articulating facets broad, not overlapping, rounded subtriangular, dorsally terminating well before axial furrow, ten terrace lines converge upwards. Thoracic dorsal exoskeletal surface smooth.

Pygidium accounts for 33-35% of total exoskeletal length; subtrapezoidal with rounded anterior corners and well-rounded posterior margin, length equal to 63-68% of maximum width, longitudinal profile initially flat, then convex backwards towards posterior end, weakly convex (tr.) medially, strongly convex (tr.) abaxially. Axis undifferentiated. Anterior ventral ridge pronounced, following curvature of the anterior pygidial margin. Articulating facet narrow (sag.), subtriangular, five terrace lines converge upwards. Dorsal surface smooth except for thin terrace lines along lateral margins, medially effaced near anterior pygidial margin.

Remarks. Raymond (1925) erected this species partly to accommodate an exoskeleton that Clarke (1897, NYSM 4158, Figs. 16A-E) identified as *Bumastus trentonesis* but which clearly was not conspecific with the types of *Bumastus trentonensis* Emmons, 1842 (see remarks under *B. milleri*). The holotype of *B. porrectus* (MCZ 101147, Figs. 15A-B, D-F) and Clarke's specimen come from the upper Trenton Group at Trenton Falls NY, and are clearly the same species. Raymond (1925) cited the 'almost total absence' of dorsal furrows from the cranidium as the primary difference between *B. porrectus* and *B. milleri*. Distinguishing between completely effaced and very faint dorsal furrows (e.g., splitting character 1, state 1, into separate bins) is nearly impossible in *Bumastoides*, especially given the varying exposure to weathering between specimens. We think it better to distinguish *B. porrectus* from morphologically similar species (e.g., *B. milleri*;

B. *holei*) based on more discrete characteristics such as the number of thoracic axial rings, and absence of sculpture.

DeMott (1987) described and figured new *Bumastoides porrectus* material from the Decorah Group of Wisconsin (Figs. 15C,G-H). We tentatively accept these as conspecific, except for the pygidia (*Bumastoides* cf. *B*. *porrectus* Fig. 15G), which was found at a different locality from the cranidia, and has a more rounded outline than other *B*. *porrectus* pygidia. DeMott (1987) stated that the median cranidial tubercle was absent in all specimens of *B*. *porrectus*. Material he illustrated (MCZ 107235, Fig. 15H) has been exfoliated in the intervening years, and shows the tubercle. Furthermore, the holotype shows the tubercle through the exoskeleton under very high magnification. Rather than lacking this feature, it seems that the tubercle is simply less conspicuous than other species. In general, *B*. *porrectus* possess more subdued sculptural features across the entire exoskeleton, so the difficulty recognizing the median tubercle is not surprising. Brett et al. (1999) and Whitely et al. (2002) reillustrated the holotype, but did not redescribe it.

Bumastoides tenuirugosus (Troedsson, 1928)

(Fig. 17)

1928 *Bumastus tenuirugosus* Troedsson: 43, pl. 15, figs. 1-10.

1983 *Bumastoides tenuirugosus* Westrop & Ludvigsen: 39-40, pl. 4, figs. 1-2, 5, 7-8; pl. 5, figs. 1-6.

Diagnosis. Path of the axial furrow straight (character 5, state 0), pitting on the cranidial internal mould absent (character 6, state 0), terrace lines present on the entire cranidial

exoskeleton (character 7, state 2), thorax of ten segments (character 8, state 2), concentric terrace lines present on pygidial exoskeleton (character 14, state 1).

Material. Figured material includes one exfoliated thoracopygon (OU 12483,Fig. 17A,C), an incomplete cranidium (OU 12495, Fig. 17B, D-E), and an exfoliated pygidium (OU 12496, Fig. 17F-G). Unfigured material includes an incomplete cranidium.

Occurrence. Upper Ordovician (Katian) Cape Calhoun Formation of Northern Greenland, and the Upper Ordovician (Katian) Selkirk Member of the Red River Formation, Garson, southern Manitoba.

Description. See Westrop & Ludvigsen (1983).

Remarks. Though *Bumastoides tenuirgusosus* has no definitive sister taxon relationship with any other species (Fig. 4), it is most similar to *B*. *billingsi* in having straight cranidial axial furrows (though they are more deeply incised in the latter), and strong, elliptical lunettes. *B*. *tenuirgusosus* shares complete terrace lines (character 7; state 2) with the Midwestern species (*B*. *beckeri* and *B*. *kimmswickensis*), but the MPTs do not indicate that this character is a synapomorphy that would unite all three taxa.

Raymond (1916) suggested that the number of thoracic segments could vary within a single species of *Bumastus* (*Bumastoides*). Troedsson (1928) took issue with this statement and while noting some degree of ontogenetic variation in *B*. *tenuirugosus*, indicated that even the smallest individuals of *B*. *tenuirugosus* have ten thoracic segments.

Westrop & Ludvigsen (1983) described specimens of *Bumastoides tenuirugosus* from the Selkirk Member of the Red River Formation that is conspecific with the Cape

Calhoun material. The sclerites illustrated here are also from the Selkirk Member at Garson, and are considered conspecific with all other specimens of *B. tenuirugosus*. Westrop & Ludvigsen (1983) noted the wide range of variation in the lunette definition and cranidial length/width ratio of the Selkirk material. These differences are likely due to preservation and ontogenetic variation (Westrop & Ludvigsen 1983), and all the material probably belongs to just the one species.

Bumastoides lenzi Chatterton & Ludvigsen, 1976

1976 *Bumastoides lenzi* Chatterton & Ludvigsen: 35, pl. 4, figs. 40-42; pl. 5, figs. 1-31.

Diagnosis. Posterior median tubercle absent (character 3, state 0), lunette predominantly crescentic (character 4, state 0), pitting on cranidial internal mould absent (character 6, state 1), concentric terrace lines absent on pygidium (character 14, state 0); cranidium subquadrate.

Occurrence. Upper Ordovician (Sandbian) of the Esbataottine Formation, of the South Nahanni River area of the District of Mackenzie, Canada.

Remarks. See *Bumastoides solangeae* below.

Bumastoides solangeae Hunda et al., 2003

2003 *Bumastoides solangeae* Hunda et al.: 11, pl. 1, figs. 1-26.

Diagnosis. Median tubercle on cranidium absent (character 3, state 0), pygidium rounded subtrapezoidal (character 12, state 1), median dorsal depression (ventral ridge) on pygidial doublure absent (character 13, state 0); librigena subtriangular, subangular genal angles, cranidium subcircular.

Occurrence. Upper Ordovician (Hirnantian) of the Whittaker Formation, Mackenzie Mountains, Canada.

Remarks.,*Bumastoides solangeae* is the only Hirnantian species known besides *B*. *beckeri*. The material from the Whittaker Formation is most similar to *B*. *lenzi*, but they differ in cranidial outline, librigena outline, and the absence of the axial furrow and median depression on the doublure of the former. The two species are not sister taxa in any of the MPTs, but they always occupy successive nodes at the base of the *Bumastoides* clade.

B. *solangeae* shares a subtriangular librigena with *B*. *kimmswickensis*, but this character was not coded due to the lack of well-preserved isolated librigena in most material.

"*Bumastoides*" *tricuspidatus* Edgecombe et al., 2006

2006 *Bumastoides tricuspidatus* Edgecombe et al.: 375, figs. 2-4.

Occurrence. Upper Ordovician (Sandbian) of the Ida Bay Limestone, Gordon Group, Ida Bay, southern Tasmania.

Remarks. *Bumastoides tricuspidatus* is a potentially important species because it is not Laurentian, and has a series of features not shared with the rest of the genus. A dicuspid doublure and subtrapezoidal to rounded subtrapezoidal pygidium are clear synapomorphies of *Bumastoides* (Fig. 5A). In contrast, *B*. *tricuspidatus* has a median projection on the inner margin of the doublure (tricuspid), and an elongate, subtriangular pygidium. The strongly pitted dorsal exoskeleton is also uncharacteristic of other *Bumastoides* species.

B. *tricuspidatus* was excluded from our analysis because the material is very fragmentary, and many taxonomically useful features are not preserved: the lunettes, number of thoracic axial rings, cranidial median tubercle etc. Further work (and better

material) is necessary to determine the position of this species within *Bumastoides*, or if it should be the basis of a new illaenid genus entirely.

Bumastoides graffhami sp. nov.

(Figs. 18-19)

1974 *Bumastoides* cf. *B*. *milleri* Shaw: 20, pl. 4, figs. 19, 20, 23.

Diagnosis. Axial furrow completely effaced (character 1, state 1), median tubercle on cranidium elliptical (character 3, state 2), ten thoracic segments (character 8, state 2), undulatory terrace lines present on pygidia (Fig. 18B) (character 15, state 0).

Derivation of Name. Named after Allen Graffham, who collected the holotype material (Shaw 1974, p. 17).

Material. Figured material includes one complete but damaged specimen (holotype OU 5204, Figs. 18A-D), one incomplete enrolled individual (OU 12497, Figs. 18F-G), one complete pygidium (OU 12498, Figs. 18F), one partially exfoliated cranidium (OU 19A-D, Figs. 19A-D), one thoracopygon (OU 12500, Fig. 19E), and one completely exfoliated cranidium (OU 12501, Fig. 19F). All figured material besides the holotype are designated here as paratypes. Unfigured material includes seven partial cranidia and three partial pygidia.

Occurrence. Upper Ordovician (Sandbian) of the lower Pooleville Member of the Bromide Formation, Arbuckle Mountains region of Oklahoma. Localities include Hwy 177, TQ, and DRa.

Description. Cranidium occupies 30% of total exoskeletal length; elliptical, length 63-69% of width at palpebral lobe; inflated, longitudinal and transverse profile strongly convex, anterior part of cranidium curving downwards strongly. Anterior margin convex

forwards, posterior margin convex backwards, flattened medially. Axial furrows completely effaced. Lunettes just forward of palpebral lobe, comprise 17-20% of cranidial length (exsag.), each equal to 6% of cranidial width opposite palpebral lobes, crescentic, deeply impressed adaxially then shallowing abaxially. Eyes crescentic, situated close to posterior margin, account for 21% of cranidial length in lateral view. Palpebral lobes semicircular, each equal to 17% of cranidial length and 5% of width; palpebral furrow extremely weak, defined largely by change in slope at fixigena, curved slightly inwards. Posterior branch of facial suture extends straight backwards to posterior margin (posterolateral projection absent). Anterior branches converge forward and downward along gently curved paths, joining rostral suture at a point approximately in front of lunette. Anterior margin of rostral plate transverse. Librigena subsemicircular with rounded genal angle, dorsal surface smooth except faint terrace lines near sutural margin, rounded lateral margin rounded with well-defined, tightly packed terrace lines. Widely spaced pits present on posterior half of cranidium, visible on internal moulds and exoskeleton, but absent anterior of palpebral lobes. Exoskeletal surface otherwise smooth posteriorly, slightly undulating, widely spaced terrace lines develop anterior of palpebral lobes, becoming tighter packed and more prominent towards anterior margin. Elongated posterior median tubercle present on cranidial internal mould.

Thorax of ten segments; strongly convex (tr.), longitudinal profile nearly flat. Axial furrows weak, bowed outwards near mid-length of thorax. Axis wide, evenly arched (tr.), subrectangular, comprising 78-79% of thoracic width. Axial rings subrectangular, maintaining equal length on all ten segments. Pleura without furrows, approximately same length (sag.) as axial rings, directed outwards and downwards

(minimally fulcrate), terminations nearly transverse. Articulating facets broad, overlapping each other; subtriangular, extend almost to axial furrow, eight to ten closely spaced chevron shaped terrace lines converge upwards. Articulating half-ring apparently long (tr.), extending laterally to axial furrow. Dorsal thoracic exoskeletal surface smooth.

Pygidium occupies 34% of total exoskeletal length; subtrapezoidal, with rounded anterior corners and well-rounded posterior margin, length equal to 63-70% of maximum width, longitudinal profile initially flat, then convex backwards towards posterior end, convex (tr.) abaxially, flat medially. Axis undifferentiated. Dorsal inner margin of pygidial doublure incompletely preserved but apparently curved backwards and dicuspid, depression present medially, transverse terrace lines mirror margin of doublure. Articulating facet subtriangular, extending upward to thoracic axial furrow, terrace lines less pronounced than on lateral margins. Four straight terrace lines follow the lateral margins, becoming fainter adaxially. Thin, undulating terrace lines extend inward and upward from lateral margins, effaced medially.

Remarks. *Bumastoides graffhami* is morphologically very similar to *B*. *milleri*, as they are sister taxa in all 8 MPT's. Shaw (1974) did not name a new species for the Oklahoma material, and instead used open nomenclature. Our revised diagnosis restricts *B*. *milleri* to exoskeletons with nine thoracic segments, so a new name is needed for the Oklahoma specimens with 10 segments. *Bumastoides graffhami* also possesses an elliptical cranidial tubercle (Fig. 19F), which further distinguishes it from *B*. *milleri*, which has a circular tubercle. *B*. *graffhami* is separated from other 10 segmented species (e.g., *B*. *porrectus*, *B*. *holei*, *B*. *billingsi*) in having undulatory terrace lines on the pygidium, completely effaced

axial furrows, lack of pygidial muscle scars, and aforementioned elliptical cranidial tubercle.

Bumastoides moundensis sp. nov.

(Figs. 20-21)

Diagnosis. Median tubercle on cranidium absent (character 3, state 0), lunettes predominantly crescentic (character 4, state 0), pitting on cranidial internal mould densely distributed (character 6, state 2), ten thoracic segments (character 8, state 2), pygidium rounded subtrapezoidal (character 12, state 1), concentric terrace lines present on pygidium (character 14, state 1), ratio of maximum pygidial length to width high (78-82%) (character 16, state 3); glabella strongly inflated, orientation of lunette and eye not parallel (Fig. 21C).

Derivation of Name. After the Effna carbonate mud-mounds, in which this species is particularly abundant.

Material. Figured material includes one damaged and exfoliated, but otherwise complete individual (holotype OU 12502, Figs. 20C-D), one thoracopygon (OU 12503, Figs. 20A-B), two exfoliated cranidia (OU 12504, Fig. 20E; OU 12506, Figs. 21A-B, D), one partial pygidium (OU 12505, Figs. 20F-H), and one complete cranidium (OU 12507, Figs. 21C, E-F). All figured material other than the holotype are designated here as paratypes. Unfigured material includes a large number of partial cranidia and pygidia.

Occurrence. Upper Ordovician (lower Sandbian) of the Effna Formation, Valley and Ridge region of Virginia. Localities include Interstate 77 and Porterfield Quarry (PQ).

Description. Cranidium occupies approximately 37% of total exoskeletal length; circular, length 73-76% of width at palpebral lobe, inflated, longitudinal and transverse

profile strongly convex, glabella overhanging anterior border. Anterior margin convex forwards, posterior margin convex backwards, flattened medially. Axial furrows very weak, converging gently forwards, terminating on adaxial side of lunette. Lunettes just forward of palpebral lobe, narrow (tr.), crescentic, impression abruptly shallowing abaxially, occupying 14% of cranidial length (exsag.), each lunette equal to 3-4% of cranidial width across palpebral lobes. Eyes crescentic, situated close to posterior margin, comprise 23-25% of cranidial length in lateral view. Palpebral lobes small, semicircular, each occupies 3% of cranidial width, equal to 7% of cranidial length; palpebral furrow weak, bowed inwards. Posterior branch of facial suture extends backwards and outwards behind the eye, extending to posterior margin, outlines a small triangular posterolateral projection, which sharply terminates behind eye. Anterior branches converge forward and downward on slightly curved paths, apparently terminating at rostral suture at a point in front of lunette. Rostral suture transverse, rostral plate rounded subtrapezoidal, deeply incised, terrace lines become progressively more chevron shaped ventrally. Librigena subsemicircular with rounded genal angle, dorsal surface smooth, some terrace lines developed near sutural margins, convex lateral margin with tightly packed terrace lines. Dorsal exoskeleton smooth until terrace lines develop at a point anterior of palpebral lobes, becoming progressively tighter and more pronounced towards anterior margin. Evenly spaced, uniformly sized pits present in internal moulds, apparently covering entire cranidium. Median tubercle absent.

Thorax of ten segments; strongly convex (tr.), longitudinal profile flat. Axial furrows weak and wide, directed backwards nearly subparallel. Axis wide, subrectangular, evenly arched (tr.), comprising 74% of thoracic width. Axial rings

subrectangular, transverse medially, curved slightly backwards at axial furrow, approximately equal in length (sag.). Pleura without furrows, approximately same length (sag.) as axial rings, directed outwards and downwards (minimally fulcrate), terminations nearly transverse. Articulating facets overlapping, broad, clearly defined, rounded subtriangular, extend almost to axial furrow, ten to twelve branching terrace lines converge upwards and towards pleural margins. Thoracic dorsal exoskeletal surface smooth.

Pygidium occupies 31% of total exoskeletal length; subcircular (rounded subtrapezoidal), anterior corners and posterior margin well rounded, length equal to 78-82% of maximum width, longitudinal profile initially gently convex backwards, then strongly convex towards posterior end, gently convex (tr.). Axis undifferentiated. Anterior ventral ridge pronounced, following curvature of anterior pygidial margin. Three pronounced terrace lines directed along lateral margins, terminating before anterior margin. Four weak, widely spaced concentric terrace lines on dorsal surface mirror pygidial outline, terminating near posterior margin. Evenly distributed pits of one size are present near posterior and anterior margins on internal moulds.

Remarks. *Bumastoides moundensis* does not have a sister taxon in any of the eight MPTs. It always occupies the node immediately above the northern Canadian species (node 6 on the strict consensus, Fig. 4), and is basal to the rest of *Bumastoides*. It differs from all other species in the degree of its glabellar inflation, and the non-parallel orientation of the lunettes and eye (likely due in part to the glabellar inflation). In terms of its overall shape, *B. moundensis* is most similar to *B. tenuirugosus* because of the rounded appearance to the pygidium, wide axis, and cephalic outline. Besides its

autapomorphies, the former differs in its lack of terrace lines on the entire cranidium, the absence of the cranidial tubercle, and crescentic lunettes.

Raymond (1925) described three species of *Bumastus* from the Effna (referred to by him as the Holston). *Bumastus dispassus* is probably best placed in *Failleana* (see Raymond 1925, pl. 7, fig. 6) because the axial furrows appear to diverge forward of the eyes, and the pygidium is elongated. *Bumastus lioderma* is known only from a damaged, partial cranidium, which is less inflated than in *Bumastoides moundensis*, and the strong, elliptical lunettes are different from the narrow, crescentic lunettes of the latter. Finally, *B*. *longiops* is morphologically very similar to *B*. *aplatus*, and based on the pygidium, almost certainly belongs to the group of species assigned here to *Stenopareia* (see *Stenopareia* remarks below).

Bumastoides kimmswickensis sp. nov.

(Figs. 22-23)

Diagnosis. Median tubercle on cranidium present (character 3, state 0), discontinuous terrace lines present on entire cranidial exoskeletal surface (character 7, state 2), nine thoracic segments (character 8; state 0), concentric terrace lines on pygidium absent (character 14, state 0), undulatory terrace lines on pygidium absent (character 15, state 1); librigena subtriangular.

Derivation of Name. After the "Kimmswick Limestone" as defined in pioneering studies of the Ordovician of Missouri (e.g. Bradley 1930).

Material. Figured material includes one thoracopygon (holotype OU 12508, Figs. 22H-J), three exfoliated cranidia (OU 12509, Figs. 22A-C; OU 12510, Figs. 22E-G; OU 12512, Figs. 23A-C), two nearly complete cranidia (OU 12513, Fig. 23D; OU 12514,

Fig. 23E), one complete pygidium (OU 12511, Fig. 22D), one exfoliated pygidium (OU 12516, Fig. 23H), and one complete librigena (OU 12515, Fig. 23F-G). All figured material besides the holotype are designated here as paratypes. Unfigured material includes a large number of partial cranidia, pygidia, and librigena.

Occurrence. Upper Ordovician (Katian) of the lower Kimmswick Limestone, Jefferson County, Missouri, Hwy M locality.

Description. Cranidium semicircular, length 68-73% of width at palpebral lobes, inflated, longitudinal profile very convex (nearly vertical), transverse profile somewhat convex. Anterior margin convex forwards, posterior margin slightly convex backwards, flattened medially. Axial furrows very weak, converging gently forwards, terminating on adaxial side of lunette. Lunettes just forward of palpebral lobe, narrow (tr.), elliptical, impression gradually shallowing abaxially, occupying 22-25% of cranidial length (exsag.), each lunette equal to 8% of cranidial width across palpebral lobes. Eyes crescentic, situated close to posterior margin. Palpebral lobes long (sag.), semicircular, each accounts for 5% of cranidial width, equal to 19-22% of cranidial length; palpebral furrow effaced. Posterior branch of facial suture extends backwards then sharply outwards behind the eye, extending to posterior margin, outlines a triangular posterolateral projection, which sharply terminates behind eye. Anterior branches converge forward and downward on slightly curved paths, apparently terminating at rostral suture at a point in front of lunette. Librigena wide (tr.), subtriangular with rounded but slightly angulate genal angle, dorsal surface covered in widely spaced, evenly sized pits. Well-developed straight terrace lines packed tightly on rounded lateral margin of librigena, more widely spaced on doublure, undulatory terrace lines migrate

inward from lateral margin towards sutural margin. Dorsal exoskeleton covered in widely spaced pits of one size, undulatory terrace lines present on entire cranidium except in a band between lunettes. Terrace lines migrating inward from lateral margins appear to deflect around lunettes, joining transverse terrace lines at posterior and anterior margins. Terrace lines generally discontinuous becoming more complete, well-incised, and transverse near anterior margin. Evenly spaced, uniformly sized pits present on internal moulds, covering entire cranidium. Posterior median tubercle circular, prominent on internal mould.

Thorax of nine segments; strongly convex (tr.), longitudinal profile flat. Axial furrows barely perceptible, only defined by very slight change in pleural angle. Axis wide, subrectangular, evenly arched (tr.). Axial rings subrectangular, transverse medially, curved slightly backwards at axial furrow, approximately equal in length (sag.). Pleura without furrows, approximately same length (sag.) as axial rings, directed outwards and downwards, slightly backwards (minimally fulcrate), terminations incomplete. Articulating facets incomplete, but dorsal extent is well below axial furrow, eight to nine terrace lines converge upwards. Thoracic dorsal exoskeletal surface smooth.

Pygidium subtrapezoidal, anterior corners and posterior margin well rounded, posterior corners sharp, length equal to 69-72% of maximum width, longitudinal profile initially gently convex backwards, then strongly convex towards posterior end, gently convex (tr.). Axis undifferentiated. One terrace ridge present along lateral margins, terminating before anterior margin, otherwise dorsal exoskeleton completely smooth. Articulating facet subtriangular, extending to just below axial furrow, six terrace lines converge upwards, border prominent. Inner margin of doublure discuspid, anterior-most

ridge follows path of inner margin, terrace lines slightly undulatory and transverse, medial depression wider anteriorly, narrows posteriorly, terminating just before posterior margin.

Remarks. *Bumastoides kimmswickensis* differs from other species found in the Kimmswick Limestone (*B*. *billingsi*, *B*. *holei*) in having one less thoracic segment, terrace lines covering the majority of the cranidium, and in the shape of the librigena. In all 8 MPTs *B*. *kimmswickensis* is the sister taxon of *B*. *beckeri* from the Maquoketa Formation of Iowa, united by their shared possession of terrace lines covering the cranidium. The details of the terrace lines are slightly different however, as *B*. *beckeri* retains transverse terrace lines between the lunettes, whereas in *B*. *kimmswickensis* they are very faint. The latter also has one fewer thoracic segment, a smoother pygidial exoskeleton, and generally more discontinuous terrace lines.

The smallest individuals of *B*. *kimmswickensis* (Figs. 22E-G; 23D, E) illustrate the range of morphological change in illaenid trilobites during holaspid ontogeny (Chatterton 1980; Ludvigsen & Chatterton 1980), observed in *Bumastoides* by Westrop & Ludvigsen (1983). In early holaspids, the lunettes are slightly narrower, the axial furrows are deeper, the terrace lines are stronger, and the glabella is less inflated. These changes are clear when viewing progressively larger specimens: Figs. 22A-C, x2.8; 23A-C, x4; 22E-G, x5; 23D, x6; 23E, x8. An ontogenetic interpretation of this variation is supported by the presence of only a single pygidium type (e.g., Fig. 22D) associated with *B*. *kimmswickensis* cranidia. As noted by Chatterton & Ludvigsen (2004), conservatism should be used when delineating new species of illaenids that change dramatically during holaspid ontogeny. In *Stenopareia grandis*, they found smaller individuals had stronger

terrace lines, a more forward genal angle, and a rounder pygidium. In agreement with Chatterton & Ludvigsen (2004) we find no larger specimens with similar morphology to the smaller individuals, and conclude that there is allometric shape change from early to late holaspids in this material. This issue is further complicated by the inability of FMC to detect discrete states in continuous shape changes in *Bumastoides*. Extreme caution should be used by workers attempting to identify new species of *Bumastoides* based on limited samples, minor differences in shape, or only with early holaspid material.

Bumastoides cf. **B**. ***milleri*** (Billings, 1859)

(Figs. 24-25)

Material. Figured material includes one mostly testate cranidium (OU 12521, Figs. 25A-B), three exfoliated cranidia (OU 12517, Fig. 24A; OU 12037, Figs. 24B-D; OU 12518, Fig. 24F) and four pygidia in different stages of exfoliation (OU 12039, Fig. 24G; OU 12519, Fig. 24E; OU 12520, Fig. 24H; OU 12522, Figs. 25C-E). Unfigured material includes a large number of partial pygidia and cranidia.

Occurrence. Upper Ordovician (Katian) of the Viola Springs Formation (Viola Group), Highway 99 section, near Fittstown, south-central Oklahoma (see Amati & Westrop 2006, figs 3 and 7).

Remarks. The Viola Springs material is nearly identical to *Bumastoides milleri* material from the Trenton. The pygidium is relatively short (sag.) and wide (tr.) with sharp posterior corners, the medial cranidial tubercle is circular and prominent, and the general shape of the cranidia is similar. Even given these similarities, we think it best to use open nomenclature on this material until a complete exoskeleton is discovered because the

number of thoracic segments is also an important diagnostic character of *Bumastoides* species.

Genus ***STENOPAREIA*** Holm, 1886

Remarks. Chatterton & Ludvigsen (1976) and Westrop & Ludvigsen (1983) both agreed that *S. aplatus* and *S. gardensis* should be moved out of *Bumastoides* based on the transverse anterior margin (semicircular) of the pygidium, and possibly based on the depth of the axial furrow. The results of our analysis support these claims, and also apply to *S. rivulus* (*S. globosus* had been revised previously by Westrop & Ludvigsen 1983). In *Bumastoides* the cranidial axial furrow is weakly incised and the glabella is not expressed by a change in slope of the glabella (in mature holaspids), whereas the opposite is true of *Stenopareia*. The latter also has a semicircular outline of the pygidium (character 12) and shorter length of the pygidial doublure (character 19). *Stenopareia* species also always retain residual expression of the pygidial axis (character 17), though in *Bumastoides*, some species (*B. billingsi*) still show some minor expression of axial furrow on the pygidium. So this character should be useful in diagnosing species of *Stenopariea*, but is of limited use in *Bumastoides*. The number of cusps on the inner margin of the pygidial doublure (character 10) is useful as a diagnostic character of *Bumastoides* (if *B. tricuspidatus* Edgecombe et al. 2006 is excluded from the genus) as all species with complete material are dicuspid, but is not likely to be useful in distinguishing between the two genera. The number of cusps is highly variable within *Stenopareia*, with anywhere from zero to two cusps claimed (e.g., compare *S. linnarssoni*, Jaaunsson 1954, fig 10F to *S. avus*, Jaaunsson 1954, fig. 10E.). As shown by Bruton & Owen (1988, p. 252), the original description of the *S. linnarssoni* doublure in Warburg (1925) was incorrect, and

it does have a single cusp. We think it is more likely these issues indicate the need for a systematic revision of *Stenopareia*, rather than demonstrating a wide variety of doublure morphologies within the genus.

Diagnoses are not provided for the species transferred provisionally to *Stenopareia*, as this is best done in a revision of *Stenopareia* that includes all nominal species. Curtis & Lane (1997) provided the most recent diagnosis of *Stenopareia*, but it is so vague that it does not exclude other species of Illaenidae: 'cephalon strongly convex longitudinally, pygidium smaller and flatter. Cranidial axial furrow shallow, only present behind shallow lateral muscle impression. Eyes small, and placed far back. Hypostome subquadrate with small triangular anterior wings. Thorax with 9 segments. Anterior sagittal margin of pygidial doublure modified, usually into cusps. Exoskeletal surface with terrace ridges; doublural surfaces with prominent terrace ridges'. This work provides criteria to distinguish between *Bumastoides* and *Stenopareia*, but the latter is still in need of a detailed revision.

"***Stenopareia***" ***aplatus*** (Raymond, 1925)

(Figs. 26C-F)

1925 *Bumastus aplatus* Raymond: 119, pl. 8, figs. 3-4.

1968 *Bumastoides aplatus* Shaw: 43, pl. 16, fig. 19; pl. 17, figs. 1-14.

Material. Figured material include one cranidium without librigena (holotype MCZ 101150, Figs. 26C-, E-F) and one complete pygidium (paratype MCZ 101151, Fig. 26D).

Occurrence. Middle Ordovician (Darriwilian) of the Day Point and Crown Point Formations (Chazy Group), Isle La Motte, Vermont, Champlain Valley of New York, and the lower Lenoir Limestone, Bluff City, Tennessee.

Remarks. Whittington (1954) questioned the placement of *Stenopareia aplatus* in *Bumastoides* based on the transverse anterior margin. Shaw (1968) stated that this assignment was fairly certain based on its flattened axis and pygidium, and smooth exoskeleton. We now know that many species of *Bumastoides* have highly sculptured surfaces, and that axial furrow of *S. aplatus* is incised much deeper than in species of *Bumastoides*.

"***Stenopareia***" ***gardensis*** (Shaw, 1968)

(Figs. 26G-J)

1968 *Bumastoides gardensis* Shaw; 44. Pl. 16, figs. 12-18.

Material. Figured material includes one exfoliated cranidium (holotype NYSM 12456, Figs. 26G, J) and one complete pygidium (paratype NYSM 12457, Figs. 26H-I).

Occurrence. Middle Ordovician (Darriwilian) of the Day Point Formation (Chazy Group), Isle La Motte, Vermont, Chazy and Valcour Island, New York.

Remarks. Shaw (1968) noted that the cranidium of *Stenopareia gardensis* was similar to *S. aplatus*. He also stated that the pygidial features (raised axis, low length to width ratio), besides the doublure, were more similar to *Nanillaenus* Jaanusson, 1954. Amati & Westrop (2004) synonymised *Thaleops* and *Nanillaenus* based on the presence of a long, high angle pygidial articulating facet. The facet of *S. gardensis* is not at a high enough angle to be placed in *Thaleops* as defined by Amati & Westrop (2004). Further, the cranidial morphology precludes the possibility that this material belongs to other *Thaleops* species in the Day Point Formation (*T. punctatus*, Raymond, 1905; *T. raymondi*, Shaw, 1968). We think these issues should be explored more, but provisionally

place *S. gardensis* in *Stenopareia* as was suggested by Chatterton & Ludvigsen (1976) and Westrop & Ludvigsen (1983).

"***Stenopareia***" ***rivulus*** (Ingham & Tripp, 1991)

(Figs. 26A-B)

1991 Bumastoides rivulus Ingham & Tripp: 42, figs. 10a-f.

Material. Figured material includes a damaged, exfoliated cranidium (holotype GLAHM A8302, Fig. 26B) and an exfoliated pygidium (paratype GLAHM A8313, Fig. 26A)

Occurrence. Upper Ordovician (Sandbian) of the Jubilation Member, Doularg Formation, (Albany Group), Girvan district, southwest Scotland.

Remarks. Ingham & Tripp (1991) were uncertain regarding their placement of *S. rivulus* in *Bumastoides*, and that hesitation seems correct, as both the pygidium and cranidium of this species more strongly resemble *Stenopareia*, and it was resolved outside the *Bumastoides* clade in all of the MPTs. The pygidium of *B. scoticus* (GLAHM A5860a, Tripp 1965, fig. 31a) is semicircular, with a narrow (sag.) doublure, strongly resembling *S. rivulus*. This species should also be placed in *Stenopareia* sensu lato.

Acknowledgements

This research was funded by NSF grant EAR-0819715 to S. Westrop and L. Amati. A. Thomas, K. Carlucci, and R. Burkhalter, assisted in fieldwork, and R. Burkhalter provided technical support in the lab. F. Read provided helpful locality information in Virginia. Loans of type material were arranged by P. Mayer at the Field Museum, Ed Landing at the New York State Museum, Neil Clark at the Hunterian Museum, Tiffany Adrain at the University of Iowa, Jessica Cundiff at the Museum of Comparative Zoology, Albert Kollar at the Carnegie Museum, and Jean Dougherty at the Geological

Survey of Canada. Thanks to Alan Owen and an anonymous reviewer for their insightful comments that greatly improved the manuscript.

References

2009 Helicon Focus 4.0.4 Pro Multiprocessor. Helicon Soft Ltd.

Akaike, H. 1974. A new look at the statistical model identification. *Automatic Control, IEEE Transactions*, **19**, 716-723.

Amati, L. & Westrop, S.R. 2004. A systematic revision of *Thaleops* (Trilobita: Illaenidae) with new species from the middle and late Ordovician of Oklahoma and New York. *Journal of Systematic Palaeontology*, **2**, 207-256.

Amati, L. & Westrop, S.R. 2006. Sedimentary facies and trilobite biofacies along an Ordovician shelf to basin gradient, Viola Group, South-Central Oklahoma. *PALAIOS*, **21**, 516-529.

Amsden, T.W. & Sweet, W.C. 1983 Upper Bromide Formation and Viola Group (Middle and Upper Ordovician) in Eastern Oklahoma. *Oklahoma Geological Survey Bulletin*, **132**, 1-76.

Billings, E. 1859. Descriptions of some new species of trilobites from the Lower and Middle Silurian rocks of Canada. *Canadian Naturalist & Geologist*, **4**, 367-383.

Bradley, J.H. 1925. Stratigraphy of the Kimmswick Limestone of Missouri and Illinois. *Journal of Geology*, **33**, 49-74.

Bradley, J.H. 1930. Fauna of the Kimmswick Limestone of Missouri and Illinois. *Walker Museum, University of Chicago Contributions*, **2**, 219-290.

Bremer, K. 1994. Branch support and tree stability. *Cladistics*, **10**, 295-304.

Brett, C.E., Whiteley, T.E., Allison, P.A. & Yochelson, E. 1999. The Walcott-Rust Quarry: a Middle Ordovician Konservat-Lagerstatten. *Journal of Paleontology*, **73**, 288-305.

Bruton, D.L. & Owen, A.W. 1988. The Norwegian Upper Ordovician illaenid trilobites. *Norsk Geologisk Tidsskrift*, **68**, 241-258.

Carlucci, J.R., Westrop, S. & Amati, L. 2010. Tetralichine trilobites from the Upper Ordovician of Oklahoma and Virginia, and phylogenetic systematics of the Tetralichini. *Journal of Paleontology*, **84**, 1099-1120.

Chatterton, B.D.E. & Ludvigsen, R. 1976. Silicified Middle Ordovician trilobites from the South Nahanni River area, District of Mackenzie, Canada. *Palaeontographica*, **154**, 1-106.

Chatterton, B.D.E. 1980. Ontogenetic studies of Middle Ordovician trilobites from the Esbataottine Formation, Mackenzie Mountains, Canada. *Palaeontographica Abt. A*, **171**, 1-74.

Chatterton, B.D.E. & Ludvigsen, R. 2004. Early Silurian trilobites of Anticosti Island, Quebec, Canada. *Palaeontographica Canadiana*, **22**, 1-264.

Clarke, J.M. 1897. The Lower Silurian trilobites of Minnesota. *Minnesota Geology and Natural History Survey*, **3**, 694-759.

Cooper, B.N. & Cooper, G.A. 1946. Lower Middle Ordovician stratigraphy of the Shenandoah Valley, Virginia. *Bulletin of the Geological Society of America*, **57**, 35-114.

Cooper, G.A. 1956. Early Middle Ordovician of the United States. Pp. 171-194 in M.G. Bassett (ed) *The Ordovician System*. University of Wales Press and National Museum of Wales.

Curtis, N.J. & Lane, P.D. 1997. The Llandovery trilobites of England and Wales, Part 1.

Monographs of the Palaeontographical Society, **605**, 1-50.

DeMott, L.L. 1987. Platteville and Decorah trilobites from Illinois and Wisconsin. Pp. 63-98 in R.E. Sloan, F.C. Shaw and R.P. Tripp (eds) *Minnesota Geological Survey, Report of Investigations* **35**, [edited by R.E Sloan, F.C. Shaw, and R.P. Tripp], 63-98.

DeQueiroz, K. & Gauthier, J. 1990. Phylogeny as a central principle in taxonomy: phylogenetic definitions of taxon names. *Systematic Zoology*, **39**, 307-322.

DeQueiroz, K. 2007. Toward an integrated system of clade names. *Systematic Biology*, **56**, 956-974.

Edgecombe, G.D., Banks, M.R. & Banks, D.M. 2006. *Bumastoides* (Trilobita: Illaenidae) from the Upper Ordovician of Tasmania. *Memoirs of the Association of Australasian Palaeontologists*, **32**, 375-381.

Emmons, E. 1842. *Geology of New York part II, comprising the survey of the second geological district*. W & A White & J. Visscher, Albany, 437 pp.

Fay, R.O., Graffham, A.A. & Sprinkle, J. 1982. Appendix: measured sections and collecting localities. Pp 335-369 in J. Sprinkle (ed) *Echinoderm faunas from the Bromide Formation (Middle Ordovician) of Oklahoma*. University of Kansas Paleontological Contributions Monograph.

Fisher, D.W. 1957. Mohawkian (Middle Ordovician) biostratigraphy of the Wells outlier, Hamilton County, New York. *New York State Museum Bulletin*, **359**, 1-33.

Foerste, A.F. 1920. The Kimmswick and Plattin Limestones of northeastern Missouri. *Denison University Bulletin, Journal of Scientific Laboratories*, **19**, 175-224.

Goloboff, P. 1993. Estimating character weights during tree search. *Cladistics*, **9**. 83-91.

Goloboff, P.A., Farris, J.S., Kallersjo, M., Oxelman, B., Ramirez, M.J. & Szumik, C.A. 2005. Improvements to resampling measures of group support. *Cladistics*, **19**, 324-332.

Goloboff, P.A., Mattoni, C.I. & Quinteros, A.S. 2006. Continuous characters analyzed as such. *Cladistics*, **22**, 589-601.

Goloboff, P., Farris, J. & Nixon, K. 2008. TNT, a free program for phylogenetic analysis. *Cladistics*, **24**, 774-786.

Harris, R.W. 1957. Ostracoda of the Simpson Group. *Oklahoma Geological Survey Bulletin*, **75**, 1-333.

Hawle, I. & Corda, A.J.C. 1847. *Prodrom einer monographie der bohmischen Trilobiten. Abhandlungen Koeniglichen Boehmischen Gesellschaft der Wissenschaften*. J.G Clave, Prague.

Holm, G. 1882. De Svenska artena af Trilobitslägtet *Illaenus* (Dalman). *Bihang till Konglungen Svenska Vetenskaps-Akademiens Handlingar*, **7**, 1-148.

Holm, G. 1886. Revision der ostbalischen silurschen Trilobiten, Abt. III, Illaeniden. *Mémoires de Impériale des Sciences de St Pétersbourg*, **33**(8), 1-173.

Hunda, B.R., Chatterton, B.D.E. & Ludvigsen, R. 2003. Silicified Late Ordovician trilobites from the Mackenzie Mountans Northwest Territories, Canada. *Palaeontographica Canadiana*, **21**, 1-87.

Ingham, J.K. & Tripp, R.P. 1991. The trilobite fauna of the Middle Ordovician Doularg Formation of the Girvan District, Scotland, and its paleoenvironmental significance. *Transactions of the Royal Society of Edinburgh: Earth Sciences*, **82**, 27-54.

Jaanusson, V. 1954. Zur Morphologie und Taxonomie der Illaeniden. *Arkiv För Mineralogie Och Geologi*, **1**, 545-583.

Jaanusson, V. 1959. Suborder Illaenina, Pp. O365-0415 in R.C. Moore (ed) *Treatise on Invertebrate Paleontology, Part O, Arthropoda I*. Geological Society of America and University of Kansas Press, Lawrence.

King, D.T. 1986. Waulsortian-type buildups and resedimented (carbonate-turbidite) facies, early Mississippian Burlington shelf, central Missouri. *Journal of Sedimentary Petrology*, **56**, 471-479.

Kobayashi, T. 1935. The Cambro-Ordovician formations and faunas of South Chosen. Palaeontology Part III. Cambrian faunas of South Chosen with special study on the Cambrian trilobite genera and families. *Journal of the faculty of science, Imperial University of Tokyo*, **4**, 49-344.

Kolata, D.R., Huff, W.D. & Bergström, S.M. 1998. Nature and regional significance of unconformities associated with the Middle Ordovician Hagan K-bentonite complex in the North American midcontinent. *Geological Society of America Bulletin*, **110**, 723-739.

Longman, M.W. 1982a. Depositional setting and regional characteristics. Pp. 6-10 in J. Sprinkle (ed) *Echinoderm Faunas from the Bromide Formation (Middle Ordovician) of Oklahoma*. The University of Kansas Paleontological Contributions, Monograph 1, Lawrence, Kansas, 360 pp.

Longman, M.W. 1982b. Depositional environments. Pp. 17-30 in J. Sprinkle (ed) *Echinoderm Faunas from the Bromide Formation (Middle Ordovician) of Oklahoma*. University of Kansas Paleontological Contributions, Monograph 1, Lawrence, Kansas, 360 pp.

Ludvigsen, R. 1979. *Fossils of Ontario part 1: The trilobites*. Royal Ontario Museum Life Sciences Miscellaneous Publications, Toronto, 96 pp.

Ludvigsen, R. & Chatterton, B.D.E. 1980. The ontogeny of *Failleana* and the origin of the Bumastinae (Trilobita). *Geological Magazine*, **117**, 471-478.

Maddison, D. & Maddison, W. 2005. MacClade: Analysis of Phylogeny and Character Evolution *4.08*. Sinauer Associates Inc, Sunderland, MA.

Murchison, R.I. 1839. *The Silurian System*. John Murray, London, 768 pp.

Raymond, P.E. 1905. Trilobites of the Chazy Limestone. *Annals of the Carnegie Museum*, **3**, 328-396.

Raymond, P.E. 1913. Notes on some new and old trilobites in the Victoria memorial Museum. *Bulletin of the Victoria Memorial Museum, Geological Survey of Canada*, **1**, 33-39.

Raymond, P.E. 1916. New and old Silurian trilobites from southeastern Wisconsin, with notes on the genera of the Illaenidae. *Harvard College Museum of Comparative Zoology Bulletin*, **60**(1), 1-41.

Raymond, P.E. 1925. Some trilobites of the lower Middle Ordovician of eastern North America. *Bulletin of the Museum of Comparative Zoology*, **67**, 1-180.

Raymond, P.E. & Narraway, J.E. 1908. Notes on Ordovician trilobites: Illaenidae from the Black River Limestone near Ottawa, Canada. *Annals of the Carnegie Museum*, **4**, 242-255.

Read, J.F. 1982. Geometry, facies, and development of Middle Ordovician carbonate buildups, Virginia Appalachians. *AAPG Bulletin*, **66**, 189-209.

Read, J.F. 1998. Phanerozoic carbonate ramps from greenhouse, transitional and ice-house worlds: clues from field and modeling studies. Pp. 107-135 in V.P. Wright and T.P. Burchette (eds) *Carbonate Ramps*. Geological Society of London Special Publications 149.

Ruppel, S. & Walker, K. 1977. The ecostratigraphy of the Middle Ordovician of the Southern Appalachians (Kentucky, Tennessee, and Virginia), U.S.A: A field excursion. *Studies in Geology, University of Tennessee Department of Geological Sciences*, **77-1**, 1-171.

Sabol, J.W. 1958. *Geology of the Porterfield Quarry area, Smyth County, Virginia*. Virginia Polytechnic Institute, 81 pp.

Shaw, F.C. 1968. Early Middle Ordovician Chazy trilobites of New York. *New York State Museum and Science Services Memoir*, **17**, 1-163.

Shaw, F. 1974. Simpson Group (Middle Ordovician) Trilobites of Oklahoma. *Journal of Paleontology Memoir*, **48**(6), 1-54.

Sheets, H.D. 2003. FMCBox-Finite Mixture Coding of continuous morphological characters. http://www3.canisius.edu/~sheets/moremorph.html.

Slocom, A.W. 1913. New trilobites from the Maquoketa beds of Fayette County, Iowa. *Field Museum of Natural History Geological Series*, **4**, 43-83.

Strait, D., Moniz, M. & Strait, P. 1996. Finite Mixture Coding: A new approach to coding continuous characters. *Systematic Biology*, **45**, 67-78.

Strong, E.E. & Lipscomb, D. 1999. Character coding and inapplicable data. *Cladistics*, **15**, 363-371.

Swofford, D.L. 2002. PAUP* Phylogentic Analysis Using Parsimony (*and other methods) *Version 4.0b10*. Sinauer Associates, Sunderland, MA.

Templeton, J.S. & Willman, H.R. 1963. Champlainian Series (Middle Ordovician) in Illinois. *Illinois State Geological Survey Bulletin*, **89**, 1-259.

Tripp, R.P. 1965. Trilobites from the Albany Division (Ordovician) of the Girvan District,

Ayrishire. *Palaeontology*, **8**, 577-603.

Tripp, R.P. 1980. Trilobites from the Ordovician Ardwell Group of the Craighead Inlier, Girvan district, Scotland. *Transactions of the Royal Society of Edinburgh: Earth Sciences*, **71**, 147-157.

Troedsson, G.T. 1928. On the Middle and Upper Ordovician faunas of northern Greenland, part II. *Meddelelser om Grønland*, **72**, 1-198.

Ulrich, E.O. 1911. Revision of the Paleozoic systems. *Geological Society of America Bulletin*, **22**, 281-680.

Walch, J.E.I. 1771. *Die Naturgeschichte der Versteinerungen, Dritter Theil. Zur Erläuterung der Knorrischen Sammlung von Merkwürdigkeiten der Natur*. P.J. FelBecker, Nürnberg, 235 pp.

Walcott, C.D. 1877. Descriptions of new species of fossils from the Chazy and Trenton Limestones. *Annual Report New York State Museum of Natural History*, **31**, 68-71.

Walter, O.T. 1927. Trilobites of Iowa and some related Paleozoic forms. *Iowa Geological Survey Annual Reports 1923 and 1924*, **31**, 1-388.

Warburg, E. 1925. The trilobites of the Leptaena Limestone in Dalarne. *Bulletin of the Geologic Institute of the University of Upsala*, **27**, 1-446.

Westrop, S.R. & Ludvigsen, R. 1983. Systematics and Paleoecology of Upper Ordovician Trilobites from the Selkirk Member of the Red River Formation, Southern Manitoba. *Manitoba Department of Energy and Mines Geological Report*, **GR 82-2**, 1-51.

Whiteley, T., Kloc, G. & Brett, C. 2002. *Trilobites of New York*. Cornell University Press, Ithaca and London, 203 pp.

Whittington, H.B. 1954. Ordovician trilobites from Stilliman's Fossil Mount. *Geological*

Society of America Memoir, **62**, 119-149.

Whittington, H.B. 1997a. Illaenidae (Trilobita): Morphology of thorax, classification, and mode of life. *Journal of Paleontology*, **71**. 878-896.

Whittington, H.B. 1997b. Morphology of the exoskeleton in R.L. Kaesler (ed) *Treatise on Invertebrate Paleontology, Pt. O, Arthropoda 1. Trilobita (revised). Volume 1. Introduction, Order Agnostida, Order Redlichiida.* Geological Society of America and University of Kansas, Lawrence.

Wilson, A.E. 1947. Trilobita of the Ottawa Formation of the Ottawa-St. Lawrence lowland. *Canada Department of Mines and Resources, Geological Survey Bulletin*, **9**, 1-86.

Figure 1. **A**, Oklahoma locality map, 177, 34.405 lat, 96.950 long, UTM NAD27 14S 0688414, 3808808, Daube (Johnston) Ranch (DRa), 34.377 lat, 97.321 long, UTM NAD27 14S 0654400, 380508085, coordinates for Tyson's Quarry (TQ) are withheld at request of the quarry owner. **B**, Missouri locality map, Hwy M, 38.359 lat, 90.465 long, UTM NAD27 15S 0721533 4248502. VA localities are not shown, as they have been illustrated elsewhere (Read 1982, fig. 1; Carlucci et al. 2010, fig. 3-2). The coordinates for I-77 are 37.745 lat, 79.513 long, UTM NAD27 17S 630905, 4178443, PQ is 36.878 lat, 81.681 long, UTM NAD27 17S 439250, 4081420.

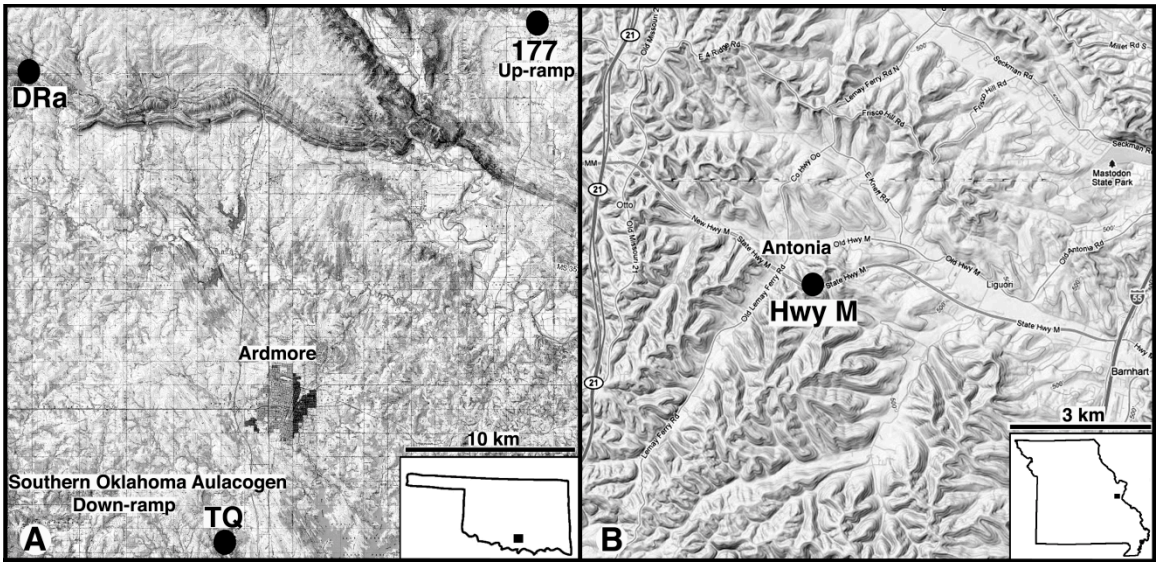
177
Up-ramp
DRa
Ardmore
10 km
Southern Oklahoma Aulacogen
Down-ramp
TQ
A
Antonia
Hwy M
Mastodon
State Park
Ottol
Liguon
Barnhart
3 km
B

Figure 2. Stratigraphic section of the 177 locality showing the upper Mountain Lake and Pooleville Members (lower Mountain Lake not shown) of the Bromide Formation. Arrows denote collection levels. Question mark (?) indicates uncertainty associated with the continuity of the shale. Key to abbreviations: ms = mudstone, ws = wackestone, ps = packstone, gs = grainstone, rs = rudstone.

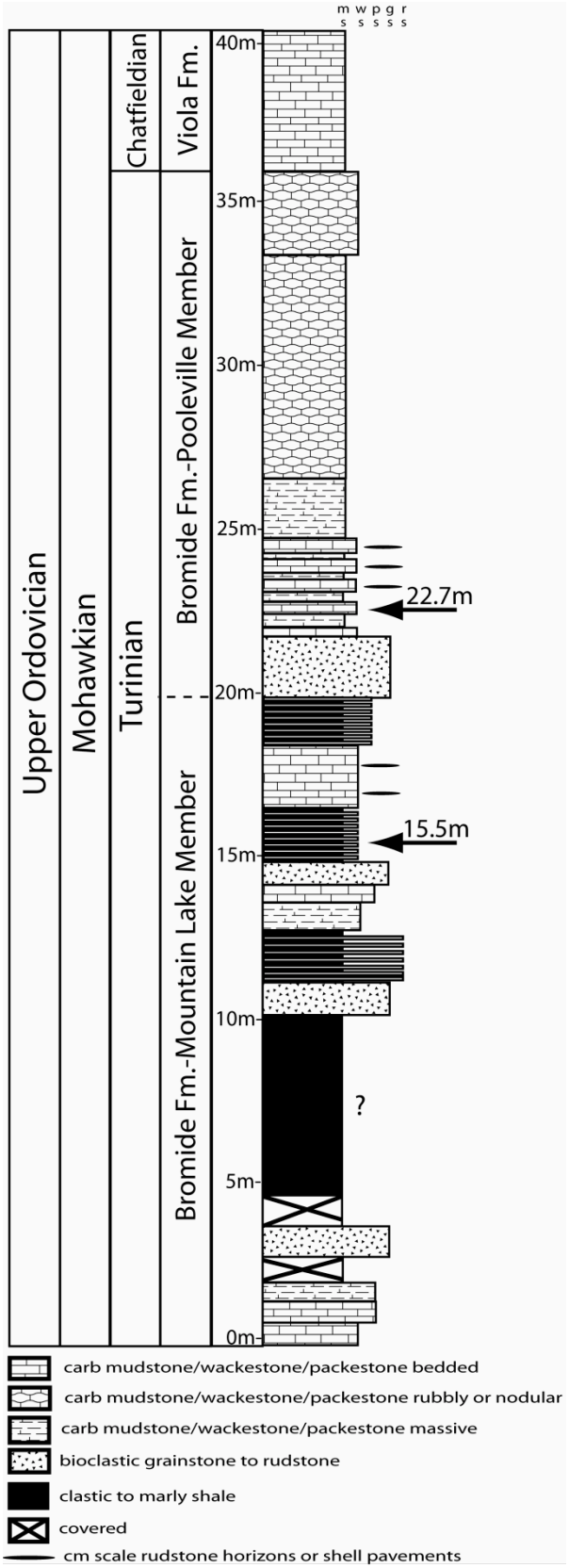
m w p g r
s s s s s
Upper Ordovician
Mohawkian
Chatfieldian
Viola Fm.
Turinian
Bromide Fm.-Pooleville Member
Bromide Fm.-Mountain Lake Member
40m
35m
30m
25m
20m
15m
10m
5m
0m
22.7m
15.5m
?
carb mudstone/wackestone/packestone bedded
carb mudstone/wackestone/packestone rubbly or nodular
carb mudstone/wackestone/packestone massive
bioclastic grainstone to rudstone
clastic to marly shale
covered
cm scale rudstone horizons or shell pavements

Figure 3. **A**-**G**, Results of the Finite Mixture Coding (FMC). Each model number refers to the number of normal distributions being evaluated (e.g., model one is one normal distribution). The relative AIC score is the goodness of fit of that model using Aikake Information Criterion (Akaike 1974). The weight is the probability of that model being correct relative to the other models. The x-axis is the percentile result of that ratio character; the y-axis is the number of taxa. The program FMCBox (Sheets 2003) was used for all calculations. See text for explanation of the characters.

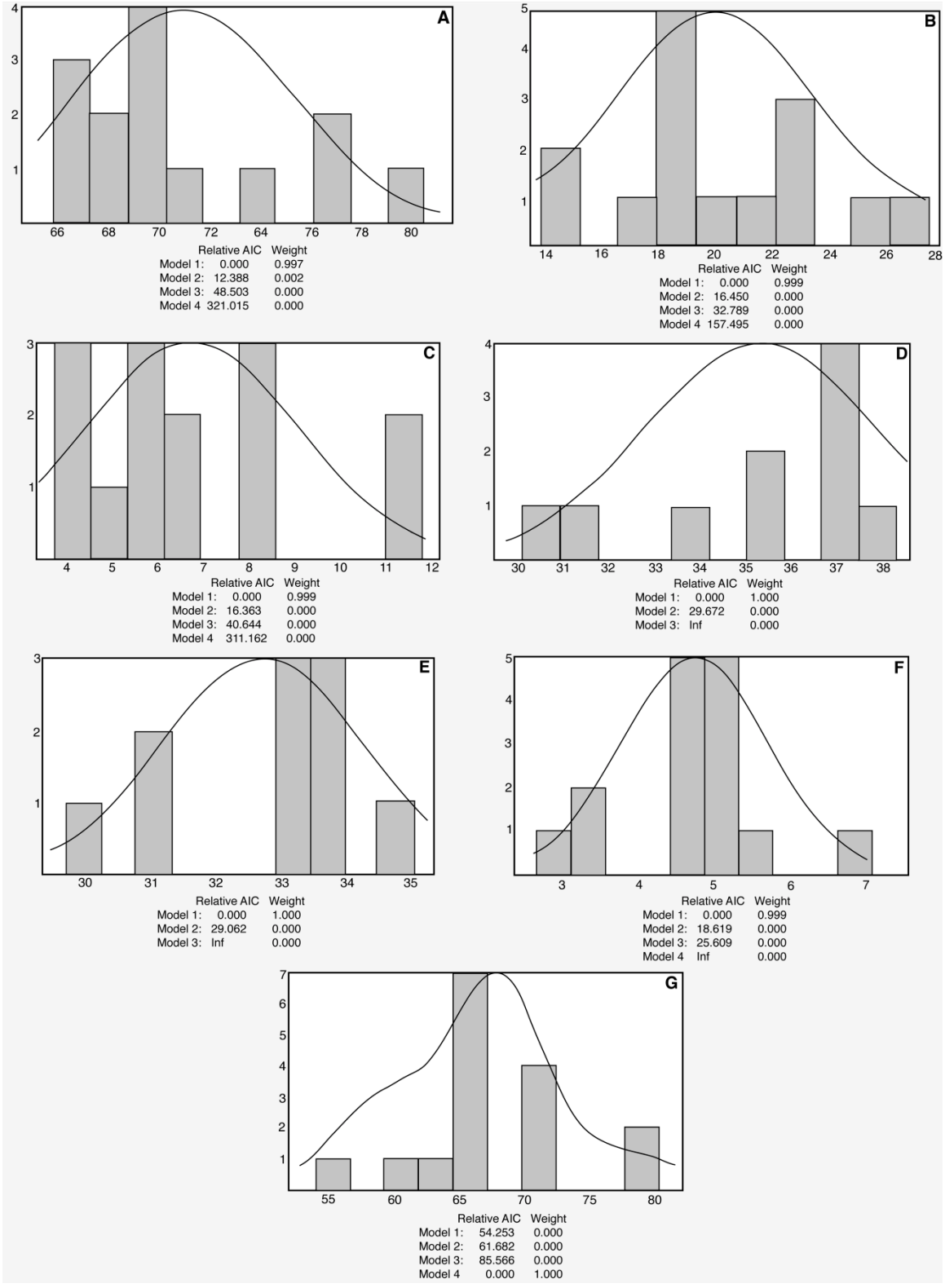
A
Relative AIC Weight
Model 1: 0.000 0.997
Model 2: 12.388 0.002
Model 3: 48.503 0.000
Model 4 321.015 0.000
B
Relative AIC Weight
Model 1: 0.000 0.999
Model 2: 16.450 0.000
Model 3: 32.789 0.000
Model 4 157.495 0.000
C
Relative AIC Weight
Model 1: 0.000 0.999
Model 2: 16.363 0.000
Model 3: 40.644 0.000
Model 4 311.162 0.000
D
Relative AIC Weight
Model 1: 0.000 1.000
Model 2: 29.672 0.000
Model 3: Inf 0.000
E
Relative AIC Weight
Model 1: 0.000 1.000
Model 2: 29.062 0.000
Model 3: Inf 0.000
F
Relative AIC Weight
Model 1: 0.000 0.999
Model 2: 18.619 0.000
Model 3: 25.609 0.000
Model 4 Inf 0.000
G
Relative AIC Weight
Model 1: 54.253 0.000
Model 2: 61.682 0.000
Model 3: 85.566 0.000
Model 4 0.000 1.000

Figure 4. Strict consensus tree of the eight MPTs retained from the first parsimony analysis, with recommended taxonomy of *Bumastoides*. *B*. *rivulus*, *B*. *aplatus*, and *B*. *gardensis* are here placed in *Stenopareia* sensu lato. Tree length is 56 steps, CI is 0.57, RI is 0.69, and RC is 0.40. The first number displayed on the top of branches is the symmetric resampling support value for the successive node; the second number is the GC value. The numbers on the bottom of the branches are the Bremer Support (if greater than one) value for the successive node. Nodes are numbered for easy reference within the text.

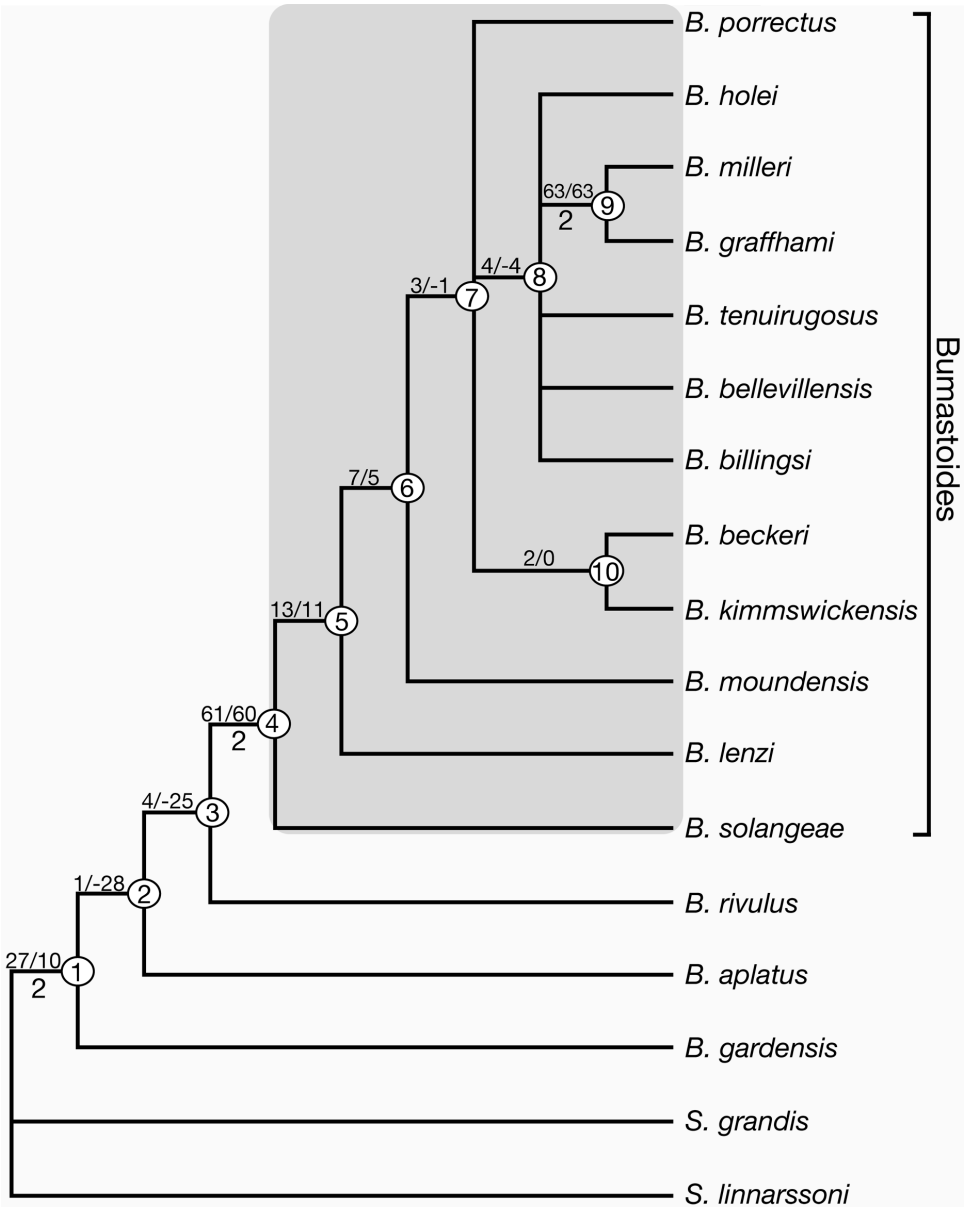
B. porrectus
B. holei
B. milleri
B. graffhami
B. tenuirugosus
B. bellevillensis
B. billingsi
B. beckeri
B. kimmswickensis
B. moundensis
B. lenzi
B. solangeae
B. rivulus
B. aplatus
B. gardensis
S. grandis
S. linnarssoni
Bumastoides
27/10
2
1
1/-28
2
4/-25
3
61/60
2
4
13/11
5
7/5
6
3/-1
7
4/-4
8
63/63
2
9
2/0
10

Figure 5. **A,** Optimized character distribution showing character states that change unambiguously on one of the eight MPTs from the first analysis. Black circles show synapomorphic character states, and white circles indicate homoplastic character states. Optimization was performed in PAUP* version 4.0b10 (Swofford 2002), and checked in TNT (Goloboff et al. 2008). **B**, The best tree found from a second parsimony analysis (implicit enumeration in TNT) that treated continuous characters as such. Implied weighting with a concavity constant (k) of three scaled characters contributions to branch length. The first number displayed to the left of branches is the symmetric resampling support value for the successive node; the second number is the GC value. Best-fit value is 8.47, CI is 0.53, RI is 0.62, and RC is 0.33 (excluding continuous data).

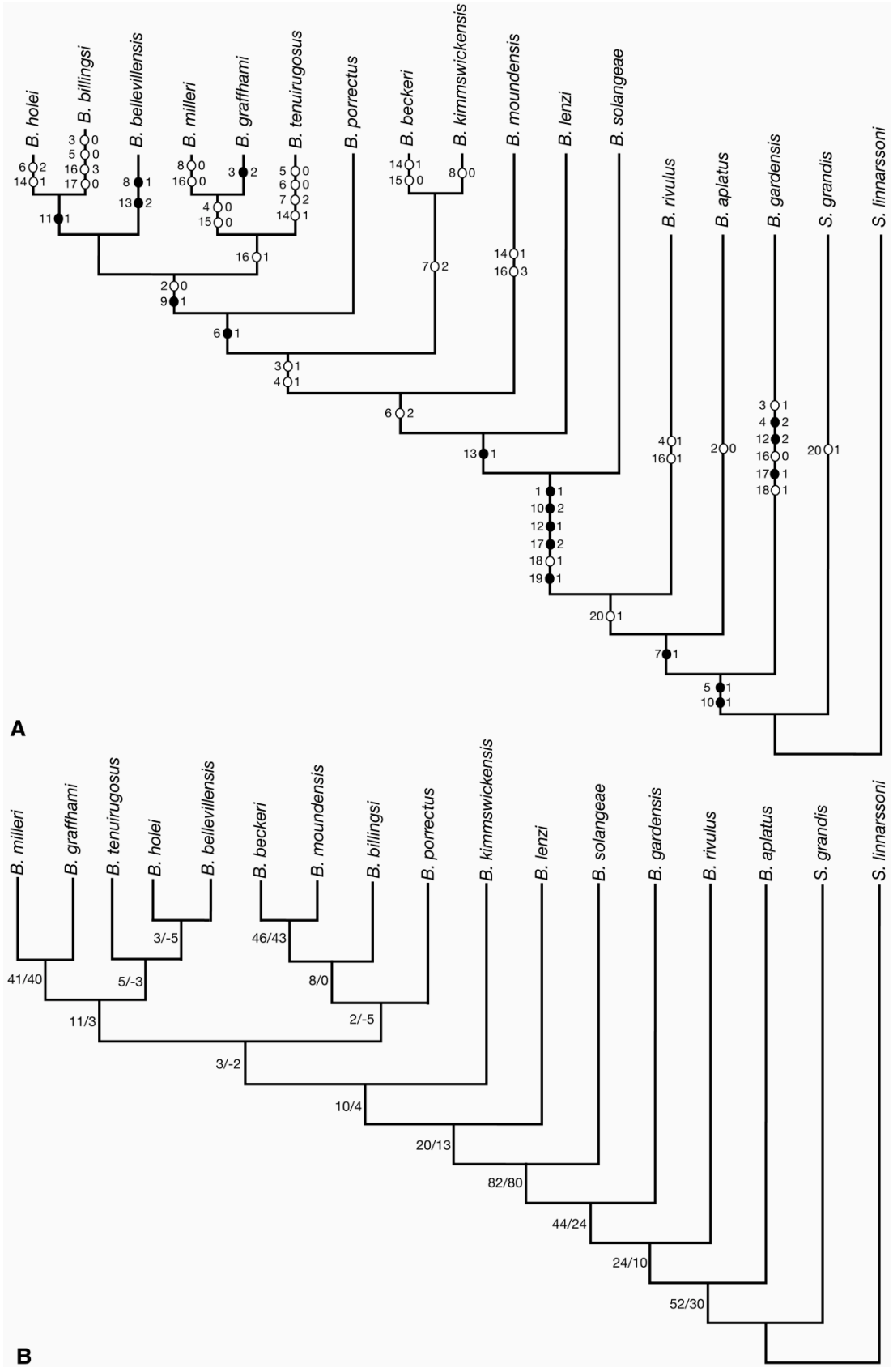
B. holei
B. billingsi
B. bellevillensis
B. milleri
B. graffhami
B. tenuirugosus
B. porrectus
B. beckeri
B. kimmswickensis
B. moundensis
B. lenzi
B. solangeae
B. rivulus
B. aplatus
B. gardensis
S. grandis
S. linnarssoni
A
B. milleri
B. graffhami
B. tenuirugosus
B. holei
B. bellevillensis
B. beckeri
B. moundensis
B. billingsi
B. porrectus
B. kimmswickensis
B. lenzi
B. solangeae
B. gardensis
B. rivulus
B. aplatus
S. grandis
S. linnarssoni
3/-5
46/43
41/40
5/-3
8/0
11/3
2/-5
3/-2
10/4
20/13
82/80
44/24
24/10
52/30
B

Figure 6. *Bumastoides milleri* (Billings, 1859). **A-D**, Upper Ordovician Selby Formation, near Ottawa, Ontario; **E-G**, Upper Ordovician Trenton Group of Herkimer County, New York. **A-D**, holotype, exfoliated dorsal exoskeleton (GSC 1319b), x 3 (Billings 1859, p. 375, fig. 10): **A**, dorsal view; **B**, posterior view; **C**, lateral view; **D**, anterior view. **E-G**, testate cranidium (MCZ 145734), x 3.5: **E**, lateral view; **F**, dorsal view; **G**, anterior views.

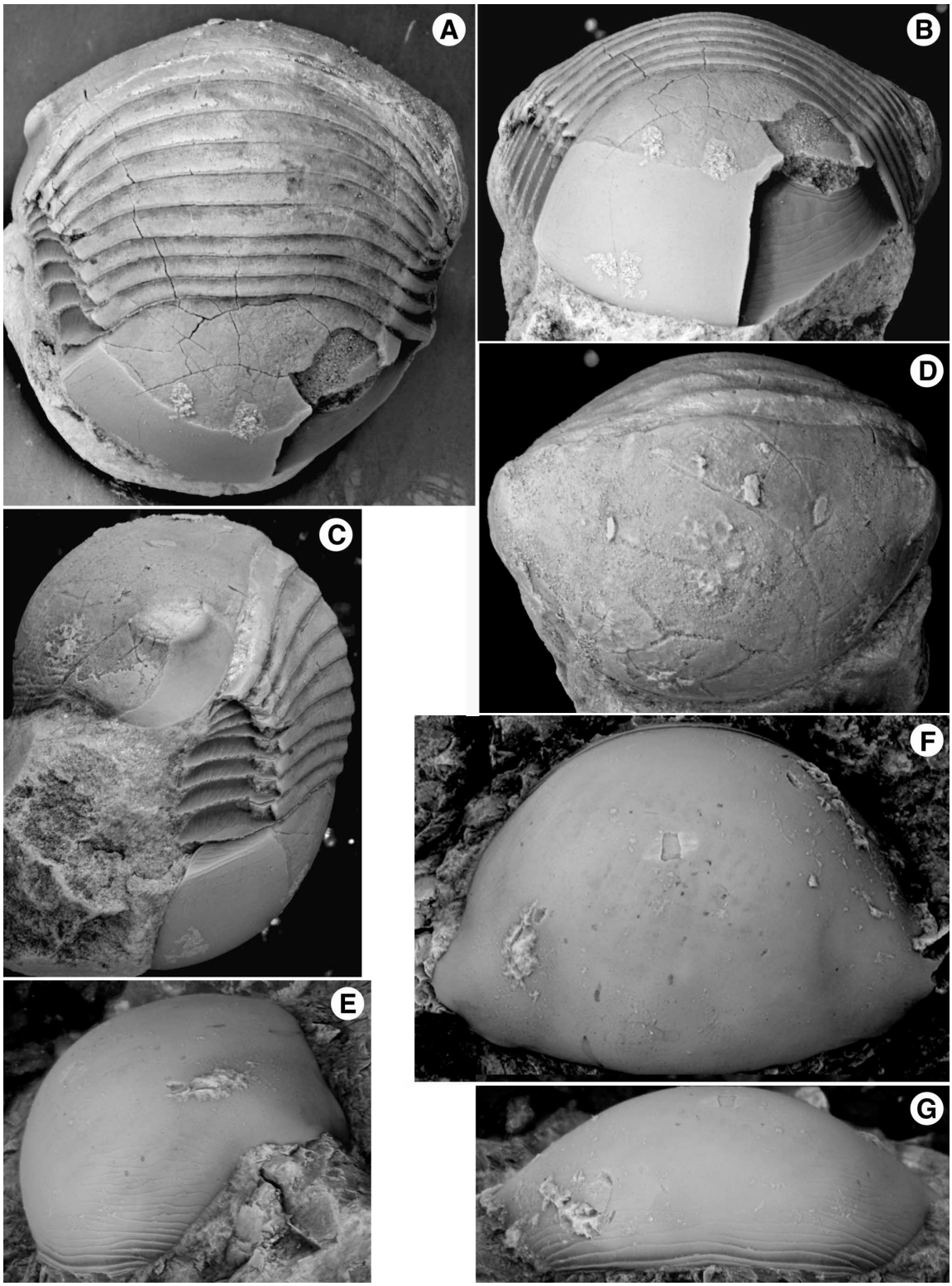
A
B
C
D
E
F
G

Figure 7. *Bumastoides milleri* (Billings, 1859) (**A-B**, **E**, **G** revised from *Bumastus trentonensis*). **A-B**, **E**, **G**, Upper Ordovician "Rockland Formation" (Trenton Group), of Hamilton County, New York; **C**, **G**, Upper Ordovician Maquoketa Formation of Iowa; **D**, **H**, Upper Ordovician Platteville Formation of Iowa. **A-B**, **E**, **F**, exfoliated, partial dorsal exoskeleton (NYSM 10757), x 1.8 (Fisher 1957, pl. 16, fig. 9): **A**, dorsal view; **B**, cranidial dorsal view; **E**, lateral view; **F** anterior view. **C**, **G**, dorsal exoskeleton (SUI 125988), x 3: **C**, lateral view; **G**, dorsal view. **D**, **H,** partially exfoliated, dorsal exoskeleton, (SUI 125975), x 1.2: **D**, lateral view; **H**, dorsal view.

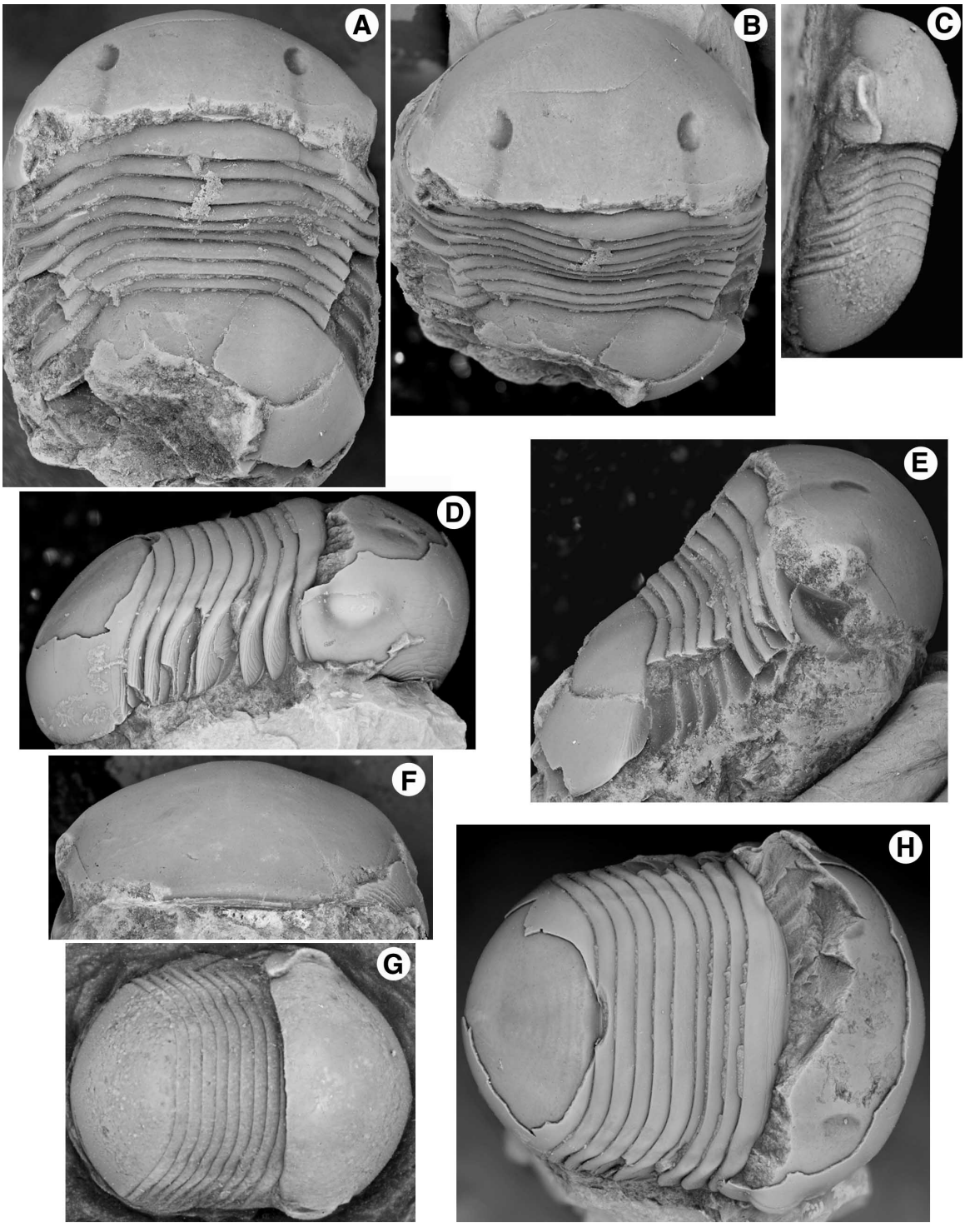
A
B
C
D
E
F
G
H

Figure 8. *Bumastoides billingsi* (Raymond & Narraway, 1908), Upper Ordovician Trenton Group, Hull Quebec. **A**-**E**, plastotype, exfoliated dorsal exoskeleton **(**CM 5472), x .95 (Raymond & Narraway 1908, pl. 62, figs. 1-2): **A**, lateral view; **B**, dorsal view; **C**, oblique lateral view; **D**, anterior view; **E**, cranidial dorsal view.

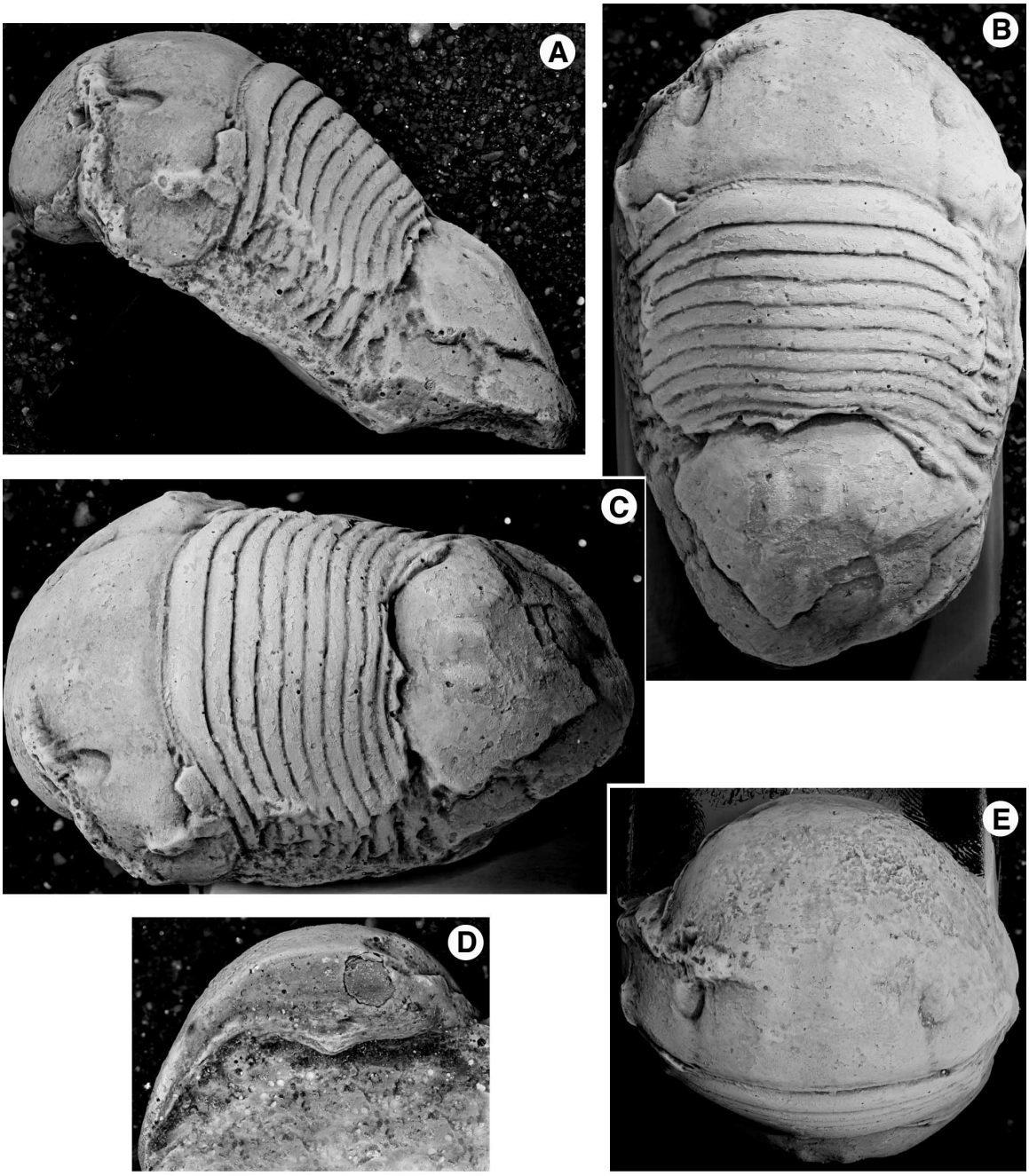
A
B
C
D
E

Figure 9. *Bumastoides billingsi* (Raymond & Narraway, 1908). **A-C**, Upper Ordovician Kimmswick Limestone of Batchtown, Illinois; **D-I**, Kimmswick Limestone of Glen Park, Missouri. **A-C**, exfoliated cranidium **(**UC 20700), x 1.5 (Bradley 1930, pl. 28, fig. 1): **A**, dorsal view; **B**, anterior view; **C**, lateral view. **D-E**, exfoliated pygidium (UC20710a), x 1.5 (Bradley 1930, pl. 28, fig. 2): **D**, posterior view; **E**, dorsal view. **G**, **H**, exfoliated pygidium **(**UC 20710b), x 1.6 (Bradley 1930, pl. 28, fig. 3): **G**, lateral view; **H**, dorsal view. **F**, **I-J** exfoliated dorsal exoskeleton **(**UC 10776), x 1.4 (Bradley, 1930, pl. 28, figs. 6-7): **F**, lateral view; **I**, dorsal view; **J**, anterior view.

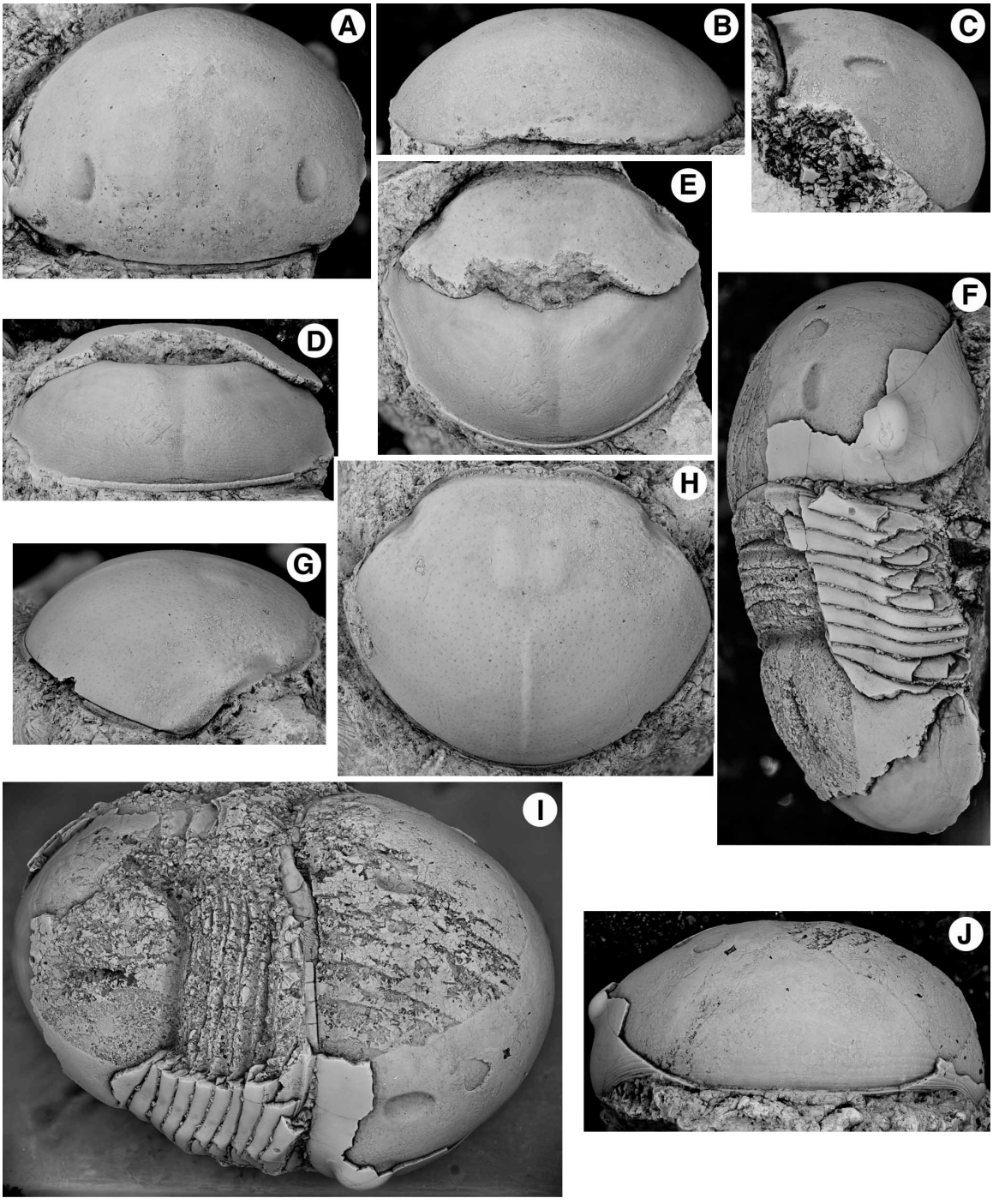
A
B
C
E
F
D
H
G
I
J

Figure 10. *Bumastoides bellevillensis* (Raymond & Narraway, 1908), Upper Ordovician Verulam Formation (Trenton Group), Belleville Ontario. **A**-**E**, holotype, partially exfoliated dorsal exoskeleton (CM 1900), x 2.6 (Raymond & Narraway 1908, pl. 61, figs. 6-7): **A**, cranidial dorsal view; **B**, anterior view; **C**, dorsal view; **D**, lateral view; **E**, posterior view.

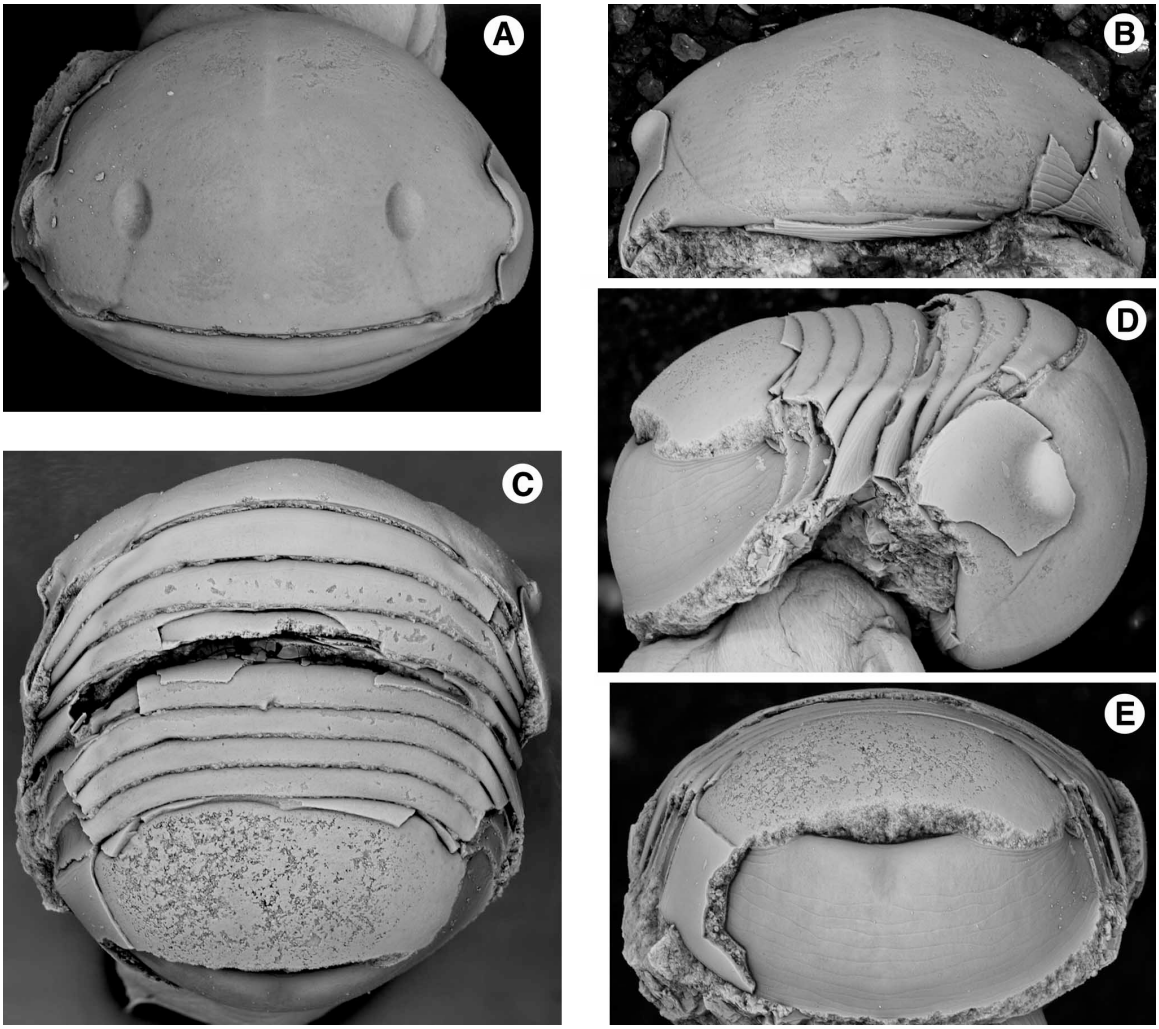
A
B
C
D
E

Figure 11. *Bumastoides beckeri* (Slocom, 1913), Upper Ordovician Maquoketa Formation, Fayette County, Iowa. **A**-**E**, holotype, enrolled dorsal exoskeleton (UC 41154), x 1.4 (Slocom 1913, pl. 14, figs. 1-3): **A**, cranidial dorsal view; **B**, dorsal view; **C**, anterior view; **D**, lateral view; **E**, posterior view. **F**-**H**, thoracopygon (P16708), x 1.6, (Slocom 1913, pl. 14, fig. 4): **F**, dorsal view; **G**, lateral view; **H**, posterior view.

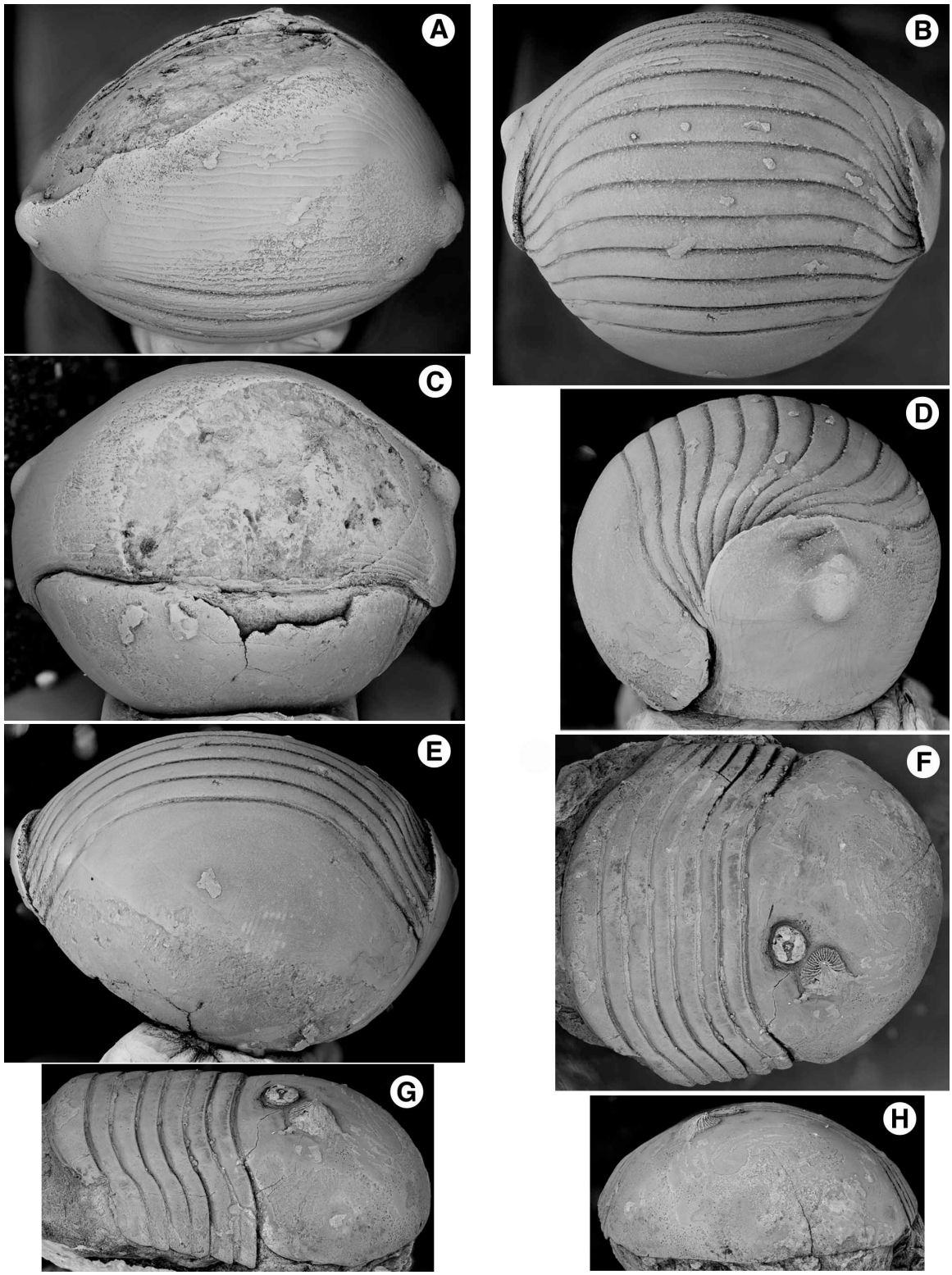
A
B
C
D
E
F
G
H

Figure 12. *Bumastoides beckeri* (Slocom, 1913), Upper Ordovician Maquoketa Formation, Fayette County, Iowa. **A**-**F**, dorsal exoskeleton (SUI 125973), x .85: **A**, anterior view; **B**, cranidial dorsal view; **C**, oblique lateral view; **D**, dorsal view; **E**, lateral view; **F**, posterior view. **G**-**H**, partially exfoliated dorsal exoskeleton (SUI 125984), x .85: **G**, lateral view; **H**, dorsal view.

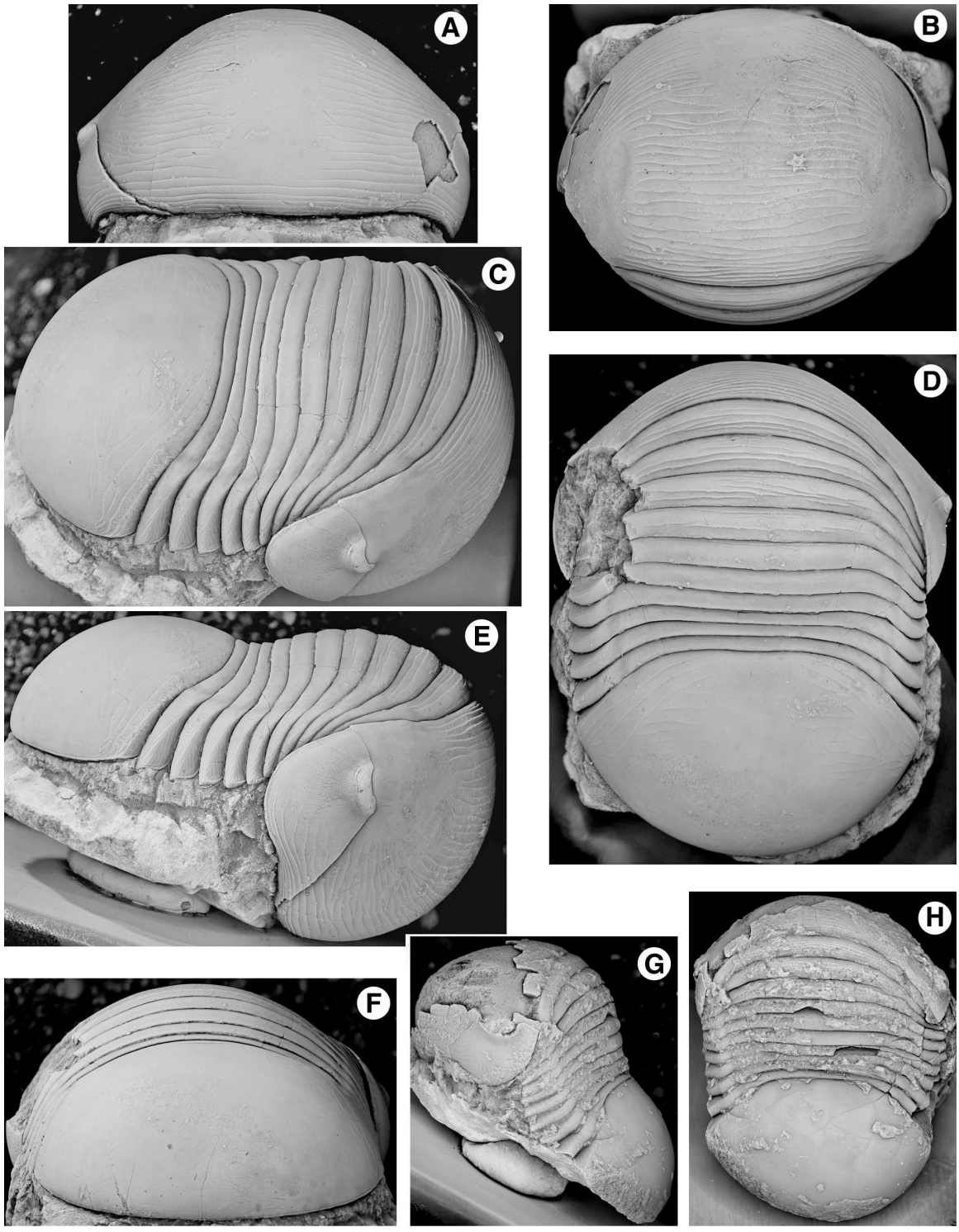
A
B
C
D
E
F
G
H

Figure 13. *Bumastoides holei* (Foerste, 1920), Upper Ordovician Rust Formation (Trenton Group) of Trenton Falls, Oneida County, New York. **A**-**D**, plesiotype, exfoliated dorsal exoskeleton **(**MCZ 101148), x 1.2 (Raymond 1925, pl. 8, figs. 5, 6, intentionally exfoliated since the Raymond illustrations?): **A**, oblique lateral view; **B**, lateral view; **C**, dorsal view; **D**, anterior view. **E**-**F**, partially exfoliated dorsal exoskeleton (MCZ 144798), x 1.5: **E**, dorsal view; **F**, lateral view.

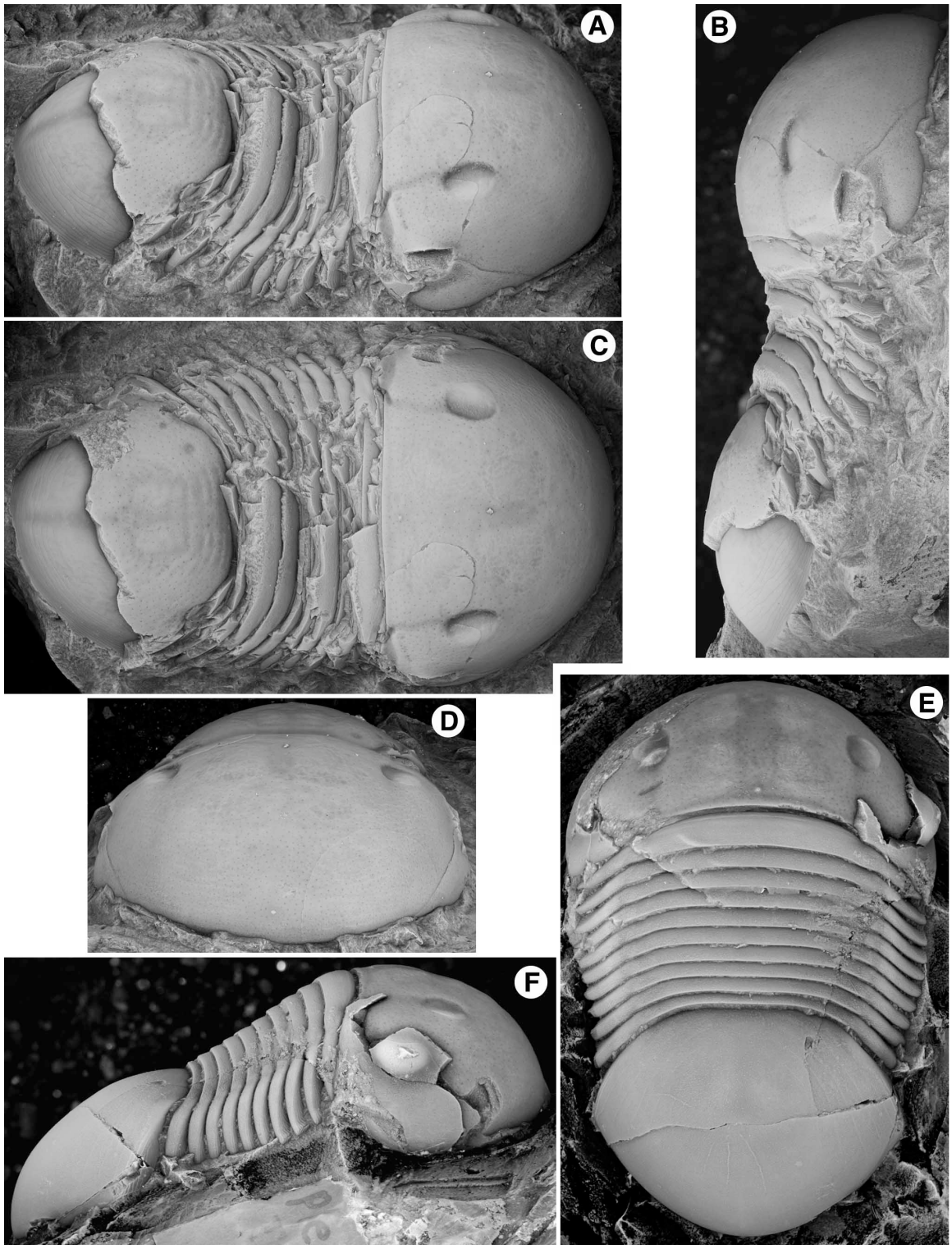
A
B
C
D
E
F

Figure 14. *Bumastoides holei* (Foerste, 1920), Upper Ordovician Rust Formation (Trenton Group) of Trenton Falls, Oneida County, New York. **A**-**C**, partially exfoliated dorsal exoskeleton (MCZ 144798), x 1.5: **A**, posterior view; **B**, oblique lateral view; **C**, anterior view. **D**-**H**, dorsal exoskeleton (MCZ 115909), x 1.5 (Brett et al. 1999, pl. 7, fig. 4): **D**, dorsal view; **E**, oblique lateral view; **F**, lateral view; **G**, posterior view; **H**, cranidial dorsal view.

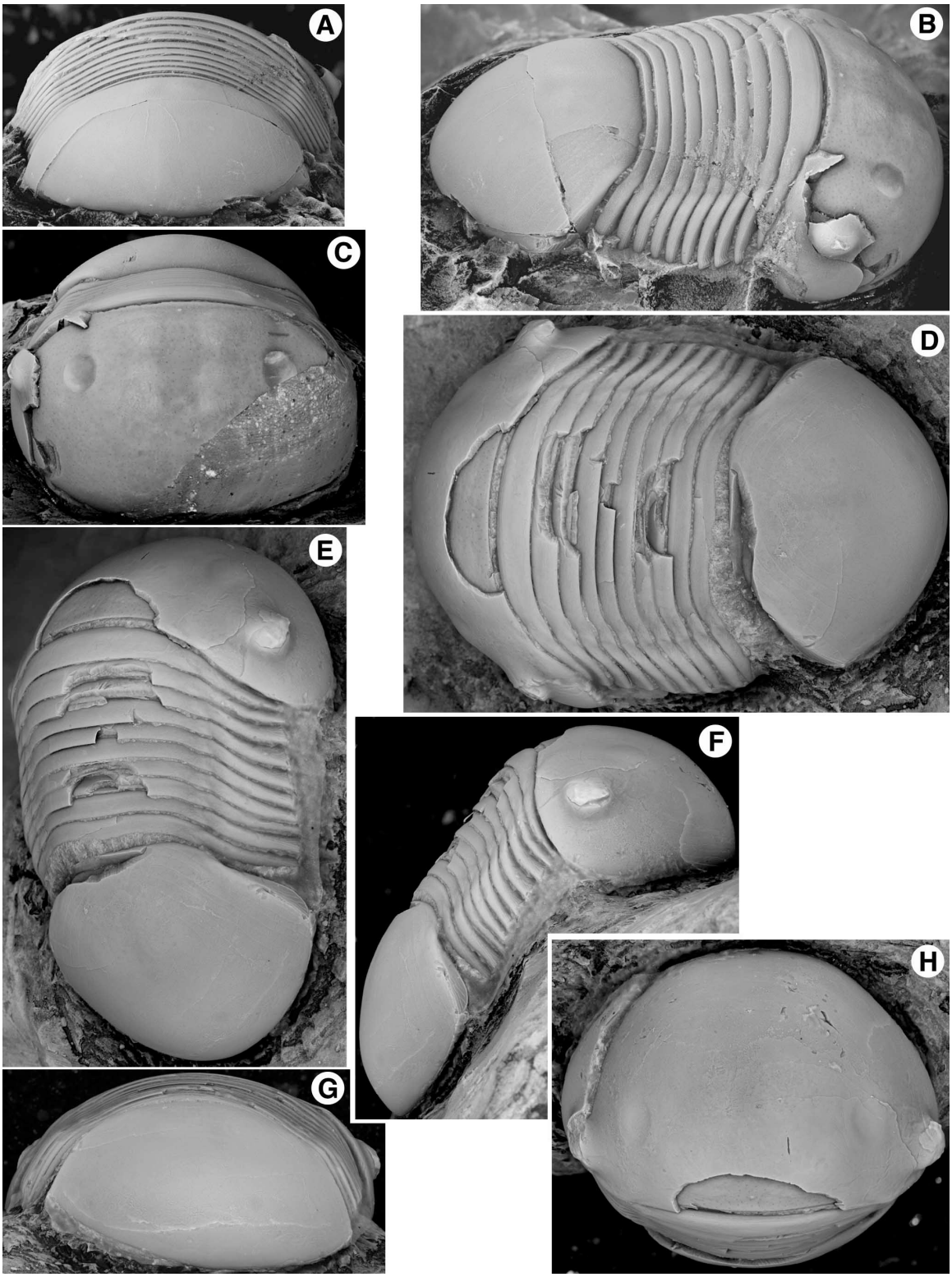
A
B
C
D
E
F
G
H

Figure 15. **A-F**, *Bumastoides porrectus* (Raymond, 1925). **A**-**B**, **D**-**F**, Upper Ordovician Denley Formation (Trenton Group) of Trenton Falls, Oneida County, New York; **C**, **H** from the Upper Ordovician Guttenberg Formation (Decorah Group), of Guttenberg and McGregor, Iowa and Fennimore West, Wisconsin. **A**-**B**, **D**-**F**, holotype, dorsal exoskeleton (MCZ 101147), x 2.5 (Raymond 1925, pl. 8, figs. 7, 8): **A**, dorsal view; **B**, oblique lateral view; **D**, lateral view; **E**, anterior view; **F**, posterior view. **C**, testate cranidium (MCZ 107234), x 2.6, dorsal view (DeMott 1987, pl. 6, figs. 24-26). **H**, exfoliated cranidium (MCZ 107235), x 3, dorsal view (DeMott 1987, pl. 6, figs. 27-28). **G**, *Bumastoides* cf. *B*. *porrectus* (Raymond, 1925), Upper Ordovician Guttenberg Formation (Decorah Group), partially exfoliated pygidium (MCZ 107236), x 2.6, dorsal view (DeMott 1987, pl. 6, figs. 29-31).

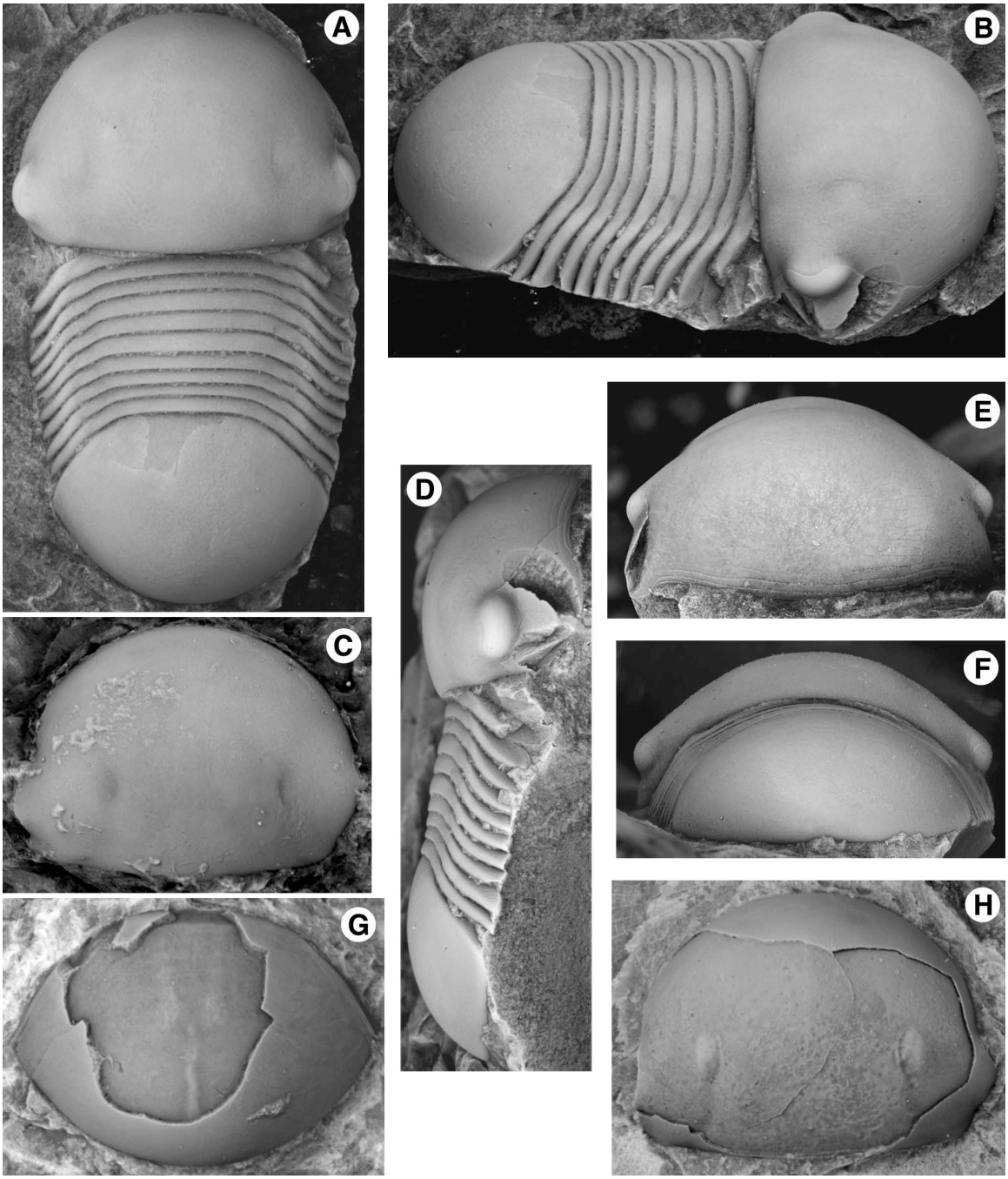
A
B
C
D
E
F
G
H

Figure 16. *Bumastoides porrectus* Raymond, 1925 (originally identified by Clarke 1897, fig. 32 as *Bumastus trentonensis*), Upper Ordovician Trenton Group of Trenton Falls, Oneida County, New York. **A-E**, dorsal exoskeleton **(**NYSM 4158), x 2 (Clarke 1897, fig. 32): **A**, anterior view; **B**, posterior view; **C**, dorsal view; **D**, oblique lateral view; **E**, lateral view.

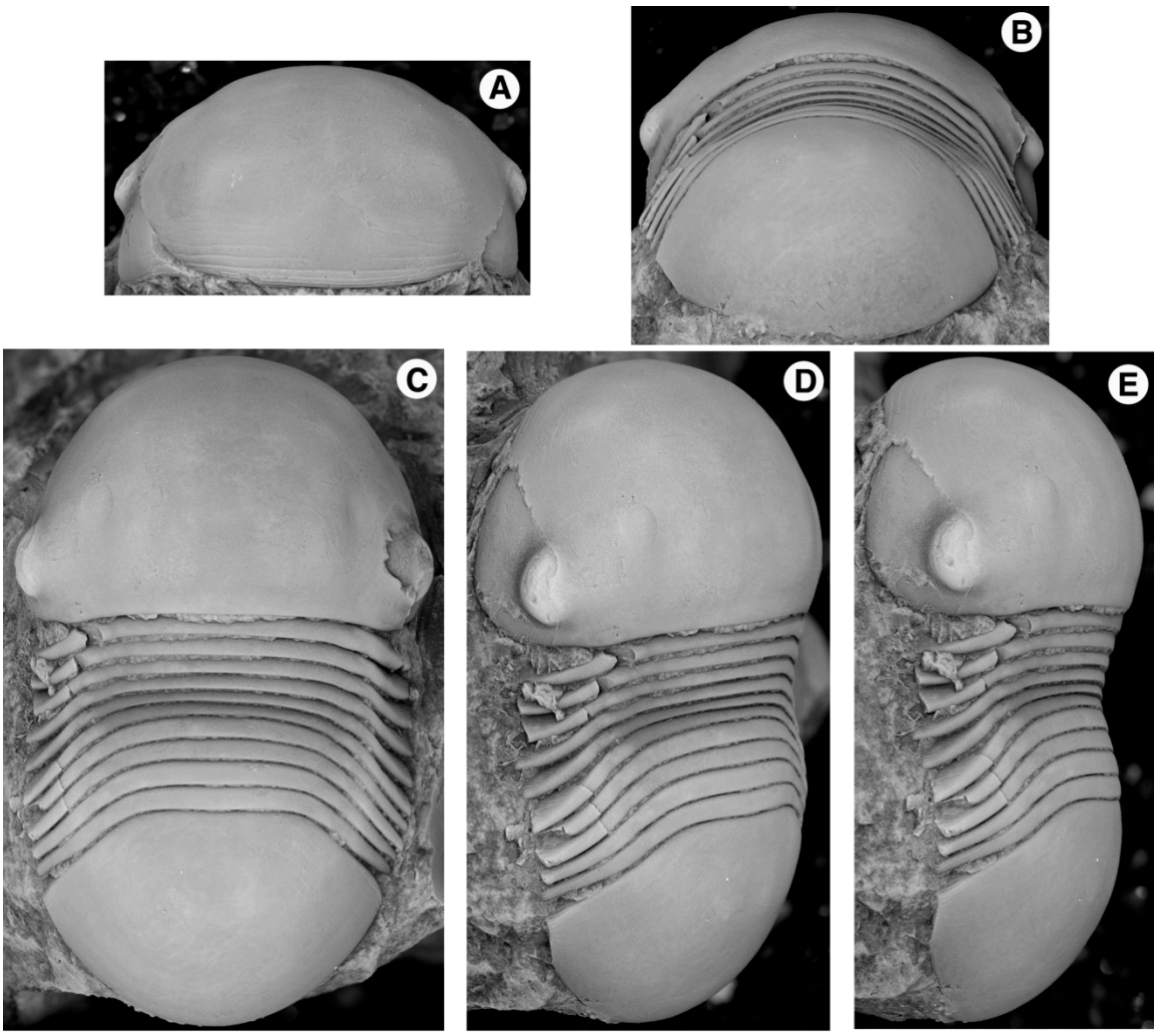
A
B
C
D
E

Figure 17. *Bumastoides tenuirugosus* Troedsson, 1928, Upper Ordovician Selkirk Member of the Red River Formation, Garson, southern Manitoba. **A**,**C**, thoracopygon (OU 12483), x 1: **A**, posterior view; **C**, lateral view; x1.2. **B**, **D**-**E**, partially exfoliated cranidium **(**OU 12495), x 2.3: **B**, anterior view; **D**, dorsal view; **E**, lateral view. **F**-**G**, exfoliated pygidium (OU 12496), x 2: **F**, dorsal view; **G**, posterior view.

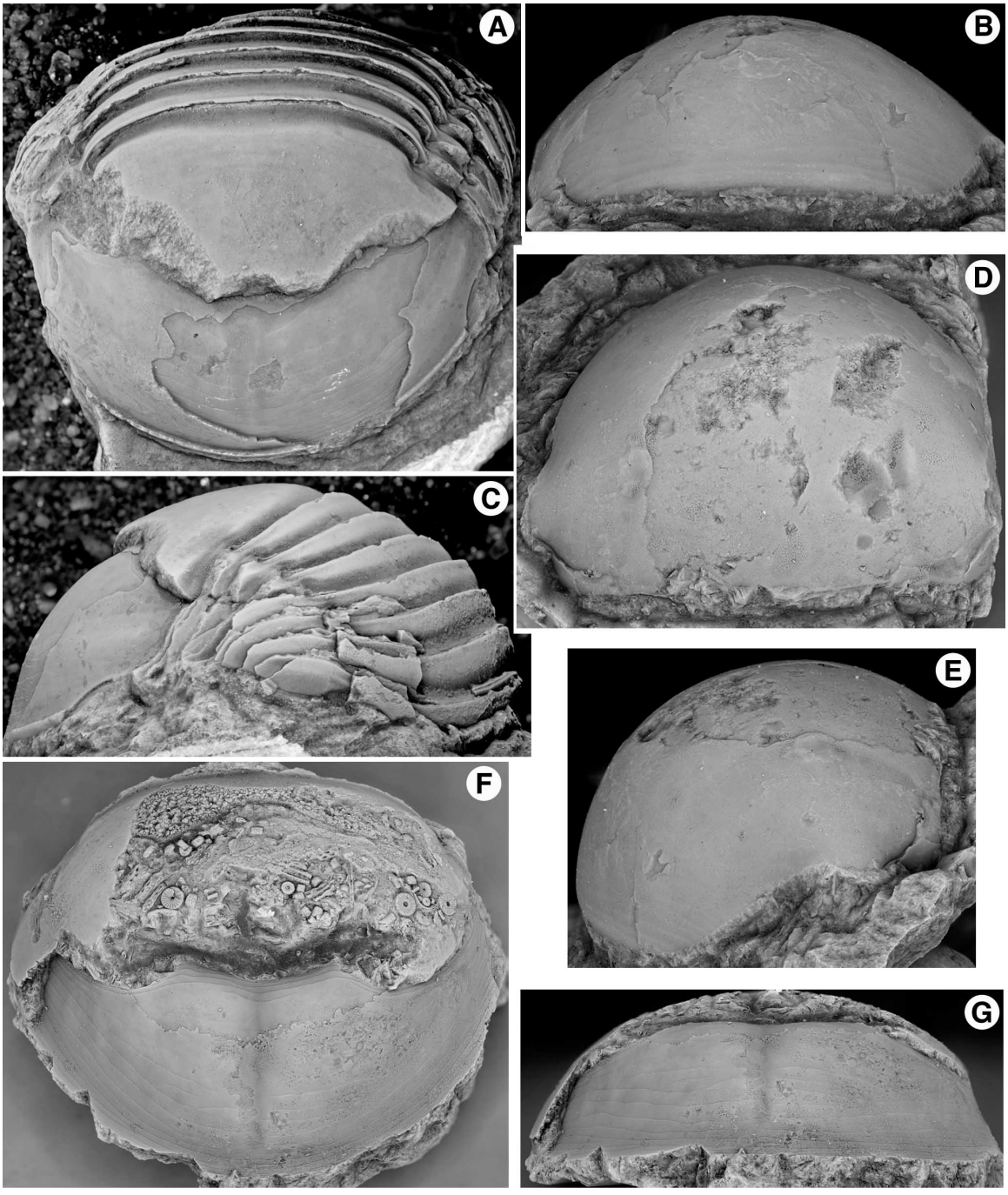
A
B
C
D
E
F
G

Figure 18. *Bumastoides graffhami* sp. nov., Upper Ordovician Bromide Formation (Simpson Group), Arbuckle Mountains region of south-central Oklahoma. **A**-**D**, holotype, dorsal exoskeleton (OU 5204), x 1.8 (Shaw 1974, pl. 4, figs. 19-20, 23): **A**, dorsal view; **B**, lateral view; **C**, oblique lateral view; x 2: **D**, posterior view. **E**, **G**, thoracopygon (OU 12497), x 1: **E**, lateral view; x 1.3: **G**, dorsal view. **F**, testate pygidium **(**OU 12498), x 1.6, dorsal view.

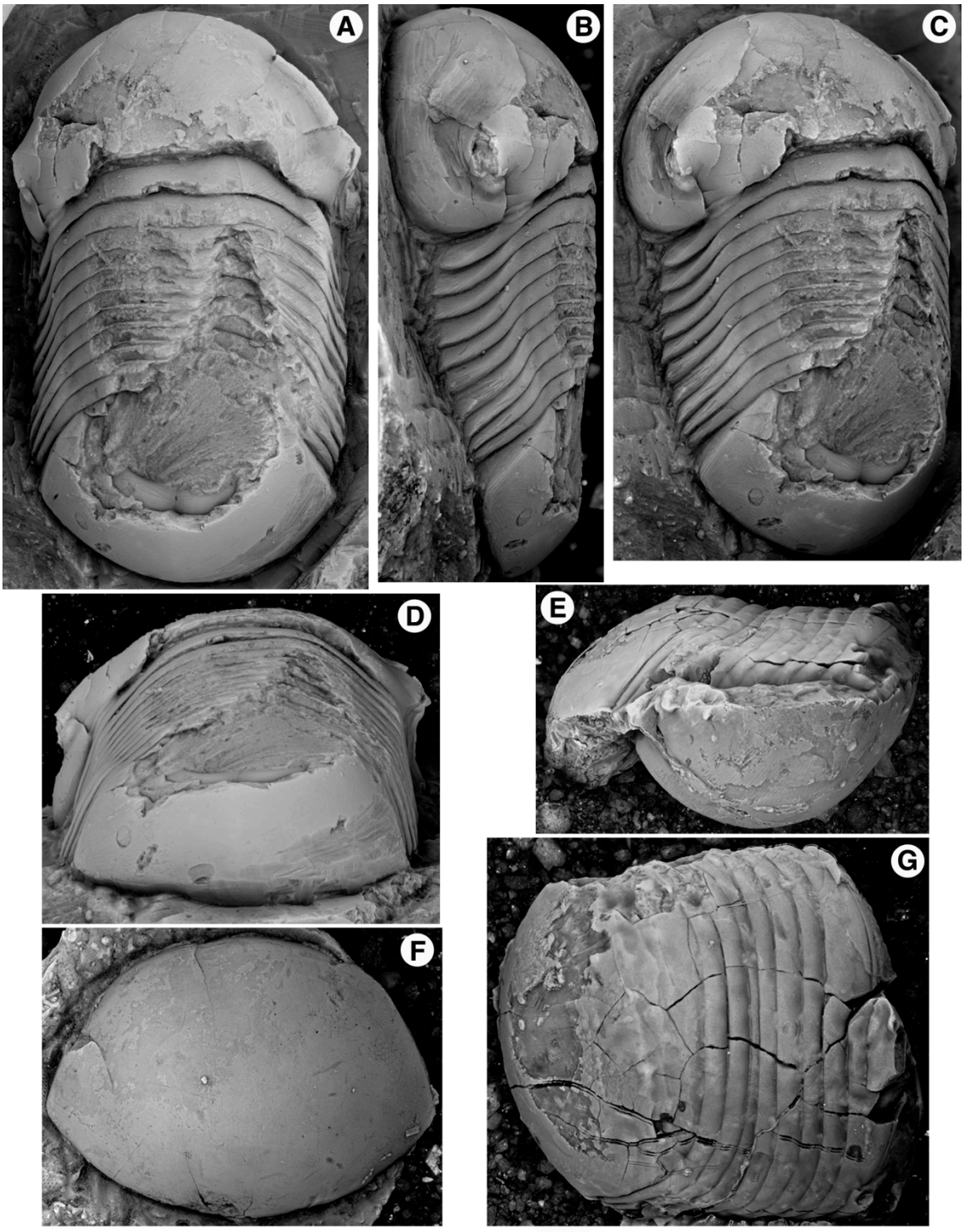
A
B
C
D
E
F
G

Figure 19. *Bumastoides graffhami* sp. nov., Upper Ordovician Bromide Formation (Simpson Group), Arbuckle Mountains region of south-central Oklahoma. **A**-**D**, partially exfoliated cranidium (OU 12499), x 2: **A**, posterior view; **C**, dorsal view; **D**, anterior view; x3: **B**, lateral view. **E**, thoracopygon **(**OU 12500), x 1.5, dorsal view. **F**, exfoliated cranidium **(**OU 12501), x 2, dorsal view.

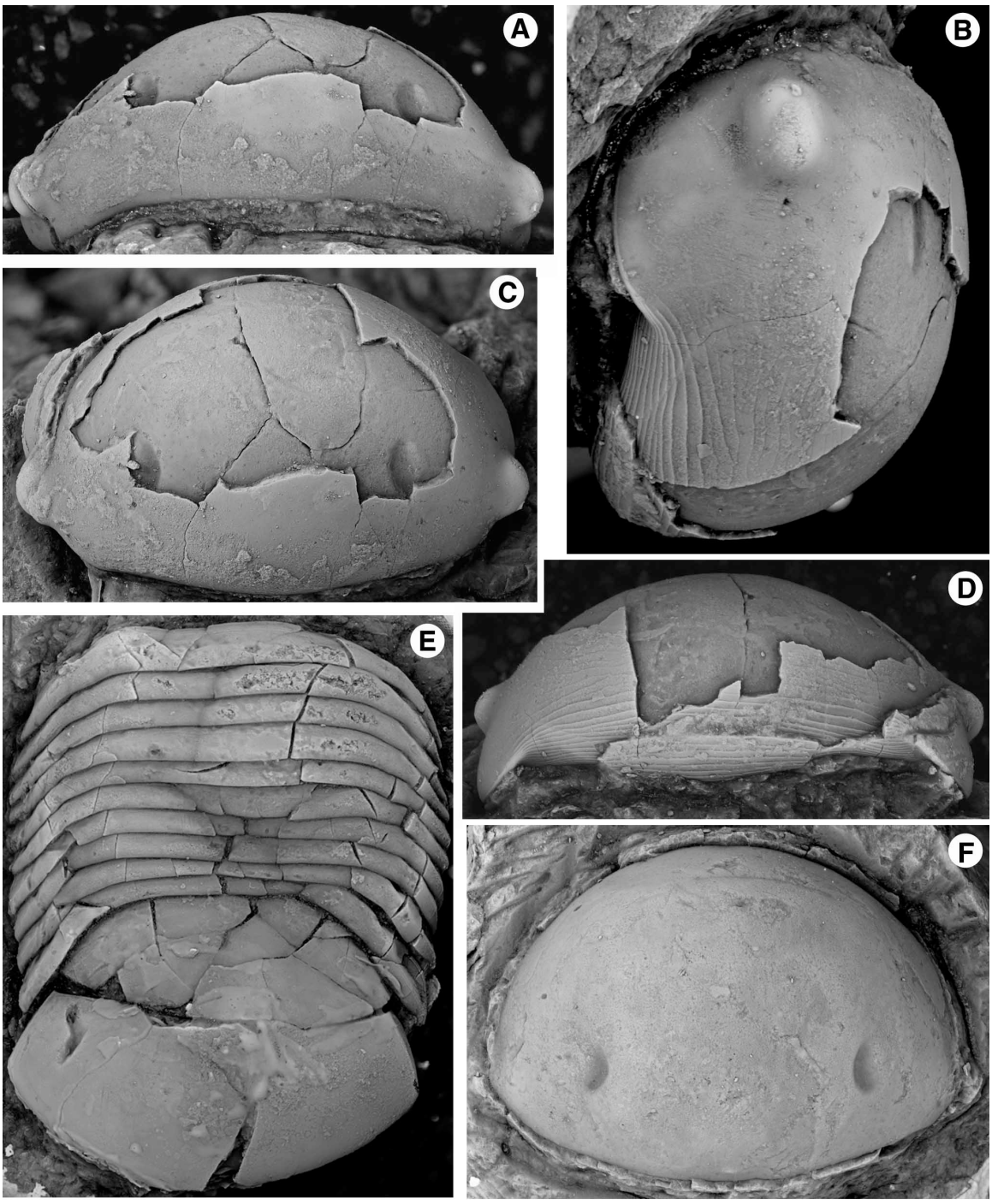
A
B
C
D
E
F

Figure 20. *Bumastoides moundensis* sp. nov., Upper Ordovician Effna Formation, Smyth County, southwestern Virginia. **A**-**B**, thoracopygon **(**OU 12503), x 1: **A**, dorsal view; **B**, lateral view. **C**-**D**, holotype, exfoliated dorsal exoskeleton (OU 12502), x 1: **C**, dorsal view; **D**, lateral view. **E**, exfoliated cranidium (OU 12504), x 1.6, dorsal view. **F-H**, testate pygidium (OU 12505), x 1.5: **F**, dorsal view; **G**, lateral view; **H**, posterior view.

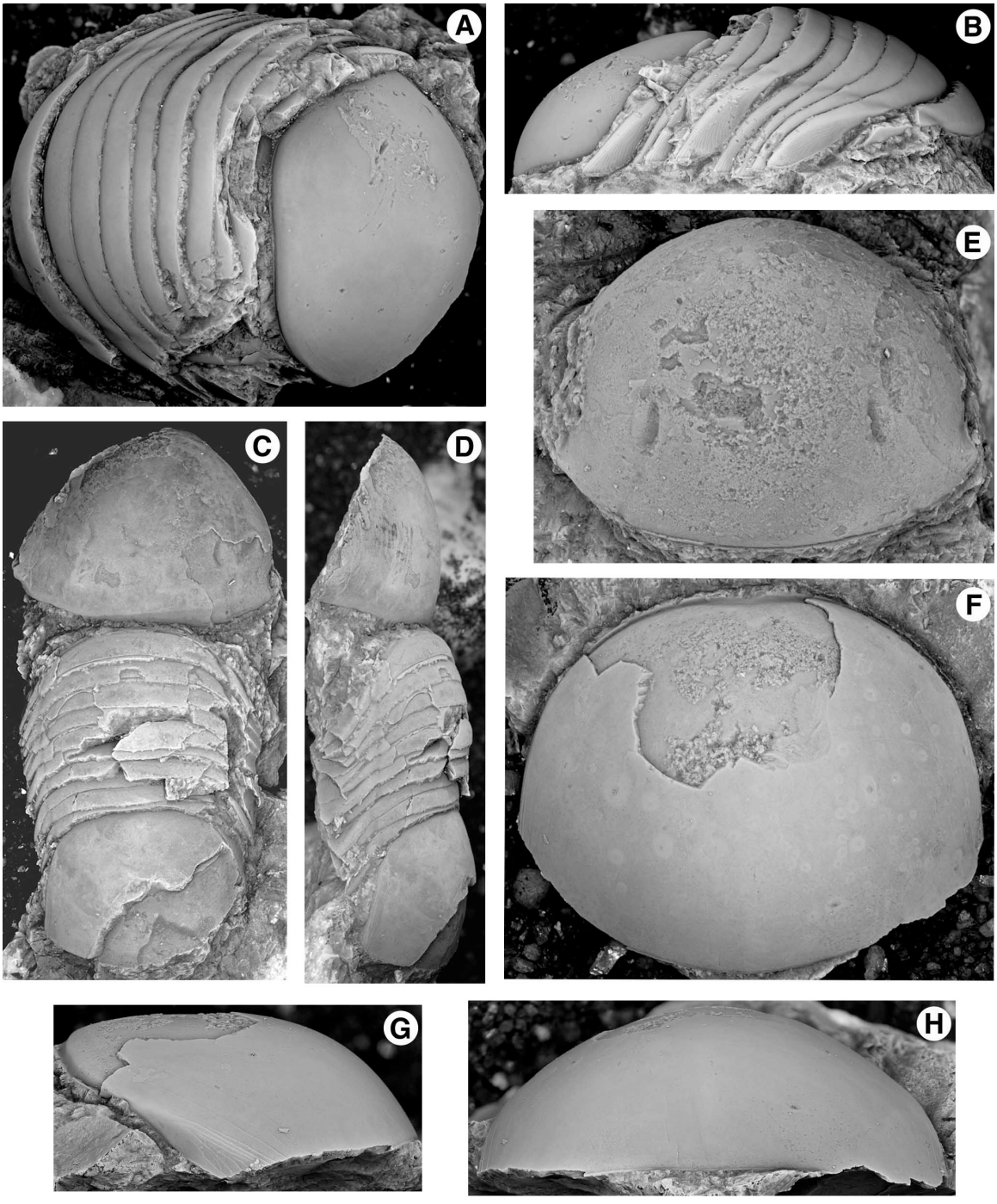
A
B
E
C
D
F
G
H

Figure 21. *Bumastoides moundensis* sp. nov., **A**-**B**, **D**, Upper Ordovician Botetourt Limestone, Bland County, Virginia; **C**, **E**-**F**, from the Upper Ordovician Effna Formation, Smyth County, southwestern Virginia. **A**-**B**, **D**, exfoliated cranidium (OU 12506), x 1.5: **A**, lateral view; **B**, dorsal view; **D**, anterior view. **C**, **E**-**F**, testate cranidium (OU 12507), x 2: **C**, lateral view; x 1.5: **E**, anterior view; **F**, dorsal view.

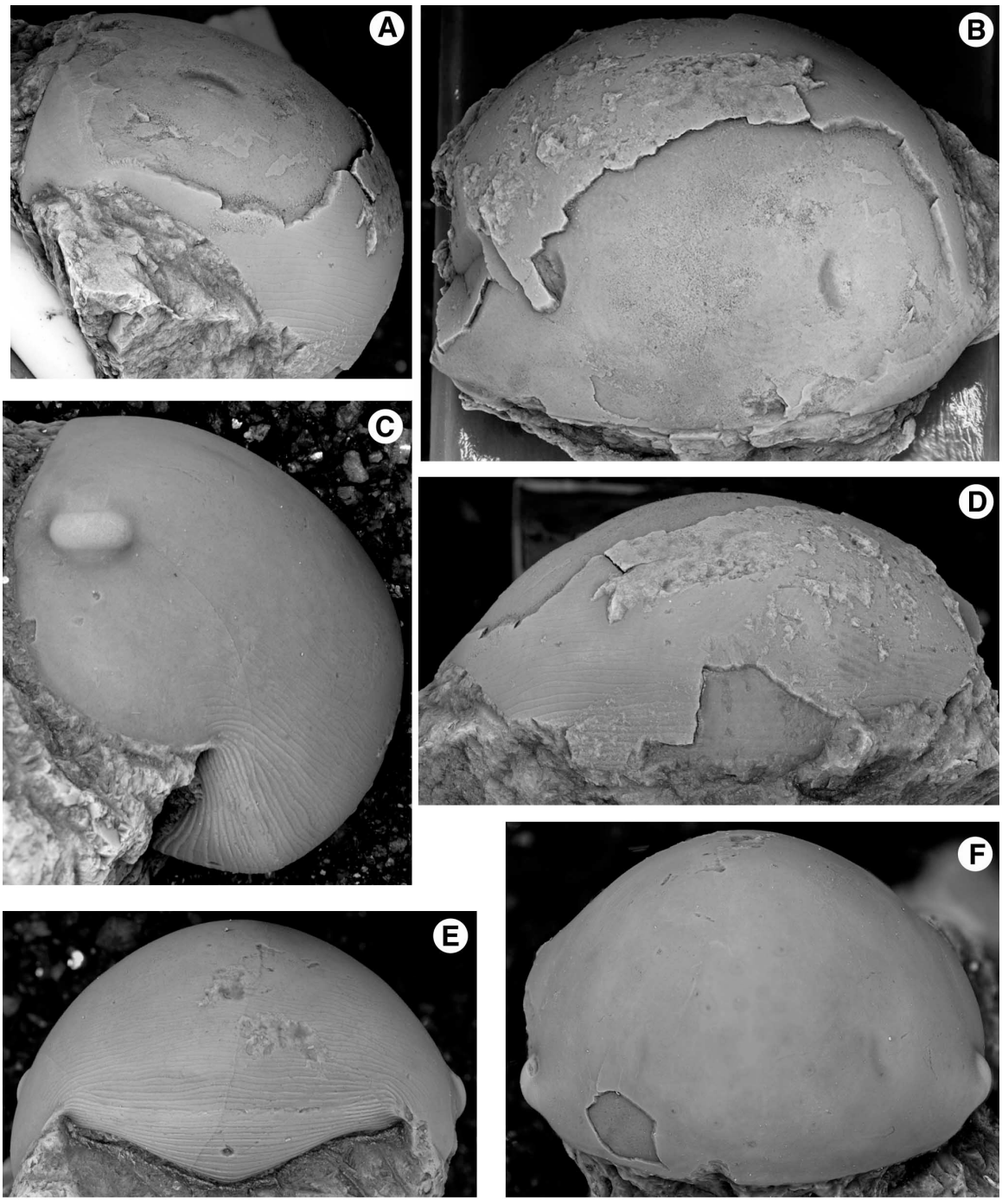
A
B
C
D
E
F

Figure 22. *Bumastoides kimmswickensis* sp. nov., Upper Ordovician Kimmswick Limestone, Jefferson County, Missouri. **A-C**, partially exfoliated cranidium (OU 12509), x 2.8: **A**, dorsal view; **B**, lateral view; **C**, anterior view. **D**, pygidium (OU 12511), x 4.1, dorsal view. **E-G**, partially exfoliated cranidium (OU 12510) x 5: **E**, lateral view; **F**, anterior view; **G**, dorsal view. **H-J**, holotype, thoracopygon (OU 12508), x 3: **H**, lateral view; **I**, dorsal view; **J**, posterior view.

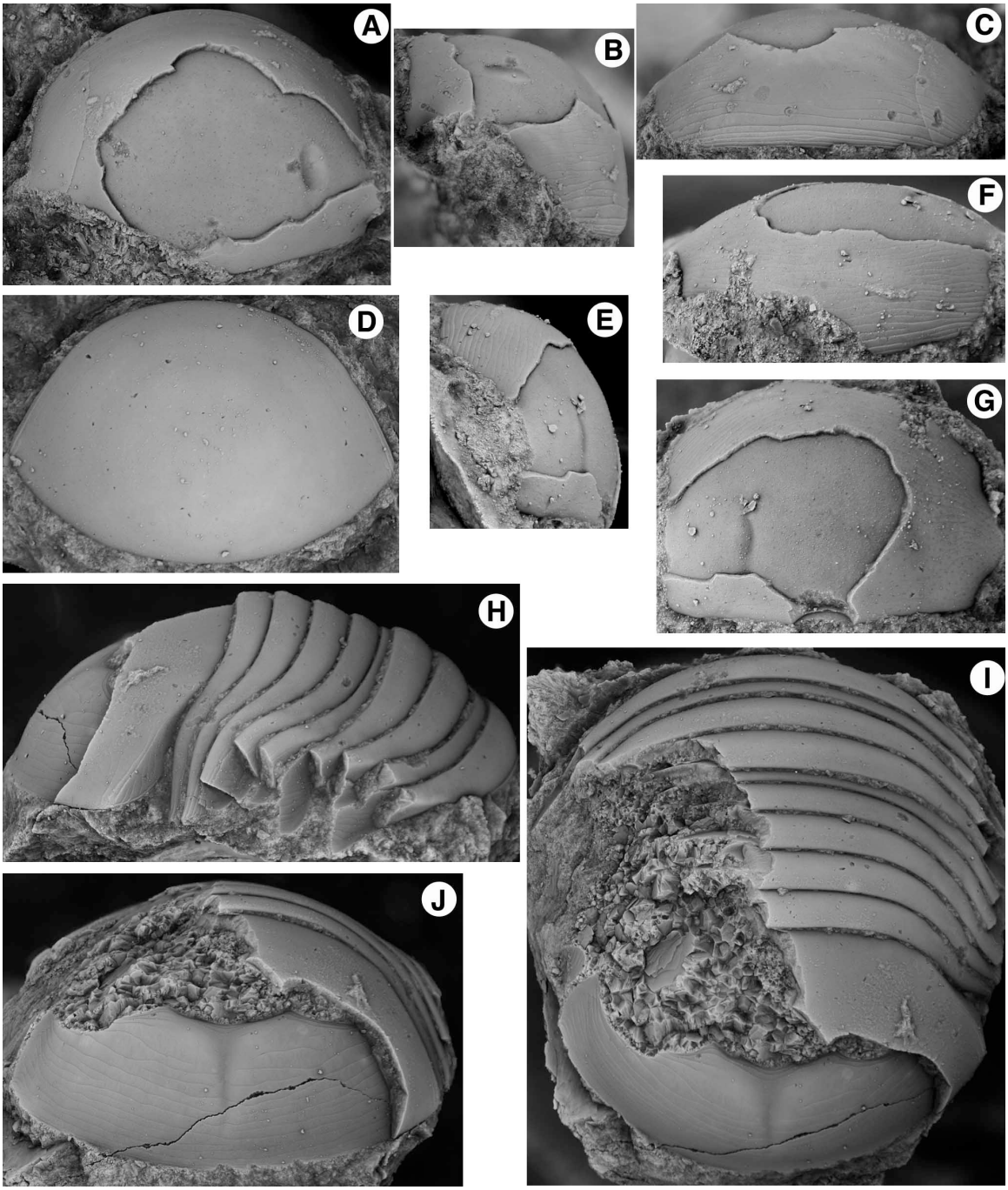
A
B
C
F
D
E
G
H
I
J

Figure 23. *Bumastoides kimmswickensis* sp. nov., Upper Ordovician Kimmswick Limestone, Jefferson County, Missouri. **A**-**C**, exfoliated cranidium (OU 12512), x 4: **A**, dorsal view; **B**, anterior view; **C**, lateral view. **D**, testate cranidium (OU12513), x 6, dorsal view. **E**, testate cranidium (OU 12514), x 8, dorsal view. **F**-**G**, librigena (OU 12515), x 8: **F**, dorsal view; **G**, lateral view. **H**, exfoliated pygidium (OU 12516), x 4, dorsal view.

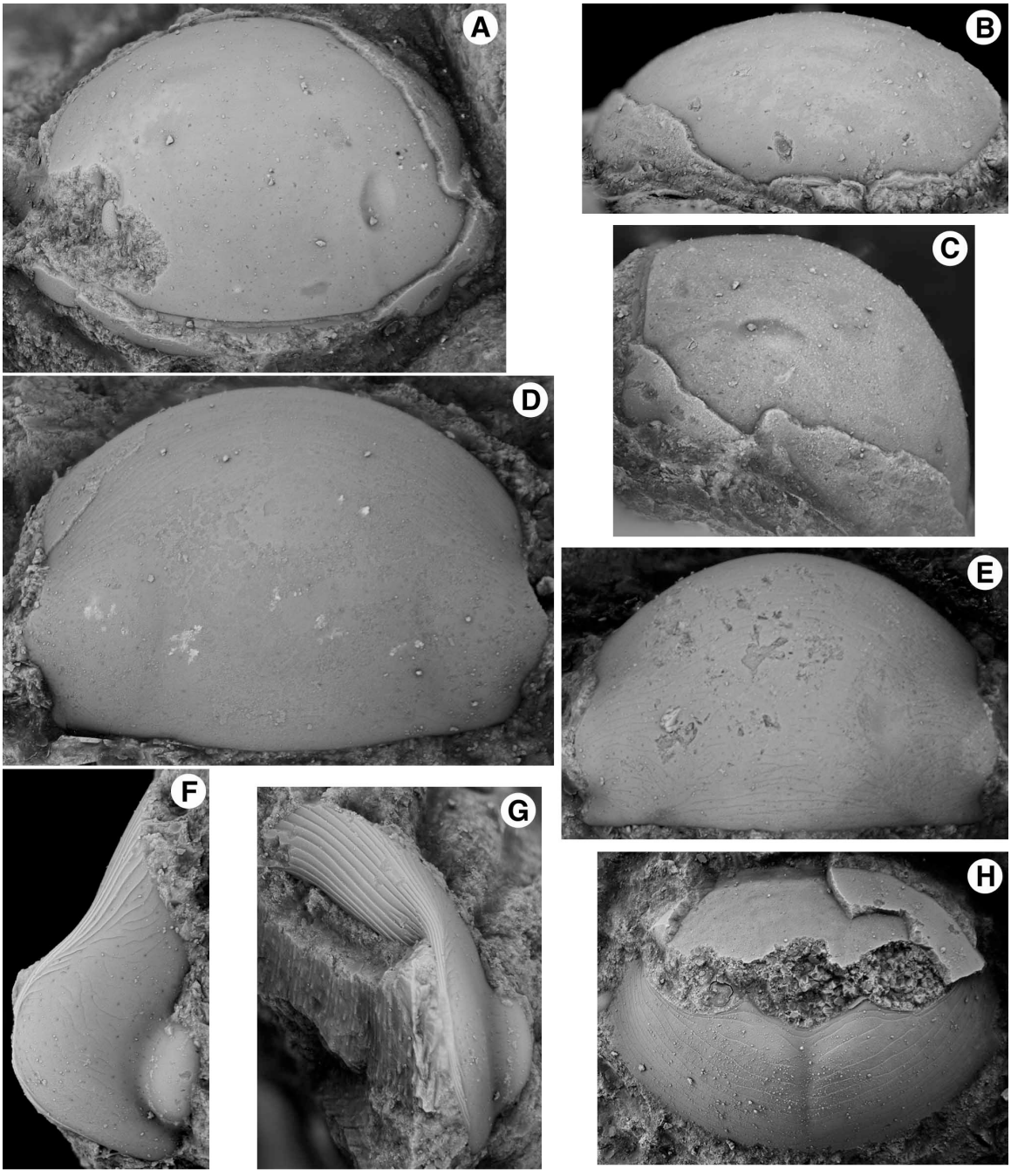
A
B
C
D
E
F
G
H

Figure 24. *Bumastoides* cf. *B*. *milleri* (Billings, 1859), Upper Ordovician Viola Springs Formation (Viola Group), near Fittstown, south-central Oklahoma. **A**, exfoliated cranidium (OU 12517), x 2, dorsal view. **B-D**, exfoliated cranidium (OU 12037), x 2: **B**, dorsal view; **C**, lateral view; **D**, anterior view. **E**, exfoliated pygidium (OU 12519), x 2, dorsal view. **F**, exfoliated cranidium (OU 12518), x 2.5, dorsal view. **G**, partially exfoliated pygidium, (OU 12039), x 2, dorsal view. **H**, partially exfoliated pygidium (OU 12520), x 3, dorsal view.

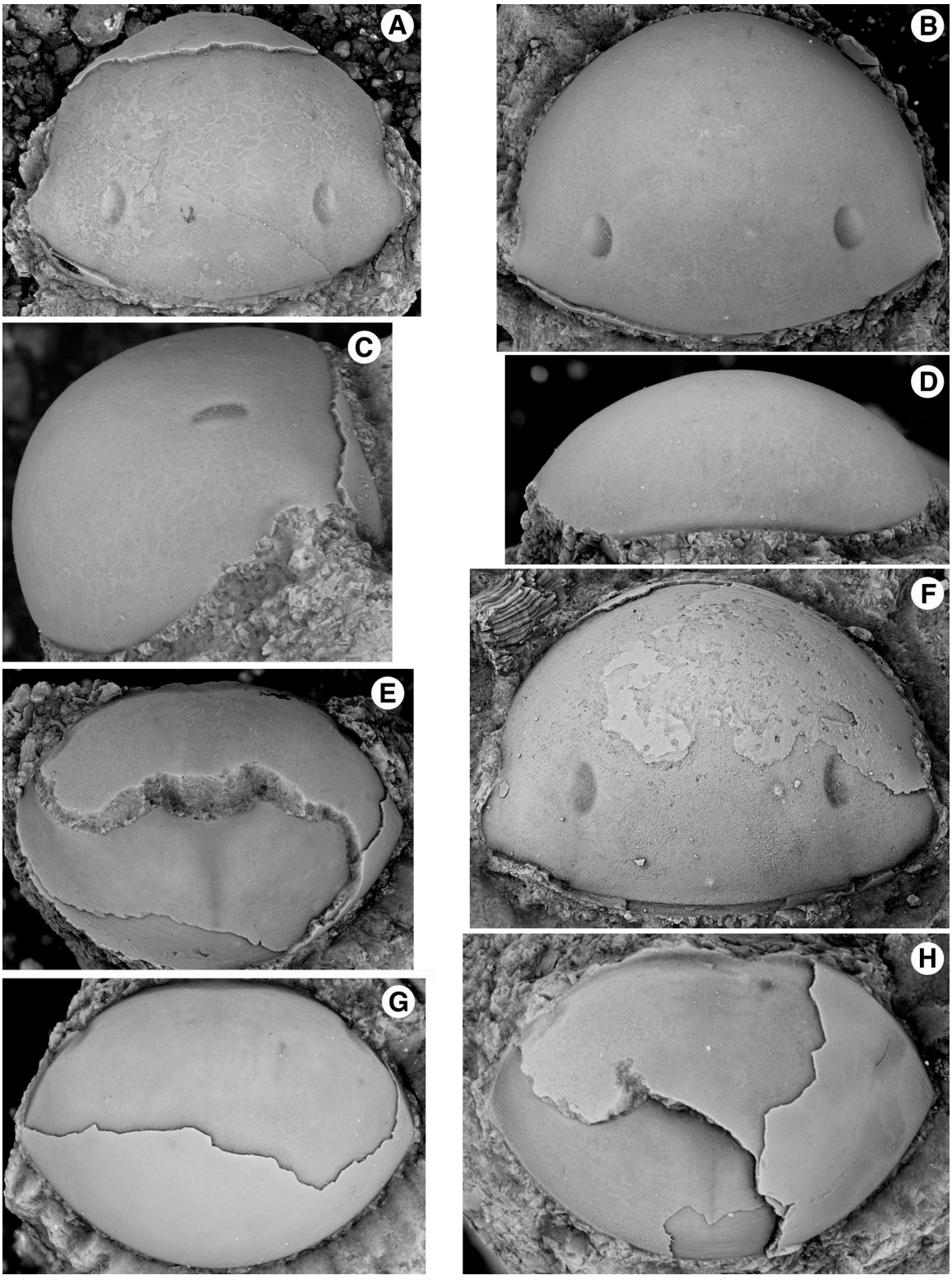
A
B
C
D
E
F
G
H

Figure 25. *Bumastoides* cf. *B*. *milleri* (Billings, 1859), Upper Ordovician Viola Springs Formation (Viola Group), near Fittstown, south-central Oklahoma. **A**-**B**, mostly testate cranidium (OU 12521) x 4.2: **A**, dorsal view; **B**, posterior view. **C**-**E**, exfoliated pygidium (OU 12522) x 2: **C**, dorsal view; **E**, posterior view; x 2.5: **D**, lateral view.

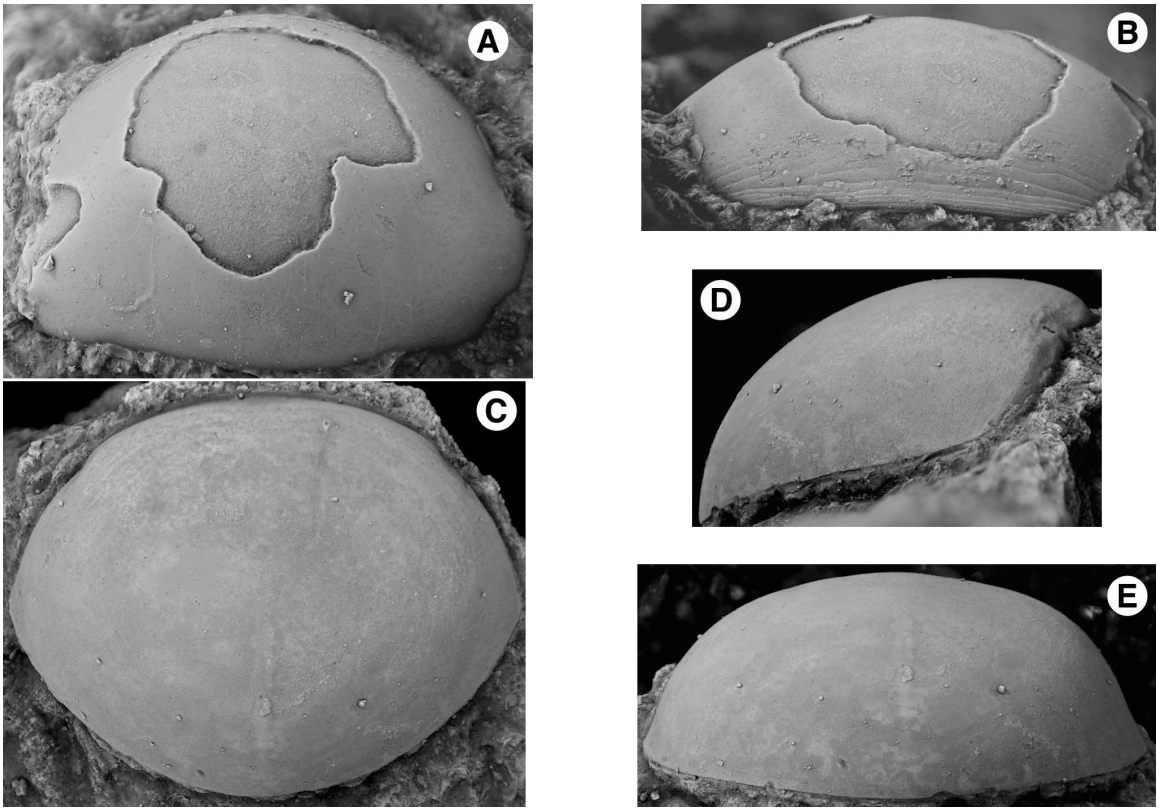
A
B
C
D
E

Figure 26. **A-B,** "*Stenopareia*" *rivulus* (Ingham & Tripp, 1991), Upper Ordovician Doularg Formation (Albany Group), southwest Scotland. **A**, exfoliated pygidium (GLAHM A8313), x 1.5, dorsal view (Ingham & Tripp 1991, fig. 10f). **B**, holotype, exfoliated cranidium, (LAHM A8302), x 3, dorsal view (Ingham & Tripp 1991, fig. 10a-b). **C-F**, "*Stenopareia*" *aplatus* (Raymond, 1925), Middle Ordovician lower Chazy Group, Isle La Motte, Vermont. **C**, **E-F**, holotype, partially exfoliated cranidium (MCZ 101150), x 2 (Raymond 1925, pl. 8, fig. 3): **C**, dorsal view; **E**, anterior view; x2.5: **F**, lateral view; x2.3. **D**, testate pygidium (MCZ 101151), x 2.5, dorsal view (Raymond 1925, pl. 8, fig. 4). **G-J**, "*Stenopareia*" *gardensis* (Shaw, 1968), Middle Ordovician Day Point Formation (Chazy Group), near Chazy New York. **G**, **J**, holotype, partially exfoliated cranidium, (NYSM 12456), x 4 (Shaw 1968, pl. 16, figs 12, 15, 17): **G**, dorsal view; **J**, lateral view. **H-I**, testate pygidium, (NYSM 12457), x 3 (Shaw 1968, pl. 16, figs. 13, 16): **H**, dorsal view; **I**, posterior view.

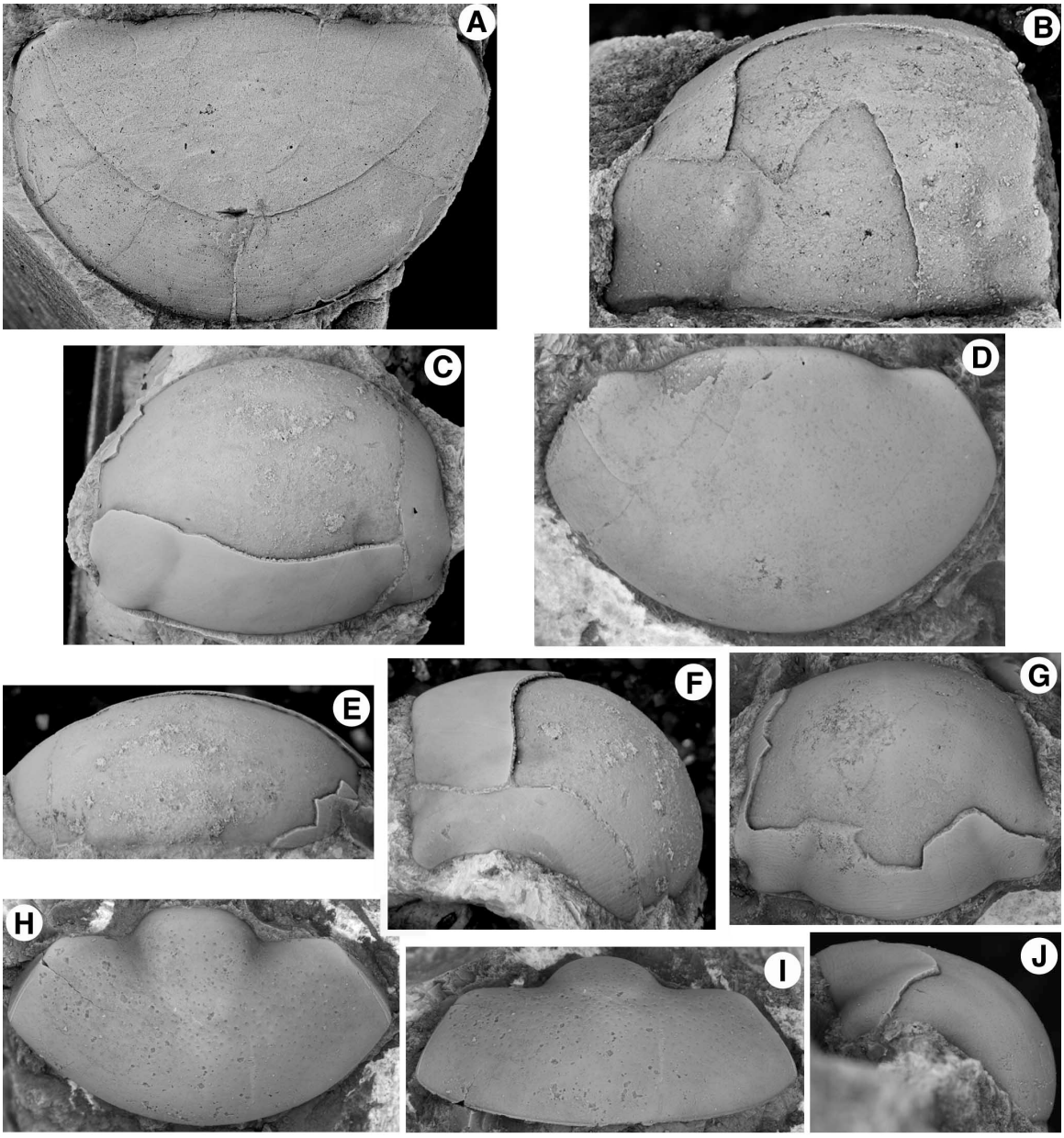
A
B
C
D
E
F
G
H
I
J

Appendix 1. Character data matrix used in the cladistic analysis. A question mark (?) denotes missing data.

Taxon	1	2	3	4	5	6	7	8	9	10	11	12	13	14	15	16	17	18	19	20
B. porrectus	1	1	1	1	1	1	1	2	0	?	?	1	1	0	1	2	2	1	?	1
B. holei	1	0	1	1	1	2	1	2	1	2	1	1	1	1	1	2	2	1	1	1
B. milleri	1	0	1	0	1	1	1	0	1	2	0	1	?	0	0	0	2	1	1	1
B. beckeri	1	1	?	1	?	2	2	2	0	?	0	1	?	1	0	2	2	1	?	1
B. tenuirugosus	1	0	1	1	0	0	2	2	1	2	0	1	1	1	1	1	2	1	1	1
B. solangeae	1	1	0	0	?	?	?	?	?	2	0	1	0	0	1	2	2	1	1	1
B. lenzi	1	1	0	0	1	0	1	?	?	2	0	1	1	0	1	2	2	1	1	1
B. bellevillensis	1	0	1	1	1	1	1	1	?	2	0	1	2	?	1	2	2	1	1	1
B. billingsi	1	?	0	1	0	1	?	2	?	2	1	1	1	0	1	3	0	1	1	1
B. graffhami	1	0	2	0	?	1	1	2	1	2	0	1	?	0	0	1	2	1	1	1
B. moundensis	1	1	0	0	1	2	1	2	0	2	0	1	?	1	1	3	2	1	1	1
B. rivulus	0	?	?	1	1	0	?	?	?	1	0	0	0	0	1	1	0	0	0	1
B. aplatus	0	0	?	0	1	0	1	?	?	1	?	0	?	0	1	2	0	0	0	0
B. gardensis	0	1	1	2	1	?	2	?	?	1	?	2	?	0	1	0	1	1	0	0
S. grandis	0	1	0	0	0	0	2	0	0	0	0	0	0	0	0	2	0	0	0	1
S. linnarssoni	0	0	0	0	0	?	0	0	0	0	0	0	?	0	?	?	0	0	0	0
B. kimmswickensis	1	1	1	1	1	2	2	0	0	2	0	1	1	0	1	2	2	1	1	1

Appendix 2. Means for measured data. Characters 1-6 were only used in the second analysis; all values expressed as percents, a question mark (?) denotes missing data. Character 1: maximum width (tr.) of one lunette in proportion to width (tr.) across palpebral lobes; character 2: cranidial length (sag.) in proportion to width (tr.) across palpebral lobes; character 3: maximum length (sag.) of lunettes in proportion to cranidial length (exsag.) in dorsal view; character 4: percentage of total exoskeletal length occupied by the cranidium (in lateral view); character 5: width of one palpebral lobe as a percentage of cranidial width across palpebral lobes; character 6: percentage of total exoskeletal length occupied by the pygidium (in lateral view); character 7: ratio of max pygidial length (sag.) to max pygidial width (tr.).

Taxon	1	2	3	4	5	6	7
B. porrectus	7	67.1	22.5	37.4	4.8	33.8	66.2
B. holei	11	69.4	26.9	35.7	5.6	33.8	72.1
B. milleri	6.6	67.9	20.7	37.2	4.8	29.7	54
B. beckeri	4.1	70.1	28.5	33.1	3.5	31.1	62.6
B. tenuirugosus	?	70	23.7	37.1	?	32.9	66.6
B. lenzi	5.5	68.7	18.5	?	7.1	?	70
B. solangeae	12	?	?	?	5.3	?	70.3
B. bellevillensis	7.9	66.4	20.8	35.6	5.2	33	65.8
B. billingsi	8.1	71.3	18.7	33.7	3.5	35	79.6
B. graffhami	5.7	65.9	18.3	30.1	5.3	33.5	66.6
B. moundensis	3.8	74.5	13.7	36.8	2.7	30.9	80.2
B. rivulus	?	?	20	?	?	?	66.6
B. aplatus	5.9	76.1	18.3	?	?	?	64.7
B. gardensis	?	?	?	?	?	?	60
S. grandis	4.3	76.7	13	38.3	4.9	33.3	64.6
S. linnarssoni	4.9	80.4	16.6	?	4.8	?	?
B. kimmensis	8	69.8	23.3	?	5	?	70.6

CHAPTER 4: SEQUENCE STRATIGRAPHY AND FACIES ARCHITECTURE OF THE UPPER ORDOVICIAN BROMIDE FORMATION, OKLAHOMA

ABSTRACT

The late Whiterockian to Mohawkian Bromide Formation succession in south-central Oklahoma was deposited along a mixed siliciclastic-carbonate ramp that distally steepened into the Southern Oklahoma Aulocogen (SOA). The depositional history and environmental context of the unit are reconsidered using lithofacies analysis and the characterization of sequence stratigraphic patterns at a variety of hierarchical scales. The dataset consists of measured sections, polished slabs and hand samples, thin sections, paleontological collections, outcrop and subsurface gamma ray, and high-resolution study of bounding surfaces and event beds. Inner-ramp (above FWWB) lithofacies suggest deposition in a range of environments: tidal flats, lagoons, shoreface, semi-restricted shallow subtidal, and bioclastic shoals. Middle-ramp environments (between FWWB and SWB) are thick and faunally diverse, and consist of rhythmically bedded marls, wackestone, packstone, and clastic shales. Outer-ramp environments (below SWB) are represented by either fissile tan-green shales or thin-bedded carbonate mudstones and shales. Ramp stratigraphy, facies associations and bounding surfaces suggest that three 3rd order depositional sequences are present in the Bromide. They demonstrate the transition from a primarily clastic ramp in the late Whiterockian to a carbonate-dominated ramp in the Mohawkian. These sequences show that the deposition of the Bromide was considerably more complex than the simple transgressive-regressive cycle traditionally used to describe accommodation dynamics in the basin. Meter and

decameter-scale cycles are common within the depositional sequences, and the Corbin Ranch Submember records an important peritidal sequence prior to a major sequence boundary with the younger Viola Formation. New correlations based on measured sections, outcrop gamma ray profiles, and subsurface well logs suggest that the middle Bromide depositional sequence expanded down-ramp, while the carbonate-dominated upper sequence shows condensation deep within the SOA. Moreover, newly documented facies associations and correlations necessitate the addition of a reference section to the Pooleville and the promotion of the lower sand unit to submember status.

INTRODUCTION

Late Whiterockian through Mohawkian deposits in the Arbuckle Mountains and Criner Hills regions of Oklahoma (Fig. 1) are recorded as the mixed carbonate-siliciclastic Bromide Formation (Ulrich 1911). Bromide strata in south-central Oklahoma were deposited along a carbonate ramp extending from the Arbuckle Platform into the Southern Oklahoma Aulacogen (SOA) (Fig. 1), a subsiding trough filled by an embayment of the Iapetus Ocean (Bambach et al. 1980). The Bromide is the youngest formation of the Simpson Group, which also includes the Joins, Oil Creek, McLish, and Tulip Creek formations (Cooper 1956; Harris 1957). Ulrich (1911) first used the term Bromide for a series of rocks between the Simpson and Viola formations, and defined the type section in the Arbuckles. Cooper (1956) divided the Bromide into the Pooleville and Mountain Lake members. The Mountain Lake is the older unit, and is characterized by a dynamic succession of quartz sandstone, interbedded sandstone and shale, and shale and limestone (primarily pelmatozoan grainstone in the lower Mountain Lake). Bauer (1994) considered the lower Mountain Lake to be Whiterockian based on the presence of the

conodont *Cahabagnathus sweeti*. In the middle and upper Mountain Lake, a Mohawkian conodont fauna replaces *C. sweeti*. These mixed carbonate-siliclastic units eventually give way to the Pooleville Member, a thick-bedded to massive unit of carbonate mud-, wacke-, and packstone. Harris (1957) noted the lithologic distinction of the fine-grained, dolomitic, and fenestral unit that capped the Pooleville at some localities in the northern Arbuckle Mountains. He defined this unit as the Corbin Ranch Formation, although it is now commonly referred to as a submember of the Bromide Formation (e.g., Derby et al. 1991). Harris (1957) considered the Corbin Ranch to be Trentonian in age because of the lack of a distinctive Black River fauna, and suggested there were significant erosional hiatuses between the Pooleville and Corbin Ranch. More recently, Bauer (1994) noted that the conodont fauna of the intertidal Corbin Ranch includes forms that range from Blackriveran (Whiterockian) to Mohawkian, and could not constrain the age of the unit.

In addition to the studies that have discussed the correlation and lithologic patterns of the Bromide (e.g., Ulrich 1911; Decker 1931; Cooper 1956; Longman 1976, 1977, 1982a 1982b; Fay and Graffham 1982b; Suhm 1997; Wahlman 2010), the subsurface patterns (Schramm 1964), diverse trilobite (e.g., Laudon 1939; Sutherland and Amsden 1959; Shaw 1974; Karim and Westrop 2002; Carlucci et al. 2010; Carlucci et al. 2012), echinoderm (e.g., Fay et al. 1982a; Sprinkle 1982), ostracod (e.g., Harris 1957; Williams 1990; Williams and Siveter 1996), conodont (e.g., Sweet 1984; Bauer 1990; Bauer 1994), chitinozoan (e.g., Grahn and Miller 1986), graptolite (e.g., Finney 1986), bryozoan (e.g., Cuffey and Cuffey 1995), and gastropod (e.g., Rohr and Johns 1990) faunas have been investigated. The most comprehensive outcrop-based studies of the Bromide were conducted by Longman (1976; 1982a, 1982b) and Fay et al. (1982b).

Based on extensive measured sections and electric logs they showed that the deposition of the Bromide thickens down-ramp from the hingeline of the SOA. They further suggested that the Bromide was deposited during a period of slow steady subsidence of the SOA, where early deposition was in storm-dominated settings, with the shallowest water to the northeast. Longman (1982a, b) noted that one complete transgressive-regressive cycle is present in the Bromide, with the transgressive basal sandstones and shales evolving to a shelf-margin carbonate buildup. Further, Longman (1982a, b) observed that episodic deposition of Bromide sandstones often exceeded the rate of subsidence during the transgression, suggesting there were complications with his simplified higher rank sequence interpretation. Above the sandstones, Longman (1982a, b) speculated that the basinal lithofacies were deposited as part of the same transgression. Eventually, water depth shallowed along the hingeline of the SOA, and a biosparite buildup developed, with a landward low-energy lagoon on the Arbuckle Platform (Longman 1982a, b). Under the Longman model, tectonic instability increased, clastic deposition shut down, and the upper Bromide was deposited as a regressive limestone sequence. Cessation of subsidence accelerated the regressive cycle of the Pooleville.

Most of the literature on the Bromide predates the development of modern sequence stratigraphy as a discipline. Here, we reconsider the facies architecture, bounding surfaces, depositional history, and correlation of the Bromide Formation, within a robust, high-resolution sequence stratigraphic framework. Multiple hierarchical levels of cyclicity in the formation were not recognized in previous work, and yield important clues about the depositional setting of the Bromide.

PALEOGEOGRAPHIC AND TECTONIC SETTING

In the late Cambrian and Ordovician, Oklahoma strata were deposited in a broad epeiric sea (Oklahoma Basin, Fig. 1) that extended across the majority of the state. Relatively simple epeirogenic processes affected the landscape of what would be Oklahoma during this time, in contrast to the complex orogenic structural basins common in the Pennsylvanian (Johnson 1991). The Oklahoma Basin lies just to the west of the margins of the Ouachita Trough, and is dominated by shallow-marine carbonates interbedded with sandstones and shales. Most authors (e.g., Longman 1982a, b; Johnson 1991) consider the SOA to be the depocenter of the Oklahoma Basin, as subsidence rates and sediment thickness are considerably higher than in shallow bank environments outside the SOA. The SOA trended to the northwest, and persisted through most of the Paleozoic, influencing the deposition of multiple formations (Longman 1982b). It extends across an area that includes the Arkoma Basin, Arbuckle Uplift, Ardmore Basin, and the Anadarko Basin, all of which contain Bromide deposits (Fig. 1). To the north, the SOA was bordered by the stable Arbuckle platform (Longman 1982b), which was a desert region that likely supplied wind-blown sand deposited as sheets in the basins. In the lower to middle Whiterockian, Simpson Group deposition began when the carbonate shelf that bordered the SOA was exposed (McPherson et al. 1988). Wind-blown sands were reworked and mantled the carbonate platform (Johnson 1988), and eventually were overlain by marine shales and carbonates. This pattern occurred during the deposition of each formation of the Simpson Group.

Subsurface isopach maps of Bromide units (Schramm 1964, figs. 14-16) show the extensive sandstone deposition on the Arbuckle Platform, suggesting sediment provenance from the north and east. To the south and west along the flanks of the Texas

arch, the sandstones become thinner, while carbonates increase in thickness. Carbonates thin laterally, in particular to the east along the Ouachita Front. Shales are thickest to the south, especially along the hinge of the SOA. The Corbin Ranch Submember is missing in parts of south-central Oklahoma, in particular near and within the SOA, and may disconformibly overlie older Bromide Strata to the east and west (Schramm figs. 3, 16). Dolomites are thickest to the northeast, above the Ouachita Front (see Wahlman 2010), and provide evidence of an arid paleoclimate (Wahlman 2010, fig. 4). In summary, Bromide deposition took place during a period of relative stability of the Oklahoma Basin, where shallow carbonate-dominated seas bordered a subsiding aulacogen, and were periodically interrupted by clastic sediment supply from the north and east.

METHODS

Nine detailed measured sections, two portable gamma ray logs, ten subsurface well logs, nine thin-sections, 19 polished slabs, over 50 field-collected paleontological collections, museum collections (Shaw 1974; Sprinkle 1982; Karim and Westrop 2002), and hundreds of lithologic samples and photographs constitute the dataset for this study. Sedimentary lithology, texture, cycles, surfaces and grain components were recorded in the field for all measured sections, at a decimeter-scale where necessary. Surfaces were correlated between measured sections by physical comparison if possible, and otherwise by stacking patterns and facies offsets. The natural radioactivity (gamma-ray) of the I-35N and 177 sections was measured in cycles per second (CPS) using a Scintrex Differential Spectrometer GRS-500 at 0.5 m intervals, averaged over a span of 30 seconds.

Sequence Terminology

The term sequences are used here to imply a succession of genetic deposits that form during a full cycle of change in accommodation and sediment supply. Meter-scale cycles are the smallest unit that can be correlated across sections, and contain both a deepening and shallowing component. We use the colloquial term "micro" (e.g., micro-HST) to denote the components of meter-scale cycles (5^{th} order) that are small-scale analogues to systems tracts of higher rank (3^{rd} order) sequences. We follow Catuneanu et al. (2009) and use the less ambiguous term "rank" when referring to hierarchical stacking levels. Stacked sets of low rank cycles are nested within systems tracts, which are the components of the higher rank sequences (Catuneanu et al. 2009). Stacked sets of low-rank cycles show consistent progradational, retrogradational or aggradational patterns that are associated with specific systems tracts. Complete high rank sequences (3^{rd} order) follow the terminology of Hunt and Tucker (1992; 1995) (i.e., depositional sequence IV of Catuneanu et al. 2009), where "normal" regressive systems tracts (HST and LST) are distinguished from forced regressions (FSST), and transgressive deposits are a distinct unit (TST).

A sequence boundary (SB) represents the lowest relative sea level, and is expressed as a subaerial unconformity or correlative conformity. In addition to sequence boundaries, we recognize three sequence stratigraphic surfaces. Transgressive surfaces (TS) (Posamentier and Vail 1988) mark the onset of marine flooding and condensation as either forced or normal regression switches to retrogradational stacking. In the former, the transgressive surface is the same as the sequence boundary and in the latter it caps the LST. The maximum flooding surface (MFS) (Van Wagoner et al. 1988) marks the onset of normal marine regression (progradational stacking), and is characterized by

considerable condensation and the farthest inferred landward extent of deep-water facies. Our forced regression surface (FRS) (McLaughlin et al. 2004) signifies the abrupt facies offset that characterizes the switch from normal to forced regression, and separates HST from FSST deposits.

LOCALITIES

Nine measured sections were taken from eight localities (see Fig. 1 caption for coordinates) in south-central Oklahoma. Six of the sections were taken from localities in the Arbuckle Mountains (HWY99, 177, I-35N, I-35S, MLQ, DRa), and three from the Criner Hills (RCS, RCL, TQ). In a paleogeographic context, the localities form a transect from south of the Arbuckle Platform (up-ramp), through the hinge of the SOA, and down into the aulacogen. We modified the nomenclature of two localities to account for new ownership. The Dunn Quarry (Fay et al. 1982b; Karim and Westrop 2002) is now the Tyson Quarry (TQ), and the Johnston Ranch (Fay et al. 1982b) is the new Daube Ranch (DRa) locality.

Ulrich (1911) first used the term “Bromide” for a unit that lay unconformably below the “Viola Limestone” (Fig. 2), but did not propose any type locality or section. Edson (1927) proposed that the type locality of the Bromide be placed at the McLish Ranch, in the town of Bromide, Coal County, Oklahoma. This locality was not accessible for this study (see Fay et al. 1982b, section 5, p. 343). The type sections of the Mountain Lake and Pooleville Members of the Bromide were proposed by Cooper (1956) to be placed at the Johnston Ranch (DRa here). Cooper defined the Mountain Lake to include the basal fine-grained quartz arenite sandstone, an overlying interbedded illitic-chloritic shale and sandstone, and an uppermost limestone and shale sequence at the top (Fay and

Graffham 1982). Cooper confined the Pooleville to the various limestones (occasionally interbedded with calcareous shales and marls) above the Mountain Lake, in particular near the SOA axis. The petroleum industry common refers to the Pooleville and Corbin Ranch as the "Bromide dense" based on its subsurface properties, though this may also include parts of the overlying Viola Springs Formation lime mudstone.

We use the I-35N section as a standard reference for correlation and discussion of sequences because it is well-preserved, nearly complete, and has previously been well-studied biostratigraphically (e.g., Bauer 1994). Our composite section utilizes the north and south sides of I-35, and the median to create a nearly complete succession of Bromide units. The I-35N locality is near the hinge of the SOA, and provides an excellent opportunity to correlate with both up-ramp and down-ramp sections. Moreover, the completeness and preservation of the I-35 section allows it to serve as an ideal "model" to characterize both meter-scale and higher rank sequences.

SEDIMENTARY FACIES

Sedimentary facies (Figs. 3-6) provide the necessary environmental information to interpret facies associations within depositional sequences, the extent of lateral change along the carbonate ramp, and preservational features (e.g., condensation) that may aid in inferring sediment supply. Depositional regime terminology of ramp systems follows Wright and Burchette (1996) and Jones (2010). Facies are not interpreted in isolation, but rather considered in relation to one another, and within their bounding surfaces. Thus, we use facies associations (Reading 1996) within sequences as the primary mode of interpreting environmental signatures. We incorporate and occasionally reconsider the facies subdivisions of previous authors (e.g., Longman 1976; Longman 1982a, b) based

on the addition of sequence stratigraphic data, and are careful to note important observations and interpretations made in other studies (e.g., Pollastro 1991). Within each member, facies are considered in order of their inferred paleobathymetric position (nearshore to basin).

Pontotoc Member

We formally (Salvador 1994, p. 14) designate the basal sandstone sequence in the Bromide Formation as the Pontotoc Member, with the HWY 99 outcrop (Figs. 1, 7) between Fittstown and Pontotoc Oklahoma, as the type locality. In his original definition of the Mountain Lake, Cooper (1956) did not place the sandstones in the member, though Fay and Graffham (1982) suggested they should be included in the unit. Our new designation is necessary to separate the primarily sandstone and siltstone unit from the largely limestone and marl succession in the Mountain Lake. Moreover, the discovery of a significant mineralized transgressive surface (RC) at the top of the sandstone sequence suggests they are temporal units, and indeed are traceable from the Arbuckle Platform into the deepest part of the SOA. In the absence of the transgressive surface, the rather abrupt transition from predominantly sandstone to limestone lithofacies is the criterion for recognition of the Pontotoc Member. The following facies descriptions serve as our characterization of the new formal unit.

Massive to Crossbedded Sandstone Facies.—Sandstone in the Pontotoc Member is composed of detrital, fine to medium grained, well-sorted, well-rounded, frosted quartz arenite (Folk 1980) grains, with small percentages of clay minerals, feldspar and other rock fragments (carbonate bioclasts). Some beds are more enriched in bryozoan and pelmatozoan bioclasts (but not to the extent of the “sandy crinoidal grainstone” of the

Mountain Lake, which are primarily limestones, Fig. 4E), and are best characterized as a sublitharenite. In a petrologic study of the Bromide sandstones, Pollastro (1991) noted a paragenetic sequence of early iron-poor calcite and quartz overgrowth cement, an intermediate transition to iron-rich calcite or dolomitic cement, and late diagenesis ferroan dolomite, ankerite and quartz cement. Bedding is generally thinner down-ramp (3-5 cm), but ranges from massive to thick-bedded (~10 cm), with ripples and hummocky cross-beds common. Up-ramp (e.g., HWY99) cross-beds are thicker bedded, tabular and almost exclusively quartz sand except for thin mud drapes that form flaser-bedded units. Large-scale (e.g.. dune-sized), unidirectional, tabular cross-beds are only present up-ramp. Down-ramp (e.g., RC), wave ripples and hummocky cross-beds are thinner bedded, have internal silt-laminae, and are finer-grained. Massive to thick-bedded, heavily bioturbated mature sandstone (e.g., I-35N) overlies the cross-bedded and thinner bedded units, and locally is present as discrete beds within the bedded sandstone.

In the most up-ramp section at HWY99, this facies is interpreted as being deposited in an upper shoreface environment, dominated by unidirectional flow of tabular dunes, where longshore bars are provided wave protection (Plint 2010). Flaser-bedded units may represent tidally-influenced foreshore environments that are the shallowest strata in the Pontotoc Member. Moving down-ramp toward the hingeline, this facies is characteristic of subtidal middle shoreface deposits, which are considerably finer-grained, and extensively bioturbated. Within the SOA, this facies is dominated by very silty, wave rippled and occasionally hummocky cross-stratified packages that are interlayered with mud, and represent the lower shoreface and offshore transition (Clifton 2006). Generally

speaking, this facies is characteristic of a prograding, normally regressive, wave-dominated shoreface.

Interbedded Sandstone and Shale Facies—This facies is similar to the thin-bedded sandstone described above, except that it is coupled with clastic shale interbeds; the sand is finer grained, and it lacks cross bedding. Abundance of silt and bioclasts (bryozoan and echinoderm) increases in this facies relative to the cross-bedded sandstones, with some beds best characterized as siltstones.

The lack of cross-bedding and ripples, and abundance of fines suggest that this rhythmic facies was transitional between shoreface and offshore deposits (inner-ramp), but likely still receiving sand from the lower shoreface.

Mountain Lake Member

Fenestral Mudstone.—Superficially similar to the Corbin Ranch (see below), a thin (~20cm) unit of fine carbonate mudstone overlies the FSST rippled grainstone in sequence 1. The unit shows very small fenestrae, internal lamination, and contains well-preserved ostracod fossils.

We interpret this unit as a restricted inner-ramp deposit from either a shallow lagoon or tidal flat environment, and the shallowest facies of the Mountain Lake Member. The fine carbonate grain size suggests very low energy conditions favorable to the accumulation of lime mud. A tidal ravinement surface separates the fenestral mudstone facies from overlying coarse brachiopod and trilobite grainstone and rudstone that were deposited early in the transgression of sequence 2.

Rippled Calcisiltite and Grainstone.—The rippled calcisiltite and grainstone facies overlies surfaces of forced regression (FSST). The facies is characterized by couplets of

white, thin-bedded (~2cm) wave rippled calcisiltite and medium bedded packstones or red-hued very coarse grainstones (Fig. 4A). The grainstones are comprised of large pelmatozoan bioclasts, but are otherwise not fossiliferous. In sequence 1, a cross-bedded crinoidal grainstone is also part of a FSST, but is interbedded with shale rather than calcisiltite.

This facies is characteristic of high energy, detached shoreface deposits (Bergman and Snedden 1999) that were deposited on a wave-dominated inner-ramp during forced regression. Rippled calcisiltites and grainstone packages sharply overlie deeper facies, with little to no transitional facies, suggesting they record relative-sea level fall (Plint 1991; Hunt and Gawthorpe 2000). Up-ramp, this facies is adjacent to tidal or lagoonal deposits (if present), and passes down-ramp into open marine wackestone and packstone (sequence 2), or interbedded grainstone, rudstone and shale (sequence 1).

Interbedded Grainstone, Rudstone and Shale.—The interbedded grainstone and shale facies (Fig. 4E, 6D) is common in the lower Mountain Lake, both within and outside the SOA. It is composed of thin to medium-bedded (cm scale), poorly sorted, nodular grainstones and rudstones interbedded with green to tan fissile shale. Packstones and mudstones (Fig. 4F) are present locally. Bioclastic grainstone and rudstone beds are often slightly sandy, containing small percentages of well-rounded quartz grains. Shales are chloritic and illitic (Longman 1982a), and weather from green to tan. Grainstone beds are highly fossiliferous, poorly sorted and show signs of condensation, such as simple bioturbated and modified firmgrounds (McLaughlin et al. 2008), and authigenic mineral crusts. Grainstones primarily consist of disarticulated crinoids and cystoids (e.g., *Diabolocrinus*, *Platycystites*, *Sinclairocystis*, *Oklahomacystis*, *Pirocystella*), and ramose

and massive bryozoans (e.g., *Batostoma*, *Dianulites*, *Lunaferamita*. *Champlainopora*). Rudstone beds within the shales consist of nearly intact colonies of massive and ramose bryozoans, brachiopods (e.g., *Sowerbyella, Bellimurina, Valcourea)* and receptaculitids, and are sharply overlain by green shales. In grainstones and rudstone, bioclasts range from lightly abraded to nearly pristine. The interbedded grainstone and shale facies shows remarkably little down-ramp facies change (Fig. 8). The primary difference is the increase in shale thickness (e.g. RC as compared to I-35) at localities well within the SOA.

The shales, grainstones and rudstones of this facies were deposited just basinward of the lower shoreface deposits of the Pontotoc Member, but likely represent a broad bathymetric range, from upper middle-ramp to upper outer-ramp. They were deposited at, or below fair weather wave base. Longman (1982) noted that early in the deposition of the Mountain Lake, the limestones in this facies succession transitioned from primarily crinoidal grainstones to beds with intact cystoids and bryozoans (rudstones). He suggested that this was a consequence of decreased current energy. While we agree, our data suggest this transition represents a 3rd order shift from a transgressive (TST), high-energy environment, to a more clastic-rich progradational sequence (HST). Moreover, Longman (1976; 1982b) suggested that the limestone beds were storm-deposited, and the shale accumulated during "quiet times" in the waning periods of storms. While there are undoubtedly some tempesite beds in this facies, they are discrete layers that do not form the entire bed. The episodic starvation model of Datillo et al. (2008) explains the genesis of the pristine rudstones during the early HST. Bryozoan colonies and cystoids are completely articulated and in life position, suggesting they were growing in-situ before

being smothered by episodic mud blanketing (obrution horizons). Further, we find no evidence of pre-existing, fair-weather mixed deposits of mud and skeletal debris that would form the raw material for storm winnowing into shell beds and shales (see Datillo et al. 2008, fig. 5). Rather, the beds are either discrete unfossiliferous green shales, or thin beds of pristine articulated fossils (Fig. 6D).

Condensed Packstone and Wackestone.—The condensed packstone, wackestone and minor grainstone beds form sharp based caps to the rhythmite facies. Generally, this facies consists of fossiliferous, amalgamated wackestone or packstone beds that are medium gray, nodular, with shales either absent or highly indurated. This facies often has heavily mineralized authigenic crusts, or capping hardgrounds indicative of highly sediment starved periods. Greater condensation of the wackestone and packstone relative to the adjacent shalier rhythmite facies is further supported by generally higher radioactivity (Fig. 9) in the former, despite the lack of shale. The fossil biota is well-preserved and similar to the rhythmite facies, with isoteline trilobites, strophomenid brachiopods, ramose bryozoans, and gastropods somewhat commonplace. Bioclasts range from moderately abraded to pristine, and burrows are conspicuous. Down-ramp from the SOA hingeline (e.g., DRa), the condensed packstone beds tend to be much thinner.

The condensed packstone and wackestone facies was deposited in a lower middle-ramp to outer-ramp environment. The wide variety of fossil preservation and presence of burrows suggests deposition between fair-weather and storm weather wave base. The bathymetric position is similar to the rhythmic limestone and shale that characterizes the Mountain Lake, with the primary difference being the direction of low rank sea-level oscillation, and therefore the reduction of the supply of siliciclastics, and degree of

condensation. The nodular fabric of this facies is likely a function of both bioturbation and pressure solution during burial. Hardgrounds, cementation by calcite-spar and authigenic pyrites and iron-oxides all suggest this facies was deposited very slowly.

Rhythmic Mudstone, Wackestone and Shale.—The limestone and shale rhythmite facies (Figs. 3A; 4C, D) is comprised of couplets of thin (3-10 cm), tan to gray, planar to nodular bedded mudstone and wackestone, with argillaceous sublaminated shale of varying thickness. Whole rock mineralogy from x-ray diffraction studies of Bromide carbonates (Pollastro 1991, table 1) indicate high percentages of acid-soluble carbonate, calcite, quartz and clay minerals (illite-smecite, kaolinite, and chlorite), and low percentages of dolomite, ankerite, plagioclase, and K-spar. Bedding is fairly regular, with the shales slightly thinner than the limestone beds. Depending on the cycle, shale interbeds thin or thicken upwards, but most often are relatively equal throughout. Sedimentary structures in the limestone beds include mottled fabrics from bioturbation (Fig. 4D), *Chondrites*, disrupted laminae (Fig. 4C), vertical burrows (often pyritized), and thin shell pavements of strophomenid brachiopods, and trilobites (*Isotelus*, *Thaleops*, *Calyptaulax*, *Remopleurides*) that have been interpreted as below storm wave base obrution horizons (Karim and Westrop 2002). Fossil material is more disarticulated up-ramp (I-35) than down-ramp (DRa, RC), but is generally well-preserved at both. Other common fossils include straight cephalopods, receptaculitids, echinoderm fragments, gastropods (e.g.,*Cyclonema*, *Eotomaria*) and ostracods (e.g., *Anisocyamus*, *Bromidella*). Shales are not nearly as fossiliferous, although cephalopods and articulated receptaculitids are found occasionally. Near or slightly within the SOA hingeline (e.g., 177, I-35, DRa), the rhythmite facies is more nodular and has a thicker shale component

when compared to the same facies within the SOA (e.g., RC, TQ), which is more evenly bedded, but less shaly. The faunas are nearly identical, except that the extraordinarily well-preserved obrution horizons are only preserved at DRa, RC, and TQ, although this may be a function of exposure and weathering. The expansion of this facies between the SOA hingeline and the Criner Hills is attributed to the drastic increase in the shale component of the unit (see isopach map, Longman 1982b, fig. 1), and the expansion of sequence 2 as a whole (see sequence stratigraphy section).

Our interpretation of the rhythmite facies differs somewhat from Longman (1976; 1982b), who suggested that the rhythmites in the Mountain Lake were only deposited along the SOA hingeline. We expand the range of the facies deeper down-ramp, which is an implication of our new correlations and condensation hypothesis of the Pooleville in the SOA (see discussion for details). This facies spans a range of environments from middle (moderate energy) to outer (low energy) ramp, with a wide degree of variation in preservation of bioclasts (tempesites to obrution horizons deeper down-ramp). Deposition was likely between fair weather and storm weather wave base, though the main character of the facies (decimeter-scale shale and marls interbedded with thicker mudstone and wackestone) is conspicuous along the gradient. Thin tempesite beds are interpreted as the distal expression of storm waves just above storm wave base, and the obrution horizons as rapid influxes of sediment which buried in-situ living organisms (Datillo et al. 2008; Brett et al. 2008). Though the facies locally becomes very thin and planar bedded, sediments are never truly laminated, suggesting that there is always at least some bioturbation along the ramp gradient. Longman notes the variability of the rhythmite facies, which he referred to as basinal, but the fauna and degree of bioturbation both

suggest deposition in a range from middle to outer-ramp. Generally speaking, the rhythmite facies is characteristic of other Ordovician outer slope deposits that are produced by pelagic carbonates and clays between fair weather and storm weather wave base (e.g., the Kope Formation, or Bromley Shale, McLaughlin et al. 2004).

Thin bedded Mudstone and Shale. —This facies is only present deep into the SOA, and consists of thin-bedded (~5cm), fine-grained lime mudstone, with very thin partings of shale and marls. Bedding is generally consistent, but eventually doubles in thickness in younger strata, as it becomes more fossiliferous. We correlate this facies with the upper rhythmite facies up-ramp at I-35N, which is a departure from the standard model of Bromide deposition (see discussion). Packstone horizons of extremely well-preserved and often articulated sclerites of the trilobite *Lonchodomas* are common at multiple levels. Other fossils include straight cephalopods, graptolites and inarticulate brachiopods.

Thin-bedded mudstones and shales in the SOA (RC) were deposited in the bathymetrically deepest unit that preserves fossils, characteristic of outer-ramp to basin deposits that were low energy, dysoxic, and typically below storm level wave base. The fauna is low in diversity, and includes extraordinarily well-preserved (e.g., *Lonchodomas),* suggesting that the deposition of lime mud and marls may have been relatively rapid. *Lonchodomas* shell horizons have not been extensively reworked, and show little to no evidence of abrasion. Sediments are not laminated, which suggests there was at least some bioturbation, but there is no significant evidence of storm scouring or reworking that would indicate a bathymetric position above storm weather wave base. Gentle sorting of *Lonchodomas* material may represent the very distal expression of

storm-generated currents. This facies grades into middle/outer-ramp rhythmites up-ramp, which are thicker bedded and more storm-influenced.

Fissile Illitic-Chloritic Shale.—This facies is characterized by a fissile, clay-rich, sublaminated green shale that weathers to a tan color. The facies is common at multiple levels within the Bromide, and is thickest in the lower Mountain Lake. There are two separate occurrences of the clay-rich green shale in the Mountain Lake. The first consists of two or three distinct units of shale (sequence 1) that generally overlie the interbedded grainstone and shale facies, and become progressively thicker down-ramp from 177 to DRa. Localities near the center of the SOA (RC) have similar thicknesses of shale as I-35. The second occurrence of clay-rich shale facies is in the upper Mountain Lake (sequence 2), where Bromide deposition was more carbonate-dominated. The uppermost occurrence of the facies is thickest near the hingeline (177), and thins both up-ramp and down-ramp from the SOA hinge (e.g., I-35, Figs. 7, 8, 9). The upper shale is not present within the Criner Hills. Whole rock mineralogy (Pollastro 1991) of the clay component of the shale facies indicates that the composition is approximately 88-100% illite-smectite, 4% chlorite, and <1% kaolinite. Quartz, pyrite, and feldspar comprised 0-14% of the shale minerologic component (Pollastro 1991, table 2). This relative proportion of clay minerals is similar in shales interbedded with Bromide carbonates (e.g., the rhythmite facies).

Pollastro (1991) suggested that the clay-rich and quartz-poor mineralogy of Bromide Formation shales indicates provenance from either modification of volcanic debris, or that silica was expelled during progressive burial in early diagenesis (possibly being transported up-dip and facilitating sandstone cementation). We cannot provide

evidence that either supports or rejects Pollastro's statements about the provenance of Bromide Formation shales; however, it is certain that there were two separate source areas for siliciclastics for the upper and lower shales. The organic-rich muds of the lower shale were deposited in anoxic to dysoxic basinal waters below storm level wave base, and it predictably thickens down-ramp. Evidence of bioturbation or fossils is absent where the shale is a continuous (i.e., not interbedded with limestone) facies. In contrast, the upper shale is similar in appearance, but it thickens along the hingeline and is thinner or potentially absent in many areas of the basin. It does not contain any sedimentary structures such as desiccation cracks, stromatolites, teepee structures, or fossils (lepertiditian ostracods, gastropods etc.) that would indicate it was a tidal flat mudstone. We tentatively suggest it may represent a lowstand deposit of siliclastics, since it directly overlies a major sequence boundary. Alternatively, it could represent the earliest portion of the overlying transgression where there was a lag time between the sequence boundary and establishment of the carbonate factory (Jones 2010). Though we feel it is unlikely to be derived from volcanic material (because of the thickness), the possibility remains that the quartz-poor mineralogy of the shale indicates an event-driven deposit.

Pooleville Member

Massive to Nodular Lime Mudstone.—This facies comprises the majority of the Pooleville Member, and consists of gray, dark blue, or tan mudstone (Fig. 5B) that is massive or nodular bedded, stylolitic, peloidal (Fig. 3C) and heavily bioturbated. Recrystallization to microspar is relatively common (see Longman 1977 for details) in burrows and mottled features. Mudstone is often interbedded with more fossiliferous and thinner bedded units of wackestone. Fossils include ostracods, gastropods, tabulate corals

(*Tetradium*), receptaculitids, and brachiopods. Steep-sided scoured channels and lenses of skeletal hash (gastropods, brachiopods) are common from up-ramp (HWY99) localities all the way down into the SOA (DRa). Bioclasts are highly abraded, and scoured lenses typically pinch out laterally. Three small bundles of an extremely fine-grained lime mudstone of slightly different character are traceable across several localities near the SOA hinge. Black chert nodules are conspicuous at the I-35 section, but are not common in the Pooleville at other localities.

The extensive evidence of bioturbation and mottled features coupled with the presence of low diversity shallow water fauna (e.g., tabulate corals, lepertiditian ostracods) suggest this facies was deposited in a shallow subtidal environment that was within the photic zone, and somewhat restricted, such as a lagoon or shallow protected inner-ramp. The presence of scour features suggests that this environment was subject to occasional large erosive storm waves, where storm winnowing could rework and concentrate bioclasts. This facies graded down-ramp into deeper, mid-ramp deposits (wackestone with rudstone pavements), and up-ramp into the Corbin Ranch tidal flats. The absence of the transgressive shoal grainstone and packstone facies in adjacent strata suggests that the distribution of transgressive sands was a mosaic, lacking significant linear trends. Both Wilkinson et al. (1999) and Wright and Burgess (2005) note that lateral migration of facies belts rarely produces idealized successions, with carbonate mosaics and frequency-area relationships being a better explanation of the spatial distribution of lithofacies.

Bioclastic Grainstone and Packstone.—The packstone and grainstone facies (Fig. 3D) in the Pooleville Member (sequence 3, TST) consists of dark blue to gray, medium-

bedded (5-10cm), thick-bedded (10-20cm) or massive beds of rubbly, fossiliferous argillaceous limestone. Packstone layers are often interbedded with grainstones, and in some instances, wavy or rubbly grainstones are interbedded with more planar beds. This facies is similar to the condensed packstone and grainstone caps of the Mountain Lake, but the former is grainstone dominated, and the latter packstone dominated. Moreover, the bioclastic grainstone and packstone facies while highly fossiliferous, is less diverse, with isoteline (*Anataphrus*) and illaenid (*Failleana*) trilobites, ramose bryozoans, and echinoderm debris as the primary constituents of the fauna. Authigenic mineral crusts of pyrite and iron oxide are common at multiple levels within the unit, particularly on the tops of grainstone beds. Far up-ramp (HWY99), this facies is considerably more massive, and exhibits low inclination cross-bedding in the correlative facies.

We interpret this facies as a transgressive package of high energy, inner-ramp shoals and mid-ramp packstones, both of which were subject to either constant wave agitation, or frequent storm reworking (above storm wave base). This mosaic blanket of carbonate sands was deposited along an energy gradient from HWY99 well up-ramp, into DRa in the aulacogen. Though there is siliclastic sediment in packstones, and in some local shale partings, the unit as a whole is considerably well-washed; suggesting much of the detrital mud was sequestered close to the shoreline. Longman (1982b) interpreted this facies as a "biosparite buildup" present along the hingeline of the aulacogen, indicating that the carbonate ramp had evolved to a platform regime with a sharp shelf-slope break (Wilson 1975). We suggest that deposition in the Pooleville is still best characterized as a ramp-dominated regime, as this facies is present well into the aulacogen (DRa), exhibits considerable bedding with no relief, and shows gradational trends along the inner-ramp,

from cross-bedded carbonate sands to thin-bedded grainstones and packstones. Previous authors have placed this facies at the top of the Mountain Lake; however, we include it in the Pooleville because it is a temporal unit that can be corrrelated across sections, and is part of the same depositional sequence as the rest of the Pooleville. Furthermore, we suggest later in this paper that much of the Pooleville is condensed down-ramp, meaning that the original designation of the Pooleville (Cooper 1956, at DRa) was based on strata that are likely equivalent to the Mountain Lake up-ramp. So, we formally propose that I-35N should become a reference section with our descriptions serving as a template to recognize our revised concept of this member.

Wackestone with Rudstone Pavements.—The primary component of this facies is a light blue-gray, medium to thick bedded (15-20 cm), slightly nodular, tan-weathering wackestone (Fig. 5C). Packstone is present locally. Beds are often capped by rudstone pavements of pristine, diverse, articulated brachiopods (e.g., *Sowerbyella*, *Strophomena*, *Plectoglossa*), trilobites (*Calyptaulax*, *Bumastoides*, *Thaleops*), ramose bryozoans, and cystoids preserved in life position. The wackestone is otherwise slightly mottled and bioturbated. The thickness of the wackestone is similar between localities near the edge of the SOA (2-4 meters), though it is not present deep within the SOA (see discussion below, our correlations diverge from those previously published). Well up-ramp (HWY99) the facies is a massive, rubbly wackestone with most bedding lost. Along the hingeline (177), the facies is interbedded with very thin marls (1-2cm), which are not present at I-35N.

The wackestone with rudstone pavement facies is interpreted as being deposited in a subtidal, moderate energy, mid-ramp environment that was between storm and fair

weather wave base, and not subject to regular wave agitation of the sea floor (i.e., fossiliferous beds are unwinnowed, Fig. 5C, Datillo et al. 2008). This interpretation is supported by the presence of known (Carlucci and Westrop 2012), open marine trilobites (e.g., *Calyptaulax* and *Thaleops*). Up-ramp this facies merges with the higher energy thin-bedded packstones and grainstones of the lowermost Pooleville. Along the SOA hingline (I-35), Longman (1982) correlated this facies with the couplets of rhythmic shale and carbonate with prominent *Isotelus* beds at DRa, RC, and TQ deep within the SOA. We disagree with this correlation for a number of reasons (see discussion), and instead correlate it with the open marine, well-bedded, fossiliferous wackestone near the top of the Pooleville at RC and TQ.

Corbin Ranch Submember

Fenestral and Microbial Laminated Mudstones—Carbonate mudstones of the Pooleville gradually grade vertically into white to dark gray, dense mudstones with fenestral cavities (Fig. 5A, D), microbial laminations, desiccation cracks, vertical tubes and oxidation marks. Cycles of well-bedded (10-20 cm) fenestral mudstone and thinner bedded (2-4 cm) rubbly wackestone are common both up-ramp on the Arbuckle Platform and near the SOA hinge. Wackestone beds have mm to cm scale shaly interbeds, and lack fenestrae. The fauna primarily consists of ostracods (e.g., *Leperditella*, *Ningulella*, *Ctenobolbina*), corals (*Tetradium*), conodonts, brachiopods (*Ancistrorhyncha*), gastropods, cyanobacteria and rarely trilobites (*Bathuyrus*). On the Arbuckle platform (HWY99), the fenestral units are slightly thicker than at I-35N, and the facies is not present in the Criner Hills. Amsden and Sweet (1983, fig. 12) showed that the Corbin Ranch fenestral facies was nearly identical at HWY99 and I-35 in terms of the relative

percentages of micrite, fenestrae, and bioclasts. Fenestral mudstones of the Corbin Ranch are predominantly calcium carbonate mud in our study areas, with generally around 1% dolomite based on whole rock mineralogy (Amsden and Sweet 1983, unpublished supplemental data). Stylolitic margins and fenestral cavities are filled with fibrous calcite, and often lined with dolomite cement (Fig. 3B), but complete dolomitization of the Corbin Ranch is restricted to areas in far eastern Oklahoma on the Ozark Uplift (Schramm 1964, fig. 16). Wahlman (2010) describes in detail the fabric-retentive microcrystalline dolomites and replacive dolomites of the Bromide in eastern Oklahoma.

The fenestral and microbial laminated mudstone facies was deposited in the low energy intertidal to supratidal zones of a tidal flat. Sedimentary structures of clotted mudstones with early fibrous cemented fenestrae, desiccation cracks, and microbial laminites unambiguously indicate deposition in both intertidal and supratidal environments (see Pratt 2010, fig. 7). This facies is gradually replaced down-ramp by the *Tetradium*-dominated inner-ramp deposits of upper Pooleville. The fenestral mudstone facies represents the shallowest bathymetric position of low rank cycles in the Corbin Ranch (see the sequence stratigraphy section for details), and together with the subtidal wackestone likely represents a complete cycle of subtidal to supratidal environments. Amsden and Sweet (1983) suggested that the restricted fauna, fenestrae, and desiccation cracks were similar to those of Andros Island (Hardie 1977) in the Bahamas, and represent deposition in high intertidal and supratidal environments.

Grainstone and packstones.—This facies and the below-wave base laminated mudstone and shale facies are previously unrecognized units within the Corbin Ranch Submember at HWY99, and may have been included in the Viola Formation in prior studies.

However, they are lithologically more similar to Bromide strata, and immediately underlie the characteristic Viola lithology. A very thin (cm-scale) packstone unit overlies fenestral beds, with corals, gastropods, and echinoderm debris overlain by an extremely irregular mineralized hardground (Fig. 5E, Fig 10E) that is either a low-rank sequence boundary or tidal ravinement surface. Fine-grained bioclastic grainstone overlies this surface and contains a similar irregular erosive surface, which is interpreted as a wave-ravinement surface (Cattaneo and Steel 2003). Just above the bioclastic grainstone, well-preserved diplograptid graptolites and trilobites (*Cryptolithus*) are present at the contact with overlying laminated mudstones.

This facies is interpreted as the expression of the landward shift of the shoreline as Corbin Ranch tidal flats and then inner-ramp shoal environments were scoured by wave action. Elsewhere in the basin, the transition from Corbin Ranch to deep subtidal Viola is unconformable, but at HWY99 it is preserved in one meter of highly condensed strata. This facies records the shallow inner-ramp as its erosional surfaces migrated landwards (Boyd 2010), and is immediately adjacent to fenestral tidal flats that were also eroded during marine transgression.

Below-wave base laminated mudstones and shale.—This facies consists of a white to light gray lime mudstone (Fig. 5F) interbedded with a fissile to marly shale. Mudstones are internally laminated, thin (3-6cm) and evenly bedded, and contain abundant diplograptid graptolites and trilobites (*Cryptolithus*). Shale interbeds thicken upwards from 1 cm to 5 cm near the base of the Viola contact.

This facies is similar to the low diversity *Lonchodomas* and graptolite dominated, thin-bedded mudstone and shale facies present deep within the SOA, and lacks the

characteristic lithology of the overlying Viola Formation. Thus, we infer that its deposition took place in a bathymetrically similar outer-ramp to basin environment, and below storm level wave base.

SEQUENCE ARCHITECTURE

Parasequences (6th order)

Mountain Lake Member.—Parasequences are recognized as gradual shoaling upward cycles of 0.5-2 meters that are present within larger, shallowing upward micro-HST's (see Figs. 10A, 11). Individual parasequences are not mappable across sections, and may represent very low rank regional progradation (allocyclic) from variation in sediment supply of terrigenous mud onto the slope. The relative thickness of the limestone beds, extent of abrasion and reworking of bioclasts, and decrease in interbedded shale are used to infer shallowing upward cyclicity. The gradual and subtle facies transitions stand in stark contrast to the abrupt boundaries of the meter-scale cycles.

Corbin Ranch Member.—Shallowing upward cycles of 0.15-0.4 meters in the Corbin Ranch are best recognized at HWY99, and generally consist of alternating units of fenestral lime mudstones and rubbly shale and wackestone. Fine lime mudstone (often with *Tetradium* and small fenestrae, Fig. 5A) shallows upward into clotted mudstones with large fenestrae (Fig. 5D) and desiccation cracks. Thus, each parasequence ranges from inner-ramp subtidal (wackestone), to possibly lagoonal intertidal (lime mudstone), and then supratidal tidal flats (clotted fenestral mudstone). There are a similar number of cycles at HWY99 and I-35 (3-4); they are similar in thickness and also show strong ordered shallowing upward trends, so we expect they are allocyclic. Autocyclic cycles that record primary signals of tidal-flat migration would likely result in laterally

discontinuous, unordered cycles with variable thickness (Pratt 2010), a trend that does not best describe peritidal beds in the Corbin Ranch. These descriptions are simplifications, as modeling experiments (e.g., Burgess et al. 2001; Burgess 2006) suggest that autocyclic processes can also form ordered cycles. Burgess (2006) also states that autocyclic generation can only truly be rejected if there is evidence of subaerial exposure of subtidal beds from relative sea-level fall.

One complete meter-scale cycle is present above Corbin Ranch parasequences, and preserves both shallowing and deepening components, as well as characteristic surfaces (see below). Cyclicity in the Corbin Ranch is best expressed as a peritidal series of asymmetrical shallowing upward cycles followed by a symmetric cycle that includes the preservation of a trangressive wave dominated coastline.

Meter-scale cycles (5^{th} order)

Mountain Lake Member.—Meter-scale cycles in the Mountain Lake Member (within 3^{rd} order sequences 1-2, Figs. 7, 8) consist of alternating micro-TST's and HST's (meter-scale analogues of systems tracts, Fig. 10A, B) that form packages of "time rich" and "time poor" deposits (Brett and Algeo 2001; Brett et al. 2008). Sequence 1 micro-HSTs range from 0.75 to 2.5 meters in thickness, and micro-TST's are 0.6 to 1 meter thick. In sequence 1, micro-HSTs are units of predominantly siliciclastic shale, interbedded with thin beds of nodular bryozoan and echinoderm grainstone. TSTs are amalgamated and nodular beds of bryozoans and echinoderm grainstone that are starved of siliciclastic sediment, and much more poorly sorted than bioclasts in the HST's. Authigenic mineral crusts (iron-oxide or pyrite) or heavily bioturbated firmgrounds (McLaughlin et al. 2008) commonly cap corroded flooding surfaces, and merged transgressive/sequence boundary

surfaces at the bases of the beds are very irregular facies offsets that show evidence of scouring. Sequence 2 meter-scale cycles are generally thicker than in sequence 1, with micro HST's that range from 0.2 to 3.8 meters in thickness, and micro-TST's from 0.5 to 6.7 meters thick. In sequence 2, micro-HSTs consist of progradational to aggradational interbedded shale and limestone rhythms, often with a thin indurated basal wackestone or packstone bed (Fig. 10B) that immediately underlies the rhythmites. Micro-HSTs are thinly planar bedded near their base, and gradually become more nodular as they decrease in siliciclastic content, and are correlatable from I-35 into the aulacogen (sequence 2, Fig. 8). Low rank transgressive surfaces/sequence boundaries sharply overlie the micro-HST's, and are often irregular erosive disconformities (e.g., Fig. 6E). Sequence 2 micro-TSTs are indurated wackestone and packstone that are shale-poor, show evidence of condensation upwards, such as high radioactivity on gamma ray (Fig. 9), poor sorting, pyritization of bioclasts, and flooding surfaces that are heavily stained with iron-oxide and pyrite mineral crusts. Throughout the Mountain Lake Member, low rank maximum flooding surfaces (MFS) signify an abrupt shift to finer-grained, more siliciclastic-rich facies, and also represent the highest degree of sediment starvation in the micro-sequence (maximum sediment starvation, Baum and Vail 1988; Brett et al. 2004).

These patterns suggest that meter-scale cycles in the Mountain Lake Member are best characterized as symmetric low rank sequences that are responding to changes in relative sea level, and contain both deepening and shallowing components. Based on work in other Ordovician meter-scale cycles (e.g., Kope Formation), alternatives include shallowing upward cycles (e.g., Jennette 1986), deepening upward cycles (e.g., Tobin 1982), or variation in the frequency and intensity of large storms (e.g., Holland et al.

1997, 2008). We reject these alternatives because of the erosive contact between micro-HST's and TST's, condensing upward features of the indurated limestones, and presence of multiple event beds (obrution and tempesites) within each cycle. Given the short duration of the cycles, the primarily signal is likely eustatic (extrinsic) rather than regional tectonics of the basin (intrinsic), but small-scale intrabasinal processes should not be discounted.

Pooleville Member.—In the Pooleville, meter-scale cycles are often lost, since much of the unit is massive, and individual beds are difficult to discern. However, the grainstone- and packstone- dominated unit (sequence 3, TST) may show similar meter-scale cyclicity as the Mountain Lake (Fig. 10C). In this case, the micro-HST (3.7 meters) is represented by slightly shaly, rubbly packstone, with thinly interbedded grainstone (Fig. 10C). Micro-TSTs are 2.6-2.9 meters in thickness, massive, and well-washed, with many sedimentary structures indicative of condensation: authigenic mineral crusts, pyrite and iron oxide halos on bioclasts, poor sorting, and high levels on gamma ray (Fig. 9). While the entire 3rd order TST in sequence 3 shows features indicative of condensation, lower rank cyclicity is evidenced by the relative degree of clastic starvation in the micro-TST compared to the micro-HST.

Corbin Ranch Submember.— Above peritidal shallowing upward cycles, and before the transition to the Viola Formation lithofacies, a complete low rank sequence is preserved (Fig. 10D) at HWY99. The micro-HST consists of rubbly wackestone and thin shale interbeds, which are overlain by a fenestral mudstone with ostracod and gastropod bioclasts. This HST unit is equivalent to the peritidal parasequences described earlier. However, in this last sequence the deepening upward TST package is preserved. The

micro-TST consists of highly condensed bioclastic packstone and grainstone (including a possible bentonite, see Rosenau et al. 2012), which preserves two highly irregular scoured surfaces. The first lies between the fenestral mudstone and bioclastic grainstone, and is interpreted as a tidal ravinement surface or a low rank sequence boundary. The second surface is within a slightly higher grainstone bed, and is interpreted as a wave ravinement surface. Finally, the packstone and grainstone beds grade into mudstone, and are abruptly overlain by a flooding surface (Fig. 5F). The overlying laminated mudstone and shale facies contains abundant cryptolithine trilobites and graptolites, and is similar to one of the deepest facies of the Mountain Lake (the low diversity *Lonchodomas* facies). Thus, the Corbin Ranch Member at HWY99 records a nearly complete package through a transgressive coastline, including most of the expected surfaces in their appropriate order (e.g., Boyd 2010, fig. 29). This transition is not preserved elsewhere in the basin that we are aware of, and we have confirmed via scintillometer the gradual transition as compared to the abrupt increase in radioactivity found at I-35 and 177 (Fig. 9).

Decameter-scale cycles (4^{th} order)

Mountain Lake Member.—In outcrops that are extremely well exposed (e.g., I-35) decameter-scale cycles are apparent. Multiple meter-scale cycles (2-5) comprise 4^{th} order cycles of generally between 4.5-13.5 meters (Fig. 11). They are comparable in thickness to 4^{th} order cycles of Vail et al (1991) and Brett et al (2004) and likely represent depositional cycles of a few hundred thousand years or less. Decameter-scale cycles are thinnest in the 3^{rd} order TST of sequences 1 and 2, and considerably thicker during the major HST interval in sequence 2. Stacked sets of meter-scale cycles form packages that

are comparatively carbonate-rich and shale-poor upward. Moreover, in all except for one decameter-scale cycle (Sequence 2, HST), the total thickness of meter-scale cycles tends to thin upward. Hence, decameter-scale cycles in the Mountain Lake are best characterized as packages of meter-scale cycles that are decreasing in total thickness upward, but increasing in the proportion of limestone thickness. Decameter-scale cycles can be split into two primary hemicycles; a lower shalier rhythmite-dominated unit, and an upper grainstone (sequence 1) or wackestone/packstone-dominated (sequence 2) unit (Fig. 11). The upper limestone hemicycle is characterized by an upward increase in fossil bioclasts, mineral staining, and hardgrounds. Since the micro-HST's in meter-scale cycles tend to thin upward, the basal portion of the rhythmite hemicycle is shaliest, and is inferred to be representative of the deepest highstand conditions of the 4th order cycles. Consequently, the primary signal of decameter-scale cycles consists of depth-related oscillations in siliclastic sediment supply that are of lower rank than those of the depositional sequences.

Depositional Sequences (3rd order)

Stacked sets of decameter-scale cycles comprise composite systems tracts that show net trends characteristic of progradational, aggradational, or retrogradational stacking, and are components of large scale, 3rd order depositional sequences in the Bromide Formation. Depositional sequences comprised of systems tracts are the highest rank of cyclicity recognized here, and our primary unit for discussions of basin architecture and large-scale depositional dynamics. They are temporally analogous to the 3rd order parasequence sets of Pope and Read (1997) and the high rank composite sequences of Brett et al (2004), and likely represent periods of approximately one million

years. The Bromide Formation encompasses a period of deposition through most of the Sandbian, which according to Finney (2005, fig. 2) is about five million years in duration. Intuitively, this makes sense with our observations, especially given the major unconformity at the Bromide/Viola contact. We outline below the major bounding surfaces of each sequence, their lateral variation (where possible), the facies of each systems tract, and the estimated relative variation in depth through each sequence.

Sequence 1.—Sequence 1 is highly condensed relative to sequences 2 and 3, and is the last depositional sequence of the Whiterockian in Oklahoma. The progradational to aggradational series of massive, hummocky cross-stratified, and rippled sandstones and siltstones (Pontotoc Member) forms the base of the Bromide and is interpreted as a 3rd order LST. Mature sands, and clay-rich silts suggest that fluvial-deltaic and eolian-derived sediment was deposited into the basin as a shallow lowstand wedge, which extended well into the SOA (the sands are still thick in the Criner Hills region). Carbonate deposition largely ceased during LST conditions in sequence 1. This wedge was deposited as massive sandstones and siltstones that conceivably downlap onto a sequence boundary. A thick unit of aggradational massive sandstone typically overlies obviously cross-stratified and flaser bedded units, suggesting the rates of aggradation increased through time, as would be expected during lowstand normal regression (Catuneanu 2006; Catuneanu et al. 2009). The relatively rapid increase in carbonate bioclasts above the sandstones implies that the shallow, siliciclastic lowstand wedge may have formed a platform that was suitable for carbonate deposition as sea levels rose (e.g., Handford and Loucks 1993, fig. 15). Lower Mountain Lake (now Pontotoc) sandstones have typically been characterized as the base of a high rank trangression, but when

considered at lower ranks, they are probably best characterized as LST deposits just prior to major condensation and transgression in sequence 1. Longman (1982a, b) noted that episodic deposition of sandstones often exceeded the rate of subsidence, and so are likely progradational in some areas of the basin.

The transgressive surface (TS) is a facies offset (and mineralized surface at RC) that shows a shift from sandstones to bioclastic grainstones that show obvious signs of condensation such as hardgrounds, firmgrounds, and authigenic mineral crusts. The TST succession in sequence 1 consists of two thin 4th order decameter-scale cycles that are grainstone-dominated, and show upward signs of increasing condensation. While not as well exposed at the 177 roadcut, our data suggest that the thickness of the sequence 1 TST is nearly identical from I-35N to 177. The MFS tops the most condensed grainstone bed, and immediately underlies an increase in siliciclastic shale. Intact massive and branching bryozoan colonies are preserved at obrution horizons in the sequence 1 HST shale sequence, whereas reworked crinoidal grainstone was more common during the TST. The increase in siliclastics suggests that a drop in the rate of sea level rise allowed for the progradation of previously sequestered sediment. The lower HST sequence is remarkably consistent from I-35 into the SOA, with the facies succession evolving from shale and rudstones to basinal shale, back into interbeds just below the FRS. The FRS is an erosive surface that corresponds to the abrupt onset of base-level fall, and a change from progradation with aggradation to progradation with downstepping attributes (Posamentier and Morris 2000; Catuneanu et al. 2009). Offshore marine shale and rudstones are abruptly overlain by rippled grainstones and shale, and then cross-bedded crinoidal grainstone (FSST) that was obviously subject to constant wave agitation of the

sea floor. A 20 cm bed of fine lagoonal mudstone, with ostracods and small fenestrae represents the shallowest facies of sequence 1, at the top of the FSST, with the SB directly on top of the bed.

Lateral facies variation within sequence 1 is relatively minor, though it encompasses the widest bathymetric range of depositional environments relative to sequences 2 and 3. LST sandstones range from upper shoreface near the Arbuckle Platform (Longman 1982b, fig. 2) to lower shoreface within the SOA, and based on isopach maps, thicken down-ramp (Schramm 1964, fig. 14). Falling stage deposits show the shallowest sedimentary structures at I-35N, but up-ramp deposits are either not preserved (HWY99) or poorly exposed (177). Given the similarity of facies stacking patterns across sequence 1, cycles of base-level rise and fall were likely uniform throughout the study area.

Sequence 2.—At the onset of sequence 2, a brachiopod hash (abraded rudstone) overlies the irregular, slightly wavy SB. Within the hash, a prominent irregular surface is interpreted as a wave ravinement surface that separates inner-ramp trangressive deposits from the backramp. The TST is dominated by trilobite packstones and crinoidal grainstones with minor shales that form two very condensed 4^{th} order decameter-scale cycles of upward thickening carbonates. The sequence 2 TST is thickest at I-35N, and slightly thinner both up-ramp (177) and down-ramp into the Criner Hills region. As in sequence 1, the MFS tops the thickest and most condensed grainstone bed just prior to the facies offset that signals a change to the rhythmite facies of the middle Mountain Lake Member. The HST deposits in sequence 2 show stacking patterns that are primarily aggradational in its early phases, and strongly progradational in later phases, indicating

decelerating base-level rise. The early HST is rich in siliclastic muds as would be expected in mixed carbonate-siliclastic systems (Mclaughlin et al. 2004). The lower portion of the HST preserves obrution beds of trilobites, echinoderms, cephalopods and brachiopods (I-35, DRa, TQ, RC) that suggest rapid deposition of mud layers. As the rate of progradation increased, the sediment influx increased from the carbonate factory (i.e., highstand shedding, Schlager et al. 1994), allowing for the preservation of thick, higher energy wackestone and packstone beds during late HST. The trilobite fauna changes considerably from early to late HST, with a low diversity *Isotelus* assemblage characteristic of outer-ramp environments (Carlucci and Westrop 2012) transitioning to a more diverse illaenid-asaphid fauna more characteristic of shallow marine settings. The sequence 2 HST is the thickest systems tract in the Bromide because, unlike sequence 1 (siliclastic dominated) and sequence 3 (carbonate dominated), it is receiving sediment both from the carbonate factory and previously sequestered clastics. The HST is thickest at DRa because it is shalier than the other localities, but it follows a similar pattern, with low energy obrution beds being gradually replaced by brachiopod dominated mudstone and rudstones within storm-level wave base. The FRS is a sharp facies offset (Plint 1991; Plint and Nummedal 2000) between the rhythmite facies and a high-energy ripplied calcisiltite and grainstone unit that represents a time period of rapid sea level fall (Cauneanu et al. 2009) not dependent on sediment supply. The FSST is missing deep within the basin, and is only present at I-35 and 177.

Similarly to sequence 1, the range in lateral facies variation between localities in sequence 2 is minor. Sequence 2 is slightly thinner up-ramp at 177, and thicker down-ramp at DRa. Within the SOA, sequence 2 ranges bathymetrically from outer-ramp to

middle-ramp, but does not show as wide a range of variation as I-35 because the FSST is not preserved. We interpret the overlying siliciclastic shale as a probable basinal LST deposit, but suggest ambiguity because of the possibility that it is a modified volcanic deposit (Pollastro 1991).

Sequence 3.—The transgressive surface of sequence 3 is a sharp-based contact between interbedded shale and limestone of the LST and a series of relatively well-washed packstones and grainstones. The sequence 3 TST is composed of a series of characteristic dark blue or tan grainstones and packstones that exhibit many features of condensation (see facies descriptions), and deepening upward patterns. The top grainstone bed is the most condensed, showing an extremely high degree of mineral crusts, pyrite replacement of bioclasts, and very poor sorting. This bed is traceable from far up-ramp (HWY99) into the SOA (DRa). In the Criner Hills, the TST is not preserved, but represented by a series of hardgrounds just prior to the rapid shallowing pattern characteristic of the Pooleville. The sequence 3 TST is thickest at 177, and would likely be thickest at HWY99 (based on the capping grainstone bed) if it were preserved. There is a general trend towards gradual thinning of the TST down-ramp until it is only represented by a strongly condensed interval of hardgrounds. The rather inconsistent pattern of the TST between basal and capping grainstones (compare I-35 and 177, Fig. 7), and its presence across most of the study area suggest that these grainstones formed a complex transgressive mosaic (Wright and Burgess 2005) rather than a shelf edge buildup as suggested by Longman (1982b).

The MFS is the stained surface between the capping grainstone bed and open marine deposits that are more enriched in lime mud. The HST deposits in sequence 3 show stacking patterns that are initially aggradational and represented by mid-ramp

wackestones (Fig. 5C) in its early phases, and then strongly progradational (inner-ramp marine to lagoonal to tidal flat facies). During the rapid shallowing of late HST and deposition of backramp (inner-ramp, shoreward of shoals) peritidal facies, down-ramp localities (e.g., RC) are represented by a very fossiliferous (e.g., *Calyptaulax*, *Isotelus*, *Lonchodomas*, *Frencrinuroides*) wackestone that is similar to the open marine wackestone at I-35N. The sequence 3 HST becomes condensed down-ramp, as the distance from the carbonate factory increases (Fig. 7, 9).

The thickness and assumed variation in bathymetric change during the sequence 3 TST is similar from 177 through DRa. The unit is remarkably similar across localities, allowing for individual beds to be traced down-ramp. The greatest lateral variation in facies during the deposition of the Bromide takes place in the sequence 3 HST, which includes the upper Pooleville and Corbin Ranch Submembers. At I-35N and South, 177, and HWY99 the HST shows a shallowing upward trend from mid-ramp to backramp deposits. In the SOA (DRa, RC), the HST is comparatively thinner, and shows shallowing upward trends from outer-ramp to storm dominated mid-ramp deposits, but never reaches the inner-ramp.

DISCUSSION

We present here updated descriptions of the facies, bounding surfaces, and cyclic architecture present within the Bromide Formation of Oklahoma. Our data provide support for three major contributions to the study of this unit: updated facies associations and basin-ramp depositional models, a much finer delineation of cyclicity and sequences, and new correlations that suggest the Pooleville is condensed down-ramp, and the Mountain Lake expanded.

Implications for the Transgressive-Regressive Model

Many authors (e.g., Longman 1976, 1982a, b; Finney 1986; Bauer 1994) have discussed the presence of a major high rank transgressive-regressive (T-R) sequence in the Bromide Formation (shown here on Figs.7 and 8 for comparison with our sequence stratigraphic interpretation). Under this model the basal sandstone unit is recording a transgression that continues until the deepest portion of the Mountain Lake (rhythmites), which then begins to infill, forming the regressive carbonate interval of the upper Bromide. T-R sequences were originally designated as a sedimentary unit deposited between the beginning of one transgression to the base of the next (Johnson and Murphy 1984; Johnson et al. 1985; Catuneanu et al. 2009). Updated models of the T-R sequence emphasize the importance of subaerial unconformities and marine maximum regression surfaces (Embry and Johannessen 1992), but are limited by the cryptic and diachronous nature of maximum regression surfaces in deep-water and the lack of differentiation between normal and forced regression (Catuneanu et al. 2009). We do not find sufficient evidence of the appropriate bounding surfaces for a formal high rank T-R sequence, and suggest that it should only be used as a general descriptor of high rank subsidence in the study area. Moreover, the traditional use of the T-R sequence to describe Bromide deposits relies on classifying the strata based on the inferred position of sea level, rather than variation in the rate of sea-level change and sedimentation.

Candelaria and Handford (1995) have suggested that the entire Bromide is part of a 3rd order sequence that includes the Tulip Creek Sandstone as early TST, and the Bromide as late TST and HST. Candelaria and Handford (1995) outlined a conceptual model of Simpson Group sequence stratigraphy that postulated that each basal sandstone

unit is trangressive, with overlying shales and carbonates as highstand. They note that their model is not based on physical evidence of bounding surfaces, and that data is still required to support their hypothesis. We do not speculate on the large-scale geometry of the entire Simpson Group as it is beyond the scope of this study. Based on estimates of global sea level (Ross and Ross 1995) that show multiple cycles of sea-level rise and fall during the Mohawkian, estimates of the duration of Bromide-aged deposits (e.g., Finney 2005), and the traditional use of 3rd order depositional sequences (e.g., Pope and Read 1997; Holland and Patzkowsky 1996; McLaughlin et al. 2004) in outcrop studies, we speculate that the patterns described by Candelaria and Handford (1995) are best characterized as higher rank than 3rd order. These geometries not seen in outcrop scale studies are likely of intermediate rank (between 3rd and 2nd order) as the Tulip Creek-Bromide interval spans a large portion of the Darriwilian and the entire Sandbian (>5 ma). Thus, our three major depositional sequences are likely nested within these potentially higher rank patterns. Sequence 2 undoubtedly reaches the deepest bathymetric extent, with sequences 1 and 3 forming shallower bookends (Fig. 12). This certainly could be interpreted as evidence of a transgressive-regressive cycle of subsidence and infilling/uplift over the span of several million years. However, we should note some concerns with the idea that most Simpson Group sandstones are components of major TST's. Isopach maps (e.g., Schramm 1964) show that Bromide sandstones thicken down-ramp towards the SOA, with thick deposits along the hingeline, and well into parts of the basin (e.g., RC). Catuneanu (2006) notes that TST deposits are typically subject to non-deposition in the shelf-edge region, with more distal marine deposits starved of terrigenous sediment. Further, as discussed here and in Longman (1981; 1982a), Bromide

sandstones show evidence of progradational stacking. At ranks higher than we can resolve here (e.g., seismic), the presence of a topset (rather than offlap and truncation) would provide evidence for large-scale lowstand wedges (Catuneanu 2006). Candeleria and Handford (1995) suggested that the sandstone sequence in the Oil Creek Formation (also Simpson Group) was more representative of LST-wedge type deposits than the Bromide because of sandstone distribution along the basin margin of the SOA.

Implications for Intrabasinal and Subsurface Correlation

Lithofacies and sequence stratigraphic analyses suggest that the upper Bromide Formation underwent significant down-ramp condensation and shut-down of carbonate production, which is in contrast to previous interpretations of massive down-ramp expansion of carbonate deposits in the Pooleville (Longman 1976, 1982; Finney 1986). Previous interpretations have suggested that the center of the aulacogen was still at moderate subtidal depth and receiving sediment while deposition was intertidal or had ceased up-ramp (Finney 1986). However, we present evidence that this pattern was true only for the upper portion of the down-ramp sections (sequence 3 HST) rather than nearly 70 meters at DRa and 40 meters at RC (see Fay et al. 1982b, fig. 78). Longman (1982a) stated that the basinal deposits in the lower Pooleville within the SOA (e.g., DRa, RC) and those of the upper Mountain Lake along the hingeline (e.g., I-35) shared the same characteristic bedding (compare Figs 4C and 4D, and 6C and 6E). We provide evidence here that they are broadly correlative. In other words, we push the correlations upwards, and place the down-ramp expansion of the Bromide thickness (see Longman 1982b, fig. 1) into the more clastic dominated Mountain Lake, rather than the primarily carbonate Pooleville Member.

Our evidence to support this assertion is multi-faceted. The correlation of the sequence 3 TST and characteristic fine mudstone beds ("C" on Figs. 7 and 8) between I-35 north and south and DRa show down-ramp compression of the upper Pooleville, which is supported by the presence of hardgrounds in a similar position during the sequence 3 TST in the Criner Hills (RC). The thin limestone sequence above the sequence 3 TST at DRa is the only unit characteristic of Pooleville lithology. The other deposits are rhythmically bedded like the Mountain Lake, and follow the same patterns of initially deepening, and then aggrading, and finally shallowing dramatically as the sequence 2 Mountain Lake deposits up-ramp. They have expanded in thickness because they are appreciably shalier. One reason this correlation may not have been considered earlier is the apparent increase in bioclasts from I-35 to DRa in the rhythmite packages. This is almost certainly an artifact of weathering, as the down-ramp localities (DRa, RC) are in creek beds, whereas I-35N is a steep vertical face. Our investigation has uncovered extremely similar strophomenid beds, straight cephalopods, and identical species of trilobites among the rhythmite packages. The same species of *Thaleops* and *Ceraurinella* trilobites occur at DRa and the lower Mountain Lake at I-35N, whereas different species of the same genera occur in the Pooleville at I-35N and TQ. Moreover, an identical species of the planktic *Remopleurides* is found in the lower to middle Mountain Lake at I-35 and the basal "Pooleville" rhythmites at RC. In other words, the species-level similarities in the trilobite faunas of the rhythmite facies of DRa and RC supports our assertion that it correlates with the same facies up-ramp, rather than with the Pooleville. There is also evidence that the rhythmites are deeper down-ramp; as they are shalier, the bioclasts are less reworked, they tend to be less nodular (compare Figs. 6C, E), and

achieve a deeper bathymetric position in sequence 2 (*Lonchodomas* mudstone, "B" on Fig. 8). Trilobites that have been considered part of the Pooleville Fauna (e.g., *Probolichas*, *Frencrinuroides*; Shaw 1974) are also present within the Mountain Lake, suggesting they are facies controlled rather than useful temporal markers. Similarly, the lower and upper echinoderm zones used by Sprinkle (1982) to aid in correlation of Bromide sections are almost certainly recurring biofacies rather than temporal units. The correlations used by Sprinkle (1982, fig. 28) stress the importance of echinoderm density as a correlation tool, even though similar assemblages of echinoderms are present almost ubiquitously throughout the Bromide. In our opinion, this has led to some erroneous suggested correlations between I-35N and DRa. Moreover, the upper and lower echinoderm zones of Sprinkle (1982) are not present within the Criner Hills, which has a considerably different echinoderm fauna, suggesting the use of these zones for correlation purposes is questionable.

Sequences 1-3 can be correlated into the subsurface (Fig. 9) based on the comparison of outcrop gamma ray scintillometer (CPS) and subsurface well logs (API). Though scintillometer measurements are point counts, and subsurface logs continuous profiles, they are sufficiently similar to permit correlation (Ettensohn et al. 1979). Gamma ray correlations were further informed by bulk density and neutron porosity, as well as comparison of facies between I-35 and 177. The correlations were done independently of the conventions used in the oil and gas industry because of nomenclatural differences. For example, much of the "Bromide" sands in the subsurface actually correspond to the Tulip Creek on the surface, and the Bromide dense is often the lower Viola Springs Formation. Therefore our correlations are based on our outcrop

gamma ray observations. For instance, where the Corbin Ranch is complete (e.g., I-35N, Fig. 9) rather than faulted out (e.g., 177, Fig. 9), there is a double-pronged excursion into the Viola, over dense, and low CPS limestones. Sequence 1 is characterized by low API sandstones (LST), which are overlain by interbedded sandstones then grainstones (TST), which result in large amplitude fluctuations of gamma ray values. The HST in sequence 1 (the lower green shale dominated unit of the Bromide) is easily traceable into the surface across the study area. Gamma ray radioactivity drops dramatically during the FSST into sequence 2, where the rhythmite packages thicken down-ramp. Individual excursions can be correlated between Healy 1-11 and Pruitt 1, showing the expansion of sequence 2 deep into the basin. Pruitt 1 is between DRa and RC, and supports our conclusion that sequence 2 expands down-ramp and sequence 3 (i.e., the Pooleville) thins. The LST shale of sequence 3 is thickest along the SOA hingeline, but traceable across the subsurface study area. The sequence 3 TST generally increases in radioactivity upwards, and has two broad excursions that are easily correlated. This is overlain by a shallowing upward sequence of dense and low radioactivity limestones (HST) that is sharply overlain by the characteristic Viola excursion. The shale excursion in Pruitt 1 corresponds to the shaly unit present at DRa (Fig. 8) during the sequence 3 HST.

Depositional Model of the Bromide

Previous workers (e.g., Longman 1976, 1982a, b) have suggested that a carbonate ramp system in the Mountain Lake evolved into a rimmed platform, with a distinct shelf edge biosparite buildup during Pooleville deposition. Our facies associations and correlations suggest that deposition of the Bromide is best characterized as an unrimmed ramp that distally steepened into the SOA (Fig. 12). The biosparites that Longman

considered a buildup show extensive evidence of condensation, and are traceable from far up-ramp into the SOA (DRa), and are best considered a transgressive mosaic rather than a buildup. Moreover, our study yielded no evidence of in situ organic buildups near the platform edge or upper slope during the deposition of the Bromide. Our new correlations all imply gradational differences between nearshore, wave-agitated facies and offshore environments. A consequence of these correlations is that the center of the SOA was not a major carbonate depocenter while inner-ramp environments were intertidal (Finney 1986). In other words, our model suggests that during deposition of the upper Pooleville, inner-ramp deposits along the SOA hingeline graded into middle-ramp environments that were farther from the carbonate factory. Thus, our facies data places a more continuous and less dramatic change in facies moving down-ramp. Isopach maps (Lonman 1982, fig. 1) show a gradual increase in thickness moving down-ramp, generally supporting this interpretation. The contour of highest thickness is about half way into the SOA (DRa Fig. 8, Pruitt 1 Fig. 9), and corresponds well to where the ramp becomes distally steepened. Under old models (Longman 1976; 1982a, b; Finney 1986) it is possible for the deepest facies of the Criner Hills (*Lonchodomas* mudstone) to be deposited at the same time as the shallowest facies (lagoonal to fenestral mudstones) up-ramp. Moreover, since there are multiple facies transitions during "Pooleville" deposition in the Criner Hills, the SOA would have to be experiencing multiple subsidence and uplift events that did not effect up-ramp localities (which shallow unidirectionally during sequence 3 HST). Williams and Siveter (1996) noted the lack of regression during much of the Pooleville deposition within the SOA, but did not suggest a reason the pattern differed so much from up-ramp localities. A strongly rimmed platform would also limit the ease in which sediment can

be transported into the basin (James et al. 2010), which contradicts the extreme expansion of the Bromide thickness down-ramp. While there was undoubtedly semi-restricted lagoonal-type deposits behind bioclastic shoals during Pooleville deposition (Fig. 12), the complexity of nearshore facies and high energy inner-ramp tempesites (Fig. 5C), are better explained by a model that allows for extensive waves and swells to move directly onto the ramp (James et al. 2010).

An updated model of Bromide deposition (Fig. 12) shows three 3rd order sequences that demonstrate the gradual transition (Fig. 9) from a siliciclastic dominated ramp (sequence 1), to a mixed siliclastic-carbonate ramp (sequence 2), to a warm-water, neritic carbonate ramp (sequence 3). Tidal environments are dominated by siliciclastic, flaser-bedded facies in sequence 1, and by sequence 3 similar environments are dominated by fenestral and microbial laminated lime muds. Middle-ramp environments are dominated by silt, sand and grainstone during the deposition of sequence 1; marls and wackestone during sequence 2, then finally to nodular limestones in sequence 3. This pattern is consistent across environments, with sequence 2 recording a transitional period between depositional regimes.

The Age of the Bromide

Holland and Patzkowsky (1996) identified six 3rd order depositional sequences in the Mohawkian of the Cincinnati Arch and Appalachian basins. In Oklahoma, the Guttenburg carbon isotope excursion (GICE) has been recognized at the Fittstown (HWY99) section in the Viola Springs Formation (Young et al. 2005; Rosenau et al. 2012), which has been associated with the M5A depositional sequence (Brett et al. 2004) in the Lexington Limestone in Kentucky, Trenton Limestone in Virginia, and the Dolly

Ridge Formation in West Virginia. This places an upper limit on the age of the Bromide Formation (equivalent to the latest Turinian; M4 in eastern North America). The lower limit has been less well discussed, though Bauer (1994) suggested that the Bromide is late Whiterockian to Mohawkian based on comparison of the conodont fauna with the range standards of Sweet (1984) and Bergström (1983). In the lower Mountain Lake, *C. sweeti* is indicative of the late Whiterockian, and is replaced by Mohawkian conodonts *Baltoniodus gerdae* and *Eoplacognathus elongatus* in the Mountain Lake. Bauer (1994, table 2) noted that *C. sweeti* showed a strong proclivity for shallower water environments, while *B. gerdae* possessed deep-water facies control. Even though *B. gerdae* has been found in multiple horizons at RC in the Criner Hills, and only in the deepest portion of the upper Mountain Lake at I-35N, it should not be taken as evidence that the deep SOA is stratigraphically younger than up-ramp localities because of the deep-water inclination of that conodont. In other words, it is expected that it would not be present in the shallow water environments of the Pooleville along the SOA hingeline. Independent estimates of the age of the upper strata in the Criner Hills compared to I-35 are inconclusive. Decker (1935, 1941) and Finney (1986) showed that graptolites from the upper Bromide (*Amplexograptus maxwelli*, *Dicellograptus flexuosus*) are diagnostic of the British *D. multidens* Zone. The *D. multidens* zone spans the Deicke, Millbrig, and Kinnekulle bentonites, and based on 40Ar/39Ar dating (Min et al. 2001) is 6.8 ± 2.8 Ma in duration. Consequently, the duration is too long to be useful in evaluating whether sequence 3 is condensed down-ramp relative to I-35N. Interestingly, both Bauer (1994) and Rosenau (2012) found *Phragmodus undatus* at HWY 99 (far up-ramp), but it has not been found in the Criner Hills. This is strong evidence that the Pooleville within the SOA

is not significantly younger, and therefore indicative of a period of deposition while up-ramp environments were subaerially exposed (Finney 1986). For simplicity's sake, we place the contact between the Whiterockian and Mohawkian (Figs. 7 and 8) at the first appearance of obviously Mohawkian conodonts (e.g., *E. elongatus*).

A high-resolution interbasinal correlation is beyond the scope of this paper, but general comparisons can be made to the depositional sequences of eastern North America. The latest Whiterockian sequence in the Appalachians (Wa-1) and the Mohawkian sequences (M1-M4) of Holland and Patzkowsky (1996) are similar in temporal scale to those of the Bromide Formation. The trilobite fauna (see Carlucci et al. 2010; Carlucci and Westrop 2012; Carlucci et al. 2012) of the Mountain Lake and Pooleville (sequences 2 and 3) show remarkable similarities to those of the Effna and Edinburgh (Botetourt and Liberty Hall facies), which span the Wa-1 through M3 sequences. Low diversity, deep-water associations of *Lonchodomas* and/or *Ampyx* with *Isotelus* are common in the Edinburgh and upper Mountain Lake. Furthermore, shallow-water fauna across the two basins are represented by closely related species of *Amphilichas*, *Probolichas*, *Thaleops*, *Bumastoides*, and *Calyptaulax*. Given the position of the Whiterockian/Mohawkian boundary and faunal similarities, it is likely that sequences 1-3 in the Bromide broadly correlate with the latest Wa-1 and M1-M4 in eastern North America. Based on their interpretation of the bentonite stratigraphy (potentially the Deicke and Millbrig) and conodont zonation, Rosenau et al. (2012) considered the Pooleville (sequence 3) as equivalent to M4 in eastern North America.

CONCLUSIONS

The late Whiterockian to Mohawkian Bromide Formation succession in south-central Oklahoma was deposited along a mixed siliciclastic-carbonate ramp that distally steepened into the Southern Oklahoma Aulocogen (SOA). Inner-ramp (above FWWB) lithofacies suggest deposition in a range of environments: tidal flats, lagoons, shoreface, semi-restricted shallow marine, and bioclastic shoals. High-energy storm deposits are common in the inner-ramp, suggesting that they were not restricted enough to limit the incursion of waves and swells onto the ramp. Middle-ramp environments (between FWWB and SWB) are thick and diverse, and consist of rhythmically bedded marls, wackestone, packstone, clastic shales and sandstones. Outer-ramp environments (below SWB) are represented by either fissile green shales or thin-bedded mudstones and shales. Ramp stratigraphy, facies associations and bounding surfaces suggest the deposition of three 3rd order depositional sequences that demonstrate the transition from a primarily clastic ramp to a carbonate-dominated ramp. Sequence stratigraphic analysis shows that the stacking patterns and cyclicity in the Bromide are considerably more complicated than the simple transgressive-regressive cycle traditionally used to describe accommodation dynamics in the basin. At lower ranks, decameter-scale packages thicken upwards in terms of their carbonate components, and often have thinning upward meter-scale cycles. Meter-scale cycles show evidence of both shallowing (micro-HST) and deepening (micro-TST) upward trends. New correlations based on measured sections, outcrop gamma ray profiles, and subsurface well logs suggest that sequence 2 expanded down-ramp, while the primarily carbonate sequence 3 exhibits strong condensation deep within the SOA. Moreover, newly documented facies associations and correlations

necessitate the addition of a reference section (I-35N) to the Pooleville, and the promotion of the lower sand unit to formal submember status (Pontotoc Member).

ACKNOWLEDGEMENTS

This research was funded by National Science Foundation grant EAR-0819715 to S. Westrop and a Geological Society of America research grant to J. Carlucci. A. Thomas, K. Carlucci, and S. Boyd assisted in fieldwork.

REFERENCES

AMSDEN, T.W., and SWEET, W.C., 1983 Upper Bromide Formation and Viola Group (Middle and Upper Ordovician) in Eastern Oklahoma: Oklahoma Geological Survey Bulletin, v. 132, p. 1-76.

BAMBACH, R.K., SCOTESE, C.R., and ZIEGLER, A.M., 1980, Before Pangea: the geographies of the Paleozoic world: American Scientist, v. 68, p. 26-38.

BAUER, J., 1990, Stratigraphy and conodont biostratigraphy of the upper Simpson Group, Arbuckle Mountains, Oklahoma, *in* Ritter, S., ed., Early to Middle Paleozoic Conodont Biostratigraphy of the Arbuckle Mountains Southern Okahoma: Norman, Oklahoma Geological Survey Guidebook 27, p. 39-54.

BAUER, J.A., 1994, Conodonts from the Bromide Formation (Middle Ordovician), south-central Oklahoma: Journal of Paleontology, v. 68, p. 358-376.

BAUM, G.R., and VAIL, P.R., 1988, Sequence stratigraphic concepts applied to Paleogene outcrops, Gulf and Atlantic basins, *in* Wilgus, C.K., Hastings, B.K., Posamentier, H.W, Wagoner, J.V., Ross, C.A., and Kendall, C.G.S.C., eds., Sea-level Changes: An Integrated Approach, Society of Economic Paleontology and Minerology Special Publication 42, p. 309-327.

BERGMAN, K.M., and SNEDDEN, J.W., 1999, Isolated Shallow Marine Sand Bodies: Sequence Stratigraphic Analysis and Sedimentologic Interpretation: Tulsa, Society for Sedimentary Geology Special Publication 64, 362 p.

BERGSTRÖM, S.M., 1983, Biogeography, evolutionary relationships, and biostratigraphic significance of Ordovician platform conodonts: Fossils and Strata, v. 15, p. 35-58.

BERGSTRÖM, S.M., XU, C., GUTIÉRREZ-MARCO, J.C., and DRONOV, A., 2008, The new chronostratigraphic classification of the Ordovician system and its relation to major regional series and stages and to $\delta^{13}C$ chemostratigraphy: Lethaia, v. 42, p. 97-107.

BOYD, R., 2010, Transgressive wave-dominated coasts, *in* James, N.P., and Dalrymple, R.W., eds., Facies Models 4, Geological Society of Canada, p. 265-294.

BRETT, C.E., and ALGEO, T.J., 2001, Sequence stratigraphy of Upper Ordovician and Lower Silurian strata of the Cincinnati Arch region., *in* Algeo, T.J., and Brett, C.E., eds., Sequence, cycle and event stratigraphy of the Upper Ordovician and Silurian Strata of the Cincinnati Arch Region. Kentucky Geological Survey Field Trip Guidebook 1, series XII.: Cincinnati OH, SEPM.

BRETT, C.E., MCLAUGHLIN, P.I., BAIRD, G.C., and CORNELL, S.R., 2004, Comparative sequence stratigraphy of the Upper Ordovician (Turinian-Edenian) of the Trenton shelf (New York-Ontario) and Lexington Platform (Kentucky, southern Ohio) successions: implications for improved paleogeographic resolution of eastern Laurentia: Palaeogeography, Palaeoclimatology, Palaeoecology, v. 210, p. 295-329.

BRETT, C.E., ALGEO, T.J., and MCLAUGHLIN, P.I., 2008, Use of event beds and sedimentary cycles in high-resolution stratigraphic correlation of lithologicaly repetitive successions: the upper Ordovician Kope Formation of northern Kentucky and southern Ohio, *in* Harries, P.J., ed., High-Resolution Approaches in Stratigraphic Paleontology, Springer Science.

BURGESS, P.M., 2006, The signal and the noise: forward modeling of allocyclic and autocyclic processes influencing peritidal carbonate stacking patterns: Journal of Sedimentary Research, v. 76, p. 962-977.

BURGESS, P.M., WRIGHT, V.P., and EMERY, D., 2001, Numerical forward modeling of peritidal carbonate parasequence development: implications for outcrop interpretation: Basin Research, v. 13, p. 1-16.

CANDELARIA, M.P., and HANDFORD, C.R., 1995, Sequence stratigraphic model for Simpson Group of the southern midcontinent, *in* Hyne, N.J., ed., Sequence Stratigraphy of the Midcontinent, Tulsa Geological Society Special Publication 4, p. 319-348.

CARLUCCI, J.R., WESTROP, S.R, and AMATI, L., 2010, Tetralichine trilobites from the Upper Ordovician of Oklahoma and Virginia, and phylogenetic systematics of the Tetralichini: Journal of Paleontology, v. 84, p. 1099-1120.

CARLUCCI, J.R., WESTROP, S.R., AMATI, L., ADRAIN, J.M., and SWISHER, R.E., 2012, A Systematic revision of the Upper Ordovician trilobite genus *Bumastoides* (Trilobita: Illaenidae) with new species from Oklahoma, Virginia, and Missouri: Journal of Systematic Palaeontology, v. 10, in press.

CARLUCCI, J.R., and WESTROP, S.R., 2012, Trilobite biofacies along an Ordovician (Sandbian) carbonate buildup to basin gradient, southwestern Virginia: PALAIOS, v. 27, p. 19-34.

CATTANEO, A., and STEEL, R.J., 2003, Transgressive deposits: a review of their variability: Earth Science Reviews, v. 62, p. 187-228.

CATUNEANU, O., 2006, Principles of Sequence Stratigraphy: Oxford, Elsevier, 375 p.

CATUNEANU, O., ABREU, V., BHATTACHARYA, J.P., BLUM, M.D., DALRYMPLE, R.W., ERIKSSON, P.G., FIELDING, C.R., FISHER, W.L., GALLOWAY, W.E., GIBLINGI, M.R., GILES, K.A., HOLBROOK, J.M., JORDAN, R., KENDALL, C.G.S.C., MACURDA, B., MARTINSEN, O.J., MIALL, A.D., NEAL, J.E., NUMMEDAL, D., POMAR, L., POSAMENTIER, H.W., PRATT, B.R., SARG, J.F., SHANLEY, K.W., STEEL, R.J., STRASSER, A., TUCKER, M.E., and WINKER, C., 2009, Towards the standardization of sequence stratigraphy: Earth Science Reviews, v. 92, p. 1-33.

CLIFTON, H.E., 2006, A reexamination of facies models for clastic shorelines, *in* Posamentier, H.W., and Walker, R.G., eds., Facies Models Revisited, Society of Economic Paleontologists and Mineralogists, Special Publication 84, p. 293-337.

COOPER, G.A., 1956, Early Middle Ordovician of the United States, *in* Bassett, M.G., ed., The Ordovician System, University of Wales Press and National Museum of Wales, p. 171-194.

CUFFEY, C.A., and CUFFEY, R.J., 1995, The Chickasaw Bryozoan reef in the middle Ordovician of south-central Oklahoma, *in* Cooper, J.D., Droser, M.L., and Finney, S.C., eds., Ordovician Odyssey: Short Papers for the Seventh International Symposium on the

Ordovician System: Fullerton, SEPM Pacific Section, p. 435-437.

DATTILO, B.F., BRETT, C.E., TSUJITA, C.J., and FAIRHURST, R., 2008, Sediment supply versus storm winnowing in the development of muddy and shelly interbeds from the Upper Ordovician of the Cincinnati region, USA: Canadian Journal of Earth Science, v. 45, p. 243-265.

DECKER, C.E., 1930, Simpson Group of Arbuckle and Wichita Mountains, Oklahoma: American Association of Petroleum Geologists Bulletin, v. 14, p. 1493-1505.

DECKER, C.E., 1935, The graptolites of the Simpson Group of Oklahoma: National Academy of Sciences Proceedings, v. 21, p. 239-243.

DECKER, C.E., 1941, Simpson Group of Arbuckle and Wichita mountains of Oklahoma: American Association of Petroleum Geologists Bulletin, v. 25, p. 650-667.

DERBY, J.R., BAUER, J.A., CREATH, W.B., DRESBACH, R.I., ETHINGTON, R.L., LOCH, J.D., STITT, J.H., MCHARGUE, T.R., MILLER, J.F., MILLER, M.A., REPETSKI, J.E., SWEET, W.C., TAYLOR, J.F., and WILLIAMS, M., 1991, Biostratigraphy of the Timbered Hills, Arbuckle, and Simpson groups, Cambrian and Ordovician, Oklahoma: A review of correlation tools and techniques available to the explorationist: Oklahoma Geological Survey Circular, v. 92, p. 15-41.

EDSON, F.C., 1927, Ordovician correlations in Oklahoma: American Association of Petroleum Geologists Bulletin, v. 11, p. 967-975.

EMBRY, A.F., and JOHANNESSEN, E.P., 1992, T-R sequence stratigraphy, facies analysis and reservoir distribution in the uppermost Triassic-lower Jurassic succession, western Sverdrup Basin, arctic Canada, *in* Vorren, T.O., Bergsager,

E., Dahl-Stamnes, O.A., Holter, E., Johansen, B., Lie, E., and Lund, T.B., eds., Arctic Geology and Petroleum Potential, Norwegian Petroleum Society Special Publication 2, p. 121-146.

ETTENSOHN, F.R., FULTON, L.P., and KEPFERLE, R.C., 1979, Use of scintillometer and gamma-ray logs for correlation and stratigraphy in homogeneous black shales: summary: Geological Society of America Bulletin, v. 90, p. 421-423.

FAY, R.O., and GRAFFHAM, A.A., 1982, Stratigraphic studies, *in* Sprinkle, J., ed., Echinoderm Faunas from the Bromide formation (Middle Ordovician) of Oklahoma, University of Kansas Paleontological Contributions, Monograph, p. 195-209.

FAY, R.O., GRAFFHAM, A.A., and SPRINKLE, J.S., 1982a, Previous studies of Bromide echinoderms, *in* Sprinkle, J., ed., Echinoderm Faunas from the Bromide formation (Middle Ordovician) of Oklahoma, University of Kansas Paleontological Contributions, Monograph, p. 35-43.

FAY, R.O., GRAFFHAM, A.A., and SPRINKLE, J., 1982b, Appendix: Measured sections and collecting localities, *in* Sprinkle, J., ed., Echinoderm faunas from the Bromide Formation (Middle Ordovician) of Oklahoma, University of Kansas Paleontological Contributions Monograph, p. 335-369.

FINNEY, S.C., 1986, Graptolite biofacies and correlation of eustatic, subsidence, and tectonic events in the Middle to Upper Ordovician of North America: PALAIOS, v. 1, p. 435-461.

FINNEY, S., 2005, Global series and stages for the Ordovician system: a progress report: Geologica Acta, v. 3, p. 309-316.

FOLK, R.L., 1980, Petrology of Sedimentary Rocks: Austin, TX, Hemphill Publishing, 184 p.

GRAHN, Y., and MILLER, M.A., 1986, Chitinozoa from the middle Ordovician Bromide Formation, Arbuckle Mountains, Oklahoma, U.S.A: Neues Jahrbuch für Geologie und Paläontologie, Abhandlungen, Abteilung B, v. 172, p. 381-403.

HAM, W.E., 1969, Regional Geology of the Arbuckle Mountains, Oklahoma, Oklahoma Geological Survey Guide Book 17, 52 p.

HANDFORD, C.R., and LOUCKS, R.G., 1993, Carbonate depositional sequences and systems tracts- response of carbonate platforms to relative sea-level changes, *in* Loucks, R.G., and Sarg, J.F., eds., Carbonate Sequence Stratigraphy: Recent Developments and Applications, American Association of Petroleum Geologists Memoir 57, p. 3-41.

HARDIE, L.A., 1977, Sedimentation on the modern carbonate tidal flats of northwest Andros Island, Bahamas: Baltimore, Johns Hopkins University Press, 202 p.

HARRIS, R.W., 1957, Ostracoda of the Simpson Group: Oklahoma Geological Survey Bulletin, v. 75, p. 1-333.

HOLLAND, S., and PATZKOWSKY, M., 1996, Sequence stratigraphy and long-term paleooceanographic changes in the Middle and Upper Ordovician of the eastern United States, *in* Witzke, B., Ludvigson, G., and Day, J., eds., Paleozoic Sequence Stratigraphy: Views from the North American Craton, GSA Special Paper 306: Boulder CO, Geological Society of America, p. 117-129.

HOLLAND, S.M., MILLER, A.I., DATTILO, B.F., MEYER, D.L., and DIEKMEYER, S.L., 1997, Cycle anatomy and variability in the storm-dominated type

Cincinnatian (Upper Ordovician): Coming to grips with cycle delineation and genesis: Journal of Geology, v. 105, p. 135-152.

HOLLAND, S.M., 2008, Climate-driven storm cyclicity: A non-eustatic mechanism for generating offshore meter-scale cycles, *in* McLaughlin, P.I., Brett, C.E., Holland, S.M., and Storrs, G.W., eds., Statigraphic Renaissance in the Cincinnati Arch, Cincinnati Museum Center Scientific Contributions 2, p. 44-57.

HUNT, D., and TUCKER, M.E., 1992, Stranded parasequences and the forced regressive wedge systems tract: deposition during base-level fall: Sedimentary Geology, v. 81, p. 1-9.

HUNT, D., and TUCKER, M.E., 1995, Stranded parasequences and the forced regressive wedge systems tract: deposition during base-level fall-reply: Sedimentary Geology, v. 95, p. 147-160.

HUNT, D., and GAWTHORPE, R.L., 2000, Sedimentary Responses to Forced Regressions: Geological Society Special Publication 172: Oxford, Geological Society of London, 400 p.

JENNETTE, D.C., 1986, Storm Dominated Cyclic Ramp Deposits of the Kope-Fairview Transition (Upper Ordovician), Southwestern Ohio and Northern Kentucky, Unpublished M.S thesis, University of Cincinnati, 210 p.

JOHNSON, K.S., AMSDEN, T.W., DENISON, R.E., DUTTON, S.P., GOLDSTEIN, A.G., RASCOE, B., SUTHERLAND, P.K., and THOMPSON, D.M., 1988, Southern midcontinent region, *in* Sloss, L.L., ed., Sedimentary cover- North American craton, U.S., Geological Society of America, The Geology of North America D-2, p. 307-359.

JOHNSON, K., 1991, Geologic overview and economic importance of late Cambrian and Ordovician rocks in Oklahoma, *in* Johnson, K., ed., Late-Cambrian-Ordovician Geology of the Southern Midcontinent 1989 Symposium: Norman, Oklahoma Geological Survey Circular 92, p. 3-14.

JOHNSON, J.G., and MURPHY, M.A., 1984, Time-rock model for Siluro-Devonian continental shelf, western United States: Geological Society of America Bulletin, v. 95, p. 1349-1359.

JOHNSON, J.G., KLAPER, G., and SANDBERG, C.A., 1985, Devonian eustatic fluctuations in Euramerica: Geological Society of America Bulletin, v. 96, p. 567-587.

JONES, B., 2010, Warm-water neritic carbonates, *in* James, N.P., and Dalrymple, R.W., eds., Facies Models 4, Geological Association of Canada, p. 341-370.

KARIM, T., and WESTROP, S., 2002, Taphonomy and Paleoecology of Ordovician Trilobite Clusters, Bromide Formation, south-central Oklahoma: PALAIOS, v. 17, p. 394-403.

LAUDON, L.R., 1939, Unusual Occurrence of *Isotelus gigas* Dekay in the Bromide Formation (Ordovician) of southern Oklahoma: Journal of Paleontology, v. 13, p. 211-213.

LONGMAN, M.W., 1976, Depositional history, paleoecology, and diagenesis of the Bromide Formation (Ordovician) Arbuckle Mountains, Oklahoma, University of Texas at Austin, 311 p.

LONGMAN, M.W., 1977, Factors controlling the formation of microspar in the Bromide Formation: Journal of Sedimentary Research, v. 47, p. 347-350.

LONGMAN, M.W., 1981, Deposition of the Bromide Formation, Arbuckle Mountains, Oklahoma: ontogeny of an ancient carbonate shelf: Shale Shaker, v. 32, p. 1-18.

LONGMAN, M.W., 1982a, Depositional environments, *in* Sprinkle, J., ed., Echinoderm Faunas from the Bromide Formation (Middle Ordovician) of Oklahoma, University of Kansas Paleontological Contributions, Monograph, p. 17-29.

LONGMAN, M.W., 1982b, Depositional setting and regional characteristics, *in* Sprinkle, J., ed., Echinoderm Faunas from the Bromide Formation (Middle Ordovician) of Oklahoma, The University of Kansas Paleontological Contributions, Monograph 1, p. 6-10.

MCLAUGHLIN, P., BRETT, C., TAHA-MCLAUGHLIN, S., and CORNELL, S., 2004, High-resolution sequence stratigraphy of a mixed carbonate-siliciclastic cratonic ramp (Upper Ordovician; Kentucky-Ohio, USA): insights into the relative influence of eustasy and tectonics through analysis of facies gradients: Palaeogeography, Palaeoclimatology, Palaeoecology, v. 210, p. 267-294.

MCLAUGHLIN, P.I., BRETT, C., and WILSON, M., 2008, Hierarchy of sedimentary discontinuity surfaces and consensed beds from the Middle Paleozoic of Eastern North America: Implications for cratonic sequence stratigraphy, *in* Pratt, B., and Holmden, C., eds., Dynamics of Epeiric Seas, Geological Association of Canada special paper 48.

MCPHERSON, J.G., DENISON, R.E., KIRKLAND, D.W., and SUMMERS, D.M., 1988, Basal sandstone of the Oil Creek Formation in the quarry of the Pennsylvania Glass Sand Corporation, Johnson County, Oklahoma, *in* Hayward, O.T., ed., Centennial Field Guide 4, Geological Society of America, South Central Section, p. 165-170.

MIN, K., RENNE, P.R., and HUFF, W.D., 2001, 40Ar/39Ar dating of Ordovician K-bentonites in Laurentia and Baltoscandia: Earth and Planetary Science Letters, v. 185, p. 121-134.

PLINT, A.G., 1991, High-frequency relative sea level oscillations in the Upper Cretaceous shelf clastics of the Alberta Foreland Basin: Evidence for a Milankovitch-scale glacio-eustatic control? *in* Macdonald, D.I.M., ed., Sedimentation, Tectonics and Eustacy: International Association of Sedimentologists, Special Publication 12: Oxford, Blackwell Science, p. 409-428.

PLINT, A.G., and NUMMEDAL, D., 2000, The falling stage systems tract: recognition and importance in sequence stratigraphic analysis, *in* Hunt, D., and Gawthorpe, R.L., eds., Sedimentary Response to Forced Regression: Geological Society of London Special Publication 172, p. 1-17.

PLINT, A.G., 2010, Wave and storm-dominated shoreline and shallow-marine systems, *in* James, N.P., and Dalrymple, R.W., eds., Facies Models 4, Geological Association of Canada, p. 167-199.

POLLASTRO, R.M., 1991, Composition, clay mineralogy, and diagenesis of the Simpson Group (Middle Ordovician), Grady County, Oklahoma: U.S. Geological Survey Bulletin, v. 1866-H, p. H1-H16.

POPE, M., and READ, J.F., 1997, High-resolution surface and subsurface sequence stratigrap hy of Late Middle to Late Ordovician (Late Mohawkian-Cincinnatian) foreland basin rocks, Kentucky and Virginia: American Association of Petroleum Geologists Bulletin, v. 81, p. 1866-1893.

POSAMENTIER, H.W., and VAIL, P.R., 1988, Eustatic controls on clastic deposition II-sequence and systems tracts models, *in* Wilgus, C.K., Hastings, B.S., Kendall, C.G.S.C., Posamentier, H.W., Ross, C.A., and Wagoner, J.C.V., eds., Sea Level Changes - An Integrated Approach. Special Publication 42, Society of Economic Paleontologists and Mineralogists, p. 125-154.

POSAMENTIER, H.W., and MORRIS, W.R., 2000, Aspects of the stratal architecture of forced regressive deposits, *in* Hunt, D., and Gawthorpe, R.L., eds., Sedimentary Responses to Forced Regressions, Geological Society of London Special Publication 172, p. 19-46.

PRATT, B.R., 2010, Peritidal carbonates, *in* James, N.P., and Dalrymple, R.G., eds., Facies Models 4, Geological Society of Canada, p. 401-420.

READING, H.G., 1996, Sedimentary Environments: Processes, Facies and Stratigraphy: London, Wiley-Blackwell, 688 p.

ROHR, D.M., and JOHNS, R.A., 1990, First occurrence of *Oriostoma* (Gastropoda) from the middle Ordovician: Journal of Paleontology, v. 64, p. 732-735.

ROSENAU, N.A., HERRMANN, A.D., and LESLIE, S.A., 2012, Conodont apatite $\delta^{18}0$ values from a platform margin setting, Oklahoma, USA: implications for initiation of late Ordovician icehouse conditions: Palaeogeography, Palaeoclimatology, Palaeoecology, v. 315-316, p. 172-180.

ROSS, C.A., and ROSS, J.R.P., 1995, North American depositional sequences and correlations, *in* Cooper, J.D., Droser, M.L., and Finney, S.C., eds., Ordovician Odyssey: Short Papers for the Seventh International Symposium on the

Ordovician System: Fullerton, California, Pacific Section Society for Sedimentary Geology, p. 309-313.

SALVADOR, A., 1994, International Stratigraphic Guide: A Guide to Stratigraphic Classification, Terminology, and Procedure: Boulder, Geological Society of America, 214 p.

SHAW, F., 1974, Simpson Group (Middle Ordovician) Trilobites of Oklahoma: Journal of Paleontology Memoir, v. 48, p. 1-54.

SCHLAGER, W., REIJMER, J.J.G., and DROXLER, A., 1994, Highstand shedding of carbonate platforms: Journal of Sedimentary Research, v. 64, p. 270-281.

SCHRAMM, M.W., 1964, Paleogeologic and quantitative lithofacies analysis Simpson Group, Oklahoma: Bulletin of the American Association of Petroleum Geologists, v. 48, p. 1164-1195.

SPRINKLE, J., 1982, Echinoderm zones and faunas, *in* Sprinkle, J., ed., Echinoderm Faunas from the Bromide Formation (Middle Ordovician) of Oklahoma, University of Kansas Paleontological Contributions, Monograph 1, p. 47-56.

SUHM, R.W., 1997, Simpson stratigraphy of the southern Midcontinent, *in* Johnson, K.S., ed., Simpson and Viola Groups in the southern midcontinent, 1994 symposium, Oklahoma Geological Survey Circular 99, p. 3-38.

SUTHERLAND, P.K., and AMSDEN, T.W., 1959, A re-illustration of the trilobite *Lonchodomas mcgeheei* Decker from the Bromide Formation (Ordovician) of southern Oklahoma: Oklahoma Geological Notes, v. 19, p. 212-218.

SWEET, W.C., 1984, Graphic correlation of upper middle and upper Ordovician rocks, North American Midcontinent Province, U.S.A, *in* Brunton, D.L., ed., Aspects of the

Ordovician System, Palaeontological Contributions from the University of Oslo 295, p. 23-35.

TOBIN, R.C., 1982, A Model for Cyclic Deposition in the Cincinnatian Series of Southwestern Ohio, Northern Kentucky, and Southeastern Indiana: Unpublished Ph.D. dissertation, University of Cincinnati.

ULRICH, E.O., 1911, Revision of the Paleozoic systems: Geological Society of America Bulletin, v. 22, p. 281-680.

VAIL, P.R., AUDEMARD, F., BOWMAN, S.A., EISNER, P.N., and PEREZ-CRUZ, G., 1991, The stratigraphic signatures of tectonics, eustasy and sedimentation - an overview, *in* Einsele, G., Ricken, W., and Seilacher, A., eds., Cycles and Events in Stratigraphy: New York, Springer-Verlag, p. 617-659.

WAGONER, J.C.V., POSAMENTIER, H.W., MITCHUM, R.M., VAIL, P.R., SARG, J.F., LOUTIT, T.S., and HARDENBOL, J., 1988, An overview of sequence stratigraphy and key definitions, *in* Wilgus, C.K., Hastings, B.S., Kendall, C.G.S.C., Posamentier, H.W., Ross, C.A., and Wagoner, J.C.V., eds., Sea Level Changes - An Integrated Approach. Special Publication 42, Society of Economic Paleontologists and Mineralogists, p. 39-45.

WAHLMAN, G.P., 2010, Reflux dolomite crystal size variation in cyclic inner-ramp reservoir facies, Bromide Formation (Ordovician), Arkoma Basin, southeastern Oklahoma: The Sedimentary Record, v. 8, p. 4-9.

WILKINSON, B.H., DRUMMOND, C.N., DIEDRICH, N.W., and ROTMAN, E.D., 1999, Poisson processes of carbonate accumulation on Paleozoic and Holocene platforms: Journal of Sedimentary Research, v. 69, p. 338-350.

WILLIAMS, M., 1990 Ostracoda (Arthropoda) of the middle Ordovician Simpson Group, Oklahoma, USA: PhD thesis, University of Leicaster, UK.

WILLIAMS, M., and SIVETER, D.J., 1996, Lithofacies-influenced ostracod associations in the middle Ordovican Bromide Formation, Oklahoma, USA: Journal of Micropalaeontology, v. 15, p. 69-81.

WILSON, J.L., 1975, Carbonate facies in geologic history: New York, Springer-Verlag, 471 p.

WRIGHT, V.P., and BURCHETTE, T.P., 1996, Shallow-water carbonate environments, *in* Reading, H.G., ed., Sedimentary Environments: Processes, Facies and Stratigraphy: London, Wiley-Blackwell, p. 368-378.

WRIGHT, V.P., and BURGESS, P.M., 2005, The carbonate factory continuum, facies mosaics and microfacies: an appraisal of some of the key concepts underpinning carbonate sedimentology: Facies, v. 51, p. 17-23.

YOUNG, S., SALTZMAN, M., and BERGSTROM, S., 2005, Upper Ordovician (Mohawkian) carbon isotope stratigraphy in eastern and central North America: Regional expression of a perturbation of the global carbon cycle: Palaeogeography, Palaeoclimatology, Palaeocology, v. 222, p. 53-76.

FIG. 1.—Paleogeographic setting and locality maps for the Bromide Formation in Oklahoma. **A)** Map of the southwestern United States showing approximate outline of the Oklahoma Basin, the SOA and other tectonic features (modified from Johnson et al. 1988; 1991). The size of the Arbuckle Mountains relative to the other features is exaggerated to show detail. **B)** Arbuckle Mountains map showing study localities, major highways, and their position relative to the SOA (modified from Ham 1969; Fay et al. 1982b).

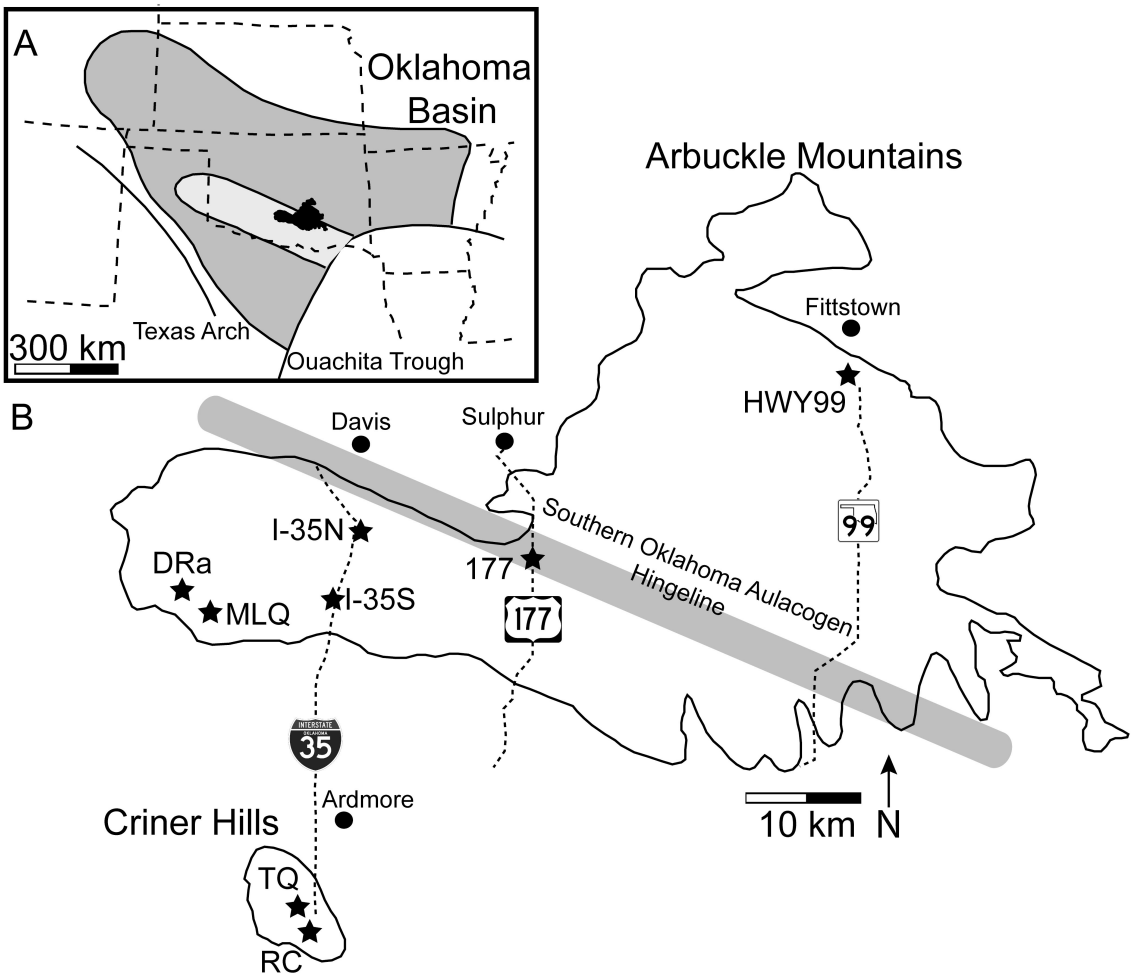
A
Oklahoma
Basin
Texas Arch
300 km
Ouachita Trough
B
Arbuckle Mountains
Fittstown
HWY99
Davis
Sulphur
Southern Oklahoma Aulacogen
Hingeline
99
I-35N
177
DRa
MLQ
I-35S
177
INTERSTATE
35
Ardmore
Criner Hills
TQ
RC
10 km
N

FIG. 2.—Stratigraphic setting of the Bromide Formation. Conodont zones from Derby et al. (1991), Bauer (1994) and Rosenau et al. (2012). Chronostratigraphy is from Derby et al. (1991) and Bergström et al. (2008).

Upper Ordovician
Dariw.
Sandbian
Katian
Whiterockian
Mohawkian
Chazyan
Turinian
GSSP
Chat
Simpson Group
Viola Gp
C. sweeti
B. gerdae
P. undatus
Viola Springs Fm.
Bromide Formation
Corbin Ranch
Pooleville
Mtn. Lake
Fittstown
Tulip Creek Fm.

FIG. 3.—Representative thin sections of various Bromide facies, scale bars = 2 mm. **A)** Marly (lime and clastic mud) wackestone with algal fragment from sequence 2 HST. **B)** Fenestral mudstone from sequence 3 HST, voids filled with coarse sparry calcite, and dolomite rhombs along rims. **C)** Peloidal, microcrystalline mudstone from sequence 3 HST. **D)** Pelmatozoan and bryozoan packstone to grainstone, showing extensive rim cementation, from sequence 3 TST. **E)** Lime mudstone with calcite intraclast and matrix filled ostracod, sequence 3 HST. **F)** Grainstone with abraded and reworked bioclasts from the backstepping sequence at HWY99, near transgressive ravinement structures (Fig. 10D).

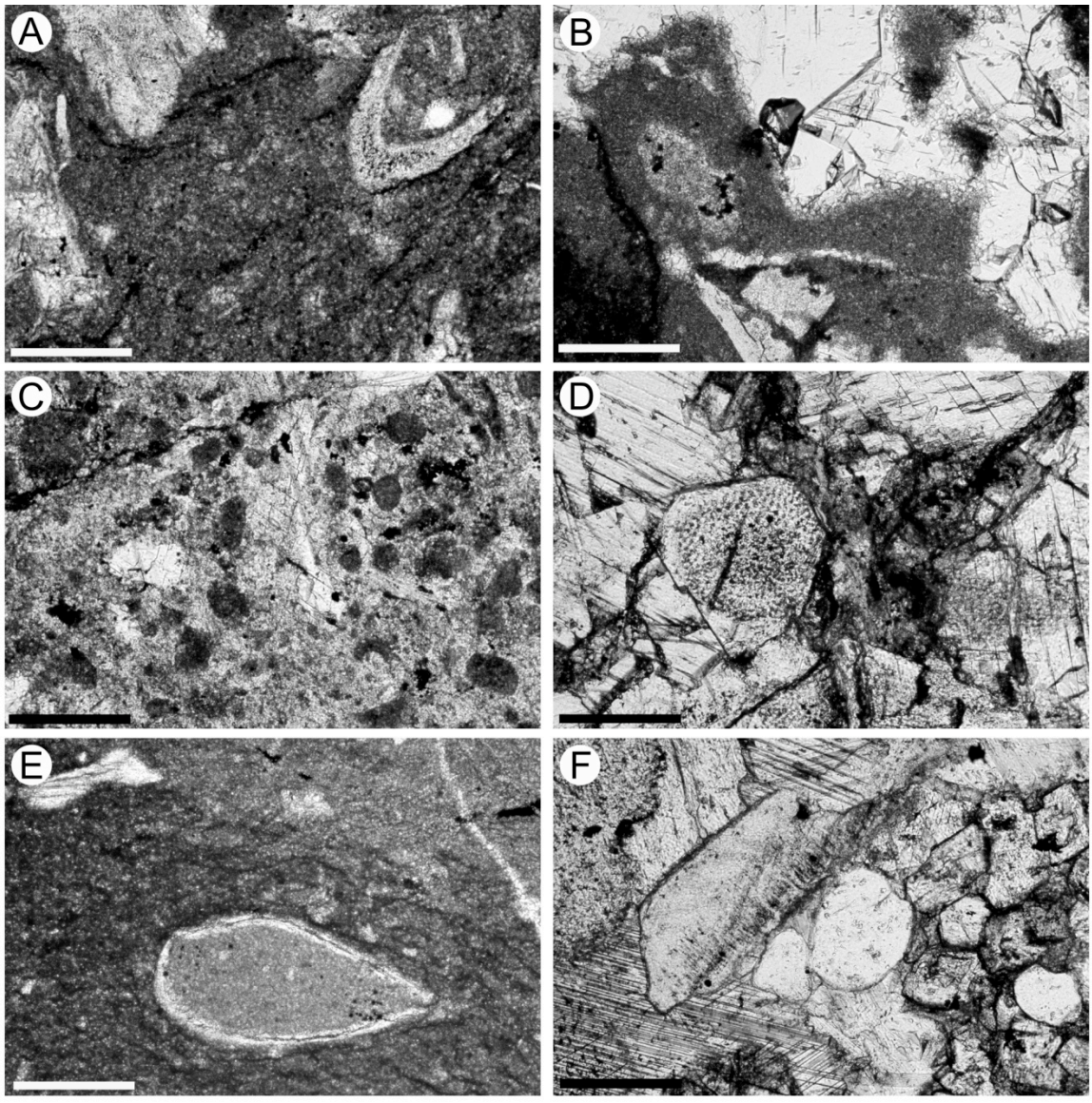
A
B
C
D
E
F

FIG. 4.—Representative polished slabs of Mountain Lake facies (except B, which is Pooleville), left is up on vertical slabs, scale bars = 2 cm. **A)** Rippled grainstone from sequence 2 FSST. **B)** Condensed fossiliferous grainstone from sequence 3 TST. **C)** down-ramp (DRa) wackestone from the rhythmite facies, with isoteline pavement, and cephalopod fragment, sequence 2 HST. **D)** Bioturbated mudstone to wackestone from the rhythmite facies at I-35N, sequence 2 HST. **E**) Condensed grainstone with ramose bryozoans in cross-section, sequence 1 TST. **F)** Heavily bioturbated and mottled mudstone, sequence 2 late HST.

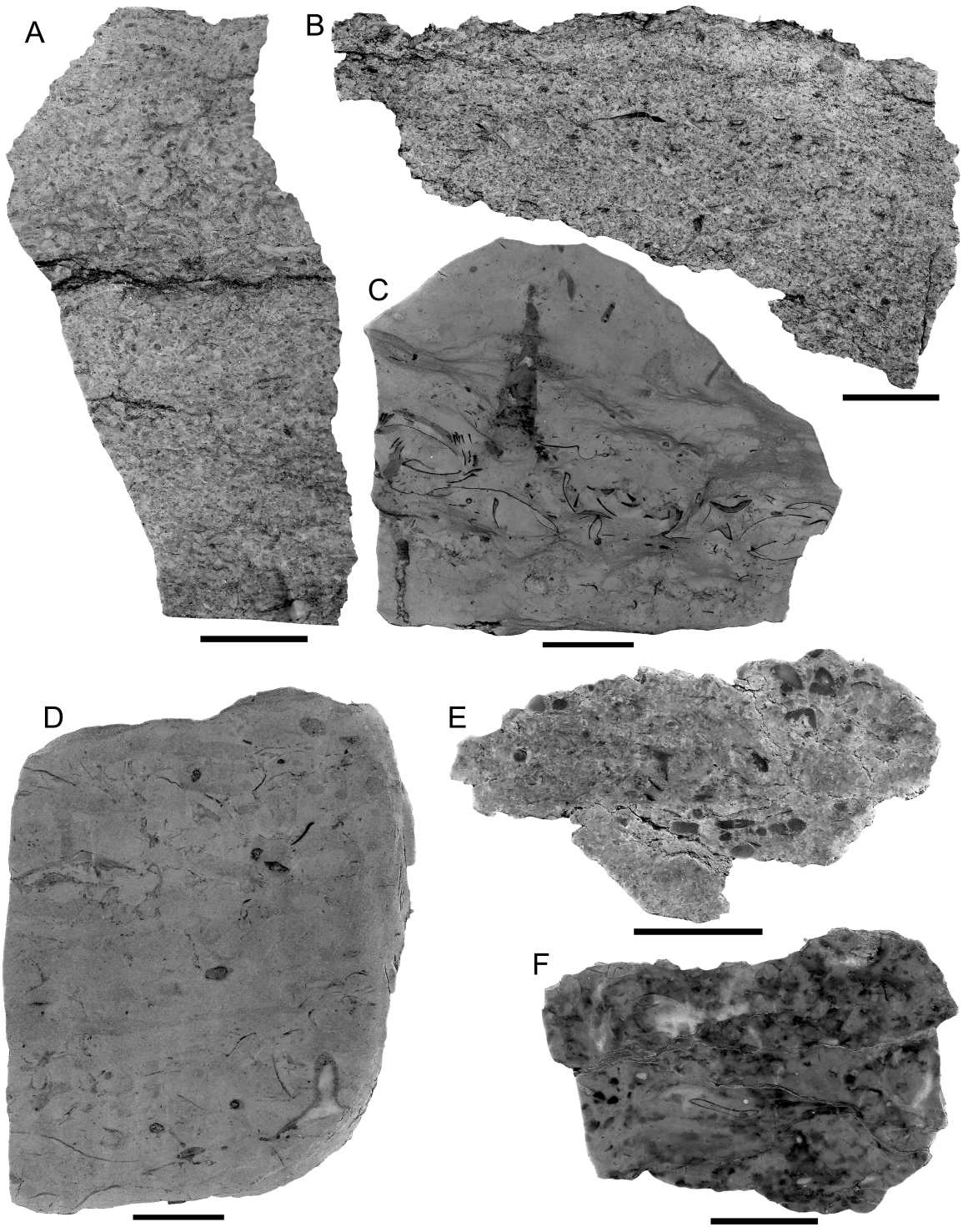
A
B
C
D
E
F

FIG. 5.— Representative polished slabs of Pooleville facies, left is up on vertical slabs, scale bars = 2 cm. **A)** *Tetradium* and cyanobacterial wackestone, showing very small fenestral pores, sequence 3 HST. **B)** Nodular, stylolitic mudstone, sequence 3 HST. **C)** Trilobite and brachiopod obrution horizon during early HST, sequence 3. **D)** Clotted mudstone with very large fenestral pores, sequence 3 HST. **E)** Ravinement surface or sequence boundary separating lagoonal or tidal mudstone from bioclastic grainstone, backstepping sequence at HWY99 (Fig. 10D). **F)** Laminated mudstone and shale in the HWY99 backstepping sequence, below Viola contact.

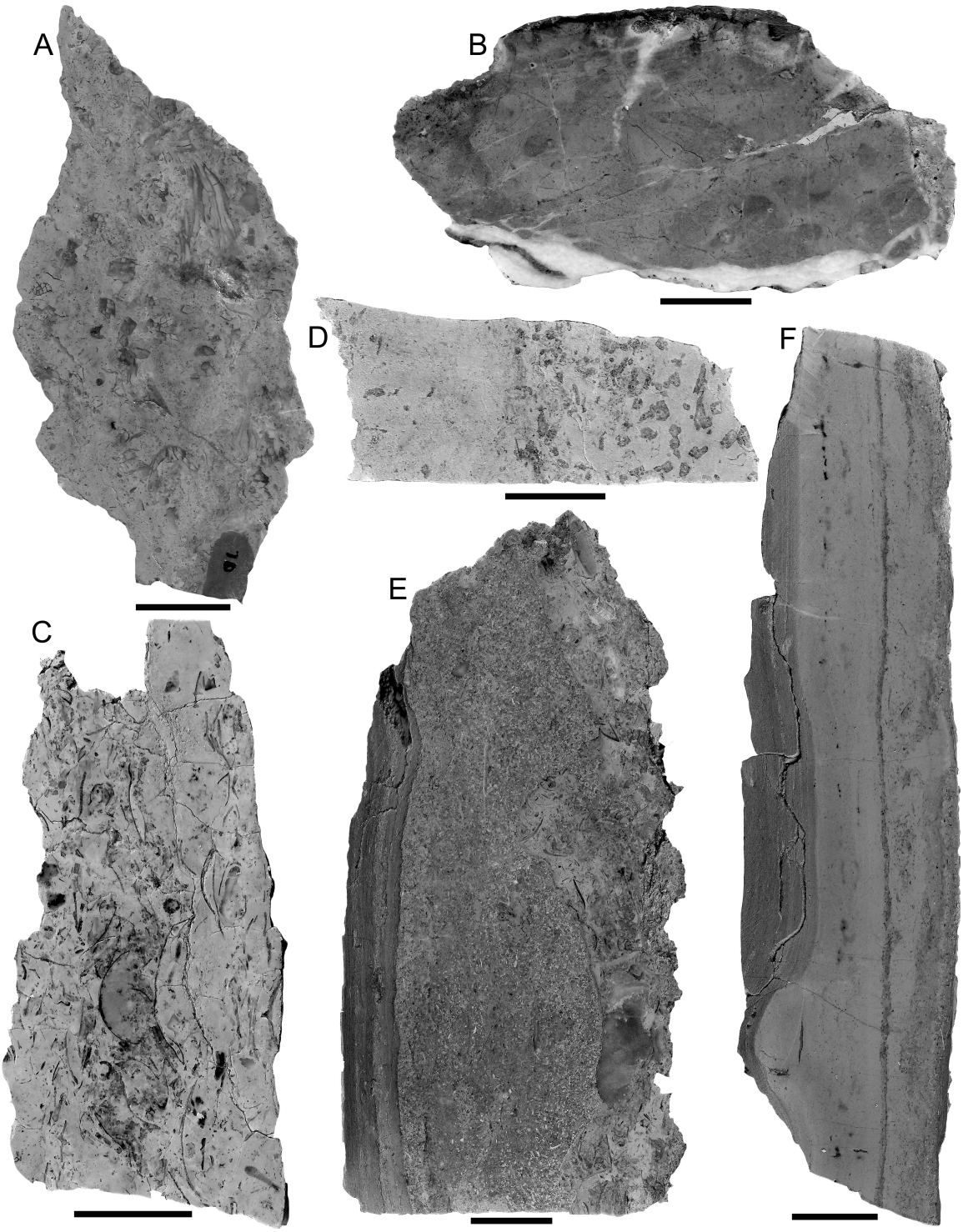
A
B
D
F
E
C

FIG. 6.—Oucrop photographs showing cyclicity and facies stacking patterns. **A)** Multiple meter-scale cycles at I-35N. The middle cycle shows two shallowing upward cycles within the micro-HST, person for scale. **B)** The nodular bedded rhythmite facies of shale and mudstone/wackestone at I-35N, rock hammer for scale. **C)** The rhythmite facies at RC, previously interpreted to be lower Pooleville, here interpreted as correlative with the Mountain Lake, scale bar = 1 m. **D)** Meter-scale cycles within the shalier sequence 1, lower Mountain Lake, I-35N, scale bar = 1 m. **E)** Contact between the micro-TST and micro-HST in a meter-scale cycle, I-35N, rock hammer for scale. **F)** Rippled grainstones and calcisiltites, sequence 2 FSST, I-35N, pencil for scale.

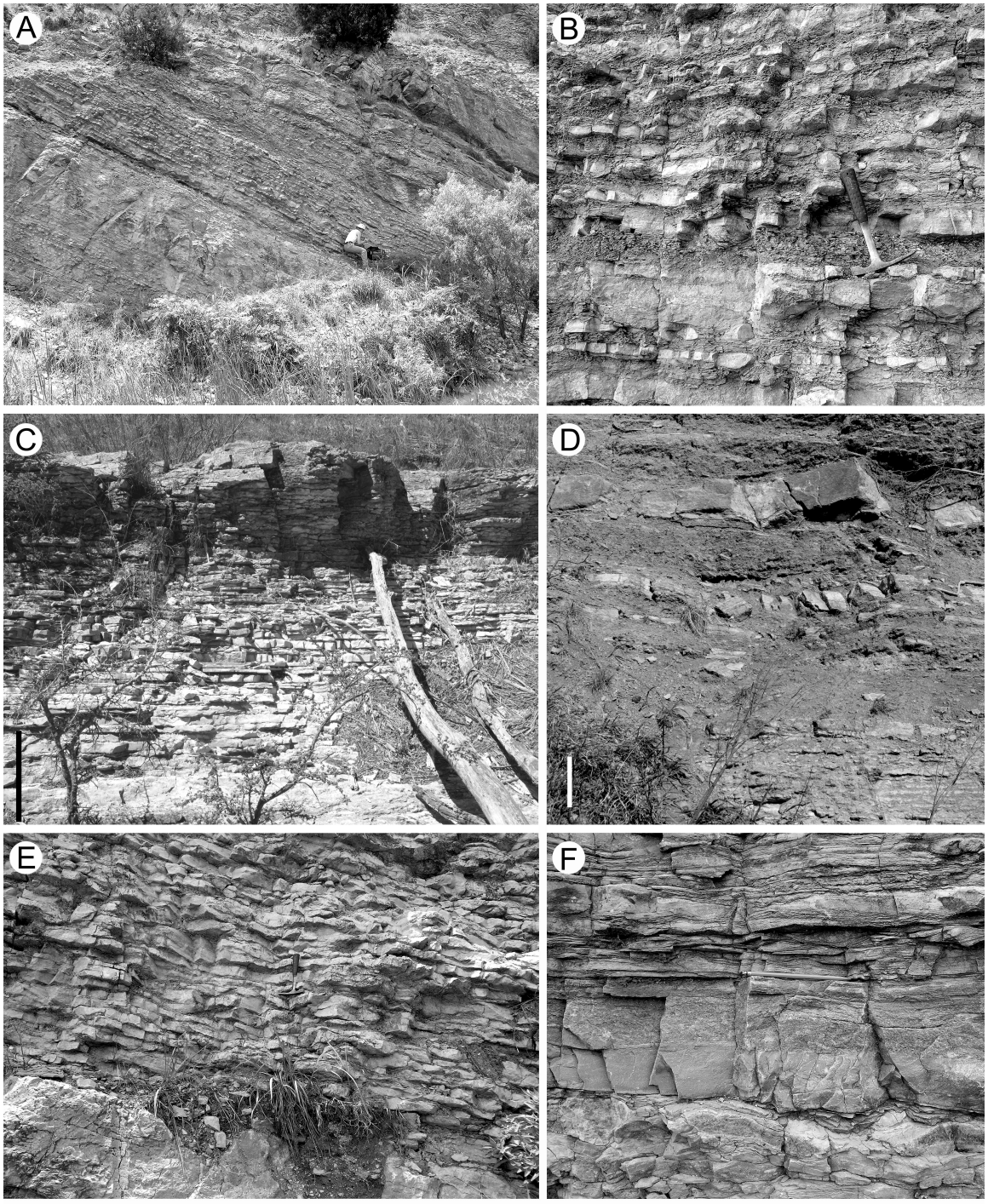
A
B
C
D
E
F

FIG. 7.—Chronostratigraphy, depositional sequences, bounding surfaces, and correlation of Bromide sections from I-35N up-ramp. See Figure 1B for horizontal scale.

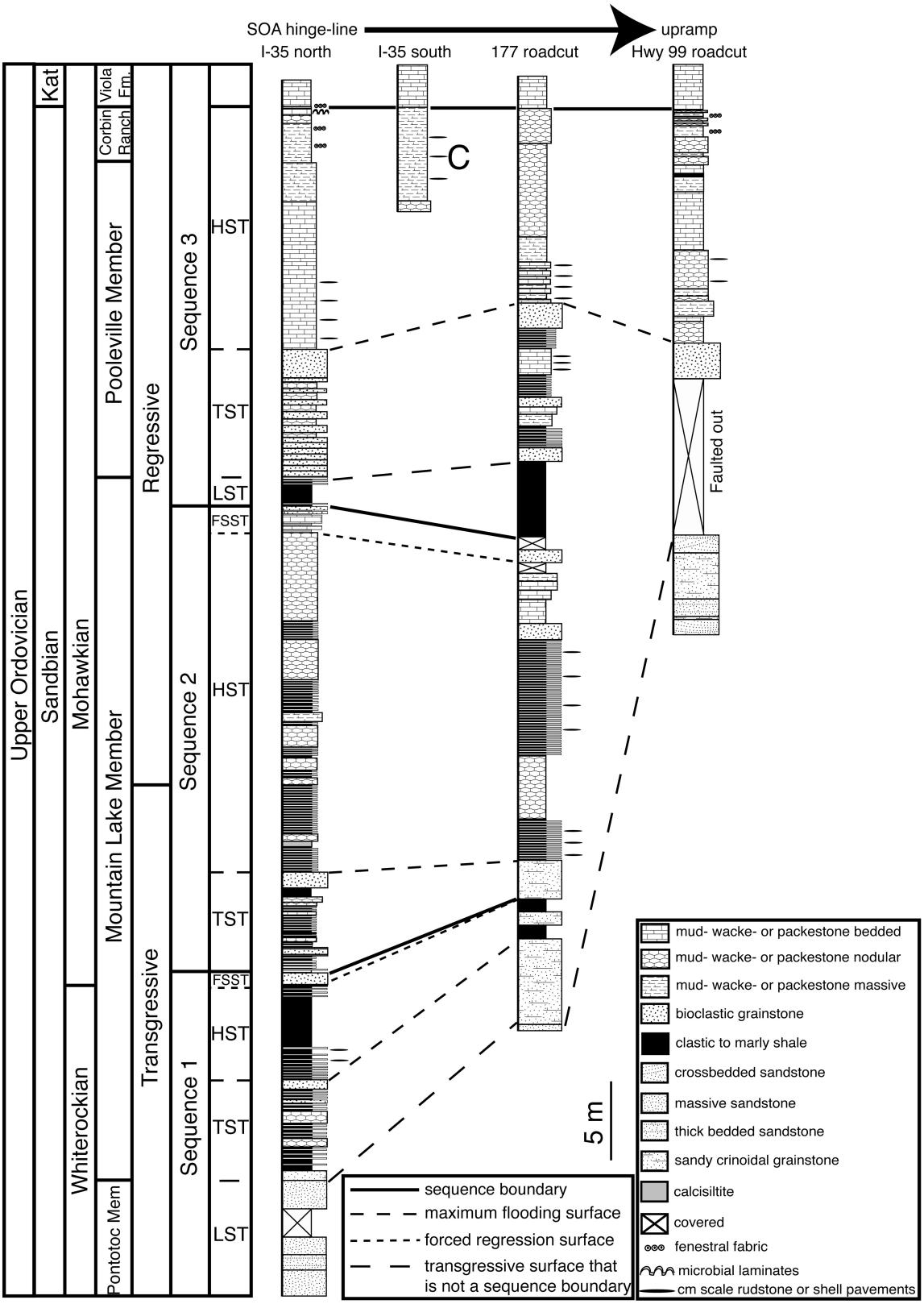
SOA hinge-line
upramp
I-35 north
I-35 south
177 roadcut
Hwy 99 roadcut
Upper Ordovician
Kat
Sandbian
Mohawkian
Whiterockian
Viola Fm.
Corbin Ranch
Pooleville Member
Mountain Lake Member
Pontotoc Mem
Regressive
Transgressive
Sequence 3
Sequence 2
Sequence 1
HST
TST
LST
FSST
HST
TST
FSST
HST
TST
LST
C
Faulted out
5 m
sequence boundary
maximum flooding surface
forced regression surface
transgressive surface that is not a sequence boundary
mud- wacke- or packestone bedded
mud- wacke- or packestone nodular
mud- wacke- or packestone massive
bioclastic grainstone
clastic to marly shale
crossbedded sandstone
massive sandstone
thick bedded sandstone
sandy crinoidal grainstone
calcisiltite
covered
fenestral fabric
microbial laminates
cm scale rudstone or shell pavements

FIG. 8.—Depositional sequences, bounding surfaces, and correlation of Bromide sections from I-35N down-ramp. See Figure 1B for horizontal scale.

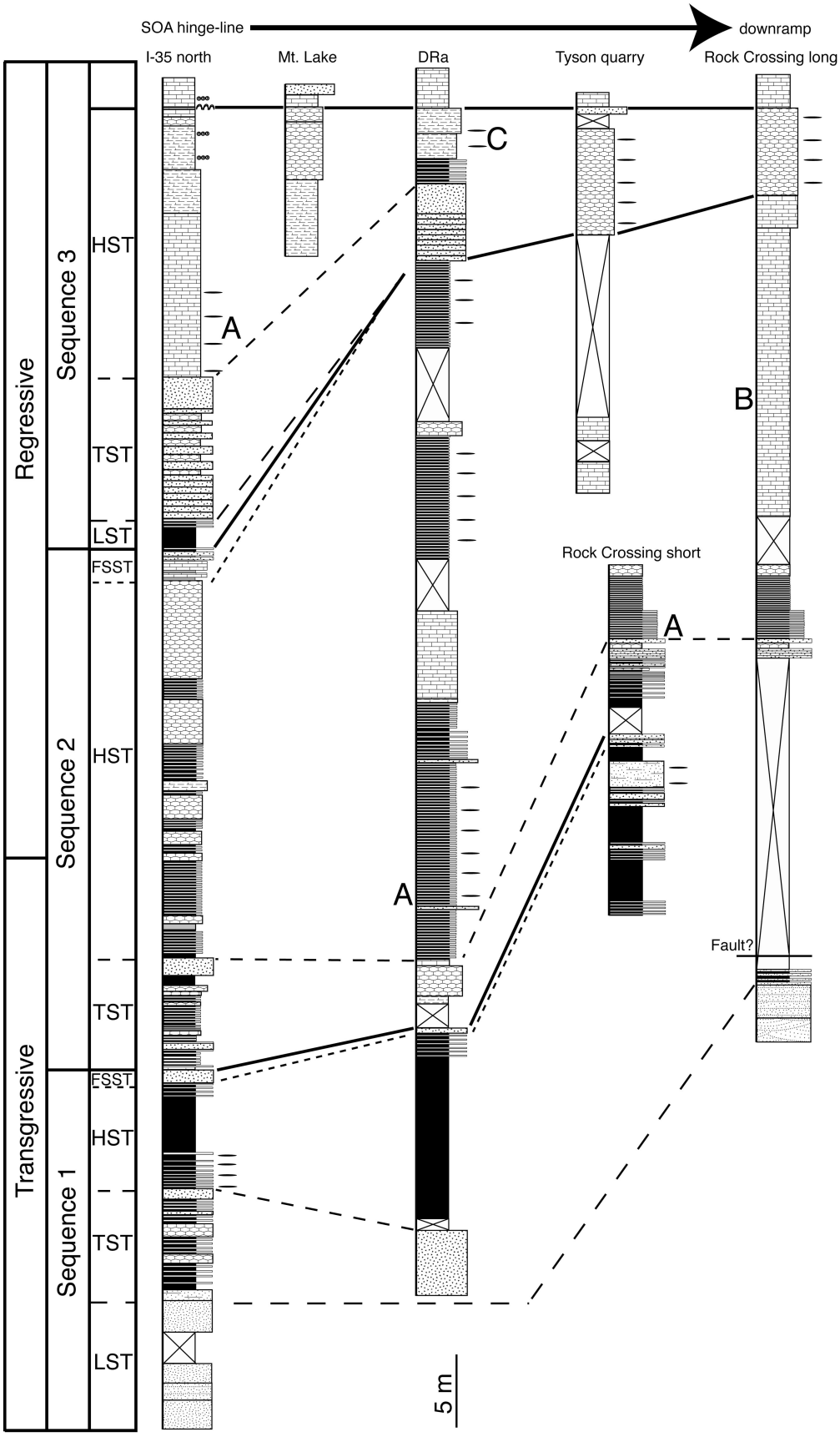
SOA hinge-line
downramp
I-35 north
Mt. Lake
DRa
Tyson quarry
Rock Crossing long
Regressive
Transgressive
Sequence 3
Sequence 2
Sequence 1
HST
TST
LST
FSST
HST
TST
FSST
HST
TST
LST
A
C
A
B
A
Rock Crossing short
Fault?
5 m

FIG. 9.—Correlation of depositional sequences into the subsurface. Note the expansion of sequence 2 moving down-ramp into the SOA. Outcrop gamma ray measured in cycles per second (Scintrex Differential Spectrometer GRS-500) at 0.5 m intervals, averaged over a span of 30 seconds. Correlations were done independently of, and differ from, naming conventions and formation tops used in the petroleum industry (see text for details). Dotted lines connect missing data points.

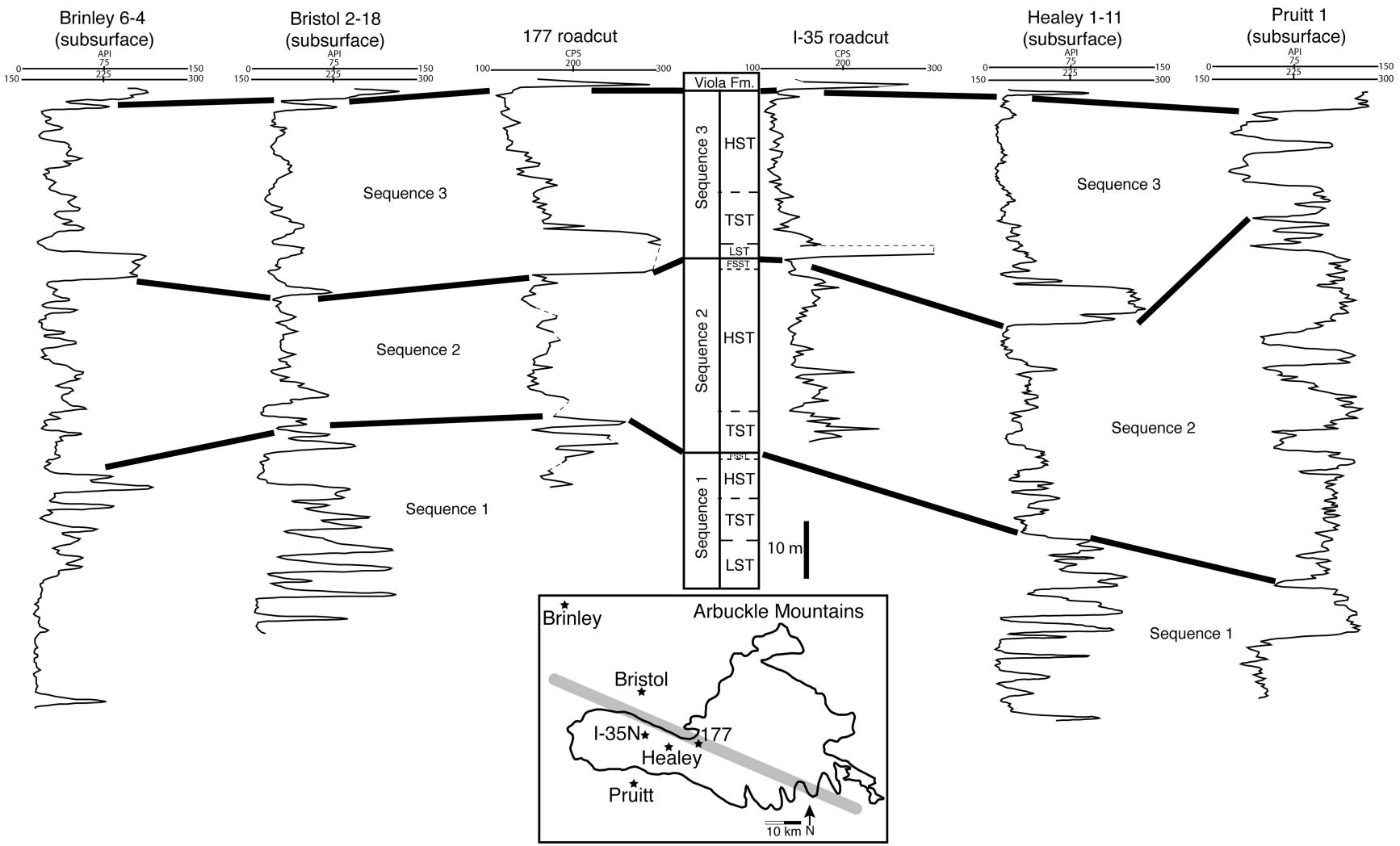
Brinley 6-4
(subsurface)
Bristol 2-18
(subsurface)
177 roadcut
I-35 roadcut
Healey 1-11
(subsurface)
Pruitt 1
(subsurface)
API
CPS
Viola Fm.
Sequence 3
Sequence 2
Sequence 1
HST
TST
LST
FSST
10 m
Brinley
Arbuckle Mountains
Bristol
I-35N
177
Healey
Pruitt
10 km
N

FIG. 10.—Meter-scale cycles and low rank sequences from the Mountain Lake and Pooleville Members and their associated lithofacies and surfaces. **A)** Meter-scale cycle from the lower Mountain Lake, sequence 1. **B)** Meter-scale cycle from the middle to upper Mountain Lake, sequence 2. **C)** Meter-scale cycle from the lower Pooleville, sequence 3. **D**) Low rank sequence at the top of the Corbin Ranch, including a transgressive coastline succession not preserved elsewhere. **E)** Facies succession during the FSST in sequence 2. LRSB = low rank sequence boundary, LRMFS = low rank maximum flooding surface, RS = ravinement surface.

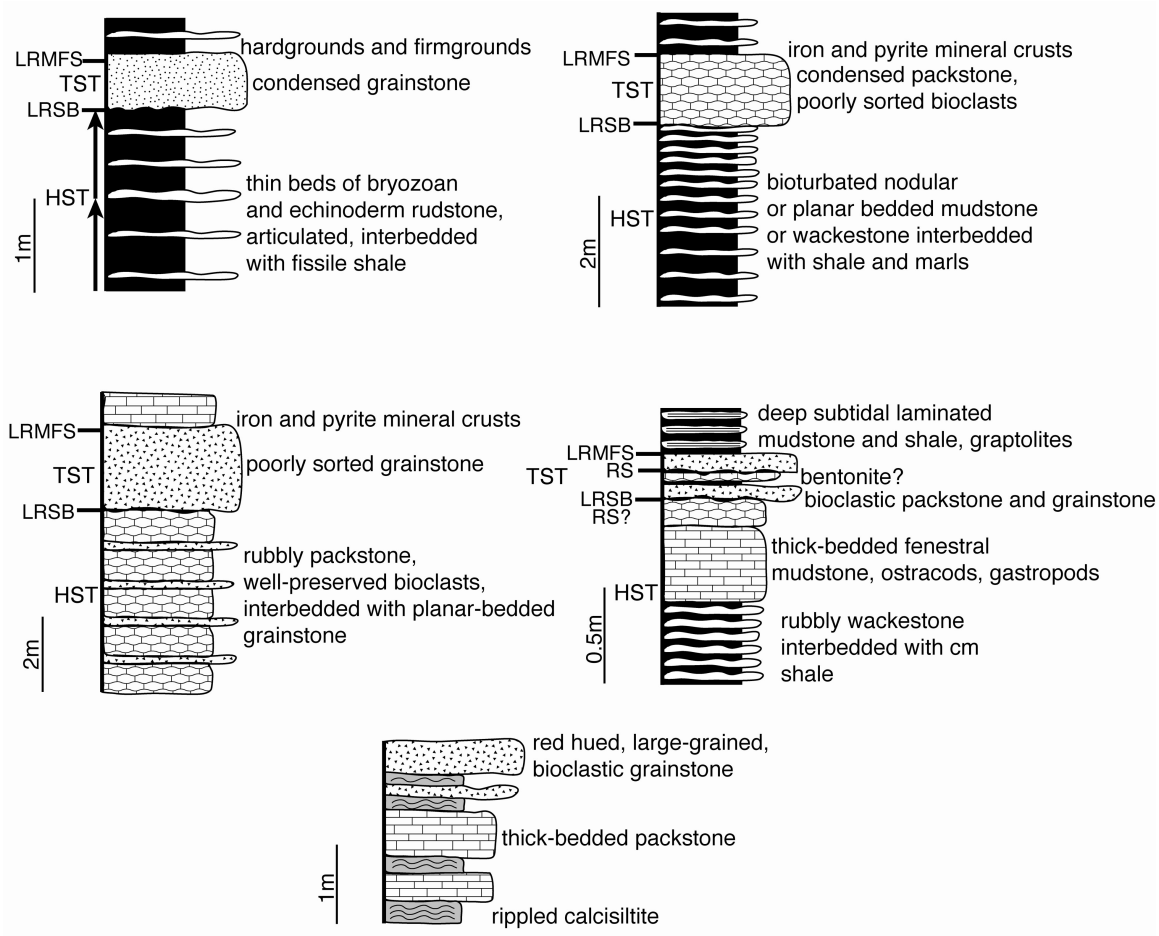
LRMFS
TST
LRSB
HST
1m
hardgrounds and firmgrounds
condensed grainstone
thin beds of bryozoan
and echinoderm rudstone,
articulated, interbedded
with fissile shale
LRMFS
TST
LRSB
HST
2m
iron and pyrite mineral crusts
condensed packstone,
poorly sorted bioclasts
bioturbated nodular
or planar bedded mudstone
or wackestone interbedded
with shale and marls
LRMFS
TST
LRSB
HST
2m
iron and pyrite mineral crusts
poorly sorted grainstone
rubbly packstone,
well-preserved bioclasts,
interbedded with planar-bedded
grainstone
deep subtidal laminated
mudstone and shale, graptolites
LRMFS
RS
TST
LRSB
RS?
bentonite?
bioclastic packstone and grainstone
thick-bedded fenestral
mudstone, ostracods, gastropods
HST
0.5m
rubbly wackestone
interbedded with cm
shale
red hued, large-grained,
bioclastic grainstone
thick-bedded packstone
1m
rippled calcisiltite

FIG. 11.—Example of low rank cyclic hierarchy (6^{th} – 4^{th} order), modeled after sequence 2 of I-35N. Ranges show the variation in thickness of each cycle across the Bromide Formation.

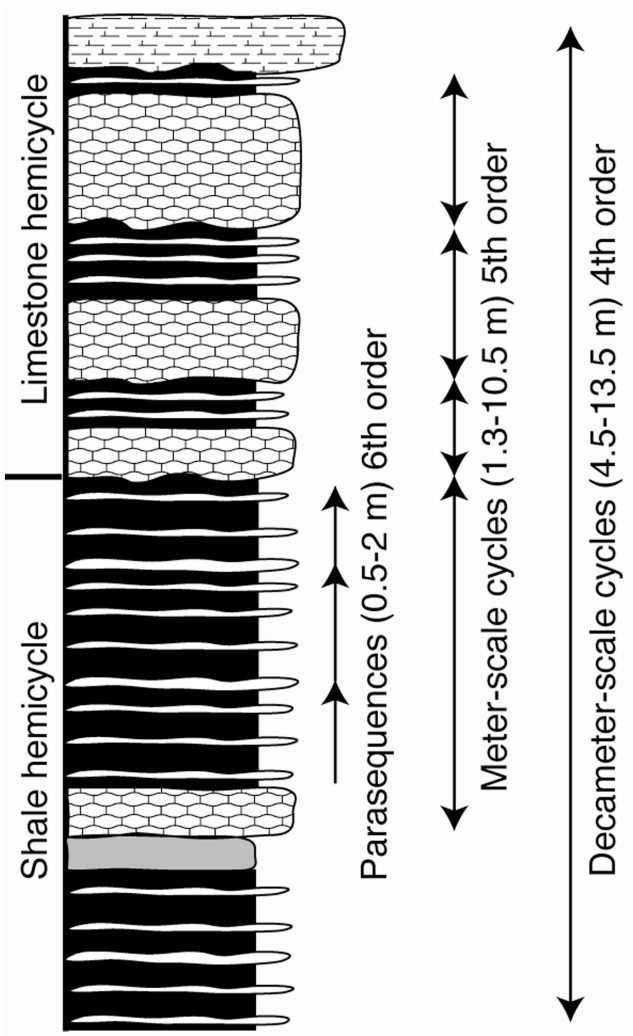
Limestone hemicycle
Shale hemicycle
Parasequences (0.5-2 m) 6th order
Meter-scale cycles (1.3-10.5 m) 5th order
Decameter-scale cycles (4.5-13.5 m) 4th order

FIG. 12.—Conceptual summary of Bromide depositional environments and associated facies in sequences 1-3, and across bathymetric settings. FWWB = fair weather wave base, SWB = storm wave base. N/A denotes the absence of a particular ramp environment within the study area during deposition of the corresponding depositional sequence.

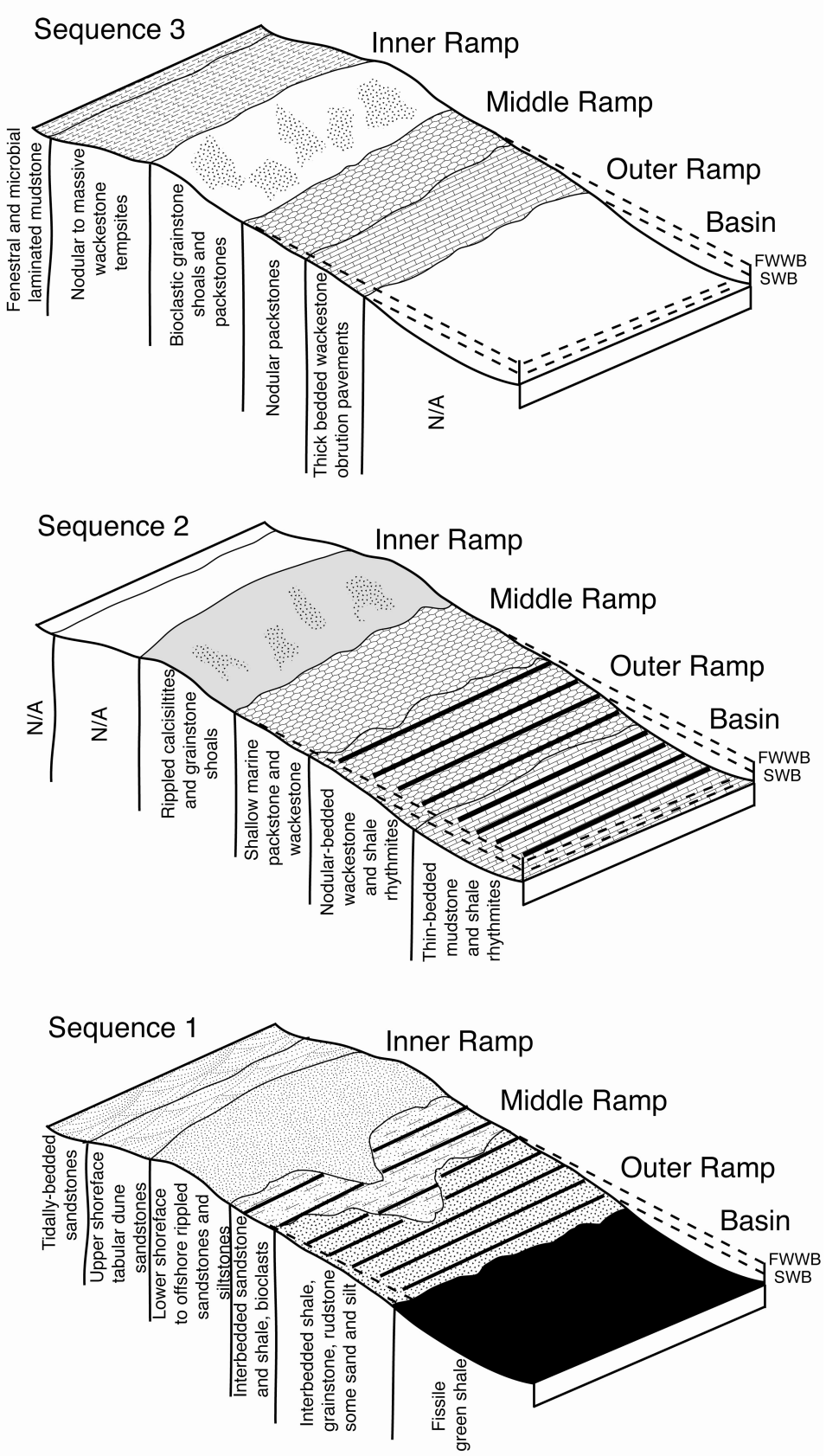
Sequence 3
Inner Ramp
Middle Ramp
Outer Ramp
Basin
FWWB
SWB
Fenestral and microbial laminated mudstone
Nodular to massive wackestone tempsites
Bioclastic grainstone shoals and packstones
Nodular packstones
Thick bedded wackestone obrution pavements
N/A
Sequence 2
Inner Ramp
Middle Ramp
Outer Ramp
Basin
FWWB
SWB
N/A
N/A
Rippled calcisiltites and grainstone shoals
Shallow marine packstone and wackestone
Nodular-bedded wackestone and shale rhythmites
Thin-bedded mudstone and shale rhythmites
Sequence 1
Inner Ramp
Middle Ramp
Outer Ramp
Basin
FWWB
SWB
Tidally-bedded sandstones
Upper shoreface tabular dune sandstones
Lower shoreface to offshore rippled sandstones and siltstones
Interbedded sandstone and shale, bioclasts
Interbedded shale, grainstone, rudstone some sand and silt
Fissile green shale

CHAPTER 5: TRILOBITE BIOFACIES ALONG AN ORDOVICIAN (SANDBIAN) CARBONATE BUILDUP TO BASIN GRADIENT, SOUTHWESTERN VIRGINIA.

ABSTRACT

The Upper Ordovician Effna, Botetourt, and Liberty Hall limestones of Virginia record deposition in several paleoenvironments along a carbonate ramp during the early history of the Taconic Foreland Basin. Four distinct lithofacies are present, i.e., biohermal mudstone and wackestone, biostromal grainstone, nodular deep flank limestone and shale, and basinal mudstones and shale, and each of these is associated with different trilobite biofacies. Cluster analysis and ordination define biofacies, and characterize gradients and patterns within the trilobite relative abundance data. Biofacies are clearly delineated along a depth gradient, with gradational compositional changes between associations. The moderate-diversity bioherm biofacies is dominated by illaenids (*Illaenus*, *Bumastoides*) and cheirurids (*Sphaerexochus*). The high-diversity biostromal biofacies is also an illaenid-cheirurid association, but is proportionally enriched in cheirurids, and includes off-bank elements not common in the bioherm. The high-diversity deep flank facies is associated with an *Ampyx-Isotelus-Nileus* assemblage that gradationally replaces the biostromal biofacies. The deep flank gives way to a low diversity *Isotelus-Calyptaulax-Raymondaspis* association of cosmopolitan trilobites in the outer slope and basin environment. These biofacies characterize local environments in the Taconic Foreland Basin just prior to, and in the initial phases of tectonically driven oceanographic change that led to regional extirpation of the buildup fauna and the reorganization of deep-water trilobite biofacies. New associations of taxa not found elsewhere in Laurentia are common within the foreland basin, suggesting that the

archetypal biofacies described here are reorganized with the onset of regional environmental change.

INTRODUCTION

During the Middle–Late Ordovician, trilobite faunas underwent a decline in relative importance to the marine biosphere, with the replacement of the Cambrian evolutionary fauna (Sepkoski, 1981; Sepkoski and Miller, 1985; Stanley, 2007) by the Paleozoic evolutionary fauna. There has been some debate as to whether trilobites underwent a real decline in absolute abundance and became displaced offshore (Sepkoski and Miller, 1985; Droser et al., 1996; Miller et al., 1998) or if the decline was an artifact of dilution (Westrop and Adrain, 1998; Adrain et al., 1998, 2000). The dilution hypothesis is supported by compilations (e.g., Adrain et al., 2000) of diversity gradients from environments across Laurentia as well as more localized studies of individual gradients (Amati and Westrop, 2006). The Appalachian foreland basin is an important area for further evaluation of biotic change in the Ordovician because patterns of diversity and turnover of trilobite faunas appear to differ from those in the rest of Laurentia (Amati and Westrop, 2006) and may reflect regional controls. During the Taconic Orogeny, changing paleoceanographic conditions (Patzkowsky and Holland, 1993, 1996) or onset of Gondwanan glaciation (Pope and Read, 1998; Pope, 2004; Saltzman and Young, 2005) caused regional biofacies replacements and extinctions in brachiopod and coral faunas in eastern North America. These changes to the biosphere coincide with increased siliciclastic influx, upwelling of cool nutrient-rich water, and a change in the style of carbonate sedimentation (Patzkowsky and Holland, 1993, 1996). In this paper, we examine trilobite biofacies associated with buildup and buildup-related

lithofacies in the Middle–Upper Ordovician boundary interval in the foreland basin. The Effna-Botetourt-Liberty Hall units span the Wa to M3 depositional sequences (latest Whiterockian–Mohawkian) of Holland and Patzkowsky (1996) and correspond to stages two and three of basin development (Read, 1980) in southwestern Virginia. The smothering of the Effna downslope carbonate buildups by basinal Liberty Hall limestone and shale are a microcosm of the regional-scale drowning of the carbonate ramp. Hence, these environments are an ideal baseline to compare with environmentally disturbed trilobite biofacies in younger foreland-basin strata. We hypothesize that these biofacies will fit the traditional paradigm of Ordovician depth-partitioned trilobite assemblages (see review below), before they are regionally extirpated and replaced by biofacies that show evidence of environmental disruption.

Further, these data allow for quantitative treatment of trilobite faunas in biohermal, biostromal, and deep-flank depositional settings, across separate buildups, and in response to depth and siliciclastic gradients. The trilobite faunas of several different Paleozoic carbonate buildups have been studied both taxonomically (e.g., Whittington, 1963; Shaw, 1968; Ross, 1972) and taphonomically (e.g., Suzuki and Bergström, 1999). Mikulic (1981) described the similarity of trilobite faunas across Paleozoic buildups (tendency for high illaenid, cheirurid, and lichid abundance), but a quantitative biofacies analysis on different subenvironments of these buildups has not been done. At small scales, Suzuki and Bergström (1999) identified spatial differentiation of trilobites between the surface and cavities within the Ordovician Boda buildups in Sweden. At larger scales, numerous authors have produced taxonomic studies (e.g., Warburg, 1925; Shaw, 1968; Ross, 1972) whose data suggest paleoecologic partitioning of trilobite

faunas between Ordovician buildups and their surrounding beds, but we provide the first quantitative evidence of this pattern.

PREVIOUS WORK ON ORDOVICIAN TRILOBITE BIOFACIES

Studies on Ordovician trilobite faunas have shown that certain taxa show consistent, long-term environmental associations that define biofacies. These biofacies traditionally are partitioned along a depth gradient, from inner- to outer-ramp environments. Fortey (1975) and Fortey and Barnes (1977) documented four trilobite "communities" in the Lower–Middle Ordovician of Spitsbergen, Norway: a high-diversity, shelf edge illaenid- and cheirurid-dominated biofacies associated with grainstone; an upper slope, high-diversity nileid-, asaphid-, and raphiophorid-dominated assemblage associated with well-oxygenated mudstones; a deep-water, lower-slope olenid biofacies associated with dark, laminated mudstones; and a pelagic biofacies dominated by telephinid trilobites that is preserved in all environments. Shaw and Fortey (1977) reviewed literature on Middle Ordovician trilobites and provided faunal lists at the generic level for most relatively well-studied units in North America (generic diversity estimated by the number of lists on which a genus occurred). They found very low generic diversity in inner shelf facies, populated by bathyurids, and relatively high diversity in outer shelf facies, with pterogometopid, isoteline, and illaenid genera particularly common. Shelf edge faunas were fairly diverse, with lichid, illaenid, and harpetid genera most represented. Upper slope faunas were also diverse, although nileid and raphiophorid genera were the most abundant trilobites in a disproportionate number of lists. Finally, lower slope faunas were of very low diversity, with only the genus *Triarthrus* and trinucleid genera present in any of the faunal lists. These data were not

treated quantitatively or with relative abundance data, but do provide a starting point for future work on Ordovician trilobite biofacies. Chatterton and Ludvigsen (1976) and Ludvigsen (1978) quantitatively showed four trilobite biofacies along a bathymetric profile of the Broken Skull, Esbataottine, Sunblood, and Road River Formations, Middle–Upper Ordovician of northern Canada. With increasing depth, four biofacies were defined: a low-diversity *Bathyurus* in peritidal facies (see also Tremblay and Westrop, 1991); a low-diversity *Isotelus* biofacies; a high-diversity *Calyptaulax-Ceraurinella* dominated biofacies; and a moderate-diversity, deep water *Dimeropyge*-dominated biofacies. Zhou et al. (2001) found evidence of a nileid biofacies in the Darriwilian-Llanvirnian of China that is associated with illaenids and interpreted as shallower than the nileid biofacies in Fortey (1975). They also found a raphiophorid (*Ampyx*, *Pytine*) biofacies in outer shelf muddy substrates and a cyclopygid biofacies in condensed graptolitic shales (Zhou et al., 2001). In a quantitative analysis of trilobite faunas along a single Ordovician Laurentian shelf-to-basin transect (Sandbian–Katian Viola Group, Oklahoma), Amati and Westrop (2006) identified a *Bumastoides*-dominated shoal biofacies in bryozoan grainstone and rudstone; farther down-ramp, they found a higher diversity *Thaleops* biofacies in wackestone and rudstone. This biofacies gave way to an outer-ramp, low-diversity, cryptolithine biofacies associated with carbonate mudstone.

GEOLOGIC SETTING

The downslope buildups are located in the Valley and Ridge province (Fig. 1) in the Appalachians of Virginia, USA, were deposited on top of shallow ramp carbonates that trended northeast (nearly parallel to the Tazewell arch), and lay just inside the

northwest margins of the Taconic Foreland Basin (Fig. 1B; Read, 1980). The buildups are part of a transgressive package (Fig. 2A, Mosheim, New Market, Lincolnshire, and Effna Limestones, and the Edinburg Formation) that unconformably overlie carbonates of the Knox and Beekmantown Groups (Read, 1980). This package is the regional onlap succession (Wa–M3 depositional sequences of Holland and Patzkowsky, 1996) that was deposited during the early and middle stages of downwarping during the development of the Taconic Foreland Basin. The downslope buildups are distributed in a broad belt (~50 km wide NW to SE) along the margins of the basin (Fig. 1B; Read, 1982, fig. 4), and were eventually infilled by Liberty Hall (Edinburg Formation) basinal shales and limestone. The Effna and Liberty Hall have informally been referred to as formations, but we follow the formal classification of Cooper and Cooper (1946) and describe the Liberty Hall as a facies of the Edinburg, and downslope buildups as the Effna Limestone. The Effna and Porterfield buildups (both Effna Limestone) (Figs. 1–3) are broadly similar to other down-ramp, Waulsortian-style (Wilson, 1975) Paleozoic mud mounds (e.g., Meiklejohn Peak; Krause, 2001) in that frame-building organisms are of little importance. High carbonate production associated with pelmatozoans, bryozoans, and calcareous algae, when coupled with extensive marine cementation, allowed the formation of rigid structures that drove buildup growth (Read, 1982).

The Effna Limestone includes the core and pod biohermal facies, and the underlying, overlying and flanking biostromal facies of the downslope buildups. The buildup cores are predominantly fine-grained mudstone and wackestone, with *Stromatactis* structures very common, and scattered bryozoan bafflestone relatively rare. Small, satellite, biohermal pods of mudstone and wackestone commonly flank the main

biohermal core of the buildups. The core and pods are underlain, interfinger with, and are often enveloped by a pelmatozoan-bryozoan biostromal grainstone (Fig. 4). The grainstone grades laterally into the Botetourt Member of the Edinburg (Cooper and Cooper, 1946); a black, nodular-bedded wacke-, packe-, and grainstone interbedded with indurated shale. Facies of the Botetourt often cut across the buildups (Fig. 2B), which Read (1982) interpreted as recording rapid drowning events. Following hardground and phosphatic crust development, upbuilding of the Effna was reinitiated, often evolving from biostromal to biohermal deposition. During the final drowning of the buildups, rate of increase in accommodation space permanently outpaced the sedimentation rate, flooding the mounds with dysoxic to anoxic basin waters of the Liberty Hall facies of the Edinburg Formation. Increased turbidity and decrease of light penetration from elevated clastic influx may have drastically decreased carbonate production, although Read (1982) argued that killing of bank biotas by anoxic basin water was the dominant process that terminated buildup development.

The Porterfield buildup is exposed at the Porterfield Quarry (PQ), an abandoned facility located 7 km southwest of Saltville, in Smyth County, Virginia (Fig. 1A). The quarry is located ~1 km down an unlabeled service road (off State Route VA 610). The PQ core buildup collections (Fig. 2B) are from boulders of biohermal mudstone left behind when the quarry ceased operation. The Effna buildup is best exposed on a roadcut along Interstate 77 (Fig. 3) near the town of Bland, in Bland County. The roadcut is less than 1 km north of the Big Walker Mountain Tunnel exit. At both localities, all non-bioherm collections were made *in situ* rather than from blocks. We visited a third downslope buildup, the Catawba, to confirm the facies relationships of Read (1982, fig.

6B), but any collectable material is completely flooded by a man-made lake, which was part of a restoration project by the quarry owners.

LITHOFACIES

We focus our observations and interpretations on the large-scale facies trends most relevant to trilobite preservation and environmental history. Read (1982, p. 198) provides a more detailed treatment of the microfabrics and thin-section petrology, including a longer discussion of uncommon bryozoan baffle- and boundstone. Tables 1 and 2 summarize our observations of the lithology, bedding, structures, fauna, and interrelationships of the Effna bioherm (core and pod) and biostrome lithofacies, the Botetourt deep flank lithofacies, and the outer ramp-to-basin Liberty Hall lithofacies (see Fig. 4 for representative examples).

Interpretations

Mudstone of the core and pod facies was likely deposited in place, where mud accumulation outpaced the deposition of skeletal grainstone. Baffling bryozoans and pelmatozoans facilitated the accumulation of lime mud by trapping fines (Read, 1982). Initial mud mound growth took place during a lower order transgression, as an increase in water depth and ocean circulation reinvigorated sediment accumulation (catch-up phase of Kendall and Schlager, 1981; Neumann and Macintyre, 1985; Emery and Myers, 1996; Reading, 1996). Extensive marine cementation formed hardgrounds and void fills that inhibited erosion and produced hard substrata for encrusting organisms. Marine cement is conspicuous throughout the core and pod facies, and likely produced surfaces that calcareous algae (see Read, 1982, fig. 10A) could encrust, which in turn produced more fine lime mud. Small pods similarly formed on the margins of the bioherms, caused by

local production of rigid mounds (overlying biostromal sands) from marine cementation and by baffling of lime mud by bryozoans.

We agree with Read (1982) that the core and pod facies is similar to Waulsortian mound core facies (Wilson, 1975; Lees and Miller, 1995) because of the extensive lime mud, lack of frame-building organisms, abundant hardgrounds and stromatactis structures, and association with pelmatozoan biostromal beds. The grainstone beds are also similar to those that separate Waulsortian-type mounds from off-bank deposits (Lees and Miller, 1995). Such biostromal units are typically interpreted as *in-situ* accumulations of grains from pelmatozoan-bryozoan assemblages that formed meadows or thickets that extended onto bank tops. Although these types of biostrome deposits are generally considered to be autochthonous, the steep slopes on the flanks of the bioherm likely produced at least some downslope movement of debris. The biostromal facies is then best characterized as a combination of *in-situ* pelmatozoan-bryozoan meadow growth and minor input of debris shed from the buildup. These meadows are often considered sea-floor stabilization communities (e.g., Batten-Hender and Dix, 2006) that facilitated buildup growth. As core complexes developed, these communities would have deposited skeletal grains on the periphery of muddy bioherms.

Botetourt limestone and shale are deeper-water deposits that are transitional between the Effna Limestone and the dysoxic to anoxic outer ramp and basin. They formed on the deep flank of the buildups or during brief drowning events prior to buildup growth (Read, 1982). Backstepping meter-scale cycles are progressively more clastic and less buildup influenced through the Botetourt Member. Abundant organics and pyrite suggests reducing conditions through the backstepping interval. The expression of the

Botetourt around deep slope buildups in southwestern Virginia is somewhat different than in northern Virginia because it was deposited on the deep flank of the biostrome, although it is likely part of the same nodular, slope-derived facies belt. The nodular fabric of the Botetourt facies is likely a function of diagenetic processes (Flügel, 2004), such as selective marine cementation around centers of nucleation, followed by compaction and grain-to-grain pressure solution of uncemented sediments. A general decrease in early cementation is evident downslope, which is supported by the extensive marine cementation on the buildups and biostrome, patchy marine cementation on the deep flank, and rare cementation in the basin. Botetourt tongues divide the buildup succession into upper and lower intervals (e.g., PQ, Fig. 2B) and were interpreted by Read (1998) as potentially recording fourth-order sea level rise. We think it is likely that the biostrome that forms the lower interval represents the transgressive systems tract (TST) and highstand systems tract (HST) phases of buildup development, whereas the Botetourt tongues record drowning and therefore the give-up phase of buildup development. The succeeding biohermal core represents a new HST phase of buildup development, followed by another drowning with the reappearance of Botetourt facies (e.g., Fig. 3), suggesting there may be two complete depositional sequences associated with buildup development (Emery and Myers, 1996). The presence of hardgrounds on the top of the Botetourt tongues supports this interpretation. Holland and Patzkowsky (1996) showed that the Effna buildup cut across the Wa and M1 depositional sequences, so the tops of the Botetourt tongues may represent a sequence boundary, though this needs to be corroborated by biostratigraphic evidence. The deep-water tongue is mappable across

some of the downslope buildups (PQ and Catawba), but is not visible at I-77 because this site only preserves the buildup crest.

Deep flank deposits eventually give way to the black mudstone and shale of the Liberty Hall facies (Edinburg Formation). The deposition of the Liberty Hall facies coincides with an increase in subsidence from widespread downwarping of the foreland basin in southwestern Virginia (Read, 1980). Clastics derived from tectonic highlands were deposited along the basin margins and fined out into outer ramp and basin environments (Read, 1980). The Liberty Hall facies is transitional between the downslope carbonate-dominated environment and the deepest part of the clastic basin (Paperville Shale; Read, 1980, fig. 1B). Slump beds and conglomerates likely indicate gravity transport along the deep slope, associated with the tectonic uplift of the eastern portion of the foreland basin (Lowry, 1974; Read, 1980). Previously unrecognized tectonic features (Table 2) of the Effna–Liberty Hall contact at PQ raise concerns about the nature of the facies changes at this locality, although a more detailed analysis is beyond the scope of this paper.

METHODS

Our dataset (Appendix 1) consists of 14 collections from the PQ and I-77 localities, six of which are from the Porterfield Buildup and associated facies and eight from the Effna buildup and associated facies (e.g., Liberty Hall beds). Of these, four are from the bioherm facies (PQEB1, PQEB1-1, PQEB1-2, PQEB2), four from the biostrome (PQEG3, I7758EG, I77EG2, I77EG3), four from the deep flank (PQBT1, I77BT1, I7760BT, I7767.5BT), and two from the outer ramp-to-basin (I7774LH, I7777LH) facies. Whenever possible, all collections were sampled laterally within units, to the greatest

extent allowed along strike (usually a few meters), and the vertical extent of sampling was less than one meter. Two of the core and pod facies collections are replicate samples from a larger collection of biohermal blocks produced by quarrying. They were randomly split into subcollections of approximately equal area in order to test for evenness in trilobite abundances within the bioherm. In other words, we wanted to test if the variation in trilobite abundances from one set of blocks was less than the variation of the bioherm as a whole.

The collections yielded 1954 trilobite sclerites that represent a minimum of 1244 individuals, with a mean sample size of 89. Generic relative abundance data was used for all analyses, and is reflective of within-habitat, time-averaged assemblages. Generic data has advantages over species-level data in biofacies analysis. Species are best used in biostratigraphic studies since their short ranges allow for fine temporal division. Biofacies are long-term, time-averaged associations of taxa in different environments so the longer temporal ranges of genera better reveal such patterns as lithofacies tracking (Ludvigsen et al., 1986). From a practical standpoint, hundreds of incomplete sclerites and those damaged either taphonomically or by splitting of rock samples can be identified to the generic level confidently, but not necessarily to individual species. All specimens are housed at the Sam Noble Oklahoma Museum of Natural History (OU), Norman, Oklahoma.

Three multivariate methods were implemented in PAST v. 2.08 (PAlaeontological STatistics; Hammer et al., 2001) to evaluate the dataset. Prior to analysis, the dataset was subject to a within-sample percent transformation (Jongman et al., 1995) in order to standardize differences in abundance among taxa. A Bray-Curtis metric (Bray and Curtis,

1957) was used in all analyses except the detrended correspondence analysis (DCA), which requires a chi-square distance matrix. Using Bray-Curtis universally allowed us to maintain consistency between analyses. Unweighted pair group with arithmetic mean (UPGMA) Q x R mode cluster analysis was used as an exploratory method to define biofacies. Ordination techniques, non-metric multidimensional scaling (NMDS), and DCA were used to detect ecologic gradients among collections and genera. There has been some debate concerning the utility of DCA in recent years (e.g., see McCune and Grace, 2002 for discussion), but it has successfully recovered the primary gradients typical of ecological (e.g., Patapova and Charles, 2002) and paleoecological studies (e.g., Holland, 2005; Holland and Patzkowsky, 2007). NMDS is particularly good at visualizing differences in taxonomic composition. Under Bray-Curtis, a Q-mode NMDS with a value of 100 shows identical sample composition with no overlap in composition at 0. In an R-mode analysis, a value of 100 means the abundances of two genera are identical, and a value of 0 means the two genera have no samples in common. In NMDS, stress values are used to assess the adequacy of the ordination results. Stress is calculated by measuring the goodness of fit between the non-parametric regression of Euclidean distance against the dissimilarities in a Bray-Curtis matrix (Clarke and Warwick, 1994) and is a measure of how well the ordination preserves the actual sample dissimilarities. Stress increases with sample size and with the degree of mismatch between the complexity of ecologic gradients and the number of specified dimensions (McCune and Grace, 2002). The implementation in PAST runs a sequence of 11 trials with random initial conditions and reports the result with the smallest stress (Hammer et al., 2001). In our dataset there was no appreciable drop in stress as we increased dimensionality from

2D to 3D, and the interpretations of the ordinations were the same in both cases, so we report the 2D results here.

Taxonomic Notes

Most taxonomic assignments are based on previous work (Cooper, 1953; Tripp and Evitt, 1986; Amati and Westrop, 2004; Adrain, 2005; Carlucci et al., 2010, 2011). Carlucci et al. (2011) revised *Bumastoides*, which necessitated the removal of some species from the genus. We place one species into "*Stenopareia*" as a placeholder, because there currently exists no genera that encompass *Bumastoides*-like trilobites with deep axial furrows on the cranidium, a subtriangularly inflated cranidium, and parallel-sided pygidia. This placement does not reflect common ancestry, but is a short-term nomenclatural solution until the Illaenidae is revised.

RESULTS

Q x R Mode Cluster Analysis

The Q mode cluster analysis shows separate groupings for biohermal, biostromal, deep flank, and outer ramp-to-basin environments (Fig. 5); however, samples from identical lithofacies of the Botetourt limestone at PQ (PQBT4) and I-77 (I77BT1, I7767.5BT, I7760BT) belong to different biofacies. Otherwise, biofacies are lithofacies specific, suggesting that the original biotic distribution is preserved in these data. All groupings record a unique trilobite biofacies, with gradational compositional changes between environments. Shallow-water collections form a distinct Q-mode cluster that corresponds to an R-mode cluster (cluster 2) composed of abundant illaenid, cheuirurid, and lichid taxa; a biostromal subcluster is differentiated from a biohermal subcluster by the presence of taxa (e.g., *Calyptaulax*, *Raymondaspis*; "*Decoroproetus*") that are also

components of the deeper water biofacies. Deeper-water collections form a distinct Q-mode cluster that corresponds to an R-mode cluster (cluster 1) of abundant isoteline, nileid, pterygometopid, and styginid taxa; a deep flank subcluster is differentiated from an outer ramp-to-basin subcluster by the retention of taxa (e.g., *Thaleops*, *Illaenus*) that are components of the shallow-water biofacies. The Botetourt deep flank at PQ clusters more closely with the bioherm and biostrome biofacies than it does with the deep flank collections from I-77. This collection contains both a shallow-water fauna (*Illaenus*, *Thaleops*), elements from the deep-water fauna (*Ampyx*), and some taxa that are not found in any other collections (e.g., *Pliomerella*, *Holdenia*). The main Botetourt deep flank cluster also contains rare elements typical of the shallow water biofacies, but is dominated by a completely new fauna (*Ampyx*, *Isotelus*, *Nileus*, *Arthrorhachis*, *Raymondaspis*). In the outer ramp-to-basin biofacies, formerly common elements become rarer (e.g., *Nileus*), and *Isotelus*, *Raymondaspis*, and *Calyptaulax* dominate the relative abundance patterns. Rare taxa include trilobites reported from deep-water facies in the literature, such as *Dionide* and *Robergia*.

Cluster analysis is used here primarily to discriminate biofacies, but a gradational pattern is still clear, as deeper biofacies in the Q-mode (Fig. 5, right to left) gradually incorporate more taxa from the deep-water R-mode cluster. Common taxa in a particular biofacies become rare in the adjacent deeper biofacies.

Ordination (NMDS and DCA)

Q-mode NMDS (Fig. 6A) with a stress value of 0.082 show that depth (i.e., position along the onbank to offbank transition) correlates well with the first axis. The extent of siliciclastic input and marine cementation also varies along the same gradient,

but it is impossible to separate these environmental signals from depth. The collections are well grouped by biofacies, with only the deep flank collections showing a large amount of variation in axis 1 scores. The collections are also clearly sorted by buildup, which suggests that the Effna and Porterfield buildups may not have been deposited coevally, or else that local factors impacted strongly on the composition of faunas. Since some facies are better exposed at the different buildups (e.g., the main buildup is not exposed at I-77, only the crest), this is only conjectural. The Botetourt at PQ (biofacies 3, Fig. 6), however, is just as close in ordination space to the buildup and biostromal collections as it is to the deep flank (Botetourt) collections at I-77. We expect this is for two reasons. Firstly, this result shows that in this case, local factors may exert a stronger control than position along the depth gradient. Secondly, this collection is from the Botetourt tongue at PQ, which represents a brief drowning event prior to development of the main biohermal core, and is therefore stratigraphically younger than the Botetourt at I-77 which overlies the buildup crest. The Q-mode DCA analysis (Fig. 6B) produced eigenvalues of 0.73 for axis 1 and 0.074 for axis 2, and is fairly similar in structure to the NMDS. The gradient along axis 1 is more evident as the transition between environments is more gradual. Under both NMDS and DCA, the large sample (PQEB1) that was split into replicate bioherm collections (PQEB1-1, PQEB1-2), and the collection from another set of boulders (PQEB2) are equidistant from each other in ordination space, suggesting an similar distribution of taxa both within and between boulders.

The R-mode NMDS (Fig. 6C) has a stress value of 0.28, indicating a moderate amount of disagreement between the rank order similarity and Euclidean distance in ordination space. The NMDS shows a strong gradient along axis 1, with taxa associated

with the deepest environments having the most negative score. Taxa that are highly constrained by lithofacies (e.g., *Probolichas*, which is only found in the bioherm) group close to their biofacies centroids, whereas more cosmopolitan taxa (e.g., *Isotelus*, *Calyptaulax*) lie between multiple biofacies centroids. The R-mode DCA (Fig. 6D) has eigenvalues of 0.73 for axis 1 and 0.19 for axis 2, and shows a similar sorting of taxa along a depth gradient (axis 1). Taxa from the bioherm and biostrome biofacies are strongly associated with each other, and those from deep flank and outer ramp-to-basin biofacies are also well grouped in ordination space, supporting the R-mode groupings (shallow and deep water fauna) found in the cluster analysis. Sorting along axis 2 in both NMDS and DCA does not appear to be related to any discernable environmental variable related to trilobite ecology.

Rarefaction

Rarefaction techniques were used to facilitate comparison of generic diversity and sampling effort between biofacies. Rarefaction curves for each biofacies (Fig. 7) show approximately three separate diversity profiles. With expected values of 90 individuals (the highest possible sample size that allows collections from all five biofacies to be included), the biohermal biofacies (*Illaenus*-*Bumastoides*-*Sphaerexochus*-*"Stenopareia"* preserves 7.87 ± 2.08 genera, the biostromal biofacies (*Sphaerexochus*-*Ilaenus*-*Thaleops*), 10.50 ± 2.78, the PQ deep flank biofacies (*Illaenus*-*Thaleops*), 10.98 ± 2.76, the I-77 deep flank biofacies (*Ampyx*-*Isotelus*-*Nileus*), 13.89 ± 2.08, and the outer ramp-to-basin biofacies (*Isotelus*-*Calyptaulax*-*Raymondaspis*), 7.0 ± 0.0. There is some overlap in the 95% confidence intervals at low sampling effort (Fig. 7, caption), but when expected diversity is rarified to 210 individuals, confidence intervals no longer overlap,

suggesting statistically different diversity profiles between the high diversity, deep flank and biostrome biofacies and the moderate diversity bioherm. Biostromal and deep flank biofacies are extremely diverse, whereas the biohermal biofacies is less diverse when rarified to any number of individuals; the outer ramp-to-basin biofacies shows the lowest diversity of any sampling effort. When rarified to 90 individuals, the outer ramp-to-basin biofacies is statistically different (95% confidence) from both the deep flank and biostromal biofacies, but not the bioherm. Qualitatively, however, we still think it is best to place the biofacies into three separate diversity profiles, given overall generic richness. The I-77 deep flank biofacies is the most diverse at any expected value in which it is present. All of the biofacies appear adequately sampled, although the PQ deep flank biofacies is comparatively under sampled. This is perhaps unsurprising since this collection did not cluster well with the other deep flank samples, and is therefore composed of fewer individuals (143). More importantly, the uneven distribution of illaenids compared to rare taxa in this biofacies is likely the primary control on the trajectory of the rarefaction curve. Interpreting curves that extensively cross others is somewhat problematic because rarefaction does not allow for any extrapolation (Raup, 1975). Hence, the relative diversity of the PQ deep flank biofacies must remain in doubt. Evenness metrics calculated in PAST (Hammer et al., 2001) confirm the uneven distribution of taxa in the PQ deep flank biofacies. Simpson evenness (1-Simpson index of dominance, Simpson, 1949) yielded values of 0.75 for the bioherm, 0.82 for the biostrome, 0.48 for the PQ deep flank, 0.86 for the I-77 deep flank, and 0.67 for the outer ramp to basin, suggesting that the probability of picking the same taxa with two random individuals from the PQ deep flank is higher. Similarly, Pielou's equitability index (J)

(Hammer and Harper, 2006) produced values of 0.68 for the bioherm, 0.70 for the biostrome, 0.43 for the PQ deep flank, 0.83 for the I-77 deep flank, and 0.73 for the basin.

TRILOBITE BIOFACIES

In his study of the Ordovician bioherm at Meiklejohn Peak, Nevada, Ross (1972) found numerous trilobite, brachiopod, and bivalve genera that were confined either to the bioherm or the biostromal flank environment, but suggested that the presence of half (16/32) of the bioherm fauna in the flank facies indicated storm sweeping and downslope transport of the bioclasts; however, we consider all trilobite biofacies defined in this study to be autochthonous assemblages that reflect environmental rather than taphonomic associations. While there was likely some downslope movement of material from the bioherm to the biostrome, we argue this has had a negligible effect on the overall biofacies patterns. Read (1982) and Ruppel and Walker (1982) both described sedimentologic features that supported an interpretation of the biostromal facies of the Effna and Holston buildups as pelmatozoan meadows or thickets, reflecting *in-situ* accumulation. Moreover, distribution patterns of many of the more abundant taxa indicate that significant transportation of trilobites between lithofacies is highly unlikely. Changes in composition between biostromal and biohermal facies include species and genera that are morphologically very similar and thus would exhibit similar taphonomic behavior. For example, *Bumastoides* is one of the dominant taxa in both the bioherm and biostrome, but "*Stenopareia*" is abundant only in the bioherm. Similarly, two different species of *Sphaerexochus* (Fig. 8C, F) both occur in similar abundance in the bioherm, but only one is well represented in the biostrome. There is no obvious taphonomic

process that would transport *Bumastoides* but not "*Stenopareia*" downslope, or one species of *Sphaerexochus* but not another. Finally, growth series of the more abundant species are found consistently together in all respective biofacies, so that there is no evidence of extensive size sorting.

In the Chazy reefs of New York, Shaw (1968) also found that numerous genera were confined to off-reef facies (*Failleana*, *Uromystrum*, *Nileoides*, *Paraceraurus*, etc.), whereas others were more common in reef than in off-reef facies (*Hyboaspis*, "*Bumastus,*" *Isotelus*, *Nieszkowskia*). Mikulic (1976) reported very similar patterns to ours on the Silurian Thornton Reef of Illinois, with the trilobite composition of the pelmatozoan flank beds showing considerable differentiation from the buildup core (more enriched in cheirurids and rarer taxa). These studies conform to our interpretation that there is an environmental gradient from buildup to basin and that overlapping taxa share similar environmental preferences. This should not be taken to imply that winnowing or small-scale transport by waves and currents does not occur in reef facies (see Westrop and Rudkin, 1999 for an example), but it does indicate that changes in faunal composition between buildups and associated flanking facies preserve the original environmental distribution patterns of trilobite taxa.

Effna Bioherm *Illaenus-Bumastoides-Sphaerexochus-*"*Stenopareia"* Biofacies

Illaenids (*Illaenus*, *Bumastoides*, *"Stenopareia"*) contributed the majority of trilobite sclerites in the biohermal environment (Fig. 8), constituting 74% of the fauna. Cheirurids (*Sphaerexochus*, *Acanthoparypha*) constitute slightly < 15% of the total and lichids (*Amphichas*, *Probolichas*) only 8%. Other taxa are a minor component of biohermal diversity. Fortey (1975) and Mikulic (1981) compiled data for Middle

Ordovician trilobite abundances in buildups. The allochthonous carbonate boulders of the Cow Head Breccia in Newfoundland yielded a fauna composed of 29% illaenids, 20% cheirurids, and 15% lichids (Whittington, 1963). The Tourmakeady Limestone (Skevington, 1971) of western Ireland possessed a fauna composed of 23% illaenids, 16% dimeropygids, and 15% cheirurids. A silicified fauna from the Tourmakeady Limestone (Adrain and Fortey, 1997) differed in composition from samples cracked out of the rock, particularly in the high abundance of *Celmus*, but still included more than 40% illaenids and cheirurids. Other studies (e.g., Shaw, 1968; Ross, 1972; Fortey, 1975) have shown similar patterns, with bathyurids, proetids, and harpetids all constituting at least some portion of buildup relative abundance. The Effna Limestone contains all the elements of the standard illaenid-cheirurid buildup biofacies, but is proportionally enriched in illaenids. The Effna bioherm is most similar compositionally to the Cow Head Breccia of Whittington (1963), though somewhat less diverse. Based on the Cow Head assemblage, Fortey (1975) noted that lichids might be an additional element that is characteristic of Ordovician buildups. More specifically, it seems that tetralichines (Carlucci et al., 2010) are associated with Ordovician buildup assemblages.

Effna Biostromal *Sphaeoroxochus-Illaenus-Thaleops* Biofacies

Illaenids comprise 57% of the total number of individuals in the biostromal pelmatozoan environment, but *"Stenopareia"* is rare and the relative abundance of *Thaleops* rises dramatically (Fig. 8). Cheirurids increase in relative abundance relative to the bioherm fauna, composing 24% of individuals. Several species of *Calyptaulax* are major new elements in the biostrome (10%), and lichids drop in relative importance (3%). Though direct comparison (e.g., with ANOSIM) of the Effna and PQ biostromal

collections is not possible because of low sample size, it is worth noting that in both the biostrome and deep flank, the dominant illaenid at PQ is *Illaenus*, while *Thaleops* is the most abundant at the I-77 site.

Ross (1972) found *Illaenus*, *Nileus*, *Arthrorhachis*, *Kawina*, and *Carrickia* in the biostromal "shallow flank" of the buildup complex at Meiklejohn Peak, suggesting broad similarities compositionally with the Effna, although *Calyptaulax* is absent from his collections. Calcarenites of the Fleury Member (Day Point Formation) have also yielded a similar fauna to the Effna biostrome: *Calyptaulax*, *Bumastoides*, *Amphilichas*, *Sphaerexochus*, *Isotelus*, and "*Encrinuroides"* (Shaw, 1968).

Botetourt Deep-Flank Biofacies

Illaenus-*Thaleops* Biofacies.—The deep flank at PQ is more similar to the bioherm than the equivalent facies at I-77, but is stratigraphically younger, as it cuts across the pelmatozoan biostrome prior to buildup development (Read, 1982). Illaenids (primarily *Illaenus* and *Thaleops*) are an astounding 90% of relative abundance, with various rare genera contributing only minor percentages (*Pliomerella*, *Calyptaulax*, *Nileus*, *Isotelus*, *Holdenia*) to the total (Fig. 9).

Ampyx-*Isotelus*-*Nileus* Biofacies (I-77 site).—Raphiophorid trilobites (*Ampyx* spp.) dominate this biofacies with 26% of the relative abundance (Fig. 9). Asaphids (*Isotelus*) and nileids (*Nileus*) are also very common, accounting for 22% of generic abundance together. Illaenids (mainly *Thaleops*) constitute 21% of relative abundance, with *Illaenus* and *Bumastoides* a more minor component of diversity than in shallower biofacies. *Raymondaspis* (6%), "*Decoroproetus*" (5%), *Arthrorhachis* (4%), and *Calyptaulax* (3%) are all somewhat common in the deep-flank association.

Compositionally and lithologically, the deep-flank biofacies is very similar to the nileid community (Valhallfonna Formation) of Fortey (1975), which was present in an upper slope environment, and associated with dark limestones and shales. In our study, the nodular limestone and shale are on the deep flank of the biostrome, but also may occupy a similar position to Fortey's fauna bathymetrically. Both the Botetourt and Valhallfonna assemblages are dominated by raphiophorids (*Ampyx* in the former; *Ampyxina* in the latter), nileids (*Nileus*; *Peraspis*), asaphids (*Isotelus*; *Niobe*), styginids (*Raymondaspis*) and agnostid arthropods (*Arthrorhachis*; *Geragnostus*, *Micragnostus*), with "leftover" elements from the illaenid-cheirurid shallow water environment. Zhou et al. (2001) found evidence of separate *Nileus*-dominated, and *Ampyx*-dominated biofacies in the Ordovician Pagoda Formation, China. The latter biofacies is expressed at deeper water depths, which they interpreted as similar bathymetrically to the nileid "community" of Fortey (1975). In our collections, the distribution of nileids and raphiophorids are strongly associated with each other. Illaenids in our deep flank biofacies are a higher proportion of relative abundance when compared to similar environments in the Valhallfonna Formation, but Zhou et al. (2001) recorded high abundance of *Panderia* associated with *Nileus*.

Liberty Hall Outer Ramp-to-Basin *Isotelus*-*Raymondaspis*-*Calyptaulax* Biofacies

Isotelus accounts for 51% of relative abundance in the outer ramp-to-basin environment (Fig. 9). *Calyptaulax* (19%) and *Raymondaspis* (14%) are also major elements of the trilobite fauna. *Dionide*, *Nileus*, *Robergia*, and *Salteria* are all proportionally rare and comprise the rest of the fauna. Cosmopolitan fauna dominate this biofacies; trilobites that show strong facies-control are notably absent. *Isotelus* is

particularly common in outer ramp, deep-water environments in the foreland basin of Virginia (Tripp and Evitt, 1986). We interpret this biofacies as the initial expression of the assemblage that exists deeper into the foreland basin. A deep-water fauna has been reported (Cooper, 1953; Bartholomew and Tillman, 1977) from the Lusters Gate and Roanoke Cement (no longer accessible) localities in the Liberty Hall, 60 and 100 km west of I-77. Cooper (1953) illustrated *Dionide*, *Porterfieldia*, *Raymondaspis*, *Robergia*, *Calyptaulax* and *Edmundsonia* from the Liberty Hall of Virginia. Preliminary data from the Liberty Hall facies of the Edinburgh Formation at Tumbling Run and Strasburg Junction in northern Virginia also suggest an association of *Isotelus* and *Calyptaulax*, in combination with rare deep-water trilobites.

DISCUSSION

Diversity Patterns

The diversity patterns shown here are similar to the trilobite communities from the Middle Ordovician Valhallfonna Formation of Spitsbergen (Fortey, 1975). The allochthonous boulders from the illaenid-cheirurid community of Fortey (1975) were likely from shelf-edge reef complexes and possessed less than half of the diversity of the autochthonous nileid-raphiophorid outer slope community. Further, the olenid lower slope community of Fortey (1975), which is analogous to our outer ramp, low diversity biofacies, was the least diverse of the Valhallfonna assemblages. Data on trilobite diversity in different buildup environments is sparse, but some authors have presented tabulations. Suzuki and Bergström (1999) noted that trilobites were diverse within the bioherms, but rare on pelmatozoan flank facies of the Boda Limestone in Dalarne, Sweden. Ross (1972, fig. 11) reported trilobite generic richness of 36 within the bioherm

at Meiklejohn Peak, Nevada, and 20 for the flanking beds. Since the present study is one of the only attempts to quantify these differences, it is uncertain if the elevated trilobite biostrome diversity of the Effna and Porterfield buildups is a unique environmental feature compared to other buildup complexes. Though Read (1982, p. 202) considered Effna biostromal facies as largely *in-situ* accumulations, it is possible that extensive downslope movement of biohermal debris could promote time-averaged mixing of biohermal and biostromal trilobites; however, we do not think that transportation played a significant role in influencing diversity in this case (see discussion under Trilobite Biofacies). A third alternative is that the biostromal facies are just less well sampled in the Boda and Meiklejohn Peak buildups.

Paleoecological Patterns

Different trilobite groups in Ordovician carbonate buildups have been shown to occupy several microenvironments on mound surfaces and cavities (Suzuki and Bergström, 1999). We show evidence herein that there is a similar paleoenvironmental partitioning at larger scales (Fig. 10), namely between bioherm, biostrome, deep flank, and possibly between buildups. In addition, we extend the work of previous authors (Fortey, 1975; Chatterton and Ludvigsen, 1976; Shaw and Fortey, 1977; Amati and Westrop, 2006), who have documented trilobite biofacies along depth transects in Laurentian environments. Amati and Westrop (2006) documented the transition from *Bumastoides*-dominated shoals to *Thaleops*-dominated midramp environments in the Viola Formation, Oklahoma. In our data from older strata, *Thaleops* is also associated with deeper environments (biostrome, deep flank) whereas *Bumastoides* is more abundant in the shallower bioherm. Thus, although separated temporally (early Sandbian in the Effna

compared to Katian in the Viola) and environmentally (buildup complex in the Effna, ramp shoals and wackestone in the Viola), species of closely related illaenid genera show consistent relative responses to water depth. Similarly, cosmopolitan genera in our study also show wide-ranging environmental tolerances in the Katian of Oklahoma (*Isotelus*, *Calyptaulax*; Amati and Westrop, 2006, fig. 8). Shaw and Fortey (1977, table 4) compiled a list of Middle–Late Ordovician Laurentian trilobite genera and their relationship to facies (environments). We are able to quantitatively support many of these relationships (e.g., *Nileus*, *Raymondaspis*, and *Ampyx* are dominant genera in upper slope environments), and also expand others (e.g., *Isotelus* and *Calyptaulax* can be dominant genera in environments deeper than shelf environments).

Our results suggest there are differences in trilobite composition between the Effna biohermal and biostromal environments within the illaenid-cheirurid association. Ross (1972) stated there were no obvious categories of reef dwellers or flank dwellers in Nevada or elsewhere in North America, but we think this signal is actually present in many other Ordovician buildups, necessitating a closer look at the biostromal portion of other buildup complexes. Mikulic (1976) presented evidence that the Silurian Thornton Reef in Illinois showed environmental differentiation between pelmatozoan peripheral beds and the buildup core. In fact, the broad patterns are very similar to what we found here (see Mikulic, 1981, tables 4–6) with larger sample sizes. Cheirurids are enriched in relative abundance relative to the bioherm, with rare taxa and those that are common downslope ("atypical buildup-dwelling trilobites" of Mikulic, 1981, p. 49) appearing only in the biostrome. Mikulic (1981) attributed this pattern to trilobites temporarily migrating to the buildup periphery, although it could simply record a general gradient in trilobite

distribution. We expect the biostromal environment in the Effna (and potentially other buildups) to be represented by a slightly deeper-water trilobite fauna, particularly if the environment is a true biostrome rather than just a flank facies associated with the main bioherm. In other words, the biostromal intermound environment is transitional between the bioherm fauna and slope fauna (*Ampyx-Isotelus-Nileus* biofacies herein). This interpretation is supported by the gradational nature of relative abundance change during the on-bank to off-bank transition.

The illaenid-cheirurid association has been identified within and outside of Laurentia and through the entirety of the Middle–Late Ordovician. The earliest occurrence of the association is in the Whiterockian (Dapingian) Tourmakeady Limestone, Ireland (Fortey, 1975; Adrain and Fortey, 1997), and it has also been found in the Darriwilian of the Table Head Formation, Newfoundland (Whittington, 1963); Meiklejohn bioherm, Nevada (Ross, 1972); Valhallfonna Formation, Spitsbergen (Fortey 1975; Fortey and Barnes, 1977); Crown Point and Valcour reefs, New York (Shaw, 1968); the Sandbian of Kazakhstan (Apollonov, 1975); Lepaena Limestone, Sweden (Warburg, 1925); the Katian of the Boda Limestone, Sweden (Warburg, 1925); and the Chair of Kildare Limestone, Ireland (Dean, 1978). Our work extends the geographic range of the association into the Taconic Foreland Basin of the early Sandbian. The illaenid-cheirurid association can also be traced into the Silurian, though many of the constituent genera change. Mikulic (1981) noted that in the early Silurian *Stenopareia* replaces *Illaenus* and *Bumastoides* as the dominant buildup illaenid, and in the late Silurian the styginid *Bumastus* replaces *Stenopareia*. There are some taxonomic issues

with *Stenopareia* (see Carlucci et al., 2011), but in general these patterns seem stratigraphically consistent.

Relationship To Foreland Basin Environmental Change

Patzkowsky and Holland (1993, 1996) recorded extinctions of brachiopod fauna at their M4–M5 sequence boundary which coincided with tectonically driven environmental change. Trilobite faunas may have undergone similar regional extinctions or biofacies replacements in response to oceanographic changes in water temperature, siliciclastic input, increased turbidity, and phosphatization (Patzkowsky and Holland, 1993, 1996; Amati and Westrop, 2006). The Liberty Hallfacies in southwestern Virginia was deposited during widespread downwarping of the Taconic Foreland Basin (stage 3 of Read, 1980, p. 1608). Highland-derived clastics were deposited into the basin margin from the east (Paperville Shale), fining down-ramp into the dysoxic and anoxic outer slope–basin deposits of the Liberty Hall facies. When carbonate production on the buildups could no longer keep pace with the creation of accommodation space, sulfide and phosphatic crusts formed on the buildups as cold, phosphatic, low oxygen basin waters smothered the buildups (Read, 1982). The biofacies we describe provide a snapshot of the trilobite faunas of southwestern Virginia prior to the major environmental changes associated with foreland basin development. They are also the youngest Ordovician buildup-related trilobite faunas documented to date in the Appalachian region of the United States. Along with buildups, the illaenid-cheirurid biofacies was essentially extirpated from eastern North America during the late Ordovician, although it persists in coeval shallow, subtidal, level-bottom settings elsewhere (e.g., Red River Formation of Manitoba; Westrop and Ludvigsen, 1983).

These faunas provide a valuable baseline that allows for comparison with trilobite biofacies adversely impacted by M4–M5 (Holland and Patzkowsky, 1996) environmental changes. More specifically they represent the depositional status quo in the foreland basin during the late Whiterockian (Dapingian) and early Mohawkian (Sandbian). The widely reported paleoecologic groupings (e.g., illaenids and cheirurids dominating buildups, raphiophorids and nileids dominating slope environments, etc.) are conspicuous. Work in progress (Carlucci and Westrop, unpublished data) in areas outside the foreland basin (e.g., the Bromide Formation of Oklahoma; Carlucci et al., 2010) during the coeval late Whiterockian–early Mohawkian interval suggest the presence of similar deep-water isoteline-raphiophorid assemblages, which also dominate the Edinburg Formation (Cooper and Cooper, 1946) of the foreland basin in northern Virginia. This deep-water association was reorganized at the M4–M5 boundary, and the similarities between areas outside the basin and those within decrease dramatically with the appearance of new associations of taxa. In Virginia, a low diversity cryptolithine biofacies spreads across the basin (Carlucci and Westrop, unpublished data) as a rapid influx of clastic sediment was deposited (Martinsburg Formation; McBride, 1962). Amati and Westrop (2006) noted that in the Sugar River Formation of New York, a similar low diversity cryptolithine biofacies emerges into a shallow water environment, with bioclastic tempesites indicative of a midramp setting. Outside the foreland basin, (e.g., Viola Springs Formation; Amati and Westrop, 2006), the low diversity crypolithine biofacies is restricted to deep-water environments, with a normal shallow-water trilobite fauna present in environments between fair-weather and storm wave base. As mentioned above, many genera show consistent relationships in response to water depth, even given temporal and geographic

variation. Preliminary evidence suggests that changing environmental conditions reorganized these relationships within the foreland basin, as well as dramatically reduced diversity when compared to similar environments outside the basin. All of the taxa extirpated from the foreland basin persist in other parts of Laurentia, suggesting that this is a regional signal unique to the foreland basin, and the biofacies we described here document persistent environmental associations immediately prior to the changes.

CONCLUSIONS

The late Whiterockian–Mohawkian (Darriwilian–Sandbian) carbonate buildup-to-basin transect in southwest Virginia was occupied by a series of trilobite biofacies. Trilobite composition gradationally changed along a depth gradient, from the bioherm, to the biostrome, deep flank, and into the outer slope–basin environment. The most abundant trilobites in the bioherm were *Illaenus*, *Bumastoides*, *"Stenopareia,"* and *Sphaerexochus*, whereas the biostromal environment was dominated by *Sphaerexochus*, *Illaenus*, and *Thaleops*. The illaenid-cheirurid association was replaced by an *Ampyx*-, *Isotelus*-, and *Nileus*-dominated biofacies in the nodular limestone of the deep flank. Outer slope and basinal mudstone and shale were occupied by a low diversity *Isotelus-Calyptaulax-Raymondaspis* association, which is interpreted as the initial expression of a deep water fauna more common in the western portion of the foreland basin. Generic diversity in the biostrome and deep flank is higher than in the bioherm, likely because the transitional environment favored a wider range of tolerances. Other Ordovician carbonate buildups may show similar patterns in trilobite distribution, even though previous studies have combined the faunas. The illaenid-cheirurid and *Nileus* biofacies associations first described by Fortey (1975) were conspicuous in Ordovician carbonate ramp deposits and

we expand their range into the Taconic Foreland basin. Later in the history of the basin, however, both buildups and the associated illaenid-cheirurid biofacies were extirpated from the basin, likely due to severe, tectonically driven environmental change.

ACKNOWLEDGMENTS

This research was funded by National Science Foundation grant EAR-0819715 to S. Westrop and a Geological Society of America research grant to J. Carlucci. A. Thomas and K. Carlucci assisted in fieldwork, and R. Burkhalter provided support both in the lab and in the field. F. Read provided helpful locality information in Virginia. Thanks to J. Adrain for his insightful comments on the affinities of some of the trilobites and to E.L. Taylor, S. Holland, J. Bonelli, and N. Heim for their comments and suggestions, which greatly improved the manuscript.

REFERENCES

ADRAIN, J.M., 2005, Aulacopleurid trilobites from the Upper Ordovician of Virginia: Journal of Paleontology, v. 79, p. 542–563.

ADRAIN, J.M., and FORTEY, R.A., 1997, Ordovician trilobites from the Tourmakeady Limestone, western Ireland: Bulletin of the Natural History Museum, London, Geology Series, v. 53, p. 79–115.

ADRAIN, J.M., FORTEY, R.A., and WESTROP, S.R., 1998, Post-Cambrian trilobite diversity and evolutionary faunas: Science, v. 280, p. 1922–1925.

ADRAIN, J.M., WESTROP, S.R., CHATTERTON, B.D.E., and RAMSKOLD, L., 2000, Silurian trilobite alpha diversity and the end-Ordovician mass extinction: Paleobiology, v. 26, p. 625–646.

AMATI, L., and WESTROP, S.R, 2004, A systematic revision of *Thaleops* (Trilobita: Illaenidae) with new species from the middle and late Ordovician of Oklahoma and New York: Journal of Systematic Palaeontology, v. 2, p. 207–256.

AMATI, L., and WESTROP, S.R., 2006, Sedimentary facies and trilobite biofacies along an Ordovician shelf to basin gradient, Viola Group, South-Central Oklahoma: PALAIOS, v. 21, p. 516–529.

APOLLONOV, M.K., 1975, Ordovician trilobite assemblages of Kazakhstan: Fossils and Strata, v. 4, p. 375–380.

BARTHOLOMEW, M.J., and TILLMAN, C.G., 1977, *Microparia*, a cyclopygid trilobite of Porterfield age from Virginia: Journal of Paleontology, v. 51, p. 131–135.

BATTEN-HENDER, K.L., and DIX, G.R., 2006, Facies, geometry and geological significance of Late Ordovician (early Caradocian) coral bioherms: Lourdes Formation, western Newfoundland: Sedimentology, v. 53, p. 1361–1379.

BRAY, J.R., and CURTIS, J.T., 1957, An ordination of upland forest communities of southern Wisconsin: Ecological Monographs, v. 27, p. 325–349.

CARLUCCI, J.R, WESTROP, S.R, and AMATI, L., 2010, Tetralichine trilobites from the Upper Ordovician of Oklahoma and Virginia, and phylogenetic systematics of the Tetralichini: Journal of Paleontology, v. 84, p. 1099–1120.

CARLUCCI, J.R., WESTROP, S.R., AMATI, L., ADRAIN, J.M., and SWISHER, R.E., 2011, A systematic revision of the Upper Ordovician trilobite genus *Bumastoides* (Trilobita: Illaenidae) with new species from Oklahoma, Virginia, and Missouri: Journal of Systematic Palaeontology, in press.

CHATTERTON, B.D.E., and LUDVIGSEN, R., 1976, Silicified middle Ordovician trilobites from the south Nahanni river area, District of Mackenzie, Canada: Palaeontographica, v. 154, p. 1–106.

CLARKE, K.R., and WARWICK, R.M., 1994, Changes in Marine Communities: an Approach to Statistical Analysis and Interpretation: Plymouth Marine Laboratory, U.K., 144 p.

Cooper, B.N., 1953, Trilobites from the lower Champlainian formations of the Appalachian Valley: Geological Society of America Memoir, v. 55, p. 1–69.

COOPER, B.N., and COOPER, G.A., 1946, Lower Middle Ordovician stratigraphy of the Shenandoah Valley, Virginia: Geological Society of America Bulletin, v. 57, p. 35–114.

DEAN, W.T., 1978, The trilobites of the Chair of Kildare Limestone (Upper Ordovician) of eastern Ireland, Pt. 3: Palaeontographical Society Monographs, v. 131, p. 99–129.

DENNISON, J.M., 1970, Carbonate bank sedimentation, eastern Shark Bay, Western Australia: American Association of Petroleum Geologists Memoirs, v. 13, p. 85–168.

DENNISON, J.M., and WOODWARD, H.P., 1963, Palinspastic maps of central Appalachians: American Association of Petroleum Geologists Bulletin, v. 47, p. 666–680.

DROSER, M.L., FORTEY, R.A., and LI, X., 1996, The Ordovician radiation: American Scientist, v. 84, p. 122–131.

EMERY, D., and MYERS, K., 1996, Sequence Stratigraphy: Wiley-Blackwell, Oxford, 297 p.

FLÜGEL, E., 2004, Microfacies of Carbonate Rocks: Analysis, Interpretation and Application: Springer-Verlag, Berlin, 976 p.

FORTEY, R.A., 1975, Early Ordovician trilobite communities: Fossils and Strata, v. 4, p. 331–352.

FORTEY, R.A., and BARNES, C.R., 1977, Early Ordovician conodont and trilobite communities of Spitsbergen: influence on biogeography: Alcheringa, v. 1, p. 297–309.

HAMMER, O., and HARPER, D., 2006, Paleontological Data Analysis: Blackwell Publishing, 351 p.

HAMMER, Ø, HARPER, D.A.T., and RYAN, P.D., 2001, PAST: Paleontological statistics software package for education and data analysis. Palaeontologia Electronica, v. 4, art 1, 9 p., 178 kb; http://palaeo-electronica.org/2001_1/past/issue1_01.htm (software available from: http://www.nhm.uio.no/norlex/past/download.html). Checked October, 2011.

HOLLAND, S.M., 2005, The signatures of patches and gradients in ecological ordinations: PALAIOS, v. 20, p. 573–580.

HOLLAND, S., and PATZKOWSKY, M., 1996, Sequence stratigraphy and long-term paleoceanographic change in the Middle and Upper Ordovician of the eastern United States, *in* Witzke, B., Ludvigson, G.A., and Day, J., eds., Paleozoic Sequence Stratigraphy: Views from the North American Craton: Geological Society of America Special Paper, v. 306, p. 117–130.

HOLLAND, S., and PATZKOWSKY, M., 2007, Gradient ecology of a biotic invasion: biofacies of the type Cincinnatian series (Upper Ordovician), Cincinnati, Ohio Region, USA.: PALAIOS, v. 22, p. 392–407.

JONGMAN, R.H.G., BRAAK, C.J.F.T., and VAN TONGEREN, O.F.R., 1995, Data Analysis in Community and Landscape Ecology: Cambridge University Press, 324 p.

KENDALL, G.S.C., and SCHLAGER, W., 1981, Carbonates and relative changes in sea level: Marine Geology, v. 44, p. 181–212.

KRAUSE, F.F., 2001, Genesis and geometry of the Meiklejohn Peak lime mud-mound, Bare Mountain Quadrangle, Nevada, USA: Ordovician limestone with submarine frost heave structures—a possible response to gas clathrate hydrate evolution: Sedimentary Geology, v. 145, p. 189–213.

LEES, A., and MILLER, J., 1995, Waulsortian banks, *in* Bosence, C.V.L., Bridges, D.W.J., Bridges, P.H., and Pratt, B.R., eds., Carbonate Mud-Mounds, Their Origin and Evolution: International Association of Sedimentologists, Special Publication, v. 23, p. 191–271.

LOWRY, W.D., 1974, North American geosynclines—test of continental-drift theory: AAPG Bulletin, v. 41, p. 643–655.

LUDVIGSEN, R., 1978, Middle Ordovician trilobite biofacies, southern Mackenzie Mountains, *in* Stelck, C.R., and Chatterton, B.D.E., eds., Western and Canadian Biostratigraphy: Geological Association of Canada Special Paper, v. 18, p. 1–33.

LUDVIGSEN, R., WESTROP, S.R., PRATT, B., TUFFNELL, P., and YOUNG, G., 1986, Dual biostratigraphy: zones and biofacies: Geoscience Canada, v. 13, p. 139–154.

MCBRIDE, E.F., 1962, Flysch and associated beds of the Martinsburg Formation

(Ordovician), central Appalachians: Journal of Sedimentary Research, v. 32, p. 39–91.

MCGUNE, B., and GRACE, J.B., 2002, Analysis of Ecological Communities: MjM Software Design, Gleden Beach, Oregon, 300 p.

MIKULIC, D.G., 1976, Distribution and community succession of trilobites, Thornton reef (Silurian, Illinois), *in* Pray, L.C., ed., The Thornton Reef (Silurian) Northeastern Illinois, 1976 Revisitation: Guidebook for the Illinois Portion of Field Trip on Silurian Reef, Inter-reef Facies, and Faunal Zones of Northern Indiana and Northeastern Illinois: Geology Society of America North Central Section and Western Michigan University, Kalamazoo, p. 1–22.

MIKULIC, D.G., 1981, Trilobites in Paleozoic carbonate buildups: Lethaia, v. 14, p. 45–56.

MILLER, A.I., HOLLAND, S.M., DROSER, M.L., and PATZKOWSKY, M.E., 1998, Dynamics of the Ordovician Radiation: a comment on Westrop and Adrain: Paleobiology, v. 24, p. 524–528.

NEUMANN, A.C., and MACINTYRE, I., 1985, Reef response to sea level rise: keep up, catch up, or give up, *in* Gabrie, C., Toffart, J.L., and Salvat, B., eds., Proceedings of the Fifth International Coral Reef Congress (Tahiti, 1985), v. 3, Symposia and Seminars (A), p. 105–110.

POTAPOVA, M.G., and CHARLES, D.F., 2002, Benthic diatoms in USA rivers: distributions along spatial and environmental gradients: Journal of Biogeography, v. 28, p. 167–187.

PATZKOWSKY, M., and HOLLAND, S., 1993, Biotic response to a Middle Ordovician paleoceanographic event in eastern North America: Geology, v. 21, p. 619–622.

PATZKOWSKY, M., and HOLLAND, S., 1996, Extinction, invasion, and sequence stratigraphy: patterns of faunal change in the Middle and Upper Ordovician of the eastern United States, *in* Witzke, B., Ludvigson, G., and Day, J., eds., Paleozoic Sequence Stratigraphy: Views from the North American Craton: Geological Society of America Special Paper, v. 306, p. 131–142.

POPE, M.C., 2004, Cherty facies of the Montoya Group, southern New Mexico and western Texas and its regional correlatives: a record of Late Ordovician paleoceanography on southern Laurentia: Palaeogeography, Palaeoclimatology, Palaeoecology, v. 210, p. 367–384.

POPE, M.C., and READ, J.F., 1998, Ordovician metre-scale cycles; implications for climate and eustatic fluctuations in the Central Appalachians during a global greenhouse, non-glacial to glacial transition: Palaeogeography, Palaeoclimatology, Palaeoecology, v. 138, p. 27–42.

RAUP, D., 1975, Taxonomic diversity estimation using rarefaction: Paleobiology, v. 1, p. 333–342.

RAYMOND, P.E., 1920, Some new Ordovician trilobites: Bulletin of the Museum of Comparative Zoology, v. 54, p. 51–69.

RAYMOND, P.E., 1925, Some trilobites of the lower Middle Ordovician of eastern North America: Bulletin of the Museum of Comparative Zoology, v. 67, p. 1–180.

READ, J.F., 1980, Carbonate ramp-to-basin transitions and foreland basin evolution, Middle Ordovician, Virginia Appalachians: AAPG Bulletin, v. 64, p. 1575–1612.

READ, J.F., 1982, Geometry, facies, and development of Middle Ordovician carbonate buildups, Virginia Appalachians: AAPG Bulletin, v. 66, p. 189–209.

READ, J.F., 1998, Phanerozoic carbonate ramps from greenhouse, transitional and ice-house worlds: clues from field and modeling studies, *in* Wright, V.P., and Burchette, T.P., eds., Carbonate Ramps: Geological Society of London Special Publications 149, p. 107–135.

READING, H.G., 1996, Sedimentary Environments: Processes, Facies and Stratigraphy: Wiley-Blackwell, Oxford, 688 p.

ROSS, J., 1972, Fossils from the Ordovician bioherm at Meiklejohn Peak, Nevada: U.S. Geological Survey Professional Paper, v. 685, p. 1–47.

RUPPEL, S.C., and WALKER, K.R., 1982, Sedimentology and distinction of carbonate buildups: Middle Ordovician, East Tennessee: Journal of Sedimentary Petrology, v. 52, p. 1055–1071.

SABOL, J.W., 1958, Geology of the Porterfield Quarry area, Smyth County, Virginia: Unpublished M.S. Thesis, Virginia Polytechnic Institute, Blacksburg, Virginia, 81 p.

SALTZMAN, M.R., and YOUNG, S.A., 2005, Long-lived glaciation in the Late Ordovician? Isotopic and sequence stratigraphic evidence from western Laurentia: Geology, v. 33, p. 109–112.

SEPKOSKI, J.J., 1981, A factor analytic description of the Phanerozoic marine fossil record: Paleobiology, v. 7, p. 36–53.

SEPKOSKI, J.J., and MILLER, A.I., 1985, Evolutionary faunas and the distribution of Paleozoic benthic communities in space and time, *in* Valentine, J.W., ed.,

Phanerozoic Diversity Patterns: Profiles in Macroevolution: Princeton University Press and the American Association for the Advancement of Science, Princeton, New Jersey, p. 153–190.

SHAW, F.C., 1968, Early Middle Ordovician Chazy trilobites of New York: New York State Museum and Science Services Memoir, v. 17, p. 1–163.

SHAW, F.C., and FORTEY, R.A., 1977, Middle Ordovician facies and trilobite faunas: Geological Magazine, v. 114, p. 409–496.

SHAW, F.C., and BOLTON, T.E., 2011, Ordovician trilobites from the Romaine and Mingan Formations (Ibexian–late Whiterockian), Mingan Islands, Quebec: Journal of Paleontology, v. 85, p. 406–441.

SIMPSON, E.H., 1949, Measurement of diversity: Nature, v. 163, p. 688–688.

SKEVINGTON, D., 1971, The age and correlation of the Rosroe Grits, Northwest Co. Galway: Proceedings of the Royal Irish Academy, Section B, v. 71, p. 75–83.

STANLEY, S.M., 2007, An analysis of the history of marine animal diversity: Paleobiology, v. 33, p. 1–55.

SUZUKI, Y., and BERGSTRÖM, J., 1999, Trilobite taphonomy and ecology in Upper Ordovician carbonate buildups in Dalarna, Sweden: Lethaia, v. 32, p. 159–172.

TREMBLAY, J.V., and WESTROP, S.R., 1991, Middle Ordovician (Whiterockian) trilobites from the Sunblood Formation, District of Mackenzie, Canada: Journal of Paleontology, v. 65, p. 801–824.

TRIPP, R.P., and EVITT, W.R., 1986, Silicified trilobites of the family Asaphidae from the Middle Ordovician of Virginia: Palaeontology, v. 29, p. 705–724.

ULRICH, E.O., and DELO, D.M., 1940, Phacopid trilobites of North America: Geological

Society of America Special Paper, v. 29, 135 p.

WARBURG, E., 1925, The trilobites of the Leptaena Limestone in Dalarne: Bulletin of the Geologic Institute of the University of Uppsala, v. 27, p. 1–446.

WESTROP, S.R., and ADRAIN, J.M., 1998, Alpha diversity and the reorganization of Ordovician benthic marine communities: Paleobiology, v. 24, p. 1–16.

WESTROP, S.R., and LUDVIGSEN, R., 1983, Systematics and paleoecology of Upper Ordovician trilobites from the Selkirk Member of the Red River Formation, southern Manitoba: Manitoba Department of Energy and Mines Geological Report, v. GR 82-2, p. 1–51.

WESTROP, S.R., and RUDKIN, D.M., 1999, Trilobite taphonomy of a Silurian reef; Attawapiskat Formation, northern Ontario: PALAIOS, v. 14, p. 389–397.

WHITTINGTON, H.B., 1963, Middle Ordovician trilobites from Lower Head, western Newfoundland: Bulletin of the Museum of Comparative Zoology, v. 129, p. 1–118.

WILSON, J.L., 1975, Carbonate Facies in Geologic History: Springer-Verlag, New York, 471 p.

ZHOU, Z., YUAN, W., and ZHOU, Z., 2001, Llanvirn–early Caradoc trilobite biofacies of western Hubei and Hunan, China: Alcheringa, v. 25, p. 69–86.

FIGURE 1—Locality and buildup maps in southwestern Virginia, USA. A) Locality map (U.S. Geological Survey) of the Porterfield Quarry (PQ) and I-77 roadcuts. I-77 coordinates: 37.745° N, 79.513° W; UTM NAD27 17S 630905, 4178443; PQ coordinates: 36.878° N, 81.681° W; UTM NAD27 17S 439250, 4081420. B) Distribution of the Effna and Porterfield buildups in relation to each other, foreland basin axis, margin, and Taconic highlands (modified from Dennison and Woodward, 1963; Dennison, 1970; Read, 1982). C) Outline of Virginia; small black rectangle shows the map location in A; gray rectangle shows the extent of coverage in B.

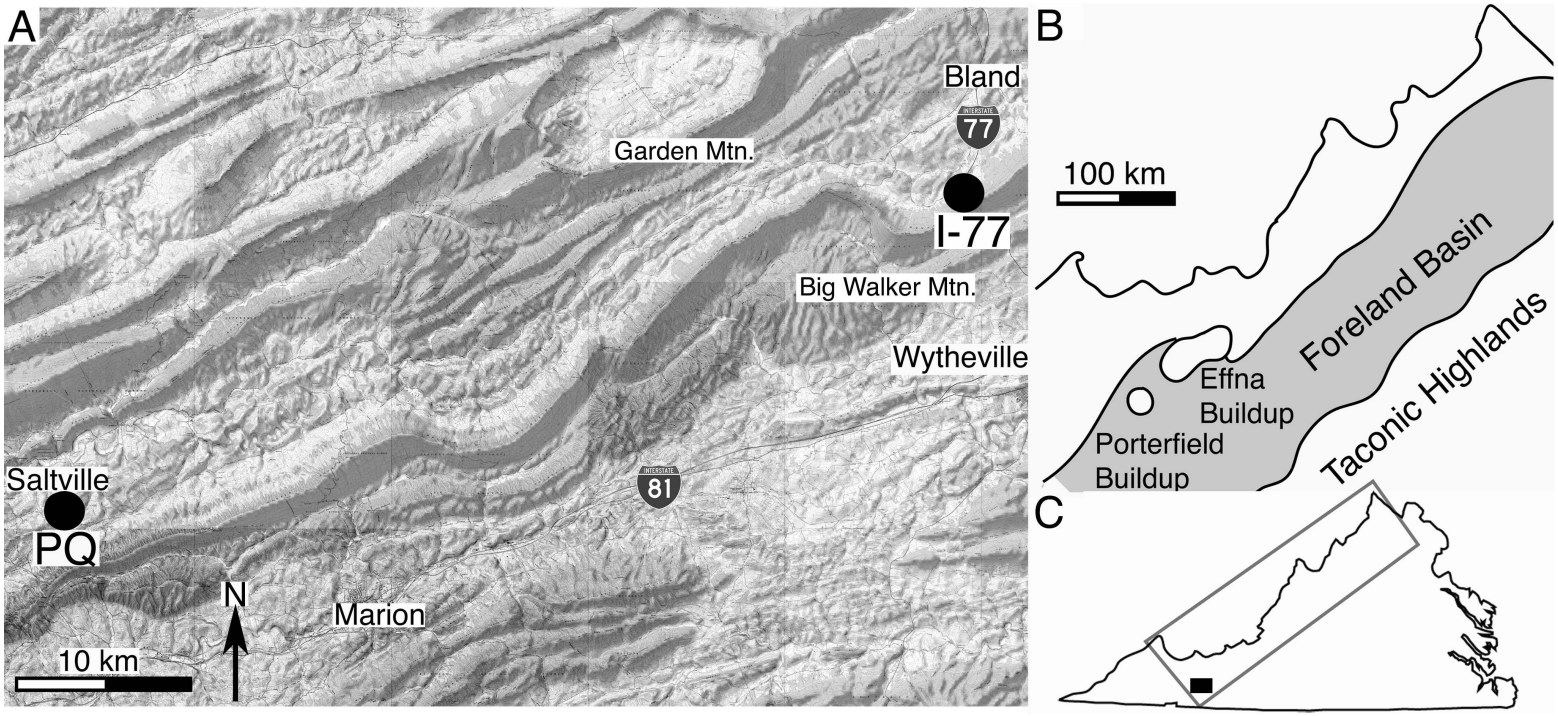
A
Bland
77
Garden Mtn.
I-77
Big Walker Mtn.
Wytheville
81
Saltville
PQ
N
Marion
10 km
B
100 km
Foreland Basin
Taconic Highlands
Effna
Buildup
Porterfield
Buildup
C

FIGURE 2—Stratigraphic setting and PQ locality maps. A) Simplified stratigraphic chart, showing Mohawkian (Sandiban) units of southwestern Virginia in approximate relation to the depositional sequences of Holland and Patzkowsky (1996). Formation names do not correspond directly with depositional sequence boundaries. B) Complete quarry map (modified from Read, 1982) based on multiple measured sections (collected and compiled by Sabol, 1958; Read, 1982; lithologic terminology modified here). Black circles = collection levels.

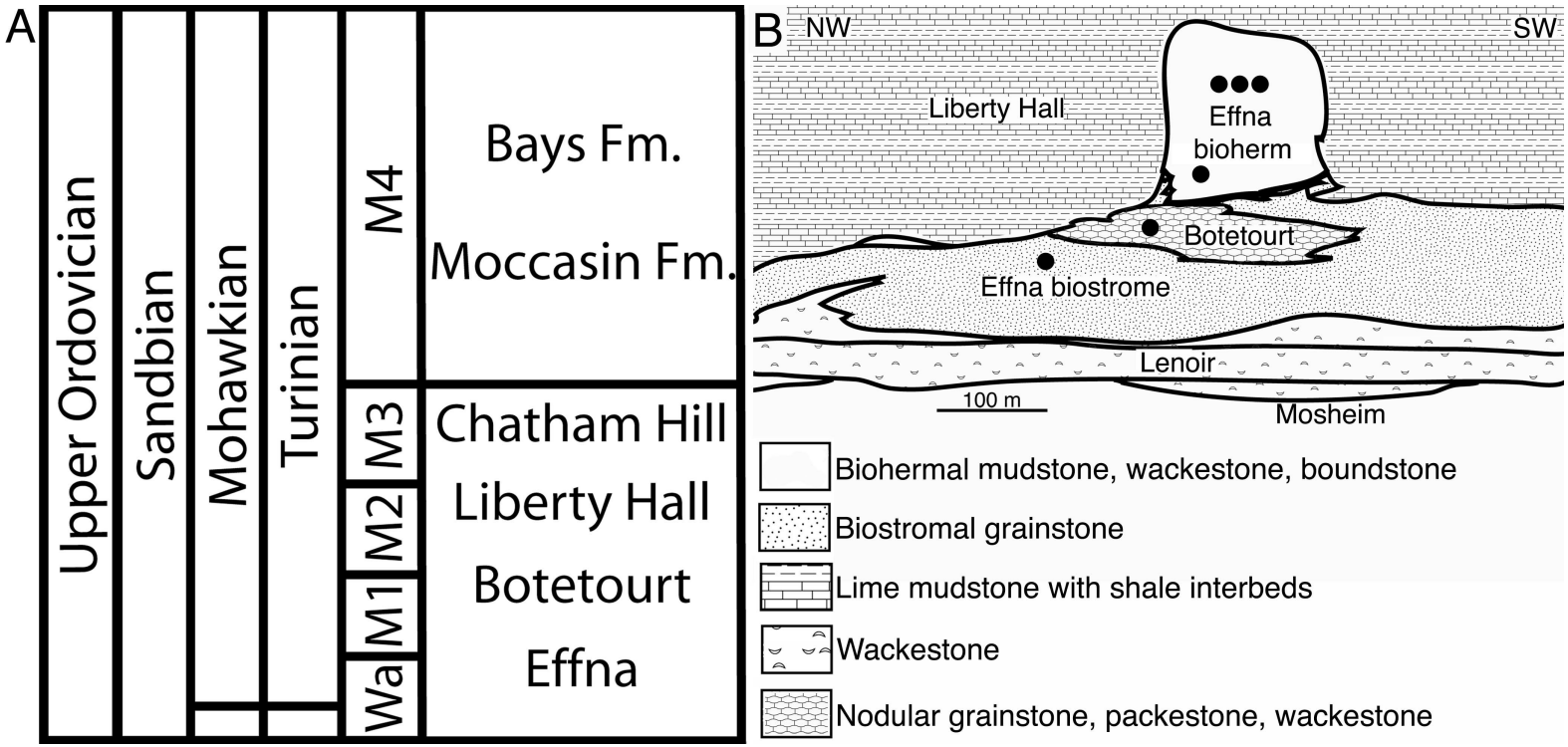
A
Upper Ordovician
Sandbian
Mohawkian
Turinian
M4
M3
M2
M1
Wa
Bays Fm.
Moccasin Fm.
Chatham Hill
Liberty Hall
Botetourt
Effna
B
NW
SW
Liberty Hall
Effna bioherm
Botetourt
Effna biostrome
Lenoir
100 m
Mosheim
Biohermal mudstone, wackestone, boundstone
Biostromal grainstone
Lime mudstone with shale interbeds
Wackestone
Nodular grainstone, packestone, wackestone

FIGURE 3—Facies mosaic of the I-77 locality showing the crest of the Effna buildup (note the complex relationship between biohermal mudstone and biostromal grainstone), the nodular Botetourt limestone, and the evenly bedded Liberty Hall beds (modified from Read, 1982). Black circles = collection levels. Note vertical exaggeration on the y axis.

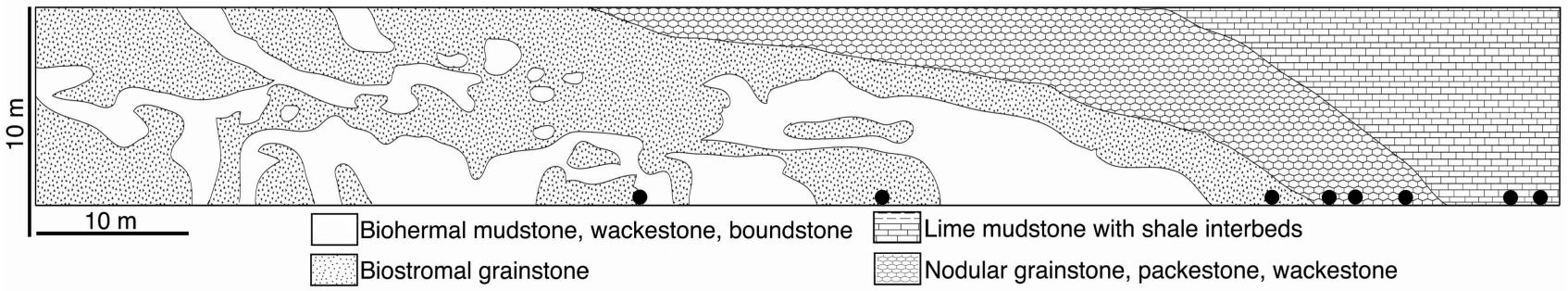
10 m
10 m
Biohermal mudstone, wackestone, boundstone
Biostromal grainstone
Lime mudstone with shale interbeds
Nodular grainstone, packestone, wackestone

TABLE 1—Effna bioherm and biostrome lithofacies.

Carbonate buildup core and pod lithofacies (Effna)

Lithology: Fine grained white lime mudstone, wackestone, and bafflestone with bryozoans that act as sediment barriers.

Bedding and structures: Massively bedded, conchoidal fracture, calcite cement forms extensive hardgrounds, pockets, stringers. *Stromatactis* structures (cm to dm) are elongate, with smooth bases, irregular digitate roofs. Void fills are equant cement or internally laminated geopetal mud, with bladed and fibrous cement on cavity margins. Wackestone commonly found in lenses or pockets within mudstone host rock, rarely interbedded with mudstone.

Fauna: Well-preserved and often articulated pelmatazoan, bryozoan (ramose, (lacy, and encrusting), trilobite, brachiopod, gastropod, ostracod, and calcareous algae bioclasts.

Interrelationships: At PQ, central mudstone and wackestone biohermal core interfingers with biostromal grainstone at the margins. Meter scale mudstone and wackestone pods flank the central bioherm, and are enveloped by Botetourt limestone. At I-77, the crest of the core and pod lithofacies forms a complex mosaic of interfingering with the biostrome (Fig. 3). Small pods of biohermal mudstone are completely enveloped by biostromal grainstone.

Biostromal grainstone lithofacies (Effna)

Lithology: Coarse grained white to light grey pelmatazoan and bryozoan grainstone, local packestone and bryozoan rudstone.

Bedding and structures: Grainstone is thick-bedded with rare cross-bedding. Calcite cement is bladed or fibrous, forming hardgrounds and stylolitic stringers. Phosphatic crusts often top thick-bedded units.

Fauna: Similar to the bioherm, with calcareous algae (*Girvanella*, *Solenopora*), echinoderms, and bryozoans proportionally enriched (see Read, 1982, table 2).

Interrelationships: At PQ, biostromal grainstone underlies and flanks the the main bioherm, interfingering with both the core and pods facies, and the Botetourt at the margins. At I-77 (Fig. 3) grainstone interfingers with, and envelops the core and pod facies at the crest of the bioherm, and occurs immediately below a sharp contact with the Botetourt.

TABLE 2—Botetourt and Liberty Hall lithofacies.

Deep flank nodular limestone and shale lithofacies (Botetourt)

Lithology: Occurs as two subfacies, black shaly mudstone, wackestone and packestone, or dark grey to black pelmatazoan grainstone (Fig. 4B).

Bedding and structures: Nodular bedded, with thin seams of indurated clastic shale and marls. Mudstone, wackestone, and packestone all show patchy marine cementation, local hardgrounds, and stylolitic stringers. Surfaces between limestone and shale are commonly sharp. Meter scale cycles are expressed as nodular limestone and shale that are in sharp contact with condensed grainstone caps. The caps become thinner upward through both successions at PQ and I-77.

Fauna: Similar to the biostrome, with calcareous algae considerably more uncommon (see Read, 1982, table 2).

Interrelationships: At PQ, the Botetourt overlies and interfingers with the Effna buildup at its margins, and overlies the biostrome laterally. A tongue of nodular limesone extends across the biostromal portion of the buildup (Fig. 2B), and was deposited prior to buildup formation. Exposed quarry walls show the Botetourt enveloping small peripheral biohermal pods. At I-77 (Fig. 3) the Botetourt is in sharp contact with the Effna grainstone at the crest, and grades into more evenly bedded Liberty Hall lithofacies.

Mudstone and shale lithofacies (Liberty Hall)

Lithology: Black lime mudstone, with thin clastic, shale partings (Edinburg Formation of Cooper and Cooper, 1949).

Bedding and structures: Thick and evenly bedded, lime mudstone internally massive to well-laminated. Mudstone beds often characterized by wackestone and packestone tops with scoured erosional bases (Fig. 4E) that are dominated by pyritized bioclasts. Pyritization is likely the product of late diagenesis, as much of the detail on trilobite sclerites is not preserved. Intraformational conglomerates have been reported by several authors (Lowry, 1974; Moshier, 1977; Read, 1980). Meter scale cycle tops are often expressed as a change to less well-bedded and more nodular beds, reminiscent of the Botetourt.

Fauna: Trilobites, small gastropods, and inarticulate brachiopods.

Interrelationships: At PQ, the contact between the Liberty Hall and the bioherm (and flanking pods) is tectonized, with crumpled beds, slickensides and fault gouges.

FIGURE 4—Representative polished slabs of lithofacies in the Effna, Botetourt, and Liberty Hall limestones. A) Effna pelmatozoan grainstone interpreted as biostromal intermound deposits. B) Botetourt grainstone, which forms meter-scale cycle tops in the backstepping unit. C) Effna mudstone, bioturbated, with numerous *Stromatactis* structures, interpreted as a biohermal deposit. D) Botetourt, nodular bedded wackestone and packstone, interbedded with indurated shale, interpreted as a deep flank (slope) deposit. E) Liberty Hall lime mudstone, with wackestone bed top on irregular surface, interpreted as an outer slope deposit.

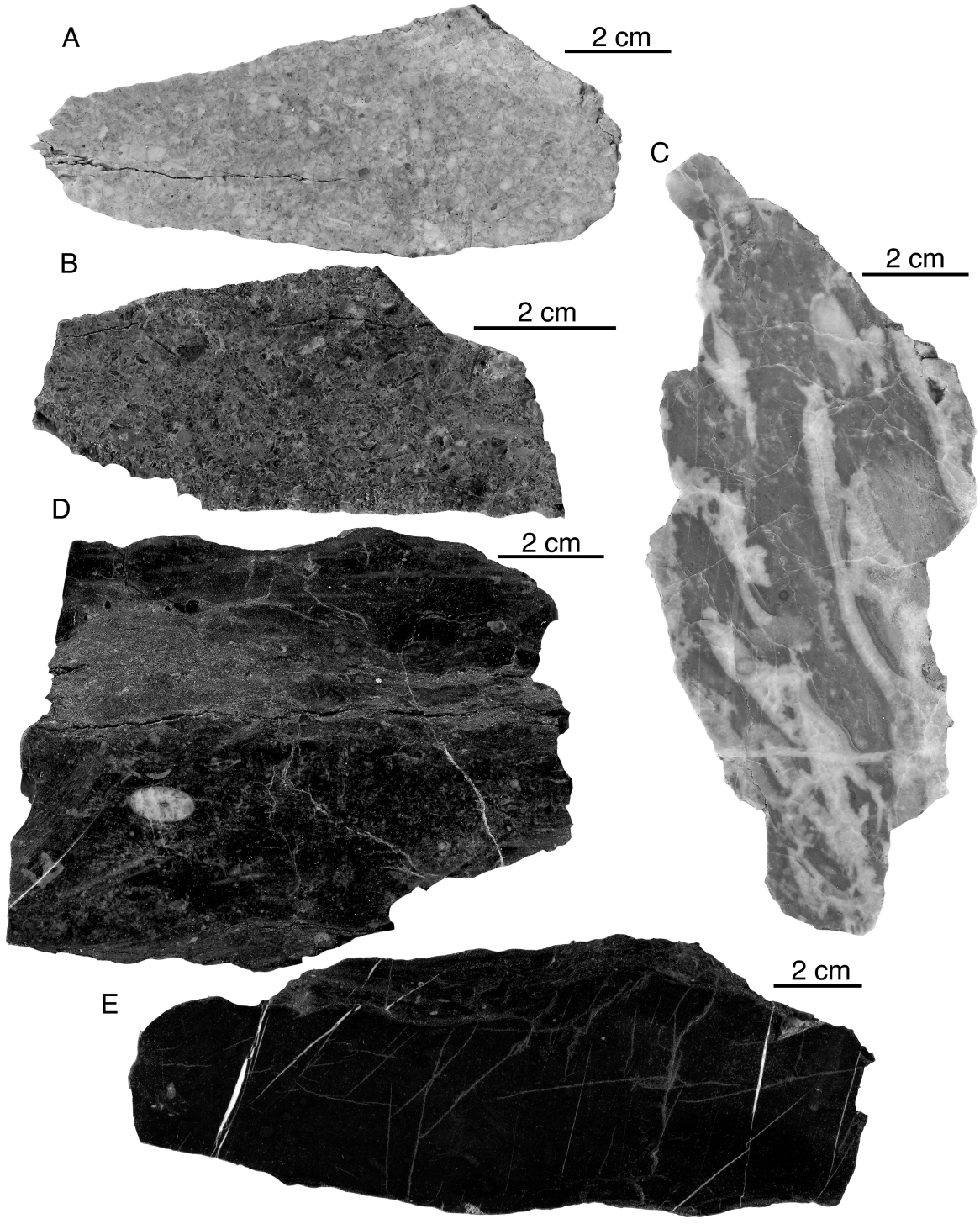
A
2 cm
B
2 cm
C
2 cm
D
2 cm
E
2 cm

FIGURE 5—Results of Q- and R-mode cluster analysis of 14 collections from PQ and I-77, southwestern Virginia. Data were transformed into percentage within sample prior to analysis. Biofacies defined by intersections of Q- and R-mode clusters. dotted lines = paleoenvironmental boundaries sorted along the Q-mode. R-mode cluster 1 = deep-water fauna, cluster 2 = shallow-water fauna, cluster 3 = rare taxa. Note how progressively deeper environments gradationally incorporate more elements from the deep-water cluster and fewer from the shallow water cluster. Shapes at terminal branches represent the biofacies that best characterizes that collection.

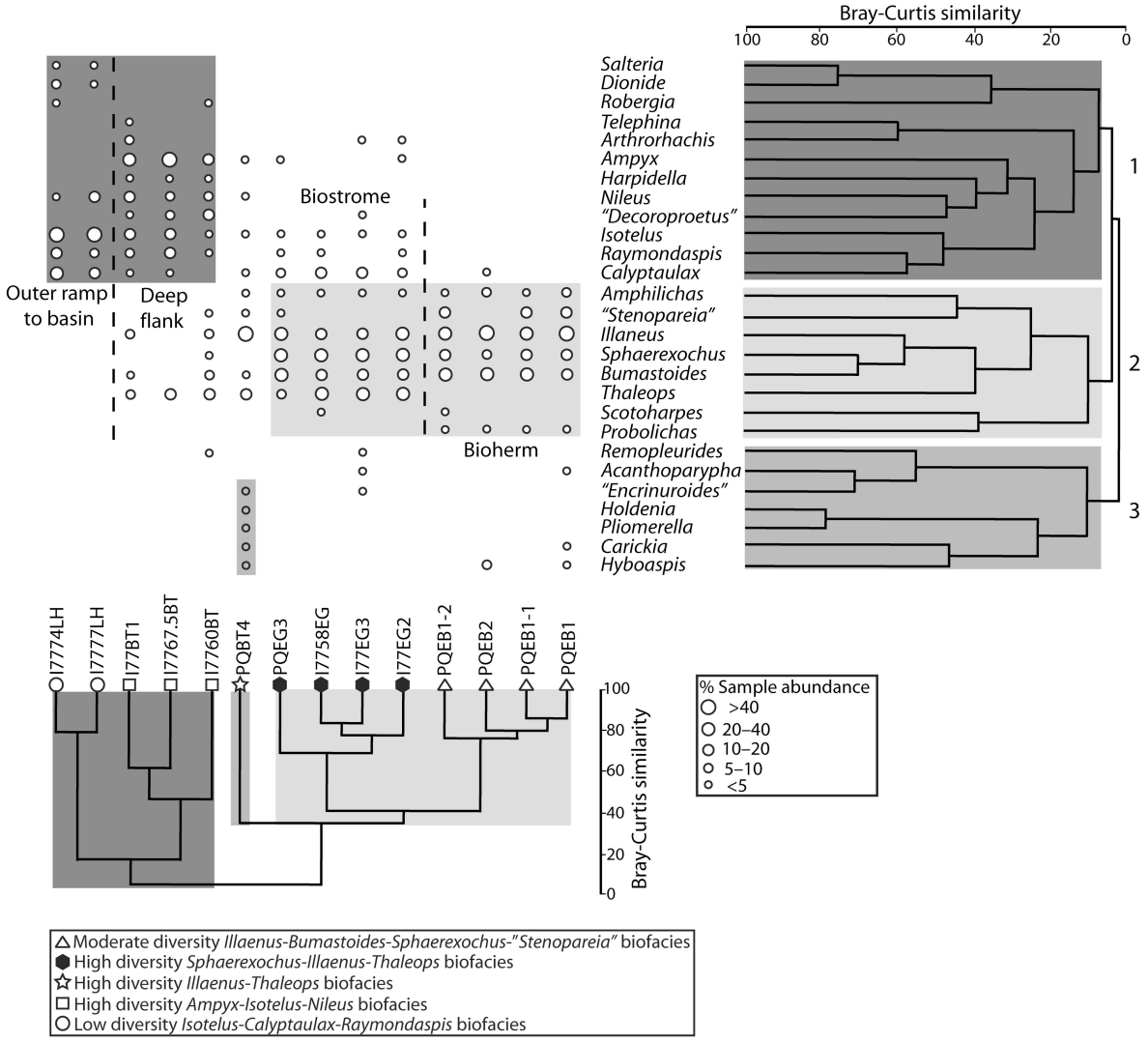
Bray-Curtis similarity
100
80
60
40
20
0
Salteria
Dionide
Robergia
Telephina
Arthrorhachis
Ampyx
Harpidella
Nileus
"Decoroproetus"
Isotelus
Raymondaspis
Calyptaulax
Amphilichas
"Stenopareia"
Illaneus
Sphaerexochus
Bumastoides
Thaleops
Scotoharpes
Probolichas
Remopleurides
Acanthoparypha
"Encrinuroides"
Holdenia
Pliomerella
Carickia
Hyboaspis
1
2
3
Outer ramp to basin
Deep flank
Biostrome
Bioherm
I7774LH
I7777LH
I77BT1
I7767.5BT
I7760BT
PQBT4
PQEG3
I7758EG
I77EG3
I77EG2
PQEB1-2
PQEB2
PQEB1-1
PQEB1
Bray-Curtis similarity
% Sample abundance
>40
20–40
10–20
5–10
<5
Moderate diversity Illaenus-Bumastoides-Sphaerexochus-"Stenopareia" biofacies
High diversity Sphaerexochus-Illaenus-Thaleops biofacies
High diversity Illaenus-Thaleops biofacies
High diversity Ampyx-Isotelus-Nileus biofacies
Low diversity Isotelus-Calyptaulax-Raymondaspis biofacies

FIGURE 6—Q- and R-mode ordination analyses showing trilobite biofacies, paleoenvironment, and buildup locality. A) Q-mode two dimensional (2D), non-metric multidimensional scaling (NMDS) with a stress of 0.082. B) Q-mode detrended correspondence analysis (DCA). C) R-mode 2D NMDS with a stress of 0.28. D) R-mode DCA. Trilobite biofacies (denoted by numbers in R-mode) correspond to approximate centroid position of inclusive genera. Generic names abbreviated to their first four letters (see Appendix 1, Figs. 8–9).

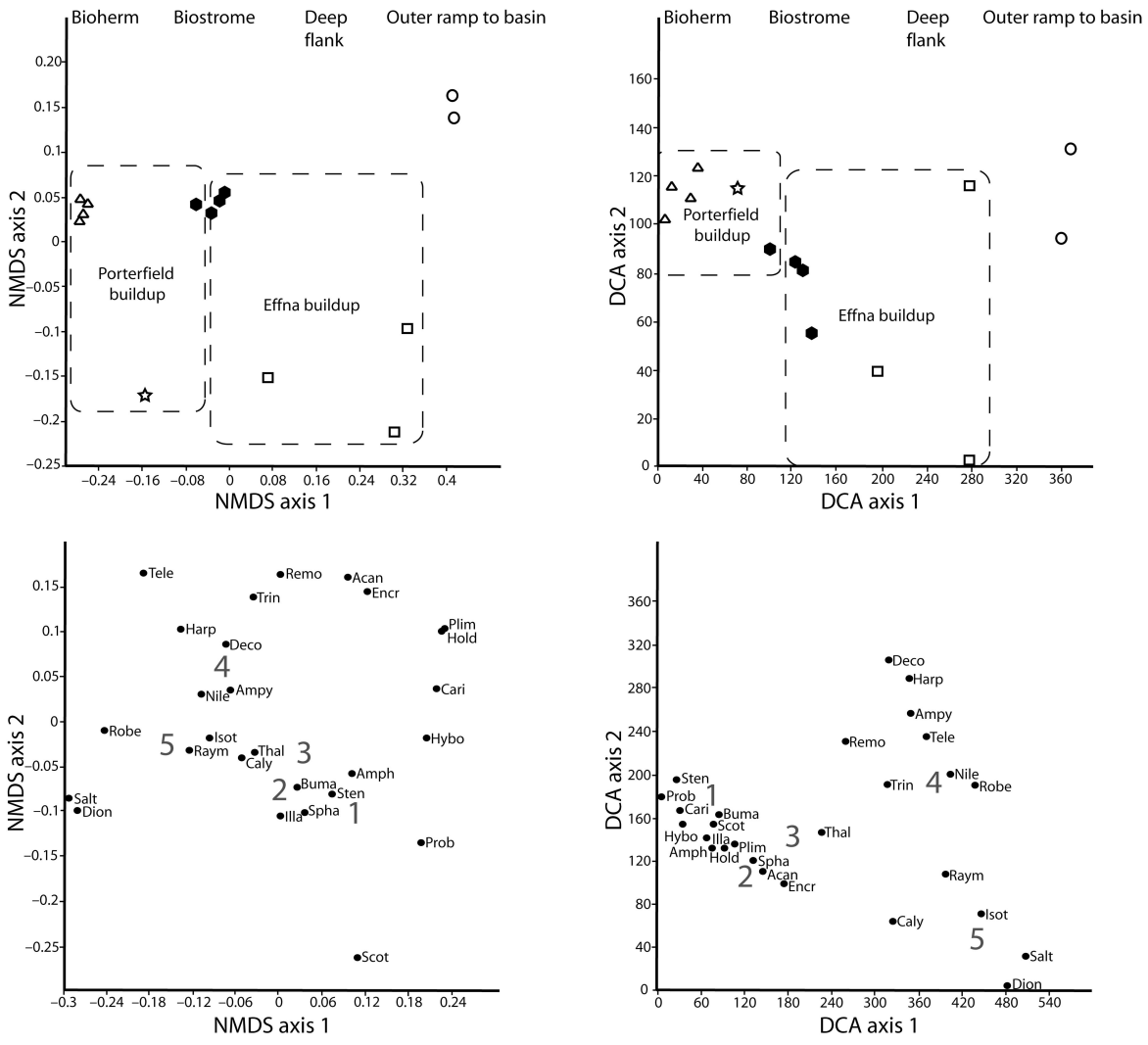

△ Moderate diversity *Illaenus-Bumastoides-Sphaerexochus-"Stenopareia"* biofacies (1)
⬢ High diversity *Sphaerexochus-Illaenus-Thaleops* biofacies (2)
☆ High diversity *Illaenus-Thaleops* biofacies (3)
□ High diversity *Ampyx-Isotelus-Nileus* biofacies (4)
○ Low diversity *Isotelus-Calyptaulax-Raymondaspis* biofacies (5)

FIGURE 7—Rarefaction curves for PQ and I-77 collections, grouped by trilobite biofacies. Three diversity profiles are described here: high diversity for the biostromal and deep flank biofacies, moderate diversity for the bioherm biofacies, and low diversity for the outer slope to basin biofacies. When expected diversity is rarified to 100 individuals, 95% confidence intervals are 8.04 ± 2.08 (biofacies 1), 10.91 ± 2.78 (biofacies 2), 11.73 ± 2.52 (biofacies 3), and 14.18 ± 2.0 (biofacies 4). When rarified to 200 individuals, confidence intervals are 9.39 ± 1.86 (biofacies 1), 13.56 ± 2.46 (biofacies 2), and 15.76 ± 0.92 (biofacies 4). At 300 individuals, confidence intervals are 10.2 ± 1.5 (biofacies 1) and 15.37 ± 1.46 (biofacies 2).

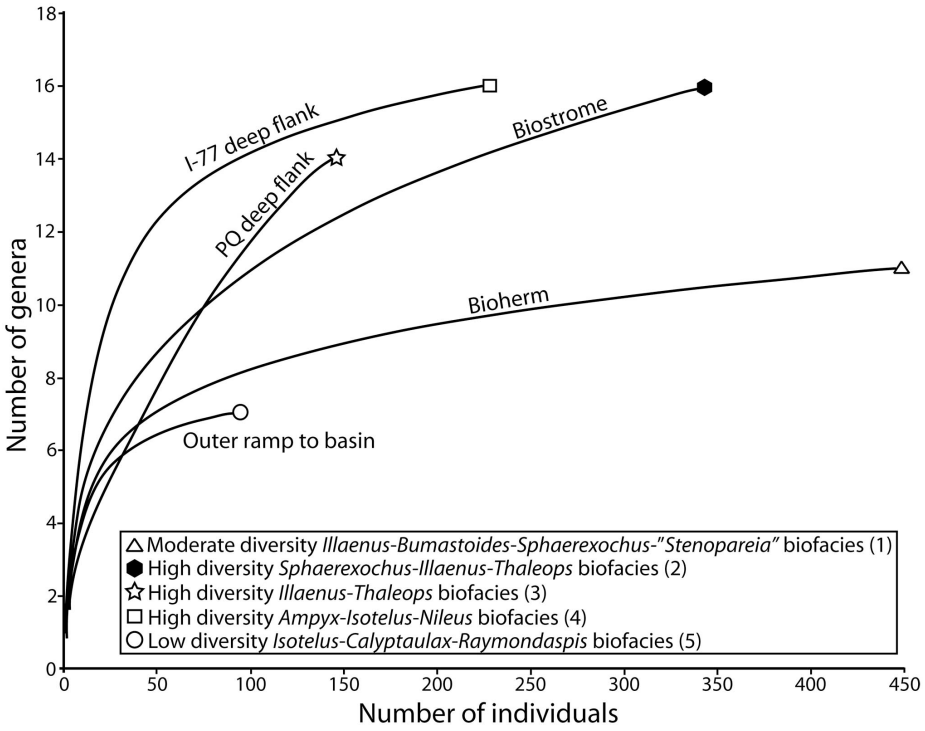
Number of genera
Number of individuals
0
2
4
6
8
10
12
14
16
18
0
50
100
150
200
250
300
350
400
450
I-77 deep flank
PQ deep flank
Biostrome
Bioherm
Outer ramp to basin
Moderate diversity Illaenus-Bumastoides-Sphaerexochus-"Stenopareia" biofacies (1)
High diversity Sphaerexochus-Illaenus-Thaleops biofacies (2)
High diversity Illaenus-Thaleops biofacies (3)
High diversity Ampyx-Isotelus-Nileus biofacies (4)
Low diversity Isotelus-Calyptaulax-Raymondaspis biofacies (5)

FIGURE 8—Trilobites common in the bioherm and biostromal biofacies. All specimens housed at the Sam Noble Oklahoma Museum of Natural History (OU). A, D) *Illaenus* sp., cranidium, OU 13972, x5 and pygidium, OU 13975, x7.9. B) *Scotoharpes* sp., cranidium, OU 13973, x3. C) *Sphaerexochus* sp. 1, cranidium, OU 13974, x6 E) *Acanthoparypha* sp., cranidium, OU 13976, x8. F) *Sphaerexochus* sp. 2, cranidium, OU 13977, x4. G, J) *Thaleops* cf. *T. fieldi* (Raymond, 1925), cranidium, OU 13978, x3.6 and pygidium, x2.7, OU 13981. H) *Probolichas* sp., median glabella, OU 13979, x4. I) *Bumastoides moundensis* (Carlucci et al., 2011), enrolled individual, OU 13980, x4. K, N) *Amphilichas effnensis* (Carlucci et al., 2010) holotype cranidium, OU 12493, x3.5 and pygidium, OU 12492, x2.4. L-M) *"Stenopareia"* (see Taxonomic Notes) sp., pygidium, OU 13982, x1.3 and cranidium, OU 13983, x1.5. Thin scale bars = 5mm, thick scale bars = 2mm.

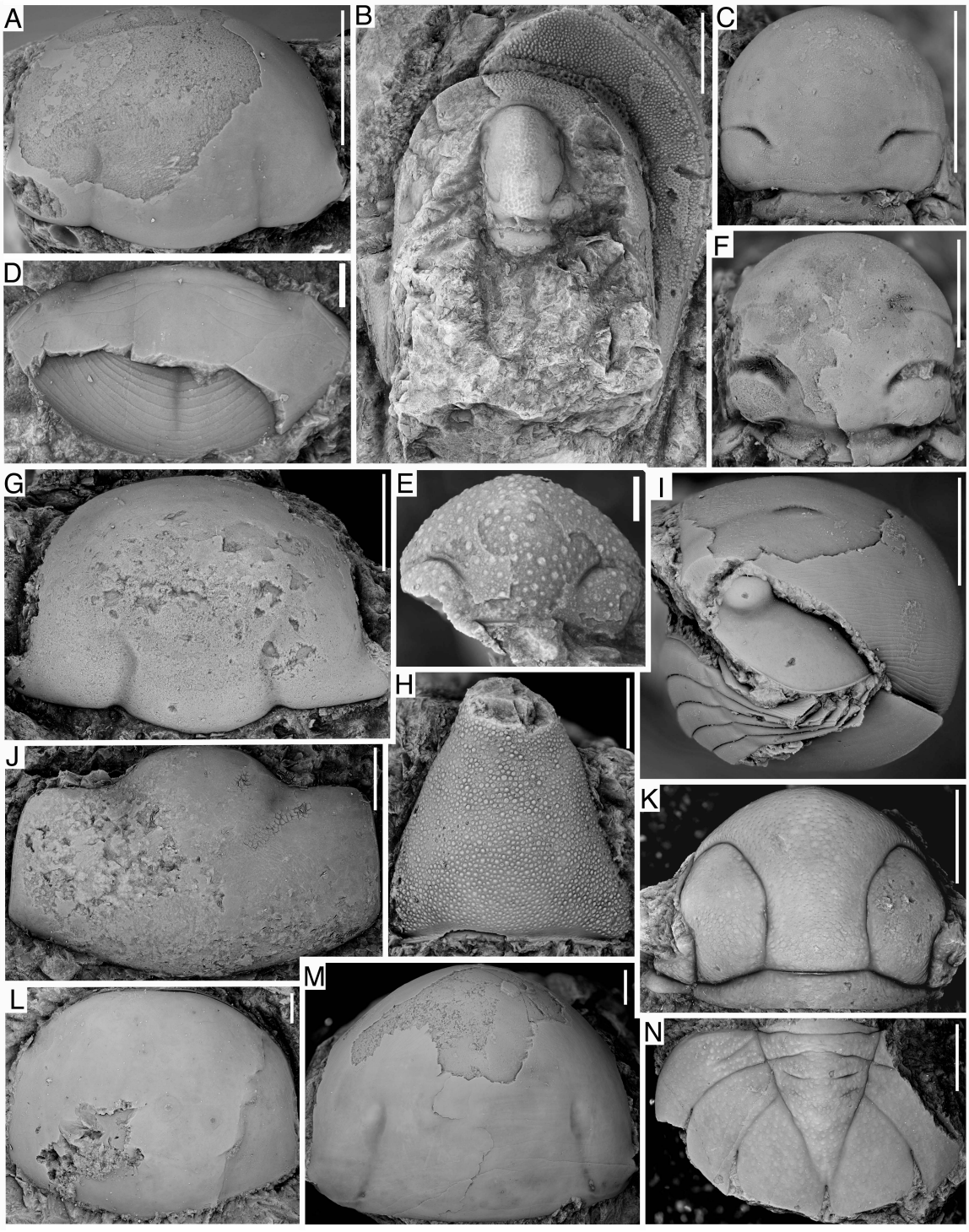
A
B
C
D
F
G
E
I
H
J
K
M
L
N

FIGURE 9—Trilobites common in the deep flank and outer slope–basin biofacies. All specimens housed at the Sam Noble Oklahoma Museum of Natural History (OU). A, D) *Isotelus* cf. *I. giselae* (Tripp and Evitt, 1986), pygidium, OU 13984, x2.4 and cranidium, OU 13971, x2.9. B) *Arthrorhachis* cf. *A. elspethi* (Raymond, 1925), pygidium, OU 13985, x7. C, F) *Nileus* sp., pygidium, OU 13986, x5.1 and cranidium, OU 13969, x2.3. E, I) *Calyptaulax* cf. *C. strasburgensis* (Ulrich and Delo, 1940), pygidium, OU 13970, x5 and cranidium, OU 13967, x5.7. G, K) *Raymondaspis gregaria* (Raymond, 1920), pygidium, OU 13965, x5.1 and cranidium OU 13968, x6.5. H, J) *Ampyx camurus* (Raymond, 1925), cranidium, OU 13966, x5.7 and pygidium, OU13964, x4.2. Thin scale bars = 5mm, thick scale bars = 2mm.

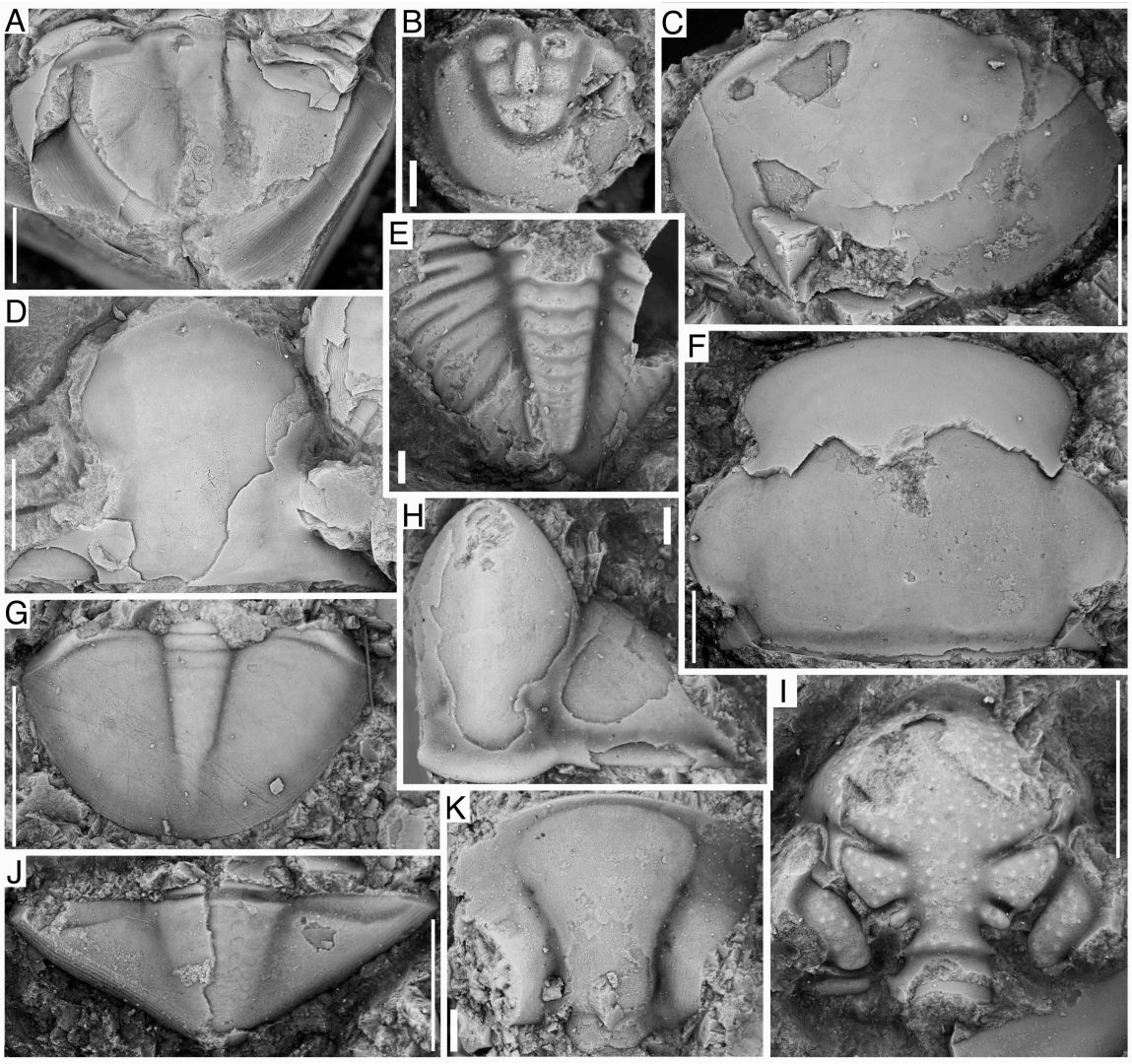
A
B
C
D
E
F
G
H
I
J
K

FIGURE 10—Conceptual diagram of an idealized downslope buildup (see also Read, 1998, fig. 4E) showing biofacies, lithofacies, and environmental interpretations. Trilobite biofacies defined by the cluster analysis (Fig. 5).

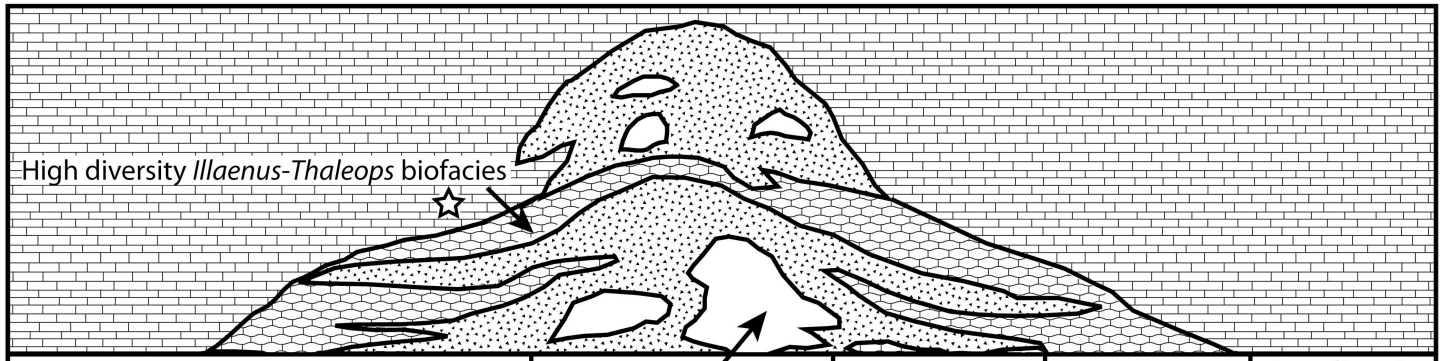

Biofacies	Moderate diversity *Illaenus-Bumastoides-Sphaerexochus-"Stenopareia"* biofacies △	High diversity *Sphaerexochus-Illaenus-Thaleops* biofacies ⬡	High diversity *Ampyx- Isotelus-Nileus* biofacies □	Low diversity *Isotelus-Calyptaulax-Raymondaspis* biofacies ○
Lithofacies	Mudstone, wackestone and boundstone	Pelmatazoan grainstone	Nodular grainstone, packestone and wackestone	Lime mudstone and shale
Environment	Biohermal	Biostromal	Deep flank	Outer ramp to basin

APPENDIX 1—Relative abundance counts for all 14 collections.

	PQEB1	PQEB1-1	PQEB1-2	PQEB2	PQEG3	PQBT4	I7758EG	I77EG2	177EG3	I77BT1	I7760BT	I7767.5BT	I7774LH	I7777LH
Illaneus	78	47	25	25	28	100	10	26	11	11	4	0	0	0
Bumastoides	34	30	22	16	19	2	7	10	6	2	7	0	0	0
“Stenopareia”	22	16	16	0	2	2	0	0	0	0	2	0	0	0
Thaleops	0	0	0	0	9	24	28	21	17	7	9	6	0	0
Sphaerexochus	25	24	9	8	21	0	18	29	13	0	2	0	0	0
Calyptaulax	0	0	0	1	8	2	8	10	7	6	0	1	11	6
Amphilichas	13	5	4	5	2	1	3	2	3	0	0	0	0	0
Hyboaspis	3	0	0	3	0	1	0	0	0	0	0	0	0	0
Carickia	3	0	0	0	0	1	0	0	0	0	0	0	0	0
Probolichas	4	1	3	1	0	0	0	0	0	0	0	0	0	0
“Decoroproetus”	0	0	0	0	0	0	0	0	1	2	9	2	0	0
Raymondaspis	0	0	0	0	3	0	2	1	0	9	2	4	9	4
Scotoharpes	0	0	2	0	0	0	1	0	0	0	0	0	0	0
”Encrinuroides”	0	0	0	0	0	1	0	0	1	0	0	0	0	0
Acanthoparypha	1	0	0	0	0	0	0	0	1	0	0	0	0	0
Pliomerella	0	0	0	0	0	3	0	0	0	0	0	0	0	0
Nileus	0	0	0	0	0	1	0	0	0	17	5	2	1	5
Ampyx	0	0	0	0	1	1	0	3	0	40	9	15	0	0
Arthrorhachis	0	0	0	0	0	0	0	1	1	8	0	0	0	0
Remopleurides	0	0	0	0	0	0	0	0	1	0	1	0	0	0
Telephina	0	0	0	0	0	0	0	0	0	5	0	0	0	0
Harpidella	0	0	0	0	0	0	0	0	0	3	2	1	0	0
Robergia	0	0	0	0	0	0	0	0	0	0	1	0	0	1
Isotelus	0	0	0	0	1	2	1	2	1	24	2	4	24	22
Dionide	0	0	0	0	0	0	0	0	0	0	0	0	3	2
Holdenia	0	0	0	0	0	2	0	0	0	0	0	0	0	0
Salteria	0	0	0	0	0	0	0	0	0	0	0	0	1	2

CHAPTER 6: TRILOBITE BIOFACIES OF THE BROMIDE FORMATION: PALEOECOLOGICAL PATTERNS, COMPARISON WITH THE VIOLA FORMATION AND INTEGRATION WITH SEQUENCE STRATIGRAPHY

Introduction

Paleoecologic studies have shown (e.g., Fortey 1975; Chatterton & Ludvigsen 1976; Amati & Westrop 2006; Carlucci & Westrop 2012) that certain groups of trilobites demonstrate consistent responses to environmental gradients in a variety of stratigraphic and depositional settings. These associations (biofacies) have only recently undergone intense study in the Upper Ordovician, a time period when the Taconic Orogeny (Read 1980) was underway in eastern Laurentia and glacial conditions may have been developing in Gondwana (Pope & Read 1998; Pope 2004; Saltzman & Young 2005). During the Upper Ordovician (Sandbian) in Oklahoma, the Bromide Formation (Ulrich 1911) was deposited in a shallow carbonate ramp that steepened into the Southern Oklahoma Aulacogen (SOA) (Carlucci 2012, chapter 4), a major depozone in the region. The depositional setting was relatively stable during the Sandbian, and three successive 3rd order depositional cycles (Carlucci 2012, chapter 4) record its evolution from a siliciclastic to a primarily carbonate ramp. In contrast to the extirpation of several trilobite associations and reorganization of deep-water cryptolithine biofacies during the development of the Taconic Foreland Basin (Amati & Westrop 2006; Carlucci & Westrop 2012), the diverse trilobite fauna of the Bromide Formation was relatively unaffected by major tectonic processes. Consequently, the trilobite fauna of the Bromide offers an excellent opportunity to quantitatively describe trilobite associations in stable

environments, which can be compared with previous work that differs both temporally (e.g., Amati & Westrop 2006) and geographically (e.g., Fortey 1975; Carlucci & Westrop 2012). Traditional models of trilobite biofacies (e.g., Fortey 1975; Fortey & Barnes 1977) in the Ordovician show that depth-related associations control the distribution and abundance of taxa, e.g., nileids and raphiophorids dominant in the outer-ramp environment. Additional quantitative treatments of Upper Ordovician biofacies are sparse and diversity trends across environments have not been adequately explored. Moreover, the sequence stratigraphy of the Bromide Formation is well documented (Longman 1982; Carlucci 2012, chapter 4) at high-resolution, and provides the opportunity to address issues of condensation bias (Brett 1998; Holland 2000), and diversity patterns within and between systems tracts and depositional sequences. Since the carbonate ramp in the Bromide spans three depositional sequences, each of which exhibits a dominant sedimentology (i.e., siliciclastic, mixed, and carbonate), similar environments can be compared between successive sequences in terms of their diversity and biofacies composition. Integration of sequence stratigraphic and biofacies data has been done on many fossil groups (e.g, Brett 1998; Holland & Patzkowsky 2007), but to our knowledge trilobites have not been analyzed in this way. The predictive framework of sequence stratigraphy allows for replacement of marine communities and tracking patterns of biofacies belts (Brett 1998) to be estimated. In addition, the relative contribution of facies, condensation, and unconformity bias (Holland 2000) in distorting biologic data can be assessed in a sequence-based predictive framework. Testable hypotheses have been suggested or modeled (Holland 1996, 2000; Abbott & Carter 1997), e.g., abrupt abundance changes are present across major flooding surfaces, transgressive systems

tracts (TST) show rapid biofacies change because of condensation, highstand systems tracts (HST) and lowstands (LST) should show more gradual replacement dynamics, and major biofacies change is expected across sequence boundaries. Amati & Westrop (2006) noted the increase in trilobite diversity in shallow subtidal environments across the boundary between the Bromide and Viola Springs Formations; a pattern that differs from the Taconic Foreland Basin (Carlucci & Westrop 2012) in similarly aged strata. Since this study focuses on the Bromide Formation, we can address the diversity and biofacies replacement dynamics across a much greater breath of depositional environments than done by Amati and Westrop (2006).

We have two objectives concerning trilobite paleoecology during the deposition of the Bromide Formation in Oklahoma. First, we analyze the trilobite fauna of the Bromide to see how the distribution of biofacies is affected by environmental gradients (e.g., depth) and sequence architecture. Secondly, we compare diversity and biofacies replacement trends in the Bromide with regions undergoing tectonically influenced bioevents, and within younger strata in the same basin. This will paint a broad picture of trilobite biofacies dynamics in Laurentia during the Mohawkian.

Materials and methods

The dataset for our study includes 19 trilobite collections from five outcrop localities in the Bromide Formation (I35N, 177, DRa, TQ, RC, see Carlucci 2012, chapter 4 for detailed measured sections and locality maps). The collections were taken from a variety of facies that were deposited along a gradient from inner-ramp storm-influenced environments to below storm-wave base outer-ramp settings. See Carlucci (2012, chapter 4) for a summary of each lithofacies, sedimentological properties, and

inferred depositional environments. Vertical variation for most collections ranged from 0-2.35 meters and was always sampled within an identical facies. Where possible, collections were sampled laterally as much as possible along strike. Of the 19 total collections, 12 are from the Mountain Lake Member of the Bromide Formation, and seven are from the Pooleville Member. Similarly, 12 were taken from depositional sequence 2, seven from depositional sequence 3, five from a 3rd order TST, and 14 from a 3rd order HST.

Relative abundance counts were taken from field collections at the generic level because the longer temporal ranges of genera better reveal patterns such as lithofacies tracking (Ludvigsen *et al*. 1986; Carlucci & Westrop 2012), whereas species level data are preferable in biostratigraphic studies. Field samples were broken down to increase surface area, whitened with ammonium chloride, and scanned under binocular microscopes to ensure that small sclerites were readily visible and counted. The final dataset consisted of 1561 trilobite sclerites that were conclusively individuals. The mean sample size per collection was 82.2 (mode of 60), and the individuals represented a total of 23 genera.

We used three quantitative techniques to study the dataset (Q and R mode Non-metric Multidimensional Scaling, NMDS; QxR mode cluster analysis; Rarefaction), which were implemented in PAST v. 2.08 (Hammer *et al*. 2001), and one qualitative tool (time-environment matrices). The dataset (Tables 1 and 2) was subject to a within-sample percent transformation (Jongman et al., 1995) to standardize differences in relative abundance among taxa. A Bray-Curtis metric (Bray & Curtis, 1957) was used to estimate similarity in the NMDS and QxR mode cluster analysis, allowing us to maintain

consistency across the different statistical treatments. Unweighted pair group with arithmetic mean (UPGMA) Q (collections) x R (genera) mode cluster analysis was used as an exploratory method to characterize and define biofacies. NMDS was used to detect paleoecologic gradients among collections (Q) and genera (R), and to visualize differences in taxonomic composition in ordination space. A Q-mode NMDS with a value of 100 shows identical sample composition with no overlap in composition at 0. Under R-mode, a value of 100 means the abundances of two genera are identical, and a value of 0 means the two genera have no samples in common (Carlucci & Westrop 2012). Stress values are used to assess the adequacy of the ordination results and are calculated by measuring the goodness of fit between the non-parametric regression of Euclidean distance against the dissimilarities in a Bray-Curtis matrix (Clarke & Warwick, 1994). Stress values are a measure of how well the ordination preserves the actual sample dissimilarities. Consequently, stress increases with sample size and with the degree of conflict between gradient complexity and the number of specified dimensions (McCune & Grace, 2002). The implementation in PAST runs a sequence of 11 trials with random initial conditions and reports the result with the smallest stress (Hammer *et al*. 2001). Since the number of ordination dimensions is arbitrary in NMDS, we evaluated the stress versus the number of dimensions to see if adding a 3rd dimension substantially lowered the stress value. Finally, rarefaction was used to estimate taxonomic diversity and sampling effort between collections of different sizes. The implementation in PAST follows an algorithm by Krebs (1989) that uses a log gamma function for computing combinatorial terms.

Time-environment analysis (Holland 1997; Brett 1998) is a qualitative method of documenting patterns of origination, extinction and migration on continental or regional scales (Holland 1997), though it can be used to describe biotic events within a single depositional basin. Here, we use systems tracts and depositional sequences as the temporal unit, and biofacies previously defined by cluster analysis as the spatial unit. Time-environment analysis allows the timing of biotic events (e.g., migration) to be considered while accounting for potential sequence stratigraphic biases.

Results

The Q-mode cluster analysis (Fig. 1) shows separate groupings for TST grainstones or packstones (biofacies 4; sequence 2 and 3), outer-ramp limestone-shale rhythmites (biofacies 3; sequence 2), lower Pooleville middle-ramp wackestones (biofacies 2; sequence 3), and outer-ramp mudstone and shale (biofacies 1; sequence 2), with inner to middle-ramp deposits (biofacies 1; sequence 3) from localities in the Criner Hills. The latter cluster indicates that the locality effect is stronger than the environmental one, whereas all of the other biofacies are lithofacies-specific. All of the collections taken from a 3rd order TST (across sequences) are clustered together, which is not surprising considering that they represent bathymetrically similar environments. In addition, the collections from condensed grainstones are less well-preserved than the other collections, and are therefore enriched in large, robust trilobites (e.g., Isotelines, *Failleana*). This suggests that there may also be a taphonomic effect on this cluster. R-mode clusters are difficult to interpret because a very large number of trilobites within the study are either highly cosmopolitan (e.g., *Isotelus*, *Thaleops*, *Calyptaulax*), present only at one locality (e.g., *Pandaspinapyga*, *Hemiarges*, *Ceratocephala*, *Sphaerocoryphe*), or are present

across a wide temporal range (e.g., *Failleana*). We include the R-mode results to easily summarize the abundances within the Q-mode clusters, but do not assign any particular meaning to the clustering patterns.

A 2D solution to the Q-mode NMDS was used (Fig. 2A) because a 3rd dimension only slightly decreased stress values (0.1595 to .1043). The first axis correlates reasonably well with depth (based on the depositional models of Carlucci 2012, chapter 4), with the exception of the Tyson Quarry collections (biofacies 1; BrTQslab1, 2), which are bathymetrically shallower than the limestone-shale rhythmites of biofacies 3 (Fig. 2A). The second axis correlates with temporal position (e.g., stratigraphy). There is a clear break between collections taken from the Pooleville (sequence 3) and Mountain Lake members (sequence 2), as modified by Carlucci (2012, chapter 4). In ordination space, Bromide collections are also well-grouped by biofacies and inferred sedimentary environment, and by 3rd order systems tract. A 2D R-mode NMDS ordination (Fig. 2B) has a fairly high stress value (0.2498), which suggests moderate levels of disagreement between the rank order similarity and Euclidean distance in ordination space. A temporal or depth gradient is not obvious in the data; however, there is a trend for more cosmopolitan taxa (e.g., *Thaleops*, *Isotelus*, *Calyptaulax*) to lie near multiple biofacies centroids. Taxa that are highly constrained by lithofacies (e.g., *Ceratocephala*) obviously group near their biofacies centroids.

Rarefaction curves were made for all four biofacies (Fig. 3) to allow for comparison of diversity estimates and sampling effort. When rarified to 159 individuals (the highest possible sample size that includes all four biofacies), biofacies 1 preserves 11.15 ± 2.64 genera, biofacies 2 preserves 9.0 ± 0, biofacies 3 preserves 9.0 ± 2.60, and

biofacies 4 preserves 6.39 ± 1.32. When rarified to 200 individuals, there are two statistically significant (95% confidence intervals) diversity profiles; high diversity (biofacies 1 and 3) and low diversity (biofacies 4). When rarified to 363 individuals, biofacies 1 and 3 have statistically significant differences in generic diversity. At both low and high sampling effort, the inner to middle ramp wackestones of the Criner Hills are the most diverse, and the condensed packstones and grainstones of TST's at I-35N retain the lowest diversity. Multiple evenness metrics (e.g., 1-Simpson index of dominance, Simpson 1949; Pielou's equitability index (J); Hammer & Harper 2006) yielded relative similar values that were not statistically different (boostrapped 95% confidence intervals).

Trilobite biofacies of the Bromide

Biofacies 1: High Diversity *Lonchodomas-Frencrinuroides*

The high diversity *Lonchodomas-Frencrinuroides* biofacies consists of two separate facies in the Criner Hills localities of the Bromide Formation (TQ, RC). The first is a thin-bedded lime mudstone and shale that we interpret as an outer-ramp deposit. This grades relatively abruptly in a shallowing upward succession of more nodular and storm-influened wackestones, packstones and shales, that shows the highest diversity facies of the Bromide. *Lonchodomas* consists of 57.6% of the relative abundance, *Frencrinuroides* 16%, *Isotelus* 9.6%, *Calyptaulax* 5.2%, *Dolichoharpes* 3.8% and *Ceraurus* 2.2%. Other elements in biofacies 1 combined constitute less than 10% of the fauna.

Biofacies 2: *Thaleops-Calyptaulax*

Biofacies 2 is associated with a middle-ramp wackestone with rudstone pavements in the Pooleville that has some elements in common with biofacies 1 (e.g.,

Holia, and the same species of *Dolichoharpes*, *Calyptaulax*, and *Thaleops*). *Thaleops* constitutes 49.1% of the biofacies 2 relative abundance; *Calyptaulax* 27.0%, *Bumastoides* and *Isotelus* 6.9%, and *Dolichoharpes* 5.7%. Other elements constitute less than 5% of the fauna.

Biofacies 3: *Isotelus-Thaleops-Failleana-Remopleurides*

Biofacies 3 is an association of cosmopolitan and deep-water trilobites with the outer-ramp limestone-shale rhythmites, which is the deepest facies of the Bromide in sequence 2 outside of the Criner Hills region. *Isotelus* is particularly abundant in this facies as it comprises 69.5% of relative abundance (see Carlucci & Westrop 2012 for another example of *Isotelus*-dominance in outer-ramp settings in the Mohawkian). *Thaleops* comprises 9.8% of relative abundance, *Failleana* 6.9%, *Remopleurides* 6.6%, and *Calyptaulax* 3.2%. All other elements constitute less than 5% of generic abundance.

Biofacies 4: Low Diversity *Anataphrus-Failleana*

The low diversity *Anataphrus-Failleana* biofacies is associated with interbedded grainstones and shales in the lower Mountain Lake, and a similar (but less shaly) interval in the lower Pooleville. Both facies were deposited during a 3rd order transgression, and show extensive signs of condensation and sediment starvation relative to Highstand deposits. *Anataphrus* represents 76% of relative abundance, *Failleana* 13.3%, *Thaleops* and *Isotelus* 4.2%. Other elements make up less than 3% of the generic abundance. The presence of almost exclusively large, robust, and convex trilobites, and general poor preservation of these facies, leads us to believe that there is likely some taphonomic bias in this biofacies. Hence, biofacies 4 may be best characterized as a "taphofacies"; though it is possible the original biologic distribution did not include smaller trilobites.

Comparison with paleoecological patterns of the Viola Formation and Taconic foreland basin

Our results here indicate that in addition to depth and depositional environment, temporal information (depositional sequence) and locality also strongly influence the similarity of biofacies composition in the Bromide Formation. There are also statistically significant differences between biofacies diversity in TST and HST deposits, though it is likely taphonomic in nature. Furthermore, collections taken from within one 3rd order TST (Fig. 2A, upper right quadrant) do not show more rapid vertical shifts in biofacies composition as compared to HST samples, as would be expected during a highly condensed interval. However, the generally poor preservation of TST packstones and grainstones may have obscured the signal. As would be expected based on predictions (Holland 2000), there is evidence of a shift in biofacies composition across sequence boundaries (Fig. 2A).

Carlucci & Westrop (2012) quantitatively described trilobite biofacies in a coeval series of environments (Fig. 4) within the Taconic foreland basin (Read 1980) during the early Mohawkian. Some of the sedimentary environments are not present in both regions (e.g., bioherms), but they can be compared to bathymetrically similar deposits (e.g., middle-ramp). Rarified to 100 individuals, there are no statistically significant compositional differences between middle-ramp wackestones (biofacies 2) in the Bromide and in the Effna Limestone of Virginia. Similarly, diverse middle-ramp wackestones of the Criner Hills of Oklahoma (biofacies 1) are not significantly different from biostromal middle-ramp deposits of Virginia when rarified to 300 individuals. Deep flank (outer-ramp) deposits of the Botetourt Member of the Edinburg Formation

(Carlucci & Westrop 2012, fig. 7) are significantly more diverse than outer-ramp rhythmites of the Bromide Formation when rarified to over 200 individuals. While they are dominated by a very similar fauna (raphiophorids, isotelines) characteristic of outer-ramp environments, there are a considerable number of faunal elements in the foreland basin that are not found in Oklahoma. Trilobites that traditionally dominate abundance in bioherms (illaenids and chierurids) are not found in the Bromide Formation, even in deposits considered by Longman (1982) to be buildup-derived. Carlucci & Westrop (2012) noted that the illaenid-chierurid association was extirpated from the Taconic foreland basin near the onset of environmental change, and that outer-ramp environments in OK and VA were populated by similar faunas. At the M4-M5 sequence boundary, these similarities diverge, and low diversity cryptolithine biofacies spread across the foreland basin (Amati & Westrop 2006). In contrast, comparison of biofacies of the Bromide Formation to the Viola Springs Formation across the same coeval sequence boundary indicates that diversity increases in similar environments. Generic diversity of the inner-ramp *Bumastoides* and middle-ramp *Thaleops* biofacies of Amati & Westrop (2006, fig. 8) is significantly (non-overlapping 95% confidence intervals) higher when compared to the inner- and middle-ramp Bromide biofacies. This difference is evident at a variety of sampling efforts. This difference is not present on rarified outer-slope biofacies data; however, the presence of abundant graptolites and internal lamination in the Viola deep-water facies suggests it was deposited at much greater depth than the Bromide.

References

ABBOTT, S.T., and CARTER, R.M., 1997, Macrofossil associations from Mid-Pleistocene cyclothems, Castlecliff Section, New Zealand: implications for sequence stratigraphy:

PALAIOS, v. 12, p. 188-210.

AMATI, L., and WESTROP, S.R., 2006, Sedimentary facies and trilobite biofacies along an Ordovician shelf to basin gradient, Viola Group, South-Central Oklahoma: PALAIOS, v. 21, p. 516-529.

BRAY, J.R., and CURTIS, J.T., 1957, An ordination of upland forest communities of southern Wisconsin: Ecological Monographs, v. 27.

BRETT, C.E., 1998, Sequence stratigraphy, paleoecology, and evolution: biotic clues and responses to sea-level fluctuations: PALAIOS, v. 13, p. 241-262.

CARLUCCI, J.R., 2012, Trilobite Biofacies, Systematics and Faunal Turnover in a Sequence Stratigraphic Framework duing the Upper Ordovician of Oklahoma and Virginia: Ph.D, University of Oklahoma, Norman OK.

CARLUCCI, J.R., and WESTROP, S.R., 2012, Trilobite biofacies along an Ordovician (Sandbian) carbonate buildup to basin gradient, southwestern Virginia: PALAIOS, v. 27, p. 19-34.

CHATTERTON, B.D.E., and LUDVIGSEN, R., 1976, Silicified middle Ordovician trilobites from the south Nahanni river area, District of Mackenzie, Canada: Palaeontographica, v. 154, p. 1-106.

CLARKE, K.R., and WARWICK, R.M., 1994, Changes in Marine Communities: an Approach to Statistical Analysis and Interpretation.: Plymouth Marine Laboratory, 144 p.

FORTEY, R.A., 1975, Early Ordovician trilobite communities: Fossils and Strata, v. 4, p. 331-352.

FORTEY, R.A., and BARNES, C.R., 1977, Early Ordovician conodont and trilobite communities of Spitsbergen: influence on biogeography: Alcheringa, v. 1, p. 297-309.

HAMMER, O., HARPER, D., and RYAN, P., 2001, PAST: Paleontological statistics software for education and data analysis: Palaeontologia Electronica, v. 4.

HAMMER, O., and HARPER, D., 2006, Paleontological Data Analysis: Blackwell Publishing, 351 p.

HOLLAND, S., and PATZKOWSKY, M., 1996, Sequence stratigraphy and long-term

paleooceanographic changes in the Middle and Upper Ordovician of the eastern United States, *in* Witzke, B., Ludvigson, G., and Day, J., eds., Paleozoic Sequence Stratigraphy: Views from the North American Craton, GSA Special Paper 306: Geological Society of America, Boulder CO.

HOLLAND, S.M., 1997, Using time-environment analysis to recognize faunal events in the Upper Ordovician of the Cincinnati Arch, *in* Brett, C.E., and Baird, G.C., eds., Paleontological Events: Stratigraphic, Ecological and Evolutionary Implications: Columbia University Press, New York, p. 309-344.

HOLLAND, S.M., 2000, The quality of the fossil record-a sequence stratigraphic perspective, *in* Erwin, D.H., and Wing, S.L., eds., Deep Time: Paleobiologies Perspective: Paleontological Society, Lawrence, KS.

HOLLAND, S., and PATZKOWSKY, M., 2007, Gradient ecology of a biotic invasion: biofacies of the type Cincinnatian series (Upper Ordovician), Cincinnati, Ohio Region, USA.: PALAIOS, v. 22, p. 392-407.

JONGMAN, R.H.G., BRAAK, C.J.F.T., and TONGEREN, O.F.R.V., 1995, Data Analysis in Community and Landscape Ecology: Cambridge University Press, 324 p.

KREBS, C.J., 1989, Ecological Methodology: Harper and Row Publishers, New York, 654 p.

LONGMAN, M.W., 1982, Depositional environments, *in* Sprinkle, J., ed., Echinoderm Faunas from the Bromide Formation (Middle Ordovician) of Oklahoma: University of Kansas Paleontological Contributions, Monograph, p. 17-29.

LUDVIGSEN, R., WESTROP, S., PRATT, B., TUFFNELL, P., and YOUNG, G., 1986, Dual biostratigraphy: Zones and biofacies: Geoscience Canada, v. 13, p. 139-154.

MCGUNE, B., and GRACE, J.B., 2002, Analysis of Ecological Communities: MjM Software Design, Gleden Beach Oregon, 300 p.

POPE, M.C., and READ, J.F., 1998, Ordovician meter-scale cycles; implications for climate and eustatic fluctuations in the Central Appalachians during a global greenhouse, non-glacial to glacial transition: Palaeogeography, Palaeoclimatology, Palaeoecology, v. 138, p. 27-42.

POPE, M.C., 2004, Cherty facies of the Montoya Group, southern New Mexico and western Texas and its regional correlatives: a record of Late Ordovician paleoceanography on

southern Laurentia: Palaeogeography, Palaeoclimatology, Palaeoecology, v. 210, p. 367-384.

SALTZMAN, M.R., and YOUNG, S.A., 2005, Long-lived glaciation in the Late Ordovician? Isotopic and sequence stratigraphic evidence from western Laurentia: Geology, v. 33, p. 109-112.

SIMPSON, E.H., 1949, Measurement of diversity: Nature, v. 163, p. 688-688.

Table 1. Relative abundance counts for 9 of 19 collections taken from the Bromide Formation.

	BrTQslab	BrRCL 51.3	BrI35N17	Br17722.7-23.3	BRI35N36.6	BrDra unlabeled	BrI35N4.5-6.85	BrI35N7.8-8.25	BrI35N7.5
Amphilichas	5	0	2	0	0	0	0	0	0
Bumastoides	0	0	0	5	0	0	0	0	0
Calyptaulax	27	0	0	8	0	5	0	0	0
Ceraurinella	0	0	1	1	0	2	1	0	0
Ceraurus	4	0	0	0	0	0	0	0	0
Dolichoharpes	19	0	0	0	0	0	0	0	0
Harpidella	8	0	0	0	0	0	0	0	0
Holia	0	0	0	1	0	0	0	0	0
Isotelus	20	30	38	5	0	70	3	3	5
Thaleops	7	0	20	21	9	3	2	0	0
Sphaerocoryphe	2	0	0	0	0	0	0	0	0
Remopleurides	0	1	17	0	0	0	0	0	0
Lonchodomas	43	253	0	0	0	0	0	0	0
Failleana	0	0	12	0	29	0	1	0	0
Frencrinuroides	73	1	0	0	0	0	0	0	0
Ceratocephala	1	0	0	0	0	0	0	0	0
Cybeloides	0	0	0	0	0	0	1	0	2
Mesotaphraspis	0	0	0	0	0	0	2	0	0
Pandaspinapyga	2	0	0	0	0	0	0	0	0
Anataphrus	0	0	2	0	30	0	29	57	55
Hemiarges	0	0	0	0	0	0	0	0	0
Illaenus	0	0	0	0	0	0	0	0	0
"Decoroproetus"	0	0	0	0	0	0	0	0	0

Table 2. Relative abundance counts for 10 of 19 collections taken from the Bromide Formation.

BrI35N18-20	BrI35N1-3	BrI35N47-48	BrTQslab2	BrI35N46.5-47	Br17724-25.5	BrRCL49.2-50.6	BrDRa33-34	BrRCS20.2	BrDRa35-36.2
0	0	0	2	1	0	0	0	0	0
0	0	1	1	1	4	0	0	0	2
0	0	14	13	19	2	0	4	0	3
1	0	1	0	0	1	0	1	0	0
0	0	0	13	0	0	0	0	0	0
0	0	4	10	5	0	0	0	0	0
0	0	0	0	0	0	0	0	0	0
0	0	0	1	0	0	0	0	0	0
20	0	1	6	2	3	17	75	31	28
3	0	19	5	7	31	0	5	3	3
0	0	0	3	0	0	0	0	0	0
7	0	0	0	0	0	0	0	1	0
0	0	0	25	0	0	118	0	0	0
14	5	0	0	0	0	0	0	0	0
1	0	0	48	0	0	0	0	0	0
0	0	0	1	0	0	0	0	0	0
0	0	0	0	0	0	0	0	0	0
0	0	0	0	0	0	0	0	0	0
0	0	0	1	0	0	0	0	0	0
2	29	0	0	0	0	0	0	0	0
0	0	0	2	0	0	0	0	0	0
0	0	0	0	0	2	0	0	0	0
0	0	0	0	0	0	0	0	1	0

Fig. 1. Results of Q- and R-mode cluster analysis of 19 collections from the Bromide Formation. Data were transformed into percentage within sample prior to analysis. Shapes at terminal branches represent the biofacies that best characterizes that collection.

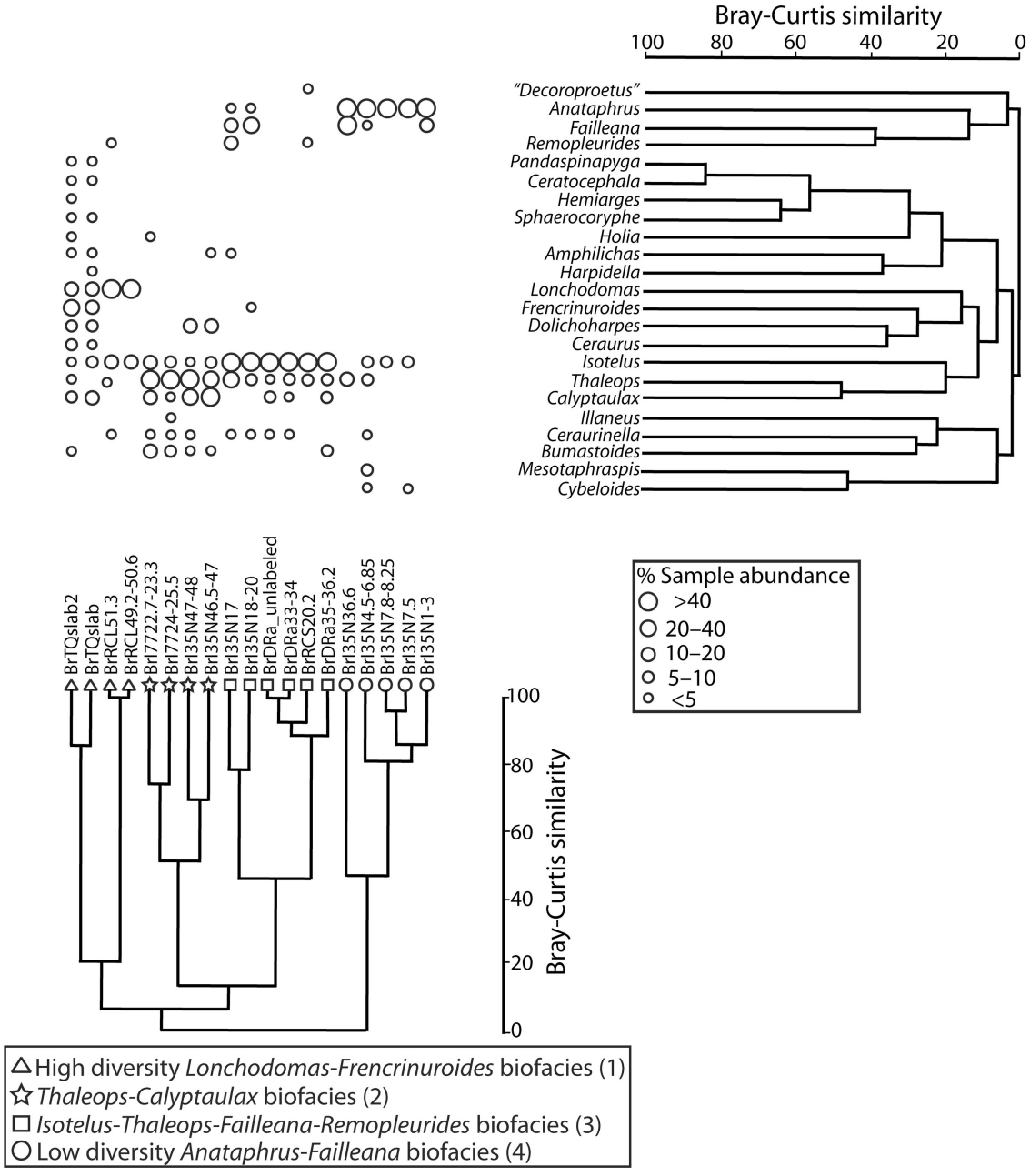
Bray-Curtis similarity
100
80
60
40
20
0
"Decoroproetus"
Anataphrus
Failleana
Remopleurides
Pandaspinapyga
Ceratocephala
Hemiarges
Sphaerocoryphe
Holia
Amphilichas
Harpidella
Lonchodomas
Frencrinuroides
Dolichoharpes
Ceraurus
Isotelus
Thaleops
Calyptaulax
Illaneus
Ceraurinella
Bumastoides
Mesotaphraspis
Cybeloides
% Sample abundance
>40
20–40
10–20
5–10
<5
BrTQslab2
BrTQslab
BrRCL51.3
BrRCL49.2-50.6
BrI7722.7-23.3
BrI7724-25.5
BrI35N47-48
BrI35N46.5-47
BrI35N17
BrI35N18-20
BrDRa_unlabeled
BrDRa33-34
BrRCS20.2
BrDRa35-36.2
BrI35N36.6
BrI35N4.5-6.85
BrI35N7.8-8.25
BrI35N7.5
BrI35N1-3
100
80
60
40
20
0
Bray-Curtis similarity
△High diversity *Lonchodomas-Frencrinuroides* biofacies (1)
☆ *Thaleops-Calyptaulax* biofacies (2)
□ *Isotelus-Thaleops-Failleana-Remopleurides* biofacies (3)
○ Low diversity *Anataphrus-Failleana* biofacies (4)

Fig. 2. Q and R-mode NMDS ordinations showing trilobite biofacies, inferred bathymetric position, depositional sequence, and systems tract of each collection. A, Q-mode 2D NMDS with a stress of 0.1595. B, R-mode 2D NMDS with a stress of 0.2498, numbers denote approximate biofacies centroid position of inclusive genera.

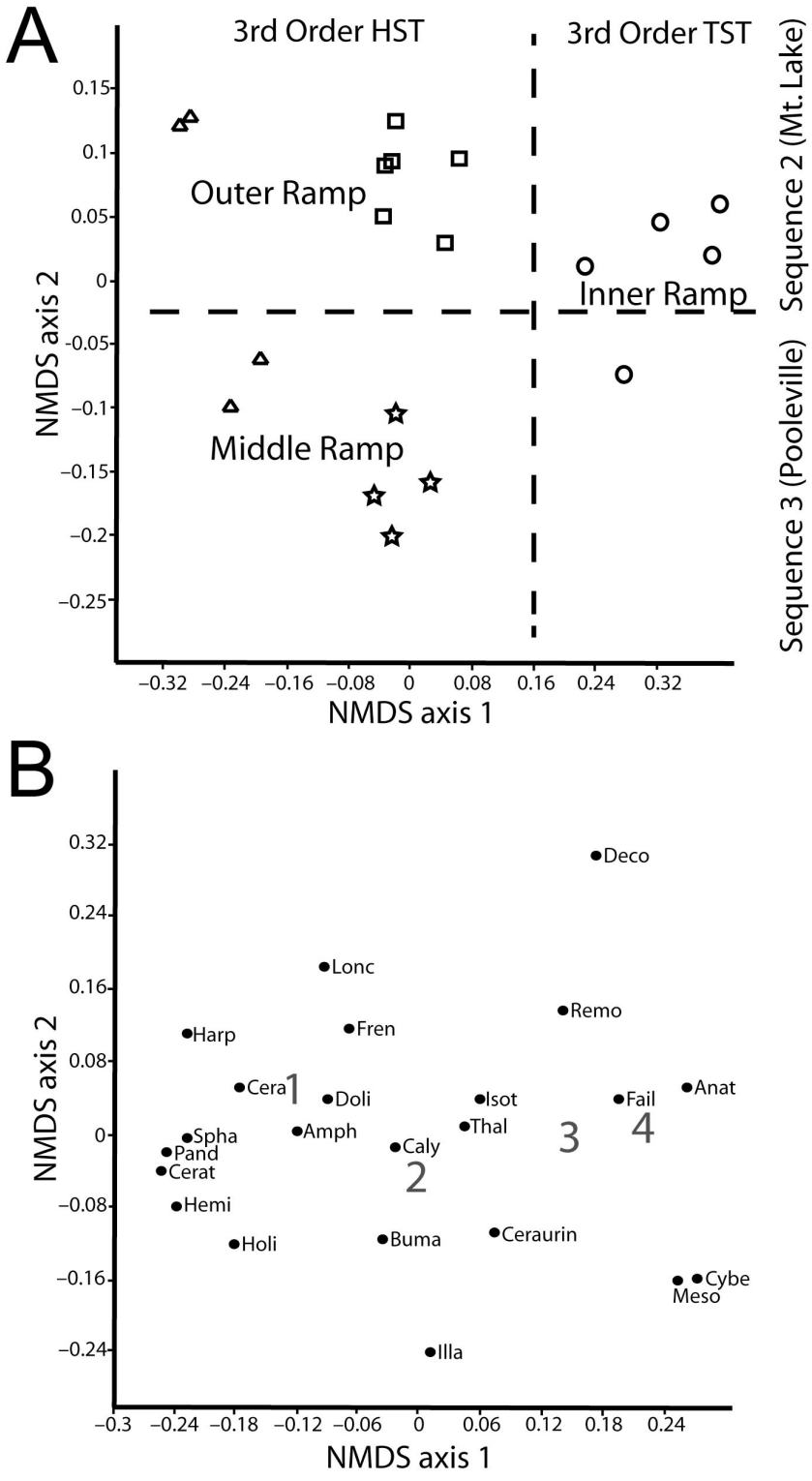

△ High diversity *Lonchodomas-Frencrinuroides* biofacies (1)
☆ *Thaleops-Calyptaulax* biofacies (2)
□ *Isotelus-Thaleops-Failleana-Remopleurides* biofacies (3)
○ Low diversity *Anataphrus-Failleana* biofacies (4)

Fig. 3. Rarefaction curves for all Bromide trilobite collections, grouped by trilobite biofacies. See text for 95% confidence intervals at select sampling efforts.

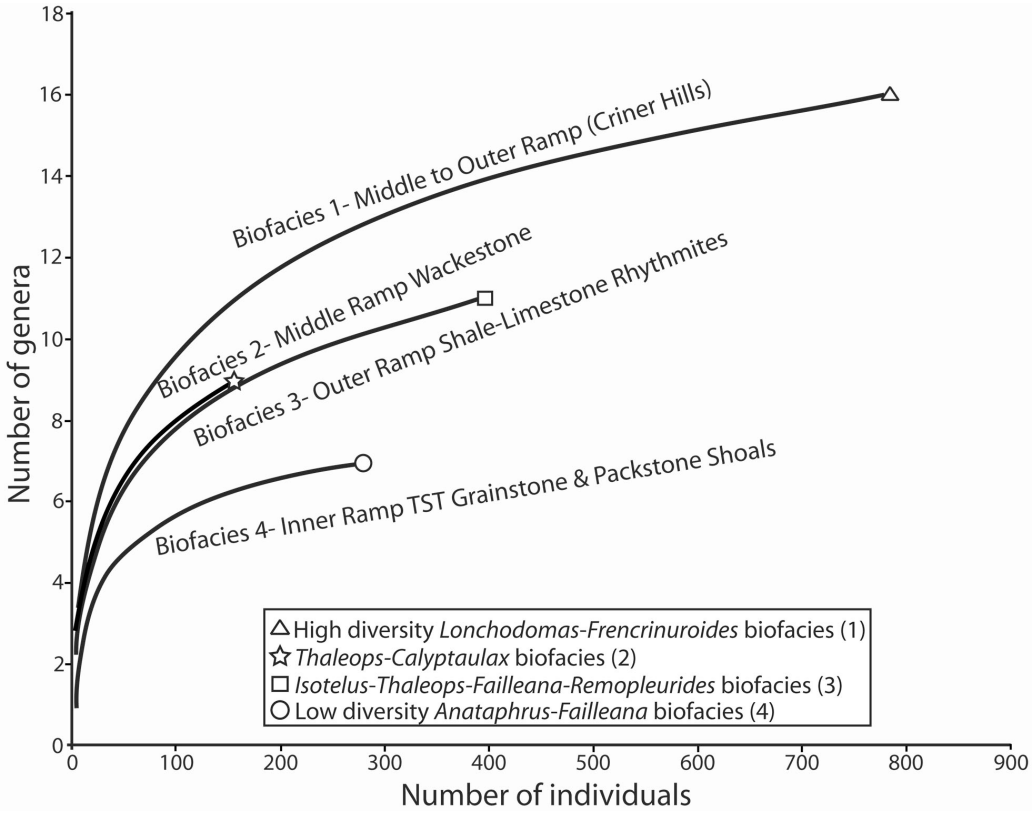
Number of genera
Number of individuals
0
2
4
6
8
10
12
14
16
18
0
100
200
300
400
500
600
700
800
900
Biofacies 1- Middle to Outer Ramp (Criner Hills)
Biofacies 2- Middle Ramp Wackestone
Biofacies 3- Outer Ramp Shale-Limestone Rhythmites
Biofacies 4- Inner Ramp TST Grainstone & Packstone Shoals
High diversity *Lonchodomas-Frencrinuroides* biofacies (1)
Thaleops-Calyptaulax biofacies (2)
Isotelus-Thaleops-Failleana-Remopleurides biofacies (3)
Low diversity *Anataphrus-Failleana* biofacies (4)

Fig. 4. Time environment matrix summarizing the relationships between trilobite biofacies, inferred depositional environment, and depositional sequence during the early to late Mohawkian in Oklahoma and Virginia. Dotted lines denote uncertain boundaries. Virginia depositional sequences from Holland & Patkowsky (1996). The peritidal biofacies in Oklahoma was not part of the analysis here, but follows Ludvigsen (1983).

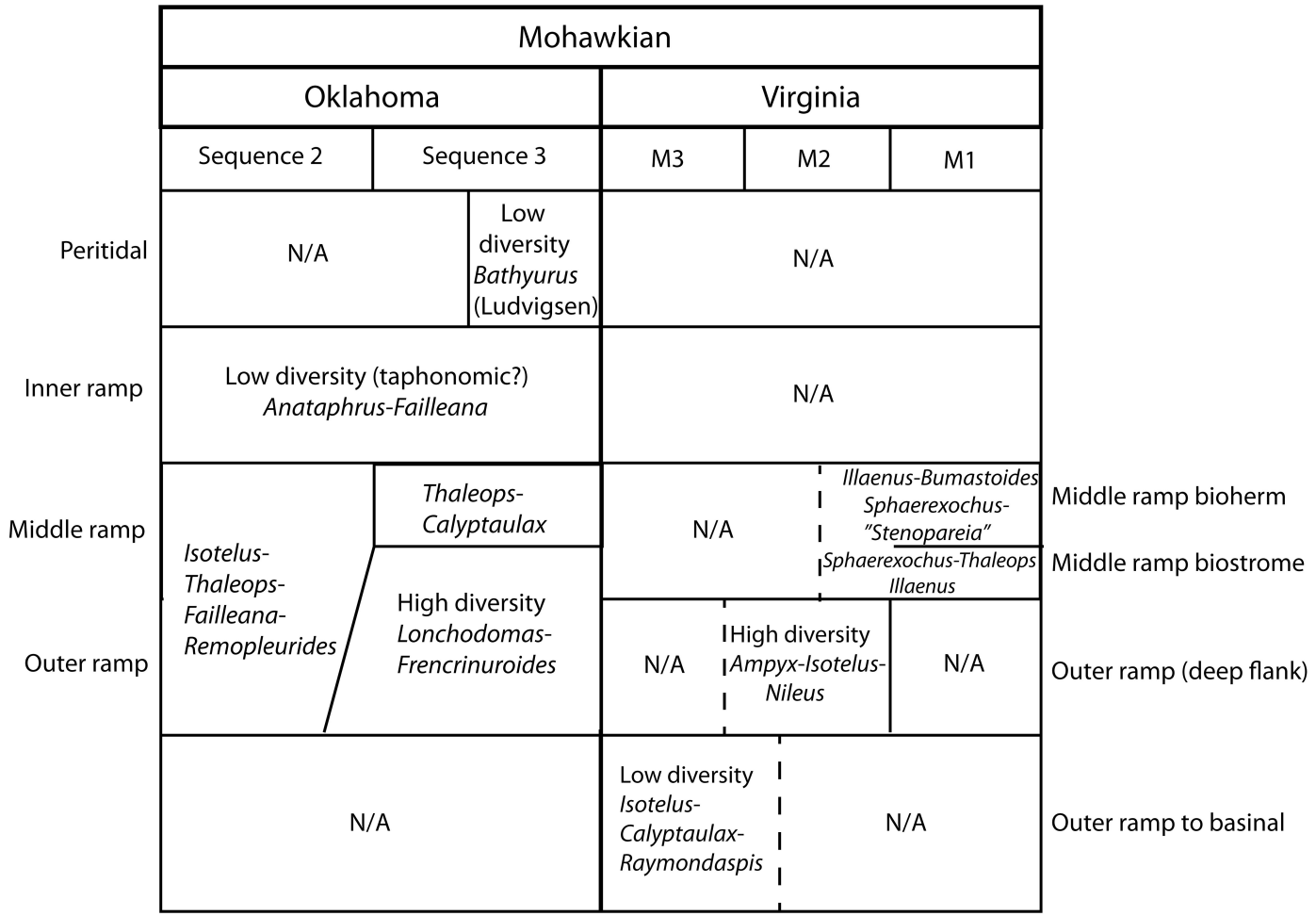
Mohawkian
Oklahoma
Virginia
Sequence 2
Sequence 3
M3
M2
M1
Peritidal
N/A
Low diversity *Bathyurus* (Ludvigsen)
N/A
Inner ramp
Low diversity (taphonomic?) *Anataphrus-Failleana*
N/A
Middle ramp
Thaleops-Calyptaulax
N/A
Illaenus-Bumastoides Sphaerexochus-"Stenopareia"
Middle ramp bioherm
Sphaerexochus-Thaleops Illaenus
Middle ramp biostrome
Isotelus-Thaleops-Failleana-Remopleurides
High diversity *Lonchodomas-Frencrinuroides*
Outer ramp
N/A
High diversity *Ampyx-Isotelus-Nileus*
N/A
Outer ramp (deep flank)
N/A
Low diversity *Isotelus-Calyptaulax-Raymondaspis*
N/A
Outer ramp to basinal

APPENDIX 1: ANNOTATED MEASURED SECTIONS

Appendix 1 is a catalog of all the sections I measured for my dissertation, including those that are figured at broader views in other chapters. In some instances (e.g., Tumbling Run, Strasburg Junction) the measured sections were not used in any chapter, but contributed towards the larger NSF EAR0819715 project. All sections are figured at a scale of 1 cm = 1 m, and are shown with younger strata to the left.

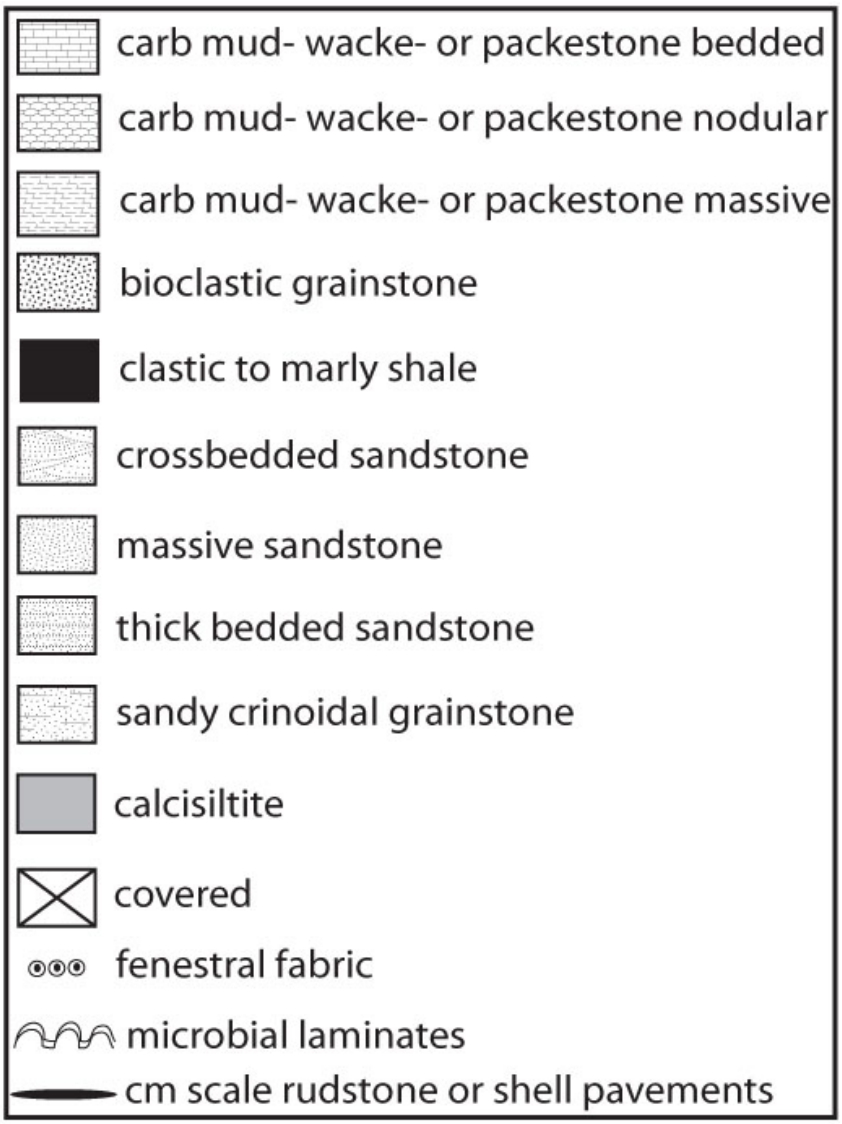

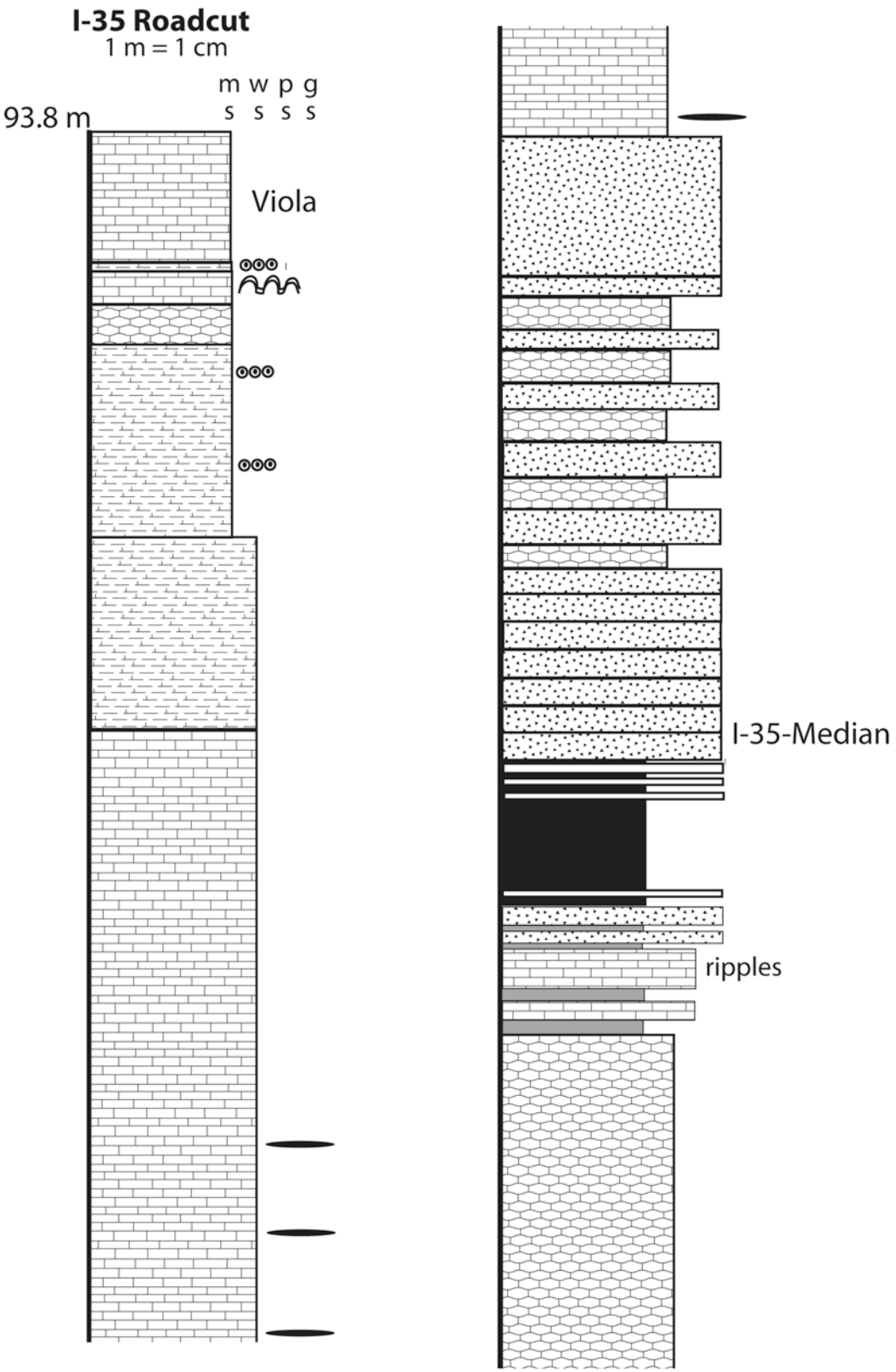
I-35 Roadcut
1 m = 1 cm
m w p g
s s s s
93.8 m
Viola
I-35-Median
ripples

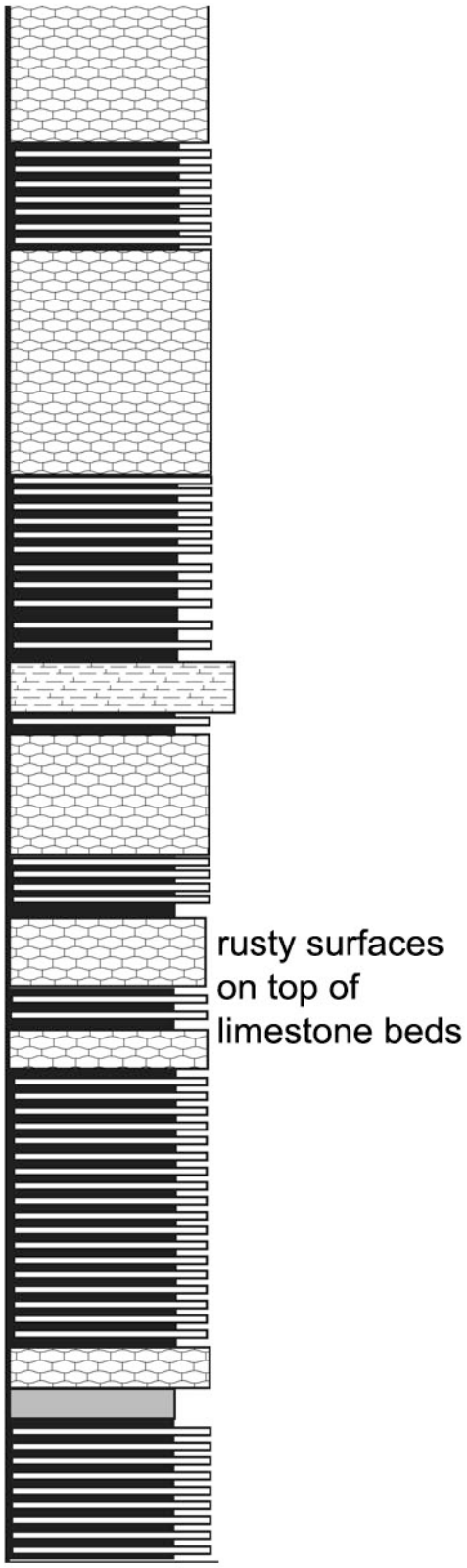
rusty surfaces
on top of
limestone beds


-I-35N
ravinement
fenestral, ostracods
x-bedding, ripples
very sharp
facies offset

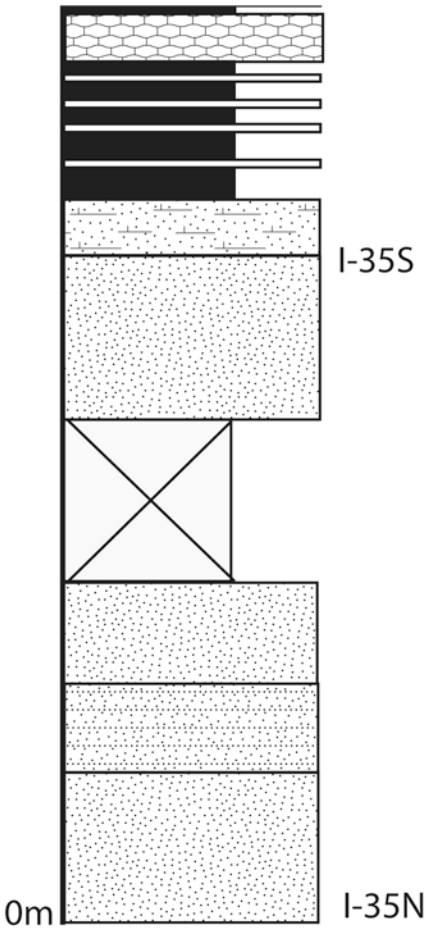
I-35S
0m
I-35N

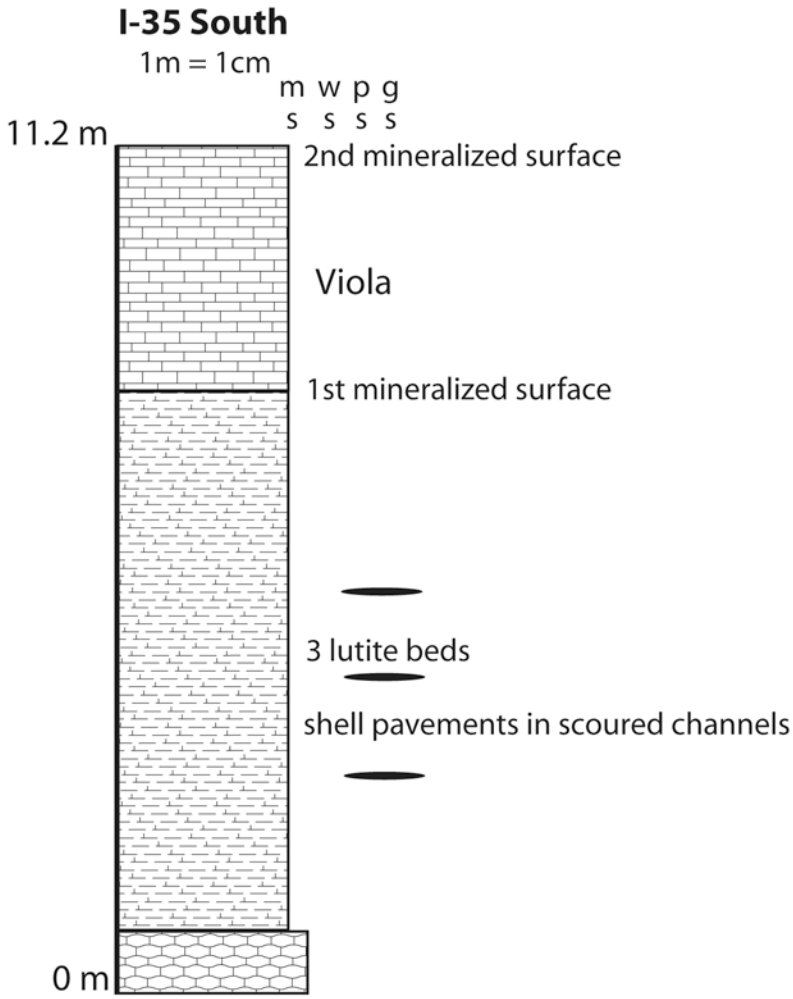
I-35 South
1m = 1cm
m w p g
s s s s
11.2 m
2nd mineralized surface
Viola
1st mineralized surface
3 lutite beds
shell pavements in scoured channels
0 m

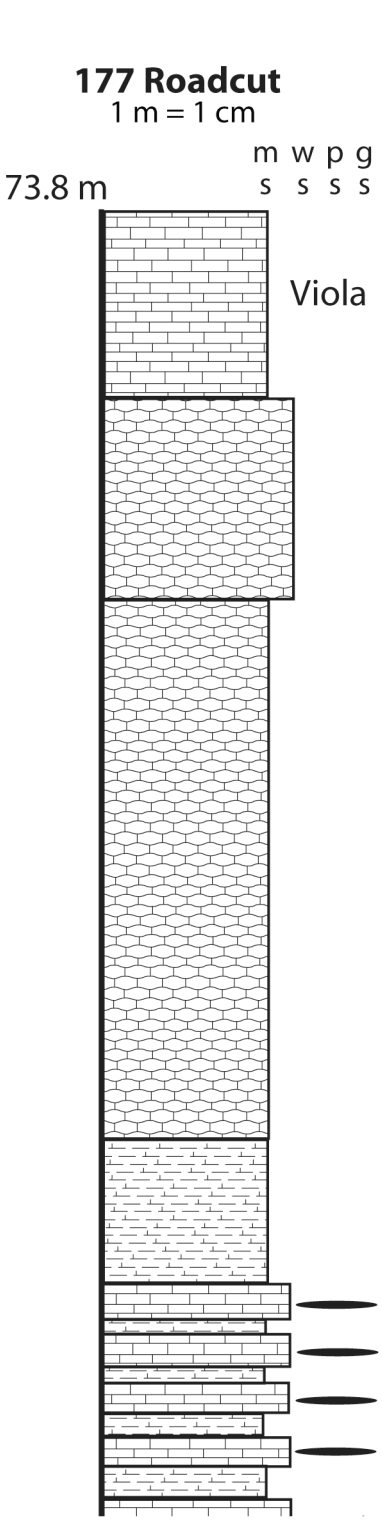
177 Roadcut
1 m = 1 cm
m w p g
s s s s
73.8 m
Viola

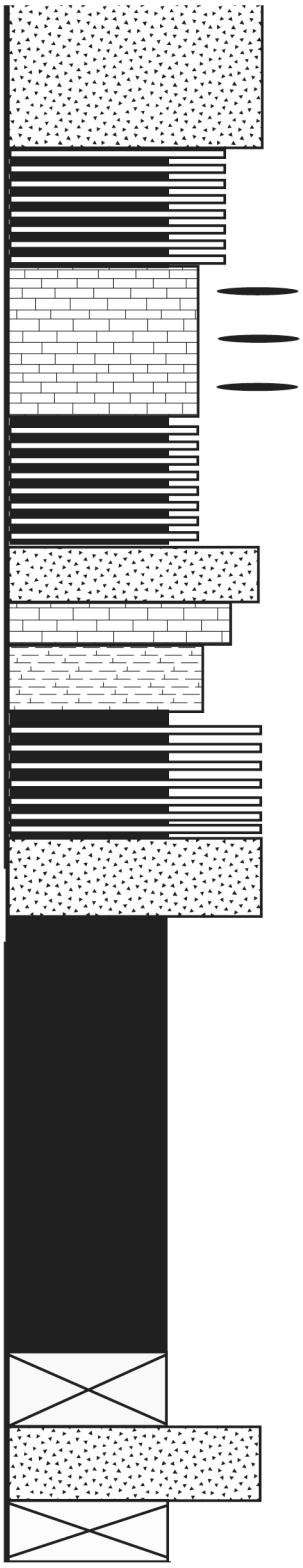

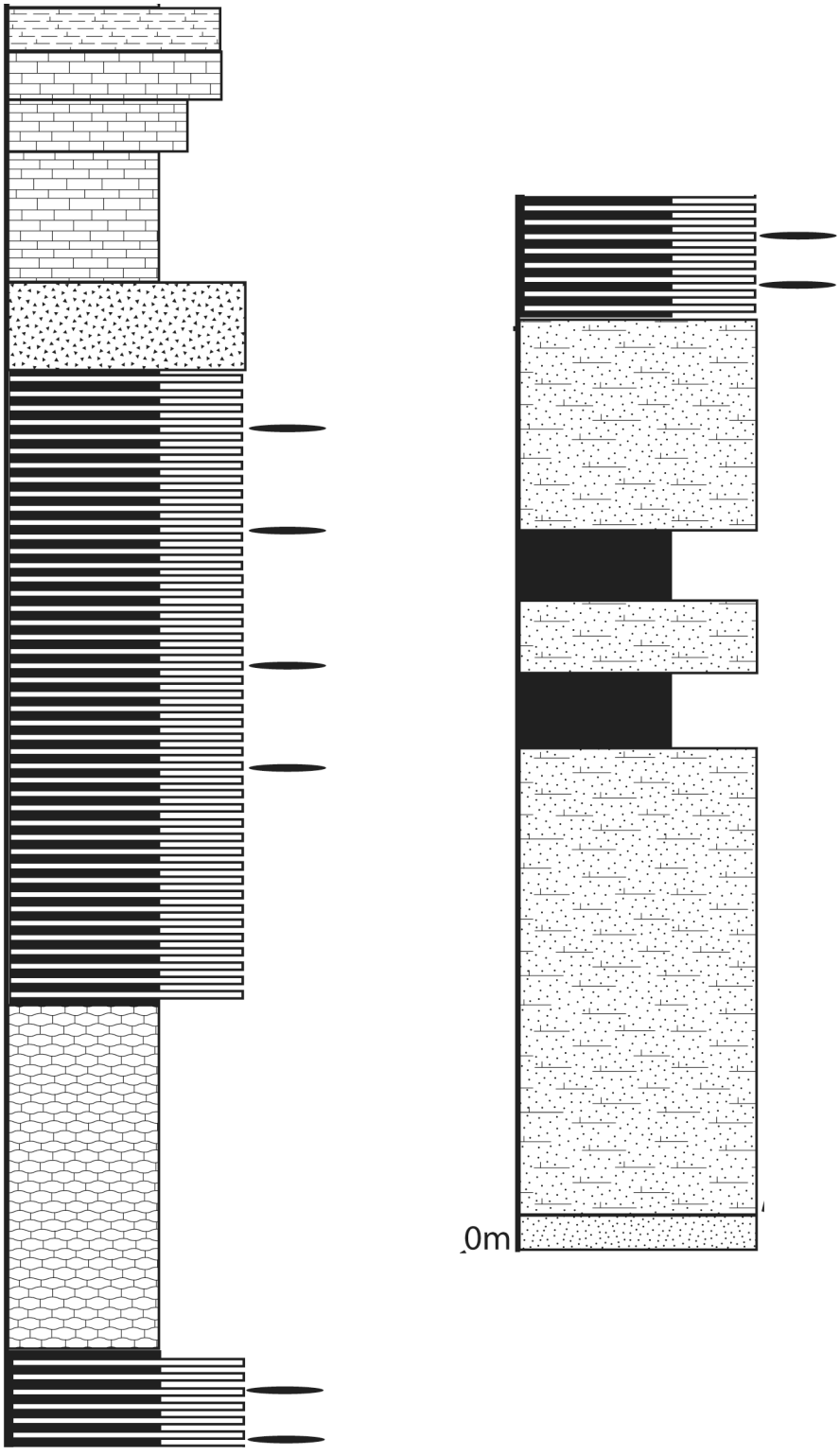
0m

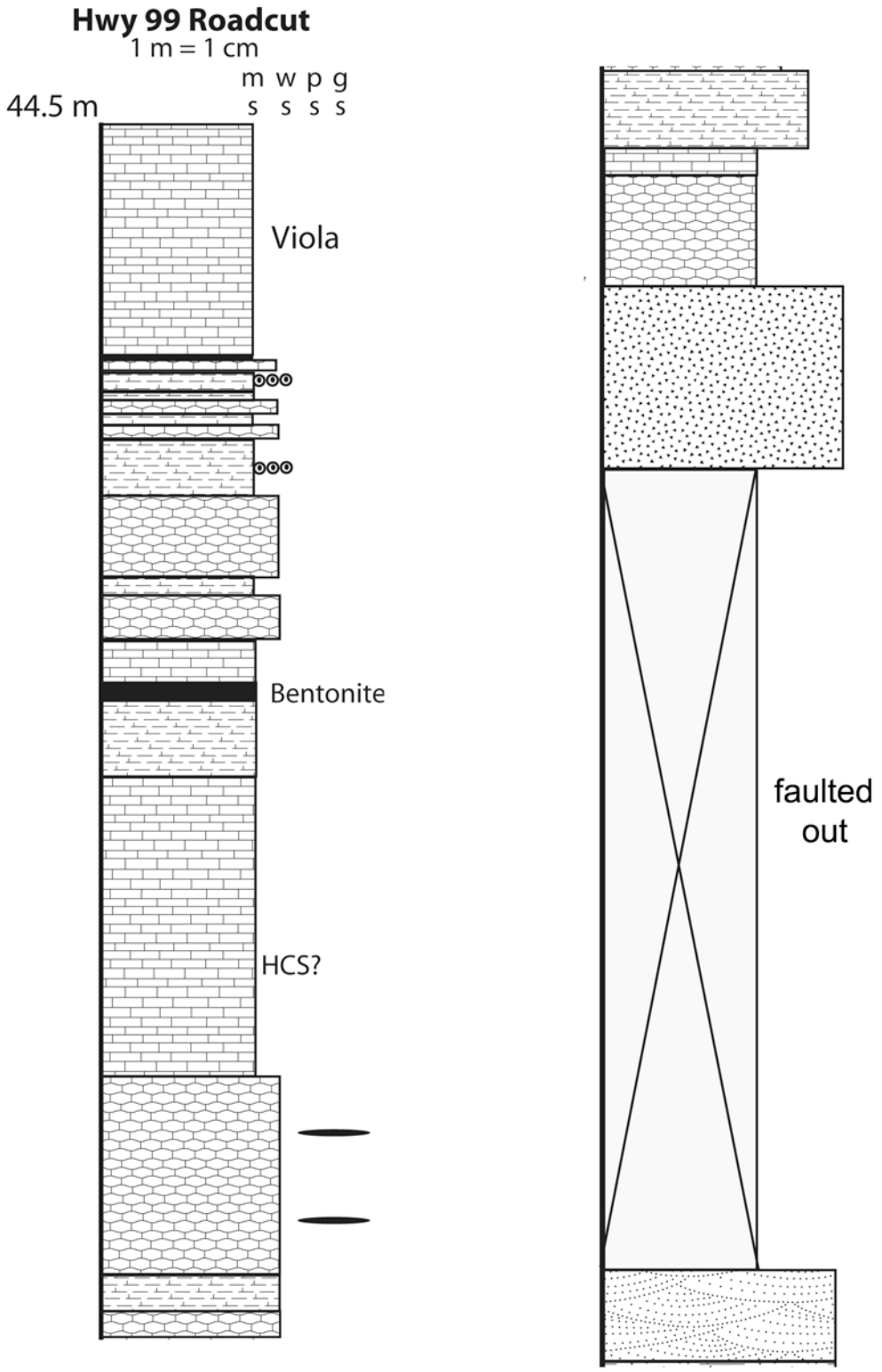
Hwy 99 Roadcut
1 m = 1 cm
m w p g
s s s s
44.5 m
Viola
Bentonite
HCS?
faulted
out

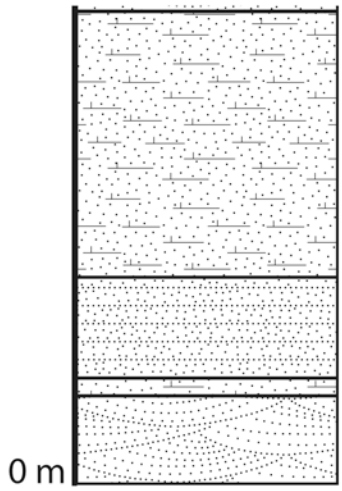
0 m

Mt. Lake Type (Quarry)

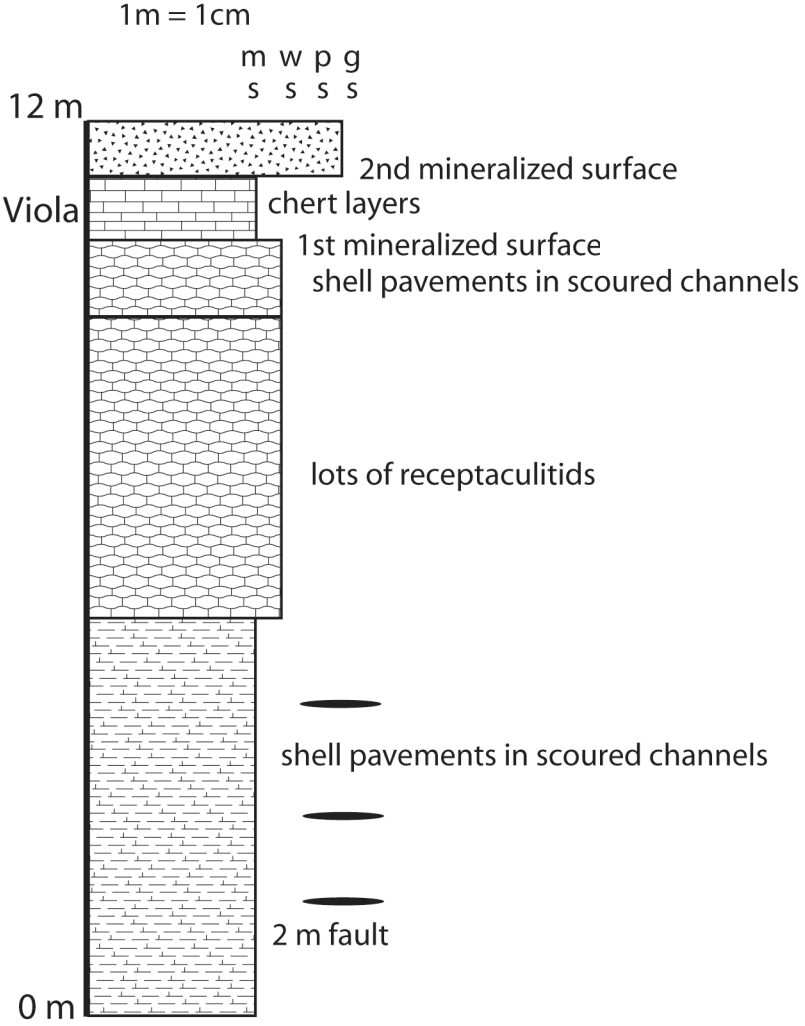

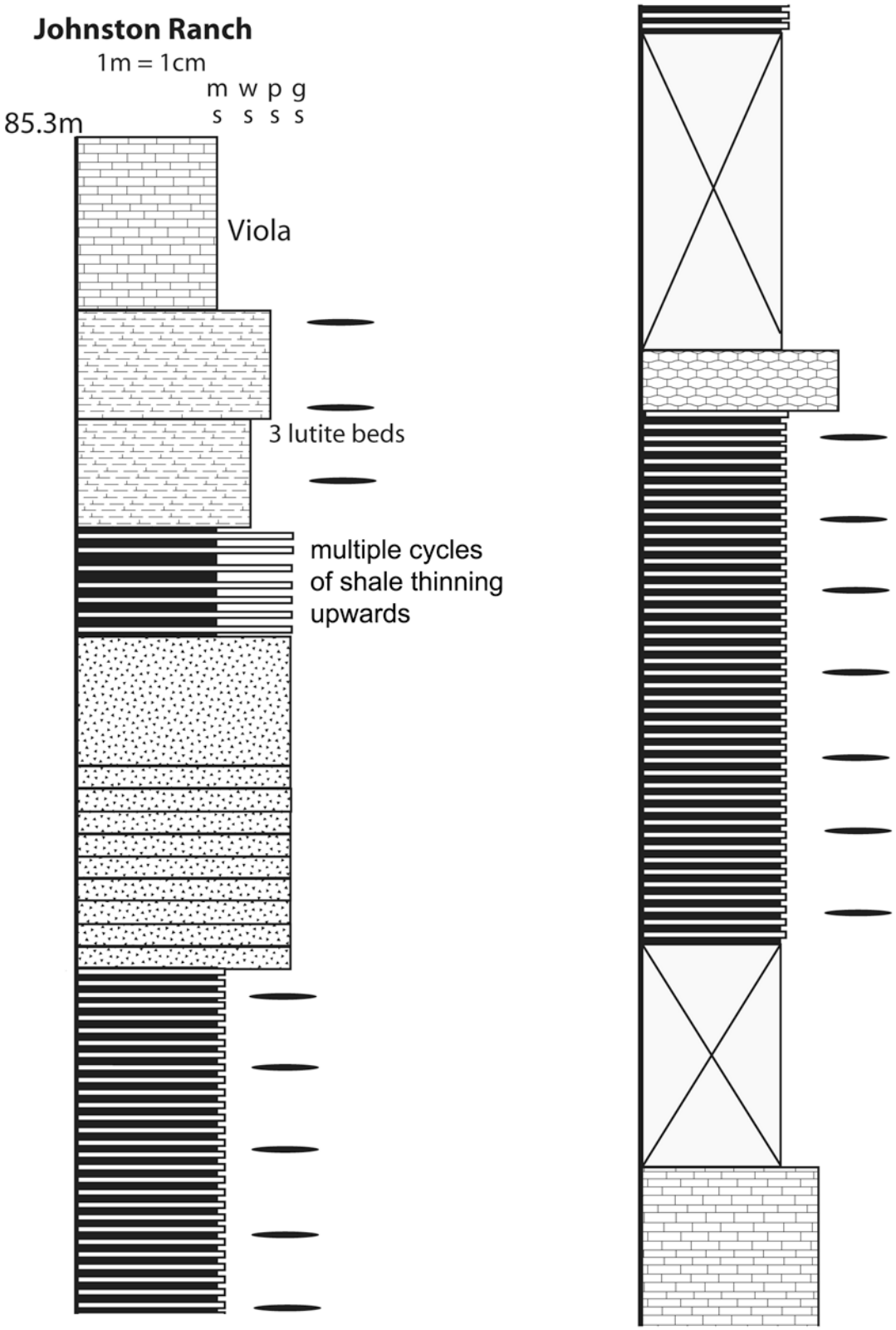
Johnston Ranch
1m = 1cm
m w p g
s s s s
85.3m
Viola
3 lutite beds
multiple cycles
of shale thinning
upwards

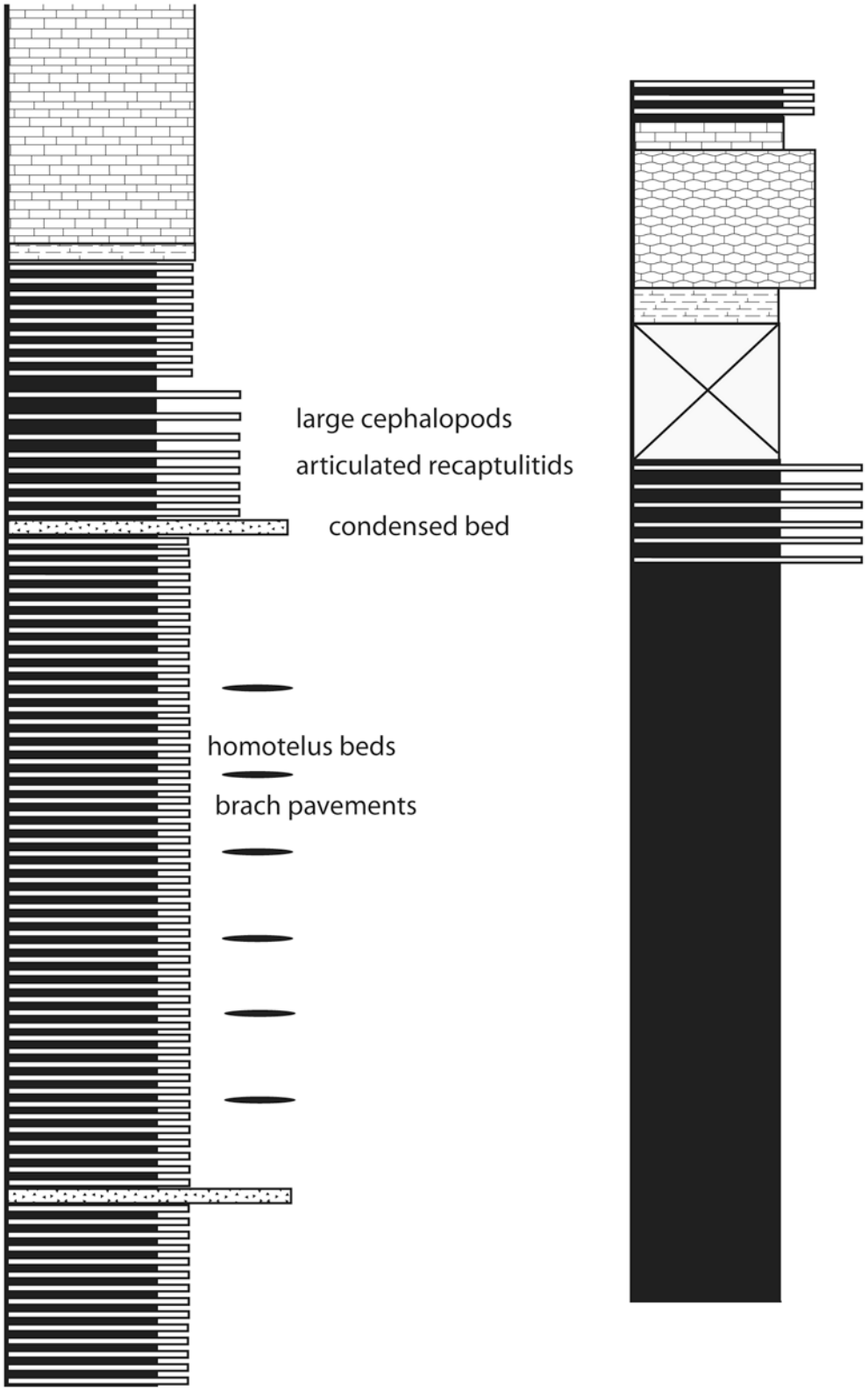
large cephalopods
articulated recaptulitids
condensed bed
homotelus beds
brach pavements

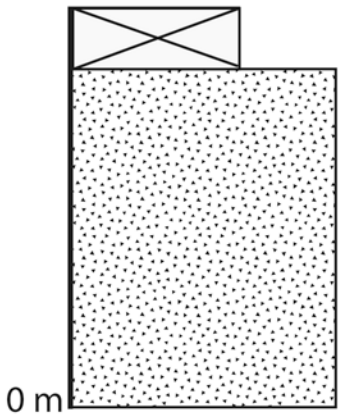
0 m

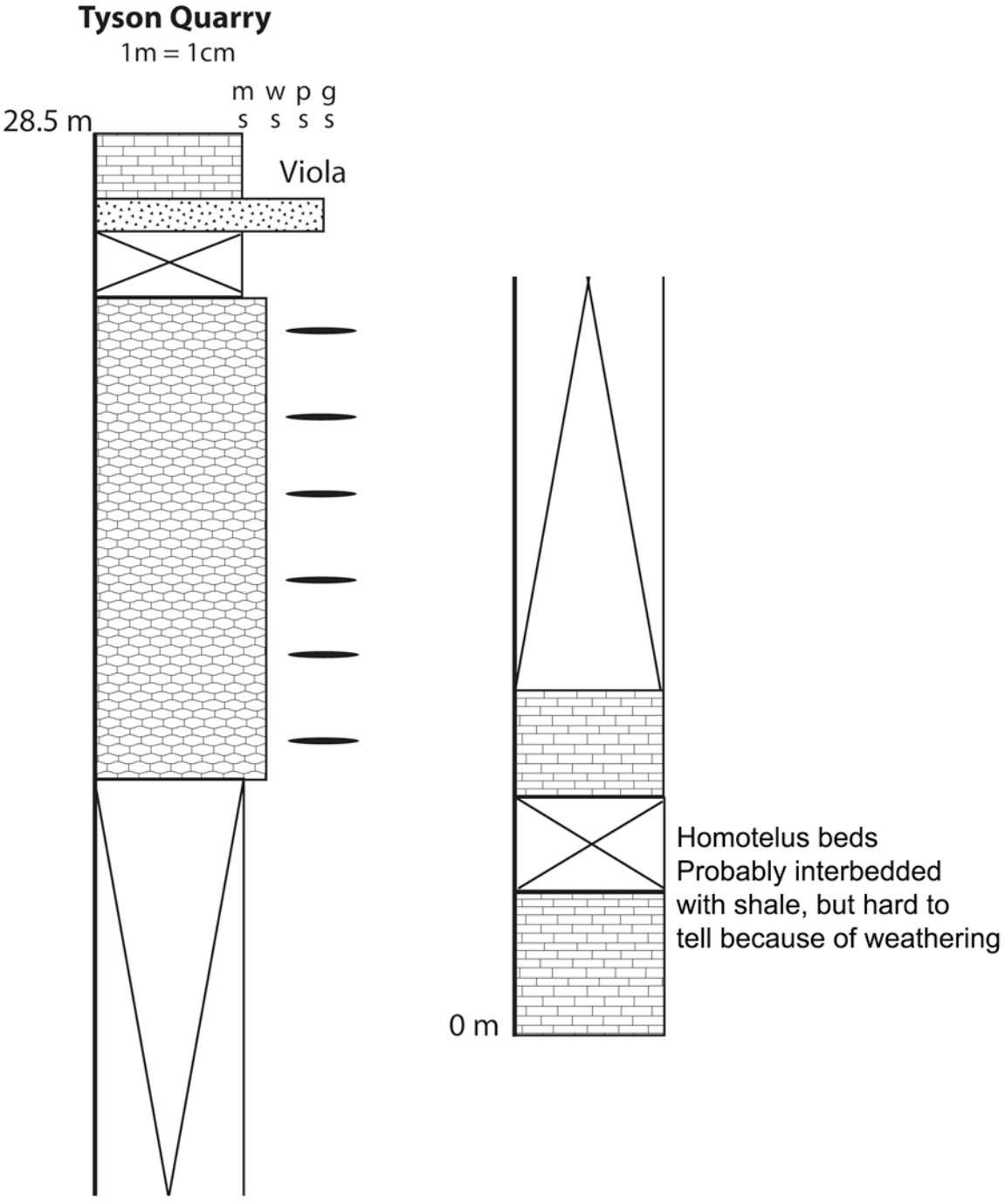
Tyson Quarry
1m = 1cm
m w p g
s s s s
28.5 m
Viola
Homotelus beds
Probably interbedded
with shale, but hard to
tell because of weathering
0 m

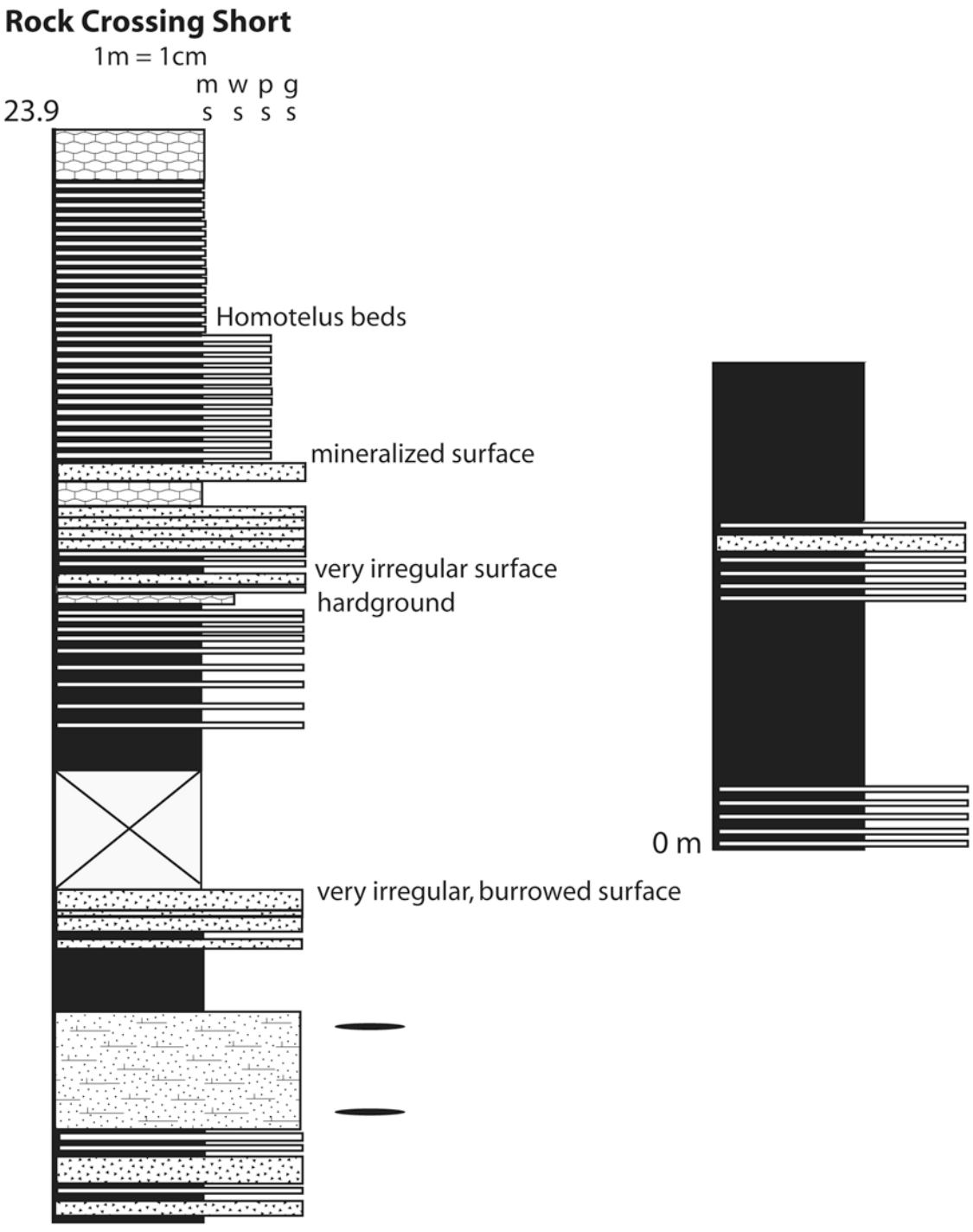
Rock Crossing Short
1m = 1cm
m w p g
s s s s
23.9
Homotelus beds
mineralized surface
very irregular surface
hardground
0 m
very irregular, burrowed surface

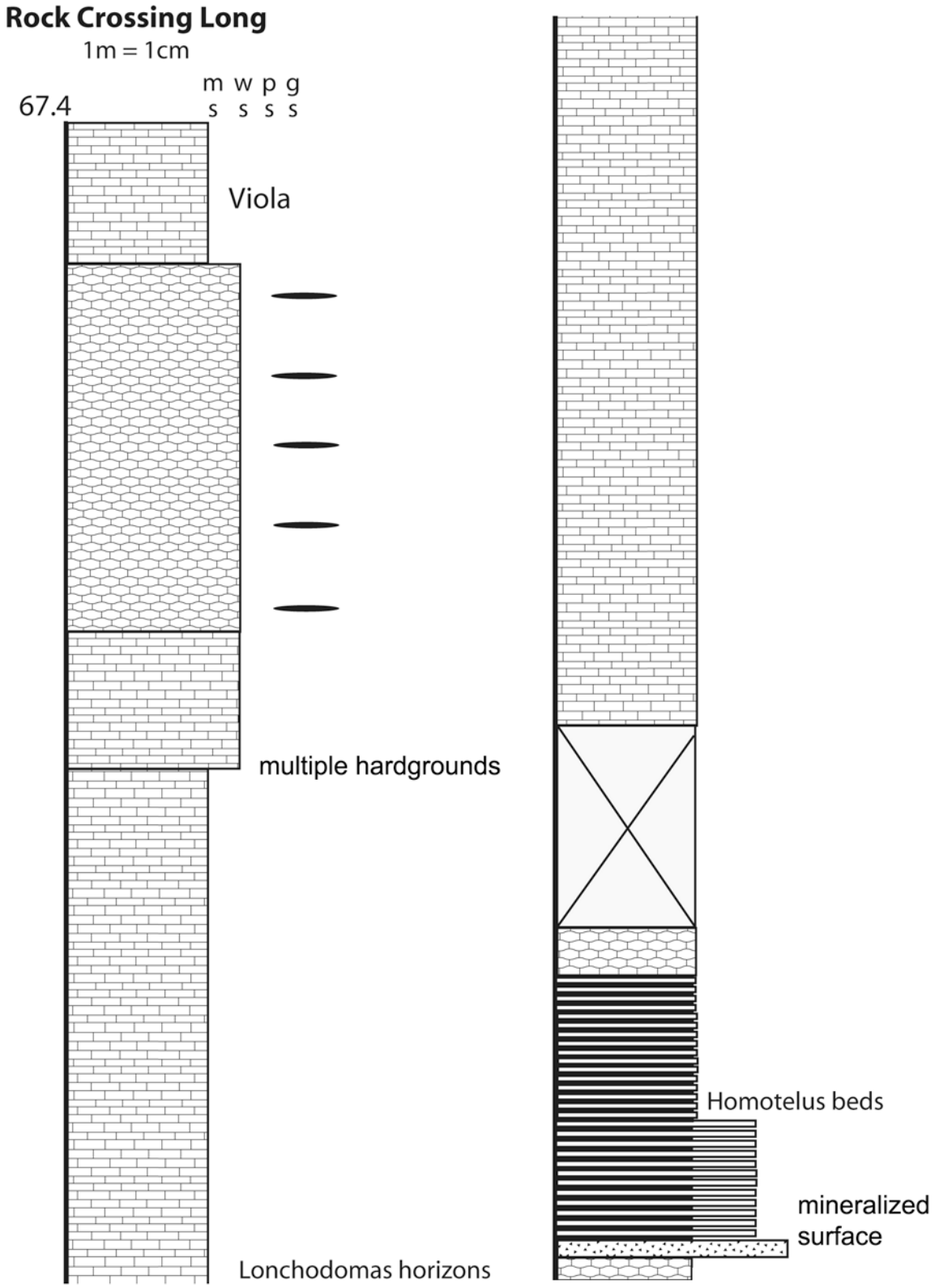
Rock Crossing Long
1m = 1cm
67.4
m w p g
s s s s
Viola
multiple hardgrounds
Lonchodomas horizons
Homotelus beds
mineralized
surface

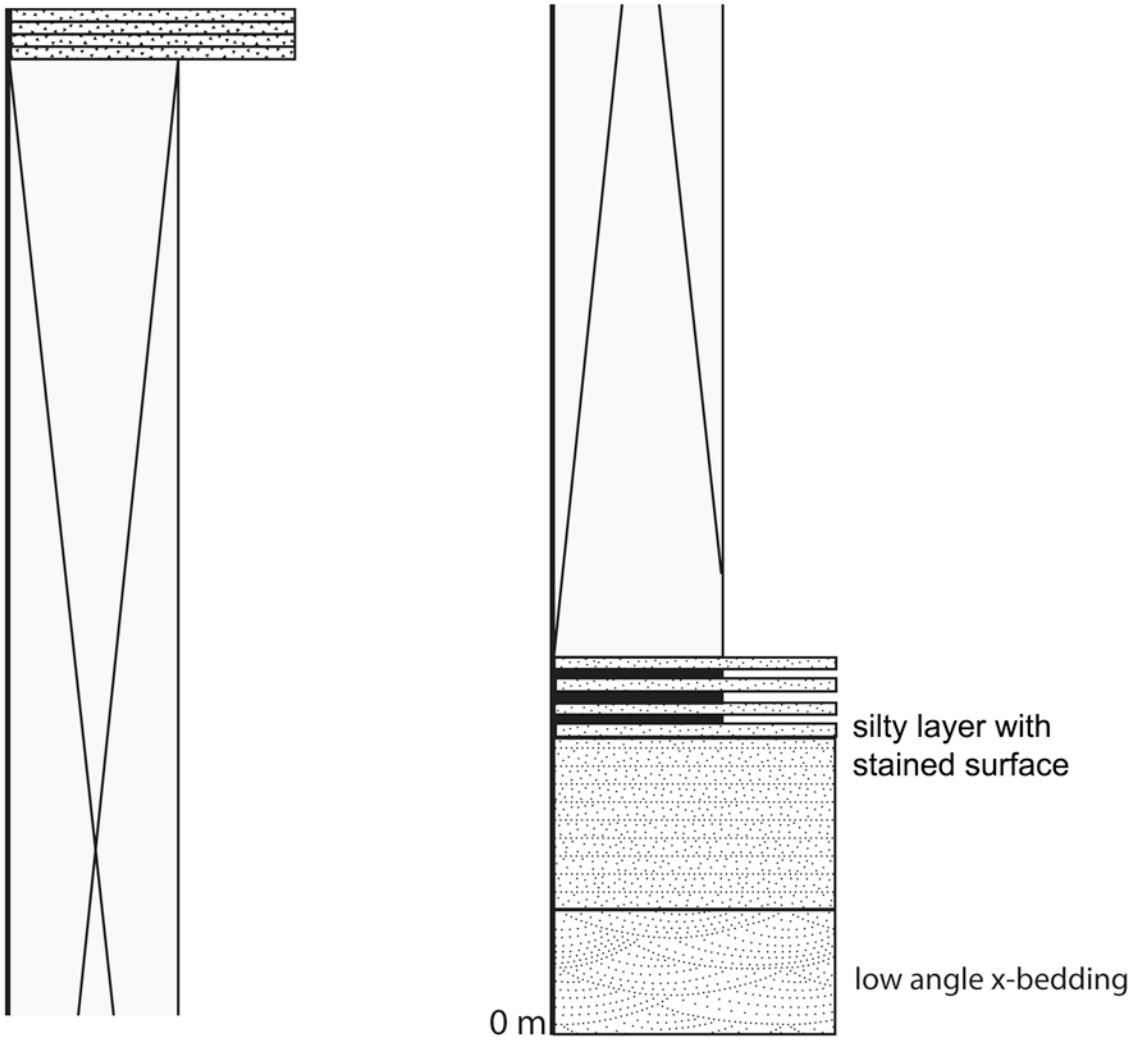
silty layer with
stained surface
low angle x-bedding
0 m

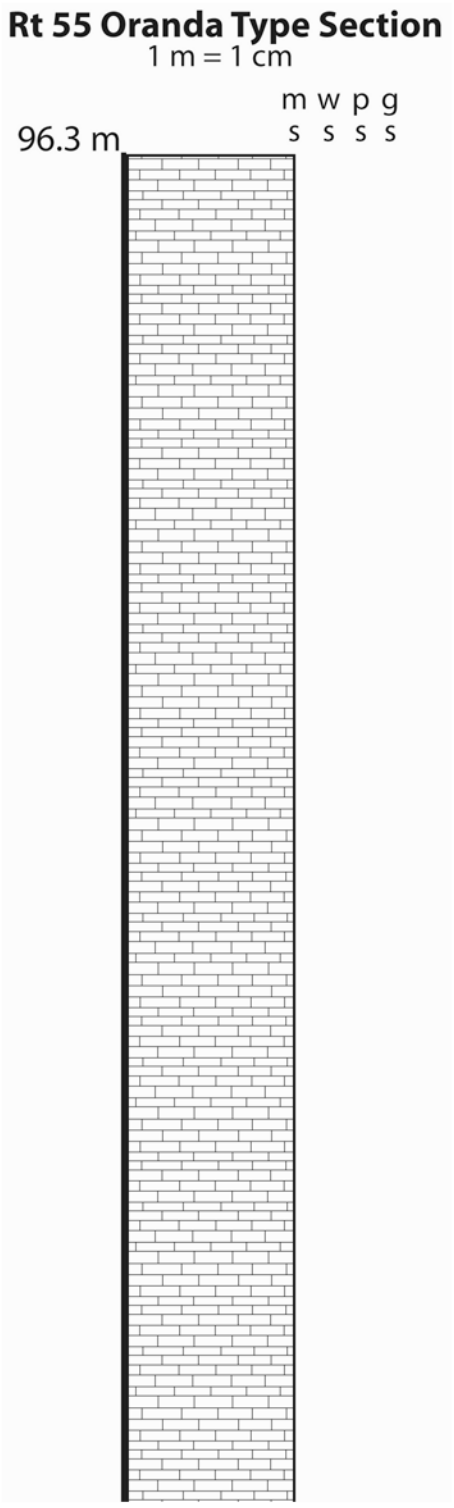
Rt 55 Oranda Type Section
1 m = 1 cm
m w p g
s s s s
96.3 m

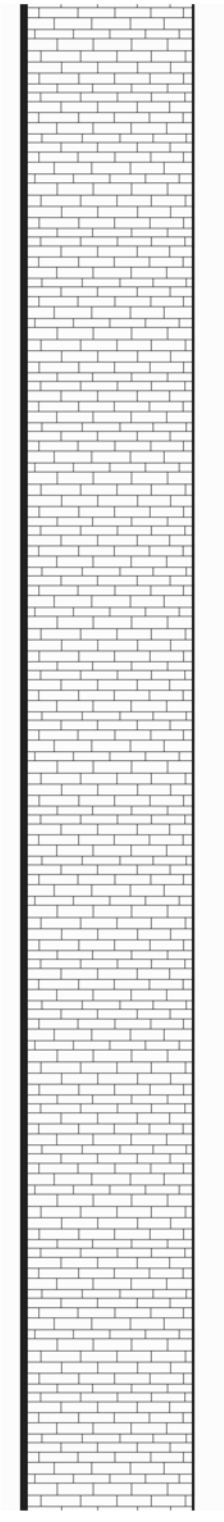

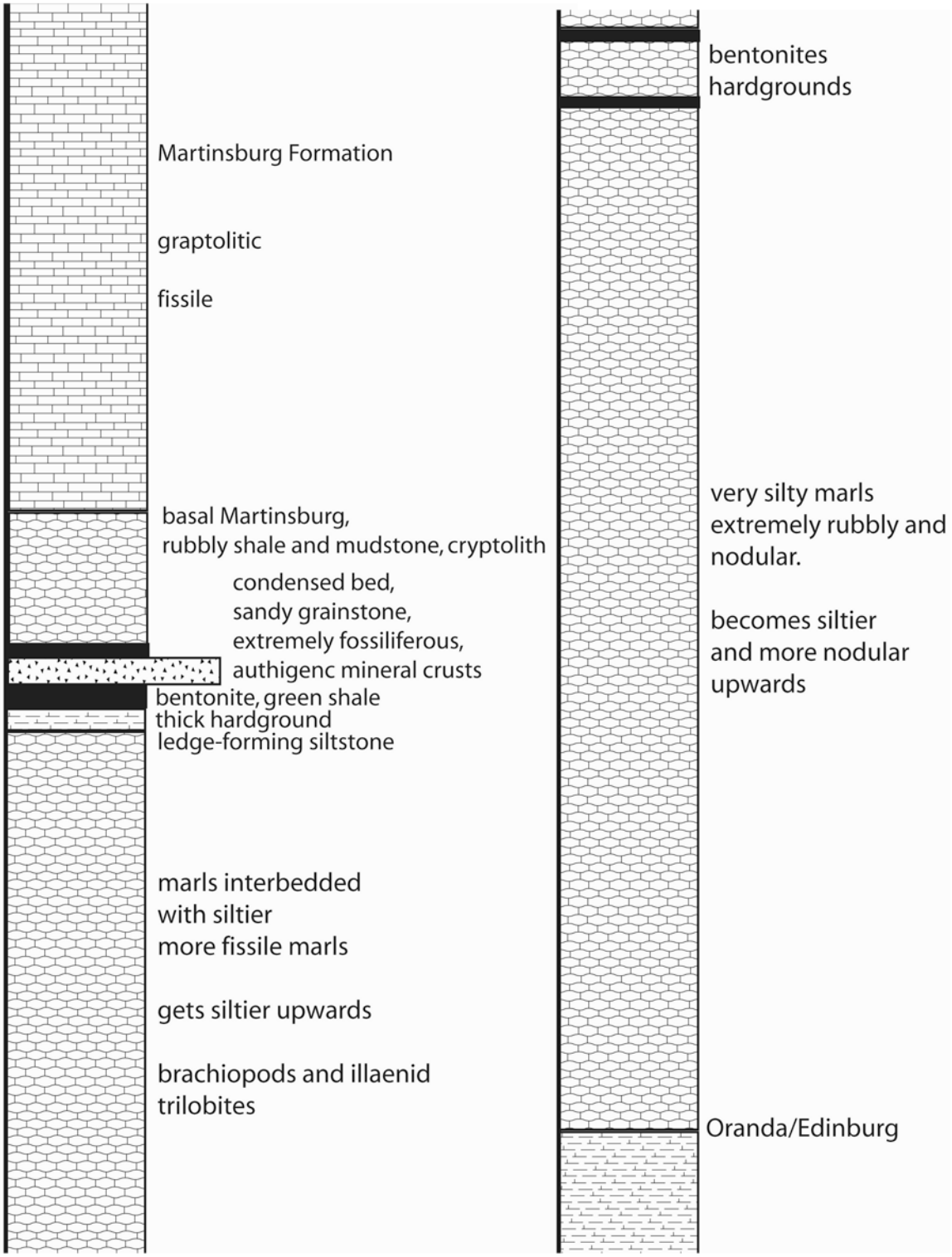
Martinsburg Formation
graptolitic
fissile
basal Martinsburg,
rubbly shale and mudstone, cryptolith
condensed bed,
sandy grainstone,
extremely fossiliferous,
authigenc mineral crusts
bentonite, green shale
thick hardground
ledge-forming siltstone
marls interbedded
with siltier
more fissile marls
gets siltier upwards
brachiopods and illaenid
trilobites
bentonites
hardgrounds
very silty marls
extremely rubbly and
nodular.
becomes siltier
and more nodular
upwards
Oranda/Edinburg

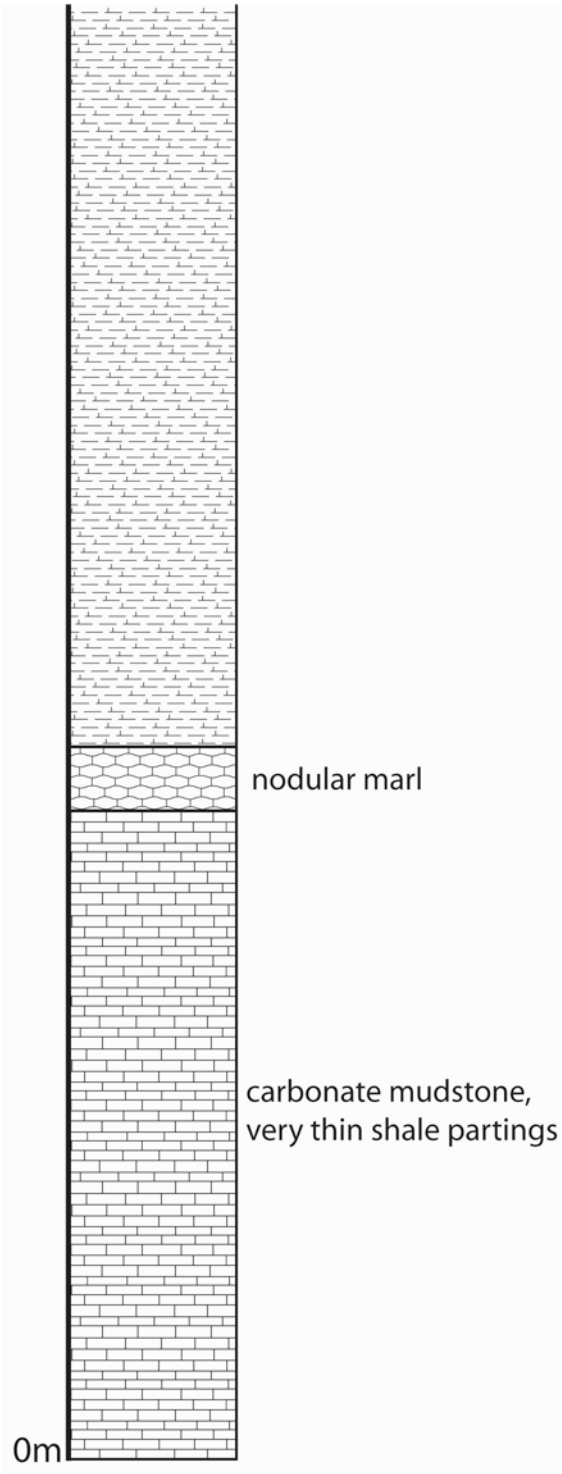
nodular marl
carbonate mudstone,
very thin shale partings
0m

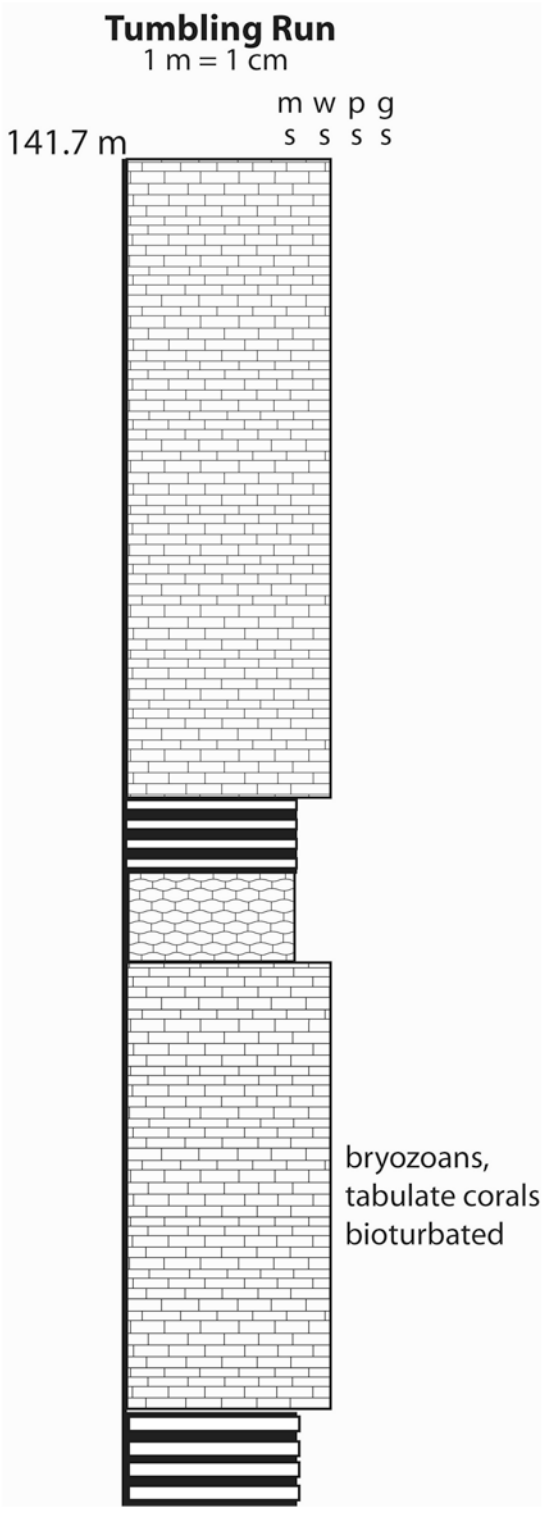
Tumbling Run
1 m = 1 cm
m w p g
s s s s
141.7 m
bryozoans,
tabulate corals
bioturbated

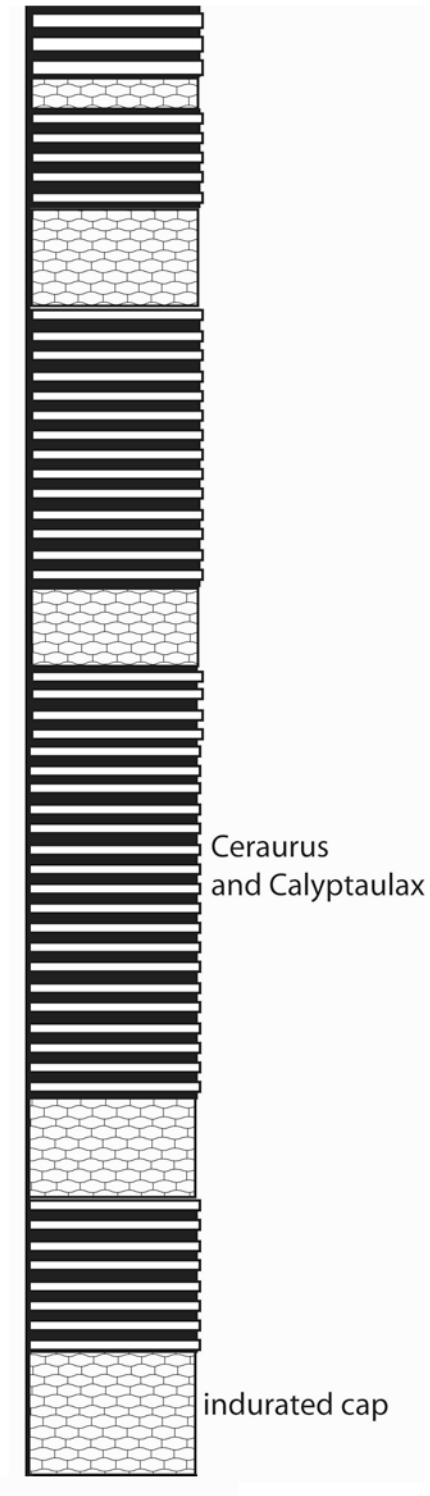
Ceraurus
and Calyptaulax
indurated cap

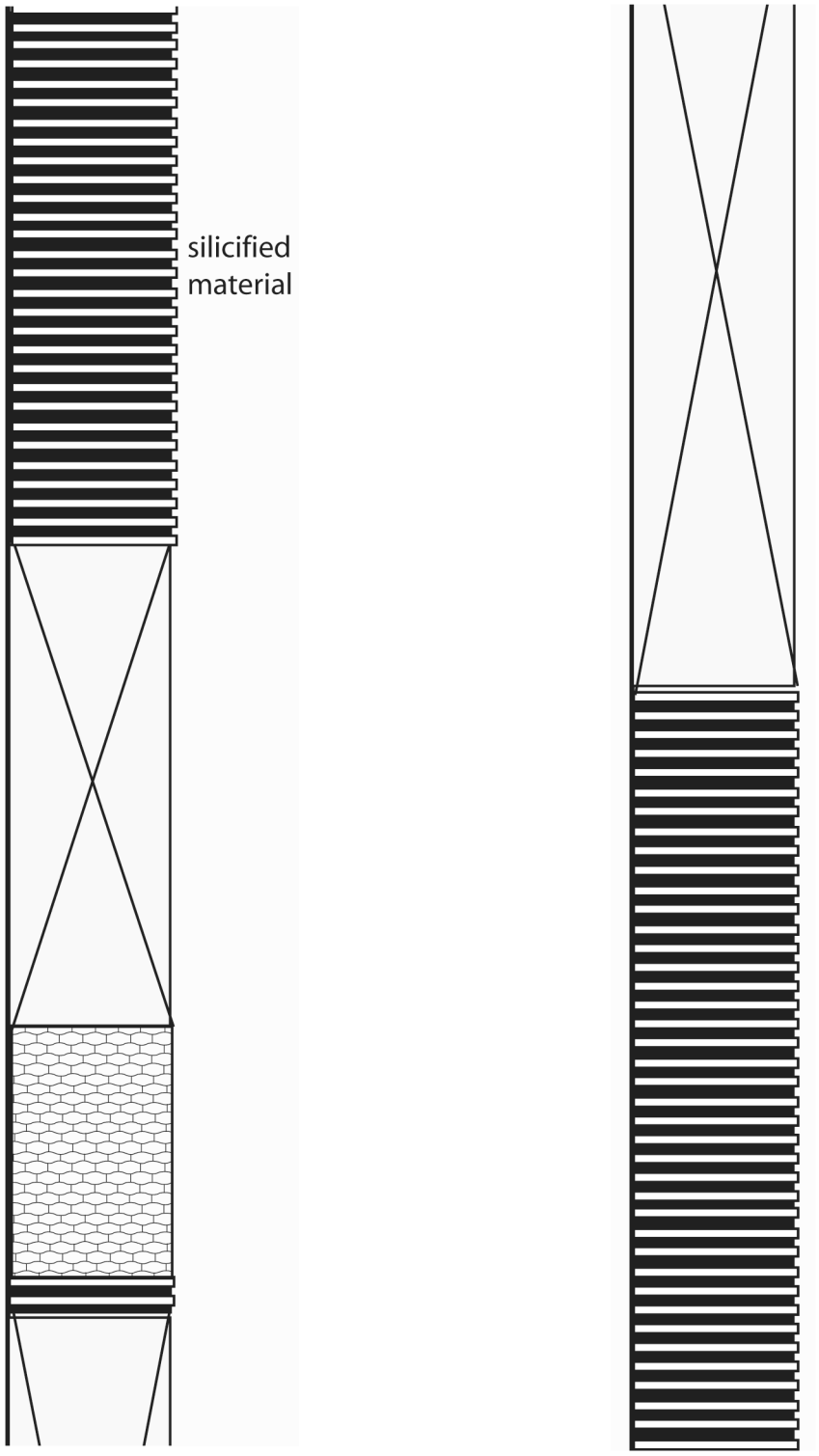
silicified
material

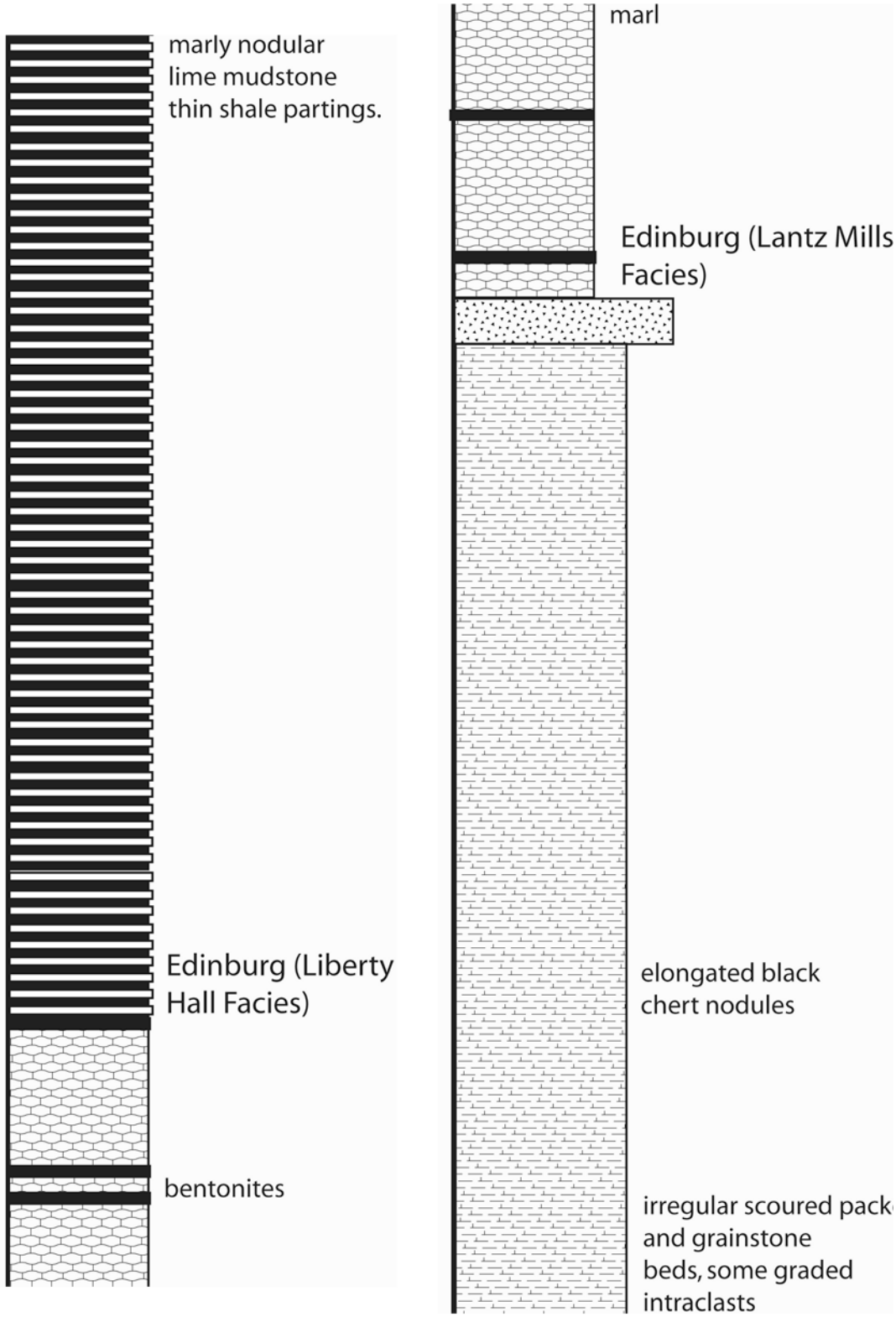
marly nodular
lime mudstone
thin shale partings.
Edinburg (Liberty
Hall Facies)
bentonites
marl
Edinburg (Lantz Mills
Facies)
elongated black
chert nodules
irregular scoured pack
and grainstone
beds, some graded
intraclasts

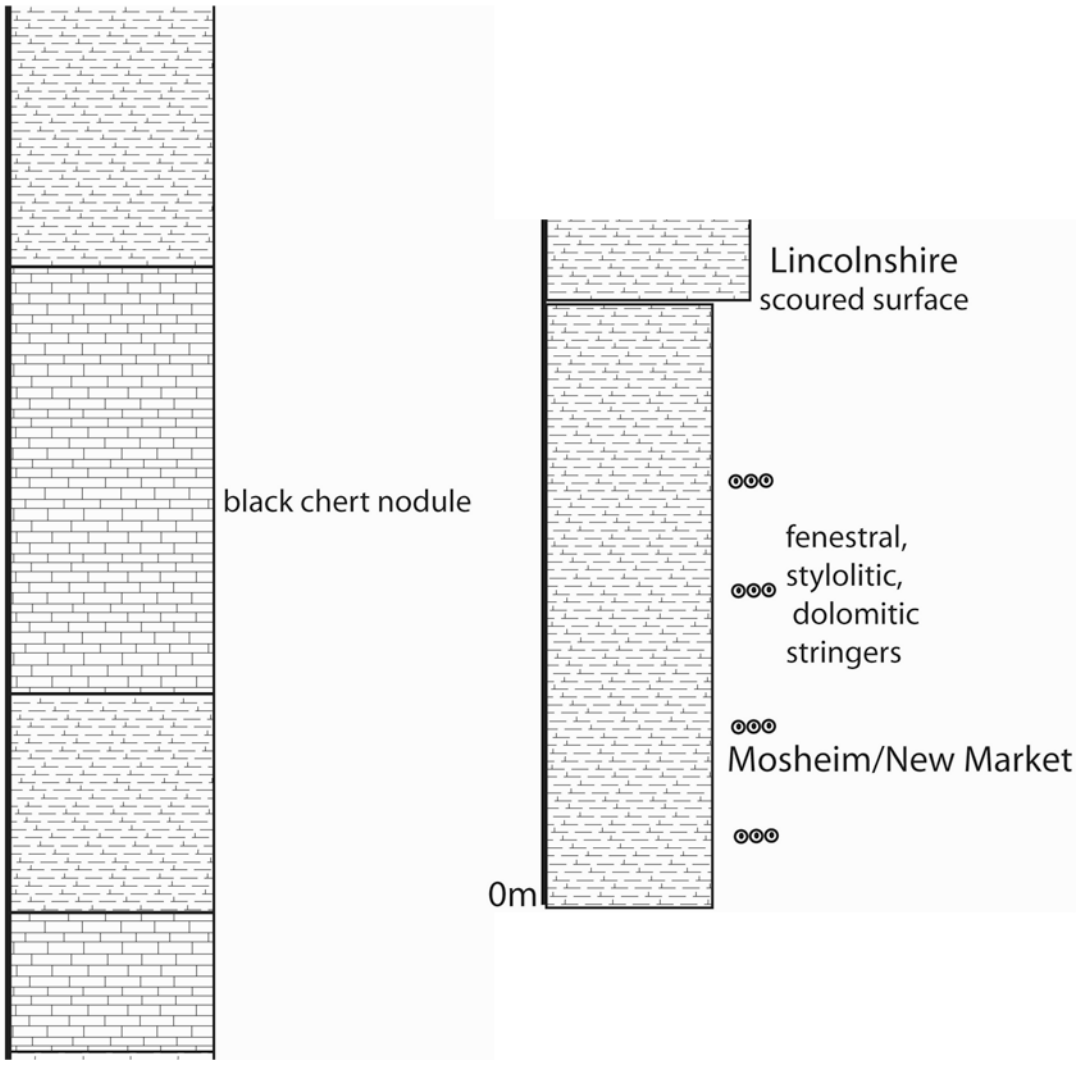
black chert nodule
Lincolnshire
scoured surface
fenestral,
stylolitic,
dolomitic
stringers
Mosheim/New Market
0m

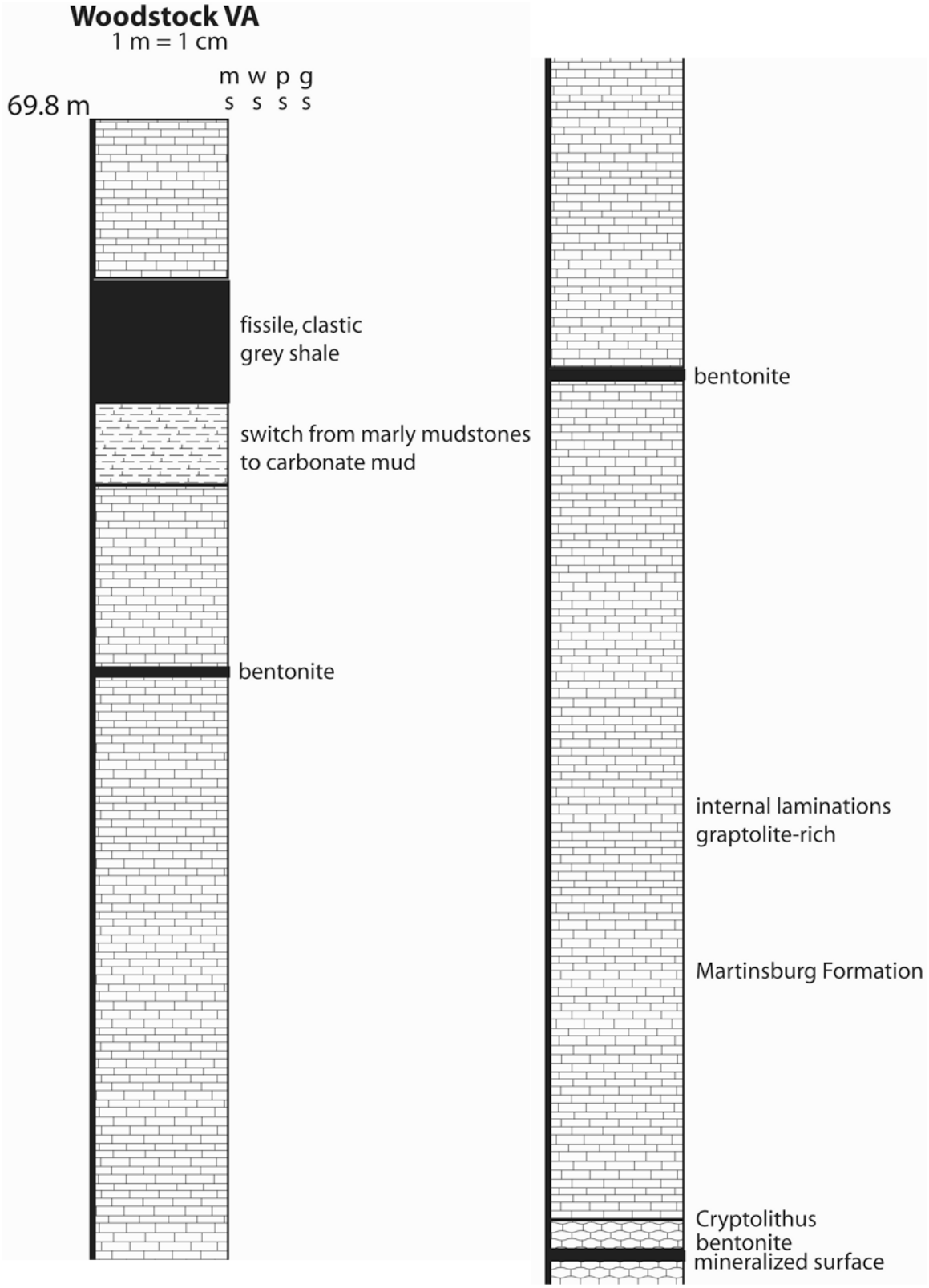
Woodstock VA
1 m = 1 cm
m w p g
s s s s
69.8 m
fissile, clastic
grey shale
switch from marly mudstones
to carbonate mud
bentonite
bentonite
internal laminations
graptolite-rich
Martinsburg Formation
Cryptolithus
bentonite
mineralized surface

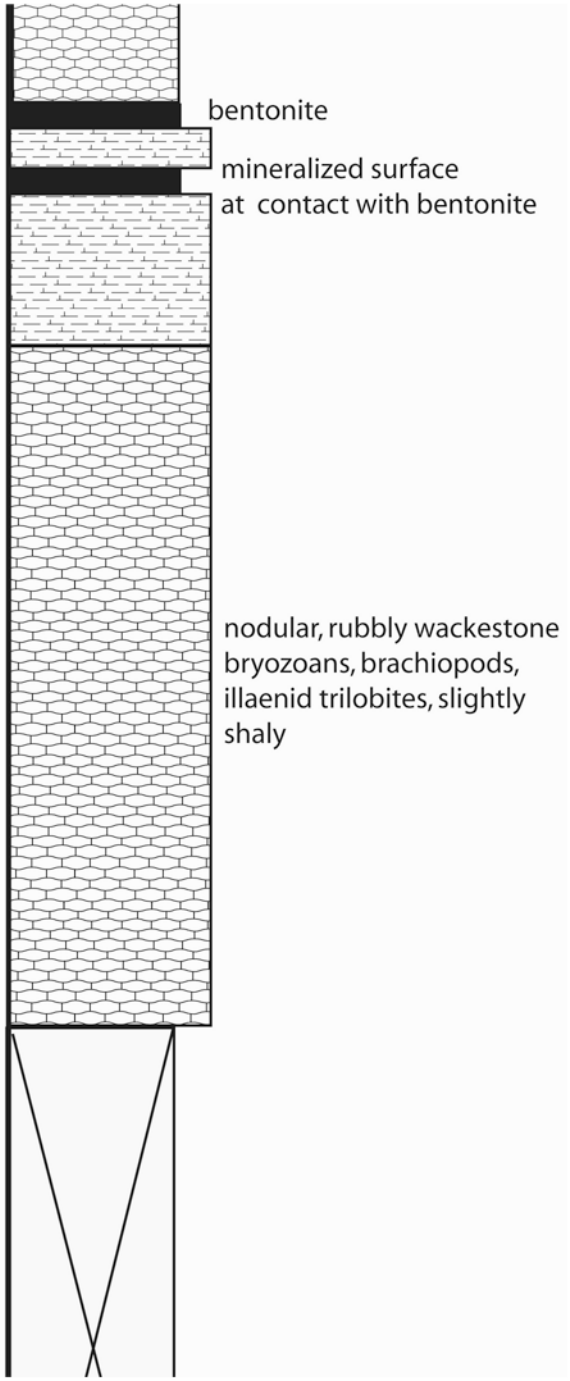
bentonite
mineralized surface
at contact with bentonite
nodular, rubbly wackestone
bryozoans, brachiopods,
illaenid trilobites, slightly
shaly

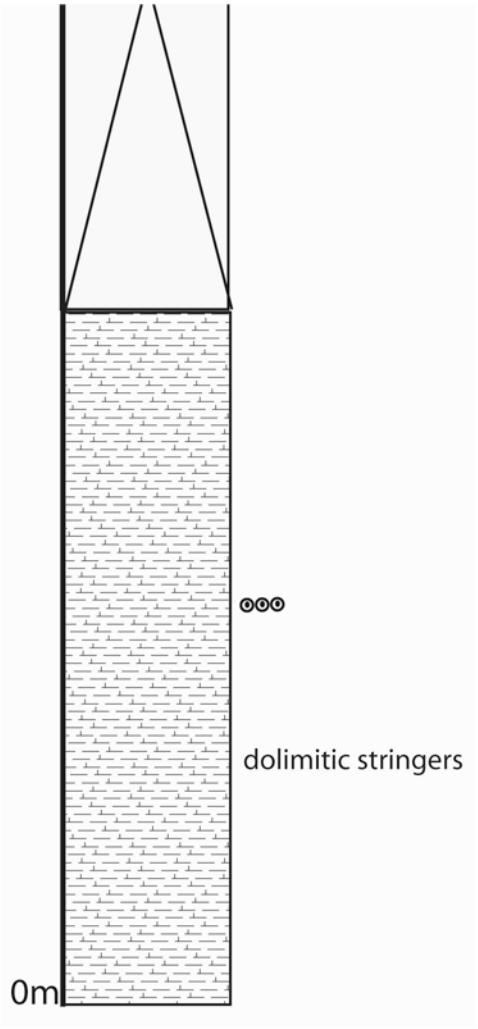
dolimitic stringers
0m

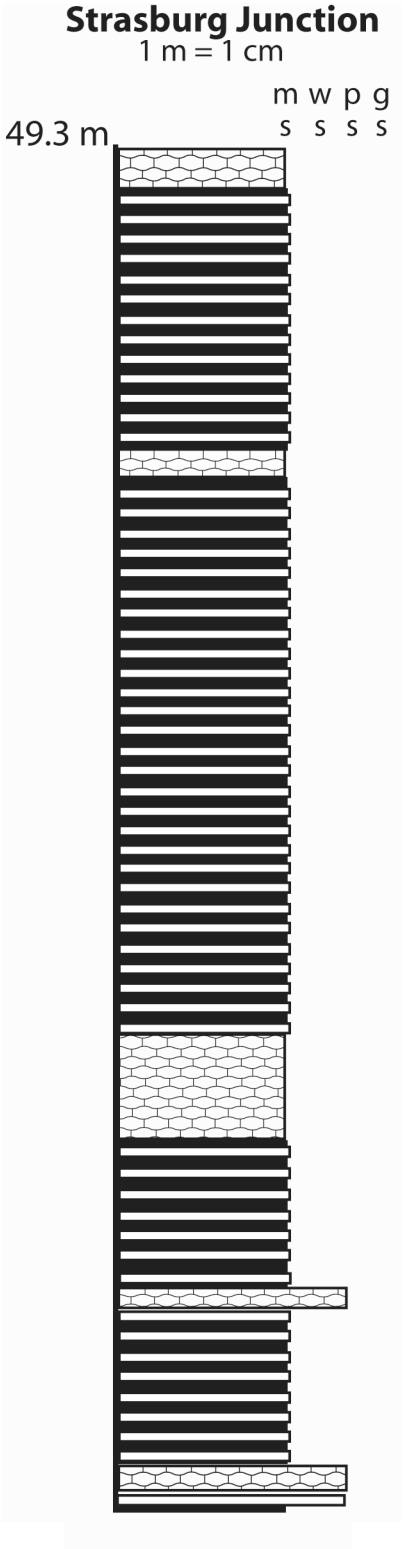
Strasburg Junction
1 m = 1 cm
m w p g
s s s s
49.3 m

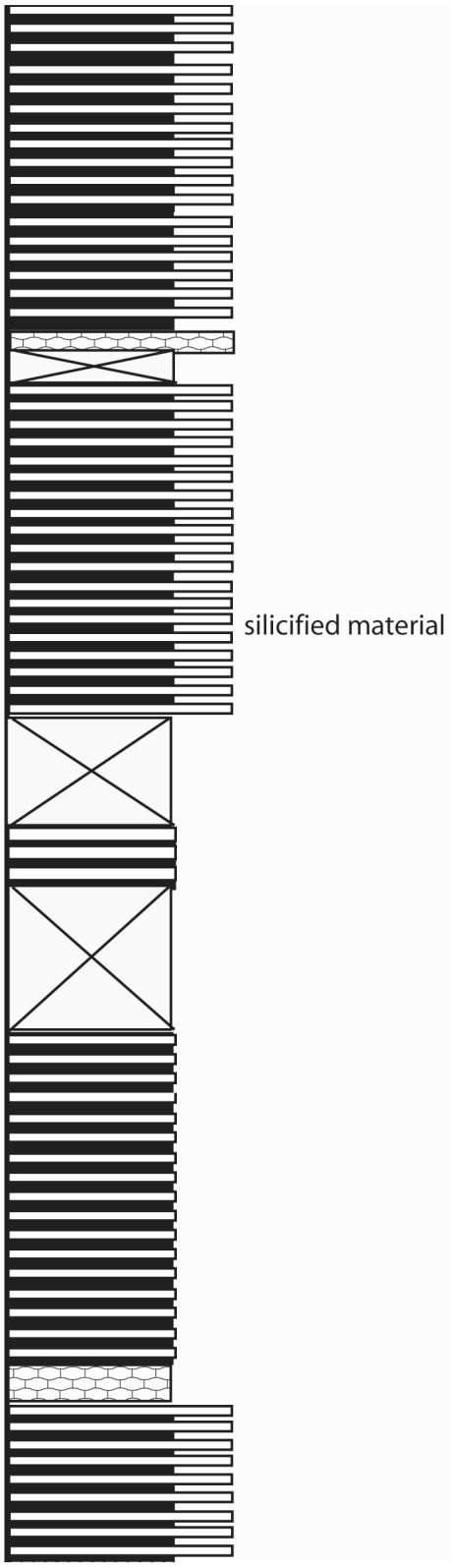
silicified material

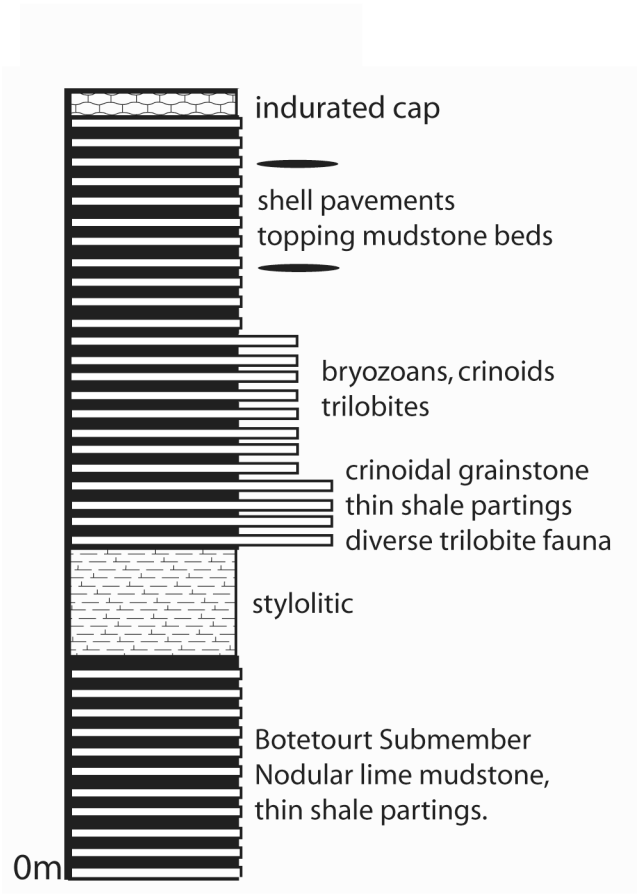
indurated cap
shell pavements
topping mudstone beds
bryozoans, crinoids
trilobites
crinoidal grainstone
thin shale partings
diverse trilobite fauna
stylolitic
Botetourt Submember
Nodular lime mudstone,
thin shale partings.
0m

APPENDIX 2: ILLUSTRATIONS AND NOTES ON REMAINING TRILOBITES OF THE BROMIDE FORMATION, OKLAHOMA

Illustrated material was photographed at 1mm intervals with a Canon E05 5D camera equipped with a 65, 80, or 120 mm lens. Images were stacked using Helicon Focus 4.04 Pro Multiprocessor (Helicon Soft, Ltd). All material is housed at the Sam Noble Oklahoma Museum of Natural History, with the OU repository acronym. Systematic nomenclature follows Jell & Adrain (2002).

Class **TRILOBITA** Walch, 1771

Order **CORYNEXOCHIDA** Kobayashi, 1935

Suborder **ILLAENINA** Jaanusson, 1959

Family **ILLAENIDAE** Hawle & Corda, 1847

Genus ***Thaleops*** Conrad, 1843

Thaleops sp. 1

(Figs. 1A-L)

Occurrence. DRa36.2 (Figs. 1A-C), I35N6.85 (Figs. 1D-I), I35N17 (Figs. 1K-L).

Remarks. *Thaleops* sp. 1 differs from other Bromide Formation species because the exoskeleton is not punctate as in *T. jaanussoni*, the axial furrows are weaker; the pygidium is narrower (sag.), with the articulating facets expressed at a flatter angle than *T. mobydicki* or *T. jaanussoni*.

Thaleops jaanussoni Amati & Westrop, 2004

(Figs. 2A-F, H-K)

Occurrence. TQ (Figs. 2A-C), I35N36.6 (Figs. 2D-F, H-K), I35N47-48 (not pictured).

Thaleops mobydicki Amati & Westrop, 2004

(Fig. 2G)

Occurrence. TQ (Fig. 2G)

Family **STYGINIDAE**

Genus ***Failleana*** Chatterton & Ludvigsen, 1976

Failleana sp. 1

(Figs. 3A-I, 4A-F, J, K)

Occurrence. I35N0-3 (Figs. 3B, F), I35N17 (Figs. 3A, C-D, G-I), Sycamore Creek (Fig. 3E), I35N18-19 (Figs. 4A-C), I35N36.6 (Figs. 4D-F, J-K).

Remarks. The morphology of *Failleana* sp. 1 is remarkably consistent throughout the Bromide Formation, even though it is found in a variety of lithofacies. It differs from *Failleana limbatus* because the path of the axial furrow is nearly straight towards the lunette, until it diverges forward on the anterior side of the lunette. In contrast, *Failleana limbatus* has an axial furrow that converges strongly inward from the genal angle, forming a sickle-shape in lateral view.

Failleana limbatus Raymond, 1910

(Figs. 4G-I)

Occurrence. TQ (Figs. 4G-I).

Order **ASAPHIDA** Burmeister, 1843

Suborder **ASAPHINA** Salter, 1864

Family A**SAPHIDAE** Burmeister, 1843

Subfamily **ISOTELINAE** Angelin, 1854

Genus ***Anataphrus*** Whittington, 1954

Anataphrus sp. 1

(Figs. 5A-B, D-F, H)

Occurrence. I35N6.85 (Figs. 5A-B, D-F, H).

Anataphrus sp. 2

(Figs. 5I-K)

Occurrence. I35N7.8 (Figs. 5I-K).

Remarks. Compared to species 1, *Anataphrus* sp. 2 has a pygidium that is proportionally shorter (sag.) and wider (tr.), with a more pronounced pygidial axis, and a narrower (sag.) pygidial border.

Anataphrus sp. 3

(Fig. 5G)

Occurrence. I35N7.8 (Fig. 5G).

Remarks. *Anataphrus* sp. 3 has a better-rounded cranidial anterior margin, larger palpebral lobes, and wider (tr.) postero-lateral projections than other *Anataphrus* species.

Anataphrus sp. 4

(Fig. 5C)

Occurrence. I35N36.6 (Fig. 5C).

Remarks. *Anataphrus* sp. 4 has regular dense pitting over the entire cranidium whereas other species develop pits only on the postero-lateral projection and near the anterior margin.

Genus ***Isotelus*** Dekay, 1824

Isotelus bromidensis Esker, 1964

(Figs 6A-D)

Occurrence. DRa36.2 (Figs. 6A-D), RCS20 (not pictured), TQ0-2.4 (not pictured).

Isotelus sp. 2

(Figs. 6E-G)

Occurrence. RCL49.2 (Figs. 6E-F), RCL51.3 (Fig. 6G).

Family **REMOPLEURIDIDAE** Hawle & Corda, 1847

Subfamily **REMOPLEURIDINAE** Hawle & Corda, 1847

Genus ***Remopleurides*** Portlock, 1843

Remopleurides sp. 1

(Figs. 7A-L)

Occurrence. I35N17 (Figs. 7A-L).

Superfamily **TRINUCLEIOIDEA** Hawle & Corda, 1847

Family **RAPHIOPHORIDAE** Angelin, 1854

Genus ***Lonchodomas*** Angelin, 1854

Lonchodomas mcgheei Decker, 1931

(Figs. 8A-H)

Occurrence. RC unlabeled (Fig. 8A-B), RCL50.6C-D, F-H), RC51.3 (Fig. 8E).

Order **HARPETIDA** Hawle & Corda, 1847

Family **HARPETIDAE** Hawle & Corda, 1847

Genus ***Dolichoharpes*** Whittington, 1949

Dolichoharpes reticulata Whittington, 1949

(Figs. 9A-C)

Occurrence. TQ (Figs.9A-C).

Order **PHACOPIDA** Salter, 1864

Suborder **PHACOPINA** Struve, 1959

Family **PTERYGOMETOPIDAE** Reed, 1905

Genus ***Calyptaulax*** Cooper, 1930

Calyptaulax annulata Raymond, 1905

(Figs. 9D-J, 10A-I)

Occurrence. I35N47-48 (Figs. 9D-J), DRa36.2 (Figs. 10A-E), TQ (Figs. 10F-I).

Family **CHEIRURIDAE** Hawle & Corda, 1847

Subfamily **CHEIRURINAE** Hawle & Corda, 1847

Genus ***Ceraurinella*** Cooper, 1953

Ceraurinella sp. 1

(Fig. 11A, F, G-H)

Occurrence. DRa36.2 (Figs. 11A, G-H), I35N17 (Fig. 11F)

"***Ceraurinella***" sp. 2

(Fig. 11B-C, E, I)

Occurrence. TQ (Fig. 11B-C, E, I).

Remarks. "*Ceraurinella*" sp. 2 differs from species 1 by having a proportionally wider (tr.) posterior area, broader genal spine, and more prominent paired tubercles on the glabella. Moreover, the pygidium is unlike any other species of *Ceraurinella*, necessitating open nomenclaure here. In this species, the most medial pair of pygidial pleural spines is not present.

Genus ***Ceraurus*** Green, 1832

Ceraurus ruidus Cooper, 1953

(Figs. 11D, J-K)

Occurrence. TQ (Figs. 11D, J-K).

Subfamily **ACANTHOPARYPHINAE** Whittington & Evitt, 1954

Genus ***Holia*** Bradley, 1930

Holia sp. 1

(Figs. 12A-B, D)

Occurrence. 17723.2-23.5 (Fig. 12A-B, D).

Holia sp. 2

(Figs. 12H-K)

Occurrence. TQ (Figs. 12H-K).

Remarks. Holia sp. 2 is clearly morphologically distinct from species 1, as it lacks a robust occipital spine. It may possesss a "thorn-like" spine (Adrain, 1998), but the specimens are damaged, so we cannot say conclusively. Species 2 also has a more pronounced anterior border, and lacks the fine, dense granules of species 1.

Genus ***Pandaspinapyga*** Esker & Levin, 1964

Pandaspinapyga salsa Esker, 1964

(Figs. 12C, F)

Occurrence. TQ (Figs. 12C, F)

Subfamily **DEIPHONINAE** Raymond, 1913

Genus ***Sphaerocoryphe*** Angelin, 1854

Sphaerocoryphe sp. 1

(Figs. 12E-G)

Occurrence. TQ (Figs. 12E-G)

Family **ENCRINURIDAE** Angelin, 1854

Genus ***Frencrinuroides*** Lespérance & Desbiens, 1995

Frencrinuroides capitonis Frederickson, 1964

(Figs. 13A-C, E-F, I-J, L)

Occurrence. TQ **(**Figs. 13A-C, E-F, I-J, L).

Subfamily **CYBELINAE** Holliday, 1942

Genus ***Cybeloides*** Slocum, 1913

***Cybeloide*s** sp. 1

(Figs. 12D, G-H, K, N)

Occurrence. I35N7.5 (Figs. 12D, G-H), I35N4.85 (Figs. K, N).

Order **ODONTOPLEURIDA** Whittington, 1959

Family **ODONTOPLEURIDAE** Burmeister, 1843

Genus ***Ceratocephala*** Warder, 1838

Ceratocephala graffhami Shaw, 1974

(Fig. 14E)

Occurrence. TQ (Fig. 14E).

Genus ***Apianurus*** Whittington, 1956

Apianurus sp. 1

(Figs. 14A, C)

Occurrence. TQ (Figs. 14A, C).

Order **LICHIDA** MOORE, 1959

Family **LICHIDAE** Hawle & Corda, 1847

Subfamily **TROCHURINAE** Phleger, 1936

Genus ***Hemiarges*** Gürich, 1901

Hemiarges sp. 1

(Figs. 14B, D, F, H)

Occurrence. TQ (Figs. 14B, D, F, H)

Order **PROETIDA** Fortey & Owens 1975

Family **DIMEROPYGIDAE** Húpe 1953

Genus ***Mesotaphraspis*** Whittington & Evitt, 1954

Mesotaphraspis sp. 1

(Fig. 14G)

Occurrence. I35N6.85 (Fig. 14G).

REFERENCES

Adrain, J.M. 1998. Systematics of the Acanthoparyphinae (Trilobita), with species from the Silurian of Arctic Canada. *Journal of Paleontology*, **72**: 698-718.

Amati, L. & Westrop, S.R. 2004. A systematic revision of *Thaleops* (Trilobita: Illaenidae) with new species from the middle and late Ordovician of Oklahoma and New York. *Journal of Systematic Palaeontology*, **2**: 207-256.

Angelin, N.P. 1854. *Palaeontologica Scandinavica Pars II*. Academiae Regiae Scientarium Suecanae (Holmiae), 21-92 pp.

Bradley, J.H. 1930. Fauna of the Kimmswick Limestone of Missouri and Illinois. *Walker Museum, University of Chicago Contributions*, **2**: 219-290.

Burmeister, H. 1843. *Die Organisation der Trilobiten aus ihren lebenden Verwandten entwickelt; nebst einer systematischen Uebersicht aller zeither beschrieben Arten*. Reimer, Berlin, 147 pp.

Chatterton, B.D.E. & Ludvigsen, R. 1976. Silicified middle Ordovician trilobites from the south Nahanni river area, District of Mackenzie, Canada. *Palaeontographica*, **154**: 1-106.

Conrad, T.A. 1843. Observations on the lead bearing limestone of Wisconsin, and description of a new genus of trilobites and fifteen new Silurian fossils. *Proceedings of the Academy of Natural Sciences of Philadelphia*, **1**: 329-335.

Cooper, B.N. 1953. Trilobites from the lower Champlainian formations of the Appalachian Valley. *Geological Society of America Memoir*, **55**: 1-69.

Decker, C.E. 1931. A new species of *Ampyx*. *Journal of Paleontology*, **5**: 153-155.

Dekay, J.E. 1864. Observations on the Structure of Trilobites, and Description of an Apparently New Genus. *Annales of the Lyceum of Natural History*, **1**: 1-174.

Esker, G.C. 1964. New species of trilobites from the Bromide Formation (Poolevillve Member) of Oklahoma. *Oklahoma Geology Notes*, **24**: 195-209.

Esker, G.C. & Levin, H. 1964. *Pandaspinapyga*, a new trilobite genus from the Kimmsick Limestone (Ordovician) of Missouri. *Journal of Paleontology*, **38**: 776-778.

Fortey, R.A. & Owens, R.M. 1975. Proetida- a new order of trilobites. *Fossils and Strata*, **4**: 227-239.

Frederickson, E.A. 1964. Two Ordovician trilobites from southern Oklahoma. *Oklahoma Geology Notes*, **24**: 71-75.

Green, J. 1832. *A monograph of the trilobites of North America*. Joseph Brano, Philadelphia, 93 pp.

Gürich, G. 1901. Ueber eine neue Lichas-art aus dem Devon von Neu-Sud Wales und uber die Gattung Lichas uberhaupt. *Neues Jahr-buch fur Mineralogie, Geologie und Palaontologie*, **14**: 519-539.

Hawle, I. & Corda, A.J.C. 1847. *Prodrom einer monographie der bohmischen Trilobiten. Abhandlungen Koeniglichen Boehmischen Gesellschaft der Wissenschaften*. J.G Clave, Prague.

Holliday, S. 1942. Ordovician trilobites from Nevada. *Journal of Paleontology*, **16**: 471-478.

Hupé, P. 1953. Classe des Trilobites. Pp. 44-246 in J. Piveteau (ed) *Traité de paléontologie 3*.

Jaanusson, V. 1959. Suborder Illaenina, O365-0415 in R.C. Moore (ed) *Treatise on Invertebrate Paleontology, Part O, Arthropoda I*. Geological Society of America and University of Kansas Press, Lawrence.

Kobayashi, T. 1935. The Cambro-Ordovician formations and faunas of South Chosen. Palaeontology Part III. Cambrian faunas of South Chosen with special study on the Cambrian trilobite genera and families. *Journal of the Faculty of Science, Imperial University of Tokyo*, **4**: 49-344.

Lespérance, P.J. & Desbiens, S. 1995. Selected Ordovician trilobites from the Lake St. John District of Quebec and their bearing on systematics. *Paleontological Society Memoir*, **42**: 1-19.

Moore, R.C. 1959. *Treatise on invertebrate paleontology, Part O, Arthropoda 1*. Geological Society of America and University of Kansas, Boulder, CO and Lawrence, KA, 560 pp.

Phleger, F. 1936. Lichadian Trilobites. *Journal of Paleontology*, **10**: 593-615.

Portlock, J.E. 1843. *Report on the Geology of the County of Londonderry, and of Parts of Tyrone and Fermanagh*. Ordnance Survey of Ireland.

Raymond, P.E. 1905. Trilobites of the Chazy Limestone. *Annals of the Carnegie Museum*, **3**: 328-396.

Raymond, P.E. 1910. Notes on Ordovician trilobites IV, new and old species from the Chazy. *Annals of the Carnegie Museum*, **7**: 60-80.

Raymond, P.E. 1913. Notes on some new and old trilobites in the Victoria memorial Museum. *Bulletin of the Victoria Memorial Museum, Geological Survey of Canada*, **1**: 33-39.

Reed, F.R.C. 1905. The classification of the Phacopidae. *Geological Magazine*, **5**: 172-178, 224-228.

Salter, J.W. 1864. A monograph of the British trilobites from the Cambrian, Silurian and Devonian formations. *Monographs of the Palaeontographical Society of London*: 1-80.

Slocum, A.W. 1913. New trilobites from the Maquoketa beds of Fayette County, Iowa. *Field Museum of Natural History Geological Series*, **4**: 43-83.

Struve, W. 1959. Suborder Phacopina, O461 in R.C. Moore (ed) *Treatise on Invertebrate Paleontology. Part O - Arthropoda (Trilobitomorpha)*. Geological Society of America and the University of Kansas Press, Lawrence.

Walch, J.E.I. 1771. *Die Naturgeschichte der Versteinerungen, Dritter Theil. Zur Erlauterung der Knorrischen Sammlung von Merkwurdigkeiten der Natur*. P.J. FelBecker, Nurnberg, 235 pp.

Whittington, H.B. 1949. Dolichoharpes and the origin of the harpid fringe. *American Journal of Science*, **247**: 276-285.

Whittington, H.B. 1954. Ordovician trilobites from Stilliman's Fossil Mount. *Geological Society of America Memoir*, **62**: 119-149.

Whittington, H.B. & Evitt, W.R. 1954. Silicified Middle Ordovician trilobites (Virginia). *Geological Society of America Memoir*, **59**: 1-137.

Whittington, H.B. 1956. Silicified Middle Ordovician trilobites: The Odontopleuridae. *Bulletin of the Museum of Comparative Zoology Harvard College*, **114**: 159-288.

Whittington, H.B. 1959. Silicified Middle Ordovician trilobites; Remopleurididae, Trinucleidae, Raphiophoridae, Endymioniidae (Virginia). *Bulletin of the Museum of Comparative Zoology*, **121**: 372-496.

Figure 1. *Thaleops* sp. 1. **A-C**, testate cranidium (OU 12495) x 6.7: **A**, dorsal view; **B**, oblique view; **C**, posterior view. **D-F**, **H**, testate cranidium (OU 12496), x 4.7: **D**, dorsal view; **E**, oblique view; **F**, anterior view; **H**, posterior view. **G**, **I**, testate pygidium (OU 12497), x 10: **G**, dorsal view; **I**, posterior view. **J**, partially exfoliated pygidium (OU 12498), x 4: **J**, dorsal view. **K**, **L**, partially foliated cranidium (OU 12499), x 2.66: **K**, dorsal view, **L**, anterior view.

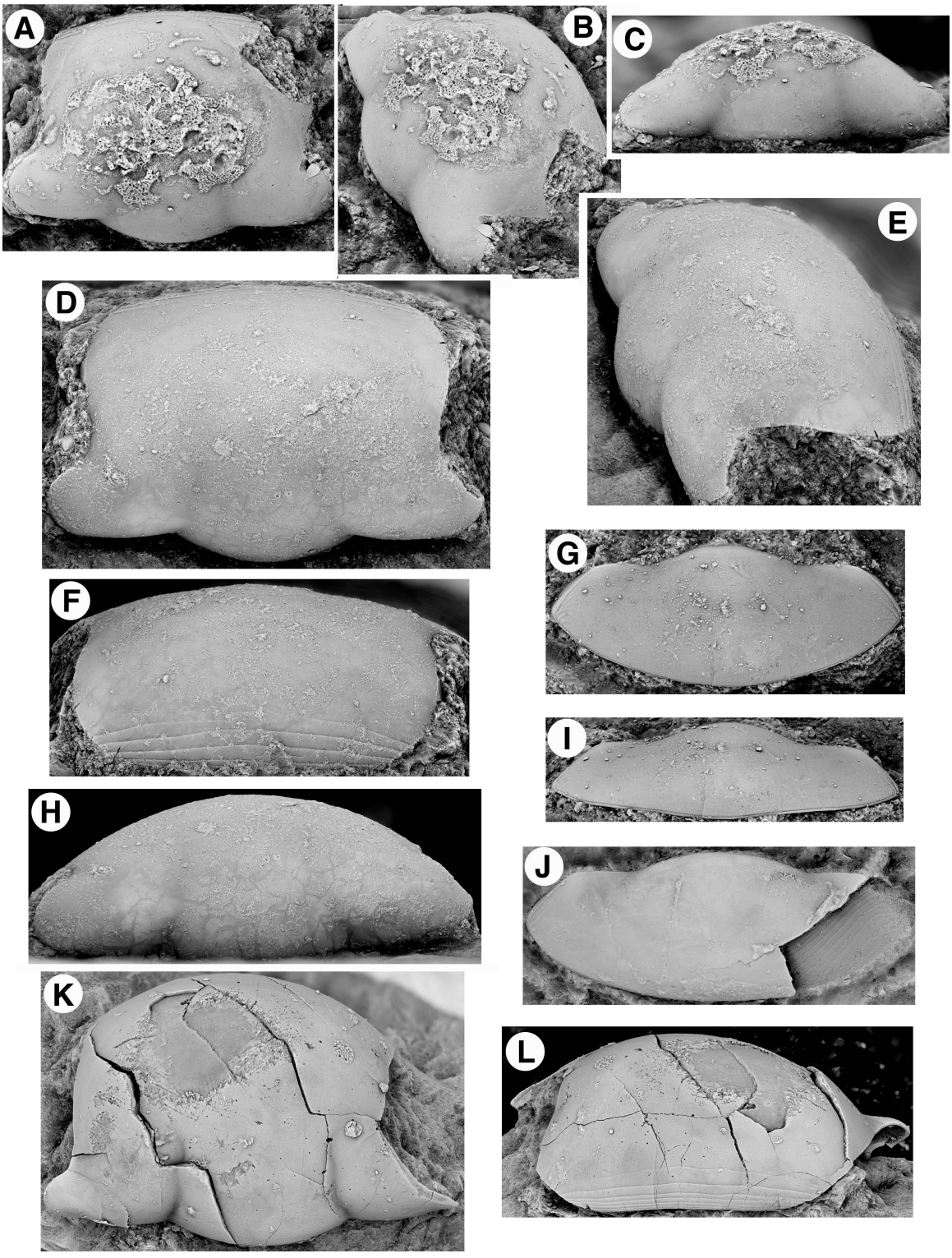
A
B
C
D
E
F
G
H
I
J
K
L

Figure 2. *Thaleops jaanussoni* (Amati & Westrop, 2004). **A-C**, partially exfoliated cranidium (OU 7995), x 6: **A**, dorsal view; **B**, posterior view; **C**, anterior view. **D**, partially exfoliated cranidium (OU 12500), x 6.7, dorsal view. **E-F**, **H-I**, testate cranidium (OU 12501), x 6.7: **E**, posterior view; **F**, lateral view; **H**, anterior view; **I**, dorsal view. **J**, exfoliated pygidium (OU 12502), x 7, dorsal view. **K**, exfoliated pygidium (OU 12503), x 6.7, dorsal view. *Thaleops mobydicki* (Amati & Westrop, 2004). **G**, testate pygidium (OU 12503), x 6.7, dorsal view.

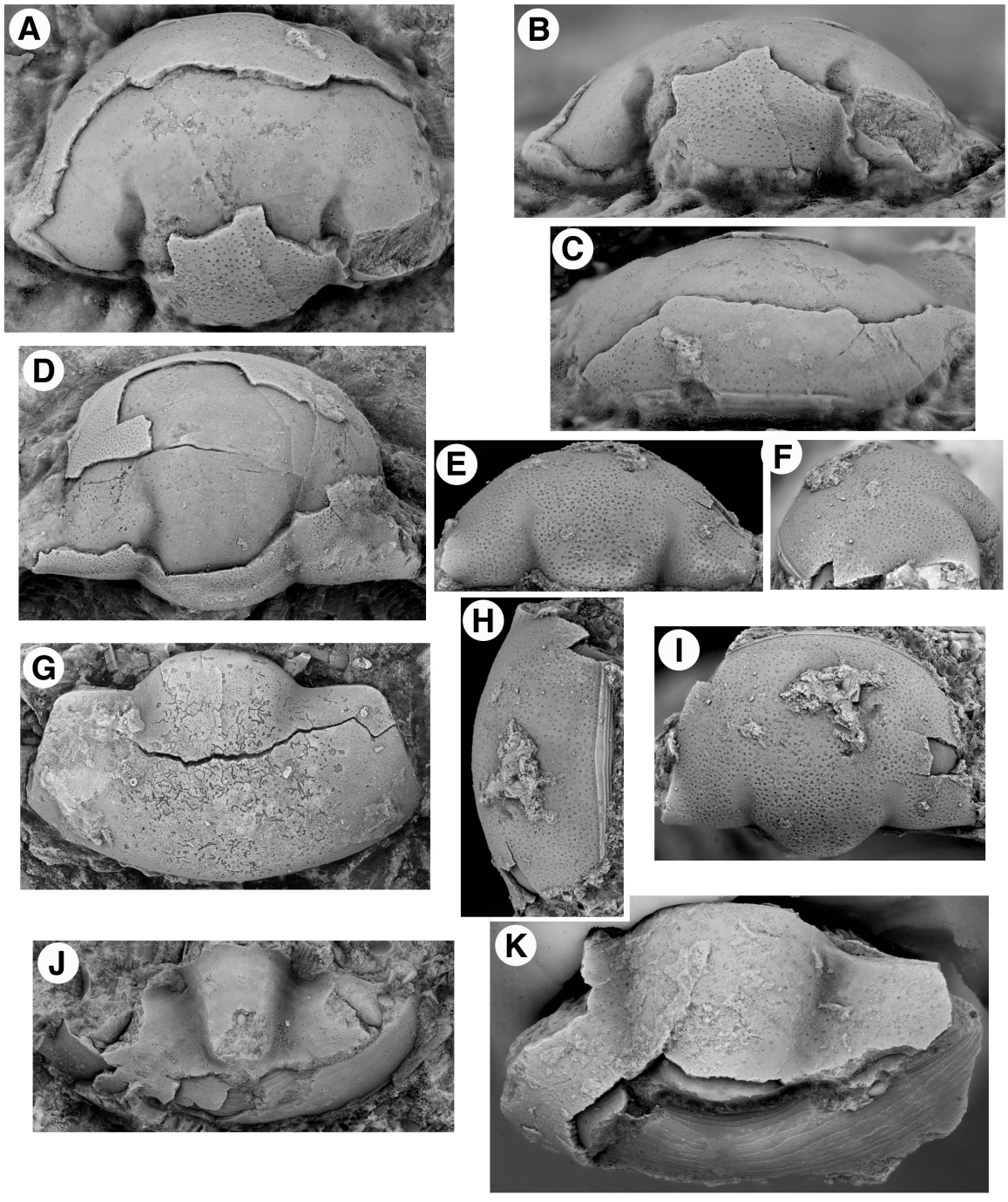
A
B
C
D
E
F
G
H
I
J
K

Figure 3. *Failleana* sp. 1. **A**, **C**-**D**, testate cranidium (OU 12504), x 3.3: **A**, dorsal view; **C**, lateral view, x 4; **D**, anterior view. **B**, **F**, exfoliated pygidium (OU 12505) x 4: **B**, dorsal view; **F**, posterior view. **E**, partially exfoliated cranidium (OU 12506), x 4.5, dorsal view. **G**-**I**, partially exfoliated pygidium (OU 12507), x 2.66: **G**, dorsal view; **H**, posterior view; **I**, lateral view.

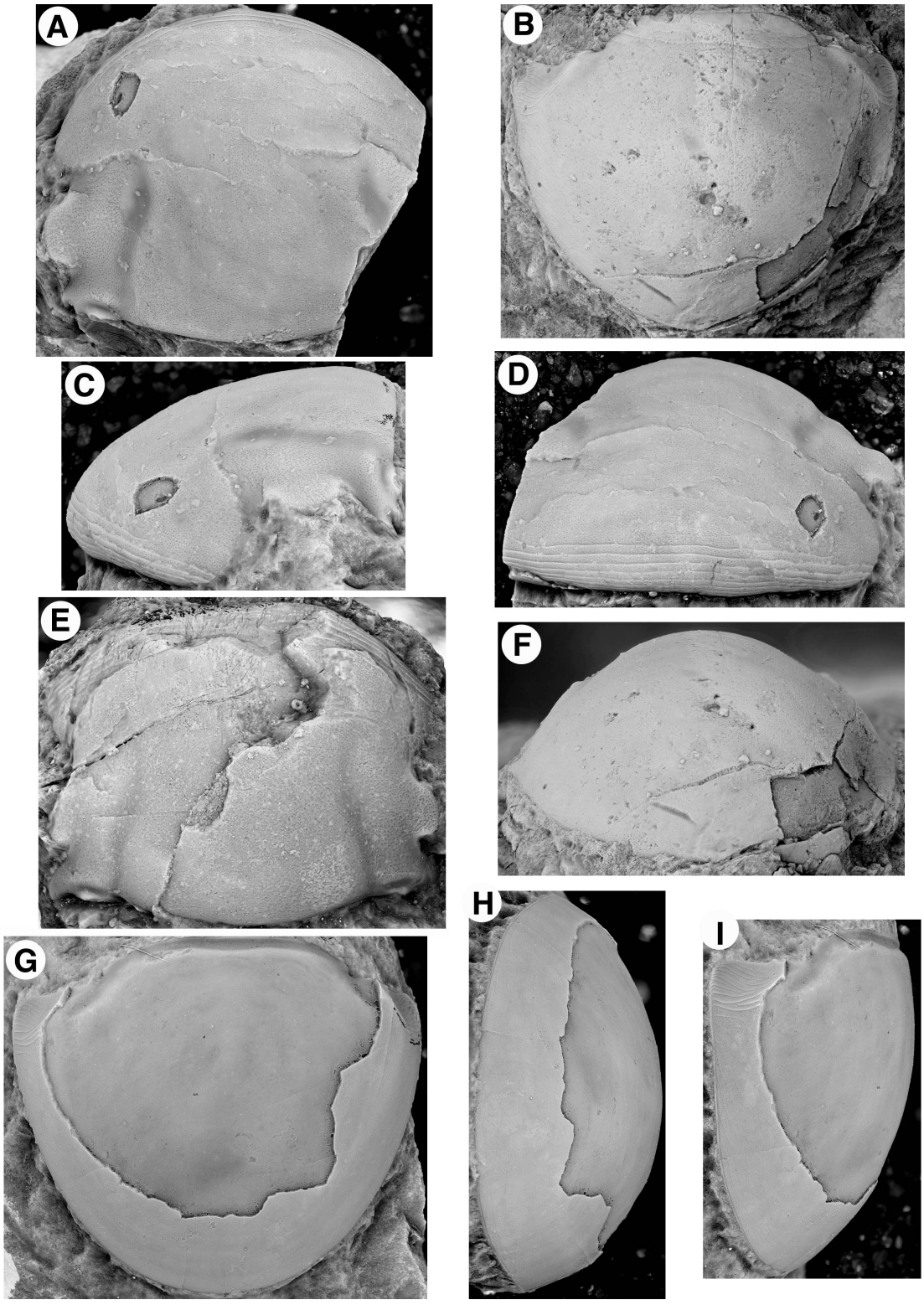
A
B
C
D
E
F
G
H
I

Figure 4. *Failleana* sp. 1. **A**, cranidium (OU 12508), x 8, dorsal view. **B-F**, partially exfoliated cranidium (OU 12509), x 6.7: **B**, anterior view; **C**, anterior view; **F**, lateral view. **D-E**, partially exfoliated cranidium (OU 12510), x 4.67: **D**, dorsal view; **E**, lateral view. **J-K**, partially exfoliated pygidium (OU 12511), x 3: **J**, posterior view; **K**, dorsal view. *Failleana limbatus* (Raymond, 1910). **G-I**, cranidium (OU 12512), x 3.1: **G**, dorsal view; **H**, lateral view; **I**, anterior view.

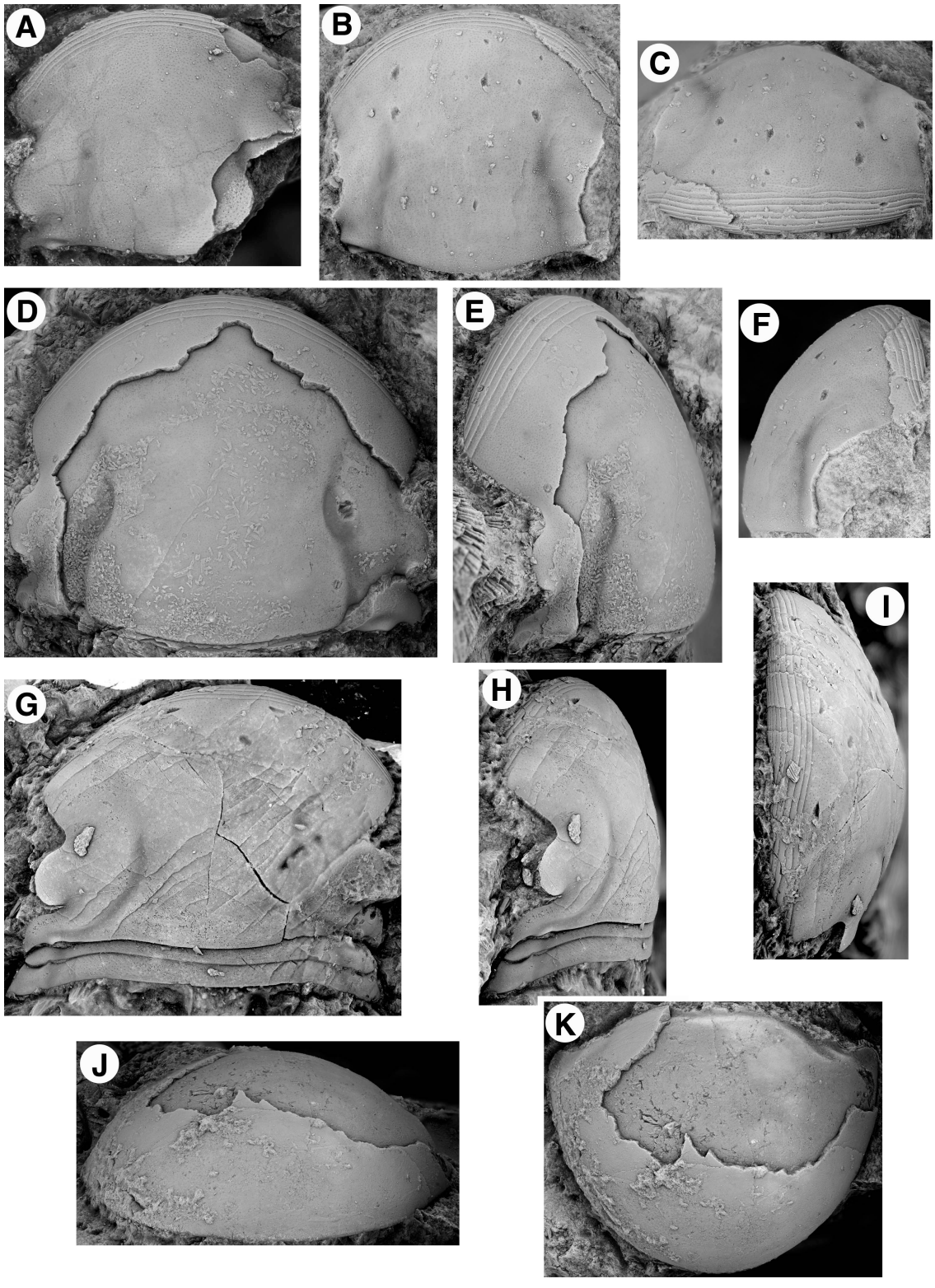
A
B
C
D
E
F
G
H
I
J
K

Figure 5. *Anataphrus* sp. 1. **A**, **D**, exfoliated cranidium (OU 12513), x 5.3: **A**, dorsal view; **D**, lateral view. **B**, **E**, testate pygidium (OU 12514), x 5.3: **B**, dorsal view; **E**, posterior view. **H**, exfoliated pygidium (OU 12515), x 5.3, dorsal view. **F**, hypostome (OU 12516) x 6.7, dorsal view. *Anataphrus* sp. 2. **I**, **K**, exfoliated pygidium (OU 12517), x 4.7: **I**, dorsal view; **K**, posterior view. **J**, testate cranidium (OU 12518), x 4, dorsal view. *Anataphrus* sp. 3. **G**, partially exfoliated cranidium (OU 12519), x 4.7, dorsal view. *Anataphrus* sp. 4. **C**, cranidium (OU 12520), x 5, dorsal view.

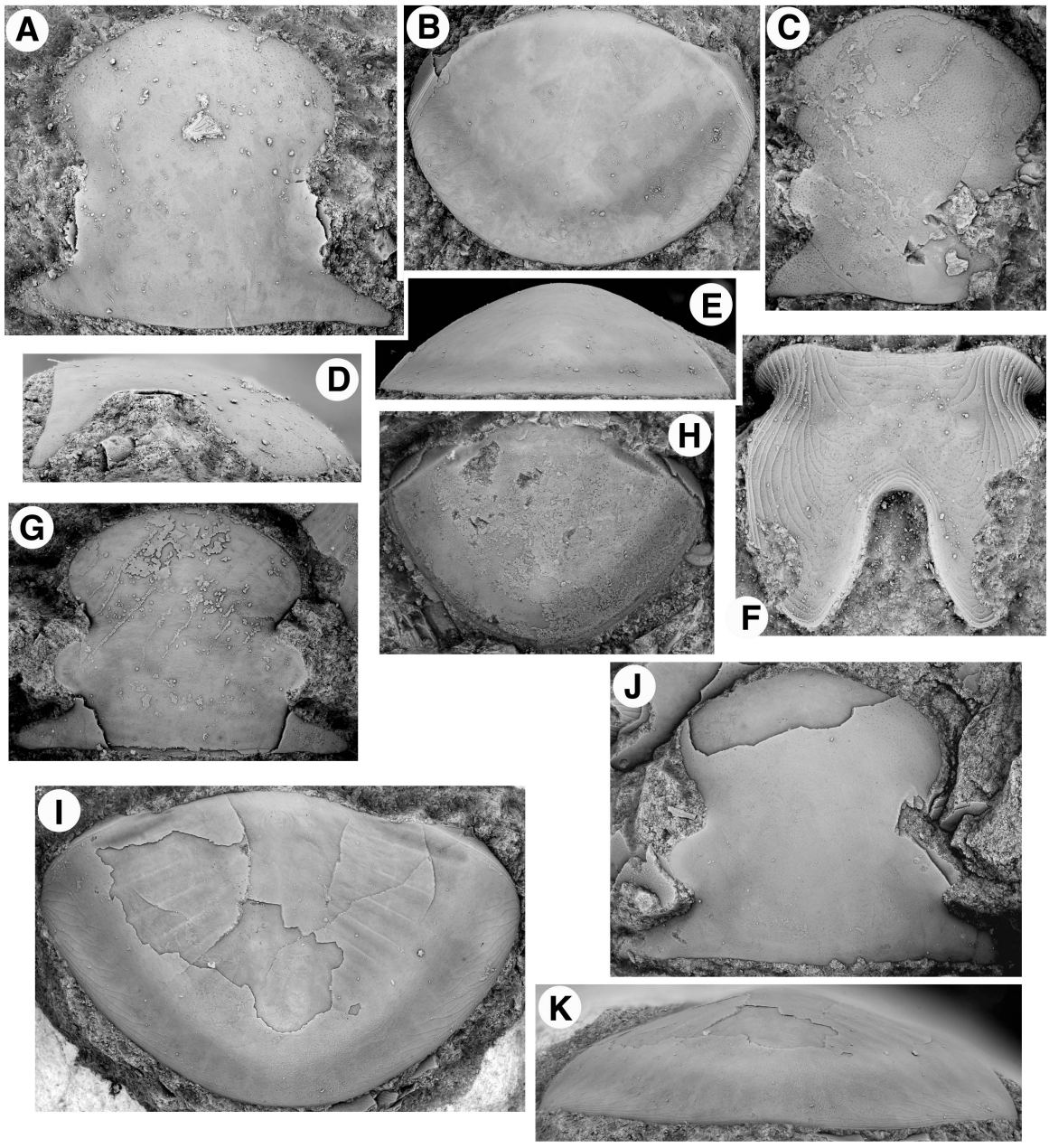
A
B
C
E
D
H
G
F
J
I
K

Figure 6. *Isotelus Bromidensis* (Esker, 1964). **A**, **C**, testate cephalon (OU 12521), x 4: **A**, dorsal view; **C**, anterior view. **B**, **D**, exfoliated pygidium (OU 12522), x 4: **B**, dorsal view; **D**, posterior view. *Isotelus* sp. 2. **E**, testate pygidium (OU 12523), x 10.6, dorsal view. **F**, transitory pygidium (OU 12524), x 14, dorsal view. **G**, testate cranidium (OU 12525), x 10.6, dorsal view.

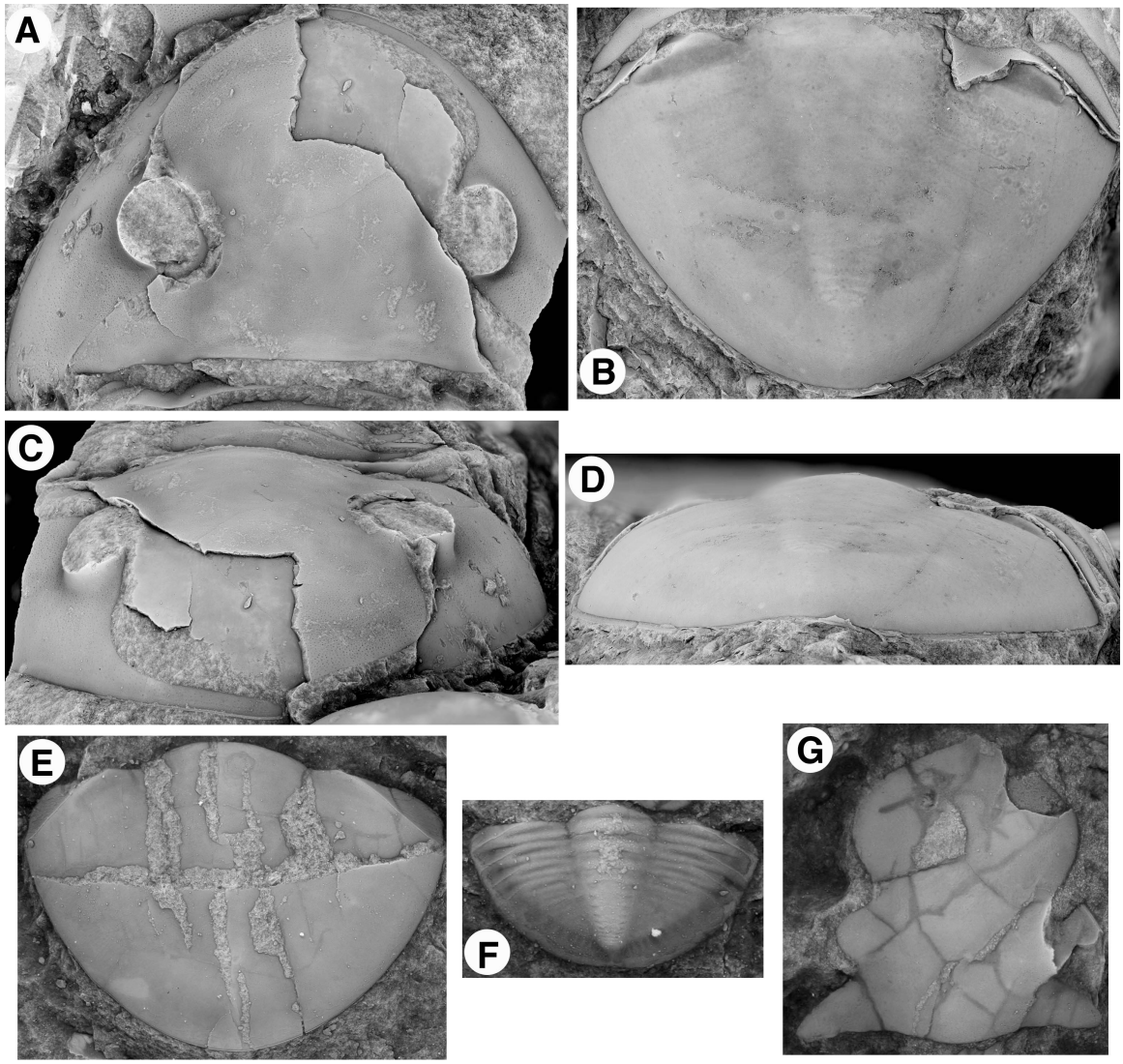
A
B
C
D
E
F
G

Figure 7. *Remopleurides* sp.1. **A-C**, thoracopygon (OU 12526), x 13.3: **A**, dorsal view; **B**, lateral view; **C**, posterior view. **D-E**, thoracopygon (OU 12527), x 9.3: **D**, dorsal view; **E**, posterior view, x 10. **F-G**, **I**, testate cranidium (OU 12528), x 6.7: **F**, dorsal view; **G**, lateral view; **I**, anterior view. **H**, **K**, **L**, testate cranidium (OU 12529), x 8: **H**, dorsal view; **K**, posterior view; **L**, lateral view. **J**, testate cranidium (OU 12530), x 8, dorsal view.

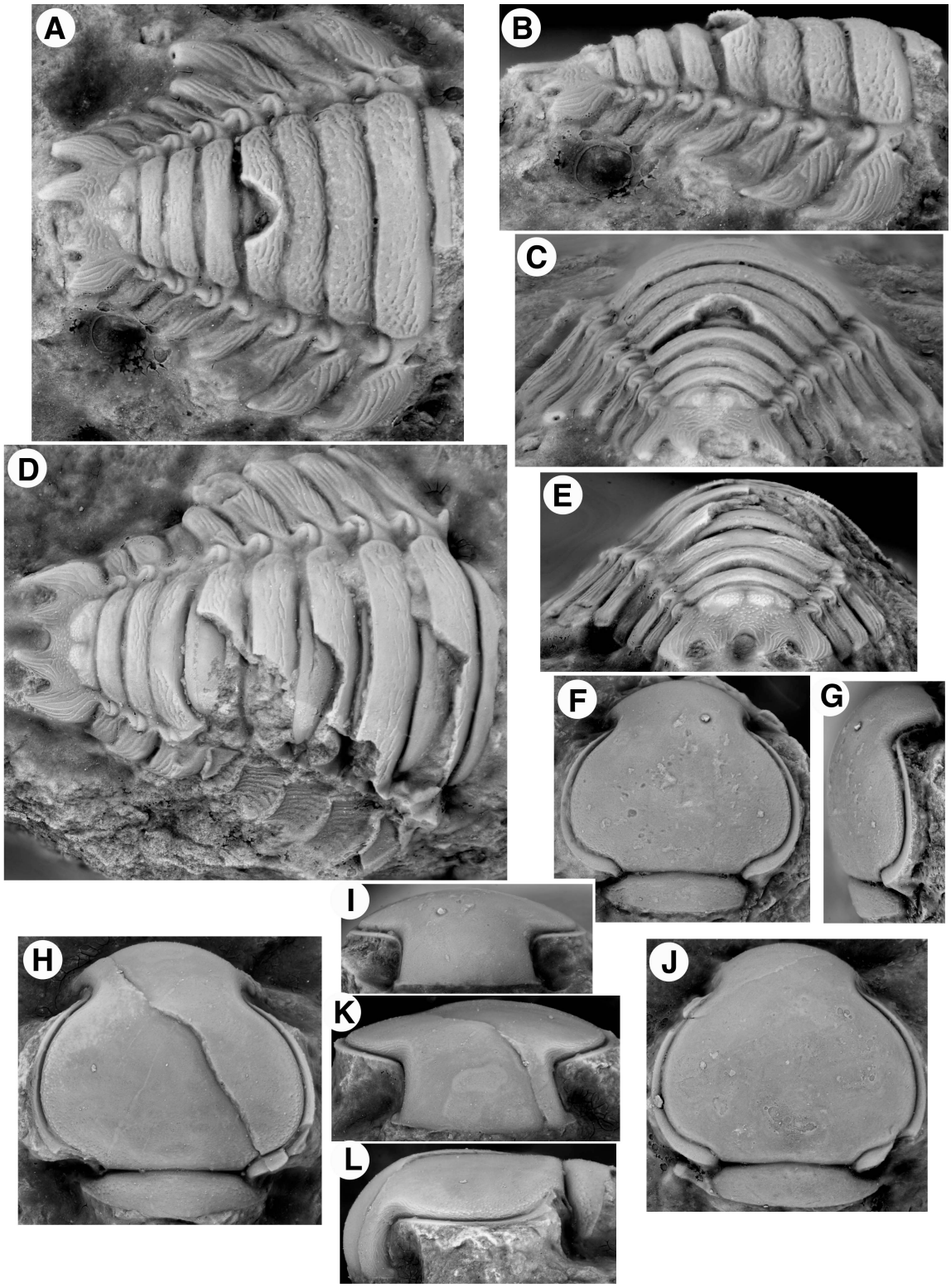
A
B
C
D
E
F
G
I
H
K
J
L

Figure 8. *Lonchodomas mcgheei* (Decker, 1931). **A**, complete individual (OU 12531), x 4, dorsal view. **B**, topotype complete individual (OU 3448), x 4.2, dorsal view. **C**-**D**, **G**, cranidium (OU 12532), x 6.7: **C**, dorsal view; **D**, lateral view, x7; **G**, anterior view. **E**, damaged individual (OU 12533), x 8, dorsal view. **F**, **H**, pygidium (OU 12534), x 10.6: **F**, dorsal view, **H**, posterior view.

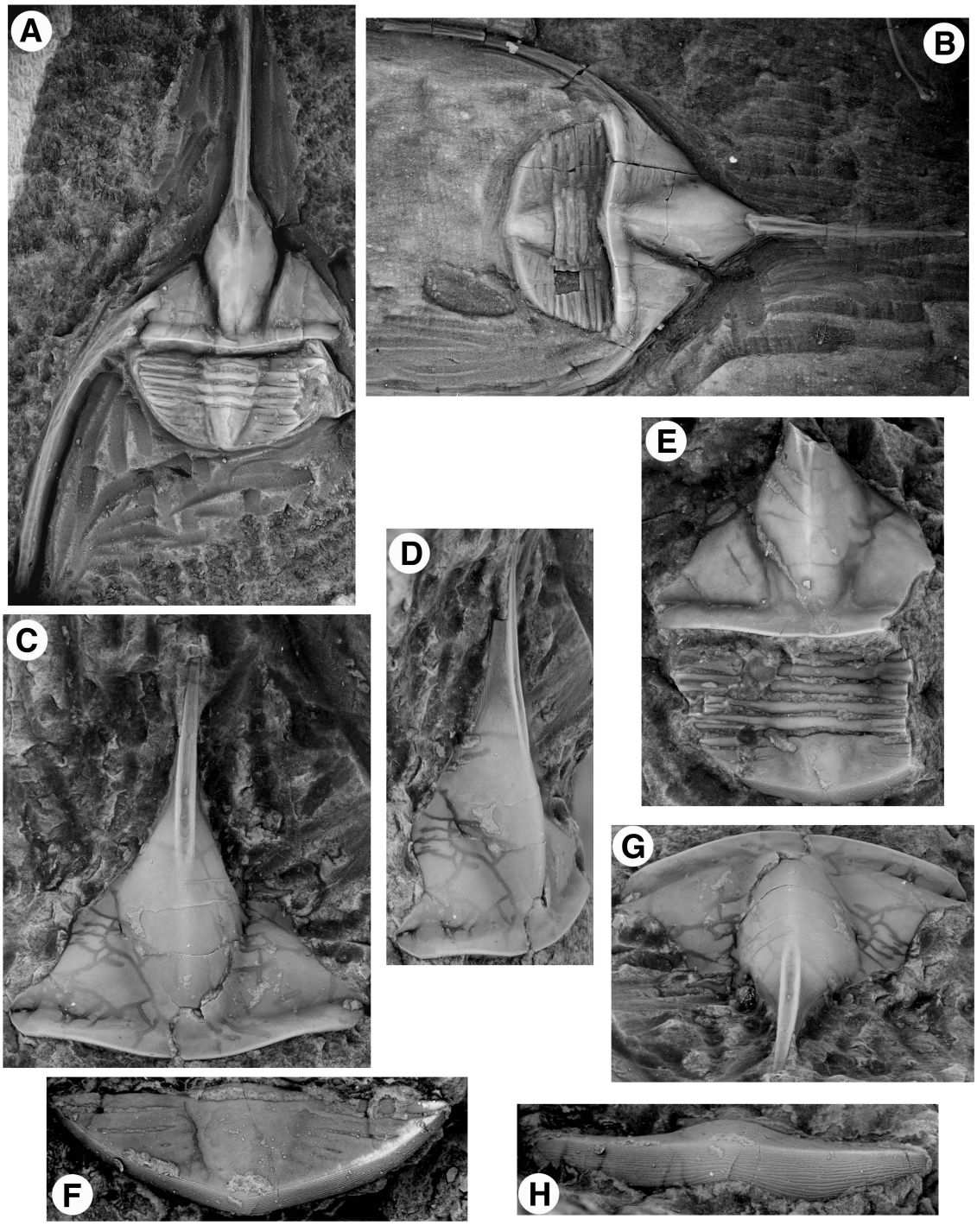
A
B
C
D
E
F
G
H

Figure 9. *Dolichoharpes reticulata* (Whittington, 1949). **A-C**, complete individual (OU 12535), x 4.6: **A**, dorsal view; **B**, anterior view; **C**, lateral view. *Calyptaulax annulata* (Raymond, 1905). **D**, **F-G**, cranidium (OU 12535), x 6.7: **D**, dorsal view; **F**, lateral view; **G**, anterior view. **E**, cranidium (OU 12537), x 4, dorsal view. **H-J**, pygidium (OU 12538), x 7: **H**, posterior view; **I**, lateral view; **J**, dorsal view.

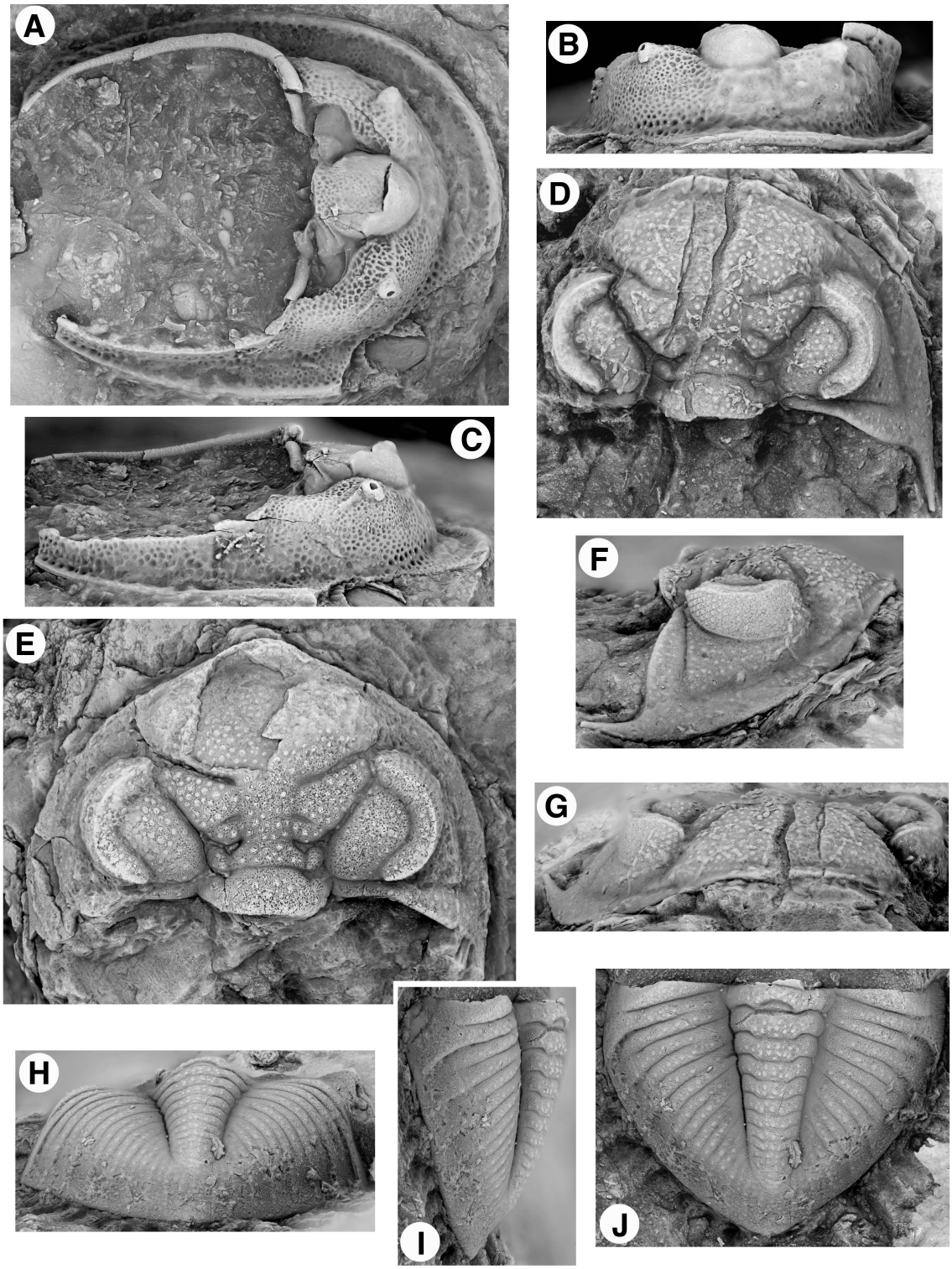
A
B
C
D
E
F
G
H
I
J

Figure 10. *Calyptaulax annulata* (Raymond, 1905). **A-B**, **E**, cranidium (OU 12539), x 6.7: **A**, dorsal view; **B**, anterior view; **E**, lateral view. **C-D**, pygidium (OU 12540), x 8: **C**, dorsal view; **D**, lateral view. **F**, pygidium (OU 12541), x 8, dorsal view. **G-I**, cranidium (OU 12542), x 6.5: **G**, dorsal view; **H**, anterior view, x6.5; **I**, lateral view, x 6.5.

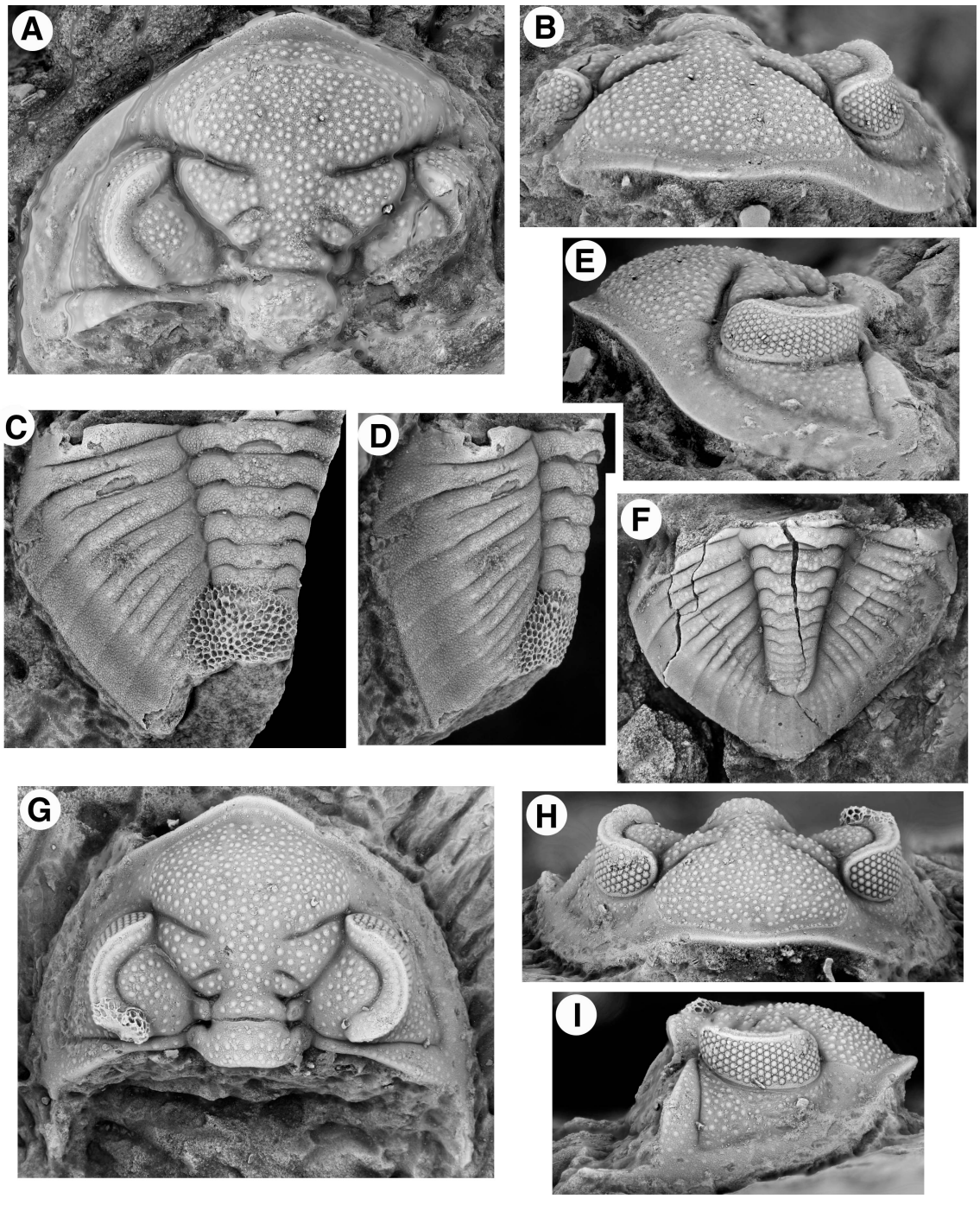
A
B
E
C
D
F
G
H
I

Figure 11. *Ceraurinella* sp. 1. **A**, cranidium (OU 12543), x 4.7, dorsal view. **F**, damaged cranidium (OU 12544), x 5.3, dorsal view. **G**, pygidium (OU 12545), x 8, dorsal view. **H**, pygidium (OU 12546), x 8, dorsal view. *Ceraurinella* sp. 2. **B**-**C**, **E**, cranidium (OU 12547), x 5.3: **B**, dorsal view; **C**, anterior view; **E**, lateral view. **I**, pygidium (OU 12548), x 3.3, dorsal view. *Ceraurus ruidus* (Cooper, 1953). **D**, cranidium (OU 12549), x 4, dorsal view. **J**-**K**, cranidium (OU 12550), x 4: **J**, dorsal view; **K**, lateral view.

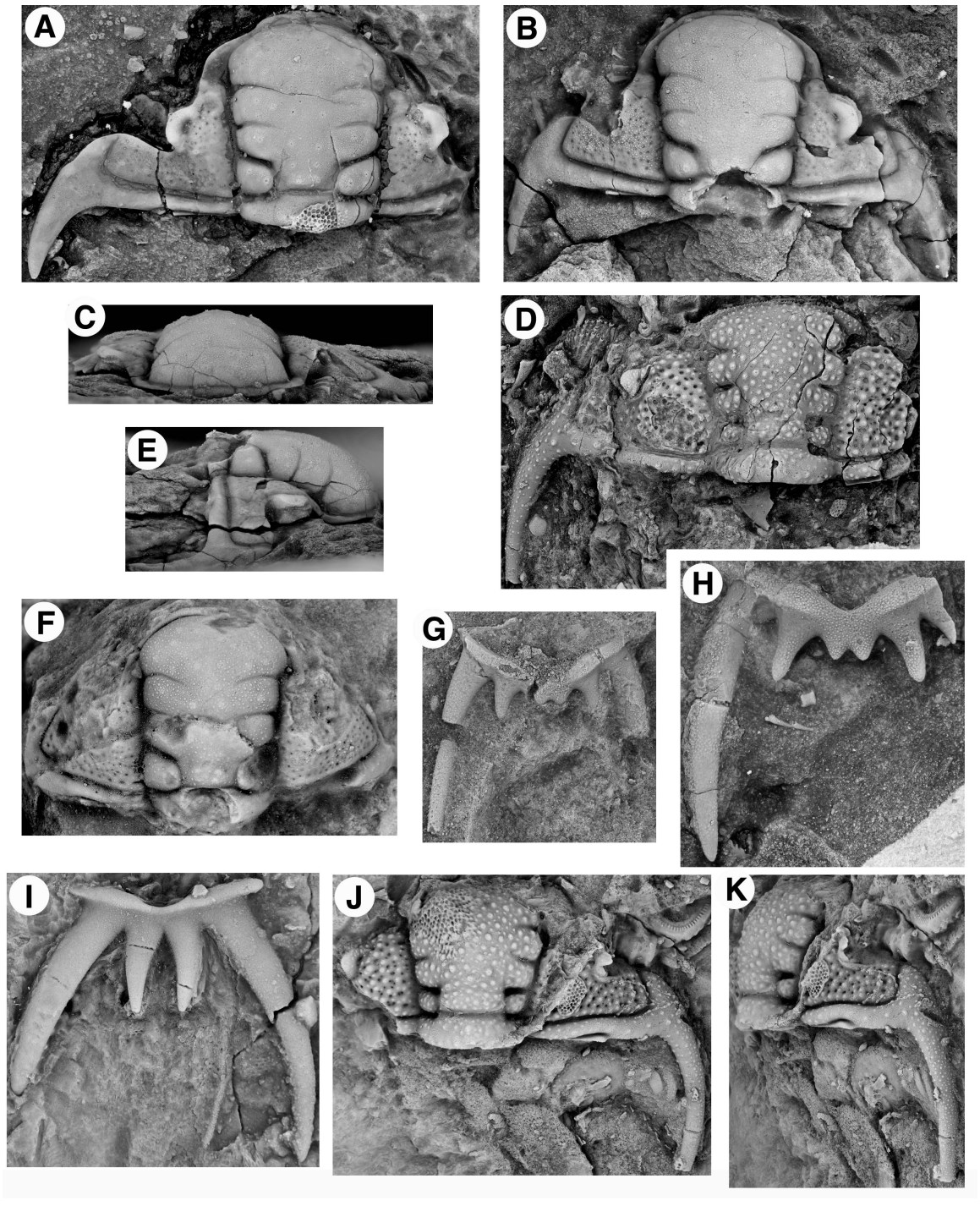
A
B
C
D
E
F
G
H
I
J
K

Figure 12. *Holia* sp. 1. **A**-**B**, **D**, cranidium (OU 12551), x 8: **A**, dorsal view; **B**, lateral view; **D**, anterior view. *Holia* sp. 2. **H**-**I**, **K**, cranidium (OU 12552), x 3.3: **H**, anterior view; **I**, dorsal view; **K**, lateral view. **J**, cranidium (OU 12553), x 4, dorsal view. *Pandaspinapyga salsa*. **C**, **F**, cranidium (OU 12554), x 4: **C**, lateral view; **F**, dorsal view. *Sphaerocoryphe* sp. 1. **E**, **G**, cranidium (OU 12555), x 8: **E**, dorsal view; **G**, lateral view, x 8.6.

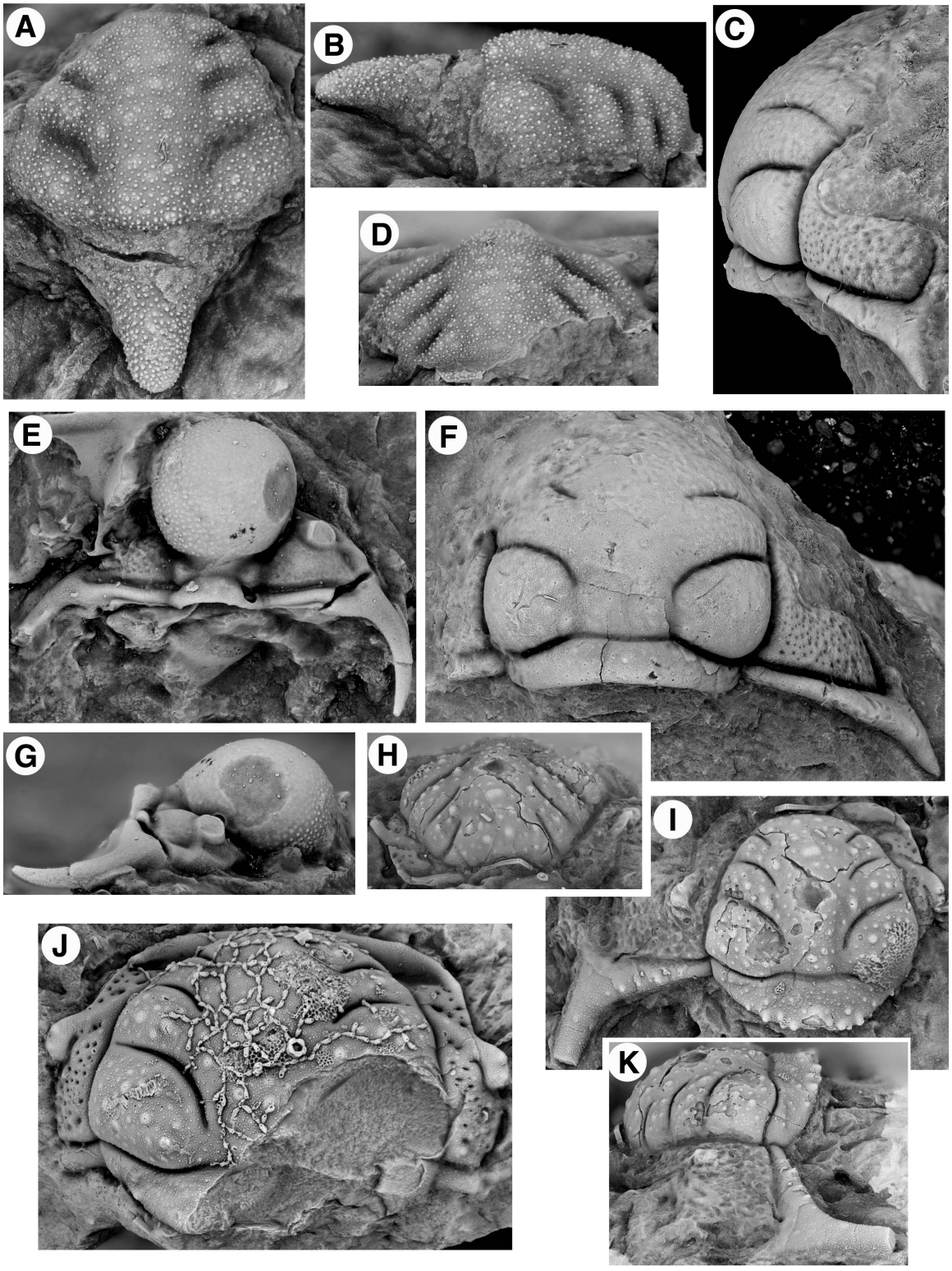
A
B
C
D
E
F
G
H
I
J
K

Figure 13. *Frencrinuroides capitonis* (Frederickson, 1964). **A**-**C**, **E**, **F**, complete individual (OU 12556), x 5.4: **A**, dorsal view; **B**, oblique lateral view; **C**, lateral view; **E**, anterior view, x 6.1; **F**, posterior view. **I**, **L**, pygidium (OU 12557), x 6.7: **I**, dorsal view; **L**, posterior view. **J**, **M**, cranidium (OU 12558), x 6.7: **J**, lateral view; **M**, dorsal view, x 5.3. *Cybeloides* sp. 1. **D**, **G**-**H**, cranidium (OU 12559), x 5.3: **D**, anterior view; **G**, dorsal view; **H**, lateral view, x 6.7. **K**, **N**, cranidium (OU 12560), x 6: **K**, dorsal view; **N**, lateral view, x 6.7.

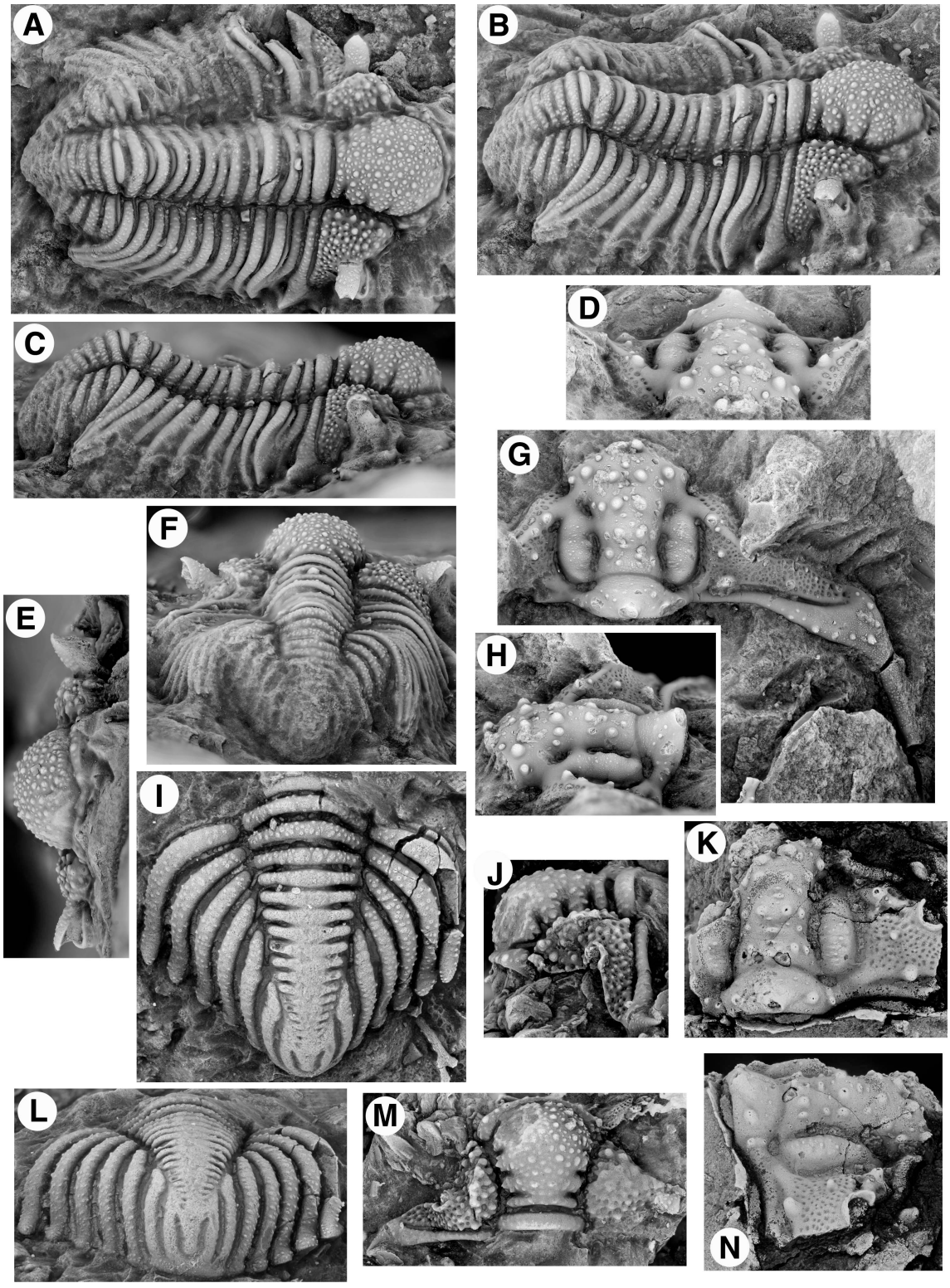
A
B
C
D
E
F
G
H
I
J
K
L
M
N

Figure 14. *Apianurus* sp. 1. **A**, **C**, cranidium (OU 12561), x 5.3: **A**, dorsal view; **C**, posterior view. *Hemiarges* sp. 1. **B**, **D**, cranidium (OU 12562), x 8: **B**, dorsal view; **D**, anterior view. **F**, **H**, cranidium (OU 12563), x 8: **F**, dorsal view; **H**, lateral view. *Ceratocephala graffhami* (Shaw, 1974). **E**, cranidium (OU 12564), x 5.3, dorsal view. *Mesotaphraspis* sp. 1. **G**, cranidium (OU 12565), x 25.3, dorsal view.

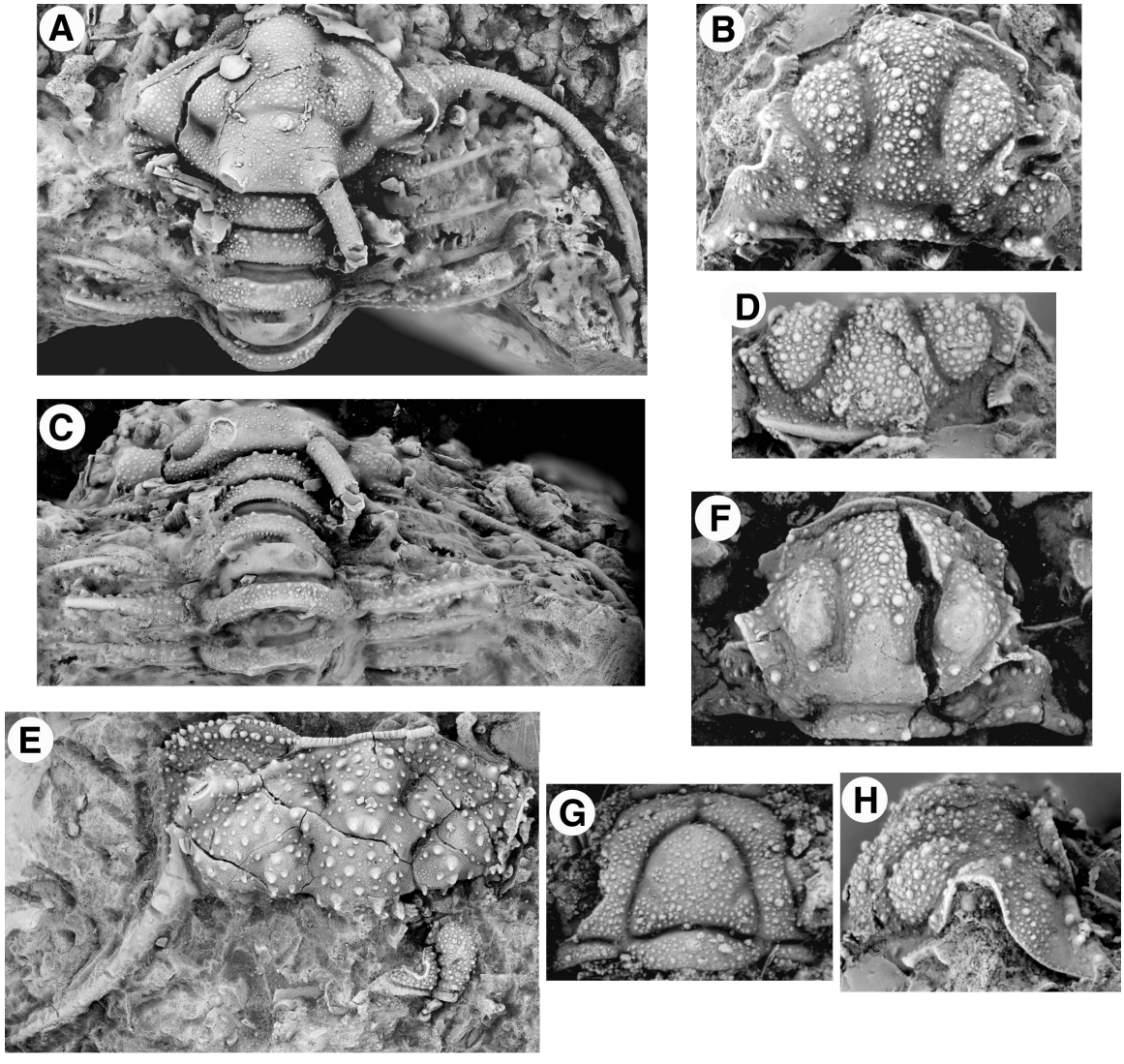
A
B
D
C
F
E
G
H

APPENDIX 3: TRILOBITE RELATIVE ABUNDANCE DATA NOT SHOWN IN CHAPTERS

This appendix shows the data for to relative abundance counts that were not part of the paleoecological studies in Chapters 5 or 6, but part of my contribution towards the larger NSF- EAR0819715 project.

	SJ34.6	WoodVA 31.8
Calyptaulax	35	0
Cryptolithus	0	47
Flexicalymene	0	2
Isotelus	2	5
Ampyx	3	0
Arthrorhachis	10	0
Remopleurides	8	0
Lonchodomas	12	0
Apianurus	1	0

TABLE 1—Relative abundance counts for two collections in Northern Virginia. SJ34.6 is from the Strasburg Junction locality (Cooper and Cooper, 1946) in the Edinburgh Formation; see measured section in appendix 1. The Woodstock VA collection is from a roadcut through the Oranda and Martinsburg Formations, on the south side of East Reservoir Road (N38° 51.997 and W78° 30.764), measured section also in appendix 1.

REFERENCES

COOPER, B.N., and COOPER, G.A., 1946, Lower Middle Ordovician Stratigraphy of the Shenandoah Valley, Virginia: Bulletin of the Geological Society of America, v. 57, p. 35-114.